

Exploration of Salvinorin A for the Development of Pain and

Addiction Therapies

By Rachel Saylor Crowley

Submitted to the graduate degree program in Medicinal Chemistry and the Graduate Faculty of the University of Kansas in partial fulfillment of the requirements for the degree of Doctor of Philosophy.

Chairperson: Thomas E. Prisinzano

Dr. Michael F. Rafferty

Dr. Brian S. J. Blagg

Dr. Michael S. Wolfe

Dr. Jeffrey P. Krise

Date Defended: June 30, 2017

The dissertation committee for Rachel Saylor Crowley certifies that
this is the approved version of the following dissertation:

Exploration of Salvinorin A for the Development of Pain and
Addiction Therapies

Chairperson: Thomas E. Prisinzano

Date Approved: June 30, 2017

Abstract

In the search for effective methods to mitigate the increasing rates of abuse and addiction of illicit substances, a variety of neurological pathways have been explored. Towards this goal of reducing drug abuse and ultimately overdose-related deaths, two avenues of research have emerged: 1) a preventative approach, the development of pain-relieving medications without the abuse and addiction liabilities associated with current therapies, and 2) a responsive approach, the development of medications for people suffering from drug abuse and addiction. The natural product salvinorin A can be manipulated towards both of these research avenues through the development of μ opioid receptor (MOR) agonists for treating pain with reduced abuse liabilities as well as through the development of κ opioid receptor (KOR) agonists with improved pharmacokinetic properties towards the development of therapies that attenuate relapse and withdrawal.

Previous structure-activity relationship (SAR) studies of salvinorin A identified that replacing the C2-acetate with a C2-benzoate results in a compound that is 4-fold selective for MORs over KORs. In an effort to increase this selectivity, to allow for probing the physiological effects induced upon activation of MORs with this non-morphine scaffold, a potent and selective MOR agonist kurkinorin (MOR $EC_{50} = 1.2 \pm 0.2$ nM, and KOR $\geq 10,000$ nM) was identified. Upon *in vivo* evaluation, kurkinorin was determined to elicit centrally-mediated antinociception with similar potency to morphine and a reduced tolerance, sedation, and reward profile in comparison to morphine. Through a SAR campaign, a variety of kurkinorin analogues were synthesized and evaluated *in vitro* for their ability to activate G-proteins and recruit β -arrestin-2 upon MOR activation. Through these studies, compounds that are more potent than kurkinorin at MORs,

compounds that are biased towards β -arrestin-2 recruitment, and compounds that are biased towards G-protein activation have been identified.

Salvinorin A suffers from poor pharmacokinetic properties, including low water solubility and rapid metabolism. In an effort to address this issue of water solubility, we sought to identify a point on the molecule through which its water solubility could be modified without sacrificing KOR activity. Previous studies indicated that salvinorin A's lactone functionality was not necessary for KOR activity; therefore, the lactone was modified to further explore its necessity and tolerance to modification. Analogues that varied in chain length, stereochemistry, and polarity at the lactone position were synthesized and evaluated for their ability to activate KORs. Overall, small linear moieties were well-tolerated, while bulkier groups were not. Salvinorin A analogues that are potent KOR agonists with polar, ionizable moieties in the C17-position have been identified, and the lactone position has been validated as a position on the molecule through which the pharmacokinetic properties can be manipulated without significant loss of KOR activity.

Salvinorin A has a very short half-life in humans (<15 minutes upon inhalation). SAR work in the past has focused on developing analogues with reduced metabolic liabilities, specifically through replacement of the acetate moiety, while maintaining KOR activity. However, the metabolism of many of these compounds had not been directly compared, to one another or to salvinorin A. Therefore, we developed a method to analyze the metabolic profiles of salvinorin A and its analogues in liver microsomes. Through screening salvinorin A and its analogues, several modifications that increase metabolic stability in comparison with salvinorin A have been identified.

Acknowledgements

I am very thankful for the support that I have had throughout graduate school, both financially and scientifically. The NIH Chemical Biology Training grant and the AFPE Fellowship have both helped to fund my training. I am also thankful for the excellent collaborators that have helped me further advance my work, particularly Dr. Bronwyn Kivell and her graduate students for their evaluation of our compounds in animals as well as Dr. Marta Filizola and her group for welcoming me as I worked with them during my rotation and for performing molecular dynamics studies of our compounds. I would like to thank the University of Kansas Department of Medicinal Chemistry for allowing me the opportunity to learn and work in this environment, and I am particularly thankful for my committee members who have given me advice and help throughout the years.

I would also like to acknowledge specific people who have supported me throughout my graduate career. To Amy, Emily, Melissa, Tammi, and Annecie, I am thankful for our friendships that have endured the long distance and for the many phone calls and texts that have gotten me through the hard days. My labmates in the Prisinzano group have always been supportive and helpful and have pushed me to become a better scientist. In particular, I'd like to thank Tammi, Mike, and Andrew for showing me how to successfully navigate the grad school life and balance having fun and working hard. To Alex, Sam, Stephanie, and Logan, thank you for always being willing to listen and talk about the good and the bad of what we do. I have also had some excellent undergraduate students who have not only helped me to become a better mentor but have also become pretty great chemists themselves, so thank you Austin and Pamela for all of your hard work. I am grateful to Deanna and the Prisinzano kids for welcoming me into their home for weekly TV dates and always bringing a smile to my face. And I would not be where or who I am today without my amazing mentor and advisor. Tom, I am so very thankful for everything that you have taught me about medicinal chemistry, but I think I am most thankful for how you have shown me that it is possible to be successful and still live every single day with faith and integrity. Thank you for pushing me to be the best that I can be and for always encouraging me to continue asking questions and searching for answers.

Lastly, I want to thank my family for always supporting me. To my new Crowley family, Matt, Vickie, and Brendo, thank you for taking me in, making me feel like family from day one, and for always providing a fun and relaxing break from the lab and Lawrence. To my brother Ryan, thanks for the Saturday morning FaceTime chats and guitar-playing while I ran columns—it always brightened my day! To my sister and best friend Beka, thanks for moving to Africa so that Kansas didn't seem too far of a move—but for real, thanks for always listening to me and making me laugh. And to my parents, you have made many sacrifices so that I can be where I am today, and I will never forget that. I am so thankful for the work ethic and values you instilled in me, and I am especially grateful for the way that you have always encouraged and supported me to live out my dreams. And last but not least, I want to thank my supportive husband, Vince. Without your friendship and encouragement, I am not sure that I would have made it here. Thanks for encouraging and helping me through the difficult days and for always bringing a smile to my face, especially when I need it most.

Table of Contents

Abstract	iii
Acknowledgements	v
Table of Contents	vi
List of Figures	viii
List of Schemes	ix
List of Tables	x
List of Abbreviations	xi
1. Introduction	1
Drug Addiction and Pain	1
The epidemic in America	1
Addiction and the reward pathway	3
The Opioid System	7
Opioid receptors	7
Functional selectivity	11
Opioids as Drugs	12
Structural classifications of current opioids	12
Targeting the opioid system: Pain therapies	14
Clinically used addiction therapies	16
Targeting the opioid system: Addiction therapies	17
Salvinorin A as a Novel Opioid	21
Issues with current opioids as therapies for pain and addiction	21
Historical use and identification	22
Metabolism	23
Structure-activity relationships	24
Proposed mode of binding	26
Needs for improvement	27
References	29
2. Project Rationale and Specific Aims	46
Overall Rationale	46
Aim 1: Development of Pain Therapies with Reduced Side Effects	48
Design and evaluation of kurkinorin <i>in vitro</i> and <i>in vivo</i>	49
Study 1: Evaluation of kurkinorin analogues with substitutions to the phenyl ring	50
Study 2: SAR-guided design and synthesis of kurkinorin analogues	51
Study 3: Evaluation of SAR-driven kurkinorin analogues	51
Aim 2: Development of New Synthetic Approaches toward Refinement of Salvinorin A's Pharmaceutical Properties	53
Study 1: Development of chemical methodology to selectively functionalize the C17 position	54
Study 2: Evaluation of compounds with C17 modifications	55
Study 3: Design, synthesis, and evaluation of analogues with C2 and C17 modifications	55
Aim 3: Understanding the Metabolism of Neoclerodane Diterpenes	55
Study 1: Development of a robust system for determining the metabolic stability of neoclerodane diterpenes	56
Study 2: Evaluation of the metabolic stability of salvinorin A and selected analogues	57

References	58
3. Development of Pain Therapies with Reduced Side Effects	65
Background: Design and evaluation of kurkinorin <i>in vitro</i> and <i>in vivo</i>	65
Results	71
Study 1: Evaluation of kurkinorin analogues with substitutions to the phenyl ring.....	71
Study 2: SAR-guided design and synthesis of kurkinorin analogues	72
Study 3: Evaluation of SAR-driven kurkinorin analogues	74
Discussion	83
References	84
4. Development of New Synthetic Approaches toward Refinement of Salvinorin A's Pharmaceutical Properties	88
Results	88
Study 1: Development of chemical methodology to selectively functionalize the C17 position.....	88
Study 2: Evaluation of compounds with C17 modifications	93
Study 3: Design, synthesis, and evaluation of analogues with C2 and C17 modifications	96
Discussion	100
References	102
5. Understanding the Metabolism of Neoclerodane Diterpenes	105
Results	105
Study 1: Development of a robust system for determining the metabolic stability of neoclerodane diterpenes	105
Study 2: Evaluation of the metabolic stability of salvinorin A and selected analogues	111
Conclusion	116
References	117
6. Overall Conclusions	120
7. Supplemental Information	124
Supplemental Tables	124
In vitro pharmacology	126
Ligand-based alignment study	128
Metabolic Stability Protocol	129
Chemistry	131
Compounds from Chapter 3:.....	132
Compounds from Chapter 4:.....	147
References	181
NMR Spectra.....	183

List of Figures

Figure 1.1: Age-adjusted rate of drug overdose deaths, by state, 2010-2015.....	1
Figure 1.2: The three stages of addiction.....	3
Figure 1.3: Opioid receptor signaling.....	10
Figure 1.4: Common opioid structural classes.....	13
Figure 1.5: Functionally selective MOR agonists.....	15
Figure 1.6: Structures of morphine and analogues.....	22
Figure 1.7: Structure of salvinorin A.....	23
Figure 1.8: Primary metabolism of salvinorin A.....	24
Figure 1.9: Salvinorin A derivatives at the C2 position.....	25
Figure 1.10: Salvinorin A furanyl-derivatives.....	25
Figure 1.11: Derivatives of salvinorin A with KOR activity.....	26
Figure 1.12: Structure of JDTC, KOR antagonist.....	27
Figure 2.1: Structures of salvinorin A and herkinorin.....	48
Figure 2.2: Chemical structure of kurkinorin.....	49
Figure 2.3: Docked structure of RB-64 (salvinorin A analogue) at the KOR.....	53
Figure 2.4: Structures of C17-modified salvinorin A analogues.....	54
Figure 3.1: X-ray crystal structures of herkinorin and herkamide.....	65
Figure 3.2: Unambiguous determination of the structure of kurkinorin.....	67
Figure 3.3: The <i>in vivo</i> effects of herkinorin, kurkinorin, and morphine.....	69
Figure 4.1: Unambiguous determination of stereochemistry at the 17-position using NMR.....	91
Figure 4.2: Ligand-based alignment of salvinorin A, 8- <i>epi</i> -salvinorin A, and 4.4	94
Figure 4.3: Proposed modifications to increase solubility through the C17 position.....	101
Figure 5.1: Layout of optimized method for microsomal stability analysis.....	109
Figure 5.2: Metabolic stability of control compounds at 150 minutes in the presence (stripes) or absence (no shading) of NADPH.....	111
Figure 5.3: Metabolic stability of salvinorin A and known C2-analogues at 150 minutes in the presence (stripes) or absence (no shading) of NADPH.....	112
Figure 5.4: Metabolic stability of MOR agonists herkinorin, herkamide, and kurkinorin at 150 minutes in the presence (stripes) or absence (no shading) of NADPH.....	113
Figure 5.5: Metabolic stability of Methyl salvinorin B and its C17-modified analogues (4.1b - 4.5b) and herkinorin and its C17-modified analogues (4.1c - 4.5c) at 150 minutes in both the presence and absence of NADPH.....	114
Figure 5.6: Novel spirobutyrolactone is more metabolically stable than salvinorin A at 150 minutes in both the presence (stripes) and absence (no shading) of NADPH.....	116
Figure 6.1: Overall conclusions and final results.....	123

List of Schemes

Scheme 3.1: Synthetic route to kurkinorin.....	66
Scheme 3.2: Synthesis of SAR-guided kurkinorin analogues.....	73
Scheme 4.1: Synthetic route to access C17 position of salvinorin A.....	89
Scheme 4.2: Synthesis of C17-derivatives of salvinorin A.....	90

List of Tables

Table 3.1: MOR, KOR, and DOR Pharmacology: Inhibition of forskolin-induced cAMP accumulation.	68
Table 3.2: MOR pharmacology: Inhibition of forskolin-induced cAMP accumulation, and scatter plot comparison of the pEC ₅₀ values of herkinorin analogues vs. kurkinorin analogues (inset).	71
Table 3.3: MOR pharmacology of SAR-driven analogues: Inhibition of forskolin-induced cAMP accumulation.	76
Table 3.4: MOR pharmacology: MOR-mediated β -arrestin recruitment.	81
Table 4.1: KOR pharmacology: Inhibition of forskolin-induced cAMP accumulation	93
Table 4.2: KOR activity of C17-derivatives: Inhibition of forskolin-induced cAMP accumulation	95
Table 4.3: KOR activity of C2/C17 derivatives: Inhibition of forskolin-induced cAMP accumulation	98
Table 4.4: MOR activity of C17-modified herkinorin derivatives.....	100
Supplemental Table 1: Calculated properties and ligand efficiencies of kurkinorin derivatives.	124
Supplemental Table 2: Calculated properties and ligand efficiencies of lactone derivatives. .	125

List of Abbreviations

cAMP	Cyclic adenosine monophosphate
C _{max}	Maximum concentration
CNS	Central nervous system
COSY	Correlation spectroscopy
CYP	Cytochrome P450 enzyme
DAMGO	[D-Ala ² , N-MePhe ⁴ , Gly-ol]-enkephalin
DIBALH	Diisobutylaluminum hydride
DMSO	Dimethylsulfoxide
DOR	Delta opioid receptor
EC ₅₀	Effective concentration eliciting 50% of maximum response
ED ₅₀	Effective dose eliciting 50% of activity
E _{max}	Maximum efficacy
EFC	Enzyme fragment complementation
EOM	Ethoxymethyl ether
ERK	Extracellular signal-regulated kinase
GDP	Guanosine monophosphate
GPCR	G-protein coupled receptor
GTP	Guanosine triphosphate
H-bond	Hydrogen bond
HAC	Heavy atom count
HCl	Hydrochloric acid
HMBC	Heteronuclear multiple-bond correlation spectroscopy
HPLC	High-performance liquid chromatography
HSQC	Heteronuclear single-quantum correlation spectroscopy
i.p.	Intraperitoneal
JNK	C-Jun amino-terminal kinase
KOR	Kappa opioid receptor
LE	Ligand efficiency
LELP	Lipophilic-adjusted ligand efficiency
MAPK	Mitogen-activated protein kinase
Mesyl	Methanesulfonyl
MOM	Methoxymethyl ether
MOR	Mu opioid receptor
NADPH	Nicotinamide adenine dinucleotide phosphate
NMR	Nuclear magnetic resonance
NOESY	Nuclear Overhauser effect spectroscopy
NOR	Nociceptin receptor
PNS	Peripheral nervous system
SAR	Structure activity relationship
SEM	Standard error of the mean
sLogP	Wildman-Crippen calculated logP
t _{1/2}	Half-life

tPSA	Total polar surface area (Å ²)
TBAF	Tetra- <i>n</i> -butylammonium fluoride
TBS	<i>tert</i> -Butyldimethylsilyl
THF	Tetrahydrofuran
TMSOTf	Trimethylsilyl trifluoromethanesulfonate
UGT	Uridine diphosphate-glucuronosyltransferase

1. Introduction

Drug Addiction and Pain

The epidemic in America

The United States is currently experiencing an opioid and drug abuse epidemic.¹ Between 2014 and 2015, the number of deaths attributed to drug overdose rose significantly, from 47,055 to 52,404.² In fact, 2015 saw the highest number of overdose deaths of any year recorded (**Figure 1.1**).³ From 2010 to 2014, the same drug classes were being abused and causing overdoses: opioids, including oxycodone, heroin, morphine, hydrocodone, fentanyl, and methadone; stimulants, cocaine and methamphetamine; and benzodiazepines, including alprazolam and diazepam. While the top ten drugs causing overdose did not vary over the five year period, the order of those drugs did. Notably, recent years have seen an increase in heroin overdose which more than tripled between 2010 and 2014, as well as overdoses attributed to fentanyl which doubled in a single year (2013-2014).⁴

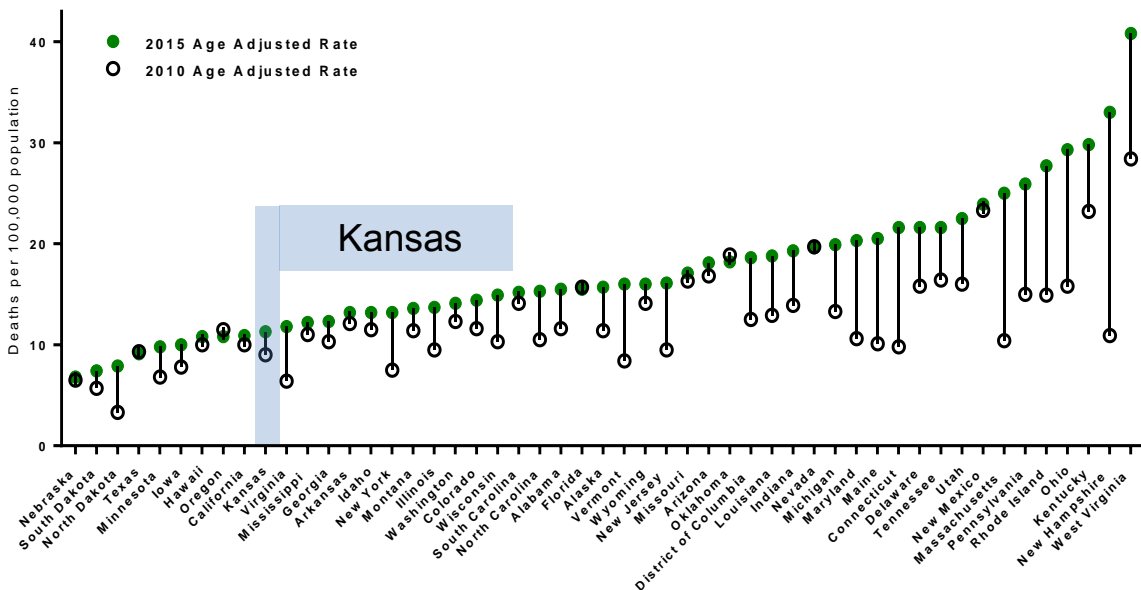


Figure 1.1: Age-adjusted rate of drug overdose deaths, by state, 2010-2015.

With over half of these overdose deaths attributed to opioids, 60.9% in 2014 to 63.1% in 2015,² the public response has been to equip law enforcement personnel with the opioid antagonist naloxone (Narcan®). The goal of this endeavor is that these first responders can administer naloxone and reverse the overdose effects, thereby preventing death.⁵ As of April 2016, thirty-three states have already implemented training and arming of the police force with naloxone, and this number continues to rise.⁵

A discussion of the opioid epidemic is incomplete without discussing the prevalence of pain and prescription opioids, as nearly half of the opioid-related deaths in 2015 involved prescription opioids.³ Pain affects about 100 million American adults, which is more than cancer, heart disease and diabetes combined.⁶ The estimated costs in the US are over \$600 billion, including healthcare, disability compensation and lost workdays; however, the personal costs in terms of suffering and quality of life cannot be measured.⁷ Opioid analgesics are the gold-standard for pain treatment and have been so for many years, despite their many adverse effects, including tolerance, dependence, and respiratory depression.⁸ The long-term use of opioids often leads to analgesic tolerance, requiring higher doses to achieve pain relief.⁹ As the opioid doses is increased, the patient is at higher risk for developing dependence and ultimately becoming addicted to the opioid therapy.¹⁰ Even so, opioids are still the most prescribed drug class for pain.¹¹ Conversely, patients who are suffering from chronic pain are often hesitant to use opioids due to the associated risks and social and legal issues associated with using opioids, which results in frequently undertreated and inadequately treated pain.¹² Therefore, the development of pain relievers without these stigmas and side effects is a critical medical need.

Addiction and the reward pathway

Overdoses are often the result of a drug addiction, the most severe form of substance abuse.¹ Drug addiction was once perceived as a character flaw or moral inadequacy, but scientific advances have now more clearly defined it as a chronic illness, with characteristics similar to other widely accepted chronic illnesses such as type 2 diabetes mellitus, asthma, and hypertension.¹³ All of these diseases, including addiction, are chronic, have no known cure, are prone to relapse, and are affected by a variety of factors including genetic, environmental, social, and behavioral. Additionally, all of these diseases have treatments with which patients often find it difficult to comply.^{1, 13}

Addictive drugs act in different ways, but their overall effect is the same—a euphoric or pleasurable experience that is the result of activation of the reward regions in the brain.¹⁴ As misuse of addictive substances continues into abuse, progressive neuroadaptations, or structural and functional changes, occur in the brain of the individual. Addiction is commonly broken down into three stages: 1) Binge and intoxication; 2) Withdrawal and negative affect; 3) Preoccupation and

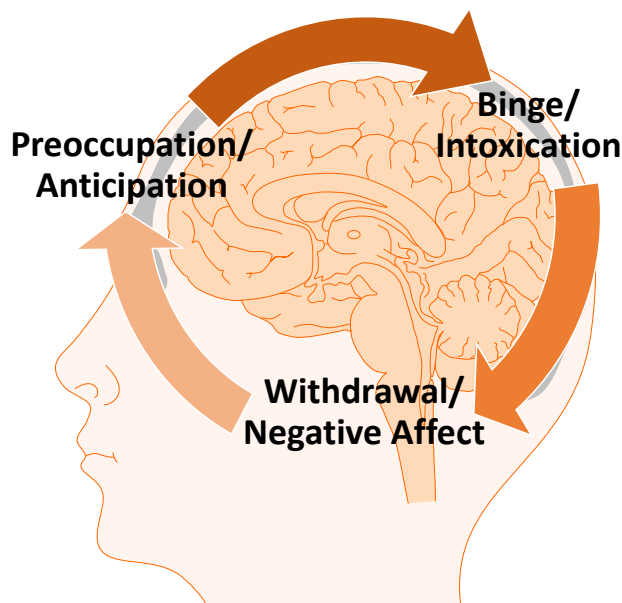


Figure 1.2: The three stages of addiction.

anticipation (**Figure 1.2**).¹⁴ Each of these stages can be traced to specific neuroadaptations in the brain that result from substance abuse.

During the first stage of addiction, binge and intoxication, consumption of the intoxicating substance occurs, and the user experiences euphoria from its activation of the reward pathways. The effects of this stage are commonly attributed to actions in the basal ganglia, more specifically activations of dopamine and opioid signaling through the nucleus accumbens.¹⁵ All addictive substances activate the reward pathway, increasing dopamine levels to produce their euphoric effects, and this response is mediated through the nucleus accumbens.¹⁶ This rewarding response to the drug motivates individuals to use the drug again. Chronic substance abuse can cause neurons to fire at the anticipation of the substance rather than the substance itself, which results in associated triggers, or cues, that promote seeking and usage of the substance.¹⁴ Ultimately, these addictive substances “hijack” the reward system of the brain, as acute administration decreases reward thresholds, increasing reward, but chronic administration increases these reward thresholds resulting in decreased reward.¹⁷

The second stage of the addiction cycle, withdrawal and negative effects, occurs after the euphoric effects of taking the substance subside and the individual feels less energetic and excited and more depressed and anxious. Addicted individuals no longer have the same motivation to pursue natural rewards because their reward systems have been conditioned to focus on the more potent dopamine release that occurs with the drug or the drug cues. Their reward pathways also become less sensitive to both drug and non-drug stimulation, so that the same amount of the substance results in a lessened degree of euphoria after long-term use. This dampened reward pathway also explains why addicted individuals are no longer motivated to pursue natural stimuli by which they had previously been motivated and found rewarding.¹⁴

These withdrawal and negative effects are modulated by the extended amygdala. Neuroadaptations in the amygdala result in increased stress reactivity and negative emotions. In non-addicted individuals, this “antireward” system helps to maintain homeostasis, but the pathway is overactive in addicted brains and results in withdrawal symptoms upon drug removal from the system.¹⁸ These withdrawal effects can present as a negative emotional state or dysphoria and increase in severity to physical illness that can be fatal in the most severe cases.^{17a} Several neurotransmitters have been shown to be under- or over-activated and together contribute to the motivational effects of withdrawal. Notably, dopamine and serotonin levels are decreased while dynorphin (the κ opioid receptor endogenous agonist) is increased which all contribute to the dysphoric effects felt during withdrawals.¹⁸ Also, the anxiolytic and stress effects of withdrawal are attributed to the decreases in GABA and neuropeptide Y and the increases in corticotropin-releasing factor and norepinephrine.¹⁸ Eventually, the brain becomes reliant on the drug to stimulate the reward pathway, and adapts in such a way that the addicted individual requires the drug to maintain relief from the negative effects experienced in the drug’s absence.¹

The final stage of the addiction cycle, preoccupation and anticipation, involves the actions of the prefrontal cortex. Neuroimaging studies have correlated prefrontal cortex dysfunction in addicted individuals to higher rates of relapse and impaired executive processes.¹⁹ The prefrontal cortex is responsible for executive function, which includes decision making, organizing thoughts, regulating social behavior (i.e. impulses, emotions, and actions), differentiating between conflicting thoughts, and selecting and initiating action. Executive processes are vital in making decisions regarding taking or stopping the drug, including the social and personal implications involved with each decision.¹ All of these processes are impaired in addicted individuals due to the down-regulated dopamine signaling. These neuroadaptations in the prefrontal cortex lower the

addicted individuals' ability to resist strong urges, such as taking the drug, as well as prevent them from following through on decisions, such as to stop taking the drug. Together, these prefrontal cortex neuroadaptations help explain how addicted individuals who genuinely desire to be free of their addiction have such difficulty resisting the impulse to take the drug.¹⁴ As these neuroadaptations remain even after the individual is able to attain abstinence, they also explain some of the difficulty that recovering drug users have to maintain their sobriety.¹⁹⁻²⁰

The three stages of addiction are a viscous cycle, with each stage increasing the addicted individual's compulsivity and decreasing their control of their addiction. The initial use of the drug activates the reward system and gives the user a "high" that they want to continue, often leading to binge intoxication. Repeated use of the drug can dampen the brain's reward system, causing the user to become tolerant to the drug which requires more of the substance to get the same euphoric effect. Similarly, this reduced sensitivity affects non-drug related rewards so that the addicted individual does not feel the same pleasure out of naturally rewarding activities as they once did. Thus the individual is more motivated to seek the "high" they get from taking drugs rather than non-drug related rewards. Upon withdrawal of the drug, an addicted individual experiences negative physical effects and dysphoric emotions, both of which lead the individual to take more drug. After long-term substance abuse, individuals become dependent upon the substance in that their bodies require the substance to relieve the dysphoria and physical withdrawal symptoms. The cycle of addiction is difficult for the user to escape, as the physical effects of withdrawal are painful and additional changes in the brain reduce the addicted individual's ability to resist the urge and impulse to use the drug. Deficits in executive function often prevent addicted individuals from accomplishing their goal to stop taking the drug, which leads to drug seeking and relapse.¹⁴

Of the 29 million American adults who will partake in using an illicit or nonmedical drug during their lifetimes, less than 20% of them (5.4 million) will progress to substance abuse and addiction.^{17a} This discrepancy between use and abuse indicates that there are risk factors for addiction and that some people are more prone than others to transition from substance use to abuse. Genetic, social, developmental, and environmental factors all play a role in determining susceptibility for drug use, abuse, and addiction. Family history of drug abuse increases the risks for developing drug addiction, possibly through genetic heritability and/or learned parenting practices.^{1, 21} Adolescence is a vulnerable point in life for the development of drug use and misuse behaviors. Individuals who are raised in environments that expose them to drug use or in high stress environments, such as being subject to physical, sexual, or emotional abuse, parental instability, neglect, or poverty, have an increased risk of developing addiction.^{1, 14} Individuals who suffer from mental illnesses are also at higher risks for misusing and abusing drugs.²² The transition from drug use to abuse to addiction requires long-term exposure to the drug and does not occur in every person who uses these addictive substances.

The Opioid System

Opioid receptors

Many drugs of abuse, particularly prescription pain killers such as morphine and oxycodone, target the opioid system. Therefore, modulation of opioid receptors carries therapeutic potential for treating pain and addiction. Opioid receptors are divided into three types, μ (MOR), κ (KOR), and δ (DOR),²³ and are expressed by neurons in the central and peripheral nervous systems (CNS and PNS), neuroendocrine cells, and immune cells.⁷ All three opioid receptors are class A G-protein coupled receptors (GPCRs) with seven transmembrane spanning helices and 50-70% genetic homology between them. The sigma and epsilon receptors were once proposed to be in the

opioid family, but DNA and sequence analysis concluded that they do not belong in the same family as the “classical” opioid receptors.⁹ However, the nociceptin receptor (NOR), is considered to be a fourth opioid receptor, of a non-opioid branch of the family. This distinction is made because the NOR does not bind, and its effects are not reversed by, the classic opioid antagonist naloxone, but it is structurally similar to the classical opioid receptors as a GPCR with a similar amino acid primary sequence.²⁴

The opioid receptors have endogenous peptides that activate them,²⁵ and just like their receptor targets, these opioid peptides are also expressed throughout the CNS and PNS.⁹ These peptides all share a common Tyr-Gly-Gly-Phe-Met/Leu sequence, which is known as the opioid sequence. The enkephalins (Met- and Leu-enkephalin) are derived from proenkephalin, β -endorphin is derived from proopiomelanocortin, and all three are potent antinociceptives that activate both MORs and DORs. The dynorphins are derived from prodynorphin and can be both pronociceptive, acting at *N*-methyl-D-aspartate (NMDA) receptors, or antinociceptive, acting at KORs.⁷ A fourth type of opioid peptide, the endomorphins, act selectively at MORs, but their precursor protein is unknown and they are unique in that they do not contain the opioid sequence.⁹ The NOR receptors also have an endogenous peptide that activates it, nociceptin/orphanin FQ, that is similarly derived from a precursor polypeptide pre-pro-nociceptin.²⁴

In 2012, the structures of all three opioid receptors were published in the inactive, antagonist-bound state: MOR bound to the morphinan antagonist β -FNA;²⁶ KOR bound to the antagonist JD1c;²⁷ and DOR bound to naltrindole²⁸ and a bifunctional DOR antagonist/MOR agonist peptide.²⁹ More recently, the crystal structure of the MOR bound to the agonist BU72 was published³⁰ as well as a NMR-based structure of the KOR bound to its endogenous peptide agonist dynorphin,³¹ but to date no active crystal structures of KOR or DOR have been solved.

Each of the three opioid receptor subtypes modulates nociception, but they all have differing roles in addiction.³² Activation of MORs not only causes analgesia, but also results in euphoria, or a feeling of well-being that can be a contributing factor towards abuse of MOR agonists. Several side effects of clinically-used opioids are the direct result of activation of MORs, such as sedation, constipation, and respiratory depression.^{9, 33} The MOR is responsible for mediation of the rewarding and addictive properties of many abused drugs, primarily due to the increases of dopamine transmission and euphoria produced upon MOR activation.^{32, 34} The rewarding effects of MOR activation are antagonized by the KOR through its suppression of dopamine release and dysphoric effects.³⁵ KOR activation also results in analgesia, but it does not mediate respiratory depression or constipation.⁹ DOR activation provides analgesia and reduces anxiety but has also been attributed to convulsions and constipation.⁹ The role of the DOR in the reward pathway and addiction is not as well defined as for MOR and KOR, but its role in anxiety reduction and attenuation of depressive-like states is well recognized. The DOR receptor does appear to be implicated in emotional processes associated with addiction.³²

The opioid receptors are inhibitory GPCRs, and as such, activation through agonist binding induces a conformational change that allows for binding of heterotrimeric $G_{i/o}$ proteins to the receptor C terminus (**Figure 1.3**). Upon displacement of GDP with GTP, the trimeric G protein dissociates into G_α and $G_{\beta\gamma}$ subunits. The G_α subunit is responsible for the inhibition of adenylyl cyclases that results in a decrease in cAMP accumulation within the cell and thus decreased cAMP-dependent Ca^{2+} influx. Prevention of action potential propagation and neuronal excitation is also achieved by the G_α subunit as it opens the G protein-coupled inwardly rectifying K^+ (GIRK) channels.³⁶ The $G_{\beta\gamma}$ subunit modulates potassium and calcium ion channels on the cell membrane.

Attenuation of neuron excitability is achieved through the modulation of Ca^{2+} concentrations, and the $\text{G}_{\beta\gamma}$ subunit suppresses Ca^{2+} influx and modulates both pre- and post-synaptic Ca^{2+} channels. All of these G-protein-mediated pathways ultimately decrease nociceptive stimulus transmission and significantly reduce pain perception.⁹

A single activated receptor can couple multiple G proteins and each, in turn, dissociate and activate downstream second messengers, ultimately resulting in signal amplification. The receptor must be desensitized in order to turn off the signal transduction process. This desensitization process is two-fold. The GPCR is first phosphorylated by a second-messenger protein kinase (i.e. protein kinase A or C) or by a GPCR kinase (GRK). Phosphorylation of intracellular regions of the receptors promotes the binding of β -arrestins.³⁷ Once β -arrestins are bound to the opioid receptor, G protein coupling can no longer occur and receptor internalization is promoted by endocytosis in clathrin-coated pits. Upon internalization, the receptor can be recycled, via

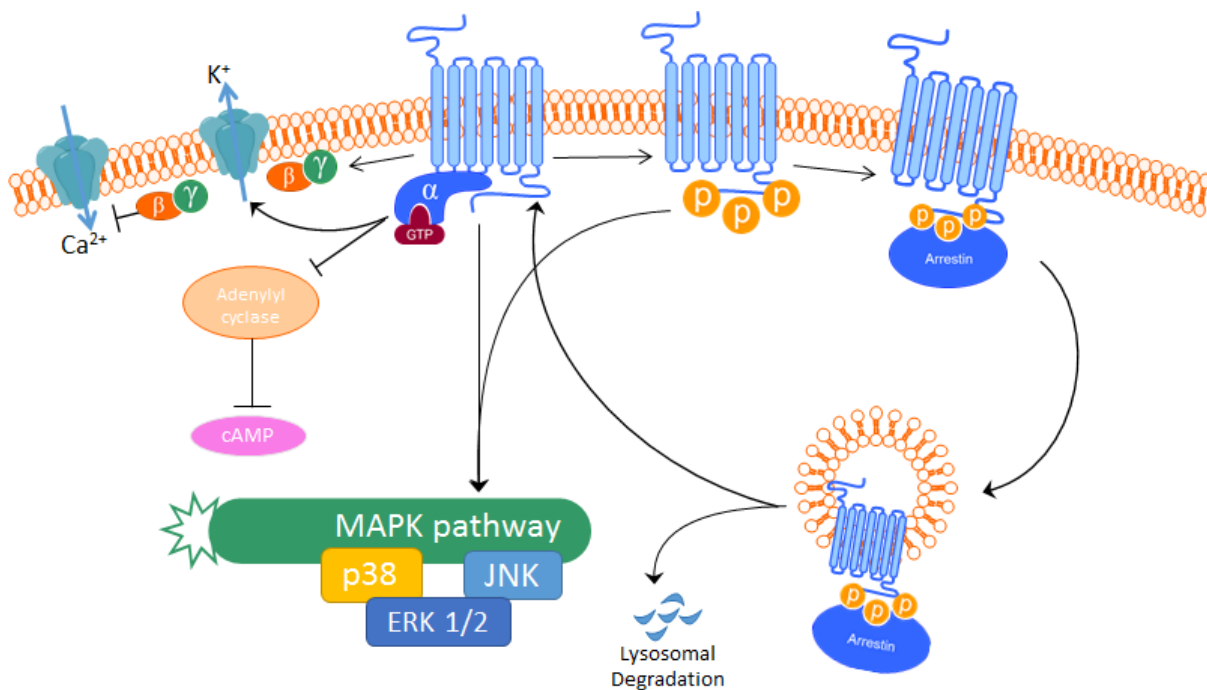


Figure 1.3: Opioid receptor signaling.

dephosphorylation and reintegration into the membrane which restores signal transduction, or it can be targeted to the lysosome where it is degraded. The phosphorylation and degradation pathways of opioid receptors are thought to contribute to the development of tolerance to opioid drugs.^{9, 36}

The opioid receptor- β -arrestin complexes have also been shown to activate signaling cascades, specifically activation of members of the mitogen-activated protein kinase (MAPK) family. These proteins include ERK 1 and 2, JNK, and p38. The mechanisms of MAPK activation for each of the specific opioid receptors have not been fully delineated, but multiple mechanisms appear to be at work, including β -arrestin-independent $G_{\beta\gamma}$ and β -arrestin-dependent mechanisms.³⁶

Recent research has indicated that, in addition to intracellular signaling and phosphorylation, opioid receptors interact with nearby proteins directly. Homo- and heterodimers of opioid receptors have been identified, where the receptors are oligomerized with another receptor of the same or different type, respectively.³⁸ Additional subtypes of receptors have also been postulated to exist from alternative splicing and posttranslational modifications.³⁹ While much work has been done to prove the existence of both the oligomerized and splice variant opioid receptors, their existence is still a debated topic among experts in the field.^{9, 40}

Functional selectivity

The idea of functional selectivity (or biased agonism) has recently been of interest in the field of GPCR research. GPCRs are dynamic systems with many structural conformations, and these different conformations activate the signaling pathways to varying extents. Functional selectivity refers to the ability of ligands to stabilize different conformations of a single receptor subtype and thus differentially regulate the downstream signaling cascades. Oftentimes the pathways being differentiated through functional selectivity are activation of G protein pathways versus β -arrestin

recruitment.³⁷ While the exact mechanisms by which functional selectivity is modulated have not been fully elucidated, studies have demonstrated that GPCRs bound to ligands biased for one pathway adopt different conformations than when they are bound to ligands biased for another pathway.⁴¹ Furthermore, biased ligands have been shown to stabilize the β -arrestin as well as the receptor in distinct conformations from unbiased ligands.⁴²

Recent work in the area of targeting GPCRs has focused on developing ligands that are functionally selective, or biased, for one pathway over another in an effort to decouple the various downstream effects of each pathway.³⁷ Identification of these biased ligands requires evaluating compounds for different pathways coupled to a single receptor and comparing the activities from those assays to a standard, unbiased or neutral compound.⁴³ This comparison is often expressed as a bias factor, or a quantitative value of the bias for one pathway over another.⁴³⁻⁴⁴

Opioid receptors have been at the forefront of the functional selectivity field. Early studies dosing mice lacking β -arrestin-2 with morphine demonstrated that the animals did not develop tolerance or other side effects associated with morphine.⁴⁵ These studies were the first to give insight into the possibility that the analgesic effects at MOR could be dissociated from the side effects through the development of functionally selective compounds.³⁷ Other studies have similarly shown that functionally selective KOR activation can dissociate some of the negative side effects from the beneficial physiological effects.⁴⁶

Opioids as Drugs

Structural classifications of current opioids

Arguably the world's oldest drug, morphine was self-administered by drinking the milk of the opium poppy dating back as early as 3400 B.C.³³ Friedrich Sertuerner identified the alkaloid

morphine as the active ingredient in opium in 1803.⁴⁷ Since the characterization of morphine's structure in 1925,⁴⁸ hundreds of derivatives of the structure have been made, and many of these derivatives have been FDA-approved for pain treatment.⁴⁷ However, most of these new opioid compounds have been unable to diverge from the morphinan or a structurally similar core. In fact, most opioids on the market can be divided into four main structural classes, all of which heavily rely on morphine's structure. These include oxymorphinans (the most similar to morphine and most common class), benzomorphans, phenylpiperidines, and diphenylheptanes (**Figure 1.4**). Morphine itself is an oxymorphinan, as are the commonly used drugs codeine, hydrocodone, hydromorphone, oxycodone, oxymorphone, buprenorphine, nalbuphine, butorphanol, and levorphanol.³³ The second most-prominent structural class are the phenylpiperidines. These drugs are synthetic but were inspired by the phenylpiperidine found in morphine. Drugs in this class include meperidine, fentanyl, remifentanyl, sufentanyl, and alfentanyl, and are very potent MOR agonists.³³ To date, only one benzomorphan, pentazocine, is FDA-approved, but others are used in opioid research. These benzomorphans have mixed activities at the MORs and KORs.³³ The diphenylheptanes include propoxyphene and methadone, both of which are MOR agonists.³³

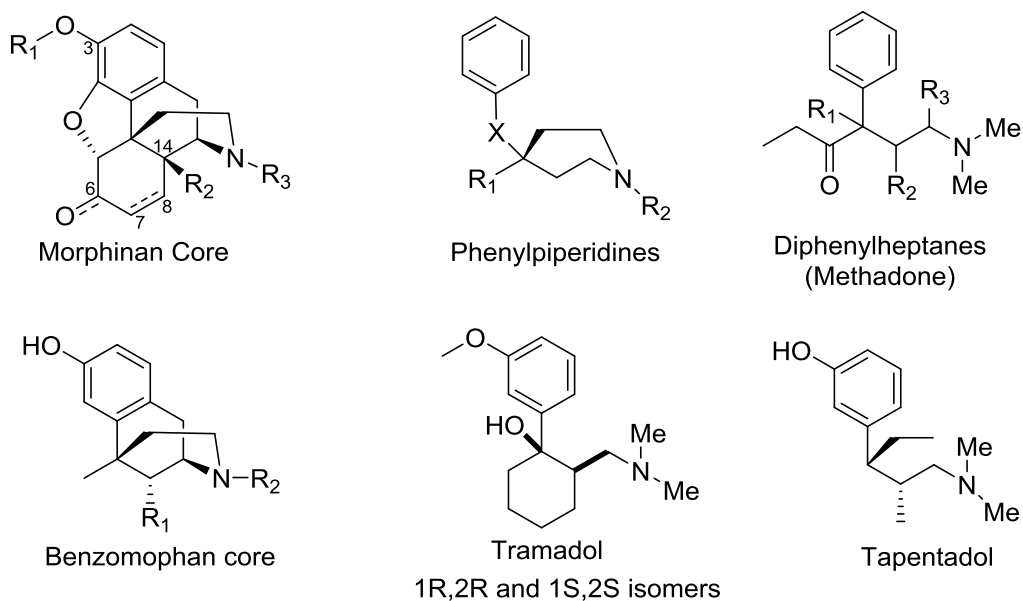


Figure 1.4: Common opioid structural classes.

Recently, two other drugs have been developed, tramadol and tapentadol, which both have MOR activity, but also mediate pain relief through other pathways, mainly the inhibition of norepinephrine reuptake.⁴⁷ These compounds are the most structurally unique in comparison to morphine, but they do still resemble the morphine core due to their phenolic or methoxyphenyl moiety, three-carbon spacers, and tertiary basic amines.⁴⁷

Research throughout the years has helped to develop strong structure-activity relationships (SARs) between the morphinan backbone and activity at the opioid receptors. Modification of the N-substituent (R_3 in **Figure 1.4**) affects the activity significantly. Creating a quaternary nitrogen restricts the compound to the periphery, while conversion of the methyl group to a cyclopropylmethyl or allyl group switches the activity from a MOR agonist to an antagonist. The phenolic hydroxyl group at C3 is required for activation of MORs. Drugs such as codeine have the phenol masked as a methoxy group ($R_1 = \text{Me}$), but it is demethylated *in vivo* by the cytochrome P450 enzyme 2D6 (CYP2D6) to the more active phenol. The 14β -substituent (R_2) can either be a hydrogen or a hydroxyl group. The non-natural 14β -OH compounds have slower penetration across the blood-brain barrier, but their slower penetration is compensated for by much higher potency at MORs. The naturally occurring allylic 6-OH-substituent can be oxidized to the ketone and the 7,8-alkene reduced with activity at MORs maintained. This modification does reduce the effectiveness of these compounds as cough suppressants, so the oxidized compounds are not used for this indication.⁴⁹

Targeting the opioid system: Pain therapies

Opium has been used for thousands of years for the treatment of pain.⁴⁷ The primary active ingredient in opium is morphine, which exerts its analgesic and euphoric effects through the MOR. Most current, clinically-used opioids also function through activation of the MOR, either

selectively or nonselectively. While the analgesic effects of these drugs are mediated through MOR activation, so too are the side effects most commonly associated with them, including sedation, nausea, respiratory depression, and constipation.⁹

Compounds with dual mechanisms of action have also been investigated. Partial agonists for MOR and compounds that have mixed MOR/KOR activity have also been targeted for pain treatments, but these compounds generally have analgesic ceilings (a dose that elicits the maximum response, and increasing the dose does not increase analgesic efficacy) and can precipitate withdrawals if given with pure MOR agonists.⁷ The dual-acting analgesic tramadol is a weak activator of the MOR, causes the release of serotonin, and inhibits the reuptake of norepinephrine. Together, these mechanisms contribute to tramadol's overall analgesic efficacy. Further, the open-chain tramadol analogue tapentadol has similar *in vivo* efficacy to oxycodone, with a reduced risk of gastrointestinal issues.⁴⁷ Additionally, recent work has shown that dual MOR/DOR agonism elicits analgesia without conditioned place preference development; however the animals did self-administer the compound, indicating that it does have abuse liabilities.⁵⁰

Although MOR activation is associated with opioid-related side effects, the MOR is still of interest in the search for better pain therapies. Decoupling the analgesic effects from the negative side effects is currently being investigated through the development of functionally selective ligands. TRV130 is G protein biased, with reduced β -arrestin-2 recruitment relative to traditional

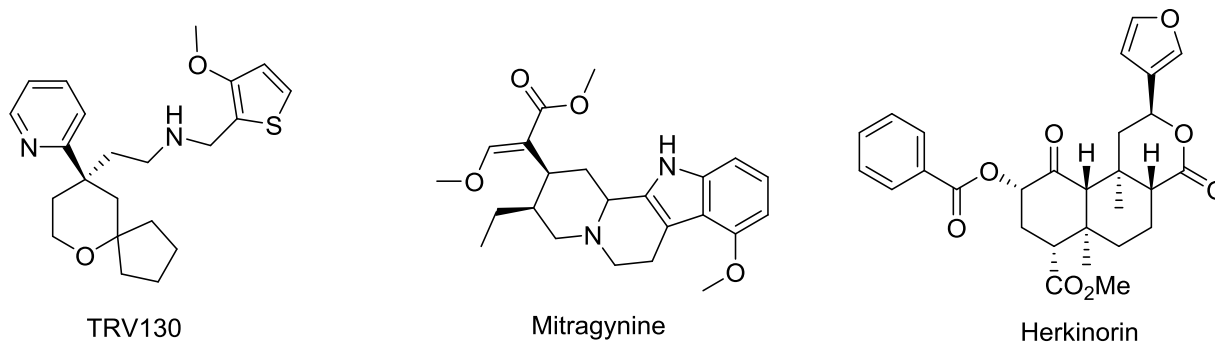


Figure 1.5: Functionally-selective MOR agonists

opioids, and is currently undergoing clinical trials (**Figure 1.5**). Thus far, TRV130 has shown reduced respiratory depression and gastrointestinal side effects.⁵¹ Other functionally selective MOR agonists have been described recently, including mitragynine⁵² and herkinorin,⁵³ among others.⁵⁴

In addition to the MOR, the DORs and KORs have been implicated as effective targets for treating nociception. Unlike the MOR, activation of the DOR does not have any reinforcing or addictive properties. DOR agonists have successfully treated chronic inflammatory nociception and bone cancer-associated nociception in animal models.⁵⁵ Co-administration of a MOR agonist with a DOR antagonist has been shown to enhance analgesia in comparison to the MOR agonist alone without an increased risk of side effects.⁸ The analgesic effects of KOR activation are limited by the KOR-induced dysphoria. However, as dysphoria only occurs upon activation of KORs in the CNS, peripheral targeting of KORs is a possible treatment option for pain therapies. Peripherally restricted KOR agonists have demonstrated analgesic efficacy in animal models of visceral and inflammatory nociception without the common MOR-associated side effects.⁴⁷ Peripheral restriction of MOR agonists has also been demonstrated to reduce the centrally-mediated side effects while maintaining analgesic efficacy in animal models of nerve damage, visceral, inflammatory, and cancer nociception.⁷

Clinically used addiction therapies

All of the few approved therapeutic options for treating drug abuse and addiction target opioid receptors. Methadone was the first approved therapeutic for long-term management of addictions to opioids.⁵⁶ It is a safer, longer-acting MOR agonist than many abused opioids, and as such, methadone therapy replaces the illicit use of opioids for a safer opioid that is administered in controlled settings. As a full MOR agonist, methadone itself is an addictive drug, but because of

its improved safety profile and longer course of action, methadone therapy is still an effective treatment for drug addiction.⁵⁷ Buprenorphine is also approved for the treatment of opioid abuse, but unlike methadone, it is a partial MOR agonist with KOR antagonism. Because of its high affinity for the MOR, buprenorphine can block the effects of the abused MOR agonists. Similarly, the MOR antagonist naltrexone is effective in treating opioid addiction, as well as alcohol dependence, but as an antagonist (lacking any agonism for MOR), it is considered safer and lacks the possibility of addiction. Therefore, naltrexone treatment is not the substitution of one addiction for another but the prevention of the rewarding properties of the abused substance. However, due to the antagonism of the MOR receptor and its lack of euphoric effects, patient compliance and retention on naltrexone treatment are reduced compared to buprenorphine and methadone.³⁴ Additionally, it is important to note that antagonism of the MOR can precipitate withdrawal symptoms if given to someone who has developed dependence to MOR agonists, and these withdrawal symptoms must be monitored, as they can be life-threatening.⁷

These currently approved addiction therapies for opioid abuse have many drawbacks. None of these substances are able to combat the neurobiological changes that have occurred in the brain due to addiction. In fact, methadone and buprenorphine are both considered maintenance therapies, as the individual is still addicted to the substance, and naltrexone simply blocks the “high” from taking the addictive drugs. Although these drawbacks may seem considerable, no other alternatives currently exist. Additionally, no medications have been approved for the treatments of other addictions, such as marijuana, cocaine, and amphetamine abuse.¹

Targeting the opioid system: Addiction therapies

The above therapeutics approved for treating opioid addiction are also being tested for their

efficacy in treating other addictions, specifically stimulant abuse. Patients on either methadone or buprenorphine maintenance treatment use less cocaine.⁵⁸ Similarly, patients treated with naltrexone have reduced amphetamine use.⁵⁹ In animal models, a combination therapy of buprenorphine and naltrexone decrease cocaine-seeking and cocaine-induced conditioned place preference without having a high abuse potential,⁶⁰ and methadone successfully prevents cocaine-induced conditioned place preference.⁶¹

While many abused substances are MOR agonists, some studies have shown promise that modulation of the MOR receptor may be a useful treatment for abuse and addiction. Some, but not all, MOR antagonists have shown success in attenuating cocaine- and heroin-seeking, cocaine-induced conditioned place preference, and cocaine self-administration.⁶² This blocking of heroin's rewarding effect can be explained simply in that heroin is a MOR agonist and blockade of the MOR prevents the rewarding properties. However, the interplay between cocaine and the MOR is more complex, as the data thus far suggest that cocaine activates MORs by increasing expression of endogenous opioid peptides.^{62b} Because MOR activation has a high potential to lead to abuse, the development of functionally selective MOR ligands may provide a way to modulate the MOR system and affect drug abuse actions without the treatment itself being addictive. Recent advances in the field of functionally selective opioid ligands have led to the identification of several biased MOR agonists, including herkinorin and mitragynine, among others (**Figure 1.5**).^{52, 54, 63}

While the MOR system has historically received the most research attention, recent research interests have shifted toward the use of DOR and KOR ligands for addiction therapies due to their lessened chance of abuse development. The DOR system's role in drug addiction is still being defined, but several studies indicate that it is a viable drug target. DOR antagonists decrease morphine-, cocaine-, and amphetamine-induced conditioned place preference,⁶⁴ and DOR agonists

increase morphine-induced conditioned place preference.⁶⁵ DOR antagonists suffer from the same depressant effects as KOR agonists. An early study evaluating the DOR antagonists in cocaine self-administration models showed that no effect was seen below the threshold where the depressant effects were seen.⁶⁶

The KOR system appears to be an attractive way to treat stimulant and other drug addictions without the high potential for abuse seen with MOR agonists. Several studies have shown that KOR agonists decrease self-administration of both cocaine and morphine while KOR antagonists do not affect the self-administration of either drug.⁶⁷ KOR activation causes dysphoria, which can result in conditioned place aversion at high enough doses. Therefore, animal studies where locomotor activity could affect the readout of the assay must confirm that the doses of KOR agonist are not causing dysphoria and affecting the animal's activity.⁶⁸ However, many of the KOR agonists have been shown to successfully prevent cocaine- and morphine-induced conditioned place preference at doses below the threshold that results in conditioned place aversion.⁶⁹ The KOR system also appears to have a role in the withdrawal mechanism, as the naloxone-induced morphine withdrawal was attenuated with KOR agonists and potentiated with KOR antagonists.⁷⁰ Additionally, cocaine reinstatement has been shown to be attenuated by both KOR agonists and antagonists.⁷¹ Of note, as these results appear to be contradictory with agonists and antagonists both eliciting the same physiological effect, it has been said that the results from the KOR antagonist studies “remain highly controversial.”^{62b}

Targeting multiple opioid receptors has also shown success in animal models of drug abuse. Ligands that are dual MOR/KOR agonists attenuate self-administration of cocaine and heroin without as many side effects as highly selective KOR agonists.⁷² Similarly, dual KOR/DOR

agonism blocked cocaine-induced conditioned place preference without causing conditioned place preference or conditioned place aversion on its own.⁷³

A recent strategy for targeting drug addiction has been to prevent the diversion of prescription pain killers, thereby restricting the source of many of the drugs being used recreationally through the development of abuse-deterrent prescription opioid formulations. These tamper-resistant and longer-acting formulations not only help prevent abuse but also ensure patient compliance.⁷⁴

Patient compliance issues have led to the development of longer-acting treatments for addiction therapies. Depot formulations that only have to be administered once a month have been developed for both naltrexone and buprenorphine. Currently, only the depot formulation of naltrexone (Vivitrol[®]) is on the market, but the depot formulation of buprenorphine recently received fast-track designation by the FDA after a successful clinical trial.⁷⁵

Several approaches to tamper-resistant formulations have also been developed; 1) The prescribed opioid is contained in a pill along with a sequestered MOR antagonist that is only released if the pill is crushed; 2) The prescribed opioid is in a gel that is too viscous or insoluble to inject by syringe; and 3) The pill itself is resistant to crushing or solvating in common solvents.⁷⁶ Another method of abuse treatment, Suboxone[®], combines the use of the partial MOR agonist buprenorphine and the MOR antagonist naloxone in a 4:1 mixture. Due to naloxone's low oral bioavailability, if Suboxone[®] is taken sublingually as prescribed, no significant antagonism by naloxone will be seen and only the partial agonism by buprenorphine will have an effect. Suboxone[®] is dosed in a film that is nearly impossible to crush into a powder and snort, but if it is dissolved, the naloxone will antagonize any effect that the buprenorphine would have.⁷⁶⁻⁷⁷

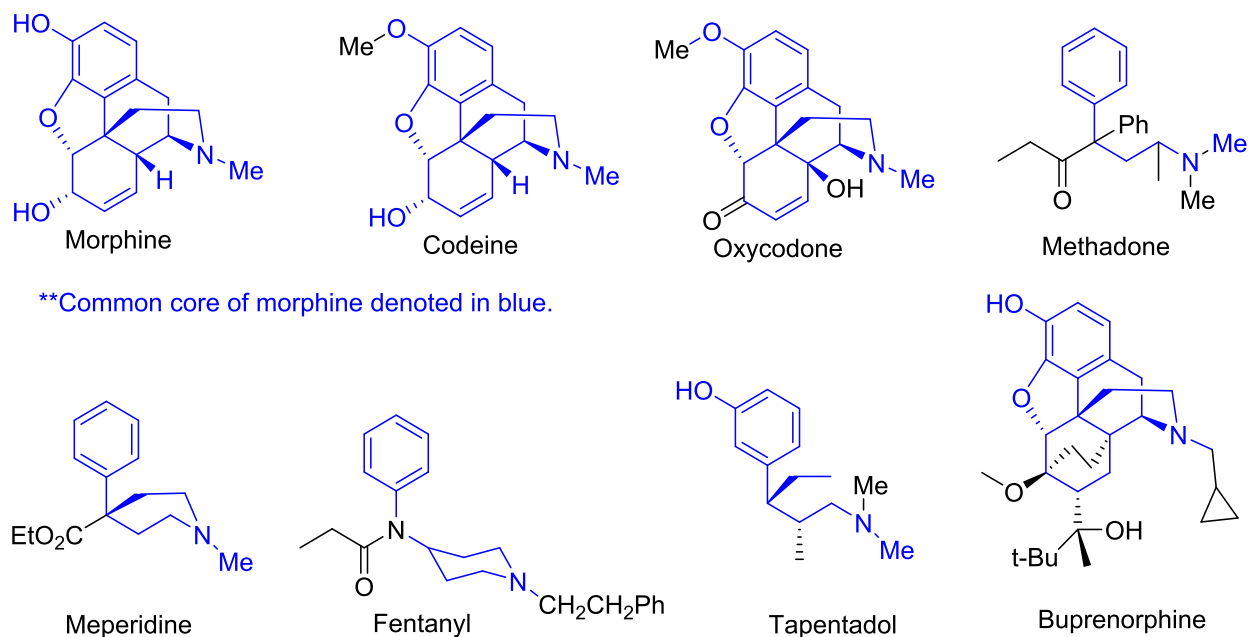
Extended-release oxycodone (OxyContin) was a heavily abused prescription drug before it was reformulated. In fact, over half of people admitted to drug treatment centers admitted to snorting

or orally taking oxycodone (53% and 55%, respectively). The reformulated pill is tamper-resistant in that it cannot be easily crushed or dissolved. As of August 9, 2010, the only form of OxyContin available is the reformulated version. The change was made with FDA approval but without notification of the general public or the prescribing physicians. In the first three years after this change was made, the rates of OxyContin-related abuse and overdoses reduced dramatically (48% and 65%, respectively). While these numbers seem like positive outcomes, some have argued that the inability to abuse prescription oxycodone has led addicted individuals to seek other drugs for their “high.” During this time when OxyContin statistics were improving, abuse of extended-release oxymorphone increased 236%.⁷⁸ Similarly, heroin overdose rates nearly tripled during those three years and are still continuing to rise.⁴ Therefore, while abuse-deterrent opioid formulations seem to have a beneficial effect of preventing the abuse of that specific drug, larger, more broadly effective solutions to the drug addiction problem are required.

Salvinorin A as a Novel Opioid

Issues with current opioids as therapies for pain and addiction

In the development of both pain and addiction therapies, a striking need for improvement over the current options is evident. Current standards of care for both pain and opioid addiction involve MORs, and the side effects from their use cannot be overlooked. Most, if not all, of these compounds are structurally similar to morphine, and although they have different pharmacological effects (full agonist, partial agonist, antagonist), they all act at the MOR in a similar fashion and result in the same side effects as morphine (**Figure 1.6**).⁴⁷ For this reason, research over the last decade has focused on identifying non-morphine-derived opioids.



**Common core of morphine denoted in blue.

Figure 1.6: Structures of morphine and analogues.

Historical use and identification

The Mexican mint plant *Salvia divinorum* has been used for many years by the indigenous Mazatec people of Oaxaca, Mexico.⁷⁹ They used the plant in spiritual divination rituals for its hallucinogenic effects, elicited with a similar potency to that of LSD. They also realized its healing properties and used small doses to treat sicknesses such as diarrhea, anemia, headaches, rheumatism, and the “semimagical” disease *panzón de borrego*, which was thought to be a sorcerer’s curse of a swollen belly.⁸⁰ To elicit these effects, *S. divinorum* can be consumed by chewing or smoking the leaves, which creates the most potent hallucinogenic effects, or by crushing the leaves and extracting the juice to drink, which does not produce significant hallucinations.⁸¹

The biological effects of *S. divinorum* prompted exploration into its active components. In the early 1980s, the active compound in *S. divinorum* was identified simultaneously by two separate groups to be the neoclerodane diterpene salvinorin A (**Figure 1.7**).^{79, 82} Although salvinorin A is responsible for the hallucinogenic effects of *S. divinorum*, it did not act at any receptor sites that

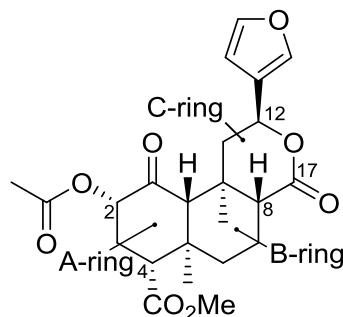


Figure 1.7: Structure of salvinorin A.

were known to mediate hallucinations.⁸¹ In 2002, Roth and colleagues determined that salvinorin A's biological activity might be due to its potent and selective activation of KORs.⁸³ This makes salvinorin A the first non-nitrogenous opioid ever discovered. In fact, prior to its discovery, a basic amine was considered to be a requirement for binding and activation of any opioid receptor.⁸⁰

Metabolism

The *in vivo* half-life ($t_{1/2}$) of salvinorin A is very short across all species studied. In rats, *i.p.* administration of salvinorin A resulted in a maximum concentration (C_{max}) in the plasma seen within 10-15 minutes of dosing.⁸⁴ A similar trend was seen for intravenous injection of salvinorin A in monkeys, with a $t_{1/2}$ of less than an hour.⁸⁵ In a human study involving smoked salvinorin A, the C_{max} in plasma was seen within 2 minutes post inhalation, and within 90 minutes, no salvinorin A was detected. This study also observed strong correlations between the subjective drug effect felt by the person and their plasma concentration of salvinorin A.⁸⁶

The short $t_{1/2}$ of salvinorin A is attributed to its rapid metabolism. The primary metabolite of salvinorin A is salvinorin B, which is formed by cleavage of the C2-acetate (**Figure 1.8**).⁸⁷ Carboxylesterases have been determined to be responsible for the salvinorin A to B conversion.⁸⁸ Additional metabolizing enzymes have been implicated in salvinorin A's metabolism, notably the cytochrome P450 enzymes (CYPs) CYP2D6, CYP1A1, CYP2C18, and CYP2E1 and the UDP-glucuronosyltransferase (UGT) UGT2B7,⁸⁴ although the specific products of these metabolic

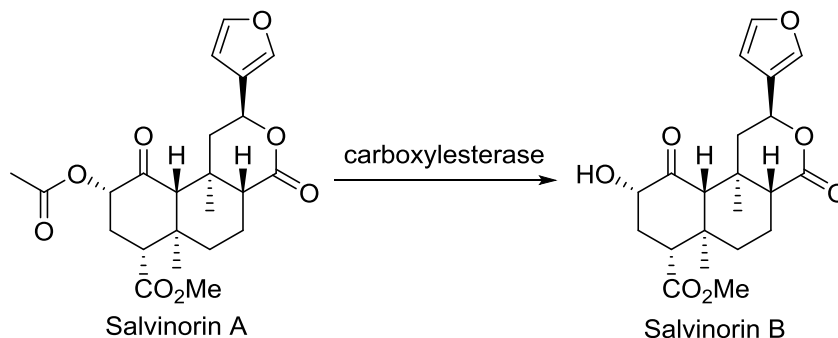


Figure 1.8: Primary metabolism of salvinorin A.

reactions have not been conclusively determined. Another specific product of metabolism has been determined to be the hydrolysis of the lactone ring by calcium-dependent lactonases to form the ring-opened products of both salvinorin A and B.⁸⁸

Structure-activity relationships

The structural complexity of salvinorin A has made the development of analogues via total synthesis challenging, although there are now several routes towards the total synthesis of salvinorin A itself.⁸⁹ All analogues of salvinorin A to date have been developed through semisynthetic methods, and although effective, the types of analogues that can be accessed via semisynthesis is limited due to the many reactive moieties within the molecule that do not tolerate harsh conditions.^{67b, 80}

Overall, most salvinorin A analogues to date have focused on modifications to the C2-acetate moiety and the furan ring. There are also a few analogues with modifications to the A-ring, C-ring, and C4-carbomethoxy moiety, although accessing these regions is generally more synthetically strenuous than the acetate and furan.

The C2 position tolerates a variety of substituents, while still maintaining KOR activity. Alkyl esters and ethers, carbamates, and sulfonates are generally well-tolerated, with the ethoxymethyl, methoxymethyl, and mesylate derivatives being more potent than or equipotent to salvinorin A

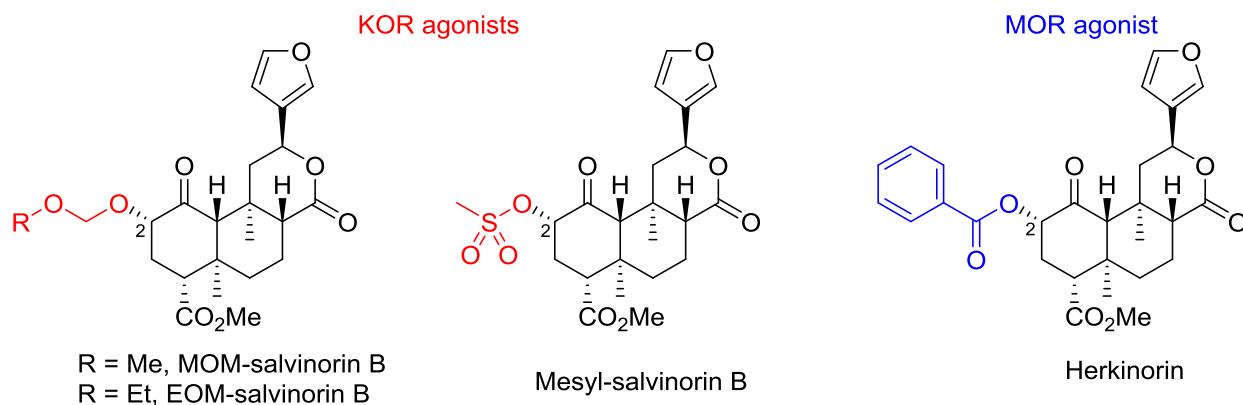


Figure 1.9: Salvinorin A derivatives at the C2 position.

itself (**Figure 1.9**). The general C2-SAR trend for KOR activity is that steric bulk is not tolerated but small, alkyl groups are.⁸⁰ While aromatic groups at the C2 position are not well-tolerated for KOR activity, substituting the acetate for a benzoate results in a MOR-selective rather than KOR-selective compound, herkinorin (**Figure 1.9**). Herkinorin was not only the first non-nitrogenous MOR agonist ever described,⁹⁰ it was also the first G-protein biased MOR agonist.⁶³ The SAR about the phenyl ring of herkinorin has been extensively explored and has been shown to tolerate meta- and para- substituted derivatives and a variety of heterocyclic substitutions. Epimerization of C2 is not well-tolerated in either the KOR agonists or the MOR agonists.⁸⁰

Furanyl derivatives of salvinorin A have also been explored, although the exploration of this position has been limited by the reaction conditions that the salvinorin A core will tolerate. Substitutions at the C16 position are possible, and generally small, linear substituents are tolerated with the 16-Br- and 16-ethynyl- derivatives being equipotent with salvinorin A (**Figure 1.10**).^{67b}

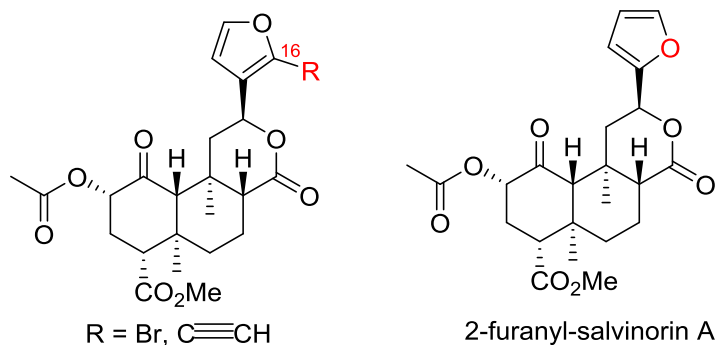


Figure 1.10: Salvinorin A furanyl-derivatives.

Modifications to the furan itself have also been accomplished, such as the 2-furanyl derivative, C12-carboxylic acid and esters, and homologated furans; however, none of these derivatives have been nearly as potent as salvinorin A.⁸⁰

In addition to these changes at the furan and acetate moieties, several other analogues of salvinorin A have been synthesized, but very few of these modifications have resulted in activity at the KORs or MORs (**Figure 1.11**). Several notable exceptions include the reduction of the C1-ketone to the deoxy compound or the reduction of the C17-lactone to either the lactol or the corresponding pyran ring, indicating that these carbonyls are not necessary parts of the decalin core for activating KORs. Additionally, limited modifications to the C4-carbomethoxy group have been accomplished, with activity maintained in the ethyl ester derivative.⁸⁰

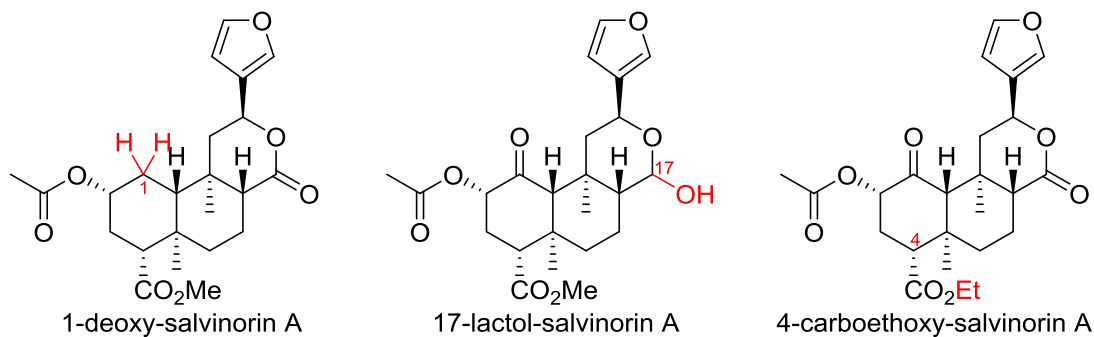


Figure 1.11: Derivatives of salvinorin A with KOR activity.

Proposed mode of binding

Because of salvinorin A's structural uniqueness as an opioid agonist, its binding at the KOR has been debated and proposed for many years. The iconic salt bridge found between the basic amines of other opioids and the aspartate residue conserved among the opioid receptors cannot be made due to the lack of basic amine in salvinorin A. Many proposed binding poses have been suggested for how salvinorin A binds at the KOR,⁹¹ but because no crystal structure exists of the active KOR, these proposed structures are simply suggestions that need to be validated with experimental evidence. Mutagenesis studies have also been conducted to selectively mutate an

amino acid in the binding pocket and evaluate salvinorin A's ability to activate the mutated receptor.^{27,91} While these studies offer some insight into which amino acids are interacting directly with the ligands at the binding site, the data can be difficult to interpret as perturbing a single amino acid can destabilize the active conformation of the structurally complex KOR. This complication is highlighted by the fact that mutating amino acids outside of or on the edge of the binding site has detrimental effects on the activity of salvinorin A at the KOR.^{91b}

In 2012, the KOR crystal structure bound to JDTC was published,²⁷ which gave insight into the binding pocket of the KOR but in an inactive state (**Figure 1.12**). However, as this is the best picture of the receptor to date, it has been used to study salvinorin A's interaction at the receptor binding pocket. The original report proposed a binding pose of a salvinorin A derivative, RB-64, which has a thiocyanate moiety that has been shown to bind covalently to cysteines in the KOR binding pocket.^{27,91e} The proposed interactions of salvinorin A and the KOR do align, for the most part, with experimental SAR data generated through the evaluation of salvinorin A analogues at the KOR *in vitro*.

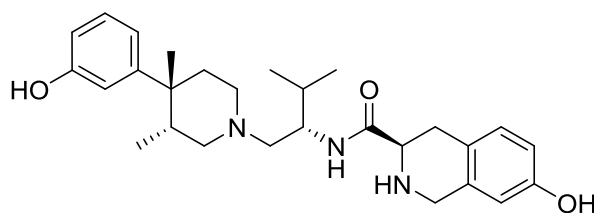


Figure 1.12: Structure of JDTC, KOR antagonist.

Needs for improvement

Salvinorin A has proven to be a structurally unique opioid scaffold that is useful in probing the effects of MORs and KORs, both *in vitro* and *in vivo*. However, the evaluation of salvinorin A and its derivatives *in vivo* has often presented with conflicting results, depending on the compound and the route of administration. Often, these discrepancies can be attributed to salvinorin A's structural

issues that prevent its further development as a drug candidate, including its rapid metabolism and low oral bioavailability.⁸⁰

In vitro evaluation indicates that the compounds are acting at KORs with similar potency, but upon administration to animals, the effects vary widely. For instance, salvinorin A showed low and inconsistent antinociceptive effects, while the 2-methoxymethyl-salvinorin B derivative showed potent antinociception in mouse models.⁹² These two compounds behave similarly *in vitro*, but the mechanisms for their significant *in vivo* differences cannot be fully delineated. In this assay, salvinorin A could be metabolized before reaching the site of action, whereas 2-methoxymethyl-salvinorin B is presumably more metabolically stable and may be able to reach the site of action to elicit the antinociceptive effects. Conversely, the two compounds could be activating the KORs in functionally selective ways that results in antinociception for the methoxymethyl-salvinorin B derivative but not for salvinorin B.⁸⁰

Salvinorin A and all of the analogues reported to date are very water insoluble.⁹³ This lack of solubility limits the doses that can be given to the animals as well as the routes of administration. In most cases, the compounds were dissolved in DMSO or other organic solvents and buffer mixtures and given via intraperitoneal (i.p.) injection.⁹³ This administration complicated the interpretation of the studies because different solvent solutions are often required to solubilize different compounds, and as organic solvents can have pharmacological effects of their own,⁹⁴ vehicle-treated animals must be treated with the specific, corresponding solvent mixtures used with each drug in order to compare the two results. The low solubility of these compounds require large volumes for delivery of the drug, which can limit the amount of dose that can be administered in animals, but the i.p. administration method is limited to low volume injections because of the small size of rodents' peritoneal cavity. These factors can limit the amount of dose that can be

administered in animals.⁹⁵ Furthermore, while i.p. administration is an effective method for research purposes, it does not correspond to any method of administration in humans, which is necessary for furthering a drug through pre-clinical trials.⁹³

Evaluation of salvinorin A and its derivatives in animals is also complicated by the potential for aversive and dysphoric effects resulting from KOR activation. Salvinorin A has been shown to attenuate cocaine-induced reinstatement of cocaine self-administration, but it has also been shown to reduce locomotor activity and elicit an aversive response in a conditioned place aversion test. Activation of the KOR and the associated decreases in dopamine release could be the cause of the positive results seen in the cocaine reinstatement models, but the KOR-related side effects must be evaluated at the specific doses in order to determine if, for example, the reduction in locomotor activity is what is actually keeping the animals from self-administering cocaine.⁸⁰

Overall, salvinorin A has proven to be a promising lead compound in the development of both pain and addiction therapies. However, improvements to the pharmacokinetic and metabolic profiles of salvinorin A derivatives as well as improved selectivity of the MOR-active compound herkinorin are still needed to further advance the therapeutic use of these compounds.

References

1. Substance Abuse and Mental Health Services Administration (US); Office of the Surgeon General (US). Facing Addiction in America: The Surgeon General's Report on Alcohol, Drugs, and Health. US Department of Health and Human Services: Washington (DC), 2016.
2. Rudd, R. A.; Seth, P.; David, F.; Scholl, L. Increases in drug and opioid-involved overdose deaths - United States, 2010-2015. *MMWR Morb. Mortal. Wkly. Rep.* **2016**, *65*, 1445-1452.

3. Centers for Disease Control and Prevention. Wide-ranging online data for epidemiologic research (WONDER). CDC, National Center for Health Statistics: Atlanta, GA, 2016. Available at <http://wonder.cdc.gov> (accessed Mar 29, 2017).
4. Warner, M.; Trinidad, J. P.; Bastian, B. A.; Minino, A. M.; Hedegaard, H. Drugs most frequently involved in drug overdose deaths: United States, 2010-2014. *Natl. Vital Stat. Rep.* **2016**, *65*, 1-15.
5. *2016 National Drug Threat Assessment Summary*; DEA-DCT-DIR-001-17; United States Drug Enforcement Administration: online: <https://www.dea.gov/resource-center/2016%20NDTA%20Summary.pdf>, November, 2016 (accessed Mar 16, 2017).
6. Institute of Medicine (US) Committee on Advancing Pain Research, Care, and Education. *Relieving Pain in America: A Blueprint for Transforming Prevention, Care, Education, and Research*. Washington (DC): National Academies Press (US); 2011.
7. Stein, C. Opioids, sensory systems and chronic pain. *Eur. J. Pharmacol.* **2013**, *716*, 179-187.
8. Dietis, N.; Guerrini, R.; Calo, G.; Salvadori, S.; Rowbotham, D. J.; Lambert, D. G. Simultaneous targeting of multiple opioid receptors: a strategy to improve side-effect profile. *Br. J. Anaesth.* **2009**, *103*, 38-49.
9. Stein, C. Opioid Receptors. *Annu. Rev. Med.* **2016**, *67*, 433-451.
10. Trang, T.; Al-Hasani, R.; Salvemini, D.; Salter, M. W.; Gutstein, H.; Cahill, C. M. Pain and poppies: the good, the bad, and the ugly of opioid analgesics. *J. Neurosci.* **2015**, *35*, 13879-13888.
11. Melnikova, I. Pain market. *Nat. Rev. Drug Discov.* **2010**, *9*, 589-590.
12. Pizzo, P. A.; Clark, N. M. Alleviating suffering 101--pain relief in the United States. *N. Engl. J. Med.* **2012**, *366*, 197-199.

13. McLellan, A. T.; Lewis, D. C.; O'Brien, C. P.; Kleber, H. D. Drug dependence, a chronic medical illness: implications for treatment, insurance, and outcomes evaluation. *JAMA* **2000**, *284*, 1689-1695.
14. Volkow, N. D.; Koob, G. F.; McLellan, A. T. Neurobiologic advances from the brain disease model of addiction. *New Engl. J. Med.* **2016**, *374*, 363-371.
15. Di Chiara, G. Nucleus accumbens shell and core dopamine: differential role in behavior and addiction. *Behav. Brain Res.* **2002**, *137*, 75-114.
16. Wise, R. A. Dopamine and reward: the anhedonia hypothesis 30 years on. *Neurotox. Res.* **2008**, *14*, 169-183.
17. (a) Koob, G. F.; Volkow, N. D. Neurocircuitry of addiction. *Neuropsychopharmacology* **2010**, *35*, 217-238; (b) Kornetsky, C.; Esposito, R. U. Euphorogenic drugs: effects on the reward pathways of the brain. *Fed. Proc.* **1979**, *38*, 2473-2476.
18. Koob, G. F.; Le Moal, M. Addiction and the brain antireward system. *Annu. Rev. Psychol.* **2008**, *59*, 29-53.
19. Goldstein, R. Z.; Volkow, N. D. Dysfunction of the prefrontal cortex in addiction: neuroimaging findings and clinical implications. *Nat. Rev. Neurosci.* **2011**, *12*, 652-669.
20. Rando, K.; Hong, K. I.; Bhagwagar, Z.; Li, C. S.; Bergquist, K.; Guarnaccia, J.; Sinha, R. Association of frontal and posterior cortical gray matter volume with time to alcohol relapse: a prospective study. *Am. J. Psychiatry* **2011**, *168*, 183-192.
21. (a) Zhong, X.; Drgonova, J.; Li, C. Y.; Uhl, G. R. Human cell adhesion molecules: annotated functional subtypes and overrepresentation of addiction-associated genes. *Ann. N. Y. Acad. Sci.* **2015**, *1349*, 83-95; (b) Demers, C. H.; Bogdan, R.; Agrawal, A. The genetics, neurogenetics and pharmacogenetics of addiction. *Curr. Behav. Neurosci. Rep.* **2014**, *1*, 33-44.

22. Burnett-Zeigler, I.; Walton, M. A.; Ilgen, M.; Barry, K. L.; Chermack, S. T.; Zucker, R. A.; Zimmerman, M. A.; Booth, B. M.; Blow, F. C. Prevalence and correlates of mental health problems and treatment among adolescents seen in primary care. *J. Adolesc. Health* **2012**, *50*, 559-564.
23. Pert, C. B.; Snyder, S. H. Properties of opiate-receptor binding in rat brain. *Proc. Natl. Acad. Sci. U. S. A.* **1973**, *70*, 2243-2247.
24. Pathan, H.; Williams, J. Basic opioid pharmacology: an update. *Br. J. Pain* **2012**, *6*, 11-16.
25. Hughes, J.; Smith, T. W.; Kosterlitz, H. W.; Fothergill, L. A.; Morgan, B. A.; Morris, H. R. Identification of 2 related pentapeptides from brain with potent opiate agonist activity. *Nature* **1975**, *258*, 577-579.
26. Manglik, A.; Kruse, A. C.; Kobilka, T. S.; Thian, F. S.; Mathiesen, J. M.; Sunahara, R. K.; Pardo, L.; Weis, W. I.; Kobilka, B. K.; Granier, S. Crystal structure of the micro-opioid receptor bound to a morphinan antagonist. *Nature* **2012**, *485*, 321-326.
27. Wu, H.; Wacker, D.; Mileni, M.; Katritch, V.; Han, G. W.; Vardy, E.; Liu, W.; Thompson, A. A.; Huang, X. P.; Carroll, F. I.; Mascarella, S. W.; Westkaemper, R. B.; Mosier, P. D.; Roth, B. L.; Cherezov, V.; Stevens, R. C. Structure of the human kappa-opioid receptor in complex with JDTic. *Nature* **2012**, *485*, 327-332.
28. Granier, S.; Manglik, A.; Kruse, A. C.; Kobilka, T. S.; Thian, F. S.; Weis, W. I.; Kobilka, B. K. Structure of the delta-opioid receptor bound to naltrindole. *Nature* **2012**, *485*, 400-404.
29. Fenalti, G.; Zatspein, N. A.; Betti, C.; Giguere, P.; Han, G. W.; Ishchenko, A.; Liu, W.; Guillemyn, K.; Zhang, H.; James, D.; Wang, D.; Weierstall, U.; Spence, J. C. H.; Boutet, S.; Messerschmidt, M.; Williams, G. J.; Gati, C.; Yefanov, O. M.; White, T. A.; Oberthuer, D.; Metz, M.; Yoon, C. H.; Barty, A.; Chapman, H. N.; Basu, S.; Coe, J.; Conrad, C. E.; Fromme,

- R.; Fromme, P.; Tourwé, D.; Schiller, P. W.; Roth, B. L.; Ballet, S.; Katritch, V.; Stevens, R. C.; Cherezov, V. Structural basis for bifunctional peptide recognition at human δ -opioid receptor. *Nat. Struct. Mol. Biol.* **2015**, *22*, 265-268.
30. Huang, W.; Manglik, A.; Venkatakrisnan, A. J.; Laeremans, T.; Feinberg, E. N.; Sanborn, A. L.; Kato, H. E.; Livingston, K. E.; Thorsen, T. S.; Kling, R. C.; Granier, S.; Gmeiner, P.; Husbands, S. M.; Traynor, J. R.; Weis, W. I.; Steyaert, J.; Dror, R. O.; Kobilka, B. K. Structural insights into micro-opioid receptor activation. *Nature* **2015**, *524*, 315-321.
31. O'Connor, C.; White, K. L.; Doncescu, N.; Didenko, T.; Roth, B. L.; Czaplicki, G.; Stevens, R. C.; Wuthrich, K.; Milon, A. NMR structure and dynamics of the agonist dynorphin peptide bound to the human kappa opioid receptor. *Proc. Natl. Acad. Sci. U. S. A.* **2015**, *112*, 11852-11857.
32. Lutz, P. E.; Kieffer, B. L. The multiple facets of opioid receptor function: implications for addiction. *Curr. Opin. Neurobiol.* **2013**.
33. Trescot, A. M.; Datta, S.; Lee, M.; Hansen, H. Opioid pharmacology. *Pain Physician* **2008**, *11*, S133-153.
34. Ross, S.; Peselow, E. The neurobiology of addictive disorders. *Clin. Neuropharmacol.* **2009**, *32*, 269-276.
35. Wang, Y. H.; Sun, J. F.; Tao, Y. M.; Chi, Z. Q.; Liu, J. G. The role of kappa-opioid receptor activation in mediating antinociception and addiction. *Acta Pharmacol. Sin.* **2010**, *31*, 1065-1070.
36. Al-Hasani, R.; Bruchas, M. R. Molecular mechanisms of opioid receptor-dependent signaling and behavior. *Anesthesiology* **2011**, *115*, 1363-1381.

37. Rankovic, Z.; Brust, T. F.; Bohn, L. M. Biased agonism: An emerging paradigm in GPCR drug discovery. *Bioorg. Med. Chem. Lett.* **2016**, *26*, 241-250.
38. Prinster, S. C.; Hague, C.; Hall, R. A. Heterodimerization of G protein-coupled receptors: Specificity and functional significance. *Pharmacol. Rev.* **2005**, *57*, 289-298.
39. Law, P. Y.; Reggio, P. H.; Loh, H. H. Opioid receptors: toward separation of analgesic from undesirable effects. *Trends Biochem. Sci.* **2013**, *38*, 275-282.
40. Dietis, N.; Rowbotham, D. J.; Lambert, D. G. Opioid receptor subtypes: fact or artifact? *Br. J. Anaesth.* **2011**, *107*, 8-18.
41. (a) Rasmussen, S. G.; DeVree, B. T.; Zou, Y.; Kruse, A. C.; Chung, K. Y.; Kobilka, T. S.; Thian, F. S.; Chae, P. S.; Pardon, E.; Calinski, D.; Mathiesen, J. M.; Shah, S. T.; Lyons, J. A.; Caffrey, M.; Gellman, S. H.; Steyaert, J.; Skiniotis, G.; Weis, W. I.; Sunahara, R. K.; Kobilka, B. K. Crystal structure of the beta2 adrenergic receptor-Gs protein complex. *Nature* **2011**, *477*, 549-555; (b) Westfield, G. H.; Rasmussen, S. G.; Su, M.; Dutta, S.; DeVree, B. T.; Chung, K. Y.; Calinski, D.; Velez-Ruiz, G.; Oleskie, A. N.; Pardon, E.; Chae, P. S.; Liu, T.; Li, S.; Woods, V. L., Jr.; Steyaert, J.; Kobilka, B. K.; Sunahara, R. K.; Skiniotis, G. Structural flexibility of the G alpha s alpha-helical domain in the beta2-adrenoceptor Gs complex. *Proc. Natl. Acad. Sci. U. S. A.* **2011**, *108*, 16086-16091.
42. Shukla, A. K.; Violin, J. D.; Whalen, E. J.; Gesty-Palmer, D.; Shenoy, S. K.; Lefkowitz, R. J. Distinct conformational changes in beta-arrestin report biased agonism at seven-transmembrane receptors. *Proc. Natl. Acad. Sci. U. S. A.* **2008**, *105*, 9988-9993.
43. Luttrell, L. M.; Maudsley, S.; Bohn, L. M. Fulfilling the promise of "biased" G protein-coupled receptor agonism. *Mol. Pharmacol.* **2015**, *88*, 579-588.

44. (a) Free, R. B.; Chun, L. S.; Moritz, A. E.; Miller, B. N.; Doyle, T. B.; Conroy, J. L.; Padron, A.; Meade, J. A.; Xiao, J.; Hu, X.; Dulcey, A. E.; Han, Y.; Duan, L.; Titus, S.; Bryant-Genevier, M.; Barnaeva, E.; Ferrer, M.; Javitch, J. A.; Beuming, T.; Shi, L.; Southall, N. T.; Marugan, J. J.; Sibley, D. R. Discovery and characterization of a G protein-biased agonist that inhibits beta-arrestin recruitment to the D2 dopamine receptor. *Mol. Pharmacol.* **2014**, *86*, 96-105; (b) Kenakin, T.; Christopoulos, A. Signalling bias in new drug discovery: detection, quantification and therapeutic impact. *Nat. Rev. Drug Discovery* **2013**, *12*, 205-216; (c) Kenakin, T.; Watson, C.; Muniz-Medina, V.; Christopoulos, A.; Novick, S. A simple method for quantifying functional selectivity and agonist bias. *ACS Chem. Neurosci.* **2012**, *3*, 193-203; (d) Zhou, L.; Lovell, K. M.; Frankowski, K. J.; Slauson, S. R.; Phillips, A. M.; Streicher, J. M.; Stahl, E.; Schmid, C. L.; Hodder, P.; Madoux, F.; Cameron, M. D.; Prisinzano, T. E.; Aube, J.; Bohn, L. M. Development of functionally selective, small molecule agonists at kappa opioid receptors. *J. Biol. Chem.* **2013**, *288*, 36703-36716.
45. (a) Bohn, L. M.; Gainetdinov, R. R.; Lin, F. T.; Lefkowitz, R. J.; Caron, M. G. Mu-opioid receptor desensitization by beta-arrestin-2 determines morphine tolerance but not dependence. *Nature* **2000**, *408*, 720-723; (b) Bohn, L. M.; Lefkowitz, R. J.; Gainetdinov, R. R.; Peppel, K.; Caron, M. G.; Lin, F. T. Enhanced morphine analgesia in mice lacking beta-arrestin 2. *Science* **1999**, *286*, 2495-2498; (c) Raehal, K. M.; Walker, J. K.; Bohn, L. M. Morphine side effects in beta-arrestin 2 knockout mice. *J. Pharmacol. Exp. Ther.* **2005**, *314*, 1195-1201.
46. (a) Berg, K. A.; Rowan, M. P.; Sanchez, T. A.; Silva, M.; Patwardhan, A. M.; Milam, S. B.; Hargreaves, K. M.; Clarke, W. P. Regulation of kappa-opioid receptor signaling in peripheral sensory neurons in vitro and in vivo. *J. Pharmacol. Exp. Ther.* **2011**, *338*, 92-99; (b) Bruchas,

- M. R.; Chavkin, C. Kinase cascades and ligand-directed signaling at the kappa opioid receptor. *Psychopharmacology* **2010**, *210*, 137-147.
47. Wolkerstorfer, A.; Handler, N.; Buschmann, H. New approaches to treating pain. *Bioorg. Med. Chem. Lett.* **2016**, *26*, 1103-1119.
48. Gulland, J. M.; Robinson, R. Constitution of codeine and thebaine. *Mem. Proc. Manchester Lit. Philos. Soc.* **1925**, *69*, 79-86.
49. Williams, D. A.; Roche, V. F.; Roche, E. B. *Foye's Principles of Medicinal Chemistry*. 7th ed.; Wolters Kluwer Health/Lippincott Williams & Wilkins: Philadelphia, 2013; p 658-699.
50. Stevenson, G. W.; Luginbuhl, A.; Dunbar, C.; LaVigne, J.; Dutra, J.; Atherton, P.; Bell, B.; Cone, K.; Giuvelis, D.; Polt, R.; Streicher, J. M.; Bilsky, E. J. The mixed-action delta/mu opioid agonist MMP-2200 does not produce conditioned place preference but does maintain drug self-administration in rats, and induces in vitro markers of tolerance and dependence. *Pharmacol. Biochem. Behav.* **2015**, *132*, 49-55.
51. Chen, X.-T.; Pitis, P.; Liu, G.; Yuan, C.; Gotchev, D.; Cowan, C. L.; Rominger, D. H.; Koblish, M.; DeWire, S. M.; Crombie, A. L.; Violin, J. D.; Yamashita, D. S. Structure–activity relationships and discovery of a G protein biased μ opioid receptor ligand, [(3-Methoxythiophen-2-yl)methyl]([2-[(9r)-9-(pyridin-2-yl)-6-oxaspiro-[4.5]decan-9-yl]ethyl])amine (TRV130), for the treatment of acute severe pain. *J. Med. Chem.* **2013**, *56*, 8019-8031.
52. Kruegel, A. C.; Gassaway, M. M.; Kapoor, A.; Váradi, A.; Majumdar, S.; Filizola, M.; Javitch, J. A.; Sames, D. Synthetic and receptor signaling explorations of the mitragyna alkaloids: Mitragynine as an atypical molecular framework for opioid receptor modulators. *J. Am. Chem. Soc.* **2016**, *138*, 6754-6764.

53. Tidgewell, K.; Groer, C. E.; Harding, W. W.; Lozama, A.; Schmidt, M.; Marquam, A.; Hiemstra, J.; Partilla, J. S.; Dersch, C. M.; Rothman, R. B.; Bohn, L. M.; Prisinzano, T. E. Herkinorin analogues with differential beta-arrestin-2 interactions. *J. Med. Chem.* **2008**, *51*, 2421-2431.
54. Manglik, A.; Lin, H.; Aryal, D. K.; McCorvy, J. D.; Dengler, D.; Corder, G.; Levit, A.; Kling, R. C.; Bernat, V.; Hübner, H.; Huang, X.-P.; Sassano, M. F.; Giguère, P. M.; Löber, S.; Da, D.; Scherrer, G.; Kobilka, B. K.; Gmeiner, P.; Roth, B. L.; Shoichet, B. K. Structure-based discovery of opioid analgesics with reduced side effects. *Nature* **2016**, *537*, 185-190.
55. Vanderah, T. W. Delta and kappa opioid receptors as suitable drug targets for pain. *Clin. J. Pain* **2010**, *26* S10-15.
56. Kreek, M. J.; Levran, O.; Reed, B.; Schlussman, S. D.; Zhou, Y.; Butelman, E. R. Opiate addiction and cocaine addiction: underlying molecular neurobiology and genetics. *J. Clin. Invest.* **2012**, *122*, 3387-3393.
57. Potenza, M. N.; Sofuoglu, M.; Carroll, K. M.; Rounsaville, B. J. Neuroscience of behavioral and pharmacological treatments for addictions. *Neuron* **2011**, *69*, 695-712.
58. (a) Montoya, I. D.; Gorelick, D. A.; Preston, K. L.; Schroeder, J. R.; Umbricht, A.; Cheskin, L. J.; Lange, W. R.; Contoreggi, C.; Johnson, R. E.; Fudala, P. J. Randomized trial of buprenorphine for treatment of concurrent opiate and cocaine dependence. *Clin. Pharmacol. Ther.* **2004**, *75*, 34-48; (b) Peles, E.; Kreek, M. J.; Kellogg, S.; Adelson, M. High methadone dose significantly reduces cocaine use in methadone maintenance treatment (MMT) patients. *J. Addict. Dis.* **2006**, *25*, 43-50.

59. Jayaram-Lindstrom, N.; Konstenius, M.; Eksborg, S.; Beck, O.; Hammarberg, A.; Franck, J. Naltrexone attenuates the subjective effects of amphetamine in patients with amphetamine dependence. *Neuropsychopharmacology* **2008**, *33*, 1856-1863.
60. (a) Wee, S.; Vendruscolo, L. F.; Misra, K. K.; Schlosburg, J. E.; Koob, G. F. A combination of buprenorphine and naltrexone blocks compulsive cocaine intake in rodents without producing dependence. *Sci. Transl. Med.* **2012**, *4*, 146ra110; (b) Cordery, S. F.; Taverner, A.; Ridzwan, I. E.; Guy, R. H.; Delgado-Charro, M. B.; Husbands, S. M.; Bailey, C. P. A non-rewarding, non-aversive buprenorphine/naltrexone combination attenuates drug-primed reinstatement to cocaine and morphine in rats in a conditioned place preference paradigm. *Addict. Biol.* **2014**, *19*, 575-586.
61. Leri, F.; Zhou, Y.; Goddard, B.; Cummins, E.; Kreek, M. J. Effects of high-dose methadone maintenance on cocaine place conditioning, cocaine self-administration, and mu-opioid receptor mRNA expression in the rat brain. *Neuropsychopharmacology* **2006**, *31*, 1462-1474.
62. (a) Giuliano, C.; Robbins, T. W.; Wille, D. R.; Bullmore, E. T.; Everitt, B. J. Attenuation of cocaine and heroin seeking by mu-opioid receptor antagonism. *Psychopharmacology* **2013**, *227*, 137-147; (b) Noble, F.; Lenoir, M.; Marie, N. The opioid receptors as targets for drug abuse medication. *Br. J. Pharmacol.* **2015**, *172*, 3964-3979.
63. Groer, C. E.; Tidgewell, K.; Moyer, R. A.; Harding, W. W.; Rothman, R. B.; Prisinzano, T. E.; Bohn, L. M. An opioid agonist that does not induce mu-opioid receptor--arrestin interactions or receptor internalization. *Mol. Pharmacol.* **2007**, *71*, 549-557.
64. (a) Kotlinska, J. H.; Gibula-Bruzda, E.; Pachuta, A.; Kunce, D.; Witkowska, E.; Chung, N. N.; Schiller, P. W.; Izdebski, J. Influence of new deltorphin analogues on reinstatement of

cocaine-induced conditioned place preference in rats. *Behav. Pharmacol.* **2010**, *21*, 638-648; (b) Billa, S. K.; Xia, Y.; Moron, J. A. Disruption of morphine-conditioned place preference by a delta2-opioid receptor antagonist: study of mu-opioid and delta-opioid receptor expression at the synapse. *Eur. J. Neurosci.* **2010**, *32*, 625-631; (c) Belkai, E.; Scherrmann, J. M.; Noble, F.; Marie-Claire, C. Modulation of MDMA-induced behavioral and transcriptional effects by the delta opioid antagonist naltrindole in mice. *Addict. Biol.* **2009**, *14*, 245-252.

65. Suzuki, T.; Tsuji, M.; Mori, T.; Misawa, M.; Endoh, T.; Nagase, H. Effect of the highly selective and nonpeptide delta opioid receptor agonist TAN-67 on the morphine-induced place preference in mice. *J. Pharmacol. Exp. Ther.* **1996**, *279*, 177-185.

66. de Vries, T. J.; Babovic-Vuksanovic, D.; Elmer, G.; Shippenberg, T. S. Lack of involvement of delta-opioid receptors in mediating the rewarding effects of cocaine. *Psychopharmacology* **1995**, *120*, 442-448.

67. (a) Glick, S. D.; Maisonneuve, I. M.; Raucci, J.; Archer, S. Kappa opioid inhibition of morphine and cocaine self-administration in rats. *Brain Res.* **1995**, *681*, 147-152; (b) Riley, A. P.; Groer, C. E.; Young, D.; Ewald, A. W.; Kivell, B. M.; Prisinzano, T. E. Synthesis and kappa-opioid receptor activity of furan-substituted salvinorin A analogues. *J. Med. Chem.* **2014**, *57*, 10464-10475; (c) Negus, S. S.; Mello, N. K.; Portoghese, P. S.; Lin, C. E. Effects of kappa opioids on cocaine self-administration by rhesus monkeys. *J. Pharmacol. Exp. Ther.* **1997**, *282*, 44-55.

68. Bruchas, M. R.; Land, B. B.; Chavkin, C. The dynorphin/kappa opioid system as a modulator of stress-induced and pro-addictive behaviors. *Brain Res.* **2010**, *1314*, 44-55.

69. (a) Bolanos, C. A.; Garmsen, G. M.; Clair, M. A.; McDougall, S. A. Effects of the kappa-opioid receptor agonist U-50,488 on morphine-induced place preference conditioning in the

developing rat. *Eur. J. Pharmacol.* **1996**, *317*, 1-8; (b) Zhang, Y.; Butelman, E. R.; Schlussman, S. D.; Ho, A.; Kreek, M. J. Effect of the kappa opioid agonist R-84760 on cocaine-induced increases in striatal dopamine levels and cocaine-induced place preference in C57BL/6J mice. *Psychopharmacology* **2004**, *173*, 146-152.

70. (a) Spanagel, R.; Almeida, O. F.; Bartl, C.; Shippenberg, T. S. Endogenous kappa-opioid systems in opiate withdrawal: role in aversion and accompanying changes in mesolimbic dopamine release. *Psychopharmacology* **1994**, *115*, 121-127; (b) Tao, Y. M.; Li, Q. L.; Zhang, C. F.; Xu, X. J.; Chen, J.; Ju, Y. W.; Chi, Z. Q.; Long, Y. Q.; Liu, J. G. LPK-26, a novel kappa-opioid receptor agonist with potent antinociceptive effects and low dependence potential. *Eur. J. Pharmacol.* **2008**, *584*, 306-311.

71. (a) Morani, A. S.; Kivell, B.; Prisinzano, T. E.; Schenk, S. Effect of kappa-opioid receptor agonists U69593, U50488H, spiradoline and salvinorin A on cocaine-induced drug-seeking in rats. *Pharmacol. Biochem. Behav.* **2009**, *94*, 244-249; (b) Beardsley, P. M.; Howard, J. L.; Shelton, K. L.; Carroll, F. I. Differential effects of the novel kappa opioid receptor antagonist, JD1c, on reinstatement of cocaine-seeking induced by footshock stressors vs cocaine primes and its antidepressant-like effects in rats. *Psychopharmacology* **2005**, *183*, 118-126.

72. (a) Archer, S.; Glick, S. D.; Bidlack, J. M. Cyclazocine revisited. *Neurochem. Res.* **1996**, *21*, 1369-1373; (b) Bowen, C. A.; Negus, S. S.; Zong, R.; Neumeyer, J. L.; Bidlack, J. M.; Mello, N. K. Effects of mixed-action kappa/mu opioids on cocaine self-administration and cocaine discrimination by rhesus monkeys. *Neuropsychopharmacology* **2003**, *28*, 1125-1139; (c) Wang, Y. J.; Tao, Y. M.; Li, F. Y.; Wang, Y. H.; Xu, X. J.; Chen, J.; Cao, Y. L.; Chi, Z. Q.; Neumeyer, J. L.; Zhang, A.; Liu, J. G. Pharmacological characterization of ATPM [(-)-3-aminothiazolo[5,4-b]-N-cyclopropylmethylmorphinan hydrochloride], a novel mixed kappa-

agonist and mu-agonist/-antagonist that attenuates morphine antinociceptive tolerance and heroin self-administration behavior. *J. Pharmacol. Exp. Ther.* **2009**, *329*, 306-313.

73. Varadi, A.; Marrone, G. F.; Eans, S. O.; Ganno, M. L.; Subrath, J. J.; Le Rouzic, V.; Hunkele, A.; Pasternak, G. W.; McLaughlin, J. P.; Majumdar, S. Synthesis and characterization of a dual kappa-delta opioid receptor agonist analgesic blocking cocaine reward behavior. *ACS Chem. Neurosci.* **2015**, *6*, 1813-1824.

74. Schaeffer, T. Abuse-deterrent formulations, an evolving technology against the abuse and misuse of opioid analgesics. *J. Med. Toxicol.* **2012**, *8*, 400-407.

75. (a) Lobmaier, P. P.; Kunoe, N.; Gossop, M.; Waal, H. Naltrexone depot formulations for opioid and alcohol dependence: a systematic review. *CNS Neurosci. Ther.* **2011**, *17*, 629-636; (b) Sigmon, S. C.; Moody, D. E.; Nuwayser, E. S.; Bigelow, G. E. An injection depot formulation of buprenorphine: extended bio-delivery and effects. *Addiction* **2006**, *101*, 420-432; (c) Nasser, A. F.; Greenwald, M. K.; Vince, B.; Fudala, P. J.; Twumasi-Ankrah, P.; Liu, Y.; Jones, J. P., 3rd; Heidbreder, C. Sustained-release buprenorphine (RBP-6000) blocks the effects of opioid challenge with hydromorphone in subjects with opioid use disorder. *J. Clin. Psychopharmacol.* **2016**, *36*, 18-26; (d) Indivior, Indivior receives FDA fast track designation for RBP-6000 buprenorphine monthly depot for the treatment of opioid use disorder.

<http://www.indivior.com/wp-content/uploads/2016/05/FDA-Fast-Track-designation-1.pdf>. Press Release, Online, 2016 (accessed Jun 26, 2017).

76. Lourenco, L. M.; Matthews, M.; Jamison, R. N. Abuse-deterrent and tamper-resistant opioids: how valuable are novel formulations in thwarting non-medical use? *Expert Opin. Drug Delivery* **2013**, *10*, 229-240.

77. Orman, J. S.; Keating, G. M. Spotlight on buprenorphine/naloxone in the treatment of opioid dependence. *CNS Drugs* **2009**, *23*, 899-902.
78. Coplan, P. M.; Chilcoat, H. D.; Butler, S. F.; Sellers, E. M.; Kadakia, A.; Harikrishnan, V.; Haddox, J. D.; Dart, R. C. The effect of an abuse-deterrent opioid formulation (OxyContin) on opioid abuse-related outcomes in the postmarketing setting. *Clin. Pharmacol. Ther.* **2016**, *100*, 275-286.
79. Ortega, A.; Blount, J. F.; Manchand, P. S. Salvinorin, a New Trans-Neoclerodane Diterpene from *Salvia-Divinatorum* (Labiatae). *J Chem Soc Perk T 1* **1982**, 2505-2508.
80. Cunningham, C. W.; Rothman, R. B.; Prisinzano, T. E. Neuropharmacology of the naturally occurring kappa-opioid hallucinogen salvinorin A. *Pharmacol. Rev.* **2011**, *63*, 316-347.
81. Siebert, D. J. *Salvia divinorum* and salvinorin A: new pharmacologic findings. *J. Ethnopharmacol.* **1994**, *43*, 53-56.
82. Valdes, L. J.; Butler, W. M.; Hatfield, G. M.; Paul, A. G.; Koreeda, M. Divinorin A, a psychotropic terpenoid, and divinorin B from the hallucinogenic Mexican mint, *Salvia divinorum*. *J. Org. Chem.* **1984**, *49*, 4716-4720.
83. Roth, B. L.; Baner, K.; Westkaemper, R.; Siebert, D.; Rice, K. C.; Steinberg, S.; Ernsberger, P.; Rothman, R. B. Salvinorin A: A potent naturally occurring nonnitrogenous κ opioid selective agonist. *Proc. Natl. Acad. Sci. U. S. A.* **2002**, *99*, 11934-11939.
84. Teksin, Z. S.; Lee, I. J.; Nemieboka, N. N.; Othman, A. A.; Upreti, V. V.; Hassan, H. E.; Syed, S. S.; Prisinzano, T. E.; Eddington, N. D. Evaluation of the transport, in vitro metabolism and pharmacokinetics of Salvinorin A, a potent hallucinogen. *Eur. J. Pharm. Biopharm.* **2009**, *72*, 471-477.

85. Schmidt, M. D.; Schmidt, M. S.; Butelman, E. R.; Harding, W. W.; Tidgewell, K.; Murry, D. J.; Kreek, M. J.; Prisinzano, T. E. Pharmacokinetics of the plant-derived kappa-opioid hallucinogen salvinorin A in nonhuman primates. *Synapse* **2005**, *58*, 208-210.
86. Johnson, M. W.; MacLean, K. A.; Caspers, M. J.; Prisinzano, T. E.; Griffiths, R. R. Time course of pharmacokinetic and hormonal effects of inhaled high-dose salvinorin A in humans. *J. Psychopharmacol.* **2016**, *30*, 323-329.
87. Schmidt, M. S.; Prisinzano, T. E.; Tidgewell, K.; Harding, W.; Butelman, E. R.; Kreek, M. J.; Murry, D. J. Determination of Salvinorin A in body fluids by high performance liquid chromatography-atmospheric pressure chemical ionization. *J. Chromatogr. B Analyt. Technol. Biomed. Life Sci.* **2005**, *818*, 221-225.
88. Tsujikawa, K.; Kuwayama, K.; Miyaguchi, H.; Kanamori, T.; Iwata, Y. T.; Inoue, H. In vitro stability and metabolism of salvinorin A in rat plasma. *Xenobiotica* **2009**, *39*, 391-398.
89. (a) Scheerer, J. R.; Lawrence, J. F.; Wang, G. C.; Evans, D. A. Asymmetric synthesis of salvinorin A, a potent kappa opioid receptor agonist. *J. Am. Chem. Soc.* **2007**, *129*, 8968-8969; (b) Bergman, Y. E.; Mulder, R.; Perlmutter, P. Total synthesis of 20-norsalvinorin A. 1. Preparation of a key intermediate. *J. Org. Chem.* **2009**, *74*, 2589-2591; (c) Line, N. J.; Burns, A. C.; Butler, S. C.; Casbohm, J.; Forsyth, C. J. Total synthesis of (-)-salvinorin A. *Chemistry (Weinheim an der Bergstrasse, Germany)* **2016**, *22*, 17983-17986; (d) Nozawa, M.; Suka, Y.; Hoshi, T.; Suzuki, T.; Hagiwara, H. Total synthesis of the hallucinogenic neoclerodane diterpenoid salvinorin A. *Org. Lett.* **2008**, *10*, 1365-1368.
90. Harding, W. W.; Tidgewell, K.; Byrd, N.; Cobb, H.; Dersch, C. M.; Butelman, E. R.; Rothman, R. B.; Prisinzano, T. E. Neoclerodane diterpenes as a novel scaffold for mu opioid receptor ligands. *J. Med. Chem.* **2005**, *48*, 4765-4771.

91. (a) Kane, B. E.; Nieto, M. J.; McCurdy, C. R.; Ferguson, D. M. A unique binding epitope for salvinorin A, a non-nitrogenous kappa opioid receptor agonist. *FEBS J.* **2006**, *273*, 1966-1974; (b) Vardy, E.; Mosier, P. D.; Frankowski, K. J.; Wu, H.; Katritch, V.; Westkaemper, R. B.; Aube, J.; Stevens, R. C.; Roth, B. L. Chemotype-selective modes of action of kappa-opioid receptor agonists. *J. Biol. Chem.* **2013**, *288*, 34470-34483; (c) Vortherms, T. A.; Mosier, P. D.; Westkaemper, R. B.; Roth, B. L. Differential helical orientations among related G protein-coupled receptors provide a novel mechanism for selectivity. Studies with salvinorin A and the kappa-opioid receptor. *J. Biol. Chem.* **2007**, *282*, 3146-3156; (d) Yan, F.; Mosier, P. D.; Westkaemper, R. B.; Stewart, J.; Zjawiony, J. K.; Vortherms, T. A.; Sheffler, D. J.; Roth, B. L. Identification of the molecular mechanisms by which the diterpenoid salvinorin A binds to kappa-opioid receptors. *Biochemistry* **2005**, *44*, 8643-8651; (e) Yan, F.; Bikbulatov, R. V.; Mocanu, V.; Dicheva, N.; Parker, C. E.; Wetsel, W. C.; Mosier, P. D.; Westkaemper, R. B.; Allen, J. A.; Zjawiony, J. K.; Roth, B. L. Structure-based design, synthesis, and biochemical and pharmacological characterization of novel salvinorin A analogues as active state probes of the kappa-opioid receptor. *Biochemistry* **2009**, *48*, 6898-6908.

92. (a) Wang, Y.; Tang, K.; Inan, S.; Siebert, D.; Holzgrabe, U.; Lee, D. Y.; Huang, P.; Li, J. G.; Cowan, A.; Liu-Chen, L. Y. Comparison of pharmacological activities of three distinct kappa ligands (Salvinorin A, TRK-820 and 3FLB) on kappa opioid receptors in vitro and their antipruritic and antinociceptive activities in vivo. *J. Pharmacol. Exp. Ther.* **2005**, *312*, 220-230; (b) Wang, Y.; Chen, Y.; Xu, W.; Lee, D. Y.; Ma, Z.; Rawls, S. M.; Cowan, A.; Liu-Chen, L. Y. 2-Methoxymethyl-salvinorin B is a potent kappa opioid receptor agonist with longer lasting action in vivo than salvinorin A. *J. Pharmacol. Exp. Ther.* **2008**, *324*, 1073-1083; (c) McCurdy, C. R.; Sufka, K. J.; Smith, G. H.; Warnick, J. E.; Nieto, M. J. Antinociceptive profile

of salvinorin A, a structurally unique kappa opioid receptor agonist. *Pharmacol. Biochem. Behav.* **2006**, *83*, 109-113.

93. Orton, E.; Liu, R. Salvinorin A: A mini review of physical and chemical properties affecting its translation from research to clinical applications in humans. *Transl. Perioper. Pain Med* **2014**, *1*, 9-11.

94. Fossum, E. N.; Lisowski, M. J.; Macey, T. A.; Ingram, S. L.; Morgan, M. M. Microinjection of the vehicle dimethyl sulfoxide (DMSO) into the periaqueductal gray modulates morphine antinociception. *Brain Res.* **2008**, *1204*, 53-58.

95. Turner, P. V.; Brabb, T.; Pekow, C.; Vasbinder, M. A. Administration of substances to laboratory animals: routes of administration and factors to consider. *J. Am. Assoc. Lab. Anim. Sci.* **2011**, *50*, 600-613.

2. Project Rationale and Specific Aims

Overall Rationale

In the search for effective methods to mitigate the increasing rates of abuse and addiction of illicit substances, a variety of neurological pathways have been explored. Towards this goal of reducing drug abuse and ultimately overdose-related deaths, two avenues of research have emerged: 1) a preventative approach, the development of pain relieving medications without the abuse and addiction liabilities associated with current therapies, and 2) a responsive approach, the development of medications for people suffering from drug abuse and addiction.¹

The opioid system in particular has been validated as a pathway through which both pain and reward are mediated.² Activation of the μ opioid receptor (MOR) results in the pain-relieving and rewarding effects of all currently-used opioid drugs, but a growing body of evidence suggests that these two effects can be dissociated, resulting in pain relief without abuse liability.³ The κ opioid receptor (KOR) is a target of interest in the development of therapeutics for a variety of diseases, including inflammation,⁴ drug addiction,⁵ pain,⁶ and depression.⁷

Current MOR agonists on the market suffer from similar, though not identical, side effect profiles.⁸ As the side effect profiles are not identical among all MOR agonists, the possibility for differentiating the beneficial pain-relieving effects from the MOR-induced side effects exists. In exploring this phenomenon, the concept of functional selectivity has emerged. Recent advances in the area of functional selectivity have indicated that multiple pathways can be activated upon agonist binding to the MOR, including G-protein activation, phosphorylation by multiple kinases, and recruitment of β -arrestins. Each of these pathways mediates a variety of downstream effects, and much work has been done to understand the physiological results of specific pathway

activation and the downstream effectors associated with each pathway.^{3c} Although tolerance, dependence, and addiction are highly complex biological responses, recent advances have been made in understanding some of the molecular pathways that contribute to their development. The fact that β -arrestin-2 contributes to MOR-mediated tolerance was demonstrated in β -arrestin-2-knock out mice treated with morphine. The antinociceptive effects were enhanced and prolonged, and morphine-induced tolerance was inhibited.^{3a, 3b} Additional studies have indicated that protein kinase C also contributes to morphine tolerance, as a protein kinase C inhibitor reversed tolerance development to morphine and other MOR agonists.⁹ Due to the high structural similarities of current MOR agonists, the development of functionally selective MOR agonists with reduced abuse liability may be realized through the exploration of different structural scaffolds.

Compounds that act at the KOR are of interest towards the development of both a preventative and a responsive approach for combating the current drug abuse and addiction epidemic. KOR activation has been shown to have both an antinociceptive effect⁶ and an antirewarding effect.¹⁰ The rewarding effects of drugs of abuse are attenuated by KOR agonists, which helps to prevent the binge and intoxication stage of the addiction cycle. This attenuation is the result of modulation of dopamine levels in the CNS.¹¹ In animal models of drug abuse, KOR agonists have shown success in reducing drug self-administration, attenuating withdrawal symptoms, and preventing relapse.¹¹⁻¹² However, many classical KOR agonists, such as U50,488 and U69,593, suffer from detrimental side effects, including sedation, aversion, dysphoria, emesis, and depression.¹¹

Salvinorin A and its analogues have been explored towards the development of a pain and drug abuse therapy targeting either the MORs or KORs, but their use has been limited by poor drug-like properties. While salvinorin A is an attractive lead in drug discovery campaigns because of its high selectivity for the KOR and its structural uniqueness in comparison to other opioids,¹³ its low

water solubility and rapid metabolism must be overcome for further development.¹⁴ Additionally, study of the antinociceptive effects of herkinorin at the MOR are complicated by its activity at the KOR.¹⁵ Thus, strategies to improve herkinorin's MOR selectivity towards the development of a pain therapy with reduced side effects as well as improvements to salvinorin A's pharmacokinetic and metabolic profiles are needed.

Aim 1: Development of Pain Therapies with Reduced Side Effects

Replacement of salvinorin A's C2-acetate moiety with a benzoate, as seen in herkinorin, shifts the activity from a KOR agonist to a MOR agonist (**Figure 2.1**).¹⁵ However the utility of herkinorin is limited by its low selectivity for the MOR, being only 4-fold selective for the MOR over KOR,¹⁶ as well as the fact that it is peripherally restricted,¹⁷ and thus cannot be used to probe centrally mediated processes. SAR campaigns to explore this interesting activity profile identified that replacing the ester linkage of herkinorin with an amide, named herkamide, eliminates KOR activity and increases the potency at the MOR.¹⁸ However, this compound was not further explored due to the complex and low-yielding synthesis required for the introduction of the amide.¹⁸

Salvinorin A analogues with activity at the MOR such as herkinorin and herkamide are interesting research probes, as they are structurally dissimilar from all other MOR agonists. The

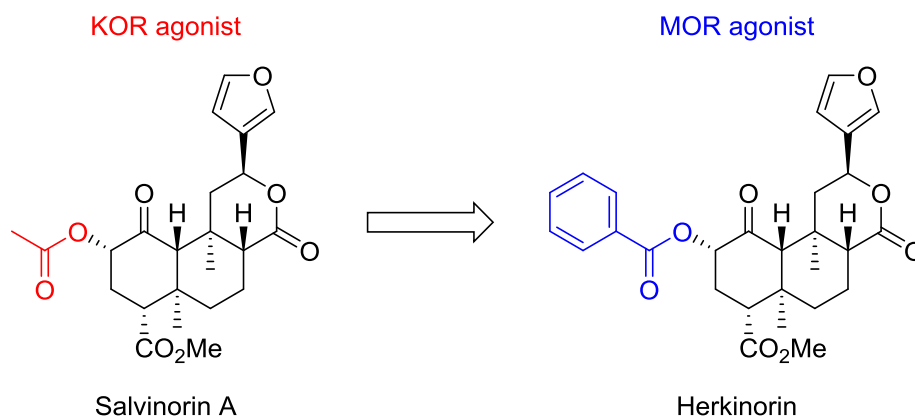


Figure 2.1: Structures of salvinorin A and herkinorin.

lack of basic nitrogen and the unique structural motif was hypothesized to be able to activate the MOR in a unique fashion that resulted in antinociception with the potential for fewer adverse effects. Therefore, the development of a potent salvinorin A-based MOR agonist that allows for further SAR exploration was a research goal.

Design and evaluation of kurkinorin *in vitro* and *in vivo*

As herkamide showed over 3,000-fold selectivity for the MOR over the KOR, the structures of herkinorin and herkamide were compared to determine what structural feature could be imparting the large selectivity differences between these structurally similar compounds. The X-ray crystal structures of these two compounds indicates that the amide and the ester adopt different orientations.¹⁶ The ester linkage holds the phenyl ring in a position that eclipses the decalin ring system while the amide linkage holds the phenyl ring planar to the decalin core. While these are not necessarily the bioactive conformations of these compounds, these X-ray structures did indicate a possible reason for the selectivity changes.

Because access to herkamide analogues is synthetically challenging, we sought to design a compound that held the phenyl ring in a similarly planar conformation to the decalin core as seen in herkamide. To accomplish this task, we envisioned the installation of a double bond between C2 and C3 would affect this planar conformation. Synthetic strategies were developed to oxidize salvinorin B to install this unsaturation, and after coupling with benzoic acid, the unsaturated analogue of herkinorin, named kurkinorin, is generated (**Figure 2.2**).¹⁶

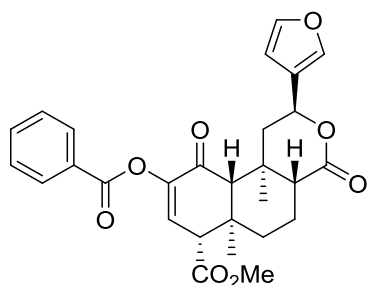


Figure 2.2: Chemical structure of kurkinorin

Initial evaluation of kurkinorin *in vitro* indicated that it was a potent and selective MOR agonist ($EC_{50} = 1.2 \text{ nM}$, $>8,000 \mu/\kappa$ selectivity). Kurkinorin was further evaluated *in vivo* for its effectiveness to elicit antinociception followed by a comparison of its side effect profile to morphine. To evaluate antinociception, male B6-SJL mice were injected with either drug or vehicle, and their tails were dropped into a hot water bath ($50 \text{ }^{\circ}\text{C}$), with a 10 s time cutoff to prevent tissue injury. The withdrawal latency was measured, and a higher withdrawal latency corresponds to a higher antinociceptive effect.¹⁹ The development of tolerance was also evaluated in this assay by generating a dose-response curve on day 1 of treatment, followed by consecutive, daily dosing, and then regenerating the dose-response curve at the end of the test. Compounds that generate tolerance result in a right-shifted dose-response curve following repeated treatments.^{3a} Sedation is an issue associated with MOR agonists and was thus of interest in this study. To evaluate sedation, animals were placed on a rotating rod and the time that they were able to stay on the rod was measured. Animals not experiencing sedation should be able to stay on the rod for the full time evaluated, 300 s, but sedated animals fall off the rod before the end point.²⁰ Lastly, the rewarding effects of MOR agonists is of concern, as they can contribute to the development of abuse and addiction. Conditioned place preference assays were used to determine rewarding effects, and in this paradigm, animals repeatedly received a dose of either vehicle or drug in one side of a two-sided chamber. On the test day, the amount of time the animal spent on the drug side versus the vehicle side was measured, and if the two are significantly different, the drug was said to be rewarding (or aversive, if the animal spent more time in the unpaired chamber).²¹

Study 1: Evaluation of kurkinorin analogues with substitutions to the phenyl ring

The effects of kurkinorin both *in vitro* and *in vivo* warranted further exploration. The developed synthetic methodology allowed for a robust SAR campaign, and analogues of herkinorin and

kurkinorin with substitutions to the 2-, 3-, and 4-positions of the phenyl ring were synthesized and evaluated for their ability to activate MORs. This was accomplished through a functional assay that measures forskolin-induced cAMP accumulation in CHO cells stably expressing MORs.²² This assay is a measurement of G-protein activation, as agonist binding to the receptor activates the G_i-protein and initiates the inhibition of adenylyl cyclase, which results in a reduction of cAMP accumulation. Forskolin is used in this assay to stimulate adenylyl cyclase and increase the signal-to-noise readout.

Study 2: SAR-guided design and synthesis of kurkinorin analogues

To further probe the MOR binding pocket, kurkinorin substituents were synthesized and evaluated based upon the results from the phenyl-substituted analogues. Although this initial SAR campaign did not yield any compounds with more favorable activity profiles at the MOR than the unsubstituted kurkinorin, we did identify trends that we were able to use to guide the next set of analogues in the search for MOR agonists with reduced side effect profiles. Notably, although no substituted phenyl compounds were more potent than the original, the substitutions at the 4- and 3-positions were generally more potent than the 2-position, and the most potent of the substituted analogues were methoxy and fluoro substituted derivatives. Using these results to guide our analogue design, we explored 1) heterocyclic derivatives in comparison to phenyl derivatives and 2) hydrogen bond possibilities off the aromatic ring. The salvinorin A core of kurkinorin and derivatives is not amenable to common deprotection methods, and thus the optimization of both protecting groups and deprotection methods was accomplished in order to synthesize several of the desired analogues.

Study 3: Evaluation of SAR-driven kurkinorin analogues

These SAR-driven analogues were evaluated *in vitro* for their ability to activate the MOR G-

protein associated pathway through inhibition of forskolin-induced cAMP accumulation. Compounds that displayed potent activation of MOR-associated G-proteins were further evaluated for their ability to recruit β -arrestin-2 through MOR activation. The DiscoverX (Fremont, CA) β -arrestin PathHunterTM technology was used for this analysis, which utilizes enzyme fragment complementation (EFC). Both the receptor and β -arrestin-2 are tagged with a fragment of β -galactosidase that is only activated upon complementation. The recruitment of β -arrestin-2 to the receptor results in the activated enzyme, and the addition of substrate that is converted into a luminescent product allows for a dose-dependent increase in luminescence. This luminescence is then used to determine the extent of β -arrestin-2 recruitment. DAMGO ([D-Ala², N-MePhe⁴, Gly-ol]-enkephalin, a potent and selective MOR peptidic probe) had previously been shown to highly recruit β -arrestin-2 through MOR activation,²³ and was thus used as the positive control to which all data were normalized.

Much work has been done to develop models for quantifying the degree of functional selectivity, or bias, that accounts for the differences between the assays and pathways,²⁴ and we employed a bias calculation equation²⁵ (**Equation 2.1**) that normalizes data to the activity of DAMGO in both assays, similar to previous work.^{24c, 24e} This equation allows for the normalization of the effective concentration eliciting 50% of maximum response (EC₅₀) and the maximum efficacy (E_{max}) of each compound to the unbiased ligand DAMGO in both the G-protein-mediated cAMP pathway as well as the β -arrestin-2 recruitment pathway. Being unbiased, DAMGO has a bias factor of 1, and bias factor values less than 1 indicate bias towards the G-protein activation pathway and those greater than 1 indicate bias towards β -arrestin-2 recruitment.

$$\log(\mathbf{Bias\ Factor}) = \left(\log \left(\frac{Emax_{test} \times EC50_{DAMGO}}{EC50_{test} \times Emax_{DAMGO}} \right) \right)_{\beta\text{-arrestin}} - \left(\log \left(\frac{Emax_{test} \times EC50_{DAMGO}}{EC50_{test} \times Emax_{DAMGO}} \right) \right)_{cAMP}$$

Equation 2.1. Bias factor equation.

Aim 2: Development of New Synthetic Approaches toward Refinement of Salvinorin A's Pharmaceutical Properties

While classical KOR agonists suffer from common side effects, salvinorin A has been shown to differ in its binding at the KOR as well as in its cellular and behavioral effects.¹¹ These results further highlight salvinorin A's potential as a structural lead towards the development of therapies for pain and drug abuse with a reduced side effect profile compared to classic opioids. The potency and selectivity of salvinorin A at the KOR does not need improvement, as is often the case in drug discovery efforts, because it activates the KOR with an EC_{50} value in the picomolar range. However, efforts to develop salvinorin A analogues with more favorable pharmacokinetic properties had not been attempted. Early into the SAR studies of salvinorin A, it was recognized that the carbonyl of the lactone moiety was not essential for KOR activity.²⁶ Additionally, the original report of the KOR crystal structure bound to JDTC modeled salvinorin A into the binding pocket and found that salvinorin A likely binds with the lactone facing the pocket opening, without any meaningful receptor interactions (**Figure 2.3**).²⁷ We hypothesized that substituting at the C17

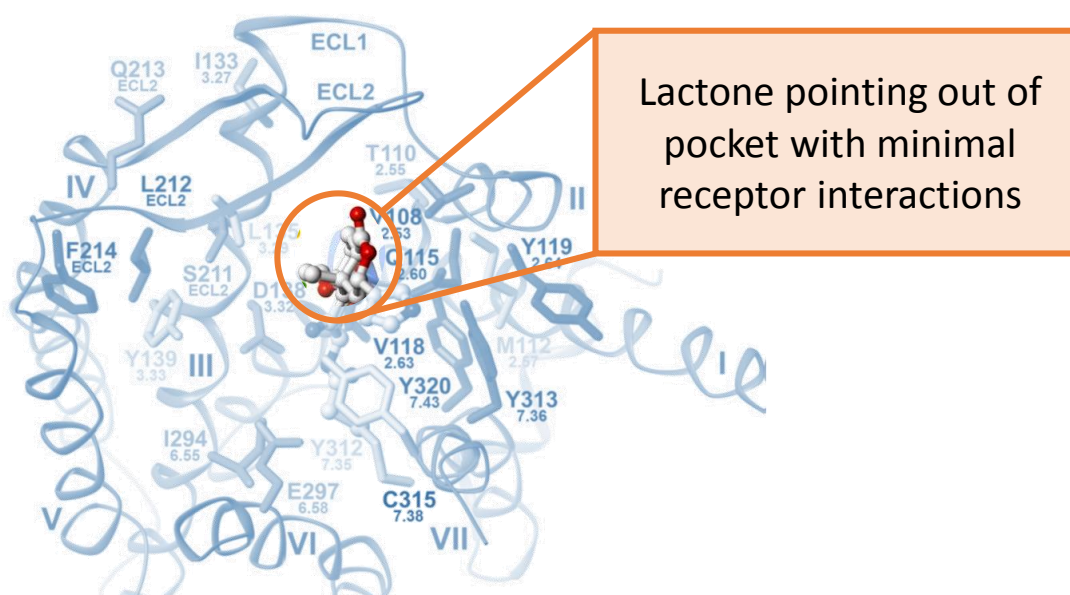


Figure 2.3: Docked structure of RB-64 (salvinorin A analogue) at the KOR. Figure adapted from Wu, H., *et. al.* Structure of the human kappa-opioid receptor in complex with JDTC. *Nature* **2012**, 485, 327-332. Used with permission.

position would be tolerated at the KOR and that this position could allow for the inclusion of water-solubilizing moieties without sacrificing KOR activity.

Study 1: Development of chemical methodology to selectively functionalize the C17 position

The initial report detailing the modification of the lactone moiety describes the synthesis of three derivatives: Salvinorin A lactol, 17-Deoxysalvinorin A, and 8,17-Didehydro-17-deoxysalvinorin A (**Figure 2.4**).²⁶ The lactol was formed through reduction of salvinorin A with diisobutylaluminum hydride; however, the reproduction of this reaction in a selective manner was not accomplished and required further optimization. The deoxygenation of the C17 position to form the two other analogues was straightforward following the published method. As no other substitutions at this position had been done, reaction conditions allowing C17 substitution also required exploration and optimization.

Reduction and substitution of the C17 carbonyl results in an additional stereogenic center on the salvinorin A core. For most compounds with C17-substitutions, these epimeric compounds were separated via simple flash column chromatography; however, some derivatives did require preparative HPLC purification to separate the epimers. Determination of the stereochemistry at the C17 position required 2D-NMR techniques, and most compounds were unambiguously identified via NOESY correlations.

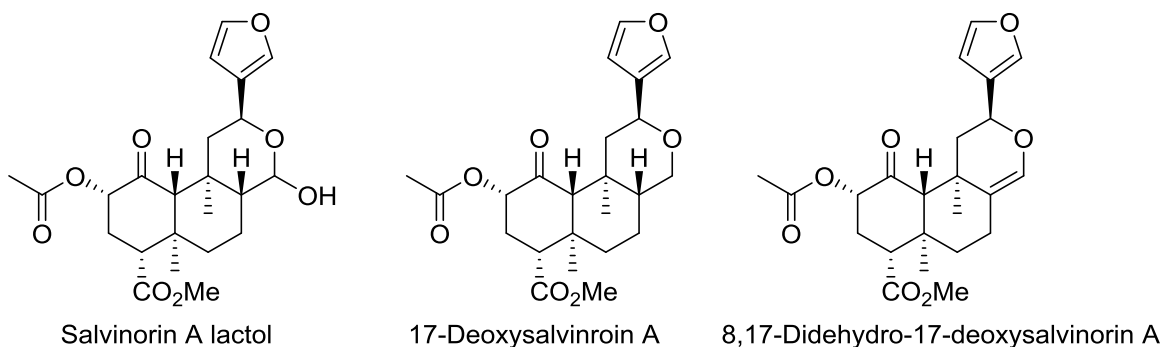


Figure 2.4: Structures of C17-modified salvinorin A analogues.

Study 2: Evaluation of compounds with C17 modifications

The analogues were evaluated for their ability to inhibit forskolin-induced cAMP accumulation through KOR activation. Evaluation of a variety of analogues, including when possible both α - and β -substituted derivatives, allowed for the generation of SAR at the C17 position. The activity values of the compounds were useful in designing further analogues.

Study 3: Design, synthesis, and evaluation of analogues with C2 and C17 modifications

Although SAR studies on the different pieces of salvinorin A have been done, no study has demonstrated that known SAR of different points can be combined to better optimize the molecule. In order to determine if changes in the structure result in corresponding activity changes, the C17 modifications were incorporated into C2-modified compounds that had previously been generated in the lab and had shown activity at KORs and MORs. These compounds would also provide insight into the binding poses at the receptor. When structural changes are made to salvinorin A, it is generally thought that the molecule maintains the same binding pose; however, as we do not have crystal structures, this assumption cannot be confirmed. By making these dual-modified compounds, the activity shifts between salvinorin A and the mono-modified compounds can be compared to those of the dual-modified compounds. If the structural modifications still allow the compounds to bind in similar poses, then the activity trends should be similar between the mono- and dual-modified compounds. Additionally, by modifying the C17 position of the MOR agonist herkinorin, the necessity of the lactone for MOR activation can be evaluated to determine if the similarities between the KOR and MOR pockets allows for the similar structural modifications.

Aim 3: Understanding the Metabolism of Neoclerodane Diterpenes

The metabolism of salvinorin A has been attributed to activity of CYP450 enzymes, UGTs, and carboxylesterases, with the most rapid effects attributed to the C2-acetate cleavage by

carboxylesterases.^{14b, 28} Due to the short $t_{1/2}$ of salvinorin A because of this rapid acetate cleavage, many salvinorin A analogues have been synthesized with modifications to the acetate in order to prevent metabolism while maintaining biological activity.²⁹ Many of these compounds have been presumed to be more metabolically stable because of these C2-modifications, but the interpretation of their *in vivo* activities is speculative without also evaluating their metabolic stability.³⁰

Study 1: Development of a robust system for determining the metabolic stability of neoclerodane diterpenes

Several previous studies have determined the metabolic stability of salvinorin A both *in vitro* and *in vivo*,³¹ but very few have evaluated the metabolism of salvinorin A analogues in comparison to salvinorin A itself.^{29a, 32} Of the studies that did include this comparison, one required the use of isotopically-labeled salvinorin A and derivatives,³² and the other was not reproducible in our lab due to the omission of key methodological details.^{29a} Therefore, we sought to develop a robust method that allowed for the evaluation of *in vitro* metabolic stability of a wide variety of neoclerodane diterpene analogues without requiring the use of radiolabeled compounds.

A method was developed using rat liver microsomes and varying the time, concentrations of compounds and proteins, buffer conditions, and quenching methods to optimize conditions for quantitative LCMS analysis. Incubation of compounds with rat liver microsomes in either the presence or absence of nicotinamide adenine dinucleotide phosphate (NADPH) followed by LCMS analysis at varying time points allowed for the evaluation of their metabolic profiles. CYP450 enzymes require NADPH for activity, and thus the metabolism seen in the presence of NADPH can be attributed to CYPs. However, in the absence of NADPH, CYP450 enzymes are inactive, and thus the metabolism observed without NADPH can be attributed to other metabolizing enzymes.

Study 2: Evaluation of the metabolic stability of salvinorin A and selected analogues

With a robust method for evaluating salvinorin A and derivatives in hand, the CYP450 enzyme-mediated and non-CYP450 enzyme-mediated metabolic stabilities were determined, allowing for direct comparison of how specific chemical modifications modulate the metabolic liabilities of salvinorin A. In the case of salvinorin A, previous reports have demonstrated that salvinorin A is a substrate for carboxylesterases.^{14b, 28} In our assay, we compared the metabolic profile of salvinorin A with its derivatives under the same conditions to determine how the change in chemical structure affects the metabolic stability of the compound. Thus using conditions without NADPH (inactive CYP450 enzymes), we monitor if esterase activity has been modulated through the chemical modifications.

These data are useful in interpreting *in vivo* results, specifically regarding a compound's duration of action and whether its ability to activate the receptor or its metabolic stability are resulting in specific changes in comparison to other compounds. Several salvinorin A analogues have been developed over the last decade that were thought to have increased stability profiles,^{15, 29c, 33} and the development of this method allows us the opportunity to directly compare the metabolic stability of salvinorin A and these analogues. This method also allows for the direct comparison of the C2-C17 modified analogues described in **Aim 2**. These analogues have modifications to the acetate and lactone moieties which have both been confirmed to be sites of metabolism in salvinorin A,^{14b} and so metabolic comparison allowed for further analysis of the role of each moiety in the metabolic stability of the compounds. The use of this method in conjunction with the ongoing synthetic and pharmacologic initiatives in the lab also led to the identification of a spirobutyrolactone moiety as a more metabolically stable bioisosteric replacement of an acetate.³⁴

References

1. Substance Abuse and Mental Health Services Administration (US); Office of the Surgeon General (US). Facing Addiction in America: The Surgeon General's Report on Alcohol, Drugs, and Health. US Department of Health and Human Services: Washington (DC), 2016.
2. (a) Lutz, P. E.; Kieffer, B. L. The multiple facets of opioid receptor function: implications for addiction. *Curr. Opin. Neurobiol.* **2013**; (b) Wolkerstorfer, A.; Handler, N.; Buschmann, H. New approaches to treating pain. *Bioorg. Med. Chem. Lett.* **2016**, *26*, 1103-1119.
3. (a) Bohn, L. M.; Gainetdinov, R. R.; Lin, F. T.; Lefkowitz, R. J.; Caron, M. G. Mu-opioid receptor desensitization by beta-arrestin-2 determines morphine tolerance but not dependence. *Nature* **2000**, *408*, 720-723; (b) Bohn, L. M.; Lefkowitz, R. J.; Gainetdinov, R. R.; Peppel, K.; Caron, M. G.; Lin, F. T. Enhanced morphine analgesia in mice lacking beta-arrestin 2. *Science* **1999**, *286*, 2495-2498; (c) Raehal, K. M.; Schmid, C. L.; Groer, C. E.; Bohn, L. M. Functional selectivity at the mu-opioid receptor: implications for understanding opioid analgesia and tolerance. *Pharmacol. Rev.* **2011**, *63*, 1001-1019; (d) Raehal, K. M.; Walker, J. K.; Bohn, L. M. Morphine side effects in beta-arrestin 2 knockout mice. *J. Pharmacol. Exp. Ther.* **2005**, *314*, 1195-1201; (e) Williams, J. T.; Ingram, S. L.; Henderson, G.; Chavkin, C.; von Zastrow, M.; Schulz, S.; Koch, T.; Evans, C. J.; Christie, M. J. Regulation of mu-opioid receptors: desensitization, phosphorylation, internalization, and tolerance. *Pharmacol. Rev.* **2013**, *65*, 223-254.
4. (a) Paton, K. F.; Kumar, N.; Crowley, R. S.; Harper, J. L.; Prisinzano, T. E.; Kivell, B. M. The analgesic and anti-inflammatory effects of Salvinorin A analogue beta-tetrahydropyran salvinorin B in mice. *Eur. J. Pain* **2017**, *21*, 1039-1050; (b) Rossi, A.; Pace, S.; Tedesco, F.; Pagano, E.; Guerra, G.; Troisi, F.; Werner, M.; Roviezzo, F.; Zjawiony, J. K.; Werz, O.; Izzo, A.

- A.; Capasso, R. The hallucinogenic diterpene salvinorin A inhibits leukotriene synthesis in experimental models of inflammation. *Pharmacol. Res.* **2016**, *106*, 64-71.
5. (a) Prisinzano, T. E. Natural products as tools for neuroscience: discovery and development of novel agents to treat drug abuse. *J. Nat. Prod.* **2009**, *72*, 581-587; (b) Graziane, N. M.; Polter, A. M.; Briand, L. A.; Pierce, R. C.; Kauer, J. A. Kappa opioid receptors regulate stress-induced cocaine seeking and synaptic plasticity. *Neuron* **2013**, *77*, 942-954.
6. Vanderah, T. W. Delta and kappa opioid receptors as suitable drug targets for pain. *Clin. J. Pain* **2010**, *26* S10-15.
7. Lalanne, L.; Ayranci, G.; Kieffer, B. L.; Lutz, P. E. The kappa opioid receptor: from addiction to depression, and back. *Front. Psychiatry* **2014**, *5*, 170.
8. Williams, D. A.; Roche, V. F.; Roche, E. B. *Foye's Principles of Medicinal Chemistry*. 7th ed.; Wolters Kluwer Health/Lippincott Williams & Wilkins: Philadelphia, 2013; p 658-699.
9. Hull, L. C.; Llorente, J.; Gabra, B. H.; Smith, F. L.; Kelly, E.; Bailey, C.; Henderson, G.; Dewey, W. L. The effect of protein kinase C and G protein-coupled receptor kinase inhibition on tolerance induced by mu-opioid agonists of different efficacy. *J. Pharmacol. Exp. Ther.* **2010**, *332*, 1127-1135.
10. Koob, G. F.; Le Moal, M. Addiction and the brain antireward system. *Annu. Rev. Psychol.* **2008**, *59*, 29-53.
11. Kivell, B. M.; Ewald, A. W.; Prisinzano, T. E. Salvinorin A analogs and other kappa-opioid receptor compounds as treatments for cocaine abuse. *Adv. Pharmacol.* **2014**, *69*, 481-511.
12. Crowley, N. A.; Kash, T. L. Kappa opioid receptor signaling in the brain: Circuitry and implications for treatment. *Prog. Neuropsychopharmacol. Biol. Psychiatry* **2015**, *62*, 51-60.

13. Prisinzano, T. E. Neoclerodanes as atypical opioid receptor ligands. *J. Med. Chem.* **2013**, *56*, 3435-3443.
14. (a) Orton, E.; Liu, R. Salvinorin A: A mini review of physical and chemical properties affecting its translation from research to clinical applications in humans. *Transl. Perioper. Pain Med* **2014**, *1*, 9-11; (b) Tsujikawa, K.; Kuwayama, K.; Miyaguchi, H.; Kanamori, T.; Iwata, Y. T.; Inoue, H. In vitro stability and metabolism of salvinorin A in rat plasma. *Xenobiotica* **2009**, *39*, 391-398; (c) Hooker, J. M.; Xu, Y.; Schiffer, W.; Shea, C.; Carter, P.; Fowler, J. S. Pharmacokinetics of the potent hallucinogen, salvinorin A in primates parallels the rapid onset and short duration of effects in humans. *NeuroImage* **2008**, *41*, 1044-1050.
15. Harding, W. W.; Tidgewell, K.; Byrd, N.; Cobb, H.; Dersch, C. M.; Butelman, E. R.; Rothman, R. B.; Prisinzano, T. E. Neoclerodane diterpenes as a novel scaffold for mu opioid receptor ligands. *J. Med. Chem.* **2005**, *48*, 4765-4771.
16. Crowley, R. S.; Riley, A. P.; Sherwood, A. M.; Groer, C. E.; Shivaperumal, N.; Biscaia, M.; Paton, K.; Schneider, S.; Provasi, D.; Kivell, B. M.; Filizola, M.; Prisinzano, T. E. Synthetic studies of neoclerodane diterpenes from *Salvia divinorum*: identification of a potent and centrally acting μ opioid analgesic with reduced abuse liability. *J. Med. Chem.* **2016**, *59*, 11027-11038.
17. Lamb, K.; Tidgewell, K.; Simpson, D. S.; Bohn, L. M.; Prisinzano, T. E. Antinociceptive effects of herkinorin, a MOP receptor agonist derived from salvinorin A in the formalin test in rats: new concepts in mu opioid receptor pharmacology: from a symposium on new concepts in mu-opioid pharmacology. *Drug Alcohol Depend.* **2012**, *121*, 181-188.
18. Tidgewell, K.; Groer, C. E.; Harding, W. W.; Lozama, A.; Schmidt, M.; Marquam, A.; Hiemstra, J.; Partilla, J. S.; Dersch, C. M.; Rothman, R. B.; Bohn, L. M.; Prisinzano, T. E.

- Herkinorin analogues with differential beta-arrestin-2 interactions. *J. Med. Chem.* **2008**, *51*, 2421-2431.
19. Le Bars, D.; Gozariu, M.; Cadden, S. W. Animal models of nociception. *Pharmacol. Rev.* **2001**, *53*, 597-652.
20. Deacon, R. M. Measuring motor coordination in mice. *J. Visualized Exp.* **2013**, e2609.
21. Feltenstein, M. W.; See, R. E. The neurocircuitry of addiction: an overview. *Br. J. Pharmacol.* **2008**, *154*, 261-274.
22. Riley, A. P.; Groer, C. E.; Young, D.; Ewald, A. W.; Kivell, B. M.; Prisinzano, T. E. Synthesis and kappa-opioid receptor activity of furan-substituted salvinorin A analogues. *J. Med. Chem.* **2014**, *57*, 10464-10475.
23. Groer, C. E.; Schmid, C. L.; Jaeger, A. M.; Bohn, L. M. Agonist-directed interactions with specific beta-arrestins determine mu-opioid receptor trafficking, ubiquitination, and dephosphorylation. *J. Biol. Chem.* **2011**, *286*, 31731-31741.
24. (a) Free, R. B.; Chun, L. S.; Moritz, A. E.; Miller, B. N.; Doyle, T. B.; Conroy, J. L.; Padron, A.; Meade, J. A.; Xiao, J.; Hu, X.; Dulcey, A. E.; Han, Y.; Duan, L.; Titus, S.; Bryant-Genevier, M.; Barnaeva, E.; Ferrer, M.; Javitch, J. A.; Beuming, T.; Shi, L.; Southall, N. T.; Marugan, J. J.; Sibley, D. R. Discovery and characterization of a G protein-biased agonist that inhibits beta-arrestin recruitment to the D2 dopamine receptor. *Mol. Pharmacol.* **2014**, *86*, 96-105; (b) Kenakin, T.; Christopoulos, A. Signalling bias in new drug discovery: detection, quantification and therapeutic impact. *Nat. Rev. Drug Discovery* **2013**, *12*, 205-216; (c) Kenakin, T.; Watson, C.; Muniz-Medina, V.; Christopoulos, A.; Novick, S. A simple method for quantifying functional selectivity and agonist bias. *ACS Chem. Neurosci.* **2012**, *3*, 193-203; (d) Luttrell, L. M.; Maudsley, S.; Bohn, L. M. Fulfilling the promise of "biased" G protein-coupled

receptor agonism. *Mol. Pharmacol.* **2015**, *88*, 579-588; (e) Zhou, L.; Lovell, K. M.; Frankowski, K. J.; Slauson, S. R.; Phillips, A. M.; Streicher, J. M.; Stahl, E.; Schmid, C. L.; Hodder, P.; Madoux, F.; Cameron, M. D.; Prisinzano, T. E.; Aube, J.; Bohn, L. M. Development of functionally selective, small molecule agonists at kappa opioid receptors. *J. Biol. Chem.* **2013**, *288*, 36703-36716.

25. Rajagopal, S.; Ahn, S.; Rominger, D. H.; Gowen-MacDonald, W.; Lam, C. M.; DeWire, S. M.; Violin, J. D.; Lefkowitz, R. J. Quantifying Ligand Bias at Seven-Transmembrane Receptors. *Mol. Pharmacol.* **2011**, *80*, 367-377.

26. Munro, T. A.; Rizzacasa, M. A.; Roth, B. L.; Toth, B. A.; Yan, F. Studies toward the pharmacophore of salvinorin A, a potent kappa opioid receptor agonist. *J. Med. Chem.* **2005**, *48*, 345-348.

27. Wu, H.; Wacker, D.; Mileni, M.; Katritch, V.; Han, G. W.; Vardy, E.; Liu, W.; Thompson, A. A.; Huang, X. P.; Carroll, F. I.; Mascarella, S. W.; Westkaemper, R. B.; Mosier, P. D.; Roth, B. L.; Cherezov, V.; Stevens, R. C. Structure of the human kappa-opioid receptor in complex with JDTic. *Nature* **2012**, *485*, 327-332.

28. Teksin, Z. S.; Lee, I. J.; Nemieboka, N. N.; Othman, A. A.; Upreti, V. V.; Hassan, H. E.; Syed, S. S.; Prisinzano, T. E.; Eddington, N. D. Evaluation of the transport, in vitro metabolism and pharmacokinetics of Salvinorin A, a potent hallucinogen. *Eur. J. Pharm. Biopharm.* **2009**, *72*, 471-477.

29. (a) Beguin, C.; Potter, D. N.; Dinieri, J. A.; Munro, T. A.; Richards, M. R.; Paine, T. A.; Berry, L.; Zhao, Z.; Roth, B. L.; Xu, W.; Liu-Chen, L. Y.; Carlezon, W. A., Jr.; Cohen, B. M. N-methylacetamide analog of salvinorin A: a highly potent and selective kappa-opioid receptor agonist with oral efficacy. *J. Pharmacol. Exp. Ther.* **2008**, *324*, 188-195; (b) Beguin, C.;

Richards, M. R.; Wang, Y. L.; Chen, Y.; Liu-Chen, L. Y.; Ma, Z. Z.; Lee, D. Y. W.; Carlezon, W. A.; Cohen, B. M. Synthesis and in vitro pharmacological evaluation of salvinorin A analogues modified at C(2). *Bioorg. Med. Chem. Lett.* **2005**, *15*, 2761-2765; (c) Prevatt-Smith, K. M.; Lovell, K. M.; Simpson, D. S.; Day, V. W.; Douglas, J. T.; Bosch, P.; Dersch, C. M.; Rothman, R. B.; Kivell, B.; Prisinzano, T. E. Potential drug abuse therapeutics derived from the hallucinogenic natural product salvinorin a. *MedChemComm* **2011**, *2*, 1217-1222.

30. Cunningham, C. W.; Rothman, R. B.; Prisinzano, T. E. Neuropharmacology of the naturally occurring kappa-opioid hallucinogen salvinorin A. *Pharmacol. Rev.* **2011**, *63*, 316-347.

31. (a) Schmidt, M. S.; Prisinzano, T. E.; Tidgewell, K.; Harding, W.; Butelman, E. R.; Kreek, M. J.; Murry, D. J. Determination of Salvinorin A in body fluids by high performance liquid chromatography-atmospheric pressure chemical ionization. *J. Chromatogr. B Analyt. Technol. Biomed. Life Sci.* **2005**, *818*, 221-225; (b) Caspers, M. J.; Williams, T. D.; Lovell, K. M.; Lozama, A.; Butelman, E. R.; Kreek, M. J.; Johnson, M.; Griffiths, R.; MacLean, K.; Prisinzano, T. E. LC-MS/MS quantification of salvinorin A from biological fluids. *Anal Methods-Uk* **2013**, *5*, 7042-7048; (c) Johnson, M. W.; MacLean, K. A.; Caspers, M. J.; Prisinzano, T. E.; Griffiths, R. R. Time course of pharmacokinetic and hormonal effects of inhaled high-dose salvinorin A in humans. *J. Psychopharmacol.* **2016**, *30*, 323-329.

32. Hooker, J. M.; Munro, T. A.; Beguin, C.; Alexoff, D.; Shea, C.; Xu, Y. W.; Cohen, B. M. Salvinorin A and derivatives: Protection from metabolism does not prolong short-term, whole-brain residence. *Neuropharmacology* **2009**, *57*, 386-391.

33. Munro, T. A.; Duncan, K. K.; Xu, W.; Wang, Y.; Liu-Chen, L. Y.; Carlezon, W. A., Jr.; Cohen, B. M.; Beguin, C. Standard protecting groups create potent and selective kappa opioids: salvinorin B alkoxymethyl ethers. *Bioorg. Med. Chem.* **2008**, *16*, 1279-1286.

34. Sherwood, A. M.; Crowley, R. S.; Paton, K. F.; Biggerstaff, A.; Neuenswander, B.; Day, V. W.; Kivell, B. M.; Prisinzano, T. E. Addressing structural flexibility at the A-ring on salvinorin A: Discovery of a potent kappa-opioid agonist with enhanced metabolic stability. *J. Med. Chem.* **2017**, *60*, 3866-3878.

3. Development of Pain Therapies with Reduced Side Effects

Background: Design and evaluation of kurkinorin *in vitro* and *in vivo*

The design of kurkinorin was based upon the comparison of the X-ray crystal structures of herkinorin and herkamide (**Figure 3.1**).¹ Specifically, the conformations of the phenyl rings of the two compounds differ significantly. In herkinorin, the phenyl ring is eclipsed relative to the decalin core; whereas the phenyl ring of herkamide sits planar to the decalin core. Although these X-ray crystal structures represent only two possible conformations of the molecules, and not necessarily the conformations bound to the receptor, they suggested that modifying the configuration of the C2 position of herkinorin might result in improved selectivity and potency for MORs.

Therefore, we hypothesized that locking the conformation of the C2 substituent would impart selectivity between the MOR and KORs. The selectivity of herkamide could be attributed to one of two different interactions occurring due to its apparent conformational restriction: 1) the

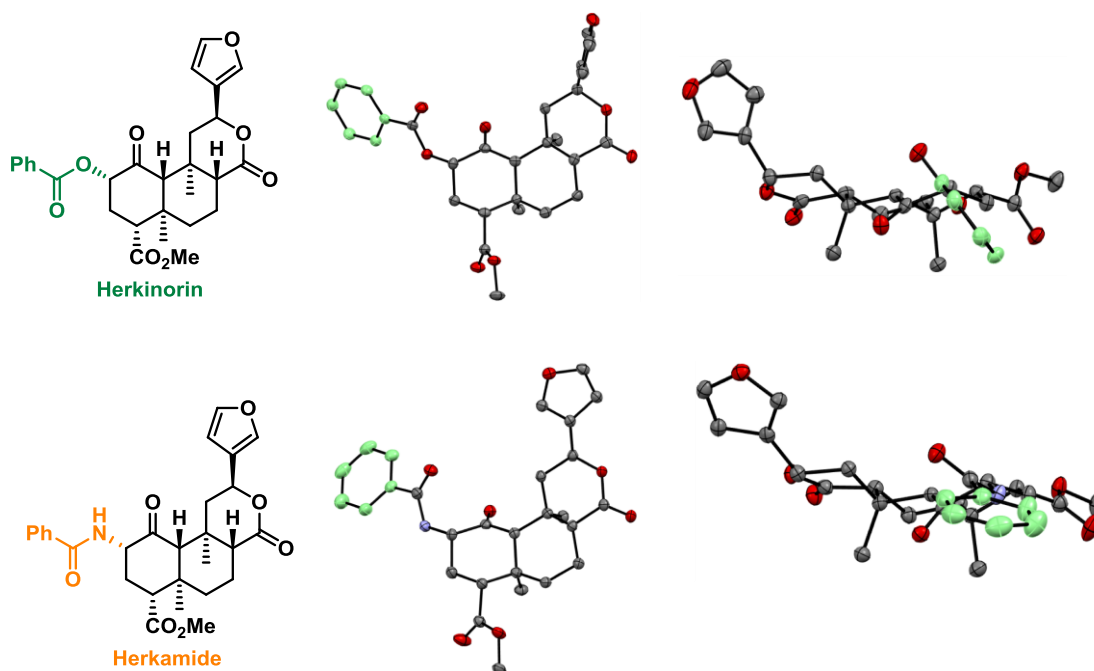
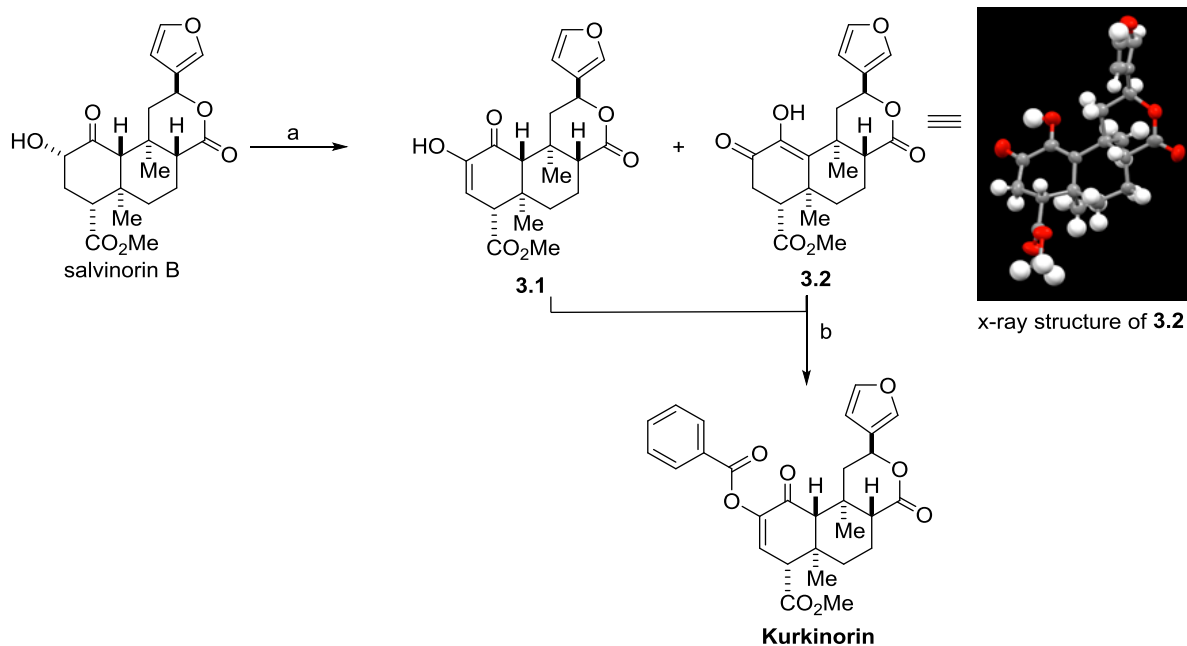


Figure 3.1: X-ray crystal structures of herkinorin and herkamide.

coplanarity of the phenyl and decalin ring systems or 2) an upward movement of the C2 substituent from the α - to the β -face of the decalin core. The inversion about C2 on salvinorin A had previously been reported to result in activity loss at KORs.² Thus, inversion of the C2 stereocenter was expected to reduce KOR activity and therefore increase MOR selectivity, and locking the C2 substituent planar to the decalin core, as seen in the crystal structure of herkamide, was anticipated to result in increased MOR activity. Accordingly, we hypothesized that a compound with this planar conformation could be generated by installing a double bond in the A-ring, as seen in kurkinorin, and in order to determine if further movement towards the β -face was tolerated, or even preferred, we inverted the C2 stereochemistry to form 2-epi-herkinorin.

In order to evaluate our hypothesis that the planarity of the ring would impart MOR selectivity, synthetic methods were required to install that unsaturation. After evaluation of a variety of methods to accomplish this transformation, it was determined that oxidation of salvinorin B with $\text{Cu}(\text{OAc})_2$ was able to produce this transformation in acceptable yields (**Scheme 3.1**).³ Of note,



Reagents and conditions: a) $\text{Cu}(\text{OAc})_2$, $\text{MeOH}/\text{CH}_2\text{Cl}_2$ (1:1), 67% yield; b) PhCOOH , DMAP, EDCI, CH_2Cl_2 , 52% yield.

Scheme 3.1: Synthetic route to kurkinorin.

the product of this isolation process is a mixture of two isomeric enols **3.1** and **3.2** that rapidly equilibrate between one another through the presumed α -diketone. Following chromatography, immediate characterization of **3.1** by NMR spectroscopy revealed a 3:1 mixture of **3.1** and **3.2**. However upon standing, solutions containing **3.1** slowly equilibrated to thermodynamically stable enol **3.2**.

Acylation of either the mixture of **3.1** and **3.2** or pure **3.2** with benzoic acid provided a single regioisomer (**Scheme 3.1**), presumably due to less steric hindrance upon addition at the preferred position over the regioisomer. The structure was confirmed to be the desired kurkinorin by 2D NMR studies. Briefly, the C3 proton correlated via COSY to the C4 proton and via HMBC to C1, C2, C4, and C5. The proton of C10 lacked any observable COSY correlations. Additionally, HSQC confirmed that carbons C3 and C10 each bear a single proton, further validating the regiochemistry of kurkinorin (**Figure 3.2**).¹

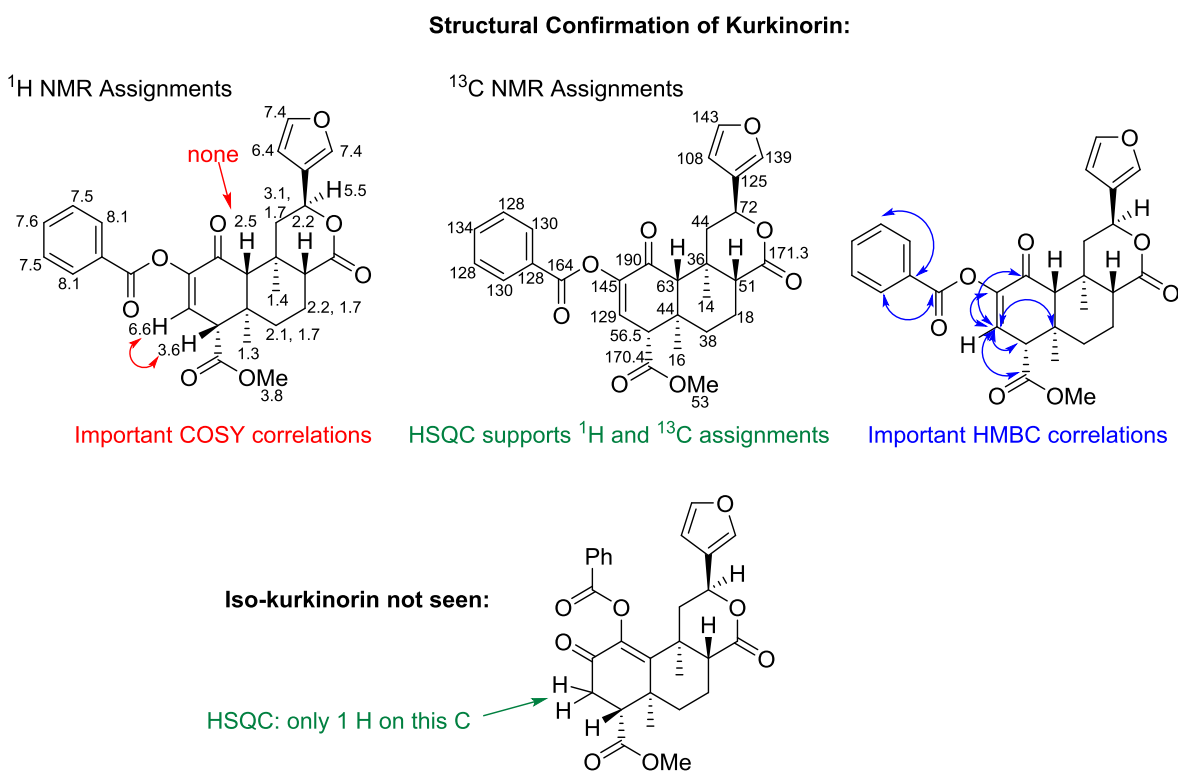


Figure 3.2: Unambiguous determination of the kurkinorin structure.

To determine how the configuration of the C2 position in herkinorin affects potency and selectivity at MORs, the 2-epi-herkinorin^{2b} and the unsaturated analogue kurkinorin were evaluated for activity at MORs, KORs, and DORs. In the forskolin-induced cAMP accumulation functional assay, the epimerization of herkinorin at the C2 position resulted in a complete loss of activity at both MOR and KORs, while kurkinorin, differing only in a degree of unsaturation from herkinorin, was determined to be a potent MOR agonist with an EC₅₀ value of 1.2 ± 0.2 nM (**Table 3.1**). Additionally, kurkinorin was extremely selective for MORs, possessing no activity at KORs at 10 μM. This impressive >8,000-fold selectivity for MORs was greater than that of both herkinorin (4.25-fold selective over KOR) and morphine (66-fold selective over KOR). Furthermore, kurkinorin is of similar potency to DAMGO, a peptidic MOR ligand commonly employed for its high potency and selectivity for MORs, as well as fentanyl, one of the most potent MOR agonists used clinically.⁴ In the same functional assay evaluating activity at DORs, kurkinorin was active with an EC₅₀ values of 74 ± 10 nM, which was unanticipated as few salvinorin-like compounds have DOR activity. Even so, kurkinorin's MOR selectivity is still greater than 60-fold. However, this result opens the possibility of identifying DOR-selective neoclerodanes in the future.

Table 3.1: MOR, KOR, and DOR Pharmacology: Inhibition of forskolin-induced cAMP accumulation.

Compound	EC ₅₀ ± SEM ^{a, b} (nM)			Selectivity	
	μ	κ	δ	κ/μ	δ/μ
DAMGO	0.6 ± 0.1	>10 000 ^c	ND ^f	>16 000	--
Morphine	3.7 ± 0.3	140 ± 10	780 ± 150 ^e	66	150
Fentanyl	0.3 ± 0.1	ND ^f	ND ^f		--
Herkinorin	39 ± 4	170 ± 20 ^d	>10 000 ^c	4.25	250
Herkamide	3.0 ± 0.4	>10 000 ^c	690 ± 50	>3 000	210
2-epi-Herkinorin	>10 000 ^c	>10 000 ^c	ND ^f	--	--
Kurkinorin	1.2 ± 0.2	>10 000 ^c	74 ± 10	>8 000	63
Salvinorin A	>10 000 ^c	0.030 ± 0.004	>10 000 ^c	< 4.0E-6	--

^aMean ± standard error of the mean; n ≥ 2 individual experiments run in triplicate. ^bE_{max} = 100% unless otherwise noted. ^cE_{max} = 0 % up to 10 μM. ^dE_{max} = 64 ± 18 %. ^eE_{max} = 90 ± 2%. ^fND = Not Determined.

With the overall goal of developing an analgesic with reduced abuse liability in mind, the *in vivo* effects of kurkinorin were explored (**Figure 3.3**). Using the hot water tail flick test in mice, which is a model of centrally mediated antinociceptive effects, herkinorin was inactive up to 10 mg/kg as it does not penetrate the CNS.⁵ Interestingly, kurkinorin did elicit significant antinociception in this same model at 5 and 10 mg/kg, and at the 10 mg/kg dose, the antinociceptive effects of kurkinorin were similar to those elicited by morphine at 30 min post-treatment. Naloxone (10 mg/kg s.c. 45 min) blocked the antinociceptive effects of kurkinorin, confirming an opioid-receptor mediated process.¹

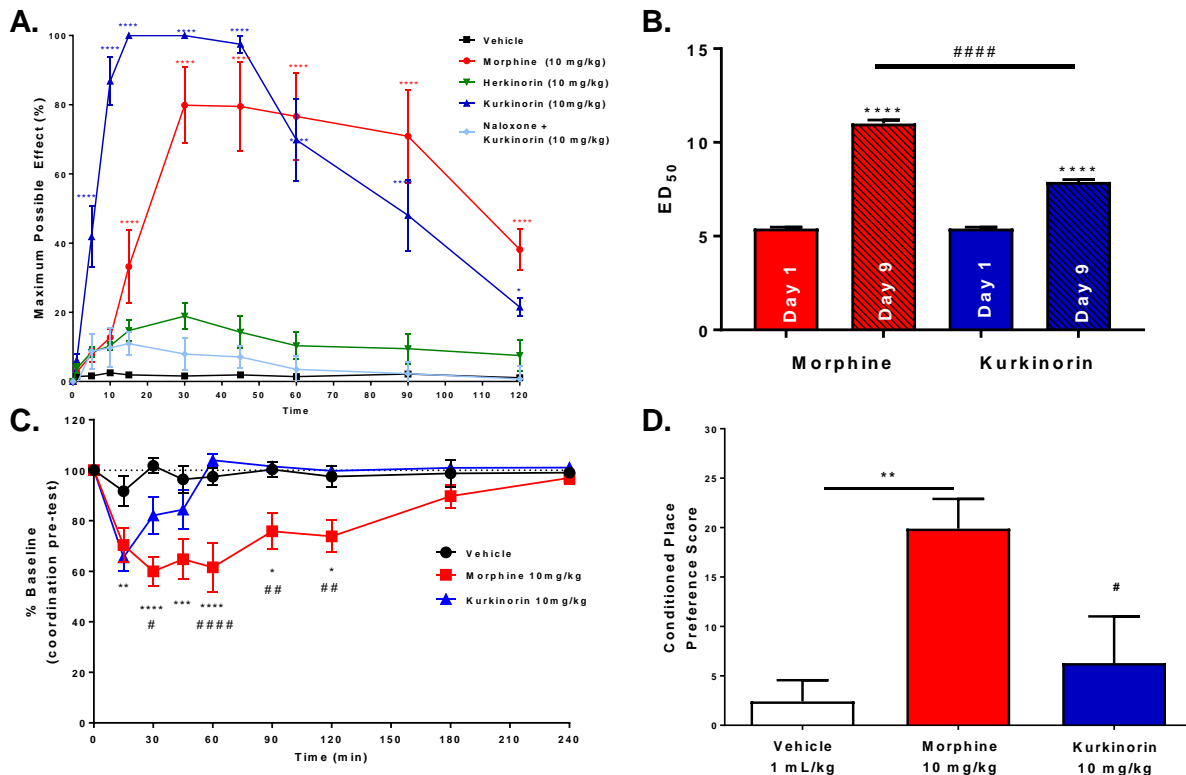


Figure 3.3: A) The antinociceptive effects of herkinorin (green), kurkinorin (dark blue), and morphine (red) as assessed in the hot-water tail-flick assay in mice at 10 mg/kg, i.p. Naloxone blocks antinociceptive effects of kurkinorin (light blue). (B) Antinociceptive effects in the hot water tail-flick assay in mice following cumulative dosing on day 1 (filled symbols) and again on day 9 (open symbols) following daily administration of 10 mg/kg/s.c. morphine or kurkinorin (n=7). (C) In mice, using a rotarod set to accelerate from 4 to 40 rpm over 300 s, morphine (10 mg/kg/i.p.) showed a significant decrease in motor coordination compared to kurkinorin (10 mg/kg/i.p.) and vehicle (n=6). (D) In mice, a significant place preference is seen in the morphine paired chamber but not with the same dose of kurkinorin when compared to vehicle. **p<0.01 compared to vehicle; #p<0.05 compared to morphine. ****p<0.0001, ***p<0.001, **p<0.01, *p<0.05, drug compared to vehicle; #####p<0.0001, ###p<0.001, ##p<0.01, #p<0.05, morphine compared to kurkinorin. Data shown as mean \pm SEM.

The CNS-penetration of kurkinorin may pose some additional risks, such as the sedation and abuse potential which are centrally mediated in morphine and other clinically used MOR agonists.⁶ Therefore, we sought to determine if kurkinorin would also produce similar negative side effects. The development of tolerance was evaluated by comparing the dose-response curves of both morphine and kurkinorin in the hot water tail flick assay. On the first day of dosing, the two compounds were equipotent, with no significant potency differences seen between morphine (ED₅₀ 5.3 mg/kg) and kurkinorin (ED₅₀ 5.0 mg/kg) (**Figure 3.3b**). On day 9, following chronic, daily administration (10 mg/kg/s.c), both morphine and kurkinorin showed the development of tolerance, but morphine showed significantly more tolerance (ED₅₀ 11.6 mg/kg) compared to kurkinorin (7.9 mg/kg). The motor coordination or sedative effects of both kurkinorin and morphine were evaluated using the rotarod test at doses that elicited the maximum antinociceptive effects (10 mg/kg) in the tail flick assay (**Figure 3.3c**). As expected, morphine induced significant sedation up to two hours post administration, while kurkinorin demonstrated slight sedation only at the 15 min time point with significantly less effect upon motor coordination compared to morphine overall.¹

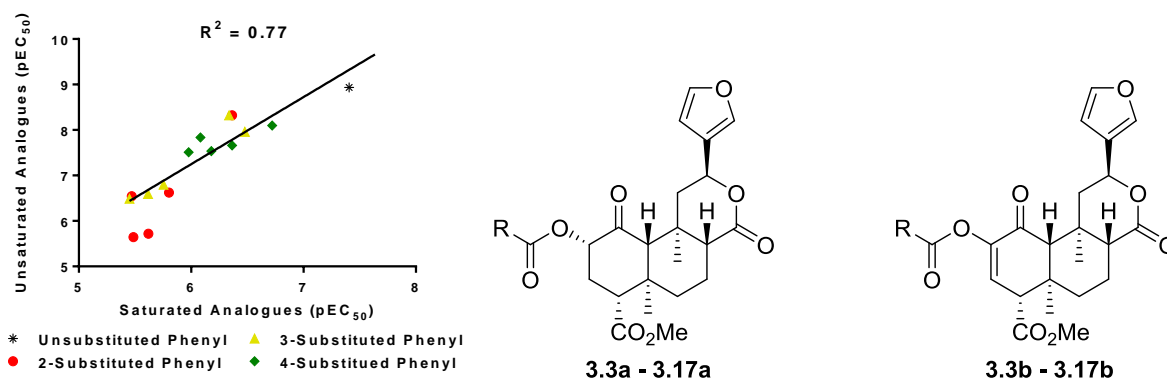
The rewarding effects were assessed using the conditioned place preference assay. Rats were paired with either drug (morphine or kurkinorin) or vehicle in daily conditioning sessions for 7 consecutive days, and the time they spent in the paired chamber was measured on the eighth day. Using this paradigm, kurkinorin resulted in a conditioned place preference score (expressed as % time spent in the drug paired chamber) similar to the vehicle control at both 5 mg/kg and 10 mg/kg and significantly less than the same doses of morphine (**Figure 3.3d**).¹

Results

Study 1: Evaluation of kurkinorin analogues with substitutions to the phenyl ring

The improved potency, selectivity, and *in vivo* activity of kurkinorin in comparison to herkinorin clearly warranted additional studies to establish SAR for compounds containing this modified core. Thus, analogues of herkinorin and kurkinorin were synthesized from salvinorin B or a mixture of **3.1** and **3.2**, respectively, following the general method in **Scheme 3.1** and were evaluated for their activity at MORs (**Table 3.2**).¹ Initial analogues were designed to provide information on the steric and electronic properties allowed in the MOR binding site as well as to

Table 3.2: MOR pharmacology: Inhibition of forskolin-induced cAMP accumulation, and scatter plot comparison of the pEC₅₀ values of herkinorin analogues vs. kurkinorin analogues (inset).



Compound	R=	EC ₅₀ ± SEM ^{a,b} (nM)	EC ₅₀ ± SEM ^{a,b} (nM)
3.3	2-F-C ₆ H ₅	400 ± 100	5 ± 1
3.4	3-F-C ₆ H ₅	460 ± 80	4.7 ± 0.4
3.5	4-F-C ₆ H ₅	800 ± 200	15 ± 2
3.6	2-Cl-C ₆ H ₅	3400 ± 200	290 ± 20
3.7	3-Cl-C ₆ H ₅	2400 ± 100	250 ± 30
3.8	4-Cl-C ₆ H ₅	660 ± 100	29 ± 8
3.9	2-CH ₃ -C ₆ H ₅	1600 ± 400	240 ± 40
3.10	3-CH ₃ -C ₆ H ₅	1800 ± 300	160 ± 30
3.11	4-CH ₃ -C ₆ H ₅	430 ± 10	21.8 ± 0.3
3.12	2-NO ₂ -C ₆ H ₅	2000 ± 1000	1910 ± 550
3.13	3-NO ₂ -C ₆ H ₅	3500 ± 200	320 ± 10
3.14	4-NO ₂ -C ₆ H ₅	1000 ± 100	31 ± 2
3.15	2-CH ₃ O-C ₆ H ₅	3300 ± 300	2000 ± 1000
3.16	3-CH ₃ O-C ₆ H ₅	330 ± 20	11 ± 2
3.17	4-CH ₃ O-C ₆ H ₅	190 ± 60	8 ± 3

^aMean ± standard error of the mean; n ≥ 2 individual experiments run in triplicate. ^bMOR Emax = 100%.

provide a direct comparison between the herkinorin and kurkinorin scaffolds. These analogues consisted of electron donating (methyl, methoxy) and electron withdrawing (halogens, nitro) substitutions in the 2-, 3-, and 4-positions of the phenyl rings.

All of these analogues retained full efficacy at MORs. In all cases, the unsaturated variants were more potent than their saturated analogues, by a factor of 1.3 to 97-fold. A scatter plot comparison of the pEC₅₀ of the two libraries shows a correlation of activity between the two series, indicating that parallel changes in structure correspond to parallel changes in activity (**Table 3.2, inset**). This correlation suggests that both the herkinorin and kurkinorin series of analogues are potentially binding at a similar location in the MORs. Generally, substitutions at the 4-position were well tolerated, with 3-substituted analogues being slightly less active, and 2-substituted analogues being considerably less active than the 4-substituted analogues. Of these substituted phenyl analogues, the chloro- and nitro-substituted analogues were the least potent, indicating that electron-poor aromatic rings may be detrimental to activity.

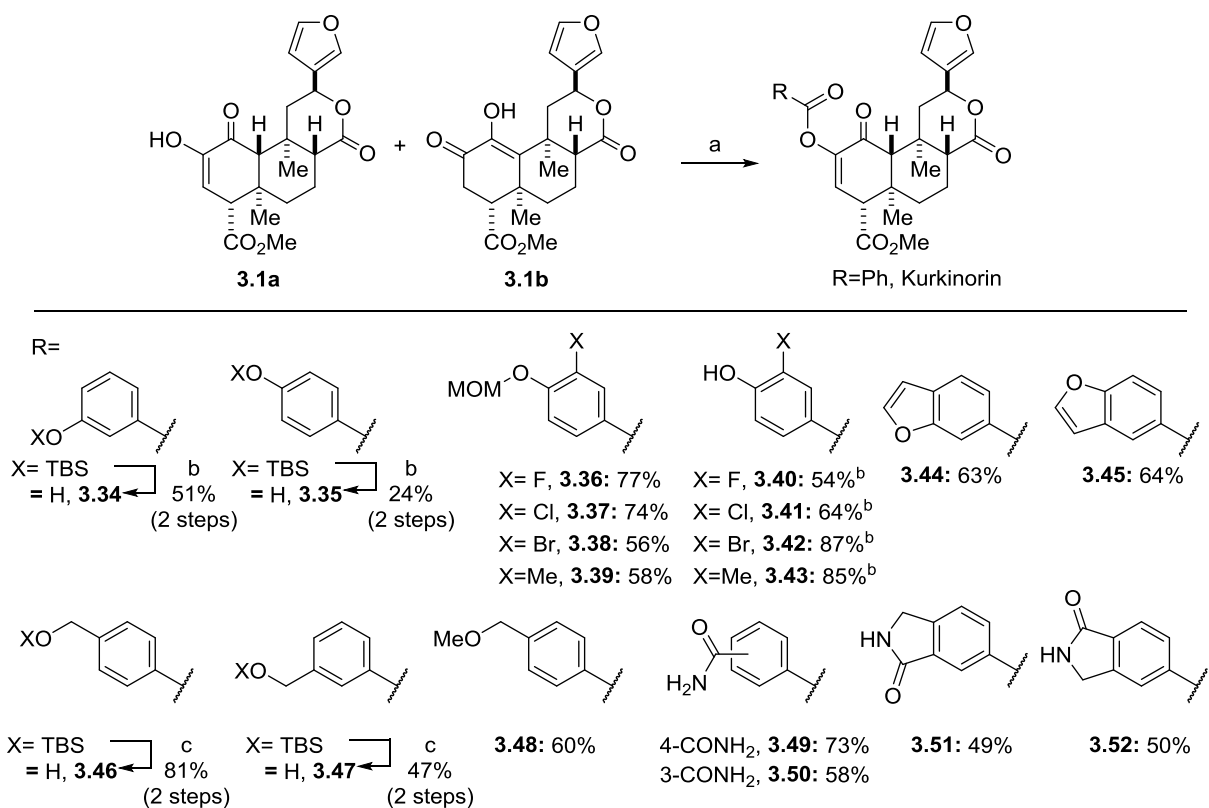
Study 2: SAR-guided design and synthesis of kurkinorin analogues

In an effort to further probe MOR binding and activation by the kurkinorin scaffold, several heterocycles (**3.18 – 3.30**) were introduced as bioisosteres in place of the phenyl ring in kurkinorin (**Table 3.3**). Analogues with varied linkers between the ester and phenyl moieties were also explored (**3.31 – 3.33**) to probe the depth and shape of the binding pocket. Additionally, due to the activity of the methoxy-substituted kurkinorin derivatives, free and protected phenols (**3.34 – 3.45**) as well as benzylic alcohols and derivatives thereof (**3.46 – 3.52**) were sought in order to probe the H-bond characteristics in the MOR binding site and to manipulate the pK_a of the ligands. The structural and activity differences between morphine and codeine highlight the role that H-bonding plays at the MOR, as the only structural difference between the two is a free phenol in morphine

and a methylated phenol in codeine, with codeine being significantly less active at the MOR than morphine.⁷

The synthesis of these kurkinorin derivatives generally followed the previously reported method for the synthesis of kurkinorin (**Scheme 3.1**).¹ However, the installation of free alcohols required protection methodology, which is not a straightforward task considering the complexity and lability of the salvinorin A core. Therefore, optimization of both protecting groups and deprotection methods was accomplished in order to synthesize a variety of the desired analogues.

Initially, *tert*-butyldimethylsilyl (TBS)-protected phenolic acids were coupled to **3.1/3.2** and then deprotected using common tetra-*n*-butylammonium fluoride (TBAF) cleavage conditions (**Scheme 3.2**). While this method was generally successful for the phenolic substrates that had



^a Reagents and conditions: a) RCO₂H, DMAP, EDCI, CH₂Cl₂; b) TBAF c) KHSO₄; H₂O, MeOH, Acetone (1:1:1). ^b Alternative reaction conditions: Prepared from corresponding MOM-protected compounds, **3.36** - **3.39**, CBr₄, PPh₃, DCE, 40 °C, overnight.

Scheme 3.2: Synthesis of SAR-guided kurkinorin analogues.

only a single substitution on the phenyl ring, it was low yielding and resulted in side products of similar retention times during the preparative HPLC separation process. This issue was more evident in subsequent derivatives with halogen moieties installed ortho to the TBS-phenol, possibly due to the manipulation of the phenol's pK_a. In fact, multiple preparative HPLC purifications were not successful in purifying these compounds to greater than 90% purity. Therefore, other protection and deprotection methods were explored that would allow for such compounds to be synthesized and purified. Ultimately, using a methoxymethyl ether protecting group and the mild triphenylphosphine and carbon tetrabromide conditions reported by Peng, *et al.* was successful.⁸ These conditions resulted in better resolution of the HPLC peaks and ultimately allowed for a better purification process. Similar purification issues were seen in the synthesis of the benzylic alcohol substituents. The TBS-protected hydroxymethyl benzoic acids were coupled to **3.1/3.2**, but TBAF deprotection again yielded low amounts of product, with side products that complicated the purification process. This deprotection was successfully accomplished using previously reported mild deprotection conditions with slight modifications to accommodate the insolubility of the kurkinorin derivatives in water.⁹ A mixture of 1:1:1 water/MeOH/Acetone, 0.5 eq. KHSO₄, and the TBS-protected benzyl alcohol kurkinorin derivative stirring overnight resulted in the desired, free benzyl alcohol derivative. Using these methods and/or the EDCI/DMAP coupling conditions described previously,¹ analogues **3.18** – **3.52** were prepared.

Study 3: Evaluation of SAR-driven kurkinorin analogues

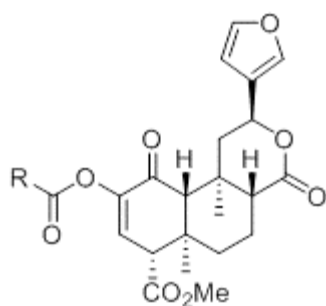
Previous SAR studies focused on herkinorin indicated that heterocyclic substitutions were well tolerated and resulted in potent MOR agonists.¹⁰ Replacement of the phenyl ring of kurkinorin with pyridines results in similar activity trends as seen for the phenyl ring substitutions with the 3-

and 4- pyridines being more potent than the 2-pyridine (**3.18** - **3.20**, **Table 3.3**). Increasing the number of nitrogen atoms in the ring, as seen in the pyrimidine analogue **3.21**, maintains potency that is equipotent to that of the 4-pyridine analogue. Additionally, modifying the pyridine ring with a methoxy group, which was previously shown to maintain activity, does not substantially increase the potency of the pyridine derivative (**3.19** $EC_{50} = 3.2 \pm 0.8$, **3.22** $EC_{50} = 2.5 \pm 0.3$ nM).

In addition to the nitrogen-containing heterocyclic analogues, heterocycles containing oxygen and sulfur atoms were also explored. The benzofuroyl-derivative of herkinorin was previously demonstrated to have modest MOR activity ($EC_{50} = 1050 \pm 80$ nM);^{10b} thus, the corresponding 2-benzofuroyl kurkinorin analogue **3.23** was evaluated and found to have a potency of 31 ± 9 nM. Modification of this moiety by substituting a sulfur atom for the oxygen atom, as seen in **3.24**, results in an increase in potency ($EC_{50} = 9 \pm 2$ nM). Because this compound was more potent than the benzofuran derivative, thiophene analogues were explored to determine if the fused benzene rings were crucial for activity or if they represented unnecessary steric bulk. The resulting 2- and 3-thiophene derivatives, **3.25** and **3.26** respectively, were the most potent heterocyclic analogues evaluated and had activities similar to kurkinorin. To probe the directionality of the possible H-bond acceptor capabilities of the sulfur and oxygen atoms of these analogues, the corresponding oxazole and thiazole derivatives were also synthesized. The 5-oxazole **3.27** and 5-thiazole **3.28** were active, with EC_{50} values nearly identical to their larger benzofuran and thianaphene counterparts. However, both the 4-oxazole **3.29** and the 4-thiazole **3.30** were completely inactive up to the highest dose tested, 10 μ M. These results indicate that while steric bulk off the 5-membered heterocyclic ring is tolerated, modifications to the directionality of the heteroatom's H-bond accepting abilities are not.

Analogues with differing linkers between the ester and phenyl moieties were also explored to further probe the depth of the binding pocket (**3.31** - **3.33**). The herkinorin analogues of these compounds, with methyl, ethyl, and ethylene linkers, have previously been evaluated for their affinity at MORs and KORs, and, interestingly, all displayed higher affinity for KORs than

Table 3.3: MOR pharmacology of SAR-driven analogues: Inhibition of forskolin-induced cAMP accumulation.



	R=	EC ₅₀ ± SEM ^{a,b} (nM)
3.18	2-Pyridinyl	410 ± 50
3.19	3-Pyridinyl	3.2 ± 0.8
3.20	4-Pyridinyl	6 ± 1
3.21	5-Pyrimidinyl	6 ± 1
3.22	6-CH ₃ O-3-Pyridinyl	2.5 ± 0.3
3.23	2-Benzofuranyl	30 ± 9
3.24	2-Thianapthenyl	9 ± 2
3.25	2-Thiophenyl	1.4 ± 0.8
3.26	3-Thiophenyl	1.3 ± 0.9
3.27	5-Oxazolyl	30 ± 2
3.28	5-Thiazolyl	5 ± 2
3.29	4-Oxazolyl	>10 000 ^c
3.30	4-Thiazolyl	>10 000 ^c
3.31	CH ₂ C ₆ H ₅	130 ± 50
3.32	CH ₂ CH ₂ C ₆ H ₅	400 ± 100
3.33	CHCHC ₆ H ₅	30 ± 10
3.34	3-OH-C ₆ H ₄	1.3 ± 0.3
3.35	4-OH-C ₆ H ₄	0.83 ± 0.04
3.36	3-F-4-OCH ₂ OCH ₃ -C ₆ H ₃	3.4 ± 0.6
3.38	3-Br-4-OCH ₂ OCH ₃ -C ₆ H ₃	1300 ± 200
3.39	3-Me-4-OCH ₂ OCH ₃ -C ₆ H ₃	170 ± 20
3.40	3-F-4-OH-C ₆ H ₃	0.6 ± 0.2
3.41	3-Cl-4-OH-C ₆ H ₃	4 ± 1
3.42	3-Br-4-OH-C ₆ H ₃	17 ± 7
3.43	3-Me-4-OH-C ₆ H ₃	60 ± 10
3.44	6-Benzofuranyl	1.5 ± 0.6
3.45	5-Benzofuranyl	9 ± 2
3.46	4-CH ₂ OH-C ₆ H ₄	0.03 ± 0.01
3.47	3-CH ₂ OH-C ₆ H ₄	2.42 ± 0.07
3.48	4-CH ₂ OCH ₃ -C ₆ H ₄	13 ± 3
3.49	4-CONH ₂ -C ₆ H ₄	0.19 ± 0.03
3.50	3-CONH ₂ -C ₆ H ₄	>10 000 ^c
3.51	3-oxoisindolinyl	2.2 ± 0.2
3.52	1-oxoisindolinyl	3.2 ± 0.7

^a Mean ± standard deviation; n ≥ 2 individual experiments run in triplicate. ^b E_{max} = 100%, unless noted otherwise. ^c E_{max} = 0 % up to 10 μM.

MORs.¹¹ The kurkinorin derivatives evaluated herein are active at MORs, but the extended linker does result in decreased MOR activity in comparison to kurkinorin. The alkyl linkers, **3.31** and **3.32**, allow for additional conformation mobility of the phenyl ring and result in over 100-fold decrease in MOR activity. The ethylene linker in **3.33** results in 25-fold loss in activity in comparison to kurkinorin, with an EC₅₀ value of 30 ± 10 nM. These results indicate that the MOR binding pocket does allow for this extension of the phenyl ring, but these analogues did not add any beneficial interactions with the receptor to achieve potent MOR activation.

Some of the most active compounds that we initially evaluated were phenyl derivatives substituted with methoxy- or fluoro-substituents (**3.3b**, **3.4b**, **3.16b**, and **3.17b**, **Table 3.2**). Unfortunately, none of these compounds were more potent than kurkinorin itself, but their activities warranted further probing of the H-bond characteristics in the receptor binding pocket. To allow for both H-bond donating and accepting, we evaluated the 3'- and 4'-phenolic kurkinorin derivatives **3.34** and **3.35**. This strategy was the first to identify a compound that showed a slight increase in potency in comparison to kurkinorin itself, with **3.34** and **3.35** having EC₅₀ values of 1.3 ± 0.3 nM and 0.83 ± 0.04 nM, respectively, vs. kurkinorin's EC₅₀ value of 1.2 ± 0.2 nM.

With the potent **3.35** in hand, we sought to further modulate the pK_a and H-bond donor capabilities of the compound by installing halogens adjacent to the phenol. Similarly to our initial results with the mono-substituted derivatives, the 3'-F-4'-OH-substitution of **3.40** was the most potent, at 0.6 ± 0.2 nM. The trend among these halogenated phenols follows the inverse of intramolecular halogen-hydrogen bond strength, with the 3'-F-4'-OH- being the strongest, followed by the 3'-Cl-4'-OH **3.41**, and the 3'-Br-4'-OH **3.42** being the weakest of the three. This trend in activity potentially indicates that the phenolic hydrogens are either coordinating with the adjacent halogens¹² or that the phenol is interacting with a weakly basic point on the receptor and the

halogens' influence on lowering its pK_a is strengthening that interaction, although the trend could also be explained by the increased bulk at the 3'-position. The installation of a methyl group ortho to the phenol, **3.43**, allowed for the evaluation of this hypothesis, with a 3'-substitution of similar molecular size to the Br of **3.42** (Taft size parameters: $CH_3 = -1.24$, $Br = -1.16$)¹³ and no modification of the phenol's pK_a or H-bond donating capabilities. The decreased activity of **3.43** compared to the halogenated phenol analogues indicates that the halogen-hydrogen bonding and pK_a manipulation is influencing the binding of **3.40** - **3.42** at the MOR more so than the steric factors. Further exploration of this interaction was accomplished by evaluating some of the MOM-protected phenols. Interestingly, **3.36** and **3.39** are 4-6-fold less active than their phenolic counterparts, but **3.38** is significantly less active at MOR than **3.42**. These results indicate that the binding site is able to accommodate the added mass of the MOM-protection and that sterically smaller 3'-substituents are preferred (3'F).

Comparison of the activities of the free phenols **3.34** and **3.35** to the corresponding methoxy analogues **3.16** and **3.17** indicated that the H-bond donating properties of the phenolic derivatives were beneficial for MOR activity. In an effort to further probe the H-bond capabilities of the oxygen in this position, we evaluated benzofuran derivatives **3.44** and **3.45** as ring-locked derivatives of the methoxy analogues with locked conformations of H-bond acceptors. Although no preference was seen between the 3'- and 4'-methoxy derivatives, the 4'OH-derivative was more potent than the 3'OH-derivative and the opposite result was seen for their corresponding ring-constrained derivatives. The benzofuran-6-carbonyl **3.44** was essentially equipotent to its 3'OH-counterpart at 1.5 ± 0.6 nM, but the benzofuran-5-carbonyl **3.45** was 12-fold less potent at 9 ± 2 nM than the 4'OH **3.35**.

Based on the activity of the phenols, we decided to probe the depth of the binding pocket with benzyl alcohol derivatives. Not only was the methylene linker tolerated in the pocket, the 4'CH₂OH derivative **3.46** was over 25-fold more potent than the 4'OH-kurkinorin derivative with an EC₅₀ value of 0.03 ± 0.01 nM. Due to this dramatic increase in potency, benzylic substitutions were further probed to determine what functionalities are tolerated in the pocket as well as what properties are mediating this increased potency. The 3'-benzylic alcohol **3.47** is not as potent as its 4'-counterpart **3.46** or the 3'phenolic compound **3.47**, suggesting that the alcohol of the 4'benzylic alcohol derivative is interacting with a residue in the back of the pocket and in space that the alcohol of the 3' derivative cannot reach. Additionally, methylating the benzylic alcohol to form **3.48** dramatically reduced potency to 13 ± 3 nM, a 433-fold potency decrease which indicates that either the H-bond donating ability of the benzyl alcohol is important or the additional methyl is not tolerated due to steric hindrance. Previously determined SAR about the phenyl ring of morphine demonstrated that replacement of morphine's phenol with a carboxamido group maintained MOR activity.¹⁴ Given these previous findings and to further explore the H-bonding requirements on the kurkinorin scaffold, the benzyl alcohols were replaced with primary amides, which are capable of both H-bond donating and accepting. This replacement resulted in the potent 4'CONH₂ derivative **3.49** and the completely inactive 3'CONH₂ derivative **3.50** (0.19 ± 0.03 nM and >10 000 nM, respectively). This dramatic difference in activity between a 3'- versus a 4'-substitution was intriguing, and warranted further exploration. We sought to determine if the directionality of the nitrogen's H-bonding abilities were the reason for the activities by evaluating the ring-locked oxoisindoline compounds. However, both the 3- and 4-oxoisindoline compounds, **3.51** and **3.52** respectively, were of similar potencies, both to one another and to the 3'CH₂OH **3.47**, with EC₅₀ values of 2.2 ± 0.2 nM and 3.2 ± 0.7 nM, respectively. Both compounds

displayed greater than 10-fold drop in activity from **3.49**, indicating that either the free carboxamido group in **3.49** is able to access a different site in the receptor that the ring-locked analogue cannot or that the added methylene unit is not tolerated sterically, but the ring locked analogue **3.52** rescued the activity from that of its inactive counterpart **3.50**.

Many of these kurkinorin analogues were further evaluated for their ability to recruit β -arrestin-2 through MOR activation (**Table 3.4**). Analogues were chosen for β -arrestin-2 recruitment analysis based upon the SAR seen in the G-protein-mediated cAMP assay, and all analogues with potencies below 10 nM were evaluated. Additionally, compounds **3.30** and **3.50** were evaluated due to their complete inactivity in the cAMP assay despite high structural similarity to potent analogues **3.28** and **3.49**, respectively, and compound **3.33** was evaluated to determine if the ethylene linker between the phenyl and ester moieties resulted in a significant conformational change in the receptor to induce signaling bias. DAMGO was previously determined to recruit β -arrestin-2 through MOR activation and was used as the positive control of the β -arrestin-2 recruitment assay.¹⁵ Morphine does not recruit to the same extent as DAMGO, and in the EFC assay utilized herein (described above, see p. 51), this trend holds true (**Table 3.4**). Herkinorin has previously been shown to activate the MOR without recruiting β -arrestin-2,^{10b, 16} however previous assays have employed fluorescent whole-cell imaging, and in this EFC assay, herkinorin does weakly recruit β -arrestin-2 with an $EC_{50} > 3 \mu\text{M}$ and an efficacy of 72%. The previously published trend that herkamide recruits β -arrestin-2 to a higher extent than herkinorin holds true in this assay, and as would be expected from its conformational similarity to herkamide, kurkinorin recruits β -arrestin-2 as well.

The functional selectivity of these compounds was evaluated by determining their bias factors (see **Equation 2.1**). As the standard to which all data are normalized, DAMGO has a bias factor

value of 1, indicating no signaling bias. The more sensitive β -arrestin-2 assay used here establishes that herkinorin does recruit β -arrestin-2, but is biased towards the G-protein coupled pathway, with a bias factor of 0.61. Compounds herkamide and kurkinorin have similar profiles, as originally

Table 3.4: MOR pharmacology: MOR-mediated β -arrestin recruitment.

Compound	EC ₅₀ \pm SEM ^a (nM) (% Efficacy) ^b	Bias Factor ^c
DAMGO	42 \pm 5 (97)	1.0
Morphine	380 \pm 40 (38)	0.36
Fentanyl	38 \pm 2 (70)	0.34
Herkinorin	3400 \pm 700 (72)	0.61
Herkamide	560 \pm 60 (85)	0.32
Kurkinorin	140 \pm 40 (96)	0.57
3.3b	63 \pm 4 (91)	5.0
3.4b	41 \pm 10 (79)	6.6
3.17b	96 \pm 30 (76)	4.6
3.19	190 \pm 20 (61)	0.76
3.20	120 \pm 30 (71)	2.71
3.21	650 \pm 90 (49)	0.32
3.22	30 \pm 10 (76)	4.42
3.24	700 \pm 100 (90)	0.90
3.25	260 \pm 30 (84)	0.33
3.26	46.2 \pm 0.1 (84)	1.69
3.28	150 \pm 10 (68)	1.64
3.30	>25 000 (0)	--
3.33	80 \pm 10 (71)	22.5
3.34	40 \pm 10 (87)	1.98
3.35	21 \pm 4 (73)	2.13
3.36	1300 \pm 80 (80)	0.15
3.38	>25 000 (0)	0.0
3.39	>25 000 (0)	0.0
3.40	24 \pm 3 (79)	1.40
3.41	180 \pm 10 (69)	1.04
3.42	1600 \pm 300 (72)	0.57
3.43	800 \pm 100 (76)	4.34
3.44	40 \pm 10 (90)	2.62
3.45	490 \pm 80 (84)	1.21
3.46	14 \pm 1 (81)	0.14
3.47	150 \pm 30 (75)	0.87
3.48	360 \pm 80 (74)	1.98
3.49	10 \pm 3 (119)	1.57
3.50	>25 000 (0)	--
3.51	190 \pm 60 (76)	0.65
3.52	260 \pm 60 (88)	0.81

^aMean \pm standard error of the mean; n \geq 3 individual experiments run in triplicate. ^bMaximum efficacy values calculated based on DAMGO maximum stimulation. ^cBias factors were calculated using **Eq. 2.1**. Values <1 indicate bias towards the cAMP pathway and values >1 indicate bias towards the β -arrestin-2 pathway. DAMGO is the reference compound, with a bias = 1.

predicted in the project rationale, having bias factor values of 0.32 and 0.57, respectively, indicating a bias towards the G-protein coupled pathway.

All of the analogues potent in the cAMP assay also recruited β -arrestin-2 to differing extents, while none of the analogues inactive in the cAMP assay (**3.30** and **3.50**) recruited β -arrestin-2. All phenyl substituted analogues were biased towards β -arrestin-2 recruitment. Interestingly, **3.21** is one of the most G-protein biased compounds, while the structurally similar **3.22** is one of the most β -arrestin-2 biased compounds, indicating that the 6-methoxy of **3.22** is able to engage in a point of contact with the receptor that favors β -arrestin-2 recruitment that **3.21** cannot. The phenolic compounds **3.40** and **3.41** are not biased, while **3.42** is slightly G-protein biased and **3.43** is β -arrestin-2 biased, indicating that the size and properties of the 3'-substituent significantly affect the β -arrestin-2 recruitment of the analogues. The MOM-protected phenol **3.36** is only a weak recruiter of β -arrestin-2 and **3.39** does not recruit β -arrestin-2 at all, which indicates that the binding pocket of the receptor in the β -arrestin-2 recruitment conformation does not tolerate the steric bulk of both a 3'-substituent and the large 4'OMOM. Conversely, **3.33** with the ethylene-linker has the highest bias factor of all analogues evaluated, at 22.5, suggesting that the spacer between the ester and phenyl moieties may allow the compound to adjust its orientation to allow for better accommodation by the different receptor conformation. The only other analogue with a similar bias factor to the MOM-protected phenols is **3.46**, but due to its high potency in the cAMP assay, its bias factor is 0.14 despite its potent β -arrestin-2 recruitment of 14 ± 1 nM. Overall, the SAR trends between β -arrestin-2 recruitment and G-protein activation are different and indicate that compounds with larger 4'-substituents may have the potential to be biased activators of the MOR-associated G-protein pathway.

To determine the efficiency of the activity of these kurkinorin derivatives, their physicochemical properties were calculated and the metrics of ligand efficiency (LE) and lipophilic-adjusted ligand efficiency (LELP) were calculated based on their EC₅₀ values in the G-protein pathway (**Supplemental Table 1**). All analogues had total polar surface areas (tPSAs) over 100 Å² and sLogP values over the ideal 2.5,¹⁷ highlighting the need for further probing of the physicochemical properties of these analogues. Analogues **3.46** and **3.49** were the most efficient analogues, with LE values of 0.38 and 0.35, respectively, and LELP values of 9.49 and 8.26.

Discussion

Through SAR studies on the naturally-occurring KOR agonist salvinorin A, we have identified kurkinorin as a potent, selective, and centrally active probe for opioid receptors. Kurkinorin's activation of MORs potently induces G-protein-mediated effects and, to a lesser extent, recruits β -arrestin-2. Kurkinorin is the first non-nitrogenous opioid to show centrally-mediated antinociceptive activity. Also of importance, kurkinorin has reduced tolerance, sedation, and rewarding properties compared to morphine.

Kurkinorin's desirable *in vivo* effects led us to explore the SAR of this scaffold at the MORs. Through this campaign, we have identified structural trends required for activating MOR-associated G-proteins, as well as for recruiting β -arrestin-2 upon MOR activation. We have identified **3.46**, a compound that is a potent and biased activator of the MOR-associated G-protein pathway with an EC₅₀ value of 0.03 ± 0.01 nM and a bias factor of 0.14. We have also identified **3.39**, which is a selective activator of the G-protein pathway without any recruitment of β -arrestin-2. Although other analogues were more potent in activating the G-protein pathway, we believe that **3.39** is an interesting starting point as a lead compound, which upon optimization, will allow for further probing of the requirements for activation of either MOR-associated pathway.

The molecular nature of kurkinorin's reduced side effect profile *in vivo* is unclear, as it does recruit β -arrestin-2 to a greater extent than morphine, but given its distinctive properties and desirable *in vivo* effects, along with the SAR-guided analogues identified through its study, kurkinorin is an attractive probe for potentially differentiating analgesia from abuse liability. Furthermore, our findings provide additional evidence that moving away from morphine-based opioid ligands may serve as a viable strategy for dissociating central antinociception from common opioid induced side effects.

References

1. Crowley, R. S.; Riley, A. P.; Sherwood, A. M.; Groer, C. E.; Shivaperumal, N.; Biscaia, M.; Paton, K.; Schneider, S.; Provasi, D.; Kivell, B. M.; Filizola, M.; Prisinzano, T. E. Synthetic studies of neoclerodane diterpenes from *Salvia divinorum*: identification of a potent and centrally acting μ opioid analgesic with reduced abuse liability. *J. Med. Chem.* **2016**, *59*, 11027-11038.
2. (a) Beguin, C.; Richards, M. R.; Li, J. G.; Wang, Y. L.; Xu, W.; Liu-Chen, L. Y.; Carlezon, W. A.; Cohen, B. M. Synthesis and in vitro evaluation of salvinorin A analogues: Effect of configuration at C(2) and substitution at C(18). *Bioorg. Med. Chem. Lett.* **2006**, *16*, 4679-4685; (b) Harding, W. W.; Schmidt, M.; Tidgewell, K.; Kannan, P.; Holden, K. G.; Gilmour, B.; Navarro, H.; Rothman, R. B.; Prisinzano, T. E. Synthetic studies of neoclerodane diterpenes from *Salvia divinorum*: semisynthesis of salvinicins A and B and other chemical transformations of salvinorin A. *J. Nat. Prod.* **2006**, *69*, 107-112.
3. (a) Shigehisa, H.; Mizutani, T.; Tosaki, S. Y.; Ohshima, T.; Shibasaki, M. Formal total synthesis of (+)-wortmannin using catalytic asymmetric intramolecular aldol condensation reaction. *Tetrahedron* **2005**, *61*, 5057-5065; (b) Kotoku, N.; Sumii, Y.; Kobayashi, M. Stereoselective synthesis of core structure of cortistatin A. *Org. Lett.* **2011**, *13*, 3514-3517.

4. Bluth, M. H.; Pincus, M. R. Narcotic analgesics and common drugs of abuse: Clinical correlations and laboratory assessment. *Clin. Lab. Med.* **2016**, *36*, 603-634.
5. Lamb, K.; Tidgewell, K.; Simpson, D. S.; Bohn, L. M.; Prisinzano, T. E. Antinociceptive effects of herkinorin, a MOP receptor agonist derived from salvinorin A in the formalin test in rats: new concepts in mu opioid receptor pharmacology: from a symposium on new concepts in mu-opioid pharmacology. *Drug Alcohol Depend.* **2012**, *121*, 181-188.
6. Trang, T.; Al-Hasani, R.; Salvemini, D.; Salter, M. W.; Gutstein, H.; Cahill, C. M. Pain and poppies: the good, the bad, and the ugly of opioid analgesics. *J. Neurosci.* **2015**, *35*, 13879-13888.
7. Williams, D. A.; Roche, V. F.; Roche, E. B. *Foye's Principles of Medicinal Chemistry*. 7th ed.; Wolters Kluwer Health/Lippincott Williams & Wilkins: Philadelphia, 2013; p 658-699.
8. Peng, Y. G.; Ji, C. Y.; Chen, Y. C.; Huang, C. Z.; Jiang, Y. Z. An efficient and selective deprotecting method for methoxymethyl ethers. *Synth. Commun.* **2004**, *34*, 4325-4330.
9. Arumugam, P.; Karthikeyan, G.; Perumal, P. T. A mild, efficient, and inexpensive protocol for the selective deprotection of TBDMS ethers using KHSO_4 . *Chem. Lett.* **2004**, *33*, 1146-1147.
10. (a) Harding, W. W.; Tidgewell, K.; Byrd, N.; Cobb, H.; Dersch, C. M.; Butelman, E. R.; Rothman, R. B.; Prisinzano, T. E. Neoclerodane diterpenes as a novel scaffold for mu opioid receptor ligands. *J. Med. Chem.* **2005**, *48*, 4765-4771; (b) Tidgewell, K.; Groer, C. E.; Harding, W. W.; Lozama, A.; Schmidt, M.; Marquam, A.; Hiemstra, J.; Partilla, J. S.; Dersch, C. M.; Rothman, R. B.; Bohn, L. M.; Prisinzano, T. E. Herkinorin analogues with differential beta-arrestin-2 interactions. *J. Med. Chem.* **2008**, *51*, 2421-2431.
11. (a) Polepally, P. R.; Huben, K.; Vardy, E.; Setola, V.; Mosier, P. D.; Roth, B. L.; Zjawiony, J. K. Michael acceptor approach to the design of new salvinorin A-based high affinity ligands for

- the kappa-opioid receptor. *Eur. J. Med. Chem.* **2014**, *85*, 818-829; (b) Tidgewell, K.; Harding, W. W.; Lozama, A.; Cobb, H.; Shah, K.; Kannan, P.; Dersch, C. M.; Parrish, D.; Deschamps, J. R.; Rothman, R. B.; Prisinzano, T. E. Synthesis of salvinorin A analogues as opioid receptor probes. *J. Nat. Prod.* **2006**, *69*, 914-918.
12. Kovács, A.; Varga, Z. Halogen acceptors in hydrogen bonding. *Coord. Chem. Rev.* **2006**, *250*, 710-727.
13. Hansch, C.; Leo, A. *Substituent Constants for Correlation Analysis in Chemistry and Biology*. Wiley-Interscience: New York, NY, 1979.
14. Wentland, M. P.; Lou, R.; Dehnhardt, C. M.; Duan, W.; Cohen, D. J.; Bidlack, J. M. 3-Carboxamido analogues of morphine and naltrexone: Synthesis and opioid receptor binding properties. *Bioorg. Med. Chem. Lett.* **2001**, *11*, 1717-1721.
15. Groer, C. E.; Schmid, C. L.; Jaeger, A. M.; Bohn, L. M. Agonist-directed interactions with specific beta-arrestins determine mu-opioid receptor trafficking, ubiquitination, and dephosphorylation. *J. Biol. Chem.* **2011**, *286*, 31731-31741.
16. (a) Groer, C. E.; Tidgewell, K.; Moyer, R. A.; Harding, W. W.; Rothman, R. B.; Prisinzano, T. E.; Bohn, L. M. An opioid agonist that does not induce mu-opioid receptor--arrestin interactions or receptor internalization. *Mol. Pharmacol.* **2007**, *71*, 549-557; (b) Xu, H.; Wang, X.; Partilla, J. S.; Bishop-Mathis, K.; Benaderet, T. S.; Dersch, C. M.; Simpson, D. S.; Prisinzano, T. E.; Rothman, R. B. Differential effects of opioid agonists on G protein expression in CHO cells expressing cloned human opioid receptors. *Brain Res. Bull.* **2008**, *77*, 49-54; (c) Rowan, M. P.; Bierbower, S. M.; Eskander, M. A.; Szteyn, K.; Por, E. D.; Gomez, R.; Veldhuis, N.; Bunnett, N. W.; Jeske, N. A. Activation of mu opioid receptors sensitizes transient receptor

potential vanilloid type 1 (TRPV1) via beta-arrestin-2-mediated cross-talk. *PLoS One* **2014**, *9*, e93688.

17. Hopkins, A. L.; Keseru, G. M.; Leeson, P. D.; Rees, D. C.; Reynolds, C. H. The role of ligand efficiency metrics in drug discovery. *Nat. Rev. Drug Discov.* **2014**, *13*, 105-121.

4. Development of New Synthetic Approaches toward Refinement of Salvinorin A's Pharmaceutical Properties

Results

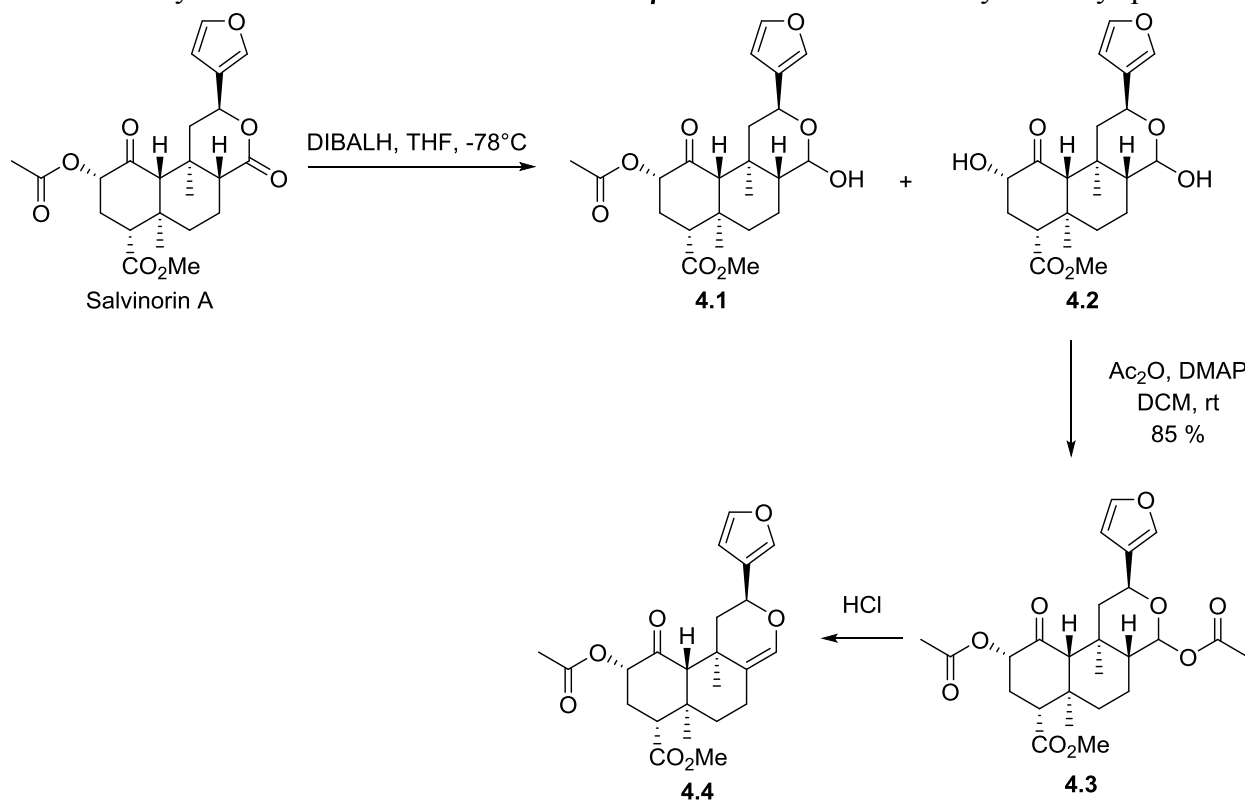
Salvinorin A's potent KOR activity and unique structural composition contribute to its attractiveness as a lead compound in the search for KOR agonists to treat pain and addiction. However, in order for salvinorin A to be further developed as a potential drug candidate, its pharmaceutical properties, including its low bioavailability, rapid metabolism, and P-gp substrate activity, require optimization. In an effort to identify a point on the molecule through which its pharmaceutical properties could be modulated, the lactone position of salvinorin A was explored. The development of chemical methodology to functionalize this position and the evaluation of these C17-derivatives for their *in vitro* KOR activity allowed for the assessment of the lactone carbonyl's necessity for KOR activity.

Study 1: Development of chemical methodology to selectively functionalize the C17 position

The original report describing the reduction of the salvinorin A lactone to the lactol **4.1** called for treatment with 13.6 eq. of diisobutylaluminum hydride (DIBALH) for 25 minutes.¹ However, this reaction was done on a small scale (36.5 μmol), and upon scale-up, this reaction was low yielding and required a large amount of DIBALH. Therefore, a full optimization of this reaction was undertaken to identify a method suitable to gram-scale reactions. Decreasing the DIBALH to 3 equivalents and increasing the time of the reaction while maintaining the temperature at -78°C accomplished this goal. A significant side reaction was determined to be the deacetylation of the C2 position to form **4.2**, but the DIBALH reduction was followed by an acetylation reaction which both acetylated the hemiacetal and re-acetylated any of the C2 position that had been deacetylated

from DIBALH (**Scheme 4.1**). This acetylated hemiacetal **4.3** was then used as the main intermediate for accessing substituents at the C17 position.

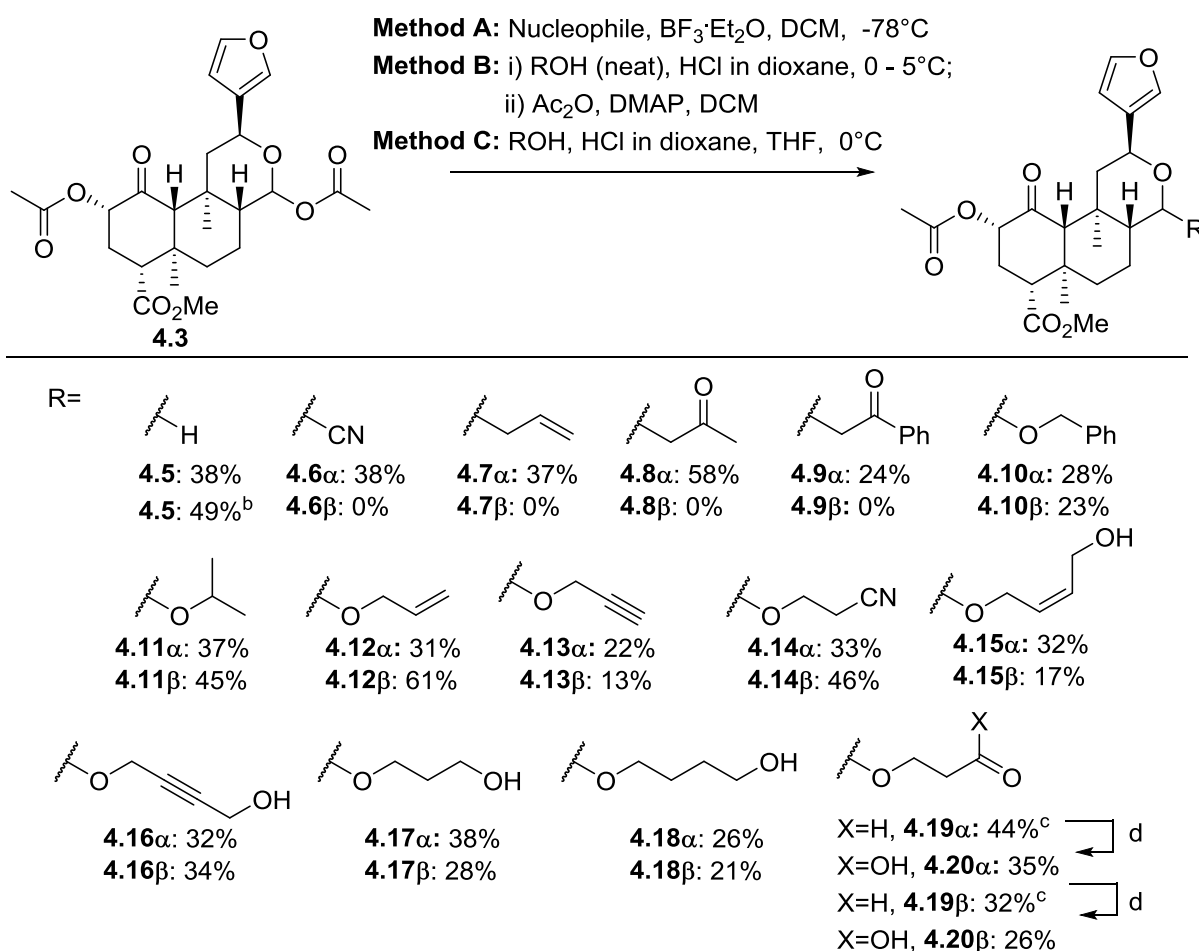
Upon attaining a method to generate **4.3** in large quantities, methods for substituting at the 17-position were explored (**Scheme 4.2**). Initially, masked nucleophiles, such as silyl-protected allyl or nitrile groups and silyl enol ethers, were added using $\text{BF}_3 \cdot \text{Et}_2\text{O}$ (General Method A) to install a carbon-carbon bond at the 17-position (**4.6 α** - **4.9 α**).² This Lewis acid catalyzed the formation of the oxocarbenium ion which allowed the masked nucleophile to add to the 17-position. However, the rest of the salvinorin A core does not tolerate the $\text{BF}_3 \cdot \text{Et}_2\text{O}$, particularly the furan, which decomposed readily, resulting in low-yielding reactions. This reaction method should produce both α - and β -substituted products, but because of the low yields, only α -substituted products could be isolated in high enough quantities for further characterization and analysis. The only exception to this selectivity was in the case of **4.10 α** and **4.10 β** which was also the only non-silyl-protected



Scheme 4.1: Synthetic route to access C17 position of salvinorin A

nucleophile added through this method. In an effort to overcome the issues with $\text{BF}_3 \cdot \text{Et}_2\text{O}$, a variety of Lewis acids were tested, but none were able to be used as a general method, as they either did not result in higher yields than the original $\text{BF}_3 \cdot \text{Et}_2\text{O}$ or were not translatable across nucleophiles. The use of trimethylsilyl trifluoromethanesulfonate (TMSOTf) as the Lewis acid³ in the formation of **4.5** did result in an increased yield, but when this method was attempted with other nucleophiles, it did not result in an enhanced formation of any other analogues.

By switching from a Lewis acid to a Brønsted-Lowry acid (hydrochloric acid, HCl) for reaction catalysis, the addition of alcohols to the 17-position was accomplished (Method B).⁴ This method



^aReagents and conditions: a) Nucleophile, $\text{BF}_3 \cdot \text{Et}_2\text{O}$, CH_2Cl_2 , -78°C ; b) i. ROH (neat), HCl in dioxane, $0 - 5^\circ\text{C}$, ii. Ac_2O , DMAP, CH_2Cl_2 ; c) ROH, HCl in dioxane, THF, 0°C ; d) OXONE monopersulfate, DMF, 3h, r.t.
^bAlternative reaction conditions: Et_3SiH , MeCN, TMSOTf, 0°C ; ^cAlternative reaction conditions: prepared from corresponding **4.17**, Dess-Martin Periodinane, CH_2Cl_2 , overnight, rt.

Scheme 4.2: Synthesis of C17-derivatives of salvinorin A.

produced both α - and β -substituted products, which, depending on the substrate, were separable by either flash column chromatography or preparative HPLC. Initially these reactions were run with the alcohol as the solvent, but removing the excess alcohol proved challenging. Additionally, a major side product was determined to be the elimination product **4.4** (**Scheme 4.1**), which was predicted to be subdued if the reaction was kept at 0 °C, but due to the presence of the dioxane from the HCl solution, the reaction would freeze upon cooling to 0 °C and the side product generation could not be inhibited. Further improvement upon this method led to the optimized Method C, whereby **4.3** and the appropriate alcohol were dissolved in THF, cooled to 0 °C, HCl in dioxane was added dropwise, and the reaction was monitored until completion and immediately quenched. This method did produce some amounts of **4.4**, but as both α - and β -substituted products were formed in high enough yields for isolation and characterization, the method was adopted.

Determining the stereochemistry around the newly formed stereocenter at C17 was accomplished using NMR coupling constants and 2D NMR methods (**Figure 4.1**). Generally, protons with J-values higher than 6 are anti and lower than 5 are syn to one another.⁵ However, the C8 proton needed for this analysis is not easily identified because it is often buried under other

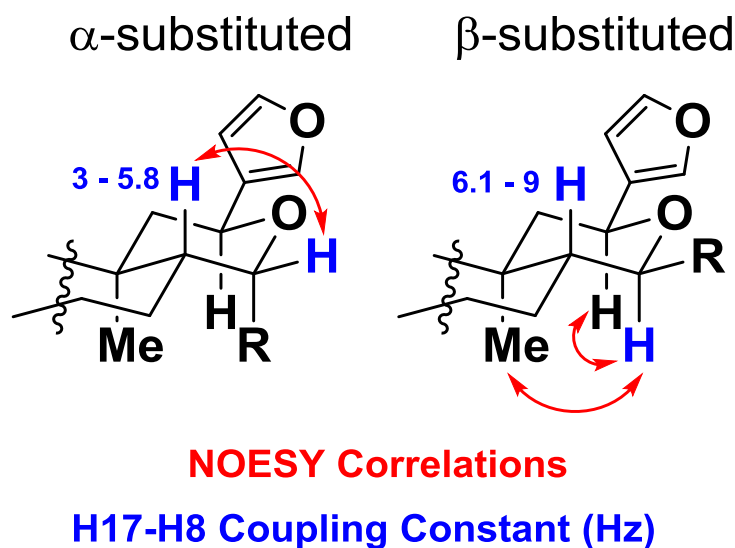


Figure 4.1: Unambiguous determination of stereochemistry at the 17-position using NMR.

aliphatic protons. Although the epimers of **4.3** were not separated, this NMR analysis revealed that the product upon acetylation was predominantly the β -epimer (C17 proton at 5.83 (d, $J = 8.0$ Hz), with NOESY correlations to the C12 proton 4.98 and the C20 methyl at 1.48). For the alcohol-substituted compounds, determining the coupling constant of the C8 and C17 protons was straightforward, as the C17 proton was a doublet with only one J value. The coupling constant alone is enough to identify the stereochemistry, but NOESY studies were done to confirm that the C17 proton in the α -substituted compounds correlated with the C8 proton, and the proton in the β -substituted compounds correlated with the C12 proton and the methyl group attached to C9. For the compounds without a C-O bond at C17 (**4.6 - 4.9**), the J -values for the C17 proton were in the ambiguous range between 5 and 6, and the J -value alone did not provide sufficient information with which to assign stereochemistry. In these cases, NOESY correlations were used to assign the stereochemistry.

The HCl substitution conditions allowed for the installation of diols to the 17-position, and these substituted diols, **4.15 - 4.18**, provided a valuable synthetic handle through which further modifications of the C17 substituent could be accessed. Oxidation of **4.17 α** and **β** under Dess-Martin oxidation conditions resulted in the aldehydes **4.19 α** and **β** . Subsequent oxidation of these aldehydes using OXONE monopersulfate resulted in the carboxylic acids **4.20 α** and **β** .

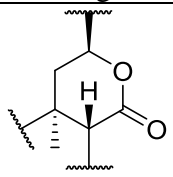
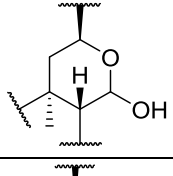
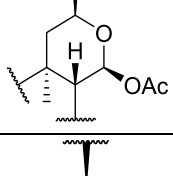
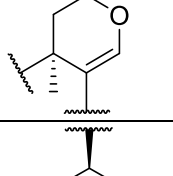
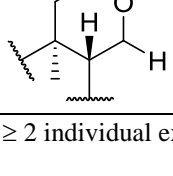
With the development of the synthetic methodology to modify the lactone core of salvinorin A, analogues were designed to probe the SAR at the KOR in an effort to determine if polar, ionizable, or solubilizing groups would be tolerated at that position. Analogues **4.1 - 4.5** were designed to evaluate the necessity of the lactone carbonyl through its reduction and removal. The introduction of stepwise modifications to the polarity and steric bulk of the substitutions in analogues **4.6 - 4.14** were used to assess the optimal substitution pattern to maintain KOR activity. Finally, analogues

4.15 – 4.20 were designed based on the SAR of the previous analogues to determine the optimal chain length of the substitution as well as the tolerability of the polar alcohols, aldehydes, and carboxylic acids.

Study 2: Evaluation of compounds with C17 modifications

The C17-analogues were evaluated for their ability to activate KORs *in vitro*. In CHO cells transfected with the KOR, the inhibition of forskolin-induced cAMP accumulation was measured. In this assay, salvinorin A is very potent with an EC₅₀ value of 0.10 ± 0.03 nM (**Table 4.1**). Reducing the lactone to the lactol (**4.1**, tested as a mixture of epimers due to the rapid epimerization of the center) and eliminating the oxygen altogether (**4.5**) resulted in equipotent compounds with EC₅₀ values of 1.2 nM. Although these compounds demonstrate a 12-fold reduction in activity,

Table 4.1: KOR pharmacology: Inhibition of forskolin-induced cAMP accumulation

Compound	C-ring:	EC ₅₀ ± SEM ^{a,b} (nM)
Salvinorin A		0.10 ± 0.03
4.1		1.2 ± 0.3
4.3		2.4 ± 0.8
4.4		2.0 ± 0.5
4.5		1.2 ± 0.4

^aMean ± standard error of the mean; n ≥ 2 individual experiments run in triplicate. ^bKOR Emax = 100%.

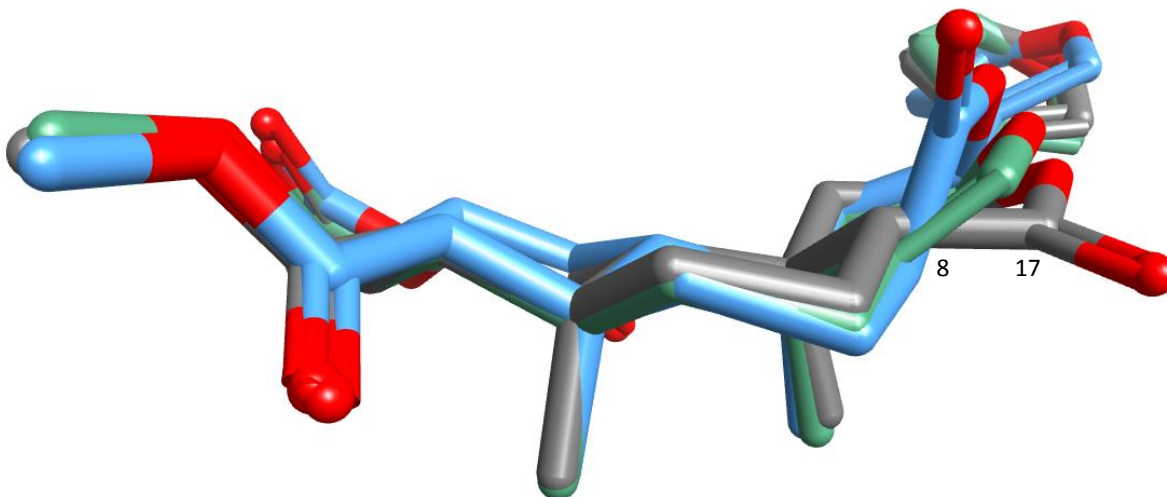
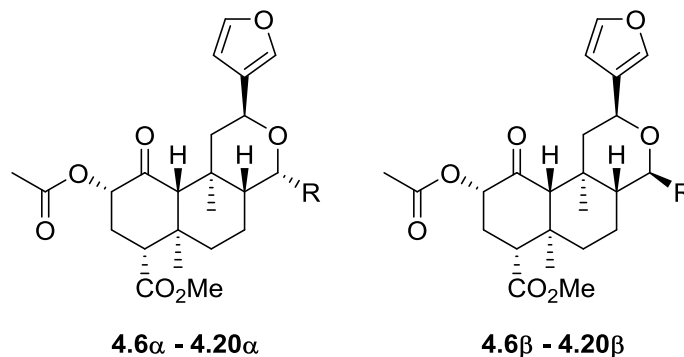


Figure 4.2: Ligand-based alignment of salvinorin A (gray), 8-epi-salvinorin A (blue), and **4.4** (green) using substructure alignment in Forge (v 10.4.2; Cresset, Litlington, Cambridgeshire, UK; <http://www.cresset-group.com/forge/>). Carbons 8 and 17 of salvinorin A numbered. See supplemental information for full method.

they indicate that the carbonyl of salvinorin A is not absolutely critical for KOR binding. Similarly, introducing unsaturation at the C8-C17 bond, **4.4**, reduces activity at KOR by 20-fold in comparison to salvinorin A with an EC_{50} value of 2.0 ± 0.5 nM. The differences in activity between **4.4** and **4.5** can potentially be attributed to the change in 3-dimensional shape that results from modifying the diterpenoid core through the installation of the double bond. The kinked diterpenoid core of **4.4** is proposed to hold the C-ring in between the conformations of salvinorin A and its epimer, 8-epi-salvinorin A (**Figure 4.2**). 8-epi-salvinorin A is significantly less potent than both **4.4** and salvinorin A at KOR ($EC_{50} = 110 \pm 30$ nM),⁶ indicating that some movement of the diterpenoid core is tolerated, but either the presence of the carbonyl in the epimerized analogue or the extension from the conformation of **4.4** to 8-epi-salvinorin A is not. Analogue **4.3** is the least active of this group, with a 24-fold reduction in activity and a potency of 2.4 ± 0.5 nM, potentially indicating that the acetylation introduces steric bulk that is not tolerated.

Table 4.2: KOR activity of C17-derivatives: Inhibition of forskolin-induced cAMP accumulation

Compound	R=	EC ₅₀ ± SEM ^{a,b} (nM)	EC ₅₀ ± SEM ^{a,b} (nM)
4.6	CN	1.3 ± 0.7	n.d.
4.7	CH ₂ CHCH ₂	45 ± 7	n.d.
4.8	CH ₂ COCH ₃	63 ± 3	n.d.
4.9	CH ₂ COC ₆ H ₅	95 ± 5	n.d.
4.10	OCH ₂ C ₆ H ₅	165 ± 1	90 ± 10
4.11	OCH(CH ₃) ₂	120 ± 20	138 ± 5
4.12	OCH ₂ CHCH ₂	20 ± 5	14 ± 3
4.13	OCH ₂ CCH	7 ± 2	3.8 ± 0.4
4.14	O(CH ₂) ₂ CN	1.1 ± 0.5	5 ± 2
4.15	OCH ₂ (CH) ₂ CH ₂ OH (z)	1.1 ± 0.5	1.2 ± 0.6
4.16	OCH ₂ CCCH ₂ OH	0.3 ± 0.1	0.5 ± 0.1
4.17	O(CH ₂) ₃ OH	0.6 ± 0.2	2.1 ± 0.8
4.18	O(CH ₂) ₄ OH	3 ± 1	23 ± 7
4.20	O(CH ₂) ₂ CO ₂ H	1.5 ± 0.6	11 ± 4

^aMean ± standard error of the mean; n ≥ 2 individual experiments run in triplicate. ^bKOR Emax = 100%.
n.d. = not determined due to limits of synthetic method.

The activity of compounds with substitutions at the C17-position appears to be dictated more by the steric bulk of the moieties rather than the stereochemistry of the C17-position. In the carbon-substituted analogues, activity decreases as the size of the moiety increases, from the small, linear nitrile (**4.6 α**), to the allyl (**4.7 α**), to the methyl and phenyl ketone derivatives (**4.8 α** and **4.9 α**), with EC₅₀ values from 1.3 ± 0.7 nM to 165 ± 1 nM (**Table 4.2**). A similar trend was seen among the substituted alcohols. The isopropyl (**4.11 α** and **β**) and benzyl (**4.10 α** and **β**) substituents were much less potent than the allyl (**4.12 α** and **β**), propargyl (**4.13 α** and **β**), and propionitrile (**4.13 α** and **β**) derivatives. The addition of diols allowed for the evaluation of polar alcohol moieties at the C17-position, and various linkers between the C17 and the alcohol were explored. These alcohols

were more potent than any of the previous analogues, with the butyne and propane linkers being the most active (0.3 ± 0.1 nM for **4.16 α** and 0.6 ± 0.2 for **4.17 α**).

As the synthetic methodology for the addition of alcohols resulted in both α and β derivatives, the activity of the epimers could be compared. However, no apparent trend in preference for either α or β epimer was seen. Additionally, substitutions at the C17-position are potentially adding new points of interaction with the receptor, as different moieties have varying degrees of activities.

Upon determining that three to four carbons was an optimal chain length for maintaining KOR activity, the carboxylic acid derivatives of the propane linkage were evaluated. These compounds, (**4.20 α** and **β**), were potent KOR agonists, with EC_{50} values of 1.5 ± 0.6 nM and 11 ± 4 nM, respectively. These compounds are the first salvinorin A derivatives with potent KOR activity to have an ionizable moiety, and they help to validate the lactone as a position through which the pharmacokinetic properties of salvinorin A could be modulated. Based upon these results, the lactone carbonyl of salvinorin A can be considered an auxophore of the scaffold, or an extraneous part of a molecule that is not essential for activity.⁷

The physicochemical properties and the metrics of ligand efficiency (LE) and lipophilic-adjusted ligand efficiency (LELP) of these lactone-modified analogues (**4.1 - 4.20**) were calculated in an effort to determine if the pharmaceutical properties of these analogues would differ from those of salvinorin A (**Supplemental Table 2**). Although none of these analogues were more efficient ligands at the KOR, several analogues are within the drug-like range (greater than 0.30 for LE and less than 10 for LELP)⁸ and further highlight the need to explore strategies to improve the pharmacokinetic properties of the salvinorin A core.

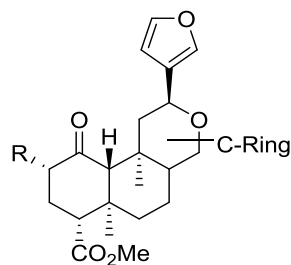
Study 3: Design, synthesis, and evaluation of analogues with C2 and C17 modifications

With chemical methods to manipulate both the C2 and C17 positions, analogues containing

modifications to both positions were synthesized and evaluated. Although many modifications have been made to the C2 position, three were chosen for this dual-modification study: methoxymethyl salvinorin B (MOM-salvinorin B), methanesulfonyl salvinorin B (Mesyl-salvinorin B), and herkinorin. These modifications were chosen because they have been evaluated in several different models and have different activity profiles. MOM-salvinorin B is more potent than salvinorin A *in vitro*, has a longer half-life *in vivo*, and has been shown to be effective in animal models of cocaine abuse.⁹ Similarly, Mesyl-salvinorin B is equipotent to salvinorin A *in vitro*, has a longer half-life *in vivo*, and has been shown to be effective in animal models of both cocaine and alcohol addiction.^{9d,10} Additionally, the sulfonate derivatives such as Mesyl-salvinorin B have been suggested to adopt a different binding mode from salvinorin A based upon the fact that parallel changes in structure (methyl to phenyl) did not result in parallel changes in activity (KOR to MOR selectivity).¹¹ Unlike the MOM- and Mesyl-salvinorin B, herkinorin acts at both KORs and MORs, being more potent at MORs. By modifying the lactone of herkinorin with modifications shown above to maintain KOR activity, the similarities of the binding poses between the MOR and the KOR can be directly compared.

Synthesis of these dual-modified analogues was accomplished using the previously described methods for generating analogues **4.1** – **4.5** with the appropriately C2-substituted analogues as the starting material (MOM-salvinorin B, Mesyl-salvinorin B, herkinorin). The only analogue synthesized differently was **4.5a**, which was synthesized from 17-deoxysalvinorin B following the previously published conditions for forming MOM-salvinorin B.^{9a} Of note, the DIBALH reduction of the lactone was successfully accomplished without cleaving the C2-substituent, further highlighting the increased stability imparted by these moieties in comparison to the acetate.

Table 4.3: KOR activity of C2/C17 derivatives: Inhibition of forskolin-induced cAMP accumulation



Compound	C-ring:	EC ₅₀ ± SEM ^{a,b} (nM)		
		4.1a - 4.5a R=	4.1b - 4.5b R=	4.1c - 4.5c R=
--		0.006 ± 0.001	0.12 ± 0.05	170 ± 20 ^c
4.1		0.06 ± 0.02	4 ± 1	310 ± 50
4.3		0.016 ± 0.006	4 ± 1	200 ± 30
4.4		0.29 ± 0.01	10 ± 2	540 ± 60
4.5		0.021 ± 0.003	4.6 ± 0.2	130 ± 20

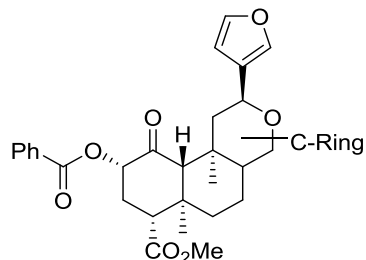
^aMean ± standard error of the mean; n ≥ 2 individual experiments run in triplicate. ^bE_{max} = 100%, unless noted otherwise. ^cE_{max} = 64 ± 18%.

These analogues were evaluated for their KOR activity using the previously described forskolin-induced cAMP accumulation assay (**Table 4.3**).¹² C17 modifications to MOM-salvinorin B (**4.1a - 4.5a**) resulted in the lowest overall fold-changes from the parent compound with all analogues being very potent KOR agonist with EC₅₀ values in the picomolar range (from

0.016 ± 0.006 nM for **4.3a** to 0.29 ± 0.01 nM for **4.4a**). As the parent MOM-salvinorin B is one of the most potent KOR analogues known to date, the fact that modifying the lactone does not seem to dramatically affect activity indicates that these analogues are binding similarly to the parent and allowing the MOM group to maintain its strong interactions with the KOR. Based upon the previous indications that the sulfonates at C2 adopt a different binding mode than the esters and ethers, it is unsurprising that the C17 modified Mesyl-salvinorin B derivatives (**4.1b** – **4.5b**) result in the largest activity changes from its parent, ranging from **4.1b**, **4.3b**, and **4.5b** being 33-fold less active to **4.4b** being 80-fold less active.

These C17 modifications to herkinorin (**4.1c** - **4.5c**) only slightly affected activity at KORs (**Table 4.3**) or MORs (**Table 4.4**). **4.4c** was the least active of the herkinorin analogues being 10-fold less active than herkinorin at both KORs and MORs, while **4.5c** was slightly more potent at KORs and **4.1c** was twice as potent at MORs than herkinorin. While the modification of the 17-position of herkinorin did not dramatically affect its activation of G-proteins associated with either MORs or KORs, it did affect its ability to recruit β-arrestin-2 upon MOR activation. Analogues **4.1c**, **4.3c**, and **4.5c** are at least 5-fold more potent in recruiting β-arrestin-2 than herkinorin, and, as such, are biased towards that pathway. The modifications found in these analogues do not affect the shape of the diterpene core in comparison to herkinorin, but the introduction of the double bond seen in **4.4c** does. This analogue, **4.4c**, is equipotent in recruiting β-arrestin-2 with herkinorin, suggesting that the kink in the diterpene core and the lactone carbonyl of herkinorin both hold the receptor in a similar conformation and the increased activities of the reduced lactone derivatives **4.1c**, **4.3c**, and **4.5c** indicates that they are able to bind more potently to a receptor conformation that recruits β-arrestin-2 than activates the G-protein pathway.

Table 4.4: MOR activity of C17-modified herkinorin derivatives.



Compound	C-ring:	Inhibition of forskolin-induced cAMP accumulation EC ₅₀ ± SEM ^{a,b} (nM)	β-arrestin-2 recruitment EC ₅₀ ± SEM ^a (nM) (% Efficacy) ^c	MOR Bias Factor
Herkinorin		39 ± 4	3400 ± 700 (72)	0.61
4.1c		19 ± 5	590 ± 60 (79)	1.90
4.3c		70 ± 30	600 ± 100 (46)	3.76
4.4c		400 ± 100	3400 ± 400 (35)	3.00
4.5c		60 ± 20	670 ± 70 (63)	4.36

^aMean ± standard error of the mean; n ≥ 2 individual experiments run in triplicate. ^b Emax = 100%. ^cMaximum efficacy values calculated based on DAMGO maximum stimulation.

Discussion

Previously determined SAR of salvinorin A at KORs led to the exploration of the lactone carbonyl as an auxophore. Through the development of chemical methodology to selectively activate and transform the lactone, analogues at this position were designed and evaluated. These

analogues allowed for validation of the hypothesis that the lactone was not critical for KOR binding and that polar, ionizable groups could be added without compromising the KOR activity. Through the development of analogues with modifications to the lactone and the C2 position, both of which were confirmed to maintain KOR activity individually, the binding modes of the analogues at the KORs and MORs were explored.

Using the chemistry described herein coupled with the SAR now understood at the C17 position, salvinorin A analogues with water solubilizing moieties appended to this position can be designed and synthesized. The free alcohol of **4.17 α/β** is not only a pharmacologically active moiety but it is also a useful chemical handle through which chemical transformations and prodrug linkers can be made.¹³ Substitutions of interest include various amines, polyethylene glycol units, and amino acid esters (**Figure 4.3**). It is expected that modification of the lactone of salvinorin A will be a viable handle through which the pharmacokinetic properties of the molecule can be modified while retaining significant KOR activity.

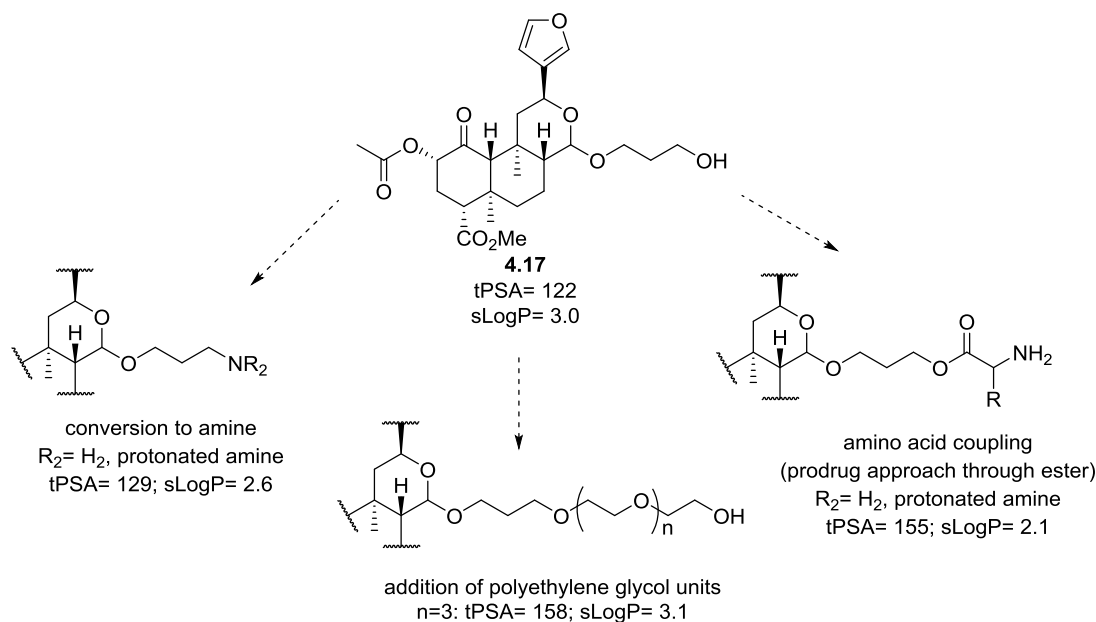


Figure 4.3: Proposed modifications to increase solubility through the C17 position. Properties calculated using Forge (v 10.4.2; Cresset, Litlington, Cambridgeshire, UK; <http://www.cresset-group.com/forge/>).

References

1. Munro, T. A.; Rizzacasa, M. A.; Roth, B. L.; Toth, B. A.; Yan, F. Studies toward the pharmacophore of salvinorin A, a potent kappa opioid receptor agonist. *J. Med. Chem.* **2005**, *48*, 345-348.
2. Beaver, M. G.; Billings, S. B.; Woerpel, K. A. C-glycosylation reactions of sulfur-substituted glycosyl donors: evidence against the role of neighboring-group participation. *J. Am. Chem. Soc.* **2008**, *130*, 2082-2086.
3. Shimokawa, J.; Harada, T.; Yokoshima, S.; Fukuyama, T. Total synthesis of gelsemoxonine. *J. Am. Chem. Soc.* **2011**, *133*, 17634-17637.
4. Schene, H.; Waldmann, H. Synthesis of deoxy glycosides under neutral conditions in LiClO₄/solvent mixtures. *Synthesis* **1999**, *1999*, 1411-1422.
5. Reich, H. J. 5-HMR-5 Vicinal Proton-Proton Coupling ³J_{HH}. <https://www.chem.wisc.edu/areas/reich/nmr/05-hmr-05-3j.htm> (accessed Apr 13, 2017).
6. Crowley, R. S.; Riley, A. P.; Sherwood, A. M.; Groer, C. E.; Shivaperumal, N.; Biscaia, M.; Paton, K.; Schneider, S.; Provasi, D.; Kivell, B. M.; Filizola, M.; Prisinzano, T. E. Synthetic studies of neoclerodane diterpenes from *Salvia divinorum*: identification of a potent and centrally acting μ opioid analgesic with reduced abuse liability. *J. Med. Chem.* **2016**, *59*, 11027-11038.
7. Silverman, R. B.; Holladay, M. W., Chapter 2 - Lead Discovery and Lead Modification. In *The Organic Chemistry of Drug Design and Drug Action (Third Edition)*, Academic Press: Boston, 2014; pp 19-122.
8. Hopkins, A. L.; Keseru, G. M.; Leeson, P. D.; Rees, D. C.; Reynolds, C. H. The role of ligand efficiency metrics in drug discovery. *Nat. Rev. Drug Discov.* **2014**, *13*, 105-121.

9. (a) Lee, D. Y. W.; Karnati, V. V. R.; He, M. S.; Liu-Chen, L. Y.; Kondaveti, L.; Ma, Z. Z.; Wang, Y. L.; Chen, Y.; Beguin, C.; Carlezon, W. A.; Cohen, B. Synthesis and in vitro pharmacological studies of new C(2) modified salvinorin A analogues. *Bioorg. Med. Chem. Lett.* **2005**, *15*, 3744-3747; (b) Wang, Y.; Chen, Y.; Xu, W.; Lee, D. Y.; Ma, Z.; Rawls, S. M.; Cowan, A.; Liu-Chen, L. Y. 2-Methoxymethyl-salvinorin B is a potent kappa opioid receptor agonist with longer lasting action in vivo than salvinorin A. *J. Pharmacol. Exp. Ther.* **2008**, *324*, 1073-1083; (c) Morani, A. S.; Ewald, A.; Prevatt-Smith, K. M.; Prisinzano, T. E.; Kivell, B. M. The 2-methoxy methyl analogue of salvinorin A attenuates cocaine-induced drug seeking and sucrose reinforcements in rats. *Eur. J. Pharmacol.* **2013**, *720*, 69-76; (d) Cunningham, C. W.; Rothman, R. B.; Prisinzano, T. E. Neuropharmacology of the naturally occurring kappa-opioid hallucinogen salvinorin A. *Pharmacol. Rev.* **2011**, *63*, 316-347.
10. (a) Simonson, B.; Morani, A. S.; Ewald, A. W. M.; Walker, L.; Kumar, N.; Simpson, D.; Miller, J. H.; Prisinzano, T. E.; Kivell, B. M. Pharmacology and anti-addiction effects of the novel κ opioid receptor agonist Mesyl Sal B, a potent and long-acting analogue of salvinorin A. *Br. J. Pharmacol.* **2014**, *172*, 515-531; (b) Zhou, Y.; Crowley, R. S.; Ben, K.; Prisinzano, T. E.; Kreek, M. J. Synergistic blockade of alcohol escalation drinking in mice by a combination of novel kappa opioid receptor agonist mesyl salvinorin B and naltrexone. *Brain Res.* **2017**, *1662*, 75-86.
11. Tidgewell, K.; Harding, W. W.; Lozama, A.; Cobb, H.; Shah, K.; Kannan, P.; Dersch, C. M.; Parrish, D.; Deschamps, J. R.; Rothman, R. B.; Prisinzano, T. E. Synthesis of salvinorin A analogues as opioid receptor probes. *J. Nat. Prod.* **2006**, *69*, 914-918.

12. Riley, A. P.; Groer, C. E.; Young, D.; Ewald, A. W.; Kivell, B. M.; Prisinzano, T. E. Synthesis and kappa-opioid receptor activity of furan-substituted salvinorin A analogues. *J. Med. Chem.* **2014**, *57*, 10464-10475.
13. Jornada, D. H.; dos Santos Fernandes, G. F.; Chiba, D. E.; de Melo, T. R.; dos Santos, J. L.; Chung, M. C. The Prodrug Approach: A Successful Tool for Improving Drug Solubility. *Molecules (Basel, Switzerland)* **2015**, *21*, 42.

5. Understanding the Metabolism of Neoclerodane Diterpenes

Results

In an effort to understand how structural changes to neoclerodane diterpenes affects their metabolic profiles, we sought to develop a robust and straightforward method that allows us to evaluate and compare the metabolic stability of salvinorin A and related diterpenes. Using rat liver microsomes, we have developed such a method as well as identified structural modifications to salvinorin A that increase its metabolic stability.

Study 1: Development of a robust system for determining the metabolic stability of neoclerodane diterpenes

Initial attempts to evaluate the metabolic stability of salvinorin A and its derivatives followed a method that was previously described by Béguin, *et. al.*¹ This method outlines 400 μ L incubations consisting of 0.25 mg/mL microsomal protein, 1 mM NADPH (omitted for control analyses), 2 mM MgCl₂, and 50 mM potassium phosphate buffer at pH 7.4 run at 37 °C from 0 to 40 minutes. Regarding the addition of the test compound, the only information specified is that “test compounds were added to the prewarmed (37 °C) incubation mixtures at the final concentration of 1 μ M.”¹ Details regarding length of the prewarming time and the compound dilution were omitted from the original procedure, and as salvinorin A is not soluble in the buffer solution used, it was presumably diluted with an organic solvent. Upon evaluation of other microsomal stability methods, we chose to employ acetonitrile as the solvent of the stock solution and a 20 min pre-incubation time.² At the specified time points after compound addition, 35 μ L of the incubation mixture was aliquoted into a quench tube containing 35 μ L of acetonitrile and tolbutamide (internal standard, 1 μ M). Samples were centrifuged and analyzed via LCMS.¹

Upon following this method to the best of our abilities given the information at hand, several limitations led us to probe the development of a more robust and reproducible method. These limitations included the large volumes of protein required for the analysis of each compound, the high number of sample tubes and thus high chance for introduction of error, and, most importantly, our inability to reproduce their results due to limited information on their exact procedural method. Using the published method as a starting point, modifications to different steps were made to determine the optimal method for metabolic stability evaluation. In the development of this new method, we identified several characteristics that our method must have to meet our needs: 1) The method should allow standardized evaluation of multiple compounds at a time with minimal intervention to limit the introduction of error; 2) The method should contain within-assay controls to quantitate the detection of the samples on each day of analysis; 3) The method should be general enough to accommodate quantitative screening of a variety of neoclerodane diterpenes without the need for radiolabeling in rat liver microsomes as well as other biological samples such as serum that may be needed in the future.

Towards the development of a more standardized approach, we quickly identified the need to move away from individual tubes for each compound at each step of the assay, including the reaction mixture, quench solution, and LCMS analysis, towards a 96-well plate for each of these steps. Microsomal stability analysis in 96-well plates have been described previously,³ although none of these methods had evaluated salvinorin A and other related diterpenes. Adapting the Béguin, *et. al.* method¹ to function in a 96-well protocol required reducing the total volume of the incubation sample to 250 μ L. With the 96-well format, the samples could all be dosed at the same time using a multi-channel pipette, and similarly, by having the quench solution ready in a separate 96-well plate, all compounds at the same time point could be quenched at exactly the same time.

This method eliminated the error previously associated between duplicate samples due to their individual tubes. It also allowed for direct analysis from the quench solution, as the HPLC is equipped to read directly from 96-well plates but not from Eppendorf tubes, which also eliminates another transfer step and potential error.

The HPLC instrument used can vary in detection limits from run to run because of its general use for not only this assay but also for other lab research. For this reason, we saw the importance of including a control within each plate to quantify the detection of each compound at the time of the run. Therefore, the first well of each row is left as a blank, with only assay buffer and the test compound added. This control allowed for the quantification of the amount of test compound added to each well, as the sample was added from the same sample plate that was used to dose the time point wells using a multi-channel pipette. Additionally, this well allowed for evaluation of the detector's signal throughout the run, as it read this control well before reading the rest of the test wells. The signal readout throughout a single plate often declined, and these control wells gave indication as to when the detection loss began as well as how the detector was functioning for that particular compound.

The most difficult characteristic to address was the ability to quantitatively measure compounds. Following the published procedure, the amount of salvinorin A was near the limit of detection of the instrument, and therefore the results were inconsistent at best. We evaluated several methods to increase the recovery of the material and therefore the quantity of compound seen by the LCMS detector. To confirm that the compounds were not adhering to the protein, the experiment was performed using the supernatant of the rat liver microsomes, but no differences were seen between these results and those using full microsomal solution. We then evaluated methods for concentrating the analysis sample, which included differing the ratio between reaction

mixture and quench solution, extractions with various organic solvents, and evaporating the buffer/quench solution followed by redissolving the residue.⁴ However, none of these methods yielded substantial improvements in detection, and as all introduced additional error and variability to the results, the LCMS sampling directly from the 1:1 assay buffer/quench solution method was continued. The analysis of the reconstituted samples did indicate that the presence of the buffer might be preventing reliable data by interfering with the internal standard's chromatography. Therefore, we introduced 1% formic acid into the quench solution and saw an improvement in the detection of the test compounds and the internal standard. Lastly, we increased the concentration of test compound in the reaction mixture to 10 μ M, which resulted in higher concentrations in the analysis solution and therefore more reproducibility from run to run.

After all of these optimizations, we were able to reproducibly generate metabolic data for neoclerodane diterpenes. However, contrary to our predicted outcomes, we did not see appreciable degradation of salvinorin A in either condition, with 80% and 100% remaining after 40 min in the presence and absence of NADPH, respectively. The high remaining values observed could potentially be attributed to the increased compound concentration that was required for optimal detection. To overcome this issue, we extended the incubation time from 40 min to 150 min in an effort to observe a differential effect between salvinorin A and its analogues while maintaining the compound amounts necessary for detection. Upon this extended incubation time, we were able to see substantial metabolism of salvinorin A in both conditions, with only 42% and 50% remaining at 150 min in the presence and absence of NADPH, respectively. Rat liver microsomes are composed of a variety of metabolizing enzymes, including CYPs, UGTs, and carboxylesterases,⁵ all of which contribute to salvinorin A's metabolism.^{4,6} In the absence of NADPH, the metabolism of salvinorin A is presumably attributed to the activity of carboxylesterases.²

The optimized method for evaluating the metabolic stability of neoclerodane diterpenes has now been established. Incubations were carried out using a total volume of 250 μL per well in 96-well plates as outlined in **Figure 5.1** in a 50 mM potassium phosphate solution with 2 mM MgCl_2 buffered to pH 7.4. Rat liver microsomes were suspended in the buffered system for a final concentration of 0.25 mg/mL. The test plate was charged with 220 μL per well of either buffer (column 1) or protein solution (columns 2-12), and the plate was stored on ice until ready to begin the assay. The quench plate was charged with 150 μL per well of the quench solution, 1 μM tolbutamide in acetonitrile with 1% formic acid, and stored on ice throughout the entirety of the experiment. A third 96-well plate was used as the aliquot source for test compound and either NADPH solution or buffer solutions in a 2:1 mixture to be added directly to the test plate. Test compound solutions were made from 5 mM acetonitrile stocks and diluted in assay buffer to 125 μM , and a 25 mM NADPH in assay buffer solution was made.

Conditions	buffer only	(-)NADPH	(+)NADPH	(-)NADPH			(+)NADPH						Conditions
Time point (min)	no protein	0	0	30	90	150	10	30	60	90	120	150	Time point
Test Plate	1	2	3	4	5	6	7	8	9	10	11	12	Well ID
Compound 1													A
													B
Compound 2													C
													D
Compound 3													E
													F
Compound 4													G
													H
Quench/ Analysis	1	2	3	4	5	6	7	8	9	10	11	12	Well ID
Compound 1													A
													B
Compound 2													C
													D
Compound 3													E
													F
Compound 4													G
													H

Figure 5.1: Layout of optimized method for microsomal stability analysis.

To begin the assay, 30 μL of corresponding test compound and NADPH or buffer mixture was added to the appropriate wells (final compound concentration of 10 μM and less than 1% acetonitrile, final NADPH concentration of 1 mM). For columns 1-3 (no protein and 0-min time points), this addition was done with the test plate on ice. For the rest of the time points, this addition was done after a 20 min pre-incubation in a 37°C incubator. At the end of each time point (0, 10, 30, 60, 90, 120, and 150 min), 150 μL of reaction mixture was removed and mixed in the corresponding wells of the quench plate. For the no protein and 0-min time points, this quench immediately followed the addition. At the end of the assay, the plates were centrifuged at 1500 rpm for 10 min to precipitate any protein remaining in the solution, followed by LCMS analysis of each of the wells.

Upon optimization of the method for determining metabolic stability of neoclerodane diterpenes, we required a straightforward analysis protocol to report our results. The published method reports their data as intrinsic clearance with the units $\frac{\mu\text{L}}{\text{min} \times \text{mg}}$, and although a similar equation for intrinsic clearance is known,⁷ we viewed this analysis readout as an overextrapolation of the data. As the goal of our work is to develop a method that allows for direct comparison of neoclerodane diterpene metabolism, a more meaningful representation of the data was warranted. The most direct method for reporting our data is to report the percent remaining at the end of the analysis period (150 min). We first determined the in-well ratio between the target peak area to internal standard peak area to normalize the amount of sample in each well. This ratio at time 0 was set to 100%, and the amount of sample present at the rest of the time points were analyzed as percent remaining. The natural log (ln) of the percent remaining was taken, and data were analyzed using linear regression analysis (GraphPad Prism 7.02; GraphPad, La Jolla, CA) to generate a linear equation. This equation was solved for $y = 150$ and the inverse ln of this value was taken to

give the percent remaining at 150 minutes. Comparison between the actual percent remaining at 150 minutes and the calculated values from the natural log curve were not significantly different. The use of the linear equation of the natural log data ensures that the data reported throughout the analysis is evaluated and reduces the chance of reporting anomalous or erroneous data from a single data point.

Statistical analysis of the percent remaining at 150 minutes was performed using a two-tailed, unpaired t-test, and p values are reported when applicable. All compounds were run in parallel assays in duplicate in ≥ 2 individual experiments. Percent remaining values are reported as the means \pm S.E.M. and represent the average of the individual experiments.

Study 2: Evaluation of the metabolic stability of salvinorin A and selected analogues

With a protocol in-hand to evaluate and report the metabolic stability of neoclerodane diterpenes, we first validated the method by evaluating dextromethorphan and verapamil, which are compounds known to be primarily metabolized by CYP450 enzymes.⁸ In our assay, we were able to distinguish significant differences between the compounds incubated in the presence and absence of NADPH (**Figure 5.2**). Both dextromethorphan and verapamil were extensively metabolized in the presence of NADPH (8.5 ± 0.9 and $26 \pm 5\%$ remaining at 150 min, respectively)

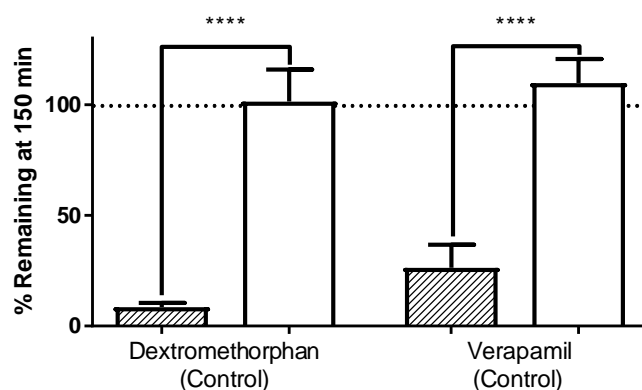
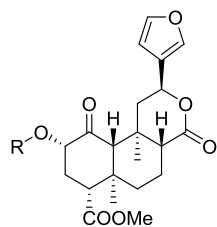


Figure 5.2: Metabolic stability of control compounds at 150 minutes in the presence (stripes) or absence (no shading) of NADPH; ****p<0.0001, via two-tailed, unpaired t-test.



R= Ac, Salvinorin A
 R= CH₂OCH₂CH₃, EOM-SVB
 R= β-tetrahydropyran, THP-SVB
 R= SO₂CH₃, Mesyl-SVB

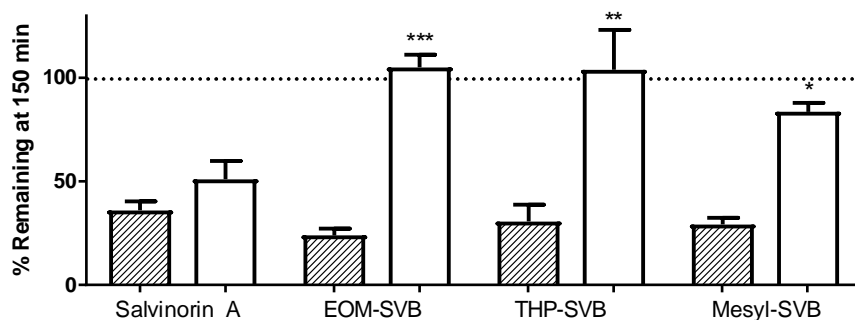


Figure 5.3: Metabolic stability of salvinorin A and known C2-analogues at 150 minutes in the presence (stripes) or absence (no shading) of NADPH; * $p < 0.05$, ** $p < 0.01$, *** $p < 0.001$ compared to salvinorin A in absence of NADPH via two-tailed, unpaired t-test.

and not in the absence of NADPH. These results confirmed that our assay is able to identify CYP450-mediated metabolism.

Upon method validation, we began the evaluation and comparison of salvinorin A and selected analogues. We began by evaluating C2-analogues of salvinorin A that had previously been confirmed as KOR agonists, and their improved metabolic stability had been presumed but not confirmed. These compounds include EOM-salvinorin B, β-tetrahydropyran salvinorin B, and Mesyl-salvinorin B (**Figure 5.3**).⁹ All three of these analogues have metabolic profiles similar to salvinorin A in the presence of NADPH, but in the absence of NADPH, they all have increased metabolic stabilities.¹⁰ Salvinorin A is extensively metabolized in the absence of NADPH (50 ± 10% remaining at 150 min), in contrast to both EOM-salvinorin B and β-THP-salvinorin B which are not readily metabolized in the absence of NADPH (105 ± 6% and 104 ± 8% remaining at 150 min, respectively) as well as Mesyl-salvinorin B which is only slightly metabolized in the absence of NADPH (84 ± 2% remaining). This method allowed us to confirm that these compounds are, in fact, more metabolically stable than salvinorin A in the absence of NADPH.

We further evaluated the salvinorin A analogues that have activity at the MOR: herkinorin, herkamide, and kurkinorin (**Figure 5.4A**). Replacing salvinorin A's acetate with a benzoate to form herkinorin significantly decreases herkinorin's metabolic stability both in the presence and

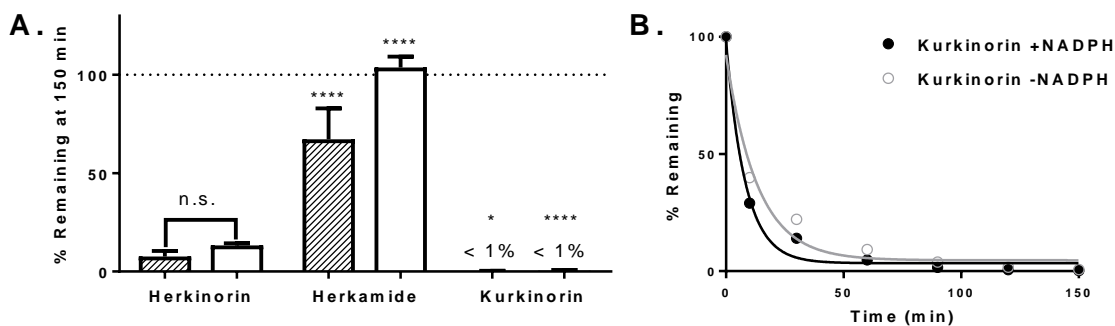


Figure 5.4: A) Metabolic stability of MOR agonists herkinorin, herkamide, and kurkinorin at 150 minutes in the presence (stripes) or absence (no shading) of NADPH; * $p < 0.05$, **** $p < 0.0001$ compared to herkinorin under the same NADPH conditions, n.s. = no significance, via two-tailed, unpaired t-test. (B) Metabolic stability curve of kurkinorin in the presence (black, filled circle) or absence (gray, open circles) of NADPH.

in the absence of NADPH (** $p < 0.01$ for both conditions, compared to salvinorin A under similar conditions, via two-tailed, unpaired t-test). Unsurprisingly with the modification of the ester to an amide linkage, herkamide is metabolically stable in the absence of NADPH, indicating an improved stability against esterases, and herkamide is also more stable than herkinorin and salvinorin A in the presence of NADPH (**** $p < 0.0001$ and ** $p < 0.01$, respectively, via two-tailed, unpaired t-test). Introduction of the unsaturation between bonds C2 and C3 as seen in kurkinorin does significantly affect the metabolic stability. In both the presence and absence of NADPH, less than 1% of kurkinorin was present after 150 min of microsomal incubation. Upon further evaluation of the metabolism curve, the majority of kurkinorin is metabolized within the first 30 min of the incubation, regardless of the NADPH conditions (**Figure 5.4B**).

Previous metabolic studies of salvinorin A that have identified metabolites indicate that the C2-acetate and the lactone are two of the most metabolically labile positions of the molecule.⁴ With the development of analogues with modifications to both of these positions (**4.1a-c – 4.5a-c**), the role of each of these moieties could be assessed through the evaluation of the metabolic stability of these dual-modified compounds. The mesyl derivatives (**4.1b – 4.5b**) and the herkinorin derivatives (**4.1c – 4.5c**) were evaluated and the results were compared to Mesyl-salvinorin B or

herkinorin, respectively, in an effort to determine how modification of the lactone affects the metabolic profile of these compounds. These analogues were chosen for this evaluation because Mesyl-salvinorin B is more stable than salvinorin A in the absence of NADPH and has a similar profile in its presence (Figure 5.3), while herkinorin is less stable than salvinorin A under both conditions (Figure 5.4).

Modifications to the lactone of Mesyl-salvinorin B have differing effects on its metabolism (Figure 5.5). The lactol derivative **4.1b** is stable to CYP450-mediated metabolism (**** $p < 0.0001$ compared to Mesyl-salvinorin B in the presence of NADPH, via two-tailed, unpaired t-test), with no significant difference in the metabolism of **4.1b** in either the presence and absence of NADPH. As would be predicted by the chemical reactivity of the acetylated hemiacetal, **4.3b** is more

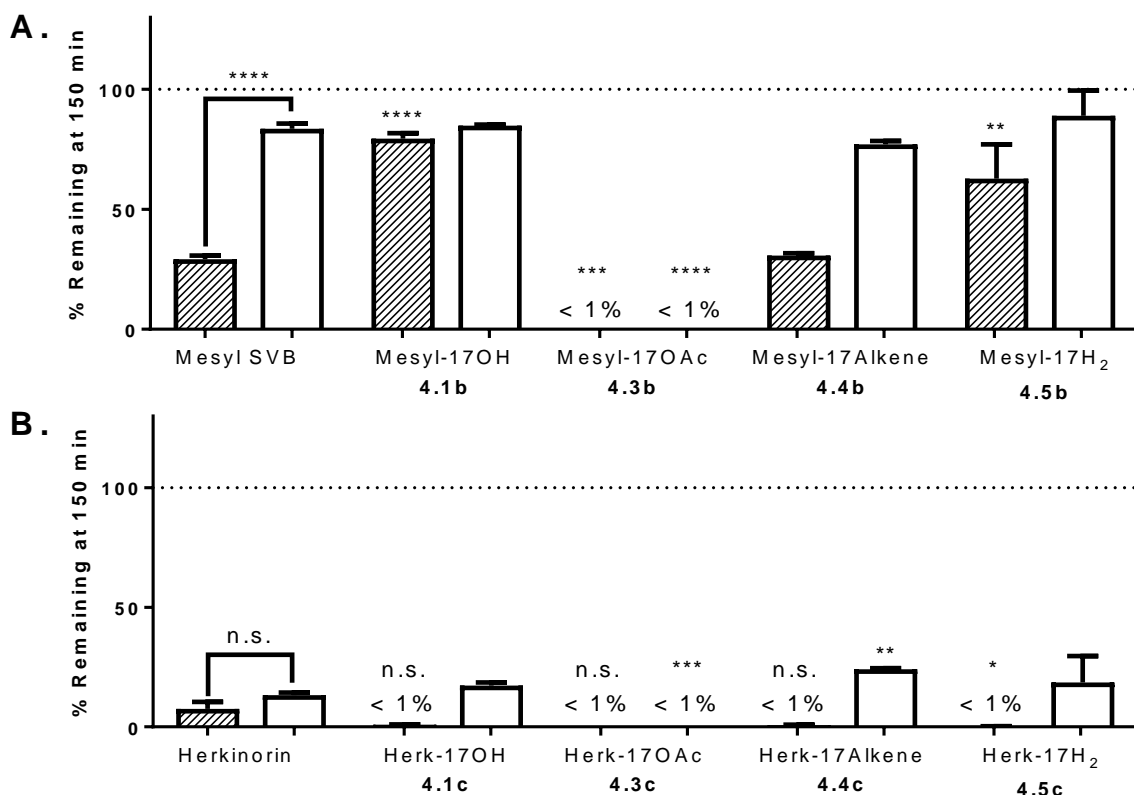
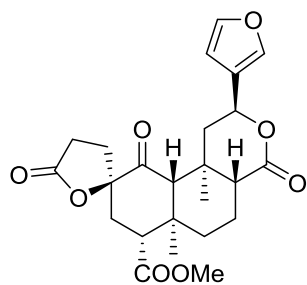


Figure 5.5: Metabolic stability of (A) Mesyl salvinorin B and its C17-modified analogues (**4.1b - 4.5b**) and (B) and herkinorin and its C17-modified analogues (**4.1c - 4.5c**) at 150 minutes in both the presence and absence of NADPH; * $p < 0.05$, ** $p < 0.01$, *** $p < 0.001$, **** $p < 0.0001$, n.s. = no significance compared to parent compound (A: Mesyl-salvinorin B or B: herkinorin) under the same NADPH conditions, via two-tailed, unpaired t-test.

significantly metabolized than the parent Mesyl-salvinorin B in both the presence and absence of NADPH. The introduction of the C8-C17 double bond in **4.4b** did not significantly affect the metabolism in either the presence or absence of NADPH compared to Mesyl-salvinorin B, indicating that the pyran moiety is metabolized similarly to the lactone. By eliminating the unstable C17-oxygen bond to form **4.5b**, the stability of the compound is increased, with a significant difference between Mesyl-salvinorin B and **4.5b** in the presence of NADPH (**p<0.01, via two-tailed, unpaired t-test). Modifying the lactone of herkinorin was not able to overcome its significant metabolism, with most of the analogues evaluated being less stable than herkinorin under similar NADPH conditions (**Figure 5.5**). **4.4c** was the only analogue to be significantly more stable than herkinorin in the absence of NADPH (**p<0.01, via two-tailed, unpaired t-test) but did not statistically differ from salvinorin A under these conditions. These results confirm that the C2-substituent is critical for metabolic stability, with the benzoate of herkinorin being readily cleaved while the mesylate of Mesyl-salvinorin B is relatively stable. Modifications to the 17-position can prevent CYP450-mediated metabolism, but these effects are not able to overcome rapid C2-metabolism.

Given that these C2-modifications have significantly improved the non-CYP450-mediated metabolic stability of salvinorin A, we set out to further explore modifications to the acetate that maintain KOR activity while improving the metabolic stability of the analogue. Through exploration of chemical modifications to the C1-C2 α -hydroxy ketone functionality, access to the spirobutyrolactone **5.1** was achieved.¹¹ This analogue is synthesized in a single step from salvinorin B and has similar potency and selectivity to salvinorin A ($EC_{50} = 0.6 \pm 0.2$ nM at KOR; >10,000 nM at MOR and DOR).



Spirobutyrolactone, **5.1**

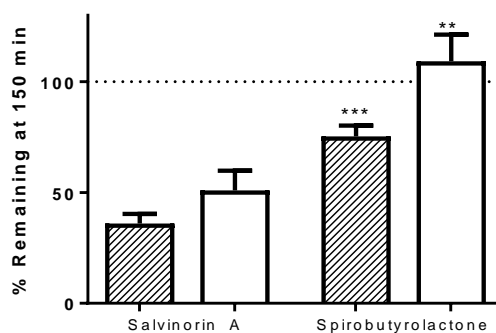


Figure 5.6: Novel spirobutyrolactone is more metabolically stable than salvinorin A at 150 minutes in both the presence (stripes, *** $p < 0.001$) and absence (no shading, ** $p < 0.01$) of NADPH, via two-tailed, unpaired t-test.

The spirobutyrolactone moiety is a rigid, conformationally constrained analogue of salvinorin A's acetate, and we hypothesized that it could provide increased metabolic liability. Using our optimized metabolic stability assay, we were able to directly compare the stability of salvinorin A to **5.1**. The metabolic stability of **5.1** in both the presence and absence of NADPH is significantly improved in comparison to salvinorin A under the same conditions ($75 \pm 5\%$ and $100 \pm 10\%$ remaining at 150 min, respectively, **Figure 5.6**). Not only does the spirobutyrolactone moiety impart resistance to non-CYP450-mediated metabolism, presumably esterases, but the CYP450-mediated oxidation is also reduced.

Conclusion

In order for salvinorin A analogues to be further investigated as drug candidates, their metabolic stability profiles must be significantly improved from that of salvinorin A. Through the development of a robust method for determining the metabolic stability of neoclerodane diterpenes, we now have the ability to directly compare the metabolic profiles of salvinorin A and its analogues. This method has allowed us to characterize the stability profiles of previously identified salvinorin A analogues as well as novel analogues recently identified and under development in our lab.

References

1. Beguin, C.; Potter, D. N.; Dinieri, J. A.; Munro, T. A.; Richards, M. R.; Paine, T. A.; Berry, L.; Zhao, Z.; Roth, B. L.; Xu, W.; Liu-Chen, L. Y.; Carlezon, W. A., Jr.; Cohen, B. M. N-methylacetamide analog of salvinorin A: a highly potent and selective kappa-opioid receptor agonist with oral efficacy. *J. Pharmacol. Exp. Ther.* **2008**, *324*, 188-195.
2. Eng, H.; Niosi, M.; McDonald, T. S.; Wolford, A.; Chen, Y.; Simila, S. T. M.; Bauman, J. N.; Warmus, J.; Kalgutkar, A. S. Utility of the carboxylesterase inhibitor bis-para-nitrophenylphosphate (BNPP) in the plasma unbound fraction determination for a hydrolytically unstable amide derivative and agonist of the TGR5 receptor. *Xenobiotica* **2010**, *40*, 369-380.
3. (a) Jayaraman, R.; Pilla Reddy, V.; Pasha, M. K.; Wang, H.; Sangthongpitag, K.; Yeo, P.; Hu, C. Y.; Wu, X.; Xin, L.; Goh, E.; New, L. S.; Ethirajulu, K. Preclinical metabolism and disposition of SB939 (Pracinostat), an orally active histone deacetylase inhibitor, and prediction of human pharmacokinetics. *Drug Metab. Dispos.* **2011**, *39*, 2219-2232; (b) Ackley, D. C.; Rockich, K. T.; Baker, T. R., Metabolic Stability Assessed by Liver Microsomes and Hepatocytes. In *Optimization in Drug Discovery: In Vitro Methods*, Yan, Z.; Caldwell, G. W., Eds. Humana Press: Totowa, NJ, 2004; pp 151-162.
4. Tsujikawa, K.; Kuwayama, K.; Miyaguchi, H.; Kanamori, T.; Iwata, Y. T.; Inoue, H. In vitro stability and metabolism of salvinorin A in rat plasma. *Xenobiotica* **2009**, *39*, 391-398.
5. Golizeh, M.; Schneider, C.; Ohlund, L. B.; Sleno, L. Dataset from proteomic analysis of rat, mouse, and human liver microsomes and S9 fractions. *Data in Brief* **2015**, *3*, 95-98.
6. Teksin, Z. S.; Lee, I. J.; Nemieboka, N. N.; Othman, A. A.; Upreti, V. V.; Hassan, H. E.; Syed, S. S.; Prisinzano, T. E.; Eddington, N. D. Evaluation of the transport, in vitro metabolism

and pharmacokinetics of Salvinorin A, a potent hallucinogen. *Eur. J. Pharm. Biopharm.* **2009**, *72*, 471-477.

7. Obach, R. S. Prediction of human clearance of twenty-nine drugs from hepatic microsomal intrinsic clearance data: An examination of in vitro half-life approach and nonspecific binding to microsomes. *Drug Metab. Disposition* **1999**, *27*, 1350-1359.

8. Thorn, H. A.; Lundahl, A.; Schrickx, J. A.; Dickinson, P. A.; Lennernas, H. Drug metabolism of CYP3A4, CYP2C9 and CYP2D6 substrates in pigs and humans. *Eur. J. Pharm. Sci.* **2011**, *43*, 89-98.

9. (a) Harding, W. W.; Tidgewell, K.; Byrd, N.; Cobb, H.; Dersch, C. M.; Butelman, E. R.; Rothman, R. B.; Prisinzano, T. E. Neoclerodane diterpenes as a novel scaffold for mu opioid receptor ligands. *J. Med. Chem.* **2005**, *48*, 4765-4771; (b) Prevatt-Smith, K. M.; Lovell, K. M.; Simpson, D. S.; Day, V. W.; Douglas, J. T.; Bosch, P.; Dersch, C. M.; Rothman, R. B.; Kivell, B.; Prisinzano, T. E. Potential drug abuse therapeutics derived from the hallucinogenic natural product salvinorin a. *MedChemComm* **2011**, *2*, 1217-1222; (c) Munro, T. A.; Duncan, K. K.; Xu, W.; Wang, Y.; Liu-Chen, L. Y.; Carlezon, W. A., Jr.; Cohen, B. M.; Beguin, C. Standard protecting groups create potent and selective kappa opioids: salvinorin B alkoxymethyl ethers. *Bioorg. Med. Chem.* **2008**, *16*, 1279-1286.

10. (a) Ewald, A. W. M.; Bosch, P. J.; Culverhouse, A.; Crowley, R. S.; Neuenswander, B.; Prisinzano, T. E.; Kivell, B. M. The C-2 derivatives of Salvinorin A, ethoxymethyl ether Sal B and β -tetrahydropyran Sal B, have anti-cocaine properties with minimal side effects. *Psychopharmacology* **2017**, DOI: 10.1007/s00213-017-4637-2; (b) Zhou, Y.; Crowley, R. S.; Ben, K.; Prisinzano, T. E.; Kreek, M. J. Synergistic blockade of alcohol escalation drinking in

mice by a combination of novel kappa opioid receptor agonist mesyl salvinorin B and naltrexone. *Brain Res.* **2017**, *1662*, 75-86.

11. Sherwood, A. M.; Crowley, R. S.; Paton, K. F.; Biggerstaff, A.; Neuenswander, B.; Day, V. W.; Kivell, B. M.; Prisinzano, T. E. Addressing structural flexibility at the A-ring on salvinorin A: Discovery of a potent kappa-opioid agonist with enhanced metabolic stability. *J. Med. Chem.* **2017**, *60*, 3866-3878.

6. Overall Conclusions

Due to the current opioid epidemic in the United States, the development of therapeutics to combat both pain and addiction is a significant medical need. Existing therapies for these disease states are in need of improvement due to a variety of side effects that often lead to under-treatment and untoward suffering of patients. The μ and κ opioid receptors (MOR and KOR, respectively) are both targets of interest in the development of pain and addiction therapies. Activation of the MOR leads to pain relief, but many agonists also elicit side effects, including tolerance and dependence that ultimately can lead to addiction. Several of these MOR-associated side effects have been attributed to the recruitment of β -arrestin-2, while the pain-relieving effects are the result of G-protein activation. Thus a compound biased towards G-protein activation over β -arrestin-2 recruitment has been pursued for the development of an analgesic therapy devoid of common side effects. Alternatively, activation of the KOR has analgesic effects without any addiction-related side effects and has been shown to reduce relapse and withdrawal symptoms in animal models of addiction, but its activation can elicit dysphoria and hallucinations. Therefore, targeting either of these receptors to elicit the beneficial effects without the associated side effects is a goal for combatting the opioid epidemic.

The natural product salvinorin A is a potent KOR that can be semisynthetically modified into a MOR agonist. As it is structurally dissimilar from the other known MOR or KOR agonists, it is an ideal lead molecule for the identification of an opioid without the side effects of the current therapies. However, several properties must be addressed in order to further pursue salvinorin A-based compounds as drug leads, including potency at the MOR and optimization of its pharmacokinetic properties.

Towards the development of a MOR agonist, the SAR about the recently-identified compound kurkinorin was undertaken, and more potent and biased analogues were identified. In particular, the 4'-benzylic alcohol derivative **3.46** (Figure 6.1) is the most potent salvinorin A-based MOR agonist identified to date, with a G-protein activation EC₅₀ value of 0.03 ± 0.01 nM. It does recruit β-arrestin-2 to a lesser extent, with an EC₅₀ value of 14 ± 1 nM in this pathway. Through exploration of the SAR of activation of these two MOR-associated pathways, the 4'-methoxymethoxy-3'-methyl derivative **3.39** was identified as a lead compound for a biased agonist as it moderately activates the G-protein pathway without any β-arrestin-2 recruitment (EC₅₀ values of 170 ± 20 nM and >25 000 nM, respectively). Based on the preliminary *in vivo* results with kurkinorin, indicating its antinociceptive activity with reduced abuse liability, and the identification of more potent and biased compounds, the kurkinorin scaffold appears to be a promising target towards the development of an analgesic therapy.

Salvinorin A's low water solubility and rapid metabolism limit its use in both animal and human studies, therefore its structure was probed in an effort towards both understanding and improving these pharmacokinetic properties. The lactone moiety was explored in the search for a point on the molecule through which the water solubility could be modulated, and the lactone carbonyl was determined to be an auxophore for both KOR and MOR binding. Analogues with polar substituents at the lactone position maintained KOR activity, and the carboxylic acid analogues **4.20α** and **4.20β** (Figure 6.1) were the first salvinorin A-based KOR agonists to have an ionizable functionality. The studies performed on the lactone of salvinorin A indicate that additional solubilizing moieties should be tolerated at this position while maintaining KOR activity. The metabolism of salvinorin A was explored through the development of a straightforward and robust method for determining the microsomal stability of salvinorin A and selected analogues. Through

this method, salvinorin A-based KOR and MOR agonists were evaluated for their metabolic stability. In comparison to salvinorin A, analogues with modifications to the C2-acetate such as EOM-salvinorin B, THP-salvinorin B, Mesyl-salvinorin B, and herkamide, were more stable to non-CYP450-dependent metabolic processes, while herkinorin and kurkinorin were not. With access to this method for evaluating metabolic stability in the laboratory, synthetic modifications can now be directly assessed for their effects on the metabolic stability of the analogues.

This work is also the first to report a systematic study of dual-modified salvinorin A analogues. The methodology developed to modify the lactone was applied to selected C2-modified salvinorin A analogues known to have unique opioid receptor activity, MOM-salvinorin B (KOR agonist), Mesyl-salvinorin B (KOR agonist with a unique binding pose from salvinorin A or MOM-salvinorin B), and herkinorin (MOR agonist). Through this systematic approach, the roles of both the lactone and the C2-derivatives were evaluated. The metabolic stability of several of these dual-modified analogues was also explored, and the analogues with a C2-mesyl and either the C17-lactol (**4.1b**) or the C17-H₂ (**4.5b**) were more stable than Mesyl-salvinorin B under CYP450-mediated metabolic conditions. These results indicate that the lactone is responsible for some of salvinorin A's CYP450-mediated degradation.

Because both of these projects compared results directly to herkinorin, the results can be extrapolated to hypothesize how kurkinorin analogues with modifications to their lactone might behave. Ultimately, as the lactone modifications to herkinorin resulted in increased β -arrestin-2 recruitment with decreased G-protein activation, the hypothesized kurkinorin lactone-modified analogue would be expected to be more biased towards β -arrestin-2 than kurkinorin. While removing the lactone from kurkinorin may prevent the metabolism at that position, the C2-ester

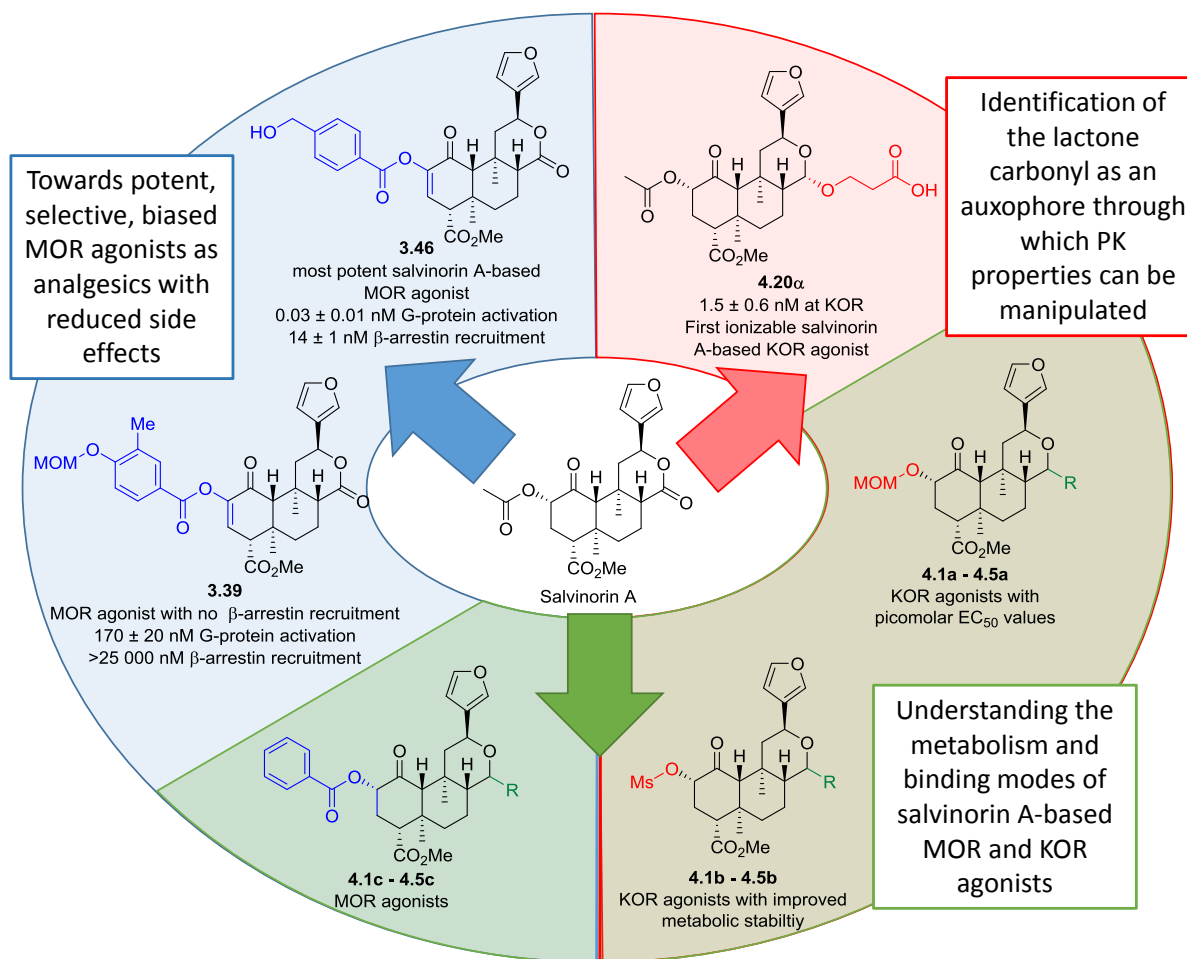


Figure 6.1: Overall conclusions and final results.

linkage is still present and very rapidly metabolized, as shown in **Figure 5.4**. Therefore the lactone modifications are not envisioned to be able to compensate for this rapid metabolism, just as they are not able to compensate for the metabolism of herkinorin.

Collectively, the studies and results described herein provide insight into the requirements of salvinorin A analogues for activation of MORs, both G-protein and β-arrestin-2 pathways, and activation of KORs, as well as functionalities that enhance or reduce metabolic stability (**Figure 6.1**). These results will help to further the exploration of salvinorin A-based compounds as potential pain and addiction therapies.

7. Supplemental Information

Supplemental Tables

Supplemental Table 1: Calculated properties and ligand efficiencies of kurkinorin derivatives.

Compound	tPSA (Å ²) ^a	sLogP ^b	HAC ^c	Ligand Efficiency ^e	LELP ^e
Herkinorin	109.1	3.7	36	0.28	13.12
Herkamide	111.9	3.3	36	0.32	10.17
Kurkinorin	109.1	3.8	36	0.34	11.19
3.18	122	3.2	36	0.24	13.16
3.19	122	3.2	36	0.32	9.90
3.2	122	3.2	36	0.31	10.23
3.21	134.9	2.6	36	0.31	8.31
3.22	131.2	3.2	38	0.31	10.32
3.23	122.2	3.9	39	0.26	14.76
3.24	109.1	5	39	0.28	17.69
3.25	109.1	3.8	35	0.35	10.96
3.26	109.1	3.8	35	0.35	10.93
3.27	135.1	2.2	35	0.29	7.47
3.28	122	3.2	35	0.32	9.85
3.29	135.1	2.2	35	N.A ^d	N.A ^d
3.30	122	3.2	35	N.A ^d	N.A ^d
3.31	109.1	3.7	37	0.25	14.51
3.32	109.1	4.1	38	0.23	17.77
3.33	109.1	4.1	38	0.27	15.12
3.34	129.3	3.5	37	0.33	10.64
3.35	129.3	3.5	37	0.34	10.39
3.36	127.6	4.2	41	0.28	14.84
3.38	127.6	4.6	41	0.23	20.34
3.39	127.6	4.1	41	0.23	18.13
3.40	129.3	3.9	38	0.33	11.73
3.41	129.3	4.2	38	0.30	13.87
3.42	129.3	4.3	38	0.28	15.35
3.43	129.3	3.8	38	0.26	14.59
3.44	122.3	3.9	39	0.31	12.58

3.45	122.3	3.9	39	0.28	13.80
3.46	129.3	3.6	38	0.38	9.49
3.47	129.3	3.6	38	0.31	11.58
3.48	118.3	3.9	39	0.28	14.08
3.49	152.2	2.9	39	0.35	8.26
3.50	152.2	2.9	39	N.A. ^d	N.A. ^d
3.51	138.2	3	40	0.30	10.12
3.52	138.2	3	40	0.29	10.31

^atPSA = total polar surface area (Å²); ^bsLogP = Wildman-Crippen calculated logP; ^cHAC = heavy atom count; ^dN.A.= not applicable. ^eProperties calculated using Forge 10.4.2 Revision: 24876, Copyright 2006-2015, Cresset BioMolecular Discovery, Ltd. Efficiency metrics calculations for herkinorin, herkamide, kurkinorin, and kurkinorin derivatives based on activity in the G-protein cAMP assay. Ligand efficiency (LE) was calculated using the following equation:

$$LE = -1.37 \times \log\left(\frac{\text{potency}, M}{\text{Heavy Atom Count}}\right).$$

Lipophilic-adjusted ligand efficiency (LELP) was calculated using the following equation: = $\frac{\text{Ligand efficiency}}{cLogP}$.

Supplemental Table 2: Calculated properties and ligand efficiencies of lactone derivatives.

Compound	tPSA (Å ²) ^a	sLogP ^b	HAC ^c	Ligand Efficiency ^e (α, if applicable)	Ligand Efficiency ^e β	LELP ^e (α, if applicable)	LELP ^e β
Salvinorin A	109	2.4	31	0.44	N.A. ^d	5.43	N.A. ^d
4.1	112	2.6	31	0.39	N.A. ^d	6.59	N.A. ^d
4.3	118	2.8	34	0.35	N.A. ^d	8.06	N.A. ^d
4.4	92	3.1	30	0.40	N.A. ^d	7.80	N.A. ^d
4.5	92	2.9	30	0.41	N.A. ^d	7.12	N.A. ^d
4.6	115.8	2.8	32	0.38	N.A. ^d	7.36	N.A. ^d
4.7	92	3.7	33	0.31	N.A. ^d	12.13	N.A. ^d
4.8	109.1	3.2	34	0.29	N.A. ^d	11.03	N.A. ^d
4.9	109.1	4.5	39	0.25	N.A. ^d	18.24	N.A. ^d
4.10	101.3	4.4	38	0.24	0.25	17.99	17.32
4.11	101.3	3.6	34	0.28	0.28	12.91	13.02
4.12	101.3	3.3	34	0.31	0.32	10.64	10.43
4.13	101.3	3	34	0.33	0.34	9.13	8.84
4.14	125	3.2	35	0.35	0.32	9.13	9.85
4.15	121.5	3	36	0.34	0.34	8.80	8.84

4.16	121.5	2.6	36	0.36	0.35	7.17	7.35
4.17	122	3	35	0.36	0.34	8.31	8.83
4.18	121.5	3.4	36	0.32	0.29	10.48	11.70
4.20	141	2.7	36	0.34	0.30	8.04	8.91

^atPSA = total polar surface area (Å²); ^bsLogP = Wildman-Crippen calculated logP; ^cHAC = heavy atom count; ^dN.A.= not applicable. ^eProperties and efficiency metrics calculated as above in **Supplemental Table 1**.

In vitro pharmacology

Cell lines and cell culture. The HitHunterTM Chinese hamster ovary cells (CHO-K1) stably expressing the human μ -opioid receptor (OPRM1, catalog # 95-0107C2) the human κ -opioid receptor (OPRK1, catalog # 95-0088C2), or the human δ -opioid receptor, (OPRD1, catalog # 95-0108C2) and the PathHunterTM Chinese hamster ovary cells stably expressing the human μ -opioid receptor β -arrestin-2 EFC cell line (catalog # 93-0213C2) were purchased from DiscoverX Corp. (Fremont, CA) and maintained in F-12 media with 10% fetal bovine serum (Life Technologies, Grand Island, NY), 1% penicillin/streptomycin/ L-glutamine (Life Technologies), and 800 μ g/mL Geneticin (Mirus Bio, Madison, WI). The media of the PathHunterTM cells was additionally supplemented with an additional 250 μ g/mL Hygromycin B (Mirus Bio). All cells were grown at 37 °C and 5% CO₂ in a humidified incubator.

Forskolin-induced cAMP accumulation. Assays proceeded as previously described.¹ Opioid receptor mediated G-protein activation was measured using the DiscoverX HitHunterTM technology. On day1, ~80% confluent CHO cells (OPRK1, OPRM1, or OPRD1) were detached from culture plates using non-enzymatic Cell Dissociation Buffer (Life Technologies) and counted using a hemocytometer. Cells were plated at 10,000 cells/well in 20 μ l Cell Plating Reagent 2 (DiscoverRx) in 384-well tissue culture plates and incubated at 37 °C overnight. On day 2, stock

solutions of all compounds were generated by dissolution in 100% DMSO to 5 mM. Stock solutions were used to make 10 serial dilutions in 100% DMSO at 100X final compound concentrations. 100X compound concentrations were diluted in assay buffer (Hank's Buffered Salt Solution (HBSS, Life Technologies) with 10 mM HEPES (Life Technologies)) containing forskolin (DiscoverX) to yield 5X compound concentrations, 100 μ M forskolin, and 5% DMSO in assay buffer. The DiscoverX HitHunter™ cAMP Assay was used according to manufacturer's instructions. Briefly, media was removed from cells, and cells were washed with 10 μ l assay buffer. Assay buffer containing antibody reagent (20 μ l/well) was added to cells. 5 μ l of 5X compound/forskolin solution were added to cells (final concentrations were 1X compound, 20 μ M forskolin, and 1% DMSO). Cells were incubated at 37 °C and 5% CO₂ for 30 minutes, followed by incubation with detection reagents according to manufacturer's instructions, and incubated at room temperature protected from light overnight. On day 3, luminescence was quantified using a Synergy 2 plate reader with Gen5 software (BioTek, Winooski, VT). Data were normalized to vehicle and forskolin only control values and analyzed using non-linear regression with GraphPad Prism 5.0.

β -arrestin-2 EFC recruitment assay. Assays proceeded as previously described.² The MOR agonist-mediated β -arrestin-2 recruitment was measured using the DiscoverX PathHunter™ technology. On day 1, ~80% confluent CHO-K1 OPRM1 β -arrestin-2 cells were detached from culture plates using nonenzymatic cell dissociation buffer (Life Technologies) and counted using a hemocytometer. Cells were plated at 5 000 cells/well in 20 μ L of Cell Plating Reagent 2 (DiscoverX) in 384-well tissue culture plates and incubated at 37 °C overnight. On day 2, stock solutions of test compounds were generated in 100% DMSO to 5 mM. The stock solutions were used to make 11 serial dilutions and then diluted to yield 5x compound concentrations in assay

buffer (Hank's Balanced Salt Solution [HBSS, Life Technologies] with 10 mM HEPES [Life Technologies]). The cells were treated with 5 μ L of the test compound solutions, final concentration of 1X compound and 1% DMSO. Cells were incubated for 90 minutes at 37°C. Cells were then treated with detection reagents, 12.5 μ L per well, according to manufacturer's instructions and incubated at room temperature for at least 1 h protected from light. Luminescence was quantified using a Synergy 2 plate reader with Gen5 Software (BioTek, Winooski, VT). Data were normalized to vehicle (no compound, 1% DMSO final concentration) to remove any background luminescence. The highest dose(s) of DAMGO was used as 100% recruitment and all data was converted to percentages based upon the DAMGO response.

Data analysis. Data were analyzed using nonlinear regression analysis in GraphPad Prism 5.0 software (GraphPad, La Jolla, CA) to generate sigmoidal dose-response curves for both the cAMP accumulation assay and the β -arrestin-2 recruitment assay. cAMP accumulation data were normalized to vehicle and forskolin only control values, and β -arrestin-2 recruitment data were normalized to vehicle and DAMGO maximum response values. All compounds were run in parallel assays in triplicate in ≥ 2 individual experiments. EC_{50} and E_{max} values are reported as the means \pm S.E.M. and represent the average of each individual experiment following nonlinear regression analysis. Bias factors were calculated using relative activity values, as shown in

Equation 2.1:

$$\log(\text{Bias Factor}) = \left(\log \left(\frac{E_{max_{test}} * EC_{50_{DAMGO}}}{EC_{50_{test}} * E_{max_{DAMGO}}} \right) \right)_{\beta\text{-arrestin}} - \left(\log \left(\frac{E_{max_{test}} * EC_{50_{DAMGO}}}{EC_{50_{test}} * E_{max_{DAMGO}}} \right) \right)_{AMP} \quad (\text{Equation 2.1})$$

Ligand-based alignment study

Ligand-based alignment studies were performed using Forge (v 10.4.2, Cresset, Litlington, Cambridgeshire, UK; <http://www.cresset-group.com/forge/>) as used previously.³ All settings were

left as default, unless noted otherwise. All compounds were imported in “use input protonation state,” as none of the compounds contain ionizable moieties. Briefly, the 2-dimensional structure of salvinorin A was imported and the preferred conformation was found using the “very accurate and slow” method in the conformation hunt mode, with a maximum of 1000 conformations evaluated. The final conformation of salvinorin A used had a conformation energy of 65.56 kcal/mol. Using the “alignment” tool, this conformation of salvinorin A was set to the “reference” role and the 2-dimensional structures of **4.4** was imported in the “prediction set.” The conformation hunt and alignment were set to “very accurate and slow” and “substructure,” respectively. The “substructure” setting weights shape similarity and alignment with the reference equally and holds the common core of the “prediction set” compounds in place while searching for the best conformation of the rest of the molecule that varies from the common core. The final conformation energies of **4.4** was 52.48 kcal/mol.

Metabolic Stability Protocol

Materials. Pooled IGS Sprague-Dawley rat liver microsomes (male, 20mg/mL) were purchased from Sekisui XenoTech, LLC (Kansas City, KS). Nicotinamide adenine dinucleotide phosphate tetrasodium salt hydrate (reduced form, NADPH, Fisher Scientific), Tolbutamide (Sigma Aldrich, St. Louis, MO), MeCN, (HPLC grade, Fisher Scientific)

In Vitro Metabolic Stability in Rat Liver Microsomes. Incubations were carried out in 96-well plates with 250 μ L per well. The reaction mixtures were in a 50 mM potassium phosphate buffer solution with 2 mM MgCl₂ and buffered to pH 7.4. Rat liver microsomes solution, 220 μ L, (protein suspended in buffered system for final concentration of 0.25 mg/mL) was added to all wells. The assay plate was pre-warmed to 37°C in an incubator (no CO₂ injection or humidity) for 20 minutes. The 0-minute time points were performed on ice, with the exception of compound **5.1** t = 0 samples

which were prewarmed to prevent compound from crashing out of solution. To begin the assay, 20 μL of test compound (5mM stock solution in MeCN [Fisher Scientific, HPLC grade] diluted in assay buffer to 125 μM , for final compound concentration of 10 μM and less than 1% MeCN in well) and 10 μL of NADPH in buffer (final concentration of 1mM) were added to the wells. At the end of each time point (0, 10, 30, 60, 90, 120, and 150 min), 150 μL of reaction mix was removed and mixed in a separate 96-well plate containing 150 μL of quench solution per well (1 μM tolbutamide in MeCN with 1% formic acid). The quench plate was stored on ice until the end of the assay. For the test samples without NADPH, the same procedure as above was conducted with the addition of 10 μL buffer instead of the NADPH solution, and time points were collected at 0, 30, 90, and 150 min. At the end of all time points, the plate was centrifuged at 1500 rpm for 10 min. to precipitate any protein remaining in the solution. The amount of compound remaining was quantified using LCMS. The plate wells were analyzed using liquid chromatography-high resolution mass spectrometry on a Waters Acquity UPLC coupled to a Waters LCT Premier TOF mass spectrometer. The chromatography utilized a Waters Acquity HSS T3 C18 column (2.1 \times 50mm, 1.8 μm) with a guard column of the same stationary phase (2.1 \times 5mm, 1.8 μm) and was run with gradient elution, using water and acetonitrile with 0.1% formic acid, from 40% to 80% acetonitrile over 3.4 minutes and held at 80% acetonitrile for 0.4 minutes. The flow rate was 0.25ml/min and the injection volume was 15 μL . Each well was sampled twice.

Data analysis. The ratio between the target area peak to internal standard peak was used throughout the data to normalize the amount of sample in each well. This ratio at time 0 was set to 100%, and the amount of sample present at the rest of the time points were analyzed as percent remaining. The \ln of the % remaining was taken, and data were analyzed using linear regression analysis in GraphPad Prism 5.0 software (GraphPad, La Jolla, CA). The linear equation generated

in GraphPad was solved for $y = 150$ and the inverse \ln of this value was taken to give the % remaining at 150 min. Statistical analysis of the % remaining at 150 min was performed using a two-tailed, unpaired t-test, and p values are reported when applicable. All compounds were run in parallel assays in duplicate in ≥ 2 individual experiments. % remaining values are reported as the means \pm S.E.M. and represent the average of each individual experiment.

Chemistry

General experimental procedures. Salvinorin A was isolated from the leaves of *Salvia divinorum* and converted to salvinorin B as previously described.⁴ All other chemical reagents were purchased from commercial suppliers and used without further purification. All solvents were obtained from a solvent purification system in which solvent was passed through two columns of activated alumina under argon. Reactions performed in standard glassware were performed under an atmosphere of argon using glassware dried overnight in an oven at 120 °C and cooled under a stream of argon. Reactions were monitored by thin-layer chromatography (TLC) on 0.25 mm Analtech GHLF silica gel plates and visualized using a UV Lamp (254 nm) and vanillin solution. Flash column chromatography was performed on silica gel (4-63 μ m) from Sorbent Technologies. ¹H and ¹³C NMR were recorded a 500 MHz Bruker AVIII spectrometer equipped with a cryogenically-cooled carbon observe probe or a 400 MHz Bruker AVIIIHD spectrometer using tetramethyl silane as an internal standard. Chemical shifts (δ) are reported in ppm and coupling constants (J) are reported in Hz. High-resolution mass spectrum (HRMS) was performed on a LCT Premier (Micromass Ltd., Manchester UK) time of flight mass spectrometer with an electrospray ion source in either positive or negative mode. Melting points were measured with a Thomas Capillary Melting Point Apparatus and are uncorrected. HPLC was carried out on either an Agilent 1100 series HPLC system with diode array detection at 209 nm on an Agilent Eclipse XDB-C18

column (250 × 10 mm, 5 mm) or a Waters Acquity UPLC with a photodiode array UV detector and an LCT Premiere TOF mass spectrometer on a Waters Acquity HSS T3 C-18 column (2.1 × 50mm, 1.8 μm). Compounds were identified as ≥90% pure by HPLC before all *in vitro* and ≥95% before all *in vivo* analyses.

Compounds from Chapter 3:

General coupling procedure using standard benchtop glassware:

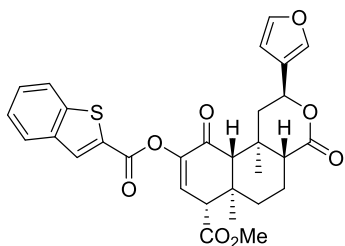
An oven-dried flask was charged with **3.1** and **3.2** (mixture) (40 mg, 0.103 mmol), EDC·HCl (29.5 mg, 0.154 mmol), DMAP (18.8 mg, 0.154 mmol), and the appropriate benzoic acid (0.154 mmol). To the flask was added CH₂Cl₂ (8 mL). After stirring overnight at r.t. the reaction was quenched with HCl (1 M, 8 mL) and the organic layer rinsed sequentially with saturated NaHCO₃ (8 mL) and brine (8 mL) then dried over Na₂SO₄. The solvent was evaporated and the resulting residue purified by FCC (30-35% EtOAc/Pentane). Compounds <95% pure as indicated by HPLC were further purified by reverse phase semi-preparatory HPLC.

General procedure for deprotection of MOM-protected phenol coupling products:

To a dry flask under Ar was added MOM-protected coupling product (0.07 mmol), carbon tetrabromide (CBr₄) (0.035 mmol, 0.5 eq.), triphenylphosphine (PPh₃) (0.035 mmol, 0.5 eq.), and dichloroethane (3mL).⁵ Reaction was heated to 40 °C overnight. If reaction was not complete as monitored by TLC the following day, a second addition of 0.5eq. of both CBr₄ and PPh₃ was added and the reaction was allowed to stir at 40 °C for a second night. Upon reaction completion as seen by TLC, the solvent was evaporated and the compound was purified via FCC (40% EtOAc/Pentane).

General procedure for deprotection of TBS-protected benzyl alcohol coupling products:

To a flask containing crude TBS-protected coupling product (0.2 mmol) was added a 1:1 mixture of MeOH and acetone (6 mL total) followed by a solution of KHSO₄ (0.1 mmol, 0.5 eq.) in 3 mL of H₂O.⁶ Reaction is a white suspension after water addition. Reaction stirred overnight at r.t. Upon reaction completion, as monitored by TLC, the solvent was evaporated and the product was extracted from water (10 mL) into EtOAc (3x 10 mL). The combined organic layers were washed with brine, dried over Na₂SO₄, and solvent was removed. The compound was purified by FCC (50% EtOAc/Pentane).



Methyl (2S,4aR,6aR,7R,10aR,10bR)-9-((benzo[b]thiophene-2-

carbonyl)oxy)-2-(furan-3-yl)-6a,10b-dimethyl-4,10-dioxo-1,4,4a,5,6,6a,7,10,10a,10b-

decahydro-2H-benzo[f]isochromene-7-carboxylate (3.24). ¹H NMR (500 MHz, CDCl₃) 8.20 (d,

J = 0.7 Hz, 1H), 7.90 (td, J = 7.5, 1.0 Hz, 2H), 7.50 (ddd, J = 8.2, 7.0, 1.3 Hz, 1H), 7.47 – 7.43 (m,

1H), 7.43 – 7.37 (m, 2H), 6.72 (d, J = 2.2 Hz, 1H), 6.39 (dd, J = 1.9, 0.9 Hz, 1H), 5.55 (dd, J =

11.5, 5.2 Hz, 1H), 3.81 (s, 3H), 3.60 (d, J = 2.2 Hz, 1H), 3.08 (dd, J = 13.7, 5.3 Hz, 1H), 2.47 (s,

1H), 2.24 – 2.17 (m, 2H), 2.15 – 2.10 (m, 1H), 1.77 – 1.72 (m, 1H), 1.71 – 1.64 (m, 2H), 1.39 (s,

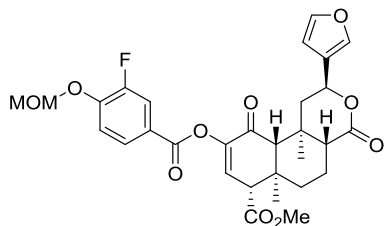
3H), 1.25 (s, 3H). ¹³C NMR (126 MHz, CDCl₃) δ 190.65, 171.36, 170.28, 160.54, 145.06, 143.67,

142.79, 139.36, 138.53, 132.51, 131.11, 130.37, 127.54, 125.85, 125.40, 125.16, 122.81, 108.44,

72.06, 63.47, 56.46, 52.51, 51.35, 44.22, 43.80, 38.44, 35.86, 17.94, 16.83, 14.85. HRMS

calculated for C₃₀H₂₈O₈S [M+Na]⁺: 549.1561 (found); 549.1578 (calcd). Melting point: 114-116

°C.



Methyl

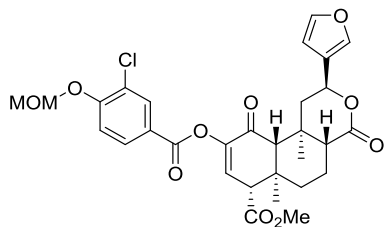
(2S,4aR,6aR,7R,10aR,10bR)-9-((3-fluoro-4-

(methoxymethoxy)benzoyl)oxy)-2-(furan-3-yl)-6a,10b-dimethyl-4,10-dioxo-

1,4,4a,5,6,6a,7,10,10a,10b-decahydro-2H-benzo[f]isochromene-7-carboxylate (3.36). ¹H

NMR (500 MHz, CDCl₃) 7.95 – 7.71 (m, 2H), 7.46 – 7.37 (m, 2H), 6.65 (d, J = 2.2 Hz, 1H), 6.39 (dd, J = 2.0, 0.9 Hz, 1H), 5.54 (dt, J = 11.6, 5.8 Hz, 1H), 5.31 (s, 2H), 3.80 (s, 3H), 3.59 (d, J = 2.3 Hz, 1H), 3.52 (d, J = 1.2 Hz, 3H), 3.06 (dd, J = 13.7, 5.4 Hz, 1H), 2.46 (s, 1H), 2.25 – 2.16 (m, 2H), 2.16 – 2.08 (m, 1H), 1.79 – 1.63 (m, 3H), 1.57 – 1.48 (m, 1H), 1.37 (s, 3H), 1.23 (s, 3H). ¹³C NMR (126 MHz, CDCl₃) δ 190.86, 171.37, 170.36, 163.34, 152.20 (d, J = 247.7 Hz), 149.99 (d, J = 10.7 Hz), 145.34, 143.68, 139.36, 130.05, 127.42, 125.41, 122.10, 118.22 (d, J = 20.5 Hz), 116.44, 108.44, 95.08, 72.05, 63.46, 56.64, 56.48, 52.49, 51.37, 44.21, 43.80, 38.45, 35.85, 17.94, 16.82, 14.86. HRMS calculated for C₃₀H₃₁O₁₀F [M+Na]⁺: 593.1788 (found); 593.1799 (calcd).

Melting point: 88-90 °C.



Methyl

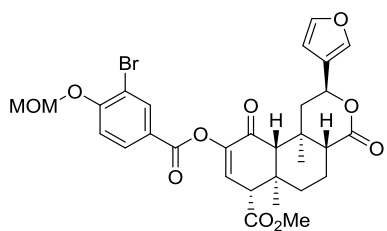
(2S,4aR,6aR,7R,10aR,10bR)-9-((3-chloro-4-

(methoxymethoxy)benzoyl)oxy)-2-(furan-3-yl)-6a,10b-dimethyl-4,10-dioxo-

1,4,4a,5,6,6a,7,10,10a,10b-decahydro-2H-benzo[f]isochromene-7-carboxylate (3.37). ¹H

NMR (500 MHz, CDCl₃) 8.14 (dd, J = 3.4, 2.2 Hz, 1H), 7.97 (dd, J = 8.7, 2.1 Hz, 1H), 7.44 – 7.36 (m, 2H), 7.24 (s, 1H), 6.65 (d, J = 2.2 Hz, 1H), 6.39 (dd, J = 1.9, 0.9 Hz, 1H), 5.54 (dd, J = 11.5, 5.5 Hz, 1H), 5.34 (d, J = 1.5 Hz, 2H), 3.80 (s, 3H), 3.59 (d, J = 2.2 Hz, 1H), 3.52 (d, J = 1.2 Hz,

4H), 3.06 (dd, $J = 13.7, 5.4$ Hz, 1H), 2.46 (s, 1H), 2.24 – 2.15 (m, 1H), 2.16 – 2.09 (m, 1H), 1.78 – 1.61 (m, 3H), 1.37 (s, 3H), 1.23 (s, 3H). ^{13}C NMR (126 MHz, CDCl_3) δ 190.85, 171.37, 170.35, 163.26, 157.28, 145.34, 143.68, 139.36, 132.45, 130.45, 130.03, 125.40, 123.62, 122.33, 115.04, 108.44, 94.79, 72.05, 63.45, 56.63, 56.48, 52.49, 51.37, 44.21, 43.79, 38.46, 35.85, 17.94, 16.82, 14.86. HRMS calculated for $\text{C}_{30}\text{H}_{31}\text{O}_{10}\text{Cl}$ $[\text{M}+\text{Na}]^+$: 587.1754 (found); 587.1679 (calcd). Melting point: 108-110 °C.



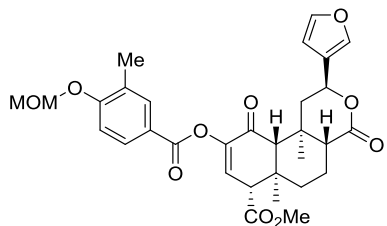
Methyl

(2S,4aR,6aR,7R,10aR,10bR)-9-((3-bromo-4-

(methoxymethoxy)benzoyl)oxy)-2-(furan-3-yl)-6a,10b-dimethyl-4,10-dioxo-

1,4,4a,5,6,6a,7,10,10a,10b-decahydro-2H-benzo[f]isochromene-7-carboxylate (3.38). ^1H

NMR (500 MHz, CDCl_3) 8.31 (dd, $J = 2.9, 2.1$ Hz, 1H), 8.06 – 7.95 (m, 1H), 7.48 – 7.35 (m, 2H), 7.21 (d, $J = 8.7$ Hz, 1H), 6.65 (d, $J = 2.2$ Hz, 1H), 6.39 (dd, $J = 2.0, 0.9$ Hz, 1H), 5.59 – 5.50 (m, 1H), 5.33 (d, $J = 1.6$ Hz, 2H), 3.80 (s, 3H), 3.73 (dd, $J = 5.3, 3.3$ Hz, 1H), 3.59 (d, $J = 2.3$ Hz, 1H), 3.52 (d, $J = 1.3$ Hz, 3H), 3.06 (dd, $J = 13.7, 5.2$ Hz, 1H), 2.47 (s, 1H), 2.24 – 2.16 (m, 2H), 1.82 – 1.52 (m, 3H), 1.37 (s, 3H), 1.23 (s, 3H). ^{13}C NMR (126 MHz, CDCl_3) δ 190.84, 171.37, 170.35, 163.11, 158.15, 145.33, 143.67, 139.36, 135.57, 131.17, 130.02, 125.40, 122.72, 114.78, 112.54, 108.44, 94.75, 72.05, 63.43, 56.63, 56.47, 52.48, 51.35, 44.21, 43.78, 38.45, 35.84, 17.94, 16.81, 14.85. HRMS calculated for $\text{C}_{30}\text{H}_{31}\text{O}_{10}\text{Br}$ $[\text{M}+\text{Na}]^+$: 631.1156 (found); 631.1173 (calcd). Melting point: 84-87 °C.

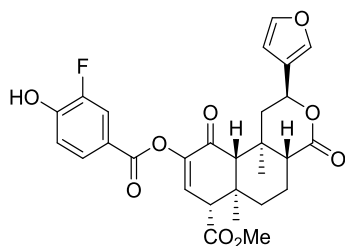


Methyl (2S,4aR,6aR,7R,10aR,10bR)-2-(furan-3-yl)-9-((4-

(methoxymethoxy)-3-methylbenzoyl)oxy)-6a,10b-dimethyl-4,10-dioxo-

1,4,4a,5,6,6a,7,10,10a,10b-decahydro-2H-benzo[f]isochromene-7-carboxylate (3.39). ¹H

NMR (500 MHz, CDCl₃) 8.01 – 7.84 (m, 2H), 7.43 – 7.35 (m, 2H), 7.15 – 7.04 (m, 1H), 6.62 (d, J = 2.2 Hz, 1H), 6.39 (dd, J = 1.9, 0.9 Hz, 1H), 5.54 (dd, J = 11.5, 5.2 Hz, 1H), 5.27 (s, 2H), 3.79 (s, 3H), 3.59 (d, J = 2.2 Hz, 1H), 3.48 (s, 3H), 3.07 (dd, J = 13.7, 5.4 Hz, 1H), 2.47 (s, 1H), 2.27 (s, 3H), 2.25 – 2.16 (m, 2H), 2.11 (dt, J = 13.0, 2.7 Hz, 1H), 1.76 – 1.60 (m, 3H), 1.37 (s, 3H), 1.23 (s, 3H). ¹³C NMR (126 MHz, CDCl₃) δ 191.05, 171.41, 170.45, 164.47, 159.93, 145.58, 143.64, 139.37, 132.91, 130.05, 129.71, 127.53, 125.47, 121.00, 112.87, 108.47, 94.04, 72.07, 63.45, 56.53, 56.21, 52.41, 51.38, 44.17, 43.81, 38.48, 35.85, 17.98, 16.81, 16.23, 14.86. HRMS calculated for C₃₁H₃₄O₁₀ [M+H]⁺: 567.2222 (found); 567.2225 (calcd). Melting point: 99-102 °C.



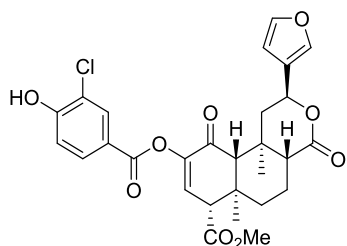
Methyl (2S,4aR,6aR,7R,10aR,10bR)-9-((3-fluoro-4-

hydroxybenzoyl)oxy)-2-(furan-3-yl)-6a,10b-dimethyl-4,10-dioxo-1,4,4a,5,6,6a,7,10,10a,10b-

decahydro-2H-benzo[f]isochromene-7-carboxylate (3.40). ¹H NMR (500 MHz, CDCl₃) 7.91 –

7.76 (m, 2H), 7.47 – 7.32 (m, 2H), 7.07 (t, J = 8.5 Hz, 1H), 6.65 (d, J = 2.2 Hz, 1H), 6.39 (dd, J = 1.9, 0.9 Hz, 1H), 5.54 (dd, J = 11.5, 5.3 Hz, 1H), 3.80 (s, 3H), 3.59 (d, J = 2.2 Hz, 1H), 3.06 (dd, J = 13.6, 5.3 Hz, 1H), 2.47 (s, 1H), 2.25 – 2.16 (m, 2H), 2.12 (dt, J = 12.9, 2.6 Hz, 1H), 1.80 – 1.56

(m, 3H), 1.37 (s, 3H), 1.23 (s, 3H). ^{13}C NMR (126 MHz, CDCl_3) δ 190.96, 171.44, 170.37, 163.30, 150.40 (d, $J = 239.3$ Hz), 148.91 (d, $J = 14.2$ Hz), 145.31, 143.68, 139.36, 130.09, 128.03, 125.37, 120.96, 117.74 (d, $J = 20.0$ Hz), 117.28, 108.43, 72.07, 63.43, 56.47, 52.50, 51.36, 44.21, 43.78, 38.45, 35.84, 17.93, 16.81, 14.86. HRMS calculated for $\text{C}_{28}\text{H}_{27}\text{O}_9\text{F}$ $[\text{M}+\text{H}]^+$: 527.173 (found); 527.1711 (calcd). Melting point: 134-136 °C.



Methyl (2S,4aR,6aR,7R,10aR,10bR)-9-((3-chloro-4-

hydroxybenzoyl)oxy)-2-(furan-3-yl)-6a,10b-dimethyl-4,10-dioxo-1,4,4a,5,6,6a,7,10,10a,10b-

decahydro-2H-benzo[f]isochromene-7-carboxylate (3.41). ^1H NMR (500 MHz, CDCl_3) 8.12 (d,

$J = 2.0$ Hz, 1H), 7.95 (dd, $J = 8.4, 1.9$ Hz, 1H), 7.45 – 7.33 (m, 2H), 7.09 (d, $J = 8.6$ Hz, 1H), 6.66

(d, $J = 2.1$ Hz, 1H), 6.39 (s, 1H), 6.26 (s, 1H), 5.55 (dd, $J = 11.6, 5.3$ Hz, 1H), 3.80 (s, 3H), 3.60

(d, $J = 2.2$ Hz, 1H), 3.49 (q, $J = 7.0$ Hz, 0H), 3.05 (dd, $J = 13.7, 5.3$ Hz, 1H), 2.48 (s, 1H), 2.24 –

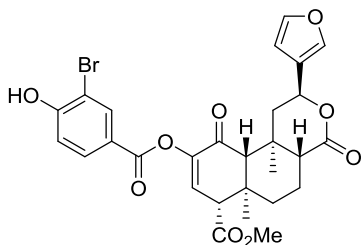
2.16 (m, 2H), 2.16 – 2.02 (m, 1H), 1.78 – 1.59 (m, 3H), 1.37 (s, 3H), 1.23 (s, 3H). ^{13}C NMR (126

MHz, CDCl_3) δ 190.99, 171.50, 170.41, 163.21, 156.17, 145.28, 143.72, 139.40, 131.63, 131.14,

130.16, 125.34, 121.60, 120.26, 116.32, 108.46, 72.10, 63.36, 56.46, 52.57, 51.36, 44.25, 43.73,

38.45, 35.83, 17.94, 16.86, 14.87. HRMS calculated for $\text{C}_{28}\text{H}_{27}\text{ClO}_9$ $[\text{M}+\text{H}]^+$: 543.1406 (found);

543.1417 (calcd). Melting point: 127-129 °C (decomp).



Methyl (2S,4aR,6aR,7R,10aR,10bR)-9-((3-bromo-4-

hydroxybenzoyl)oxy)-2-(furan-3-yl)-6a,10b-dimethyl-4,10-dioxo-1,4,4a,5,6,6a,7,10,10a,10b-

decahydro-2H-benzo[f]isochromene-7-carboxylate (3.42). ^1H NMR (500 MHz, CDCl_3) 8.27 (d,

$J = 2.1$ Hz, 1H), 7.99 (dd, $J = 8.6, 2.1$ Hz, 1H), 7.45 – 7.35 (m, 2H), 7.09 (d, $J = 8.5$ Hz, 1H), 6.65

(d, $J = 2.2$ Hz, 1H), 6.39 (dd, $J = 1.9, 0.9$ Hz, 1H), 5.54 (dd, $J = 11.5, 5.3$ Hz, 1H), 3.80 (s, 3H),

3.59 (d, $J = 2.2$ Hz, 1H), 3.06 (dd, $J = 13.6, 5.3$ Hz, 1H), 2.47 (s, 1H), 2.20 (td, $J = 10.7, 9.6, 4.8$

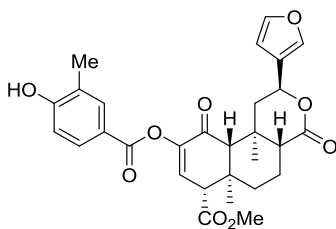
Hz, 2H), 2.15 – 2.09 (m, 1H), 1.77 – 1.60 (m, 3H), 1.37 (s, 3H), 1.23 (s, 3H). ^{13}C NMR (126 MHz,

CDCl_3) δ 190.91, 171.35, 170.33, 162.98, 157.00, 145.30, 143.67, 139.36, 134.63, 131.84, 130.06,

125.39, 122.04, 116.06, 110.32, 108.43, 72.04, 63.43, 56.47, 52.49, 51.36, 44.22, 43.79, 38.46,

35.84, 17.94, 16.81, 14.86. HRMS calculated for $\text{C}_{28}\text{H}_{27}\text{O}_9\text{Br}$ $[\text{M}+\text{H}]^+$: 587.0909 (found);

587.0911 (calcd). Melting point: 144-147 °C.



Methyl (2S,4aR,6aR,7R,10aR,10bR)-2-(furan-3-yl)-9-((4-

hydroxy-3-methylbenzoyl)oxy)-6a,10b-dimethyl-4,10-dioxo-1,4,4a,5,6,6a,7,10,10a,10b-

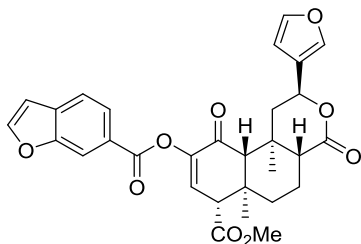
decahydro-2H-benzo[f]isochromene-7-carboxylate (3.43). ^1H NMR (500 MHz, CDCl_3) 7.90

(dd, $J = 2.2, 0.9$ Hz, 1H), 7.85 (dd, $J = 8.4, 2.2$ Hz, 1H), 7.45 – 7.33 (m, 2H), 6.82 (d, $J = 8.4$ Hz,

1H), 6.62 (d, $J = 2.2$ Hz, 1H), 6.38 (dd, $J = 2.0, 0.9$ Hz, 1H), 5.54 (dd, $J = 11.5, 5.3$ Hz, 1H), 3.80

(s, 3H), 3.59 (d, $J = 2.3$ Hz, 1H), 3.07 (dd, $J = 13.7, 5.4$ Hz, 1H), 2.47 (s, 1H), 2.28 (s, 3H), 2.25 –

2.15 (m, 2H), 2.11 (dt, $J = 12.9, 2.5$ Hz, 1H), 1.76 – 1.63 (m, 3H), 1.38 (s, 3H), 1.23 (s, 3H). ^{13}C NMR (126 MHz, CDCl_3) δ 191.16, 171.46, 170.47, 164.43, 158.90, 145.55, 143.66, 139.37, 133.59, 130.30, 129.78, 125.45, 124.18, 120.55, 114.93, 108.46, 72.10, 63.47, 56.54, 52.43, 51.41, 44.20, 43.82, 38.50, 35.85, 17.97, 16.82, 15.61, 14.88. HRMS calculated for $\text{C}_{29}\text{H}_{30}\text{O}_9$ $[\text{M}+\text{H}]^+$: 523.1963 (found); 593.1938 (calcd). Melting point: 124-127 °C (decomp).



Methyl

(2S,4aR,6aR,7R,10aR,10bR)-9-((benzofuran-6-

carbonyloxy)-2-(furan-3-yl)-6a,10b-dimethyl-4,10-dioxo-1,4,4a,5,6,6a,7,10,10a,10b-

decahydro-2H-benzo[f]isochromene-7-carboxylate (3.44). ^1H NMR (500 MHz, CDCl_3) 8.28 (p,

$J = 0.8$ Hz, 1H), 8.01 (dd, $J = 8.2, 1.5$ Hz, 1H), 7.80 (d, $J = 2.2$ Hz, 1H), 7.68 (dd, $J = 8.2, 0.6$ Hz,

1H), 7.49 – 7.36 (m, 2H), 6.85 (dd, $J = 2.2, 1.0$ Hz, 1H), 6.68 (d, $J = 2.2$ Hz, 1H), 6.39 (dd, $J = 1.9,$

0.9 Hz, 1H), 5.60 – 5.46 (m, 1H), 3.81 (s, 3H), 3.61 (d, $J = 2.2$ Hz, 1H), 3.08 (dd, $J = 13.7, 5.3$ Hz,

1H), 2.49 (s, 1H), 2.26 – 2.17 (m, 1H), 2.13 (dt, $J = 13.2, 2.7$ Hz, 1H), 1.79 – 1.58 (m, 2H), 1.39

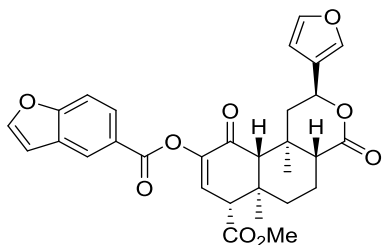
(s, 3H), 1.26 (d, $J = 2.2$ Hz, 5H). ^{13}C NMR (126 MHz, CDCl_3) δ 190.96, 171.39, 170.40, 164.78,

154.30, 148.44, 145.52, 143.65, 139.36, 132.69, 129.94, 125.42, 124.74, 124.25, 121.15, 113.87,

108.45, 106.92, 72.07, 63.46, 56.51, 52.47, 51.38, 44.20, 43.80, 38.46, 35.85, 17.96, 16.84, 14.86.

HRMS calculated for $\text{C}_{30}\text{H}_{28}\text{O}_9$ $[\text{M}+\text{H}]^+$: 533.1819 (found); 533.1806 (calcd). Melting point: 156-

157 °C (decomp).



Methyl (2S,4aR,6aR,7R,10aR,10bR)-9-((benzofuran-5-

carbonyl)oxy)-2-(furan-3-yl)-6a,10b-dimethyl-4,10-dioxo-1,4,4a,5,6,6a,7,10,10a,10b-

decahydro-2H-benzo[f]isochromene-7-carboxylate (3.45). ^1H NMR (500 MHz, CDCl_3) 8.46 –

8.40 (m, 1H), 8.08 (dd, $J = 8.7, 1.8$ Hz, 1H), 7.71 (d, $J = 2.2$ Hz, 1H), 7.57 (dt, $J = 8.7, 0.8$ Hz,

1H), 7.48 – 7.34 (m, 2H), 6.86 (dd, $J = 2.2, 1.0$ Hz, 1H), 6.68 (d, $J = 2.2$ Hz, 1H), 6.39 (dd, $J = 2.0,$

0.9 Hz, 1H), 5.62 – 5.47 (m, 1H), 3.80 (s, 3H), 3.61 (d, $J = 2.2$ Hz, 1H), 3.08 (dd, $J = 13.7, 5.3$ Hz,

1H), 2.49 (s, 1H), 2.20 (ddt, $J = 12.6, 6.9, 3.5$ Hz, 2H), 2.12 (dt, $J = 13.1, 2.7$ Hz, 1H), 1.79 – 1.63

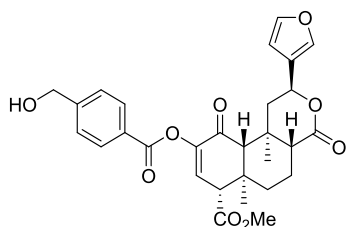
(m, 3H), 1.39 (s, 3H), 1.25 (s, 3H). ^{13}C NMR (126 MHz, CDCl_3) δ 191.04, 171.39, 170.42, 164.76,

157.96, 146.54, 145.52, 143.65, 139.36, 129.92, 127.66, 126.67, 125.41, 124.67, 123.18, 111.63,

108.45, 107.13, 72.06, 63.45, 56.51, 52.47, 51.38, 44.20, 43.80, 38.47, 35.85, 17.96, 16.84, 14.86.

HRMS calculated for $\text{C}_{30}\text{H}_{28}\text{O}_9$ $[\text{M}+\text{H}]^+$: 533.1797 (found); 533.1806 (calcd). Melting point: 112-

115 $^\circ\text{C}$.



Methyl (2S,4aR,6aR,7R,10aR,10bR)-2-(furan-3-yl)-9-

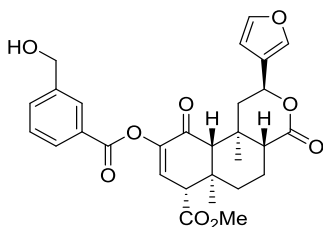
((4-(hydroxymethyl)benzoyl)oxy)-6a,10b-dimethyl-4,10-dioxo-1,4,4a,5,6,6a,7,10,10a,10b-

decahydro-2H-benzo[f]isochromene-7-carboxylate (3.46). ^1H NMR (500 MHz, CDCl_3) 8.14 –

8.02 (m, 2H), 7.48 (d, $J = 8.3$ Hz, 2H), 7.45 – 7.36 (m, 2H), 6.66 (d, $J = 2.2$ Hz, 1H), 6.39 (dd, $J =$

1.9, 0.9 Hz, 1H), 5.54 (dd, $J = 11.5, 5.3$ Hz, 1H), 4.80 (d, $J = 2.6$ Hz, 2H), 3.80 (s, 3H), 3.60 (d, J

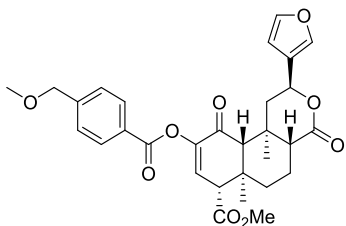
= 2.3 Hz, 1H), 3.06 (dd, J = 13.7, 5.3 Hz, 1H), 2.47 (s, 1H), 2.24 – 2.16 (m, 2H), 2.12 (dt, J = 13.4, 2.7 Hz, 1H), 1.90 (s, 1H), 1.77 – 1.64 (m, 3H), 1.37 (s, 3H), 1.24 (s, 3H). ¹³C NMR (126 MHz, CDCl₃) δ 190.90, 171.40, 170.39, 164.40, 147.14, 145.42, 143.66, 139.37, 130.53, 129.99, 127.37, 126.55, 125.40, 108.44, 72.06, 64.57, 63.44, 56.49, 52.48, 51.36, 44.19, 43.79, 38.45, 35.84, 17.94, 16.82, 14.85. HRMS calculated for C₂₉H₃₀O₉ [M+H]⁺: 523.1964 (found); 523.1963 (calcd). Melting point: 115-118 °C.



Methyl (2S,4aR,6aR,7R,10aR,10bR)-2-(furan-3-yl)-9-((3-

(hydroxymethyl)benzoyl)oxy)-6a,10b-dimethyl-4,10-dioxo-1,4,4a,5,6,6a,7,10,10a,10b-

decahydro-2H-benzo[f]isochromene-7-carboxylate (3.47). ¹H NMR (500 MHz, CDCl₃) 8.11 (d, J = 1.7 Hz, 1H), 8.03 (d, J = 7.8 Hz, 1H), 7.64 (d, J = 7.6 Hz, 1H), 7.48 (t, J = 7.7 Hz, 1H), 7.43 – 7.37 (m, 2H), 6.66 (d, J = 2.1 Hz, 1H), 6.39 (d, J = 1.8 Hz, 1H), 5.54 (dd, J = 11.5, 5.3 Hz, 1H), 4.77 (s, 2H), 3.80 (s, 3H), 3.60 (d, J = 2.1 Hz, 1H), 3.06 (dd, J = 13.7, 5.4 Hz, 1H), 2.47 (s, 1H), 2.24 – 2.07 (m, 3H), 1.85 (s, 1H), 1.77 – 1.63 (m, 3H), 1.37 (s, 3H), 1.24 (s, 3H). ¹³C NMR (126 MHz, CDCl₃) δ 190.87, 171.38, 170.37, 164.47, 145.45, 143.67, 141.56, 139.38, 132.31, 129.98, 129.49, 128.90, 128.56, 128.52, 125.44, 108.45, 72.06, 64.63, 63.49, 56.51, 52.46, 51.38, 44.22, 43.82, 38.48, 35.86, 17.97, 16.82, 14.86. HRMS calculated for C₂₉H₃₀O₉ [M+H]⁺: 523.1959 (found); 523.1963 (calcd). Melting point: 104-106 °C.



Methyl (2S,4aR,6aR,7R,10aR,10bR)-2-((4-

(methoxymethyl)benzoyl)oxy)-6a,10b-dimethyl-4,10-dioxo-1,4,4a,5,6,6a,7,10,10a,10b-

decahydro-2H-benzo[f]isochromene-7-carboxylate (3.48). ^1H NMR (500 MHz, CDCl_3) 8.17 –

8.00 (m, 2H), 7.47 – 7.43 (m, 2H), 7.41 (dd, $J = 1.6, 0.9$ Hz, 1H), 7.39 (t, $J = 1.7$ Hz, 1H), 6.66 (d,

$J = 2.1$ Hz, 1H), 6.39 (dd, $J = 1.9, 0.9$ Hz, 1H), 5.60 – 5.48 (m, 1H), 4.54 (s, 2H), 3.80 (s, 3H), 3.60

(d, $J = 2.3$ Hz, 1H), 3.42 (s, 3H), 3.07 (dd, $J = 13.7, 5.3$ Hz, 1H), 2.47 (s, 1H), 2.20 (ddd, $J = 12.2,$

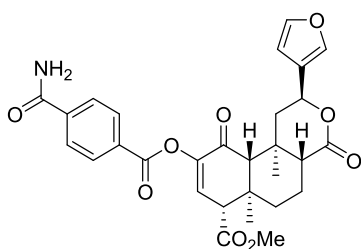
6.4, 3.1 Hz, 2H), 2.12 (dt, $J = 13.1, 2.7$ Hz, 1H), 1.80 – 1.62 (m, 3H), 1.38 (s, 3H), 1.24 (s, 3H).

^{13}C NMR (126 MHz, CDCl_3) δ 190.90, 171.38, 170.38, 164.42, 145.43, 144.74, 143.66, 139.36,

130.42, 129.97, 127.42, 127.28, 125.41, 108.44, 73.90, 72.05, 63.45, 58.45, 56.49, 52.47, 51.37,

44.19, 43.80, 38.45, 35.84, 17.95, 16.82, 14.85. HRMS calculated for $\text{C}_{30}\text{H}_{32}\text{O}_9$ $[\text{M}+\text{Na}]^+$:

559.1922 (found); 559.1944 (calcd). Melting point: 135-140 $^\circ\text{C}$.



Methyl

(2S,4aR,6aR,7R,10aR,10bR)-9-((4-

carbamoylbenzoyl)oxy)-2-((furan-3-yl)-6a,10b-dimethyl-4,10-dioxo-

1,4,4a,5,6,6a,7,10,10a,10b-decahydro-2H-benzo[f]isochromene-7-carboxylate (3.49). ^1H

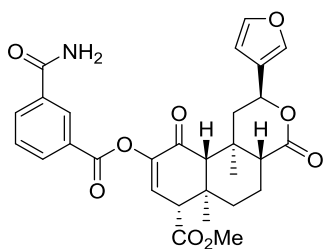
NMR (500 MHz, CDCl_3) 8.26 – 8.09 (m, 2H), 7.96 – 7.84 (m, 2H), 7.47 – 7.30 (m, 2H), 6.70 (d,

$J = 2.2$ Hz, 1H), 6.39 (dd, $J = 1.9, 0.9$ Hz, 1H), 6.11 (d, $J = 21.1$ Hz, 1H), 5.67 (s, 1H), 5.55 (dd, J

$= 11.6, 5.5$ Hz, 1H), 3.81 (s, 3H), 3.80 (s, 1H), 3.61 (d, $J = 2.2$ Hz, 1H), 3.06 (dd, $J = 13.7, 5.3$ Hz,

1H), 2.48 (s, 1H), 2.26 – 2.14 (m, 2H), 2.16 – 2.09 (m, 1H), 1.46 (s, 1H), 1.38 (s, 3H), 1.35 (s,

1H), 1.25 (s, 3H). ¹³C NMR (126 MHz, CDCl₃) δ 190.73, 171.45, 170.31, 167.89, 163.67, 145.28, 143.70, 139.37, 137.95, 131.36, 130.58, 130.26, 127.60, 125.38, 108.43, 72.02, 63.48, 56.47, 52.53, 51.36, 44.25, 43.81, 38.45, 35.86, 17.94, 16.83, 14.86. HRMS calculated for C₂₉H₃₀NO₉ [M+Na]⁺: 558.1728 (found); 558.1740 (calcd). Melting point: 201-203 °C.



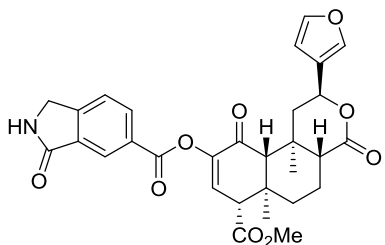
Methyl

(2S,4aR,6aR,7R,10aR,10bR)-9-((3-

carbamoylbenzoyl)oxy)-2-(furan-3-yl)-6a,10b-dimethyl-4,10-dioxo-

1,4,4a,5,6,6a,7,10,10a,10b-decahydro-2H-benzo[f]isochromene-7-carboxylate (3.50). ¹H

NMR (500 MHz, CDCl₃) 8.51 (dt, J = 4.1, 1.7 Hz, 1H), 8.25 (ddt, J = 7.8, 3.2, 1.4 Hz, 1H), 8.14 (dq, J = 7.8, 1.4 Hz, 1H), 7.59 (td, J = 7.8, 1.5 Hz, 1H), 7.44 – 7.36 (m, 2H), 6.68 (d, J = 2.2 Hz, 1H), 6.54 – 6.40 (m, 1H), 6.38 (dt, J = 1.8, 0.9 Hz, 1H), 6.19 – 5.99 (m, 1H), 5.53 (ddd, J = 13.2, 8.3, 5.4 Hz, 1H), 3.80 (d, J = 4.1 Hz, 3H), 3.62 (d, J = 2.2 Hz, 1H), 3.04 (td, J = 13.5, 12.9, 5.3 Hz, 1H), 2.50 (s, 1H), 2.20 (ddd, J = 16.0, 9.1, 3.2 Hz, 2H), 2.12 (dd, J = 13.3, 3.6 Hz, 1H), 1.81 – 1.62 (m, 2H), 1.44 (s, 1H), 1.36 (s, 3H), 1.23 (s, 3H). ¹³C NMR (126 MHz, CDCl₃) δ 190.82, 171.43, 170.35, 168.05, 163.77, 145.24, 143.68, 139.40, 133.96, 133.46, 133.07, 130.31, 129.21, 128.84, 128.70, 125.35, 108.44, 72.02, 63.34, 56.40, 52.52, 51.26, 44.24, 43.71, 38.40, 35.82, 17.93, 16.82, 14.84. HRMS calculated for C₂₉H₃₀NO₉ [M+Na]⁺: 558.1754 (found); 558.1740 (calcd). Melting point: 199-201 °C.

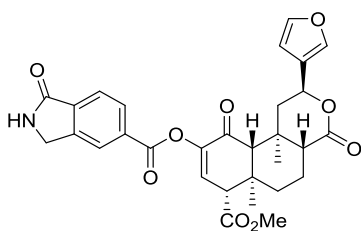


(2S,4aR,6aR,7R,10aR,10bR)-2-(furan-3-yl)-7-

(methoxycarbonyl)-6a,10b-dimethyl-4,10-dioxo-1,4,4a,5,6,6a,7,10,10a,10b-decahydro-2H-

benzo[f]isochromen-9-yl 3-oxoisindoline-5-carboxylate (3.51). ¹H NMR (500 MHz, CDCl₃)

8.69 – 8.56 (m, 1H), 8.31 (ddd, J = 7.9, 2.8, 1.6 Hz, 1H), 7.61 (dd, J = 7.9, 0.9 Hz, 1H), 7.55 (s, 1H), 7.42 (ddt, J = 2.6, 1.8, 0.8 Hz, 1H), 7.39 (t, J = 1.7 Hz, 1H), 6.70 (d, J = 2.2 Hz, 1H), 6.39 (dd, J = 1.9, 0.9 Hz, 1H), 5.58 – 5.51 (m, 1H), 4.56 (d, J = 2.7 Hz, 2H), 3.81 (s, 2H), 3.62 (d, J = 2.2 Hz, 1H), 3.06 (dd, J = 13.8, 5.5 Hz, 1H), 2.49 (s, 1H), 2.25 – 2.17 (m, 2H), 2.16 – 2.08 (m, 1H), 2.01 (s, 1H), 1.84 – 1.61 (m, 3H), 1.38 (s, 3H), 1.25 (s, 3H). ¹³C NMR (126 MHz, CDCl₃) δ 190.72, 171.39, 170.54, 170.30, 163.77, 148.90, 145.30, 143.67, 139.36, 133.48, 132.80, 130.23, 128.75, 126.06, 125.40, 123.69, 108.44, 72.04, 63.41, 56.43, 52.50, 51.32, 45.89, 44.22, 43.75, 38.40, 35.85, 17.94, 16.81, 14.84. HRMS calculated for C₃₀H₂₉O₉N [M+H]⁺: 548.1910 (found); 548.19151 (calcd). Melting point: 189-194 °C.



(2S,4aR,6aR,7R,10aR,10bR)-2-(furan-3-yl)-7-

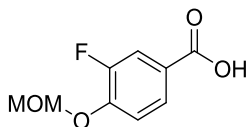
(methoxycarbonyl)-6a,10b-dimethyl-4,10-dioxo-1,4,4a,5,6,6a,7,10,10a,10b-decahydro-2H-

benzo[f]isochromen-9-yl 1-oxoisindoline-5-carboxylate (3.52). ¹H NMR (500 MHz, CDCl₃)

8.26 – 8.19 (m, 2H), 7.97 (d, J = 8.3 Hz, 1H), 7.60 (s, 1H), 7.45 – 7.25 (m, 3H), 6.71 (d, J = 2.1 Hz, 1H), 6.39 (dd, J = 2.0, 0.9 Hz, 1H), 5.54 (dd, J = 11.5, 5.4 Hz, 1H), 4.54 (s, 2H), 3.81 (s, 3H), 3.62 (d, J = 2.2 Hz, 1H), 3.07 (td, J = 13.5, 6.8 Hz, 1H), 2.50 (s, 1H), 2.20 (td, J = 11.5, 10.0, 4.7

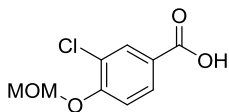
Hz, 2H), 2.14 – 2.09 (m, 1H), 2.01 (s, 0H), 1.76 (ddd, J = 14.3, 10.7, 5.4 Hz, 2H), 1.69 (d, J = 13.1 Hz, 1H), 1.38 (s, 3H), 1.25 (s, 3H).z ¹³C NMR (126 MHz, CDCl₃) δ 190.79, 171.32, 170.48, 170.32, 163.90, 145.27, 143.69, 143.57, 139.37, 136.85, 131.43, 130.30, 130.20, 125.37, 125.31, 124.05, 108.43, 72.00, 63.42, 56.43, 52.53, 51.31, 45.65, 44.26, 43.76, 38.42, 35.85, 17.93, 16.82, 14.84. HRMS calculated for C₃₀H₂₉O₉N [M+NH₄]⁺: 565.2198 (found); 565.2186 (calcd). Melting point: 229-232 °C.

General procedure for MOM-protection of benzoic acids: Protection of the phenolic acids were accomplished following the published protection method.⁷ To a solution of 3'-X-4'-hydroxybenzoic acid (1.6 mmol) in DCM (5 mL) stirring under Ar at 0 °C was added N,N-diisopropylethylamine (DIPEA) (1.5 mL, 5.5 eq.) followed by the dropwise addition of methoxymethylchloride (0.7 mL, 5.5 eq.). This reaction was allowed to stir at r.t. for 48 h before being quenched with sat. aq. NH₄Cl solution (20 mL) and extracted into DCM (3x). The combined organic layers were dried over Na₂SO₄ and the solvent was removed under reduced pressure to afford the crude ether ester. To a solution of the crude ester in MeOH (20mL), a 15% aq. NaOH solution was added and the mixture was heated for 70 °C for 3 h. After cooling the reaction to 0 °C, the pH was adjusted to 5 with 6M HCl to precipitate a white solid. This solid was filtered to give the desired MOM-protected phenolic acid.



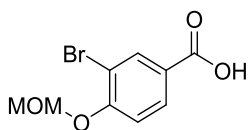
3-Fluoro-4-(methoxymethoxy)benzoic acid. ¹H NMR (400 MHz, CDCl₃)

7.90 – 7.80 (m, 2H), 7.26 (d, J = 16.5 Hz, 1H), 5.31 (s, 2H), 3.53 (s, 3H). ¹³C NMR (101 MHz, DMSO) δ 165.99, 151.48 (d, J = 245.0 Hz), 148.21 (d, J = 10.7 Hz), 126.44 (d, J = 3.1 Hz), 124.69 (d, J = 6.2 Hz), 116.85 (d, J = 19.6 Hz), 116.67, 94.67, 56.09. HRMS calculated for C₉H₉O₄F [M-H]⁻: 199.0457 (found); 199.0412 (calcd). Melting point: 163-164 °C.



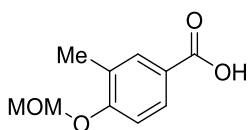
3-Chloro-4-(methoxymethoxy)benzoic acid. ^1H NMR (400 MHz, CDCl_3) δ

8.14 (d, $J = 2.1$ Hz, 1H), 7.97 (dd, $J = 8.8, 2.1$ Hz, 1H), 7.24 (d, $J = 8.7$ Hz, 1H), 5.34 (s, 2H), 3.53 (s, 3H). ^{13}C NMR (101 MHz, CDCl_3) δ 169.80, 157.22, 132.43, 130.36, 123.56, 123.29, 114.98, 94.85, 56.63. HRMS calculated for $\text{C}_9\text{H}_9\text{O}_4\text{Cl}$ $[\text{M}-\text{H}]^-$: 215.0154 (found); 215.0117 (calcd). Melting point: 169-170 $^\circ\text{C}$.



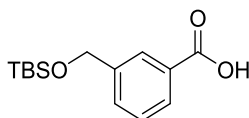
3-Bromo-4-(methoxymethoxy)benzoic acid. ^1H NMR (400 MHz, CDCl_3)

8.30 (d, $J = 2.1$ Hz, 1H), 8.00 (dd, $J = 8.7, 2.1$ Hz, 1H), 7.20 (d, $J = 8.7$ Hz, 1H), 5.33 (s, 2H), 3.53 (s, 3H). ^{13}C NMR (101 MHz, CDCl_3) δ 169.88, 158.11, 135.58, 131.09, 123.70, 114.70, 112.51, 94.81, 56.64. HRMS calculated for $\text{C}_9\text{H}_9\text{O}_4\text{Br}$ $[\text{M}-\text{H}]^-$: 258.9652 (found); 258.9611 (calcd). Melting point: 167-168 $^\circ\text{C}$.



4-(methoxymethoxy)-3-methylbenzoic acid. ^1H NMR NMR (400 MHz,

$\text{DMSO}-d_6$) δ 7.80 – 7.70 (m, 2H), 7.10 (d, $J = 9.2$ Hz, 1H), 5.30 (s, 2H), 3.39 (s, 3H), 2.51 (p, $J = 1.9$ Hz, 3H). ^{13}C NMR (101 MHz, DMSO) δ 167.07, 158.32, 131.75, 128.80, 126.44, 123.36, 112.92, 93.72, 55.78, 15.89. HRMS calculated for $\text{C}_{10}\text{H}_{12}\text{O}_4$ $[\text{M}-\text{H}]^-$: 195.0708 (found); 195.0657 (calcd). Melting point: 136-138 $^\circ\text{C}$.

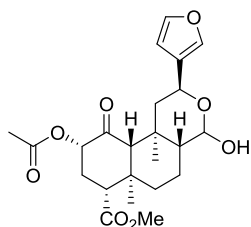


3-(((tert-butyl dimethylsilyl)oxy)methyl)benzoic acid. To a mixture of 3-

hydroxymethyl benzoic acid (304 mg, 2.0 mmol) in DMF (4mL) was added *tert*-Butyldimethylsilyl chloride (724 mg, 4.8 mmol), and imidazole (300 mg, 4.4 mmol). The reaction

mixture was stirred at r.t. overnight before being quenched with acetone (20mL). The reaction mixture was chilled in the refrigerator for 20 minutes and then the white precipitate was filtered. The solvent was evaporated, and the crude product was dissolved in THF (10mL) and sat. aq. NaHCO₃ solution (10mL) to hydrolyze the formed silyl ester. The reaction was allowed to stir at r.t. overnight followed by evaporation of the THF. The resulting mixture was acidified with 1N HCl (30 mL) and extracted with Et₂O (3x 20mL). The combined organic extracts were washed with brine (50 mL), dried (Na₂SO₄) and concentrated. The resulting clear, pale yellow oil was used without further purification. ¹H NMR (400 MHz, CDCl₃) δ 8.06 (dp, J = 1.5, 0.8 Hz, 1H), 8.00 (ddt, J = 7.9, 1.9, 1.0 Hz, 1H), 7.61 (ddq, J = 7.6, 2.0, 0.9 Hz, 1H), 7.45 (t, J = 7.7 Hz, 1H), 4.80 (t, J = 0.8 Hz, 2H), 0.96 (d, J = 0.8 Hz, 9H), 0.12 (d, J = 0.6 Hz, 6H). ¹³C NMR (101 MHz, CDCl₃) δ 171.94, 142.04, 131.46, 129.22, 128.80, 128.46, 127.74, 64.46, 25.94, 18.47, -5.25. HRMS calculated for C₁₄H₂₂O₃Si [M-H]⁻: 265.1302 (found); 265.1265 (calcd). Melting point: 40-42 °C.

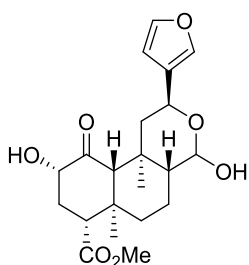
Compounds from Chapter 4:



Methyl (2S,4aR,6aR,7R,9S,10aR,10bS)-9-acetoxy-2-(furan-3-yl)-4-hydroxy-6a,10b-dimethyl-10-oxododecahydro-2H-benzo[f]isochromene-7-carboxylate (4.1).

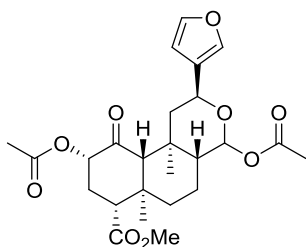
To a dry flask flushed with Ar salvinorin A (1g, 2.31 mmol) was added and dissolved in THF (100mL). The reaction mixture was cooled with a dry ice/acetone bath to -78°C. Upon cooling completely, a 1M solution of DIBALH in hexanes was added dropwise (18.5 mmol, 18.5 mL). The reaction mixture was kept stirring and maintained at -78°C until TLC indicated complete consumption of starting material, usually 4 hours. Reaction flask was moved to an ice/water bath and was quenched at 0 °C with sat. aq. NH₄Cl solution (100mL). The resulting mixture stirred for

20 minutes and was allowed to reach room temperature. The mixture was then extracted with EtOAc (3 x 150 mL). The combined organic extracts were washed with brine (200 mL), dried (Na₂SO₄) and concentrated. The crude mixture of lactols (**4.1** and **4.2**, 0.830g) was carried into the next acetylation reaction without further purification. Compound previously described; characterization matches literature. **4.1** was purified via FCC (40% EtOAc in DCM) for pharmacological assays. HRMS calculated for C₂₃H₃₀O₈ [M+Na]⁺: 457.1825 (found); 457.1838 (calcd). Melting point: 170-171 °C.



Methyl (2S,4aR,6aR,7R,9S,10aR,10bS)-2-(furan-3-yl)-4,9-dihydroxy-

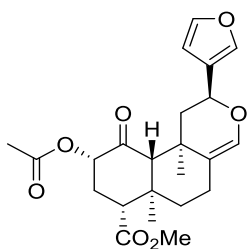
6a,10b-dimethyl-10-oxododecahydro-2H-benzo[f]isochromene-7-carboxylate (4.2). ¹H NMR (400 MHz, CDCl₃) 7.40 – 7.35 (m, 2H), 6.52 – 6.27 (m, 1H), 5.34 – 5.07 (m, 1H), 4.91 (dd, J = 11.6, 2.4 Hz, 1H), 4.83 (dd, J = 8.7, 6.1 Hz, 1H), 4.26 – 3.95 (m, 1H), 3.70 (s, 3H), 3.67 (dd, J = 13.4, 3.4 Hz, 1H), 3.05 (d, J = 6.2 Hz, 1H), 2.70 (dt, J = 13.8, 3.0 Hz, 1H), 2.43 (dtd, J = 13.4, 7.9, 3.2 Hz, 1H), 2.20 (ddd, J = 33.5, 13.0, 2.4 Hz, 1H), 2.08 (s, 1H), 2.05 (s, 1H), 2.04 – 1.96 (m, 1H), 1.83 (dq, J = 13.6, 3.5 Hz, 1H), 1.72 (dt, J = 13.3, 3.4 Hz, 1H), 1.65 (s, 1H), 1.57 (dd, J = 13.4, 4.2 Hz, 1H), 1.42 (s, 3H), 1.22 – 1.13 (m, 1H), 1.06 (s, 2H).



(2S,4aR,6aR,7R,9S,10aR,10bS)-2-(furan-3-yl)-7-

(methoxycarbonyl)-6a,10b-dimethyl-10-oxododecahydro-2H-benzo[f]isochromene-4,9-diyl

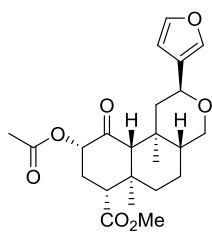
diacetate (4.3). To a flask containing the crude mix of **4.1** and **4.2** (0.83g, 2.1 mmol) in DCM (100mL) was added DMAP (0.516 g, 4.2 mmol) and Ac₂O (0.4mL, 4.2mmol). The reaction mixture was stirred at r.t. overnight and was then quenched with MeOH (25mL). The quenched reaction was allowed to stir for 20 min. and followed by solvent evaporation. The crude residue was dissolved in DCM (100mL) and sat. aq. NaHCO₃ solution (100mL) and organic layers separated. Following further extraction with DCM (2 x 50 mL) the organic layers were combined and washed with H₂O (90 mL) and 1M HCl (10 mL). The combined organic extracts were washed with brine (100 mL), dried (Na₂SO₄) and concentrated to afford **4.3** (0.933 g, 93% yield). ¹H NMR (400 MHz, CDCl₃) δ 7.38 – 7.31 (m, 2H), 6.37 (s, 1H), 5.83 (d, J = 8.0 Hz, 1H), 5.22 – 5.06 (m, 1H), 4.95 (dd, J = 11.2, 2.1 Hz, 1H), 3.71 (d, J = 1.1 Hz, 3H), 2.76 (dd, J = 11.1, 5.9 Hz, 1H), 2.27 (dd, J = 13.6, 8.7 Hz, 2H), 2.15 (d, J = 1.2 Hz, 3H), 2.10 (d, J = 1.2 Hz, 3H), 2.08 (s, 1H), 1.72 (d, J = 13.2 Hz, 1H), 1.62 (d, J = 12.1 Hz, 0H), 1.55 (d, J = 5.1 Hz, 3H), 1.46 (s, 3H), 1.37 (d, J = 8.6 Hz, 2H), 1.30 – 1.16 (m, 2H), 1.09 (s, 2H). ¹³C NMR (126 MHz, CDCl₃) δ 202.24, 171.84, 169.97, 169.67, 143.05, 139.39, 125.62, 108.94, 92.46, 75.06, 66.98, 65.40, 53.76, 51.90, 49.62, 44.34, 42.44, 38.70, 35.96, 30.89, 21.17, 20.68, 17.58, 16.81, 14.89. HRMS calculated for C₂₅H₃₂O₉ [M+Na]⁺: 499.1937 (found); 499.1944 (calcd). Melting point: 184-185 °C.



Methyl (2S,6aR,7R,9S,10aS,10bR)-9-acetoxy-2-(furan-3-yl)-6a,10b-dimethyl-10-oxo-1,5,6,6a,7,8,9,10,10a,10b-decahydro-2H-benzo[f]isochromene-7-

carboxylate (4.4). Compound previously described; characterization matches literature. ¹H NMR (400 MHz, CDCl₃) δ 7.46 – 7.33 (m, 2H), 6.37 (dd, J = 1.9, 0.9 Hz, 1H), 6.27 (d, J = 1.7 Hz, 1H),

5.12 (ddd, $J = 10.6, 8.6, 1.0$ Hz, 1H), 4.78 (dd, $J = 11.6, 1.9$ Hz, 1H), 3.70 (s, 3H), 2.79 – 2.66 (m, 1H), 2.39 – 2.22 (m, 4H), 2.16 (s, 3H), 2.13 (s, 1H), 1.94 (ddd, $J = 14.6, 4.6, 2.6$ Hz, 1H), 1.70 (ddd, $J = 13.0, 4.3, 2.5$ Hz, 1H), 1.53 (d, $J = 0.7$ Hz, 3H), 1.49 (dd, $J = 13.4, 4.6$ Hz, 1H), 1.44 – 1.34 (m, 1H), 1.15 (s, 3H). ^{13}C NMR (126 MHz, CDCl_3) δ 202.97, 172.01, 169.91, 143.20, 139.31, 137.05, 125.80, 117.01, 108.66, 75.17, 66.59, 65.44, 53.45, 51.80, 44.34, 42.76, 40.01, 34.06, 30.59, 22.74, 22.59, 20.66, 15.39. HRMS calculated for $\text{C}_{23}\text{H}_{28}\text{O}_7$ $[\text{M}+\text{Na}]^+$: 439.1727 (found); 439.1733 (calcd). Melting point: 77-79 °C.



Methyl (2S,6aR,7R,9S,10aR,10bS)-9-acetoxy-2-(furan-3-yl)-6a,10b-

dimethyl-10-oxododecahydro-2H-benzo[f]isochromene-7-carboxylate (4.5). Synthesized as previously described, following General Method A (below) using triethylsilane. Alternate reaction conditions: To a flask containing **4.3** (0.105 mmol, 0.05 g) under Ar was added CH_3CN (3 mL) and triethylsilane (0.315 mmol, 3 equiv.). The reaction flask was cooled to 0°C with an ice bath and trimethylsilyl trifluoromethanesulfonate (0.21 mmol, 2 equiv.) was added dropwise. Reaction was monitored by TLC for consumption of starting material, generally within an hour, at which time it was quenched with sat. aq. NaHCO_3 solution (3 mL) and extracted with EtOAc (3x 5 mL). The combined organic extracts were washed with brine (50 mL), dried (Na_2SO_4) and concentrated. Purification by FCC (30% EtOAc in Pentane) afforded **4.5** as a white solid (49% yield). Compound previously described; characterization matches literature. ^1H NMR (400 MHz, CDCl_3) δ 7.33 (d, $J = 1.4$ Hz, 2H), 6.35 (t, $J = 1.5$ Hz, 1H), 5.22 – 5.07 (m, 1H), 4.71 (dd, $J = 11.5, 2.4$ Hz, 1H), 3.71 (s, 3H), 3.58 (d, $J = 7.6$ Hz, 2H), 2.83 – 2.70 (m, 1H), 2.36 – 2.21 (m, 2H), 2.16 (s, 3H), 2.13 (dd, $J = 13.1, 2.5$ Hz, 1H), 2.10 (d, $J = 2.3$ Hz, 1H), 1.73 – 1.59 (m, 2H), 1.54 – 1.41 (m, 1H), 1.39 (s,

3H), 1.38 – 1.24 (m, 2H), 1.24 – 1.16 (m, 1H), 1.09 (s, 3H). HRMS calculated for C₂₃H₃₀O₇ [M+Na]⁺: 441.1873 (found); 441.1889 (calcd). Melting point: 126-128 °C.

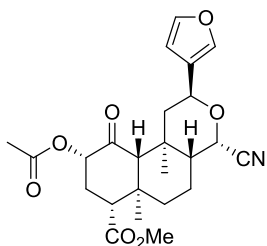
General Methods of Substituting at 17:

General Method A: A solution of **4.3** (40 mg) and the appropriate nucleophile (5 equiv.) in DCM (3mL) was cooled to -78 °C with a dry ice/acetone bath. BF₃•Et₂O (0.02 mL, 1.2 equiv.) was added dropwise to the stirring reaction. Reaction was kept at -78 °C and monitored for consumption of **4.3** by TLC, usually 1h, and was then transferred to ice water bath for another hour. Reaction was quenched at 0 °C with sat. aq. NaHCO₃ solution. The resulting mixture stirred for 30 minutes and was then extracted with DCM (3 x 25 mL). The combined organic extracts were washed with brine (50 mL), dried (Na₂SO₄) and concentrated. The resulting solid was purified by flash column chromatography.

General Method B: A solution of **4.3** (40 mg) in the appropriate alcohol (neat, 3mL) was cooled to 0-5°C with an ice/water bath. HCl in dioxane (4M solution, 20 equiv.) was added dropwise to the stirring reaction. Reaction was kept between 0-5 °C (to prevent dioxane freezing) and monitored for consumption of **4.3** by TLC, usually 20-40 min. Reaction was quenched at 0 °C with solid K₂CO₃ (0.150 g) and stirred for 20 min. The resulting mixture was filtered through a short pad of celite, washed with DCM, and concentrated. The K₂CO₃ cleaved the C2 acetate, so the resulting crude mixture was acetylated with Ac₂O and DMAP (1.1 equiv. each, 0.01 mL and 0.12 g, respectively) in DCM (4 mL) overnight. MeOH (5mL) was added to quench Ac₂O, the reaction mixture stirred for 20 min, and the solvent was evaporated. The reaction mixture was purified by flash column chromatography.

General Method C: A solution of **4.3** (40 mg) and the appropriate alcohol (10 equiv.) in THF (1mL) was cooled to 0 °C with an ice bath. HCl in Dioxane (4M solution, 10 equiv.) was added

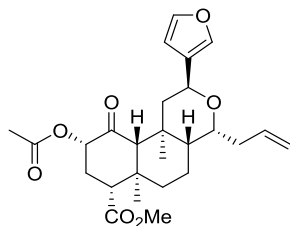
dropwise to the stirring reaction. Reaction was kept at 0°C until **4.3** and monitored for consumption of **4.3** by TLC, usually 20-40 min. Reaction was quenched at 0 °C with sat. aq. NaHCO₃ solution. The resulting mixture stirred for 10 minutes and was then extracted with EtOAc (3 x 25 mL). The combined organic extracts were washed with brine (50 mL), dried (Na₂SO₄) and concentrated. The resulting mixture was purified by flash column chromatography.



Methyl (2S,4S,4aR,6aR,7R,9S,10aR,10bS)-9-acetoxy-4-cyano-2-

(furan-3-yl)-6a,10b-dimethyl-10-oxododecahydro-2H-benzo[f]isochromene-7-carboxylate

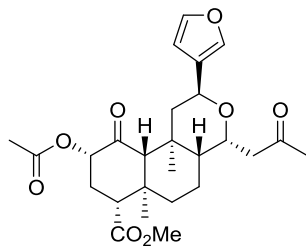
(4.6α). Compound **4.6α** was prepared using General Method A, described above, with Trimethylsilyl cyanide as the nucleophile. FCC (30% EtOAc in Pentane) to afford **4.6α** as a white solid (38% yield). ¹H NMR (500 MHz, CDCl₃) δ 7.42 – 7.32 (m, 2H), 6.36 (dd, J = 1.9, 0.9 Hz, 1H), 5.12 (ddd, J = 10.7, 9.0, 1.0 Hz, 1H), 5.08 (dd, J = 11.6, 2.2 Hz, 1H), 4.62 (d, J = 4.9 Hz, 1H), 3.72 (s, 3H), 3.49 (d, J = 5.1 Hz, 1H), 2.80 – 2.71 (m, 1H), 2.32 – 2.30 (m, 1H), 2.29 – 2.26 (m, 2H), 2.16 (s, 3H), 2.03 (s, 1H), 1.83 – 1.66 (m, 2H), 1.66 – 1.65 (m, 3H), 1.47 – 1.43 (m, 1H), 1.32 – 1.19 (m, 2H), 1.14 (s, 3H). ¹³C NMR (126 MHz, CDCl₃) δ 201.54, 171.58, 169.91, 143.29, 139.52, 125.28, 117.67, 108.63, 74.89, 65.70, 65.60, 65.57, 53.68, 51.96, 46.46, 43.85, 42.61, 38.77, 34.91, 30.69, 20.60, 19.64, 16.90, 14.85. IR: peak at 1730.03. HRMS calculated for C₂₄H₂₉NO₇ [M+NH₄]⁺: 461.2290 (found); 461.2288 (calcd). Melting point: 71-73 °C (dec).



Methyl (2S,4R,4aR,6aR,7R,9S,10aR,10bS)-9-acetoxy-4-allyl-2-

(furan-3-yl)-6a,10b-dimethyl-10-oxododecahydro-2H-benzo[f]isochromene-7-carboxylate

(4.7α). Compound **4.7α** was prepared using General Method A, described above, with allyltrimethylsilane as the nucleophile. FCC (10% →20% EtOAc in Pentane) to afford **4.7α** as a white solid (37% yield). ¹H NMR (500 MHz, CDCl₃) δ 7.33 (d, J = 2.0 Hz, 2H), 6.39 – 6.29 (m, 1H), 5.86 (ddt, J = 17.0, 10.1, 6.8 Hz, 1H), 5.12 (dd, J = 10.9, 9.6 Hz, 1H), 5.08 (dd, J = 17.1, 1.8 Hz, 1H), 5.04 (dd, J = 10.1, 1.7 Hz, 1H), 4.80 (dd, J = 11.4, 2.2 Hz, 1H), 3.84 (ddd, J = 11.5, 5.6, 3.0 Hz, 1H), 3.71 (s, 3H), 2.80 – 2.71 (m, 1H), 2.71 – 2.60 (m, 1H), 2.29 – 2.25 (m, 2H), 2.24 (d, J = 5.1 Hz, 0H), 2.21 (dd, J = 13.1, 2.2 Hz, 1H), 2.15 (s, 3H), 2.08 (s, 1H), 1.74 – 1.61 (m, 4H), 1.52 (qd, J = 12.7, 4.0 Hz, 1H), 1.45 (s, 3H), 1.38 – 1.30 (m, 1H), 1.19 (t, J = 12.2 Hz, 1H), 1.09 (s, 3H). ¹³C NMR (126 MHz, CDCl₃) δ 202.32, 171.95, 169.86, 142.86, 139.05, 136.59, 127.04, 116.13, 109.06, 77.61, 75.04, 66.59, 60.68, 53.68, 51.78, 48.30, 44.60, 42.81, 39.63, 35.03, 32.87, 30.80, 20.82, 20.63, 17.15, 16.71. HRMS calculated for C₂₆H₃₄O₇ [M+H]⁺: 459.2381 (found); 459.2377 (calcd). Melting point: 66-68 °C.

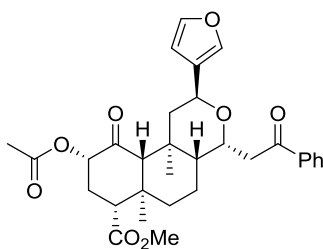


Methyl (2S,4R,4aR,6aR,7R,9S,10aR,10bS)-9-acetoxy-2-(furan-3-

yl)-6a,10b-dimethyl-10-oxo-4-(2-oxopropyl)dodecahydro-2H-benzo[f]isochromene-7-

carboxylate (4.8α). Compound **4.8α** was prepared using General Method A, described above, with 2-(Trimethylsiloxy)propene as the nucleophile. FCC (40% EtOAc in Pentane) to afford **4.8α**

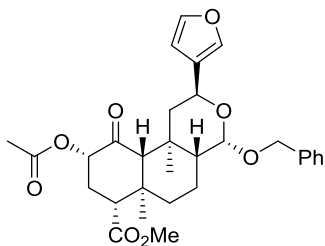
as a white solid (57% yield). ^1H NMR (500 MHz, CDCl_3) δ 7.33 (dq, $J = 4.7, 1.6$ Hz, 2H), 6.34 – 6.30 (m, 1H), 5.14 – 5.06 (m, 1H), 4.79 (ddd, $J = 33.7, 11.5, 2.2$ Hz, 1H), 4.07 (s, 1H), 3.87 (dd, $J = 10.8, 5.7$ Hz, 1H), 3.71 (d, $J = 1.6$ Hz, 3H), 2.83 (d, $J = 17.6$ Hz, 1H), 2.79 – 2.71 (m, 1H), 2.64 – 2.48 (m, 1H), 2.30 – 2.20 (m, 2H), 2.14 (s, 3H), 2.06 (d, $J = 27.0$ Hz, 1H), 1.95 (s, 2H), 1.78 – 1.55 (m, 3H), 1.53 – 1.43 (m, 1H), 1.40 (s, 2H), 1.29 (s, 0H), 1.18 (s, 3H), 1.13 (t, $J = 12.4$ Hz, 1H), 1.07 (s, 3H). ^{13}C NMR (126 MHz, CDCl_3) δ 210.54, 202.17, 171.88, 169.90, 142.97, 139.25, 126.76, 108.81, 74.88, 71.59, 66.38, 61.03, 53.73, 51.76, 48.43, 45.37, 42.77, 39.46, 37.97, 34.93, 31.28, 30.74, 27.27, 20.61, 16.65, 16.42. HRMS calculated for $\text{C}_{26}\text{H}_{34}\text{O}_8$ $[\text{M}+\text{H}]^+$: 475.2325, (found); 475.2327 (calcd). Melting point: 109-111 $^\circ\text{C}$.



Methyl (2S,4R,4aR,6aR,7R,9S,10aR,10bS)-9-acetoxy-2-(furan-3-

yl)-6a,10b-dimethyl-10-oxo-4-(2-oxo-2-phenylethyl)dodecahydro-2H-benzof[]isochromene-7-carboxylate (4.9 α). Compound **4.9 α** was prepared using General Method A, described above, with 1-Phenyl-1-trimethylsiloxyethylene as the nucleophile. FCC (30% EtOAc in Pentane) to afford **4.9 α** as a white solid (24% yield). ^1H NMR (500 MHz, CDCl_3) 8.01 – 7.88 (m, 2H), 7.61 – 7.53 (m, 1H), 7.52 – 7.43 (m, 2H), 7.28 (t, $J = 1.7$ Hz, 1H), 7.23 (dd, $J = 1.6, 0.8$ Hz, 1H), 6.21 (dd, $J = 1.8, 0.9$ Hz, 1H), 5.20 – 5.07 (m, 1H), 4.88 (dd, $J = 11.5, 2.1$ Hz, 1H), 4.60 (ddd, $J = 9.4, 5.6, 3.4$ Hz, 1H), 3.71 (s, 3H), 3.64 (dd, $J = 15.3, 9.6$ Hz, 1H), 2.91 (dd, $J = 15.4, 3.4$ Hz, 1H), 2.84 – 2.69 (m, 1H), 2.35 – 2.20 (m, 3H), 2.16 (s, 3H), 2.10 (s, 1H), 1.81 – 1.73 (m, 1H), 1.73 – 1.66 (m, 1H), 1.55 (s, 3H), 1.50 – 1.40 (m, 2H), 1.25 (s, 1H), 1.25 – 1.18 (m, 1H), 1.10 (s, 3H). ^{13}C NMR (126 MHz, CDCl_3) δ 202.33, 198.75, 171.90, 169.87, 142.81, 139.10, 137.16, 133.15,

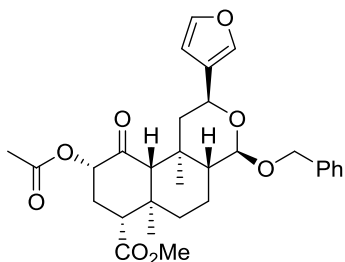
128.67, 128.20, 126.59, 108.91, 75.03, 73.72, 66.34, 61.41, 53.60, 51.84, 47.96, 44.30, 42.75, 39.39, 37.82, 34.91, 30.79, 20.64, 20.59, 16.83, 16.73. HRMS calculated for C₃₁H₃₆O₈ [M+Na]⁺: 559.2274 (found); 559.2307(calcd). Melting point: 185-186 °C.



Methyl

(2S,4S,4aR,6aR,7R,9S,10aR,10bS)-9-acetoxy-4-

(benzyloxy)-2-(furan-3-yl)-6a,10b-dimethyl-10-oxododecahydro-2H-benzo[f]isochromene-7-carboxylate (**4.10α**). Compound **4.10α** was prepared using General Method A, described above, with Benzyl alcohol as the nucleophile. FCC (18% →20% EtOAc in Pentane) to afford **4.10α** as a white solid (28% yield). ¹H NMR (500 MHz, CDCl₃) δ 7.37 – 7.31 (m, 6H), 7.28 (ddd, J = 6.8, 3.4, 2.1 Hz, 1H), 6.35 (dd, J = 1.8, 0.9 Hz, 1H), 5.12 (ddd, J = 10.7, 9.1, 0.9 Hz, 1H), 5.00 (dd, J = 11.7, 2.2 Hz, 1H), 4.79 (dd, J = 7.9, 4.6 Hz, 2H), 4.47 (d, J = 12.4 Hz, 1H), 3.70 (s, 3H), 2.74 (dd, J = 9.3, 7.5 Hz, 1H), 2.26 (td, J = 9.5, 2.1 Hz, 2H), 2.21 (dd, J = 13.1, 2.3 Hz, 1H), 2.15 (s, 3H), 2.04 (s, 1H), 1.82 – 1.72 (m, 1H), 1.69 (dt, J = 13.3, 3.2 Hz, 1H), 1.65 – 1.58 (m, 2H), 1.45 (ddd, J = 12.6, 3.5, 1.9 Hz, 1H), 1.39 (dq, J = 13.7, 2.7 Hz, 1H), 1.29 – 1.21 (m, 2H), 1.12 (s, 3H). ¹³C NMR (126 MHz, CDCl₃) δ 202.19, 171.98, 169.93, 143.02, 139.19, 138.51, 128.29, 127.33, 127.18, 126.65, 108.89, 100.66, 75.03, 69.59, 66.15, 60.99, 53.85, 51.79, 48.63, 44.61, 42.76, 39.46, 34.67, 30.76, 20.65, 20.14, 16.93, 16.72. HRMS calculated for C₃₀H₃₆O₈ [M+Na]⁺: 547.2308 (found); 547.2308 (calcd). Melting point: 66-68 °C.



Methyl

(2S,4R,4aR,6aR,7R,9S,10aR,10bS)-9-acetoxy-4-

(benzyloxy)-2-(furan-3-yl)-6a,10b-dimethyl-10-oxododecahydro-2H-benzo[f]isochromene-

7-carboxylate (4.10β). Compound **4.10β** was prepared using General Method A, described above,

with Benzyl alcohol as the nucleophile. FCC (25% EtOAc in Pentane) to afford **4.10β** as a white

solid (23% yield). ¹H NMR (500 MHz, CDCl₃) δ 7.39 – 7.31 (m, 6H), 7.29 (ddd, J = 7.9, 6.0, 3.2

Hz, 1H), 6.39 (dd, J = 1.9, 0.9 Hz, 1H), 5.13 (ddd, J = 10.5, 8.8, 0.9 Hz, 1H), 4.91 (d, J = 12.1 Hz,

1H), 4.82 (dd, J = 11.5, 2.4 Hz, 1H), 4.59 (d, J = 2.2 Hz, 1H), 4.57 (d, J = 6.1 Hz, 1H), 3.70 (s,

3H), 2.79 – 2.70 (m, 1H), 2.30 – 2.21 (m, 2H), 2.15 (s, 3H), 2.12 (d, J = 2.4 Hz, 1H), 2.08 (s, 1H),

1.95 – 1.86 (m, 1H), 1.74 – 1.64 (m, 1H), 1.37 (s, 3H), 1.36 – 1.33 (m, 0H), 1.31 (dd, J = 8.9, 2.4

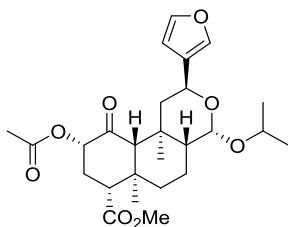
Hz, 2H), 1.25 (s, 1H), 1.24 – 1.17 (m, 1H), 1.07 (s, 3H). ¹³C NMR (126 MHz, CDCl₃) δ 202.58,

171.96, 169.88, 142.87, 138.91, 138.02, 128.31, 127.62, 127.55, 126.59, 108.88, 99.03, 75.06,

70.19, 66.18, 65.56, 53.67, 51.77, 50.70, 45.01, 42.40, 38.87, 35.74, 30.90, 20.63, 17.54, 16.75,

15.13. HRMS calculated for C₃₀H₃₆O₈ [M+Na]⁺: 547.2318 (found); 547.2308 (calcd). Melting

point: 71-73 °C.

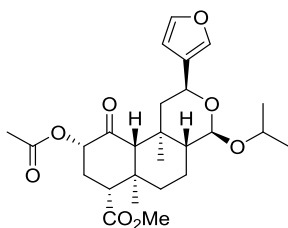


Methyl (2S,4S,4aR,6aR,7R,9S,10aR,10bS)-9-acetoxy-2-(furan-3-yl)-

4-isopropoxy-6a,10b-dimethyl-10-oxododecahydro-2H-benzo[f]isochromene-7-carboxylate

(4.11α). Compound **4.11α** was prepared using General Method B, described above, with isopropyl

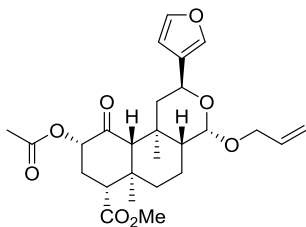
alcohol. FCC (20% EtOAc in Pentane) followed by preparative HPLC (75% MeCN in H₂O; *t_R* = 9.12 min) to afford **4.11α** as a white solid (37 % single epimer, 82% both epimers). ¹H NMR (500 MHz, CDCl₃) δ 7.35 (d, *J* = 1.4 Hz, 2H), 6.36 (t, *J* = 1.4 Hz, 1H), 5.16 – 5.08 (m, 1H), 5.01 (dd, *J* = 11.6, 2.3 Hz, 1H), 4.76 (d, *J* = 3.3 Hz, 1H), 3.83 (p, *J* = 6.2 Hz, 1H), 3.71 (s, 3H), 2.78 – 2.70 (m, 1H), 2.25 (td, *J* = 9.6, 2.2 Hz, 2H), 2.21 – 2.17 (m, 1H), 2.15 (s, 3H), 2.03 – 2.00 (m, 1H), 1.71 – 1.59 (m, 3H), 1.52 (d, *J* = 0.7 Hz, 3H), 1.41 – 1.30 (m, 2H), 1.26 (t, *J* = 1.8 Hz, 1H), 1.21 (d, *J* = 6.2 Hz, 3H), 1.11 (s, 3H), 1.08 (d, *J* = 6.1 Hz, 3H). ¹³C NMR (126 MHz, CDCl₃) δ 202.27, 172.04, 169.93, 142.98, 139.06, 126.96, 108.95, 99.36, 75.04, 69.46, 66.27, 60.67, 53.88, 51.76, 48.59, 44.72, 42.76, 39.43, 34.75, 30.78, 23.64, 21.62, 20.66, 20.13, 16.92, 16.58. HRMS calculated for C₂₆H₃₆O₈ [M+Na]⁺: 499.2314 (found); 499.2308 (calcd). Melting point: 69-70 °C.



Methyl (2S,4R,4aR,6aR,7R,9S,10aR,10bS)-9-acetoxy-2-(furan-3-yl)-4-isopropoxy-6a,10b-dimethyl-10-oxododecahydro-2H-benzo[f]isochromene-7-

carboxylate (4.11β). Compound **4.11β** was prepared using General Method B, described above, with isopropyl alcohol. FCC (20% EtOAc in Pentane) followed by preparative HPLC (75% MeCN in H₂O; *t_R* = 12.65 min) to afford **4.11β** as a white solid (45 % single epimer, 82% both epimers). ¹H NMR (500 MHz, CDCl₃) δ 7.37 – 7.29 (m, 2H), 6.36 (dd, *J* = 1.9, 0.9 Hz, 1H), 5.18 – 5.05 (m, 1H), 4.80 (ddd, *J* = 11.5, 2.5, 1.0 Hz, 1H), 4.55 (d, *J* = 8.6 Hz, 1H), 3.94 (p, *J* = 6.2 Hz, 1H), 3.70 (s, 3H), 2.79 – 2.68 (m, 1H), 2.31 – 2.20 (m, 2H), 2.15 (s, 3H), 2.14 – 2.09 (m, 1H), 2.06 – 2.03 (m, 1H), 1.82 (ddt, *J* = 13.4, 5.1, 2.8 Hz, 1H), 1.68 (dt, *J* = 13.5, 3.4 Hz, 1H), 1.58 (td, *J* = 13.0, 4.1 Hz, 1H), 1.43 (s, 1H), 1.42 – 1.39 (m, 3H), 1.33 – 1.27 (m, 1H), 1.24 (d, *J* = 6.2 Hz, 3H), 1.18 (ddd, *J* = 12.2, 2.7, 1.5 Hz, 1H), 1.13 (d, *J* = 6.1 Hz, 3H), 1.08 (s, 3H). ¹³C NMR (126 MHz, CDCl₃)

δ 202.65, 172.01, 169.87, 142.73, 138.79, 126.83, 108.90, 98.48, 75.07, 71.18, 66.02, 65.69, 53.70, 51.75, 50.65, 44.92, 42.44, 38.94, 35.79, 30.93, 23.73, 22.13, 20.65, 17.50, 16.77, 15.16. HRMS calculated for $C_{26}H_{36}O_8$ $[M+Na]^+$: 499.2308 (found); 499.2308 (calcd). Melting point: 66-67 °C.



Methyl (2S,4S,4aR,6aR,7R,9S,10aR,10bS)-9-acetoxy-4-(allyloxy)-

2-(furan-3-yl)-6a,10b-dimethyl-10-oxododecahydro-2H-benzo[f]isochromene-7-carboxylate

(4.12 α). Compound **4.12 α** was prepared using General Method B, described above, with allyl

alcohol. FCC (20% EtOAc in Pentane) followed by preparative HPLC (60% MeCN in H_2O ; t_R =

26.31 min) to afford **4.12 α** as a white solid (31 % single epimer, 92.4% both epimers). 1H NMR

(400 MHz, $CDCl_3$) δ 7.35 (s, 2H), 6.37 (s, 1H), 5.90 (ddt, J = 16.1, 10.5, 5.2 Hz, 1H), 5.28 (d, J =

17.1 Hz, 1H), 5.22 – 5.09 (m, 2H), 4.98 (d, J = 11.6 Hz, 1H), 4.73 (d, J = 3.0 Hz, 1H), 4.22 (dd, J

= 13.2, 4.3 Hz, 1H), 3.92 (dd, J = 13.5, 5.6 Hz, 1H), 3.71 (s, 3H), 2.74 (t, J = 8.5 Hz, 1H), 2.32 –

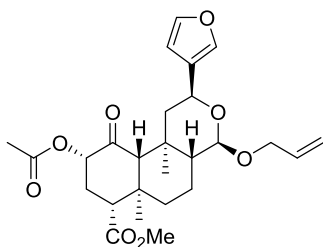
2.17 (m, 3H), 2.15 (s, 3H), 2.03 (s, 1H), 1.70 (d, J = 11.0 Hz, 1H), 1.42 (q, J = 11.9, 8.7 Hz, 2H),

1.26 (s, 5H), 1.22 (d, J = 11.7 Hz, 1H), 1.12 (s, 3H). ^{13}C NMR (126 MHz, $CDCl_3$) δ 202.21, 172.00,

169.94, 143.03, 139.12, 134.68, 126.74, 116.00, 108.89, 100.49, 75.03, 68.39, 66.17, 60.88, 53.87,

51.80, 48.62, 44.64, 42.75, 39.46, 34.68, 30.77, 20.65, 20.12, 16.91, 16.63. HRMS calculated for

$C_{26}H_{34}O_8$ $[M+Na]^+$: 497.2162 (found); 497.2151 (calcd). Melting point: 66-67 °C.

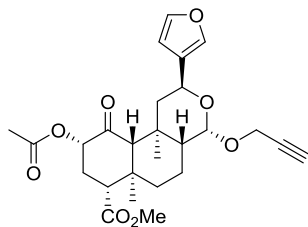


Methyl

(2S,4R,4aR,6aR,7R,9S,10aR,10bS)-9-acetoxy-4-

(allyloxy)-2-(furan-3-yl)-6a,10b-dimethyl-10-oxododecahydro-2H-benzo[f]isochromene-7-

carboxylate (4.12 β). Compound **4.12 β** was prepared using General Method B, described above, with allyl alcohol. FCC (20% EtOAc in Pentane) followed by preparative HPLC (60% MeCN in H₂O; t_R = 21.57 min) to afford **4.12 β** as a white solid (61.2% single epimer, 92.4% both epimers). ¹H NMR (400 MHz, CDCl₃) δ 7.36 – 7.30 (m, 2H), 6.37 (s, 1H), 5.91 (ddt, J = 16.4, 10.7, 5.5 Hz, 1H), 5.27 (d, J = 17.3 Hz, 1H), 5.21 – 5.03 (m, 2H), 4.80 (d, J = 11.2 Hz, 1H), 4.53 (d, J = 8.3 Hz, 1H), 4.36 (dd, J = 13.1, 5.0 Hz, 1H), 4.04 (dd, J = 13.1, 6.0 Hz, 1H), 3.70 (s, 3H), 2.75 (dd, J = 10.7, 6.3 Hz, 1H), 2.26 (t, J = 10.9 Hz, 2H), 2.15 (s, 3H), 2.11 (s, 1H), 2.07 (s, 1H), 1.86 (d, J = 13.5 Hz, 1H), 1.74 – 1.63 (m, 1H), 1.58 (td, J = 13.0, 4.0 Hz, 1H), 1.40 (s, 3H), 1.26 (s, 2H), 1.18 (t, J = 12.4 Hz, 1H), 1.09 (s, 3H). ¹³C NMR (126 MHz, CDCl₃) δ 202.59, 171.96, 169.88, 142.85, 138.90, 134.48, 126.57, 116.81, 108.88, 99.07, 75.07, 69.41, 66.11, 65.58, 53.68, 51.78, 50.69, 44.95, 42.41, 38.87, 35.75, 30.92, 20.64, 17.49, 16.76, 15.13. HRMS calculated for C₂₆H₃₄O₈ [M+Na]⁺: 497.2162 (found); 497.2151 (calcd). Melting point: 74-76°C.

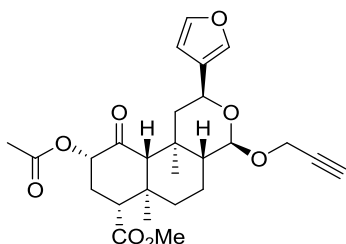


Methyl (2S,4S,4aR,6aR,7R,9S,10aR,10bS)-9-acetoxy-2-(furan-3-

yl)-6a,10b-dimethyl-10-oxo-4-(prop-2-yn-1-yloxy)dodecahydro-2H-benzo[f]isochromene-7-

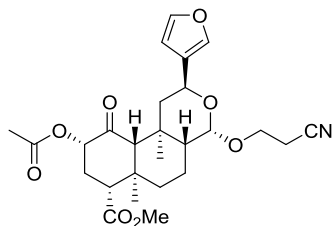
carboxylate (4.13 α). Compound **4.13 α** was prepared using General Method B, described above, with propargyl alcohol. FCC (20% EtOAc in Pentane) followed by preparative HPLC (60% MeCN in H₂O; t_R = 14-16 min) to afford **4.13 α** as a white solid (22.2 % single epimer, 35.3% both epimers). ¹H NMR (500 MHz, CDCl₃) δ 7.37 – 7.30 (m, 2H), 6.38 (dd, J = 1.9, 0.9 Hz, 1H), 5.16 – 5.06 (m, 1H), 4.99 (dd, J = 11.6, 2.3 Hz, 1H), 4.87 (d, J = 3.1 Hz, 1H), 4.23 (dd, J = 3.4, 2.4 Hz, 2H), 3.71 (s, 3H), 2.74 (dd, J = 9.2, 7.7 Hz, 1H), 2.37 (t, J = 2.4 Hz, 1H), 2.26 (dd, J = 9.2, 1.6 Hz,

2H), 2.23 (dd, $J = 6.0, 2.4$ Hz, 1H), 2.20 (d, $J = 2.3$ Hz, 1H), 2.15 (s, 3H), 2.02 (s, 1H), 1.75 – 1.66 (m, 2H), 1.54 – 1.51 (m, 3H), 1.44 (tdd, $J = 15.9, 4.3, 2.8$ Hz, 2H), 1.24 – 1.19 (m, 1H), 1.11 (s, 3H). ^{13}C NMR (126 MHz, CDCl_3) δ 202.14, 171.96, 169.94, 143.04, 139.17, 126.54, 108.86, 99.74, 79.85, 75.02, 73.88, 66.10, 61.25, 54.67, 53.86, 51.80, 48.34, 44.55, 42.75, 39.43, 34.62, 30.75, 20.64, 19.91, 16.90, 16.49. HRMS calculated for $\text{C}_{26}\text{H}_{32}\text{O}_8$ $[\text{M}+\text{Na}]^+$:495.2008 (found); 495.1995 (calcd). Melting point: 74-76 °C.



Methyl (2S,4R,4aR,6aR,7R,9S,10aR,10bS)-9-acetoxy-2-(furan-

3-yl)-6a,10b-dimethyl-10-oxo-4-(prop-2-yn-1-yloxy)dodecahydro-2H-benzo[f]isochromene-7-carboxylate (4.13 β). Compound **4.13 β** was prepared using General Method B, described above, with propargyl alcohol. FCC (20% EtOAc in Pentane) followed by preparative HPLC (60% MeCN in H_2O ; $t_R = 12.5$ -14 min) to afford **4.13 β** as a white solid (13.1% single epimer, 35.3% both epimers). ^1H NMR (500 MHz, CDCl_3) δ 7.38 – 7.31 (m, 2H), 6.37 (dd, $J = 1.9, 0.9$ Hz, 1H), 5.17 – 5.07 (m, 1H), 4.83 (dd, $J = 11.5, 1.8$ Hz, 1H), 4.70 (d, $J = 8.7$ Hz, 1H), 4.35 (d, $J = 5.1$ Hz, 1H), 3.71 (s, 3H), 2.79 – 2.70 (m, 1H), 2.41 (t, $J = 2.4$ Hz, 1H), 2.31 – 2.23 (m, 2H), 2.15 (s, 3H), 2.13 (d, $J = 2.5$ Hz, 1H), 2.08 (d, $J = 1.0$ Hz, 1H), 1.89 – 1.81 (m, 1H), 1.73 – 1.66 (m, 1H), 1.59 (d, $J = 9.1$ Hz, 2H), 1.42 (d, $J = 0.8$ Hz, 3H), 1.36 (dd, $J = 13.2, 3.7$ Hz, 1H), 1.27 – 1.24 (m, 2H), 1.09 (s, 3H). ^{13}C NMR (126 MHz, CDCl_3) δ 202.53, 171.93, 169.88, 142.91, 138.95, 126.38, 108.83, 97.84, 79.58, 75.07, 74.21, 66.28, 65.53, 55.24, 53.69, 51.80, 50.46, 44.88, 42.42, 38.78, 35.80, 30.92, 20.63, 17.32, 16.77, 15.13. HRMS calculated for $\text{C}_{26}\text{H}_{32}\text{O}_8$ $[\text{M}+\text{Na}]^+$:495.2008 (found); 495.1995 (calcd). Melting point: 78-80°C.



Methyl (2S,4S,4aR,6aR,7R,9S,10aR,10bS)-9-acetoxy-4-(2-

cyanoethoxy)-2-(furan-3-yl)-6a,10b-dimethyl-10-oxododecahydro-2H-benzo[f]isochromene-

7-carboxylate (4.14α). Compound **4.14α** was prepared using General Method B, described above,

with 3-hydroxypropionitrile. FCC (30% EtOAc in Pentane) to afford **4.14α** as a white solid (33 %

single epimer, 79% both epimers). ¹H NMR (500 MHz, CDCl₃) δ 7.40 – 7.31 (m, 2H), 6.37 (dd, J

= 1.9, 0.9 Hz, 1H), 5.11 (ddd, J = 10.9, 9.1, 0.9 Hz, 1H), 5.03 (dd, J = 11.7, 2.3 Hz, 1H), 4.74 (d,

J = 3.3 Hz, 1H), 3.92 (ddd, J = 10.1, 6.4, 5.5 Hz, 1H), 3.71 (s, 3H), 3.60 (ddd, J = 10.0, 6.9, 5.5

Hz, 1H), 2.74 (dd, J = 9.3, 7.5 Hz, 1H), 2.63 (ddd, J = 6.3, 5.4, 3.7 Hz, 2H), 2.31 – 2.23 (m, 2H),

2.20 (d, J = 2.4 Hz, 1H), 2.15 (s, 3H), 2.02 (s, 1H), 1.80 – 1.69 (m, 2H), 1.63 (dd, J = 13.5, 4.3 Hz,

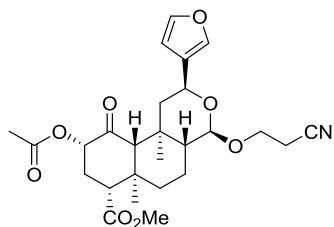
1H), 1.55 (s, 3H), 1.50 – 1.39 (m, 2H), 1.24 – 1.18 (m, 1H), 1.12 (s, 3H). ¹³C NMR (126 MHz,

CDCl₃) δ 202.01, 171.91, 169.95, 143.15, 139.26, 126.37, 117.93, 108.74, 101.71, 75.00, 66.02,

63.01, 61.43, 53.85, 51.82, 48.40, 44.57, 42.73, 39.36, 34.53, 30.73, 20.64, 19.97, 19.16, 16.92,

16.42. HRMS calculated for C₂₆H₃₃NO₈ [M+Na]⁺: 510.2101 (found); 510.2104 (calcd). Melting

point: 76-78 °C.



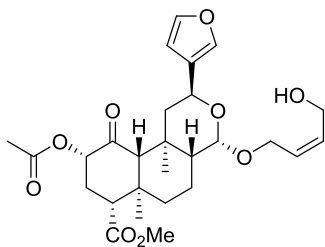
Methyl (2S,4R,4aR,6aR,7R,9S,10aR,10bS)-9-acetoxy-4-(2-

cyanoethoxy)-2-(furan-3-yl)-6a,10b-dimethyl-10-oxododecahydro-2H-benzo[f]isochromene-

7-carboxylate (4.14β). Compound **4.14β** was prepared using General Method B, described above,

with 3-hydroxypropionitrile. FCC (30% EtOAc in Pentane) followed by preparative HPLC (60%

MeCN in H₂O; *t_R* = 10.6 min) to afford **4.14β** as a white solid (46 % single epimer, 79% both epimers). ¹H NMR (500 MHz, CDCl₃) δ 7.35 (d, *J* = 1.9 Hz, 2H), 6.36 (dd, *J* = 1.7, 1.0 Hz, 1H), 5.13 (ddd, *J* = 10.9, 8.4, 0.9 Hz, 1H), 4.82 (dd, *J* = 11.5, 2.5 Hz, 1H), 4.55 (d, *J* = 8.7 Hz, 1H), 4.05 (ddd, *J* = 10.0, 6.0, 5.0 Hz, 1H), 3.71 (s, 3H), 2.79 – 2.72 (m, 1H), 2.71 – 2.55 (m, 2H), 2.31 – 2.23 (m, 2H), 2.15 (s, 3H), 2.08 (s, 1H), 1.87 (dt, *J* = 10.9, 3.2 Hz, 1H), 1.71 (dt, *J* = 13.5, 3.4 Hz, 1H), 1.65 – 1.53 (m, 4H), 1.42 – 1.38 (m, 3H), 1.39 – 1.33 (m, 0H), 1.25 (s, 1H), 1.23 – 1.13 (m, 1H), 1.08 (s, 3H). ¹³C NMR (126 MHz, CDCl₃) δ 202.48, 171.90, 169.90, 143.01, 138.94, 126.26, 117.83, 108.78, 100.31, 75.06, 66.27, 65.47, 63.56, 53.67, 51.81, 50.54, 44.79, 42.39, 38.80, 35.63, 30.87, 20.63, 19.20, 17.32, 16.75, 15.02. HRMS calculated for C₂₆H₃₃NO₈ [M+Na]⁺: 510.2091 (found); 510.2104 (calcd). Melting point: 95-97 °C.



Methyl (2S,4S,4aR,6aR,7R,9S,10aR,10bS)-9-acetoxy-2-(furan-3-

yl)-4-(((Z)-4-hydroxybut-2-en-1-yl)oxy)-6a,10b-dimethyl-10-oxododecahydro-2H-

benzo[f]isochromene-7-carboxylate (4.15α). Compound **4.15α** was prepared using General

Method C, described above, with *cis*-2-butene-diol. FCC (10→40% EtOAc in CH₂Cl₂) followed

by preparative HPLC (60% MeCN in H₂O; *t_R* = 8.4 min) to afford **4.15α** as a white solid (32%

single epimer, 49% both epimers). ¹H NMR (500 MHz, CDCl₃) δ 7.39 – 7.24 (m, 3H), 6.37 (dd, *J*

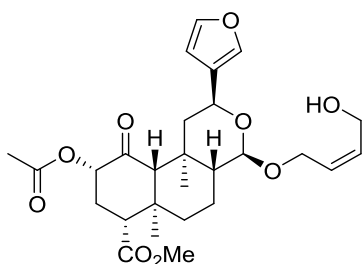
= 1.9, 0.9 Hz, 1H), 5.82 (dddd, *J* = 12.7, 8.0, 4.6, 1.4 Hz, 1H), 5.74 – 5.61 (m, 1H), 5.11 (ddd, *J* =

10.0, 9.2, 0.9 Hz, 1H), 4.97 (dd, *J* = 11.7, 2.2 Hz, 1H), 4.74 (d, *J* = 3.3 Hz, 1H), 4.24 – 4.17 (m,

2H), 4.17 – 4.09 (m, 2H), 3.71 (s, 3H), 2.79 – 2.70 (m, 1H), 2.30 – 2.16 (m, 3H), 2.15 (s, 3H), 2.03

– 2.00 (m, 1H), 1.78 (q, *J* = 13.1, 9.9 Hz, 1H), 1.75 – 1.63 (m, 2H), 1.52 (s, 3H), 1.47 – 1.32 (m,

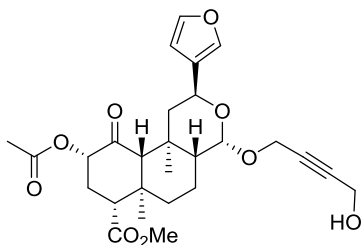
2H), 1.25 (s, 1H), 1.24 – 1.19 (m, 1H), 1.11 (s, 3H). ¹³C NMR (126 MHz, CDCl₃) δ 202.17, 171.96, 169.94, 143.13, 139.11, 132.31, 128.16, 126.52, 108.81, 100.06, 75.02, 66.09, 62.82, 61.09, 58.50, 53.84, 51.81, 48.47, 44.71, 42.74, 39.43, 34.66, 30.75, 20.64, 20.02, 16.91, 16.55. HRMS calculated for C₂₇H₃₆O₉ [M+Na]⁺: 527.2255 (found); 525.2257 (calcd). Melting point: 62-64 °C.



Methyl (2S,4R,4aR,6aR,7R,9S,10aR,10bS)-9-acetoxy-2-

(furan-3-yl)-4-(((Z)-4-hydroxybut-2-en-1-yl)oxy)-6a,10b-dimethyl-10-oxododecahydro-2H-benzo[f]isochromene-7-carboxylate (4.15β). Compound **4.15β** was prepared using General

Method C, described above, with *cis*-2-butene-diol. FCC (10→40% EtOAc in CH₂Cl₂) followed by preparative HPLC (60% MeCN in H₂O; *t_R* = 7.4 min) to afford **4.15β** as a white solid (17 % single epimer, 49% both epimers). ¹H NMR (500 MHz, CDCl₃) δ 7.38 – 7.31 (m, 2H), 6.37 (dd, *J* = 1.8, 0.9 Hz, 1H), 5.81 (dtt, *J* = 11.2, 6.6, 1.4 Hz, 1H), 5.73 – 5.65 (m, 1H), 5.15 – 5.08 (m, 1H), 4.86 – 4.77 (m, 1H), 4.53 (d, *J* = 8.6 Hz, 1H), 4.45 – 4.37 (m, 1H), 4.23 – 4.18 (m, 2H), 4.18 – 4.14 (m, 1H), 3.70 (s, 3H), 2.78 – 2.70 (m, 1H), 2.31 – 2.22 (m, 2H), 2.15 (s, 3H), 2.12 (d, *J* = 2.4 Hz, 1H), 2.07 (d, *J* = 1.9 Hz, 1H), 1.81 (dq, *J* = 13.5, 3.1 Hz, 1H), 1.69 (dt, *J* = 13.5, 3.4 Hz, 1H), 1.43 – 1.37 (m, 3H), 1.34 (qd, *J* = 12.9, 3.7 Hz, 1H), 1.25 (s, 3H), 1.22 – 1.14 (m, 1H), 1.08 (s, 3H). ¹³C NMR (126 MHz, CDCl₃) δ 202.54, 171.94, 169.89, 142.94, 138.92, 132.16, 128.16, 126.43, 108.82, 99.15, 75.06, 66.21, 65.52, 64.10, 58.70, 53.67, 51.80, 50.64, 44.96, 42.39, 38.82, 35.74, 30.91, 20.64, 17.44, 16.76, 15.11. HRMS calculated for C₂₇H₃₆O₉ [M+Na]⁺: 527.2275 (found); 525.2257 (calcd). Melting point: 76-78 °C.



Methyl (2S,4S,4aR,6aR,7R,9S,10aR,10bS)-9-acetoxy-2-

(furan-3-yl)-4-((4-hydroxybut-2-yn-1-yl)oxy)-6a,10b-dimethyl-10-oxododecahydro-2H-

benzo[f]isochromene-7-carboxylate (4.16α). Compound **4.16α** was prepared using General

Method C, described above, with 1,4-butyndiol. FCC (25% EtOAc in CH₂Cl₂) to afford **4.16α** as

a white solid (32% single epimer, 66% both epimers). ¹H NMR (500 MHz, Chloroform-*d*) 7.40 –

7.32 (m, 2H), 6.37 (dd, *J* = 1.8, 0.9 Hz, 1H), 5.11 (ddd, *J* = 10.1, 9.2, 0.9 Hz, 1H), 4.99 (dd, *J* =

11.6, 2.3 Hz, 1H), 4.85 (d, *J* = 3.2 Hz, 1H), 4.31 – 4.22 (m, 4H), 3.71 (s, 3H), 2.74 (dd, *J* = 9.2, 7.7

Hz, 1H), 2.26 (dd, *J* = 9.2, 1.6 Hz, 1H), 2.23 (dd, *J* = 6.9, 2.5 Hz, 1H), 2.20 (d, *J* = 2.3 Hz, 0H),

2.18 (s, 1H), 2.15 (s, 3H), 2.02 (s, 1H), 1.73 – 1.67 (m, 2H), 1.65 – 1.59 (m, 1H), 1.54 – 1.52 (m,

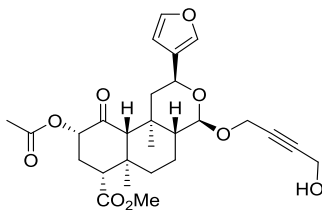
3H), 1.47 – 1.39 (m, 2H), 1.27 – 1.25 (m, 1H), 1.24 – 1.20 (m, 1H), 1.11 (s, 3H). ¹³C NMR (126

MHz, CDCl₃) δ 202.15, 171.96, 169.94, 143.09, 139.13, 126.60, 108.81, 99.91, 83.96, 82.03,

75.02, 66.08, 61.28, 55.05, 53.85, 51.82, 51.19, 48.39, 44.62, 42.74, 39.43, 34.64, 30.75, 20.65,

19.97, 16.91, 16.53. HRMS calculated for C₂₇H₃₄O₉ [M+Na]⁺: 525.2108 (found); 525.2101

(calcd). Melting point: 99-101 °C



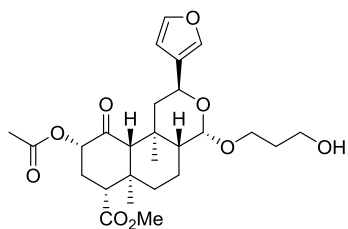
Methyl (2S,4R,4aR,6aR,7R,9S,10aR,10bS)-9-acetoxy-2-(furan-3-

yl)-4-((4-hydroxybut-2-yn-1-yl)oxy)-6a,10b-dimethyl-10-oxododecahydro-2H-

benzo[f]isochromene-7-carboxylate (4.16β). Compound **4.16β** was prepared using General

Method C, described above, with 1,4-butyndiol. FCC (25% EtOAc in CH₂Cl₂) to afford **4.16β** as

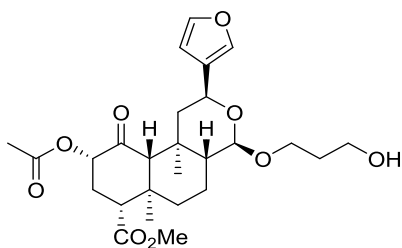
a white solid (34% single epimer, 66% both epimers). ^1H NMR (500 MHz, CDCl_3) δ 7.36 (dt, $J = 1.7, 0.8$ Hz, 1H), 7.34 (t, $J = 1.7$ Hz, 1H), 6.37 (dd, $J = 1.9, 0.9$ Hz, 1H), 5.17 – 5.05 (m, 1H), 4.83 (dd, $J = 11.7, 2.4$ Hz, 1H), 4.65 (d, $J = 8.7$ Hz, 1H), 4.46 – 4.33 (m, 2H), 4.31 (t, $J = 1.8$ Hz, 2H), 3.71 (s, 3H), 2.78 – 2.69 (m, 1H), 2.32 – 2.22 (m, 2H), 2.15 (s, 3H), 2.15 – 2.09 (m, 1H), 2.08 (d, $J = 1.1$ Hz, 1H), 1.84 (dq, $J = 13.7, 3.3$ Hz, 1H), 1.72 – 1.67 (m, 1H), 1.42 – 1.40 (m, 3H), 1.35 (dd, $J = 13.3, 3.6$ Hz, 1H), 1.25 (d, $J = 1.4$ Hz, 3H), 1.22 – 1.17 (m, 1H), 1.09 (s, 3H). ^{13}C NMR (126 MHz, CDCl_3) δ 202.53, 171.92, 169.90, 142.92, 138.95, 126.37, 108.83, 98.12, 84.28, 81.75, 75.07, 66.25, 65.51, 55.60, 53.68, 51.81, 51.20, 50.48, 44.88, 42.41, 38.77, 35.78, 30.91, 20.63, 17.36, 16.78, 15.14. HRMS calculated for $\text{C}_{27}\text{H}_{34}\text{O}_9$ $[\text{M}+\text{Na}]^+$: 525.2130 (found); 525.2101 (calcd). Melting point: 92-94 °C.



Methyl (2S,4S,4aR,6aR,7R,9S,10aR,10bS)-9-acetoxy-2-(furan-3-yl)-4-(3-hydroxypropoxy)-6a,10b-dimethyl-10-oxododecahydro-2H-benzo[f]isochromene-7-carboxylate (4.17 α). Compound **4.17 α** was prepared using General Method C, described above, with 1,3-propanediol. FCC (20 \rightarrow 40% EtOAc in CH_2Cl_2) to afford **4.17 α** as a white solid (38% single epimer, 66% both epimers). ^1H NMR (500 MHz, CDCl_3) δ 7.45 – 7.30 (m, 2H), 6.37 (dd, $J = 1.8, 0.9$ Hz, 1H), 5.11 (dd, $J = 10.6, 9.3$ Hz, 1H), 4.96 (dd, $J = 11.6, 2.3$ Hz, 1H), 4.70 (d, $J = 3.1$ Hz, 1H), 3.94 (ddd, $J = 9.8, 6.3, 4.9$ Hz, 1H), 3.83 – 3.76 (m, 2H), 3.71 (s, 3H), 3.46 (ddd, $J = 9.8, 6.8, 5.0$ Hz, 1H), 2.78 – 2.69 (m, 1H), 2.29 – 2.24 (m, 1H), 2.24 – 2.18 (m, 1H), 2.15 (s, 3H), 2.05 (d, $J = 25.1$ Hz, 1H), 1.97 (s, 1H), 1.90 – 1.82 (m, 2H), 1.76 – 1.66 (m, 2H), 1.66 – 1.57 (m, 1H), 1.52 (s, 3H), 1.43 (ddt, $J = 11.6, 8.3, 2.7$ Hz, 2H), 1.28 – 1.19 (m, 2H), 1.10 (s, 3H). ^{13}C NMR (126 MHz, CDCl_3) δ 202.15, 171.93, 169.95, 143.08, 139.14, 126.60, 108.84, 101.42, 75.01,

66.80, 66.09, 61.63, 60.92, 53.84, 51.82, 48.45, 44.49, 42.72, 39.38, 34.62, 32.16, 30.75, 20.64, 20.05, 16.90, 16.57. HRMS calculated for C₂₆H₃₆O₉ [M+Na]⁺: 515.2255 (found); 515.2257 (calcd).

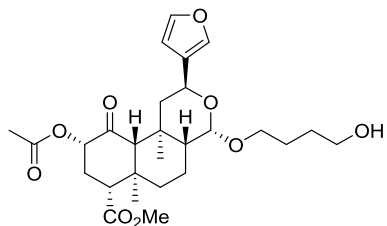
Melting point: 69-72 °C (dec).



Methyl (2S,4R,4aR,6aR,7R,9S,10aR,10bS)-9-acetoxy-2-

(furan-3-yl)-4-(3-hydroxypropoxy)-6a,10b-dimethyl-10-oxododecahydro-2H-

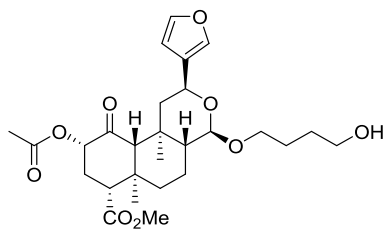
benzo[f]isochromene-7-carboxylate (4.17β). Compound **4.17β** was prepared using General Method C, described above, with 1,3-propanediol. FCC (20→40% EtOAc in CH₂Cl₂) to afford **4.17β** as a white solid (28% single epimer, 66% both epimers). ¹H NMR (500 MHz, CDCl₃) δ 7.40 – 7.31 (m, 2H), 6.36 (dd, J = 1.9, 0.9 Hz, 1H), 5.25 – 5.04 (m, 1H), 4.82 (dd, J = 11.3, 2.3 Hz, 1H), 4.50 (d, J = 8.7 Hz, 1H), 4.01 (ddd, J = 9.8, 6.8, 5.4 Hz, 1H), 3.76 (dd, J = 11.1, 5.2 Hz, 1H), 3.70 (s, 3H), 3.71 – 3.63 (m, 1H), 2.81 – 2.67 (m, 1H), 2.32 – 2.21 (m, 3H), 2.15 (s, 4H), 2.08 (d, J = 1.3 Hz, 1H), 1.82 (tdd, J = 9.0, 7.9, 4.5, 1.9 Hz, 2H), 1.69 (dt, J = 13.5, 3.3 Hz, 1H), 1.63 (d, J = 5.0 Hz, 2H), 1.55 (d, J = 15.0 Hz, 0H), 1.40 (s, 3H), 1.35 (td, J = 13.2, 3.8 Hz, 1H), 1.25 – 1.16 (m, 2H), 1.08 (s, 3H). ¹³C NMR (126 MHz, CDCl₃) δ 202.53, 171.93, 169.88, 142.99, 138.90, 126.35, 108.76, 100.09, 75.06, 67.06, 66.22, 65.50, 60.74, 53.67, 51.79, 50.61, 44.88, 42.38, 38.82, 35.70, 32.14, 30.89, 20.64, 17.50, 16.75, 15.07. HRMS calculated for C₂₆H₃₆O₉ [M+Na]⁺: 515.2251 (found); 515.2257 (calcd). Melting point: 99-101 °C.



Methyl (2S,4S,4aR,6aR,7R,9S,10aR,10bS)-9-acetoxy-2-

(furan-3-yl)-4-(4-hydroxybutoxy)-6a,10b-dimethyl-10-oxododecahydro-2H-

benzo[f]isochromene-7-carboxylate (4.18α). Compound **4.18α** was prepared using General Method C, described above, with 1,4-butanediol. FCC (20→40% EtOAc in CH₂Cl₂) to afford **4.18α** as a white solid (26% single epimer, 47% both epimers). ¹H NMR (500 MHz, CDCl₃) δ 7.42 – 7.31 (m, 2H), 6.37 (dd, J = 1.8, 0.9 Hz, 1H), 5.16 – 5.07 (m, 1H), 4.95 (dd, J = 11.6, 2.3 Hz, 1H), 4.68 (d, J = 3.2 Hz, 1H), 4.11 (t, J = 6.5 Hz, 2H), 3.71 (s, 3H), 3.69 (d, J = 10.8 Hz, 2H), 3.39 – 3.30 (m, 1H), 2.79 – 2.68 (m, 2H), 2.29 – 2.21 (m, 2H), 2.22 – 2.18 (m, 1H), 2.17 (d, J = 2.4 Hz, 1H), 2.15 (s, 3H), 2.06 (s, 3H), 1.76 – 1.70 (m, 3H), 1.52 (s, 3H), 1.49 – 1.38 (m, 2H), 1.11 (s, 3H). ¹³C NMR (126 MHz, CDCl₃) δ 202.20, 171.98, 169.94, 143.05, 139.10, 126.74, 108.87, 101.22, 75.03, 67.99, 64.27, 62.41, 53.86, 51.80, 48.62, 44.64, 42.75, 39.45, 34.70, 30.77, 29.93, 29.11, 26.24, 25.06, 20.65, 16.93, 16.58. HRMS calculated for C₂₇H₃₈O₉ [M+Na]⁺: 529.2405 (found); 529.2414 (calcd). Melting point: 110-113 °C.

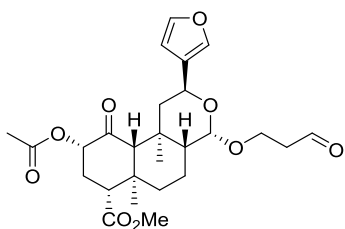


Methyl (2S,4R,4aR,6aR,7R,9S,10aR,10bS)-9-acetoxy-2-

(furan-3-yl)-4-(4-hydroxybutoxy)-6a,10b-dimethyl-10-oxododecahydro-2H-

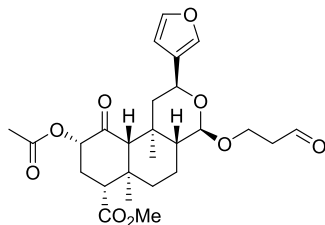
benzo[f]isochromene-7-carboxylate (4.18β). Compound **4.18β** was prepared using General Method C, described above, with 1,4-butanediol. FCC (20→40% EtOAc in CH₂Cl₂) to afford **4.18β** as a white solid (21% single epimer, 47% both epimers). ¹H NMR (500 MHz, CDCl₃) δ 7.37

– 7.30 (m, 2H), 6.36 (dd, $J = 1.8, 0.9$ Hz, 1H), 5.16 – 5.08 (m, 1H), 4.81 (dd, $J = 11.5, 2.3$ Hz, 1H), 4.48 (d, $J = 8.6$ Hz, 1H), 4.00 – 3.92 (m, 1H), 3.92 – 3.82 (m, 2H), 3.70 (s, 3H), 3.67 – 3.64 (m, 2H), 3.51 – 3.38 (m, 2H), 2.77 – 2.69 (m, 1H), 2.31 – 2.21 (m, 2H), 2.17 – 2.16 (m, 2H), 2.12 (dd, $J = 13.2, 2.4$ Hz, 1H), 2.11 – 2.04 (m, 1H), 1.91 – 1.77 (m, 3H), 1.73 – 1.65 (m, 2H), 1.40 (s, 3H), 1.08 (s, 3H). ^{13}C NMR (126 MHz, CDCl_3) δ 202.57, 171.97, 169.88, 142.87, 138.88, 126.55, 108.84, 99.99, 75.07, 67.21, 65.55, 62.66, 53.67, 51.78, 50.70, 44.98, 42.39, 38.87, 35.71, 32.35, 30.90, 30.17, 26.39, 23.46, 20.64, 16.76, 15.09. HRMS calculated for $\text{C}_{27}\text{H}_{38}\text{O}_9$ $[\text{M}+\text{Na}]^+$: 529.2422 (found); 529.2414 (calcd). Melting point: 101-105 °C.



Methyl (2S,4S,4aR,6aR,7R,9S,10aR,10bS)-9-acetoxy-2-(furan-3-yl)-6a,10b-dimethyl-10-oxo-4-(3-oxopropoxy)dodecahydro-2H-benzo[f]isochromene-7-carboxylate (4.19 α). To a dry flask under Ar, **4.17 α** (34.6 mg, 0.07 mmol) and Dess-Martin periodinane (41.5mg, 0.098 mmol) in DCM (1mL) was added and the reaction stirred overnight at r.t. Upon reaction completion as monitored by TLC, the reaction was quenched with sat. aq. NaHCO_3 (2mL) and sat. aq. $\text{Na}_2\text{S}_2\text{O}_3$ (2mL). The reaction mixture allowed to stir for 20 min. before being extracted into DCM (3x 10mL). The combined organic extracts were washed with brine (30 mL), dried (Na_2SO_4) and concentrated to yield crude aldehyde which was purified by FCC (8% EtOAc in DCM) to afford **4.19 α** as a white solid (44% yield). ^1H NMR (500 MHz, CDCl_3) δ 9.81 (q, $J = 1.8$ Hz, 1H), 7.46 – 7.32 (m, 2H), 6.38 (dd, $J = 1.8, 0.9$ Hz, 1H), 5.21 – 5.05 (m, 1H), 4.96 (dd, $J = 11.6, 2.3$ Hz, 1H), 4.70 (d, $J = 3.2$ Hz, 1H), 4.09 (dt, $J = 10.2, 5.8$ Hz, 1H), 3.71 (s, 3H), 3.67 (dt, $J = 10.2, 5.7$ Hz, 1H), 2.79 – 2.71 (m, 1H), 2.67 (td, $J = 5.9, 1.9$ Hz, 2H), 2.25 (td, $J = 10.2, 9.5, 2.2$ Hz, 2H), 2.22 – 2.16 (m, 1H), 2.15 (s, 3H), 2.01 (s, 1H), 1.71 – 1.62 (m,

1H), 1.60 (t, J = 4.9 Hz, 3H), 1.45 (s, 3H), 1.42 – 1.34 (m, 1H), 1.23 – 1.19 (m, 1H), 1.09 (s, 3H). ¹³C NMR (126 MHz, CDCl₃) δ 202.10, 200.96, 171.94, 169.93, 143.09, 139.19, 126.57, 108.82, 101.49, 75.00, 66.07, 61.95, 61.04, 53.84, 51.80, 48.44, 44.56, 43.76, 42.72, 39.37, 34.61, 30.74, 20.64, 19.99, 16.89, 16.44. HRMS calculated for C₂₆H₃₄O₉ [M+H]⁺: 491.2235 (found); 491.2276 (calcd). Melting point: 221-223 °C.

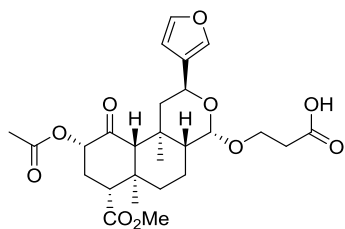


Methyl (2S,4R,4aR,6aR,7R,9S,10aR,10bS)-9-acetoxy-2-(furan-3-

yl)-6a,10b-dimethyl-10-oxo-4-(3-oxopropoxy)dodecahydro-2H-benzo[f]isochromene-7-

carboxylate (4.19β). To a dry flask under Ar, **4.17β** (30 mg, 0.061 mmol) and Dess-Martin periodinane (36.2 mg, 0.085 mmol) in DCM (1mL) was added and the reaction stirred overnight at r.t. Upon reaction completion as monitored by TLC, the reaction was quenched with sat. aq. NaHCO₃ (2mL) and sat. aq. Na₂S₂O₃ (2mL). The reaction mixture allowed to stir for 20 min. before being extracted into DCM (3x 10mL). The combined organic extracts were washed with brine (30 mL), dried (Na₂SO₄) and concentrated to yield crude aldehyde which was purified by FCC (8% EtOAc in DCM) to afford **4.19β** as a white solid (32% yield). ¹H NMR (500 MHz, CDCl₃) δ 9.78 (d, J = 3.3 Hz, 1H), 7.34 (dt, J = 6.3, 1.8 Hz, 2H), 6.36 (dd, J = 1.8, 0.9 Hz, 1H), 5.19 – 5.06 (m, 1H), 4.81 (dd, J = 11.5, 2.4 Hz, 1H), 4.51 (d, J = 8.7 Hz, 1H), 4.18 (ddd, J = 10.3, 6.2, 5.0 Hz, 1H), 3.84 (ddd, J = 10.2, 7.8, 4.8 Hz, 1H), 3.70 (s, 3H), 2.74 (dt, J = 17.2, 10.1, 7.3 Hz, 1H), 2.78 – 2.68 (m, 1H), 2.64 (dddd, J = 17.3, 6.4, 4.8, 1.8 Hz, 1H), 2.29 – 2.22 (m, 2H), 2.15 (s, 3H), 2.16 – 2.09 (m, 1H), 2.08 – 2.03 (m, 1H), 1.70 (ddt, J = 26.5, 13.5, 3.5 Hz, 2H), 1.56 (td, J = 13.1, 4.2 Hz, 1H), 1.40 (s, 3H), 1.38 – 1.25 (m, 1H), 1.22 – 1.14 (m, 2H), 1.08 (s, 3H). ¹³C NMR (126 MHz, CDCl₃) δ 202.52, 201.08, 171.92, 169.89, 142.92, 138.91, 126.42, 108.84,

100.17, 75.05, 66.12, 65.52, 62.72, 53.67, 51.78, 50.56, 44.84, 43.87, 42.38, 38.81, 35.65, 30.88, 20.63, 17.34, 16.75, 15.06. HRMS calculated for C₂₆H₃₄O₉ [M+H]⁺: 491.2165 (found); 491.2276 (calcd). Melting point: 114-118 °C.



3-(((2S,4S,4aR,6aR,7R,9S,10aR,10bS)-9-acetoxy-2-(furan-3-yl)-

7-(methoxycarbonyl)-6a,10b-dimethyl-10-oxododecahydro-2H-benzo[f]isochromen-4-

yl)oxy)propanoic acid (4.20α). To a solution of **4.19α** (19.6 mg, 0.04 mmol) in DMF (1mL) was

added OXONE (24.6 mg, 0.04 mmol). The reaction mixture was stirred at r.t. for 3h. Upon

consumption of the starting material, as monitored by TLC, 1M HCl (3mL) was added and the

mixture was extracted into EtOAc (3x 10mL). The combined organic extracts were washed with

brine (30 mL), dried (Na₂SO₄) and concentrated. The resulting mixture was purified by preparative

HPLC to afford **4.20α** as a white solid (7.0 mg, 35 % yield). ¹H NMR (500 MHz, CDCl₃) δ 7.41

– 7.32 (m, 2H), 6.38 (dd, J = 1.8, 0.9 Hz, 1H), 5.13 – 5.08 (m, 1H), 5.00 (dd, J = 11.7, 2.2 Hz, 1H),

4.70 (d, J = 3.2 Hz, 1H), 4.03 (dt, J = 9.9, 6.3 Hz, 1H), 3.70 (s, 3H), 3.59 (dt, J = 9.9, 5.8 Hz, 1H),

2.80 – 2.69 (m, 1H), 2.62 (d, J = 6.0 Hz, 1H), 2.25 (td, J = 10.0, 9.5, 2.2 Hz, 2H), 2.18 (dd, J =

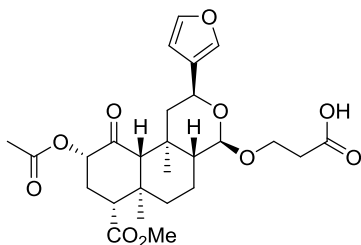
13.1, 2.3 Hz, 1H), 2.15 (s, 3H), 2.02 (d, J = 8.5 Hz, 2H), 1.70 – 1.58 (m, 3H), 1.47 (s, 3H), 1.38

(tt, J = 12.2, 2.6 Hz, 2H), 1.26 – 1.19 (m, 1H), 1.10 (s, 3H). ¹³C NMR (126 MHz, CDCl₃) δ 202.15,

175.85, 171.98, 169.95, 143.03, 139.28, 126.57, 108.90, 101.37, 75.03, 66.12, 63.47, 60.91, 53.84,

51.80, 48.47, 44.47, 42.74, 39.42, 34.85, 34.62, 30.75, 20.64, 19.94, 16.90, 16.38. HRMS

calculated for C₂₆H₃₄O₁₀ [M+NH₄]⁺: 524.2480 (found); 524.2490 (calcd). Melting point: 92-93 °C.



3-(((2S,4R,4aR,6aR,7R,9S,10aR,10bS)-9-acetoxy-2-(furan-3-

yl)-7-(methoxycarbonyl)-6a,10b-dimethyl-10-oxododecahydro-2H-benzo[f]isochromen-4-

yl)oxy)propanoic acid (4.20β). To a solution of **4.19β** (16.2 mg, 0.033 mmol) in DMF (1mL) was

added OXONE (16.2 mg, 0.033 mmol). The reaction mixture was stirred at r.t. for 3h. Upon

consumption of the starting material, as monitored by TLC, 1M HCl (3mL) was added and the

mixture was extracted into EtOAc (3x 10mL). The combined organic extracts were washed with

brine (30 mL), dried (Na₂SO₄) and concentrated. The resulting mixture was purified by preparative

HPLC to afford **4.20β** as a white solid (4.3 mg, 26 % yield). ¹H NMR (500 MHz, CDCl₃) δ 7.41

– 7.31 (m, 2H), 6.36 (dd, J = 1.9, 0.9 Hz, 1H), 5.22 – 5.06 (m, 1H), 4.82 (dd, J = 11.5, 2.3 Hz, 1H),

4.53 (d, J = 8.6 Hz, 1H), 4.11 (dt, J = 10.2, 5.8 Hz, 1H), 3.79 (ddd, J = 10.2, 7.5, 5.5 Hz, 1H), 3.70

(s, 3H), 2.75 (dd, J = 9.3, 7.6 Hz, 1H), 2.68 – 2.56 (m, 1H), 2.24 (td, J = 9.5, 2.1 Hz, 2H), 2.15 (s,

3H), 2.12 (dd, J = 13.2, 2.5 Hz, 1H), 2.08 (d, J = 7.2 Hz, 1H), 2.03 (s, 1H), 1.76 (dt, J = 13.4, 3.5

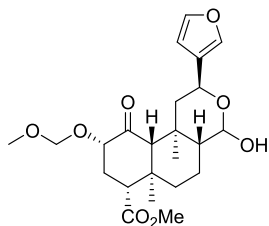
Hz, 1H), 1.67 (dt, J = 13.5, 3.3 Hz, 1H), 1.56 (td, J = 13.1, 4.2 Hz, 1H), 1.39 (s, 3H), 1.32 (qd, J =

12.8, 3.7 Hz, 1H), 1.25 – 1.15 (m, 2H), 1.07 (s, 3H). ¹³C NMR (126 MHz, CDCl₃) δ 202.60,

175.20, 171.96, 169.90, 142.93, 138.94, 126.36, 108.81, 100.38, 75.09, 66.23, 65.36, 64.53, 53.60,

51.78, 50.44, 44.72, 42.38, 38.78, 35.65, 34.94, 30.88, 20.64, 17.29, 16.76, 15.04. HRMS

calculated for C₂₆H₃₄O₁₀ [M+NH₄]⁺: 524.2477 (found); 524.2490 (calcd). Melting point: 95-96 °C.



Methyl (2S,4aR,6aR,7R,9S,10aR,10bS)-2-(furan-3-yl)-4-hydroxy-9-

(methoxymethoxy)-6a,10b-dimethyl-10-oxododecahydro-2H-benzo[f]isochromene-7-

carboxylate (4.1a). Synthesized following procedure for **4.1** using methoxymethyl-salvinorin B

(0.188 mmol, synthesized as previously described⁸) as the starting material, yielding **4.1a** (51.4

mg, 63% yield, mixture of lactol epimers). ¹H NMR (500 MHz, CDCl₃) δ 7.43 – 7.33 (m, 2H),

6.40 (dd, J = 1.9, 0.9 Hz, 1H), 5.23 – 5.14 (m, 0H), 4.90 (dd, J = 11.6, 2.4 Hz, 1H), 4.83 (dd, J =

8.7, 5.2 Hz, 1H), 4.75 – 4.62 (m, 2H), 4.14 – 4.06 (m, 1H), 3.70 (d, J = 1.1 Hz, 3H), 3.37 (d, J =

1.1 Hz, 3H), 2.94 (d, J = 6.1 Hz, 1H), 2.69 (dt, J = 13.4, 3.5 Hz, 1H), 2.61 – 2.56 (m, 0H), 2.32

(dddd, J = 14.8, 11.3, 7.3, 3.4 Hz, 1H), 2.26 (dd, J = 13.0, 2.4 Hz, 0H), 2.22 – 2.11 (m, 2H), 1.98

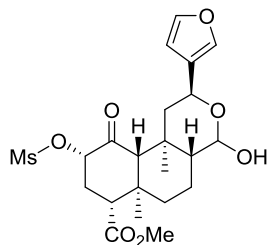
(s, 1H), 1.92 (s, 0H), 1.82 (dp, J = 13.8, 3.0 Hz, 1H), 1.71 (dt, J = 13.3, 3.4 Hz, 1H), 1.60 (s, 1H),

1.42 (s, 2H), 1.25 (s, 1H), 1.23 – 1.13 (m, 1H), 1.12 (s, 1H), 1.09 (s, 2H). ¹³C NMR (126 MHz,

CDCl₃) δ 206.32, 172.21, 143.10, 139.12, 126.35, 108.75, 95.71, 94.24, 77.93, 66.28, 65.61, 55.78,

54.02, 52.24, 51.74, 44.97, 42.33, 38.87, 35.72, 32.73, 17.70, 16.75, 15.02. HRMS calculated for

C₂₃H₃₂O₈ [M+H]⁺: 437.2264 (found); 437.2170 (calcd). Melting point: 87-91 °C.



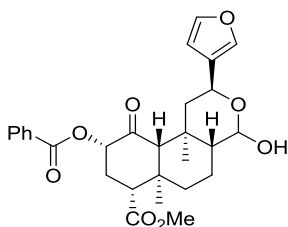
Methyl (2S,4aR,6aR,7R,9S,10aR,10bS)-2-(furan-3-yl)-4-hydroxy-

6a,10b-dimethyl-9-((methylsulfonyl)oxy)-10-oxododecahydro-2H-benzo[f]isochromene-7-

carboxylate (4.1b). Synthesized following procedure for **4.1** using methanesulfonyl-salvinorin B

(0.271 mmol, synthesized as previously described⁹) as the starting material, yielding **4.1b** as a

mixture of lactol epimers which was carried through without further purification. ^1H NMR (500 MHz, CDCl_3) δ 7.43 – 7.32 (m, 2H), 6.42 – 6.38 (m, 1H), 5.26 – 5.11 (m, 1H), 5.02 (ddd, $J = 14.8$, 12.3, 7.5 Hz, 1H), 4.87 (ddd, $J = 29.4$, 10.1, 4.2 Hz, 1H), 3.72 (d, $J = 1.1$ Hz, 3H), 3.22 (d, $J = 3.0$ Hz, 3H), 2.82 – 2.67 (m, 2H), 2.46 (ddq, $J = 14.4$, 7.0, 3.6 Hz, 1H), 2.38 (dd, $J = 14.3$, 12.1 Hz, 1H), 2.25 – 2.10 (m, 1H), 2.04 (s, 1H), 1.86 (dd, $J = 14.0$, 3.4 Hz, 1H), 1.73 (dt, $J = 13.5$, 3.4 Hz, 1H), 1.59 (s, 1H), 1.41 (s, 2H), 1.25 (s, 2H), 1.24 – 1.19 (m, 1H), 1.13 (s, 1H), 1.10 (s, 2H). ^{13}C NMR (126 MHz, CDCl_3) δ 201.88, 171.37, 143.25, 139.24, 126.10, 108.80, 94.14, 80.69, 66.16, 65.59, 53.52, 52.02, 44.74, 42.26, 39.56, 38.66, 35.82, 32.24, 29.74, 17.62, 16.86, 15.03. HRMS calculated for $\text{C}_{22}\text{H}_{30}\text{O}_9\text{S}$ $[\text{M}+\text{H}]^+$: 471.1819. (found); 471.1683 (calcd). Melting point: 155-156 $^\circ\text{C}$.

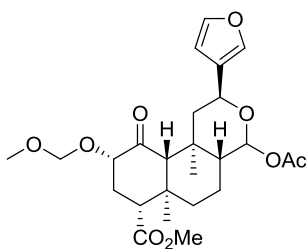


Methyl (2S,4aR,6aR,7R,9S,10aR,10bS)-9-(benzoyloxy)-2-(furan-3-

yl)-4-hydroxy-6a,10b-dimethyl-10-oxododecahydro-2H-benzo[f]isochromene-7-carboxylate

(4.1c). Synthesized following procedure for **4.1** using herkinorin (0.404 mmol, synthesized as previously described⁹) as the starting material, yielding **4.1c** as a mixture of lactol epimers (190 mg, 94% yield) Mixture of epimers: ^1H NMR (500 MHz, CDCl_3) δ 8.08 (dd, $J = 8.4$, 1.3 Hz, 2H), 7.57 (tt, $J = 7.2$, 1.4 Hz, 1H), 7.45 (ddt, $J = 8.8$, 7.6, 1.5 Hz, 2H), 7.40 – 7.30 (m, 2H), 6.38 (ddd, $J = 8.7$, 1.9, 0.9 Hz, 1H), 5.42 – 5.35 (m, 1H), 5.22 – 5.16 (m, 0H), 4.87 (ddd, $J = 21.4$, 10.1, 4.1 Hz, 2H), 3.73 (d, $J = 1.3$ Hz, 3H), 2.89 – 2.77 (m, 1H), 2.68 (d, $J = 6.2$ Hz, 1H), 2.48 – 2.38 (m, 2H), 2.26 (dd, $J = 13.2$, 2.4 Hz, 0H), 2.20 – 2.14 (m, 2H), 2.05 (s, 0H), 1.90 – 1.85 (m, 1H), 1.79 – 1.73 (m, 1H), 1.62 (s, 2H), 1.61 (s, 1H), 1.45 – 1.37 (m, 3H), 1.26 (t, $J = 7.1$ Hz, 1H), 1.15 (s, 2H). ^{13}C NMR (126 MHz, CDCl_3) δ 202.27, 201.91, 172.01, 171.95, 165.44, 143.08, 139.12,

133.36, 133.32, 129.88, 129.24, 128.41, 126.21, 108.81, 95.81, 94.20, 77.21, 75.48, 75.44, 66.33, 66.09, 65.50, 60.99, 53.92, 53.78, 52.27, 51.87, 51.84, 48.45, 44.92, 44.81, 42.52, 39.52, 38.91, 35.76, 34.61, 31.07, 30.94, 20.23, 17.72, 17.01, 16.85, 16.57, 15.03. HRMS calculated for $C_{28}H_{32}O_8$ $[M+NH_4]^+$: 514.2458 (found); 514.2435 (calcd). Melting point: 119-121 °C.



Methyl (2S,4aR,6aR,7R,9S,10aR,10bS)-4-acetoxy-2-(furan-3-yl)-

9-(methoxymethoxy)-6a,10b-dimethyl-10-oxododecahydro-2H-benzo[f]isochromene-7-

carboxylate (4.3a). Synthesized following procedure for **4.3** using **4.1a** (0.03 mmol) as starting

material, yielding **4.3a** (11.1 mg, 77% yield). 1H NMR (500 MHz, $CDCl_3$) δ 7.46 – 7.34 (m, 2H),

6.40 (dd, $J = 1.9, 0.9$ Hz, 1H), 5.85 (d, $J = 8.8$ Hz, 1H), 4.99 (dd, $J = 11.4, 2.4$ Hz, 1H), 4.75 – 4.68

(m, 3H), 4.15 (dd, $J = 12.0, 7.6$ Hz, 1H), 3.72 (s, 3H), 3.39 (s, 3H), 2.73 (dd, $J = 13.5, 3.4$ Hz, 1H),

2.42 – 2.28 (m, 1H), 2.26 – 2.16 (m, 2H), 2.12 (s, 3H), 2.03 (s, 1H), 1.77 – 1.67 (m, 2H), 1.65 –

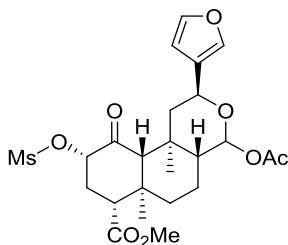
1.52 (m, 1H), 1.49 (s, 3H), 1.38 (d, $J = 7.7$ Hz, 1H), 1.23 (t, $J = 12.3$ Hz, 1H), 1.11 (s, 3H). ^{13}C

NMR (126 MHz, $CDCl_3$) δ 205.99, 172.09, 169.60, 143.06, 139.35, 125.81, 108.83, 95.75, 92.48,

77.93, 66.93, 65.56, 55.81, 54.05, 51.73, 49.67, 44.56, 42.32, 38.71, 35.97, 32.70, 21.11, 17.57,

16.76, 14.87. HRMS calculated for $C_{25}H_{34}O_9$ $[M+Na]^+$: 501.2094 (found); 501.2101 (calcd).

Melting point: 149-152 °C.



Methyl (2S,4aR,6aR,7R,9S,10aR,10bS)-4-acetoxy-2-(furan-3-yl)-

6a,10b-dimethyl-9-((methylsulfonyl)oxy)-10-oxododecahydro-2H-benzo[f]isochromene-7-

carboxylate (4.3b). Synthesized following procedure for **4.3** using **4.1b** (crude, 0.271 mmol) as

starting material, yielding **4.3b** (102 mg, 73% yield over two steps). ¹H NMR (500 MHz, CDCl₃)

δ 7.40 – 7.30 (m, 2H), 6.39 (dd, J = 1.9, 0.9 Hz, 1H), 5.83 (d, J = 8.7 Hz, 1H), 5.04 (ddd, J = 12.4,

7.5, 0.9 Hz, 1H), 4.97 (dd, J = 11.6, 2.4 Hz, 1H), 3.71 (s, 3H), 3.22 (s, 3H), 2.74 (dd, J = 13.5, 3.5

Hz, 1H), 2.48 (ddd, J = 13.3, 7.6, 3.5 Hz, 1H), 2.37 (td, J = 13.4, 12.3 Hz, 1H), 2.18 (dd, J = 13.1,

2.5 Hz, 1H), 2.10 (s, 3H), 2.05 (d, J = 5.6 Hz, 1H), 1.73 (dt, J = 14.8, 3.5 Hz, 1H), 1.64 – 1.57 (m,

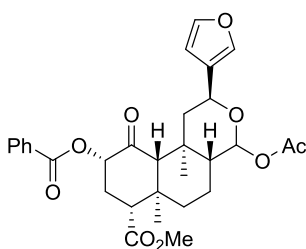
1H), 1.49 – 1.42 (m, 3H), 1.41 – 1.33 (m, 2H), 1.30 – 1.21 (m, 1H), 1.21 (t, J = 7.0 Hz, 1H), 1.10

(s, 3H). ¹³C NMR (126 MHz, CDCl₃) δ 201.56, 171.20, 169.58, 143.15, 139.45, 125.53, 108.86,

92.29, 80.49, 76.75, 66.80, 65.50, 53.53, 51.98, 49.51, 44.35, 42.22, 39.55, 38.48, 36.02, 32.19,

21.10, 17.46, 16.82, 14.83. HRMS calculated for C₂₄H₃₂O₁₀S [M+NH₄]⁺: 530.2053 (found);

530.5054 (calcd). Melting point: 140-141 °C.



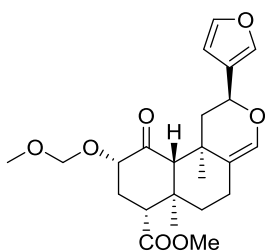
Methyl (2S,4aR,6aR,7R,9S,10aR,10bS)-4-acetoxy-9-(benzoyloxy)-

2-(furan-3-yl)-6a,10b-dimethyl-10-oxododecahydro-2H-benzo[f]isochromene-7-carboxylate

(4.3c). Synthesized following procedure for **4.3** using **4.1c** (0.20 mmol) as starting material,

yielding **4.3c** (75.6 mg, 70% yield). ¹H NMR (500 MHz, CDCl₃) δ 8.11 – 8.06 (m, 2H), 7.61 –

7.55 (m, 1H), 7.48 – 7.42 (m, 2H), 7.37 (dt, J = 1.6, 0.8 Hz, 1H), 7.33 (t, J = 1.7 Hz, 1H), 6.38 (dd, J = 1.9, 0.8 Hz, 1H), 5.86 – 5.82 (m, 1H), 5.43 – 5.37 (m, 1H), 4.96 (dd, J = 11.7, 2.3 Hz, 1H), 3.73 (s, 3H), 2.88 – 2.82 (m, 1H), 2.48 – 2.41 (m, 2H), 2.23 – 2.19 (m, 2H), 2.11 (s, 3H), 1.78 – 1.73 (m, 1H), 1.47 (s, 3H), 1.41 (td, J = 9.3, 3.3 Hz, 2H), 1.33 – 1.24 (m, 2H), 1.15 (s, 3H). ¹³C NMR (126 MHz, CDCl₃) δ 201.97, 171.84, 169.61, 165.44, 143.03, 139.36, 133.39, 129.89, 129.20, 128.42, 125.62, 108.90, 92.43, 75.41, 66.96, 65.40, 53.77, 51.87, 49.61, 44.36, 42.48, 38.72, 35.96, 31.03, 21.13, 17.57, 16.85, 14.85. HRMS calculated for C₃₀H₃₄O₉ [M+NH₄]⁺: 556.2549 (found); 556.2541 (calcd). Melting point: 171-172 °C.



Methyl

(2S,6aR,7R,9S,10aS,10bR)-2-(furan-3-yl)-9-

(methoxymethoxy)-6a,10b-dimethyl-10-oxo-1,5,6,6a,7,8,9,10,10a,10b-decahydro-2H-

benzo[f]isochromene-7-carboxylate (4.4a). Synthesized following procedure previously

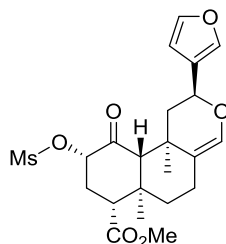
described for **4.4** using **4.1a** (0.046 mmol) as starting material, yielding **4.4a** (5.0 mg, 26.3% yield).

¹H NMR (500 MHz, CDCl₃) δ 7.43 – 7.34 (m, 2H), 6.38 (d, J = 1.9 Hz, 1H), 6.28 (d, J = 1.8 Hz, 1H), 4.85 – 4.78 (m, 2H), 4.78 – 4.66 (m, 1H), 4.03 (ddd, J = 12.2, 7.6, 1.3 Hz, 1H), 3.70 (s, 3H),

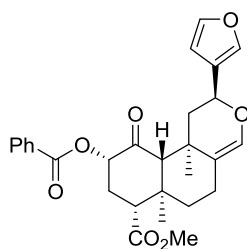
3.38 (s, 1H), 2.68 (dd, J = 13.5, 3.2 Hz, 1H), 2.44 (ddd, J = 13.3, 7.6, 3.1 Hz, 1H), 2.39 – 2.24 (m, 3H), 2.14 (s, 1H), 2.11 – 2.00 (m, 1H), 2.00 – 1.90 (m, 1H), 1.70 (ddd, J = 12.9, 4.4, 2.6 Hz, 1H),

1.63 (q, J = 8.8, 8.1 Hz, 2H), 1.55 (d, J = 3.3 Hz, 3H), 1.53 – 1.34 (m, 1H), 1.13 (s, 3H). ¹³C NMR (126 MHz, CDCl₃) δ 206.70, 172.31, 143.21, 139.28, 136.88, 126.00, 117.38, 108.60, 95.80, 78.14, 66.59, 65.65, 55.78, 53.78, 51.67, 44.67, 42.66, 40.09, 34.13, 32.41, 22.75, 22.63, 15.38.

HRMS calculated for C₂₃H₃₀O₇ [M+H]⁺: 419.2082 (found); 419.2065 (calcd). Melting point: 60-62 °C.

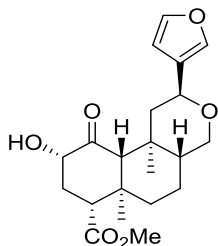


Methyl (2S,6aR,7R,9S,10aS,10bR)-2-(furan-3-yl)-6a,10b-dimethyl-9-((methylsulfonyl)oxy)-10-oxo-1,5,6,6a,7,8,9,10,10a,10b-decahydro-2H-benzo[f]isochromene-7-carboxylate (4.4b). ¹H NMR (500 MHz, CDCl₃) δ 7.39 (d, J = 1.9 Hz, 1H), 6.38 (d, J = 1.8 Hz, 1H), 6.28 (d, J = 1.7 Hz, 1H), 5.01 (dd, J = 12.3, 7.5 Hz, 1H), 4.85 – 4.71 (m, 1H), 3.71 (s, 3H), 3.22 (s, 3H), 2.70 (dd, J = 13.2, 3.7 Hz, 1H), 2.50 – 2.42 (m, 1H), 2.42 – 2.32 (m, 2H), 2.27 (dt, J = 13.9, 3.2 Hz, 1H), 2.07 (s, 1H), 1.96 (ddd, J = 14.7, 4.9, 2.8 Hz, 1H), 1.71 (dt, J = 13.2, 3.7 Hz, 1H), 1.53 (s, 3H), 1.48 (dd, J = 13.4, 4.6 Hz, 1H), 1.39 (t, J = 12.6 Hz, 1H), 1.16 (s, 3H). ¹³C NMR (126 MHz, CDCl₃) δ 202.29, 171.44, 143.31, 139.39, 137.31, 125.78, 116.66, 108.63, 80.74, 66.55, 65.70, 53.31, 51.93, 44.48, 42.59, 39.84, 39.55, 34.19, 31.98, 22.73, 22.51, 15.46. HRMS calculated for C₂₂H₂₈O₈S [M+H]⁺:453.1602 (found); 453.1578 (calcd). Melting point: 108-109 °C.



Methyl (2S,6aR,7R,9S,10aS,10bR)-9-(benzoyloxy)-2-(furan-3-yl)-6a,10b-dimethyl-10-oxo-1,5,6,6a,7,8,9,10,10a,10b-decahydro-2H-benzo[f]isochromene-7-carboxylate (4.4c). ¹H NMR (500 MHz, CDCl₃) δ 8.09 (dd, J = 7.9, 1.4 Hz, 2H), 7.63 – 7.52 (m, 1H), 7.45 (t, J = 7.7 Hz, 2H), 7.41 – 7.34 (m, 2H), 6.41 – 6.33 (m, 1H), 6.28 (d, J = 1.6 Hz, 1H), 5.38 (dd, J = 12.3, 7.6 Hz, 1H), 4.84 – 4.73 (m, 1H), 3.72 (s, 3H), 2.81 (dd, J = 12.8, 4.0 Hz, 1H), 2.52 – 2.34 (m, 3H), 2.34 – 2.26 (m, 1H), 2.21 (s, 1H), 1.97 (ddd, J = 14.6, 4.7, 2.6 Hz, 1H), 1.73

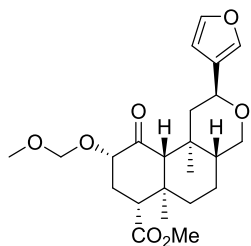
(ddd, $J = 13.1, 4.3, 2.6$ Hz, 1H), 1.58 (s, 1H), 1.54 (s, 3H), 1.21 (s, 3H), 1.18 (d, $J = 7.2$ Hz, 1H). ^{13}C NMR (126 MHz, CDCl_3) δ 202.73, 172.06, 165.44, 143.18, 139.30, 137.08, 133.34, 129.90, 129.32, 128.42, 125.85, 117.09, 108.70, 75.60, 66.67, 65.50, 53.54, 51.81, 44.43, 42.87, 40.10, 34.13, 30.81, 22.78, 22.64, 15.49. HRMS calculated for $\text{C}_{28}\text{H}_{30}\text{O}_7$ $[\text{M}+\text{H}]^+$: 479.2044 (found); 479.2065 (calcd). Melting point: 74-76 °C.



Methyl (2S,4aR,6aR,7R,9S,10aR,10bS)-2-(furan-3-yl)-9-hydroxy-6a,10b-

dimethyl-10-oxododecahydro-2H-benzo[f]isochromene-7-carboxylate. To a flask containing **4.5** (0.05 mmol) in MeOH (2mL) was added Na_2CO_3 (0.20 mmol, 4 equiv.). Reaction stirred at r.t. until starting material consumed as seen by TLC. Upon reaction completion, solvent was evaporated. The crude residue was dissolved in CH_2Cl_2 (10 mL) and HCl (1 M, 8 mL), and the organic layer separated. Following further extraction with DCM (2 x 10 mL), the organic layers were combined and washed with brine (8 mL) then dried over Na_2SO_4 , and concentrated to afford 17-deoxysalvinorin B (0.016 g, 83% yield). ^1H NMR (500 MHz, CDCl_3) δ 7.35 (t, $J = 1.5$ Hz, 2H), 6.35 (dd, $J = 1.8, 1.0$ Hz, 1H), 4.74 (dd, $J = 11.5, 2.4$ Hz, 1H), 4.06 (dd, $J = 11.8, 7.8$ Hz, 1H), 3.70 (s, 3H), 3.59 (d, $J = 7.6$ Hz, 2H), 2.74 (dd, $J = 13.5, 3.2$ Hz, 1H), 2.45 (ddd, $J = 13.4, 7.7, 3.3$ Hz, 1H), 2.16 (dd, $J = 12.9, 2.4$ Hz, 1H), 2.10 (d, $J = 1.1$ Hz, 1H), 2.00 (td, $J = 13.5, 11.9$ Hz, 1H), 1.72 – 1.55 (m, 2H), 1.49 (dtt, $J = 12.0, 8.0, 4.2$ Hz, 1H), 1.42 (d, $J = 0.8$ Hz, 3H), 1.38 – 1.28 (m, 3H), 1.19 – 1.12 (m, 1H), 1.06 (s, 3H). ^{13}C NMR (126 MHz, CDCl_3) δ 209.44, 172.20, 143.04, 138.91, 127.07, 108.61, 77.27, 74.21, 67.46, 67.09, 65.22, 53.35, 51.73, 46.45, 45.58, 43.30, 38.96, 34.60,

34.42, 19.57, 16.92, 13.81. HRMS calculated for C₂₁H₂₈O₆ [M+Na]⁺: 399.1774 (found); 399.1784 (calcd). Melting point: 57-59 °C.

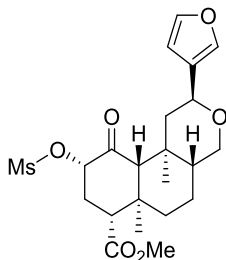


Methyl

(2S,4aR,6aR,7R,9S,10aR,10bS)-2-(furan-3-yl)-9-

(methoxymethoxy)-6a,10b-dimethyl-10-oxododecahydro-2H-benzo[f]isochromene-7-

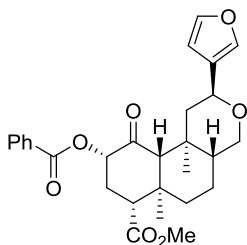
carboxylate (**4.5a**). To a flask containing 17-deoxysalvinorin B (0.02 g, 0.053 mmol) under Ar was added CH₂Cl₂ (2 mL), diisopropylethylamine (0.372 mmol, 7 equiv.) and chloromethyl methyl ether (0.372 mmol, 7 equiv.). Reaction stirred at r.t. for 48 h, until starting material had been consumed as monitored by TLC, and was quenched with saturated NaHCO₃ (4 mL) and extracted with CH₂Cl₂ (3x 5 mL). The combined organic extracts were washed with brine (50 mL), dried (Na₂SO₄) and concentrated. Purification by FCC (40% EtOAc in Pentane) afforded **4.5a** as a white solid (32% yield). ¹H NMR (500 MHz, CDCl₃) δ 7.35 (dd, J = 2.7, 1.3 Hz, 2H), 6.36 (dd, J = 1.9, 0.9 Hz, 1H), 4.73 (dd, J = 8.5, 3.0 Hz, 1H), 4.70 (d, J = 3.6 Hz, 2H), 4.12 (ddd, J = 12.2, 7.3, 0.9 Hz, 1H), 3.70 (s, 3H), 3.60 – 3.57 (m, 2H), 3.37 (s, 3H), 2.72 (dd, J = 13.5, 3.4 Hz, 1H), 2.33 (ddd, J = 13.4, 7.3, 3.5 Hz, 1H), 2.24 – 2.11 (m, 2H), 1.99 (s, 1H), 1.73 – 1.60 (m, 2H), 1.46 (tdt, J = 12.5, 6.2, 3.4 Hz, 1H), 1.42 – 1.39 (m, 3H), 1.38 – 1.27 (m, 2H), 1.19 – 1.11 (m, 1H), 1.08 (s, 3H). ¹³C NMR (126 MHz, CDCl₃) δ 206.28, 172.26, 142.99, 138.91, 127.16, 108.66, 95.73, 77.93, 67.54, 67.13, 65.76, 55.77, 54.13, 51.70, 46.49, 45.64, 42.64, 39.04, 34.61, 32.68, 19.60, 16.83, 13.71. HRMS calculated for C₂₃H₃₂O₇ [M+H]⁺: 421.2236 (found); 421.2221 (calcd). Melting point: 120-123 °C.



Methyl (2S,4aR,6aR,7R,9S,10aR,10bS)-2-(furan-3-yl)-6a,10b-dimethyl-

9-((methylsulfonyl)oxy)-10-oxododecahydro-2H-benzo[f]isochromene-7-carboxylate (4.5b).

Synthesized following procedure for **4.5** using **4.3b** (0.082 mmol) as starting material, yielding **4.5b** (18.6 mg, 50% yield). ^1H NMR (500 MHz, CDCl_3) δ 7.36 (d, $J = 1.4$ Hz, 2H), 6.37 (t, $J = 1.4$ Hz, 1H), 5.03 (ddd, $J = 12.4, 7.6, 0.9$ Hz, 1H), 4.72 (dd, $J = 11.5, 2.4$ Hz, 1H), 3.71 (s, 3H), 3.62 (d, $J = 25.1$ Hz, 1H), 3.58 (d, $J = 1.8$ Hz, 1H), 3.21 (s, 3H), 2.76 (dd, $J = 13.4, 3.5$ Hz, 1H), 2.47 (ddd, $J = 13.3, 7.6, 3.5$ Hz, 1H), 2.37 (td, $J = 13.4, 12.3$ Hz, 1H), 2.13 (dd, $J = 13.0, 2.4$ Hz, 1H), 2.05 (d, $J = 1.0$ Hz, 1H), 1.73 – 1.58 (m, 3H), 1.54 – 1.44 (m, 1H), 1.39 (s, 3H), 1.36 – 1.28 (m, 1H), 1.24 – 1.15 (m, 1H), 1.09 (s, 3H). ^{13}C NMR (126 MHz, CDCl_3) δ 201.81, 171.37, 143.07, 139.02, 126.92, 108.70, 80.64, 67.44, 67.05, 65.72, 53.62, 51.94, 46.34, 45.44, 42.52, 39.53, 38.82, 34.73, 32.23, 19.48, 16.91, 13.70. HRMS calculated for $\text{C}_{22}\text{H}_{30}\text{O}_8\text{S}$ $[\text{M}+\text{H}]^+$: 455.1740 (found); 455.1734 (calcd). Melting point: 90-91 °C.



Methyl (2S,4aR,6aR,7R,9S,10aR,10bS)-9-(benzoyloxy)-2-(furan-3-yl)-

6a,10b-dimethyl-10-oxododecahydro-2H-benzo[f]isochromene-7-carboxylate (4.5c).

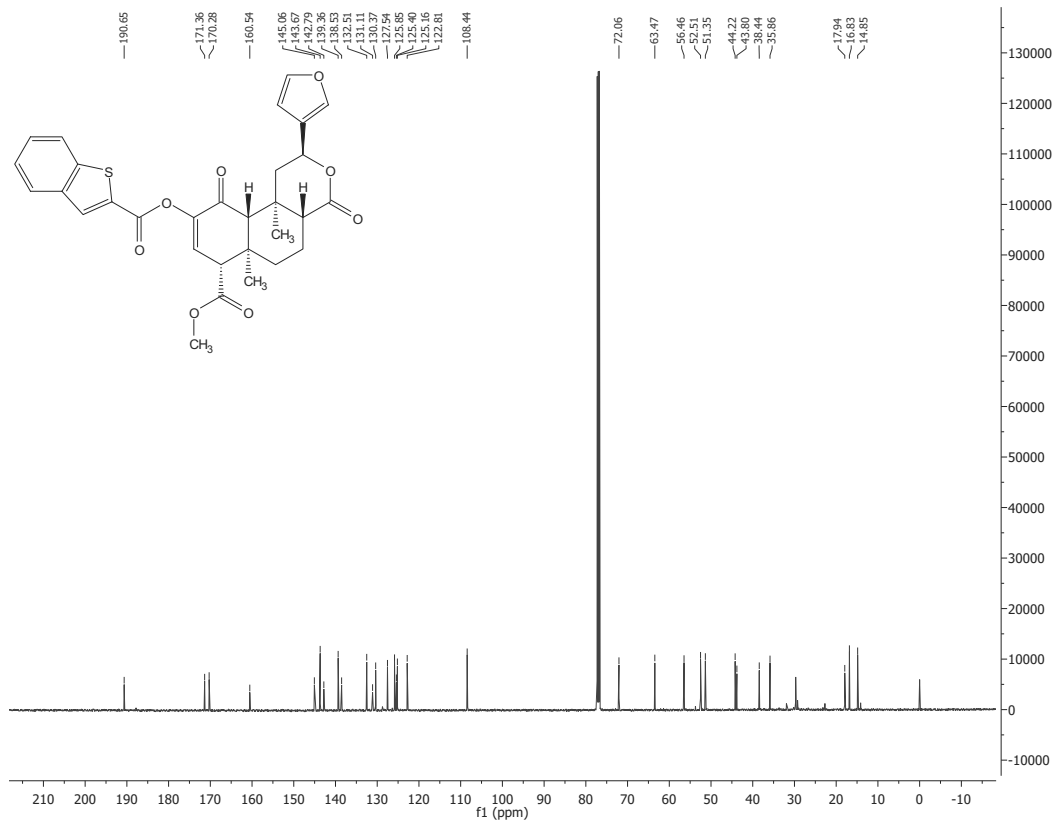
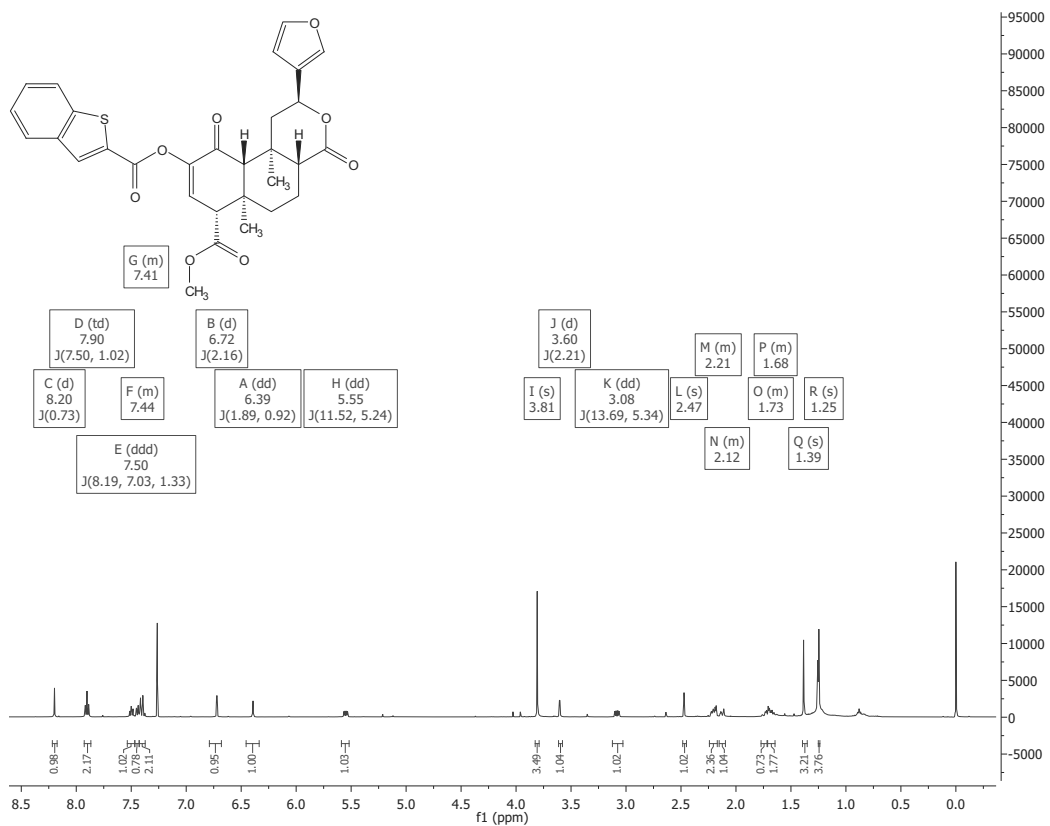
Synthesized following procedure for **4.5** using **4.3c** (0.080 mmol) as starting material, yielding **4.5c** (21.2 mg, 55% yield). ^1H NMR (500 MHz, CDCl_3) δ 8.15 – 8.02 (m, 2H), 7.57 (ddt, $J = 8.7, 7.1, 1.3$ Hz, 1H), 7.47 – 7.41 (m, 2H), 7.34 (d, $J = 1.5$ Hz, 2H), 6.35 (t, $J = 1.4$ Hz, 1H), 5.46 – 5.35

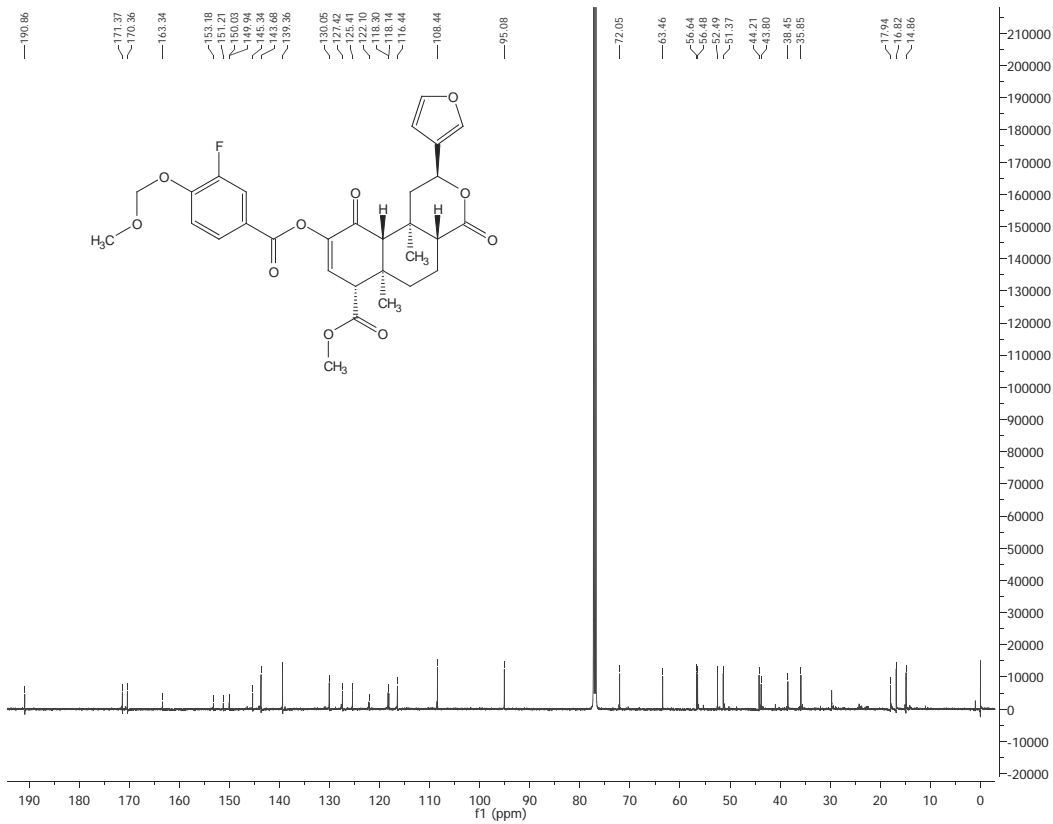
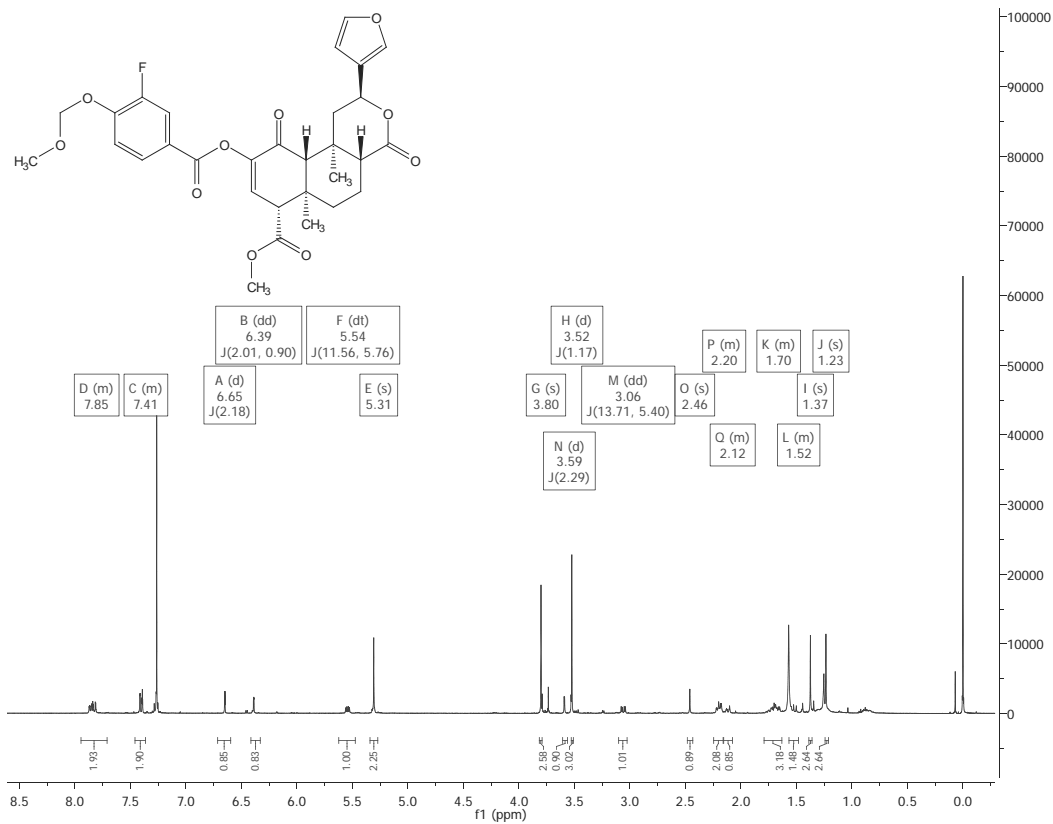
(m, 1H), 4.71 (dd, J = 11.5, 2.4 Hz, 1H), 3.73 (s, 3H), 3.63 – 3.51 (m, 2H), 2.90 – 2.82 (m, 1H), 2.48 – 2.37 (m, 2H), 2.18 (s, 1H), 2.18 – 2.14 (m, 1H), 1.74 – 1.68 (m, 2H), 1.52 (qd, J = 7.6, 3.8 Hz, 1H), 1.40 (s, 3H), 1.34 – 1.29 (m, 1H), 1.26 (d, J = 3.1 Hz, 2H), 1.14 (s, 3H). ¹³C NMR (126 MHz, CDCl₃) δ 202.26, 172.00, 165.44, 142.95, 138.93, 133.33, 129.89, 129.29, 128.40, 127.00, 108.75, 75.47, 67.57, 67.10, 65.63, 53.86, 51.83, 46.44, 45.48, 42.80, 39.06, 34.64, 31.04, 19.62, 16.94, 13.72. HRMS calculated for C₂₈H₃₂O₇ [M+NH₄]⁺: 498.2492 (found); 498.2486 (calcd). Melting point: 120-121 °C.

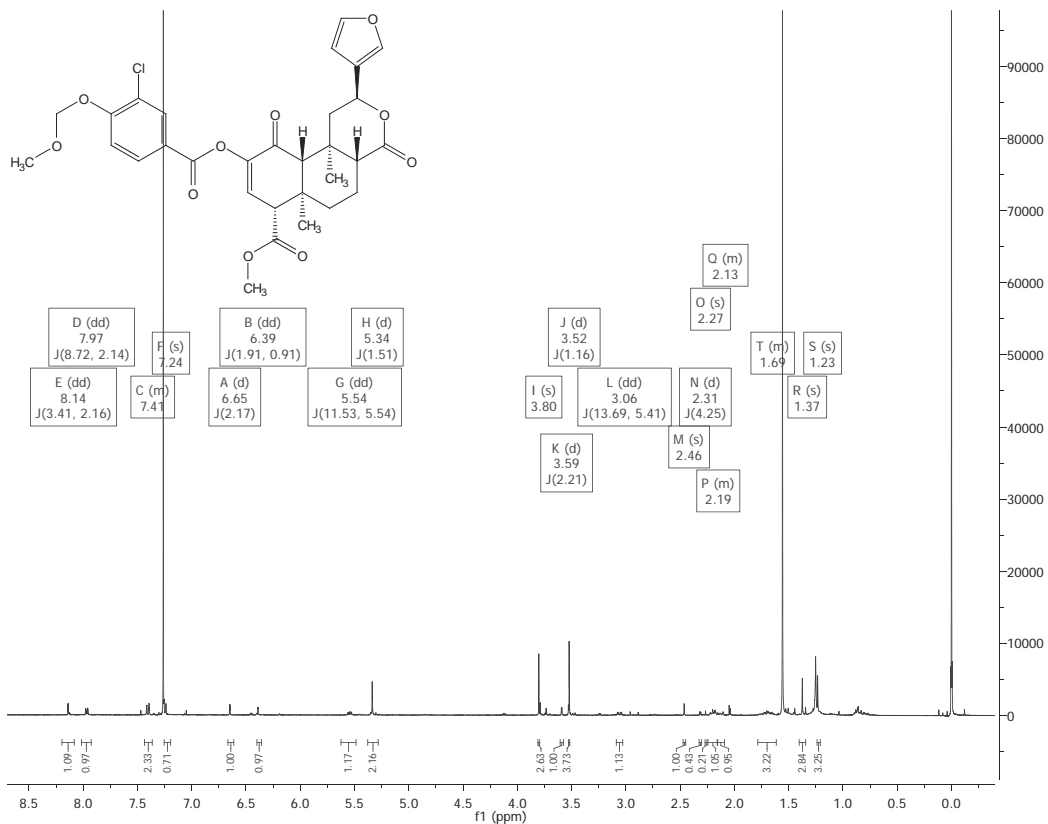
References

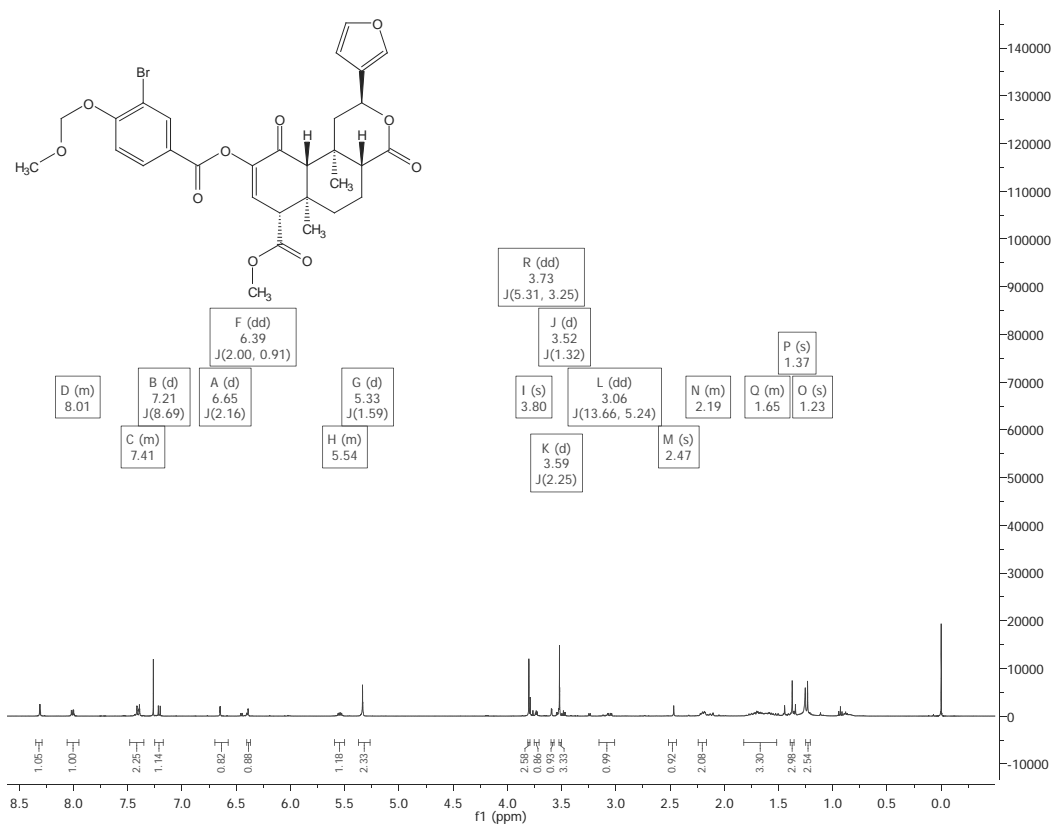
1. Riley, A. P.; Groer, C. E.; Young, D.; Ewald, A. W.; Kivell, B. M.; Prisinzano, T. E. Synthesis and kappa-opioid receptor activity of furan-substituted salvinorin A analogues. *J. Med. Chem.* **2014**, *57*, 10464-10475.
2. Crowley, R. S.; Riley, A. P.; Sherwood, A. M.; Groer, C. E.; Shivaperumal, N.; Biscaia, M.; Paton, K.; Schneider, S.; Provasi, D.; Kivell, B. M.; Filizola, M.; Prisinzano, T. E. Synthetic studies of neoclerodane diterpenes from *Salvia divinorum*: identification of a potent and centrally acting μ opioid analgesic with reduced abuse liability. *J. Med. Chem.* **2016**, *59*, 11027-11038.
3. (a) Iconaru, L. I.; Ban, D.; Bharatham, K.; Ramanathan, A.; Zhang, W.; Shelat, A. A.; Zuo, J.; Kriwacki, R. W. Discovery of small molecules that inhibit the disordered protein, p27(Kip1). *Sci. Rep.* **2015**, *5*, 15686; (b) Chessari, G.; Buck, I. M.; Day, J. E.; Day, P. J.; Iqbal, A.; Johnson, C. N.; Lewis, E. J.; Martins, V.; Miller, D.; Reader, M.; Rees, D. C.; Rich, S. J.; Tamanini, E.; Vitorino, M.; Ward, G. A.; Williams, P. A.; Williams, G.; Wilsher, N. E.; Woolford, A. J. Fragment-based drug discovery targeting inhibitor of apoptosis proteins: Discovery of a non-alanine lead series with dual activity against cIAP1 and XIAP. *J. Med. Chem.* **2015**, *58*, 6574-6588; (c) Cheeseright, T.; Mackey Phd, M.; Rose Phd, S.; Vinter Phd,

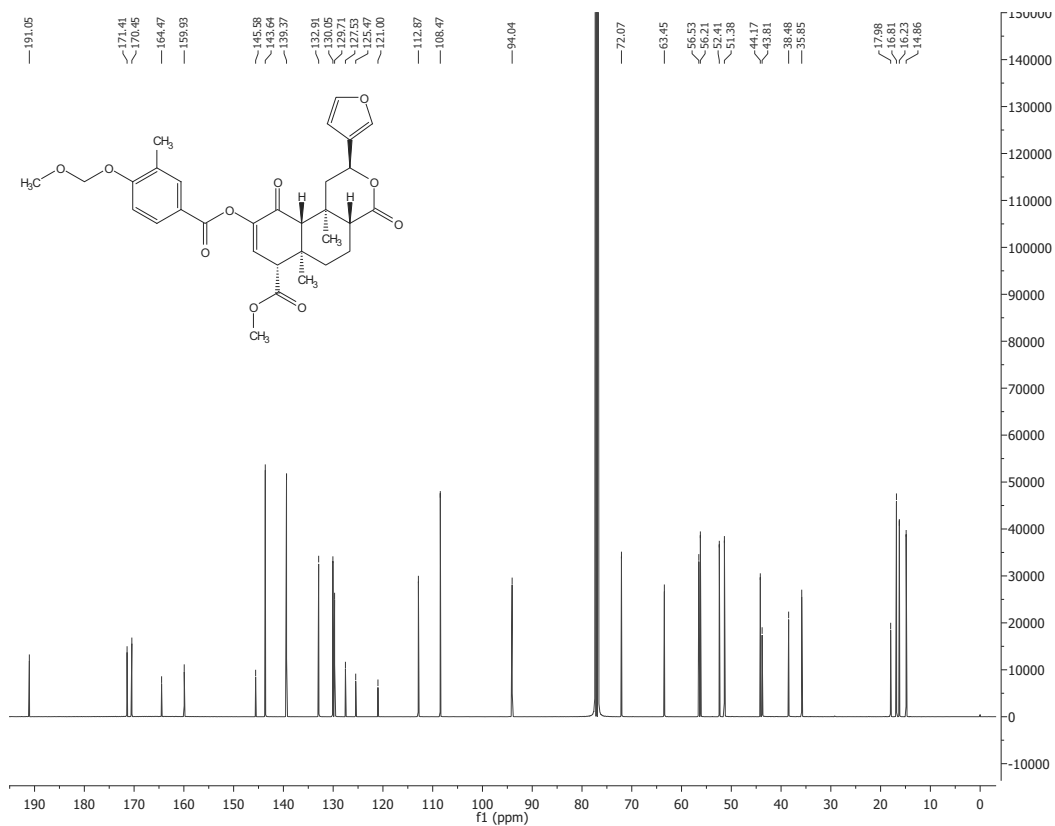
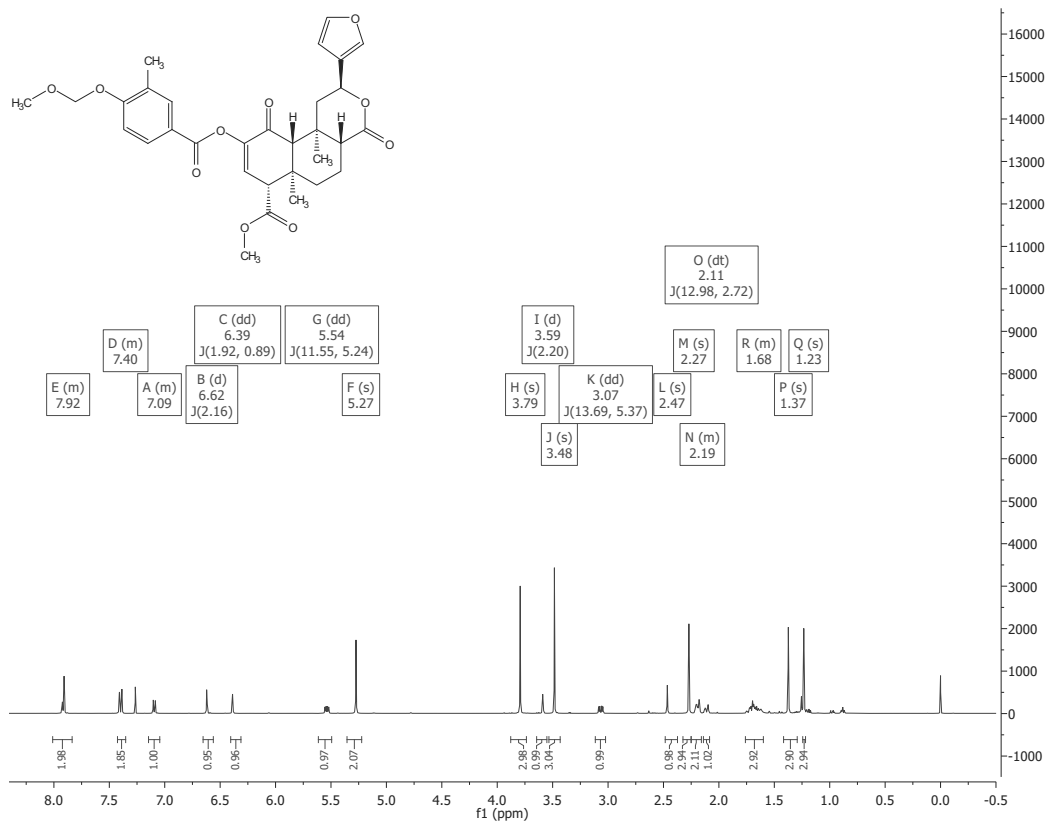
- A. Molecular field technology applied to virtual screening and finding the bioactive conformation. *Expert Opin. Drug Discovery* **2007**, *2*, 131-144.
4. Harding, W. W.; Schmidt, M.; Tidgewell, K.; Kannan, P.; Holden, K. G.; Gilmour, B.; Navarro, H.; Rothman, R. B.; Prisinzano, T. E. Synthetic studies of neoclerodane diterpenes from *Salvia divinorum*: semisynthesis of salvinicins A and B and other chemical transformations of salvinorin A. *J. Nat. Prod.* **2006**, *69*, 107-112.
 5. Peng, Y. G.; Ji, C. Y.; Chen, Y. C.; Huang, C. Z.; Jiang, Y. Z. An efficient and selective deprotecting method for methoxymethyl ethers. *Synth. Commun.* **2004**, *34*, 4325-4330.
 6. Arumugam, P.; Karthikeyan, G.; Perumal, P. T. A mild, efficient, and inexpensive protocol for the selective deprotection of TBDMS ethers using KHSO_4 . *Chem. Lett.* **2004**, *33*, 1146-1147.
 7. Lampe, J. W.; Biggers, C. K.; Defauw, J. M.; Foglesong, R. J.; Hall, S. E.; Heerding, J. M.; Hollinshead, S. P.; Hu, H.; Hughes, P. F.; Jagdmann, G. E.; Johnson, M. G.; Lai, Y.-S.; Lowden, C. T.; Lynch, M. P.; Mendoza, J. S.; Murphy, M. M.; Wilson, J. W.; Ballas, L. M.; Carter, K.; Darges, J. W.; Davis, J. E.; Hubbard, F. R.; Stamper, M. L. Synthesis and protein kinase inhibitory activity of balanol analogues with modified benzophenone subunits. *J. Med. Chem.* **2002**, *45*, 2624-2643.
 8. Lee, D. Y. W.; Karnati, V. V. R.; He, M. S.; Liu-Chen, L. Y.; Kondaveti, L.; Ma, Z. Z.; Wang, Y. L.; Chen, Y.; Beguin, C.; Carlezon, W. A.; Cohen, B. Synthesis and in vitro pharmacological studies of new C(2) modified salvinorin A analogues. *Bioorg. Med. Chem. Lett.* **2005**, *15*, 3744-3747.
 9. Harding, W. W.; Tidgewell, K.; Byrd, N.; Cobb, H.; Dersch, C. M.; Butelman, E. R.; Rothman, R. B.; Prisinzano, T. E. Neoclerodane diterpenes as a novel scaffold for mu opioid receptor ligands. *J. Med. Chem.* **2005**, *48*, 4765-4771.

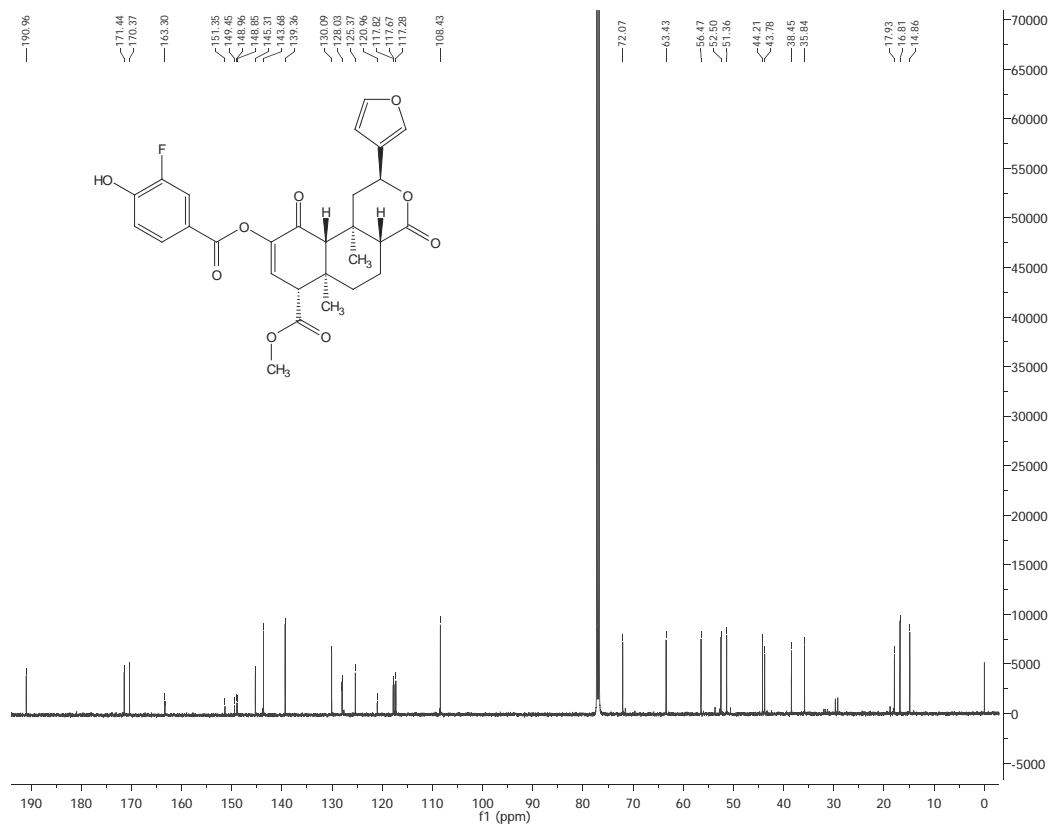
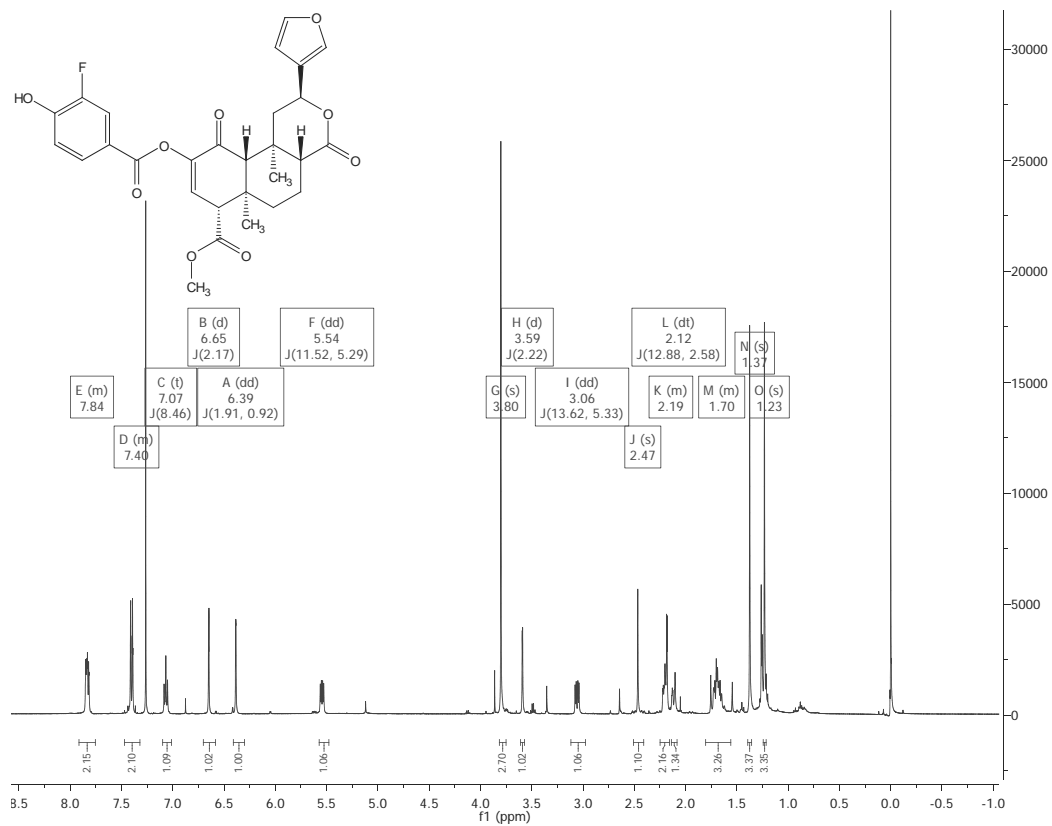


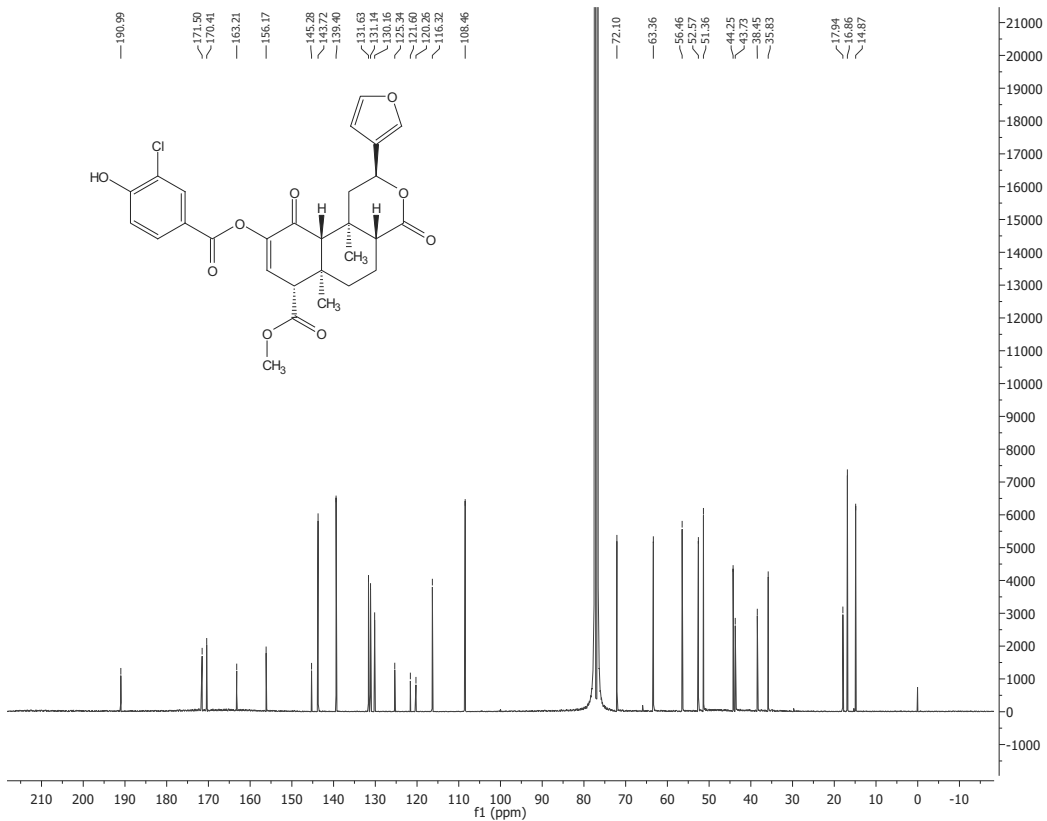
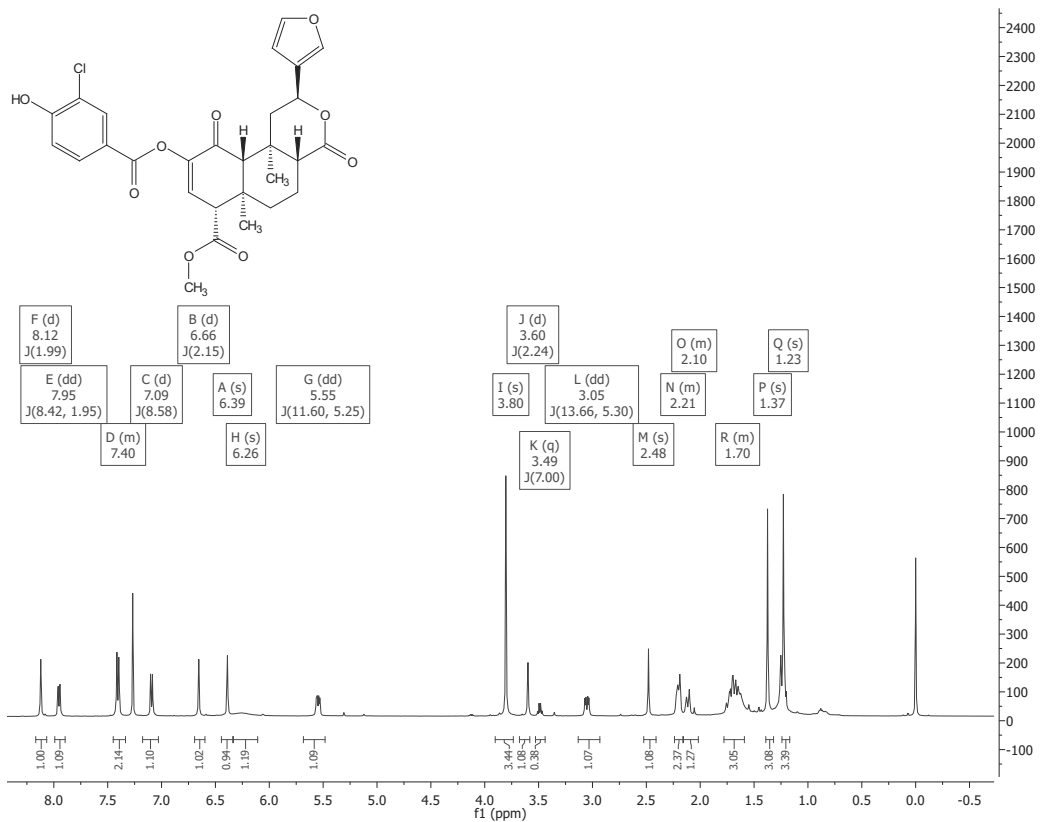


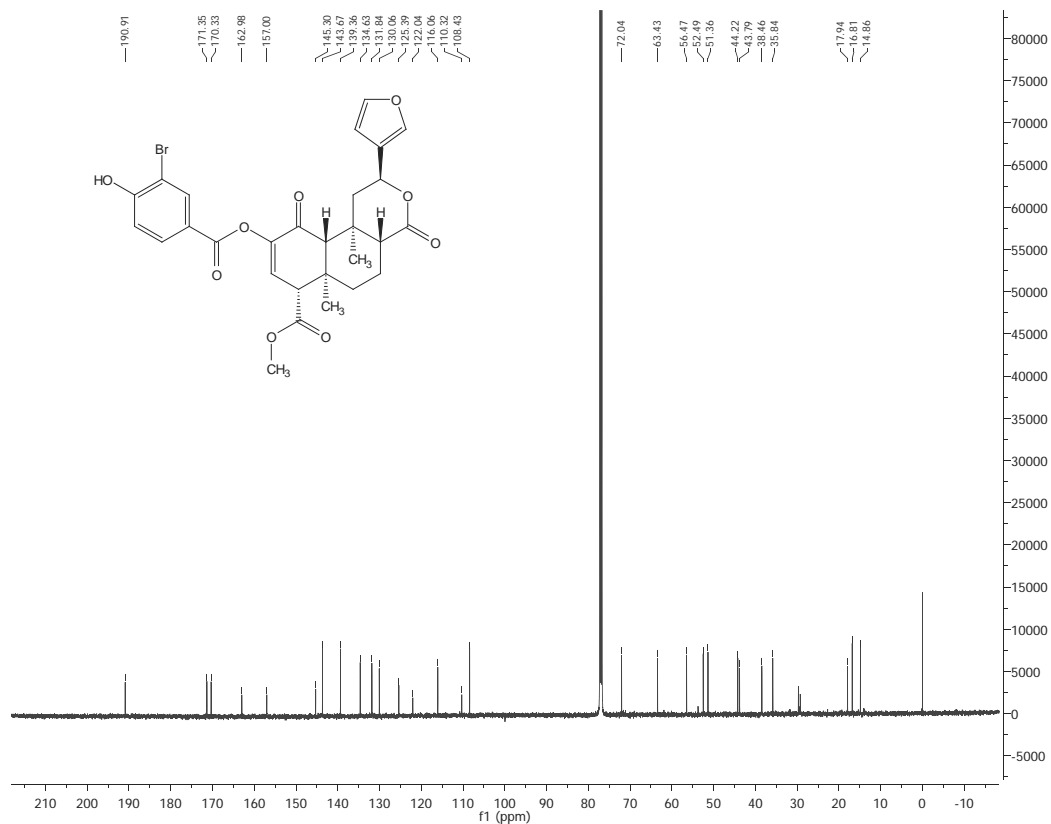
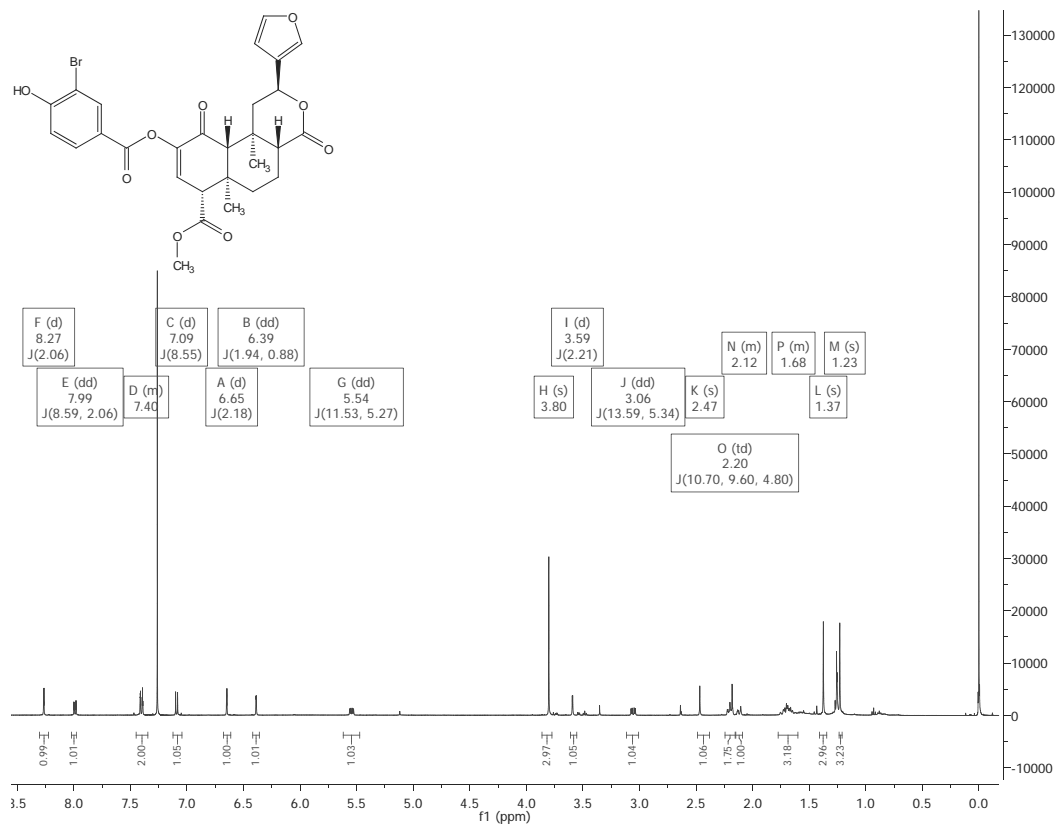


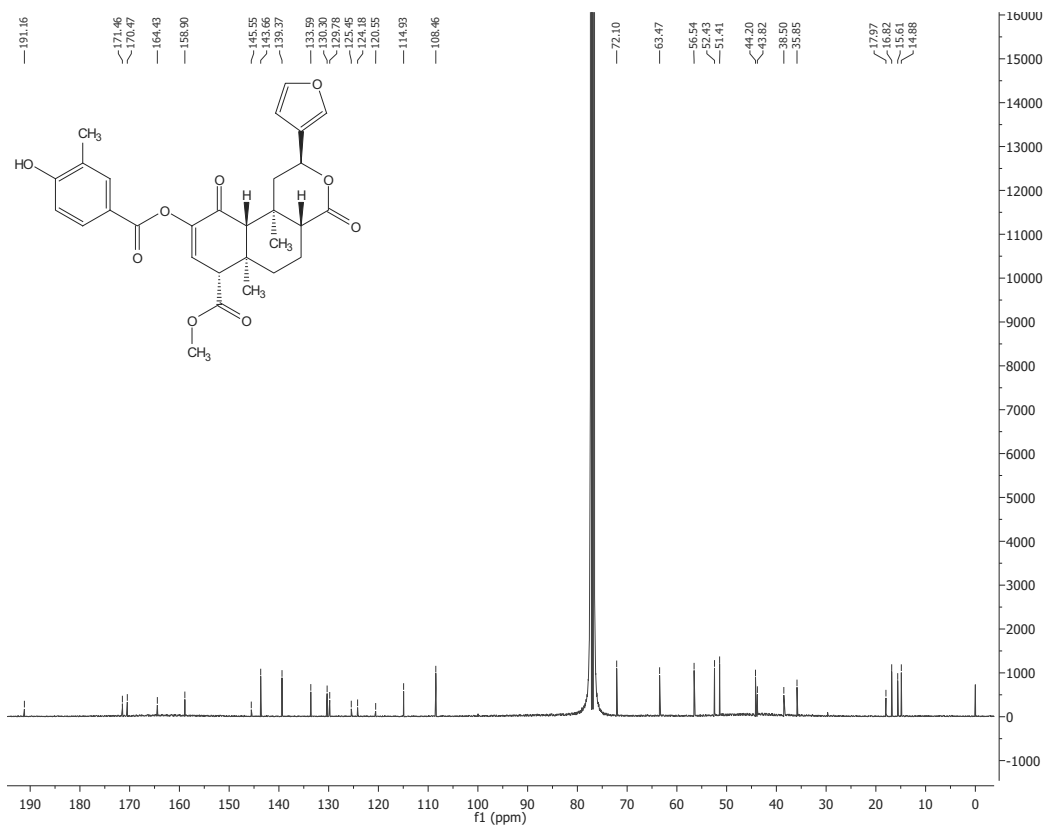
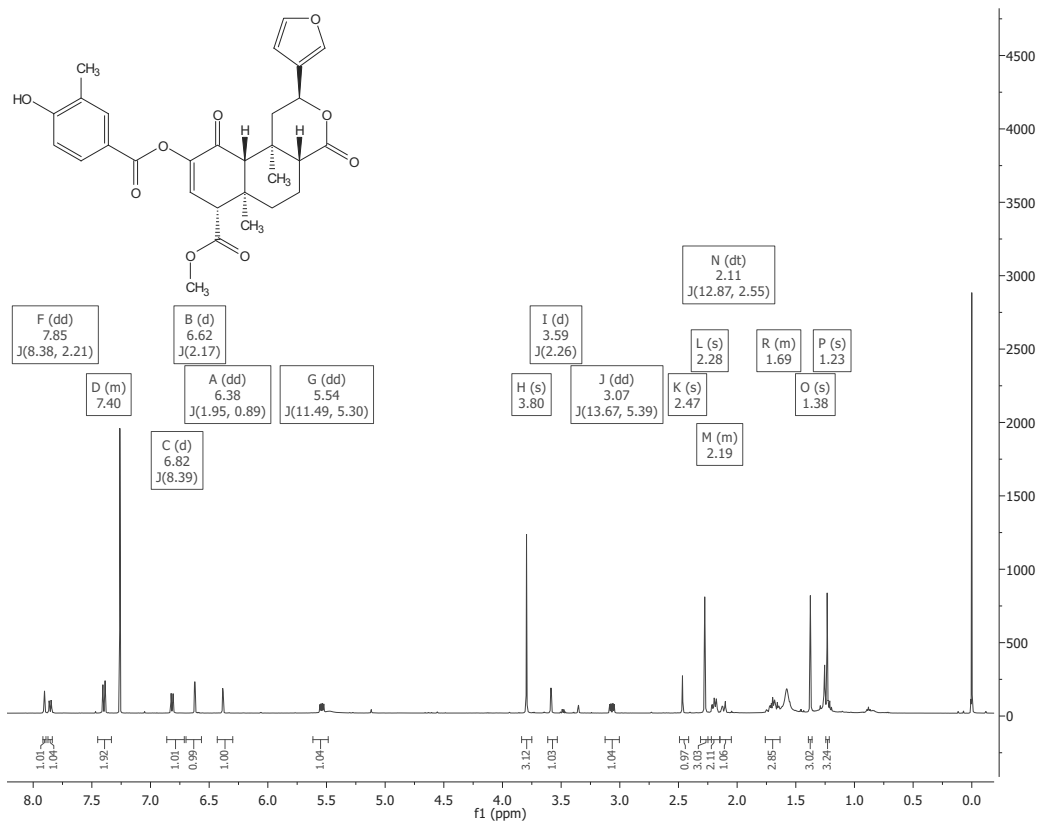


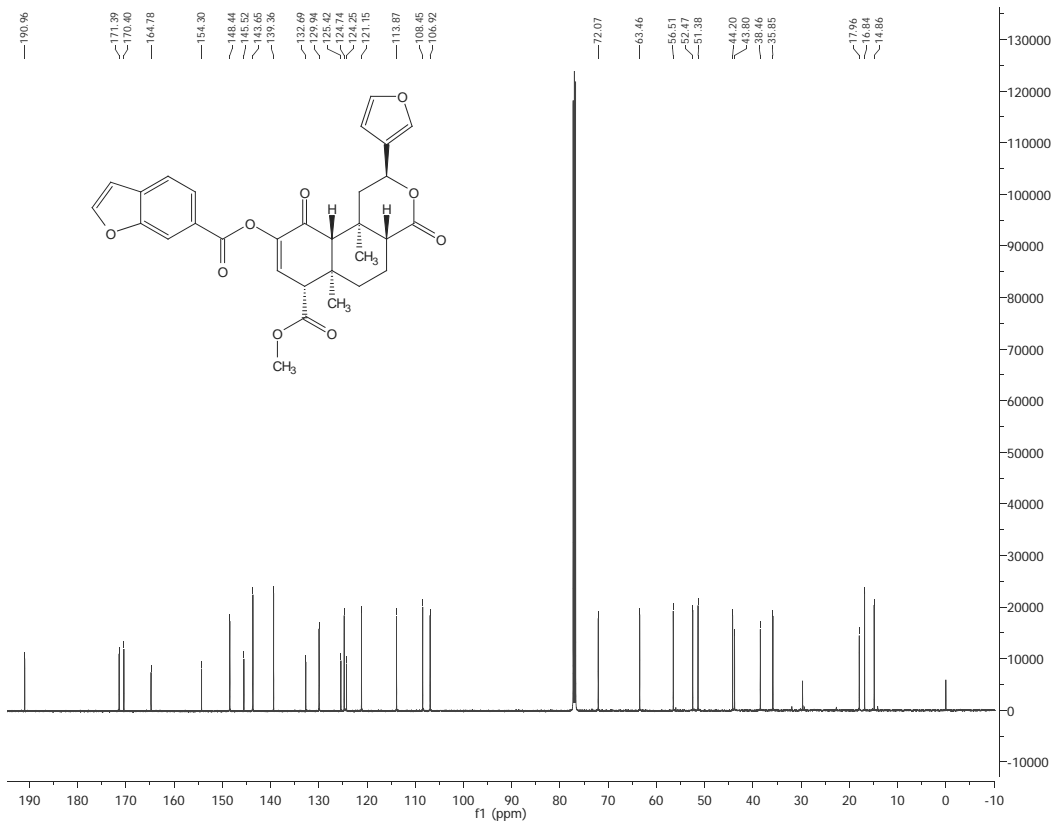
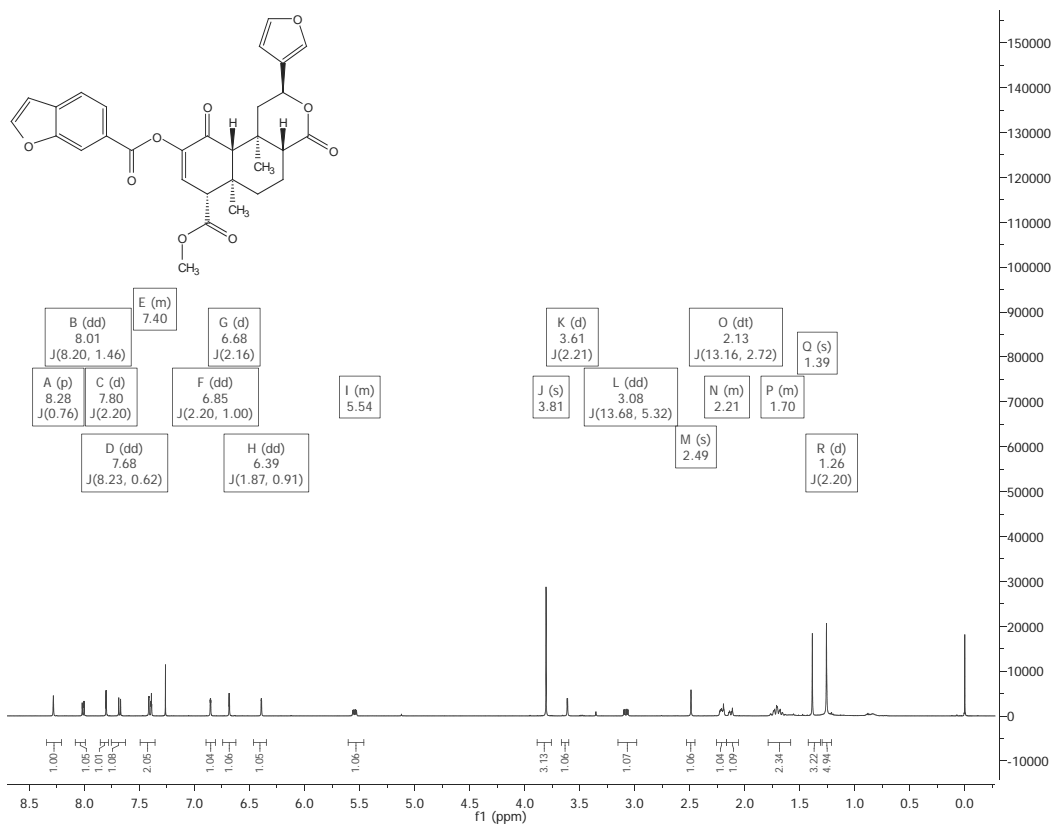


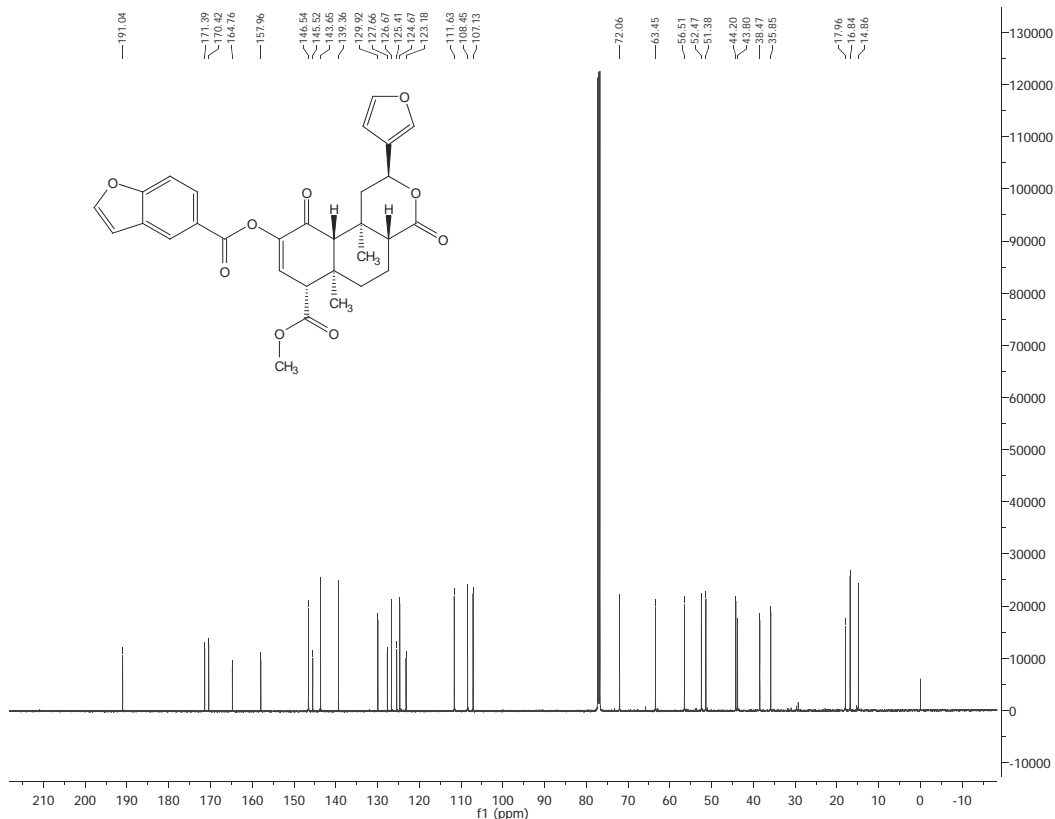
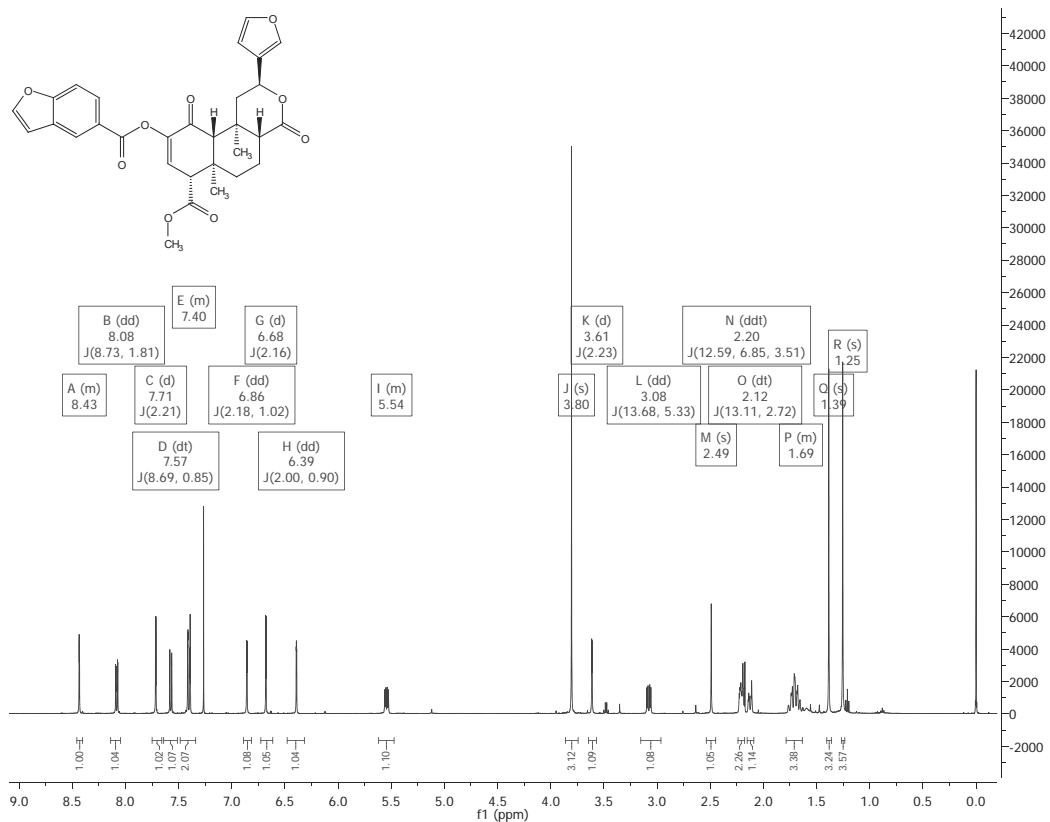


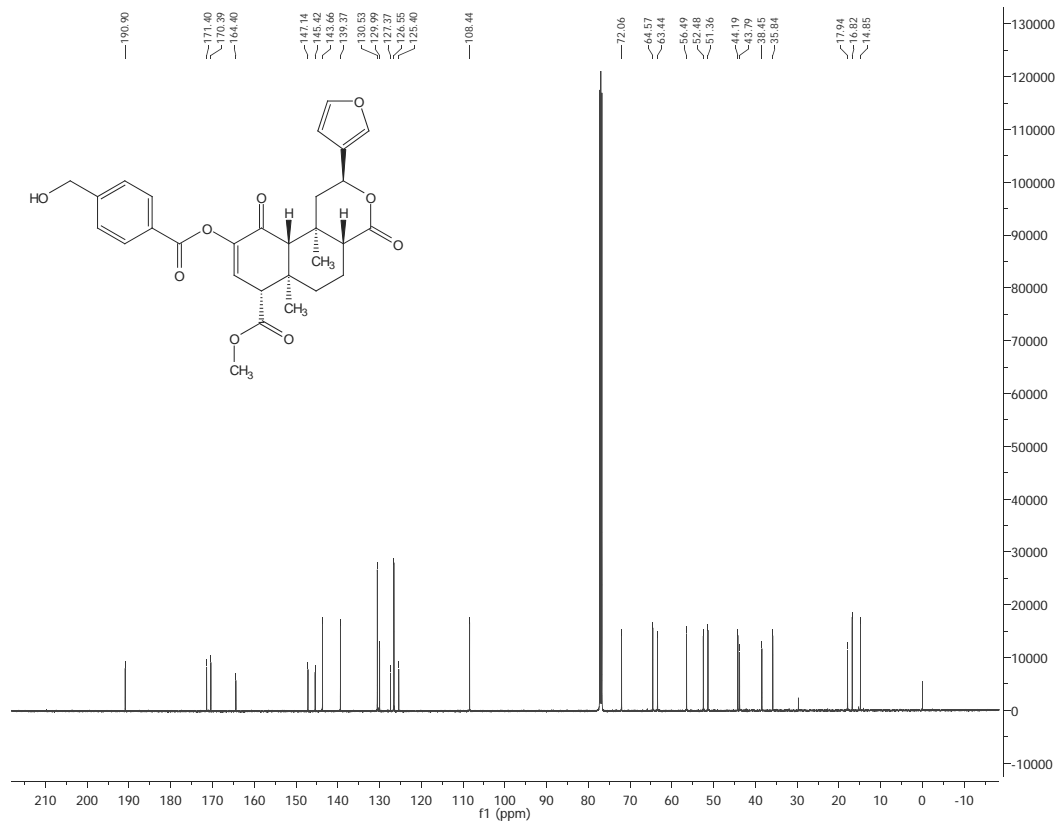
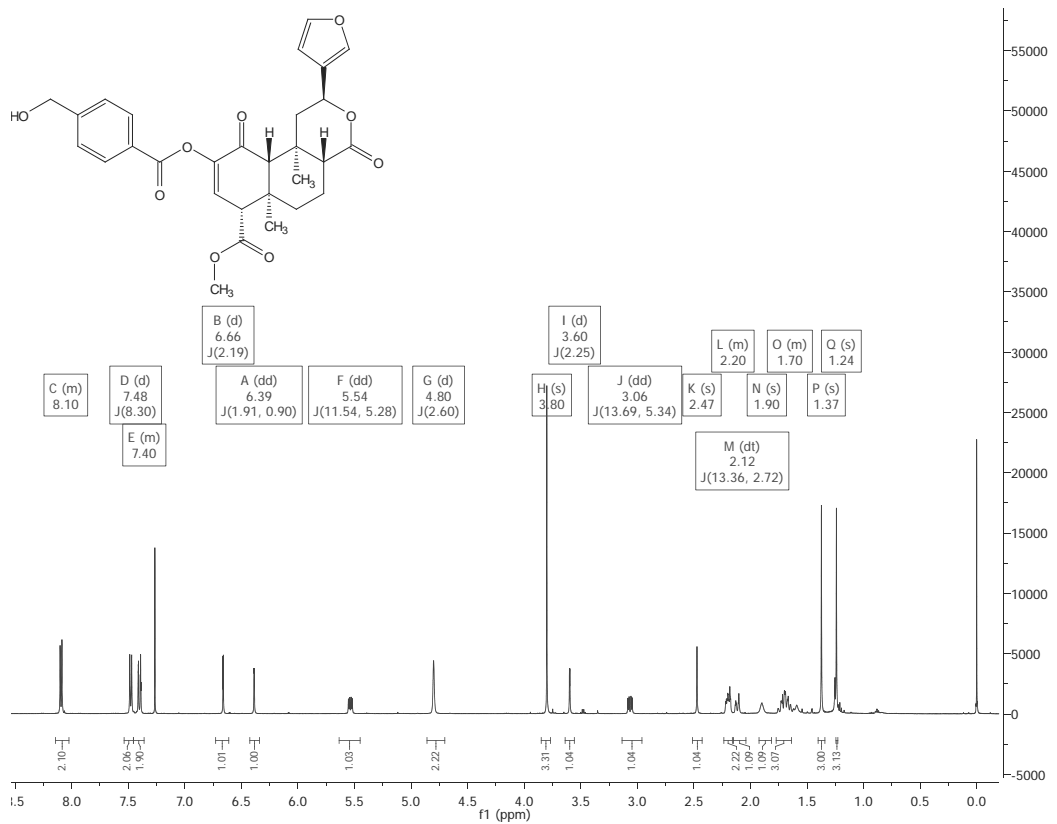


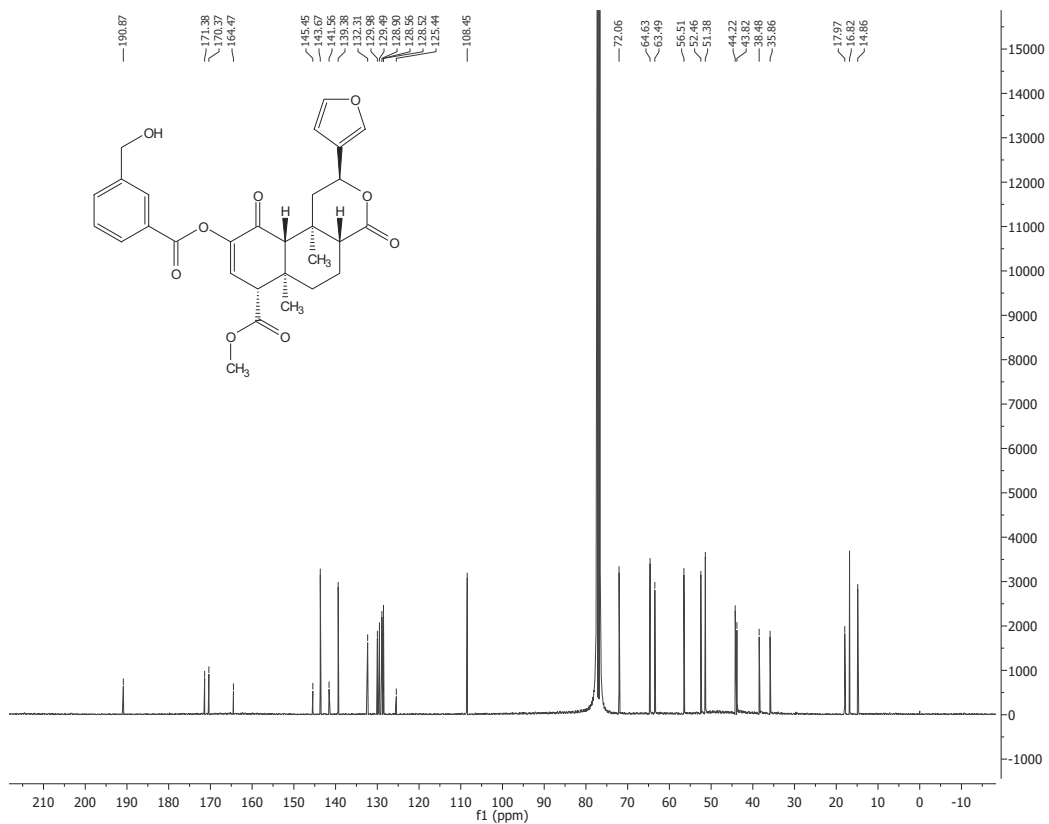
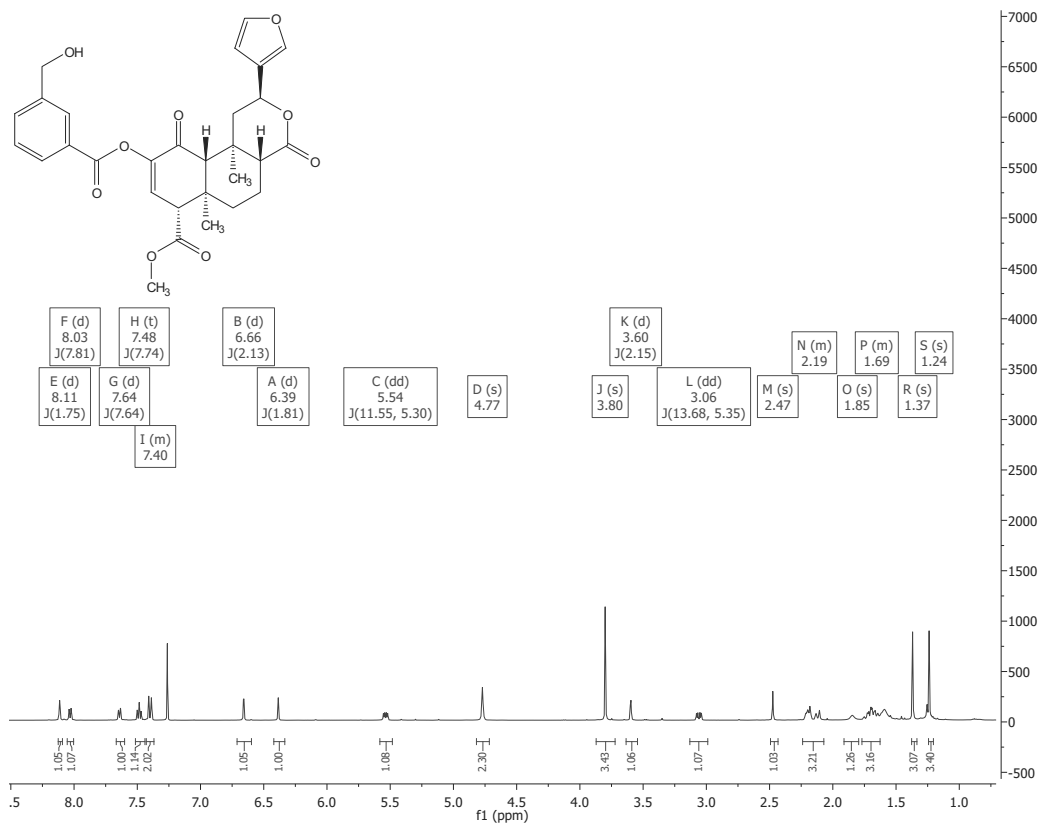


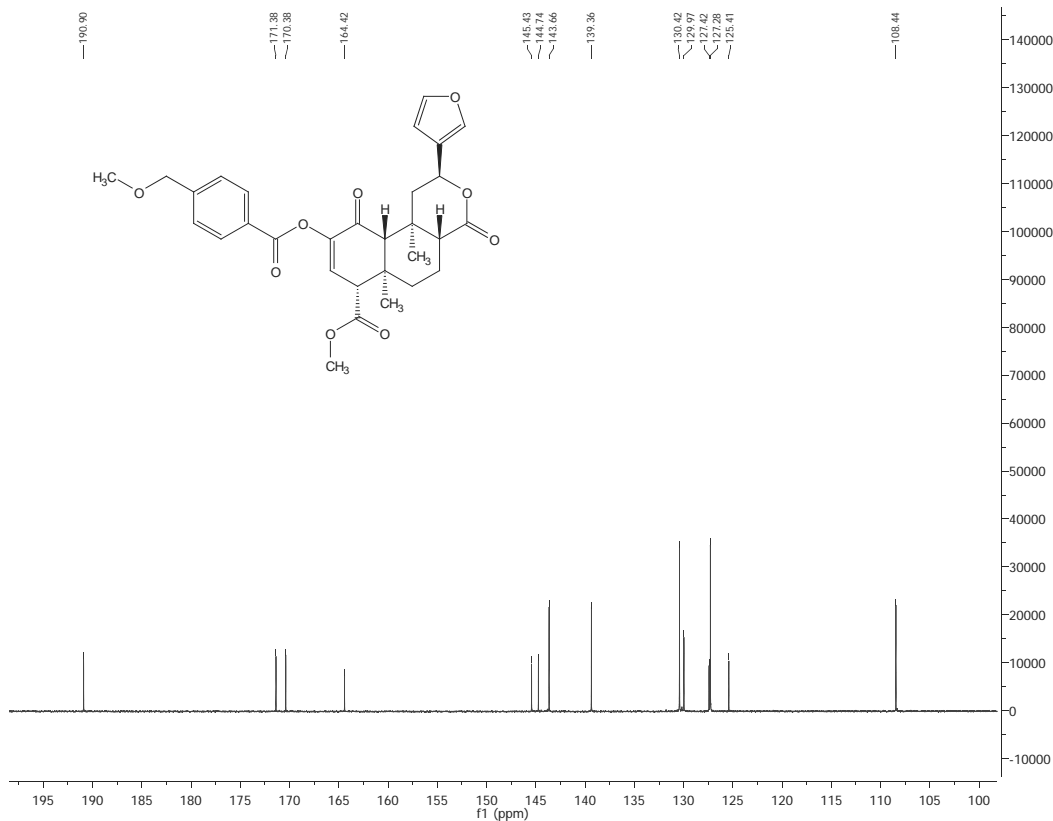
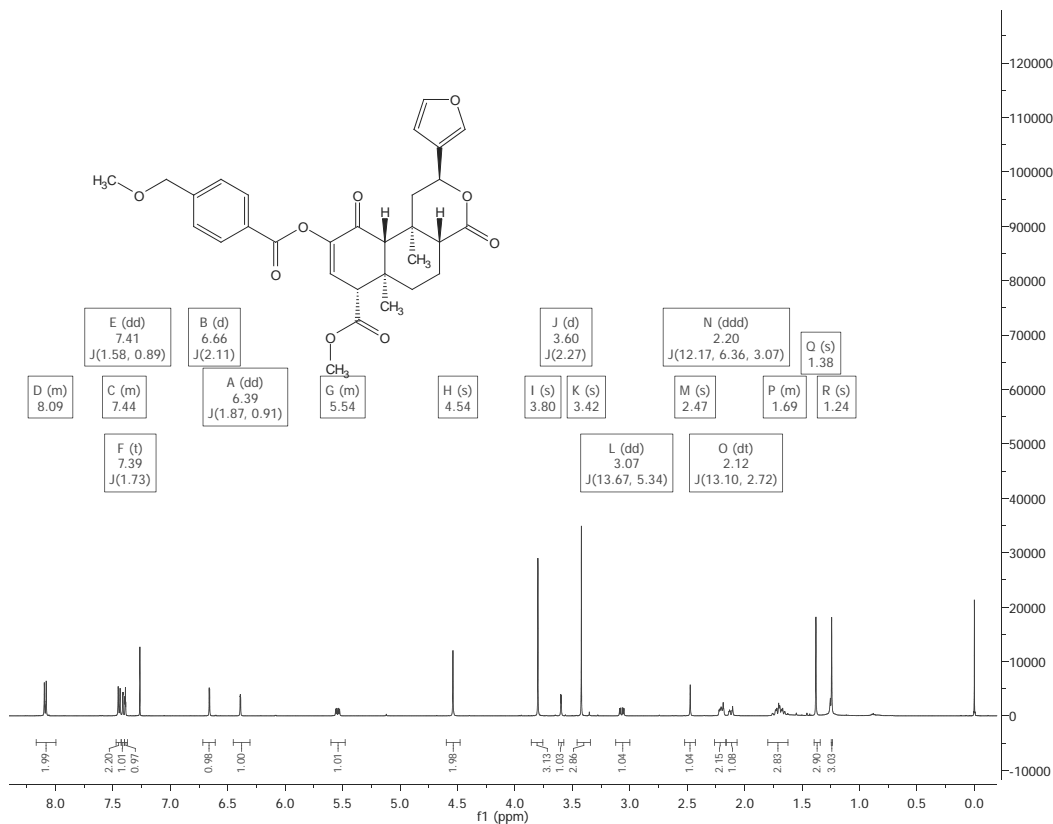


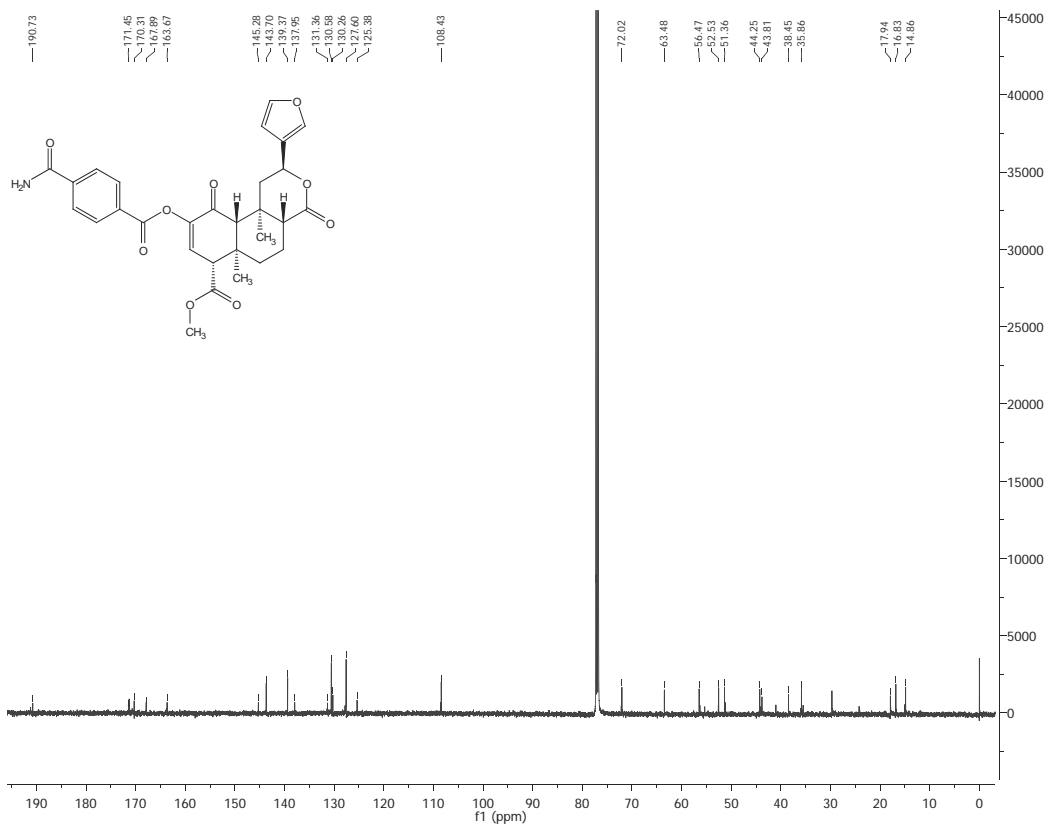
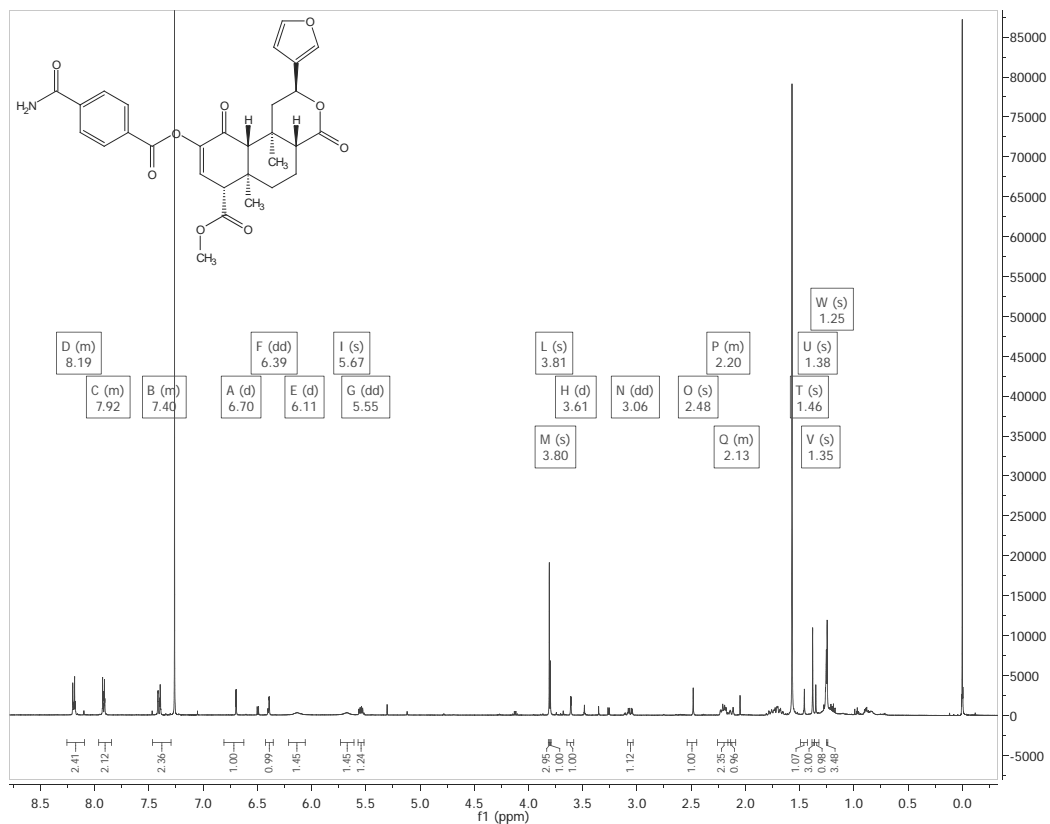


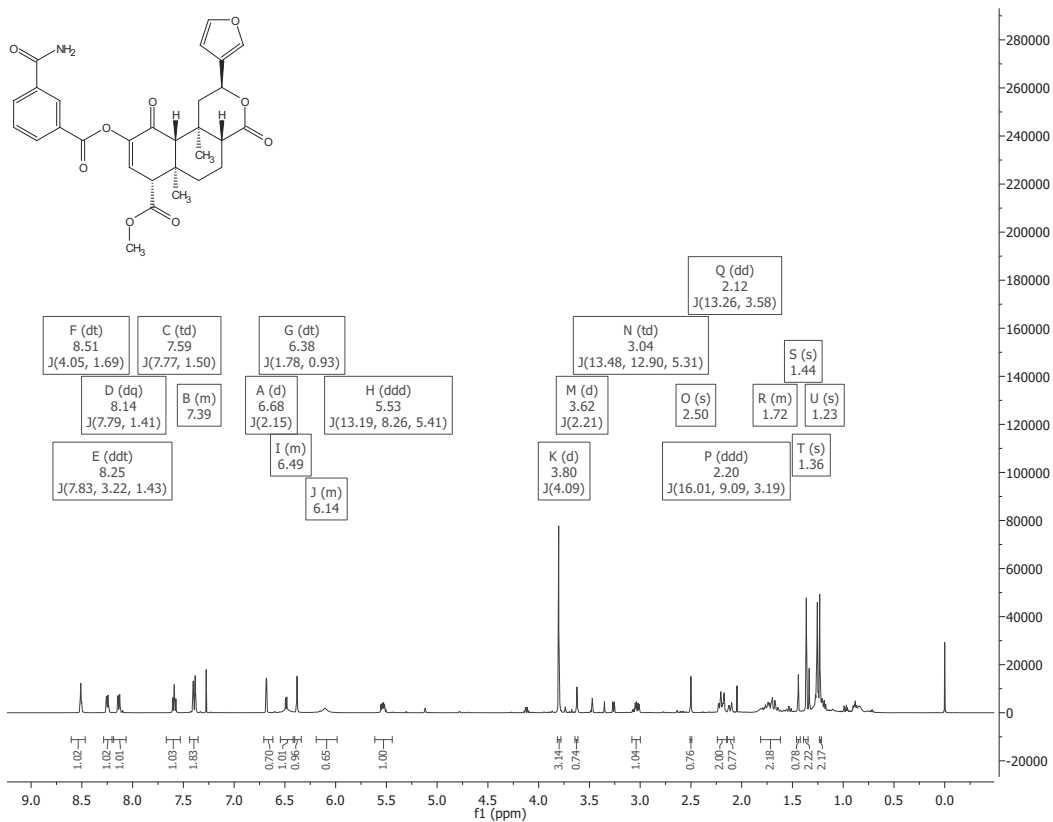


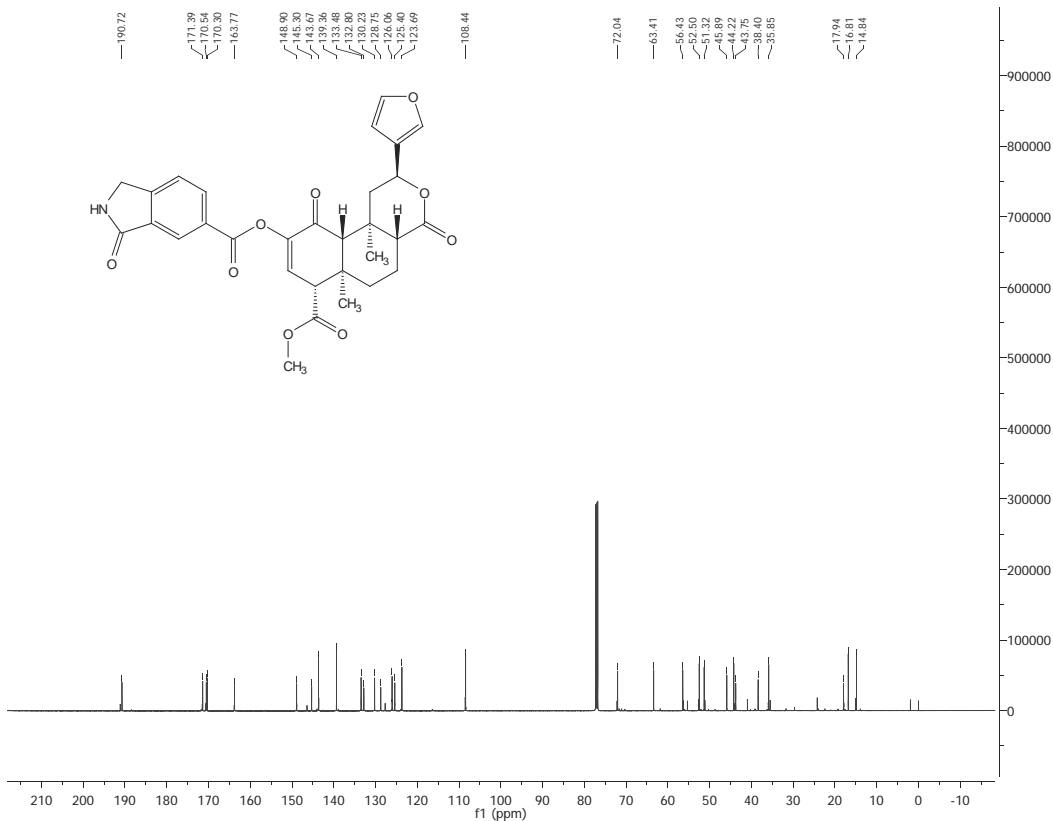
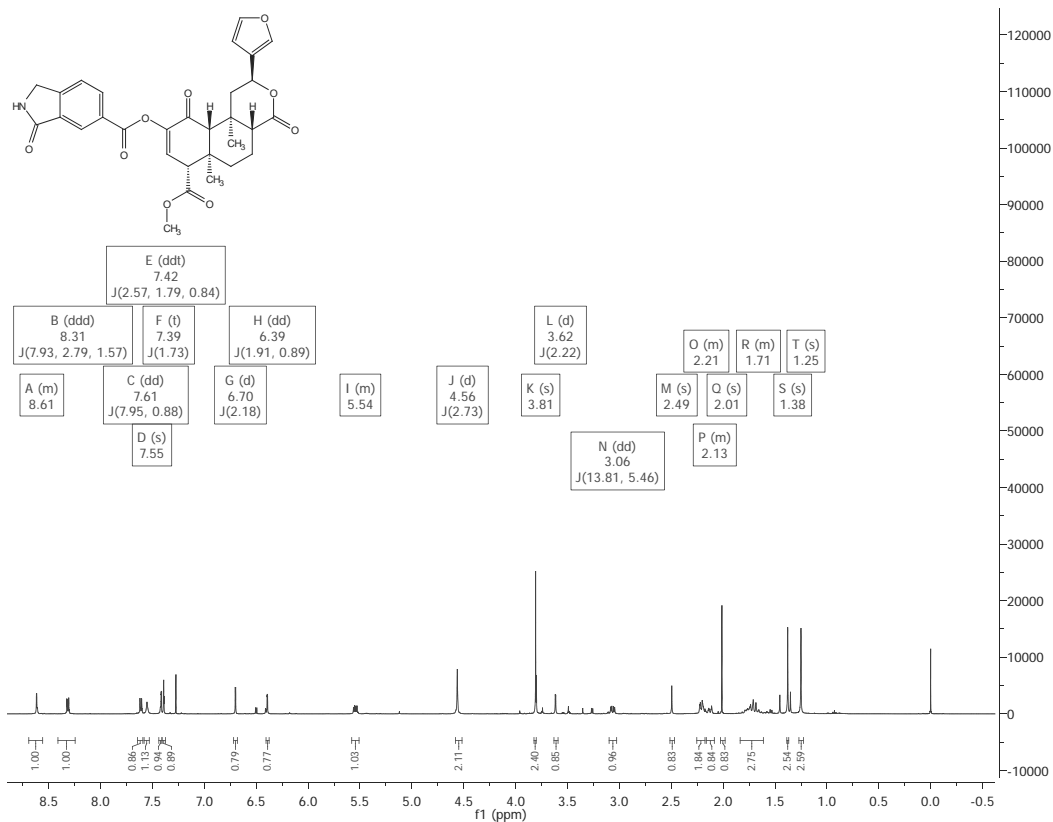


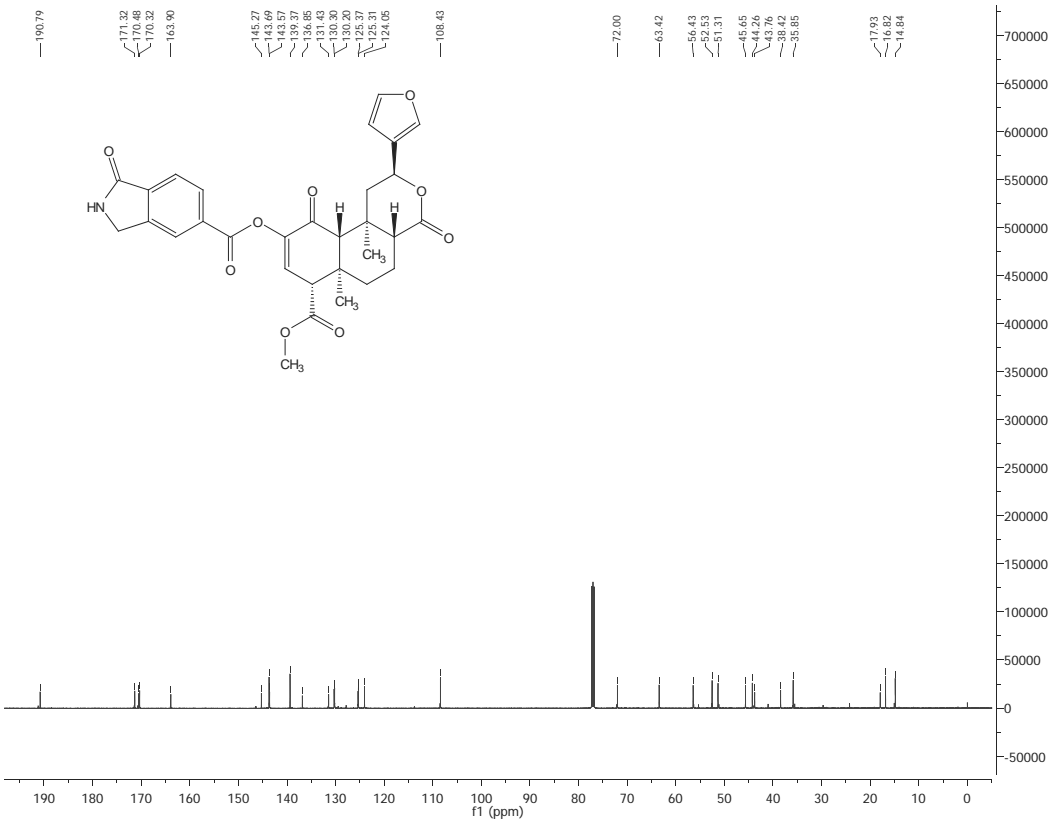
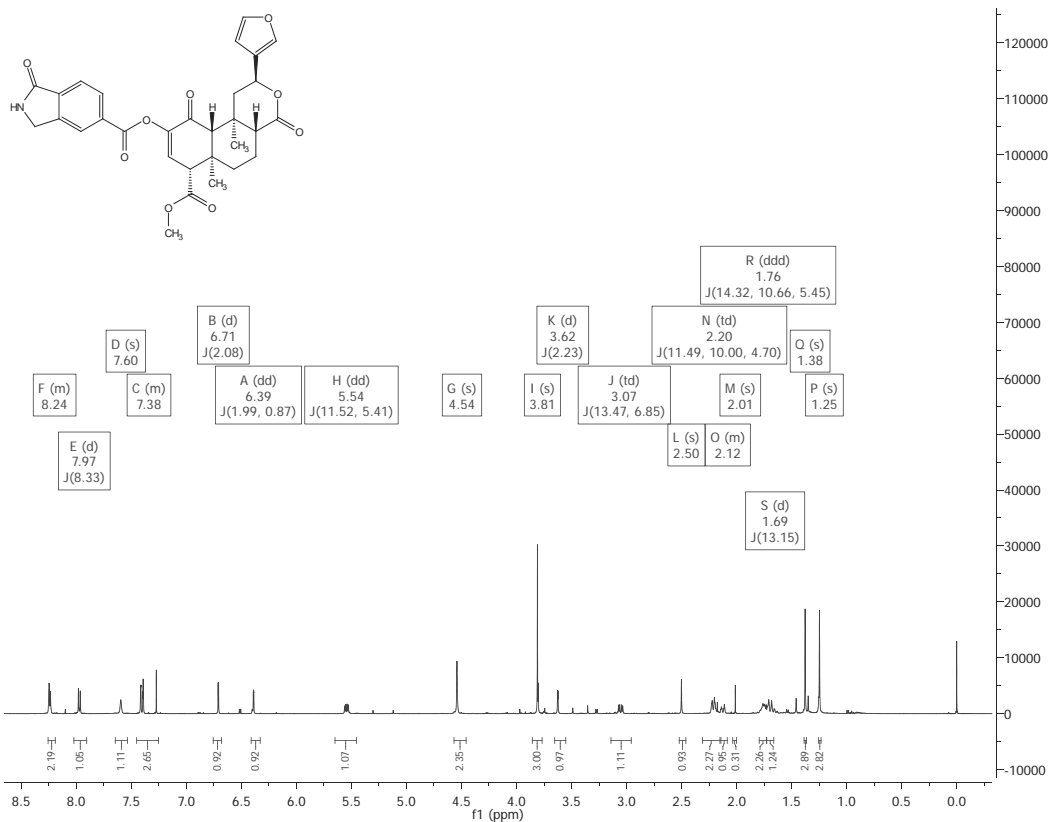


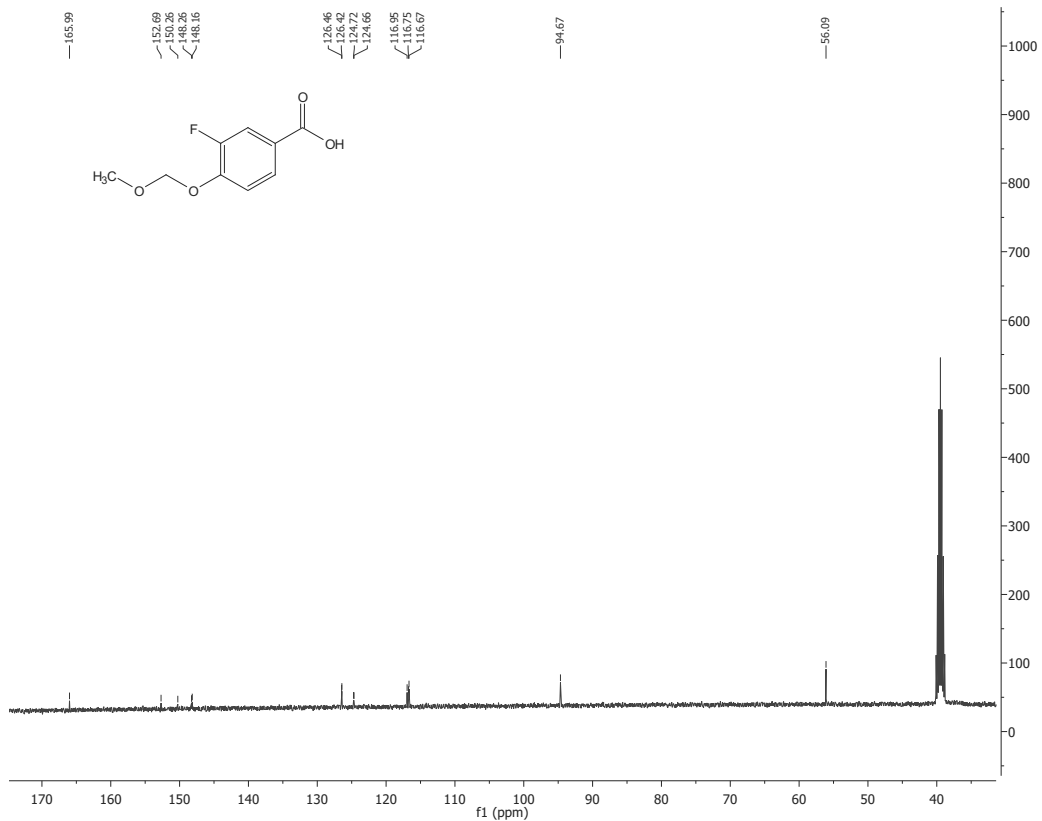
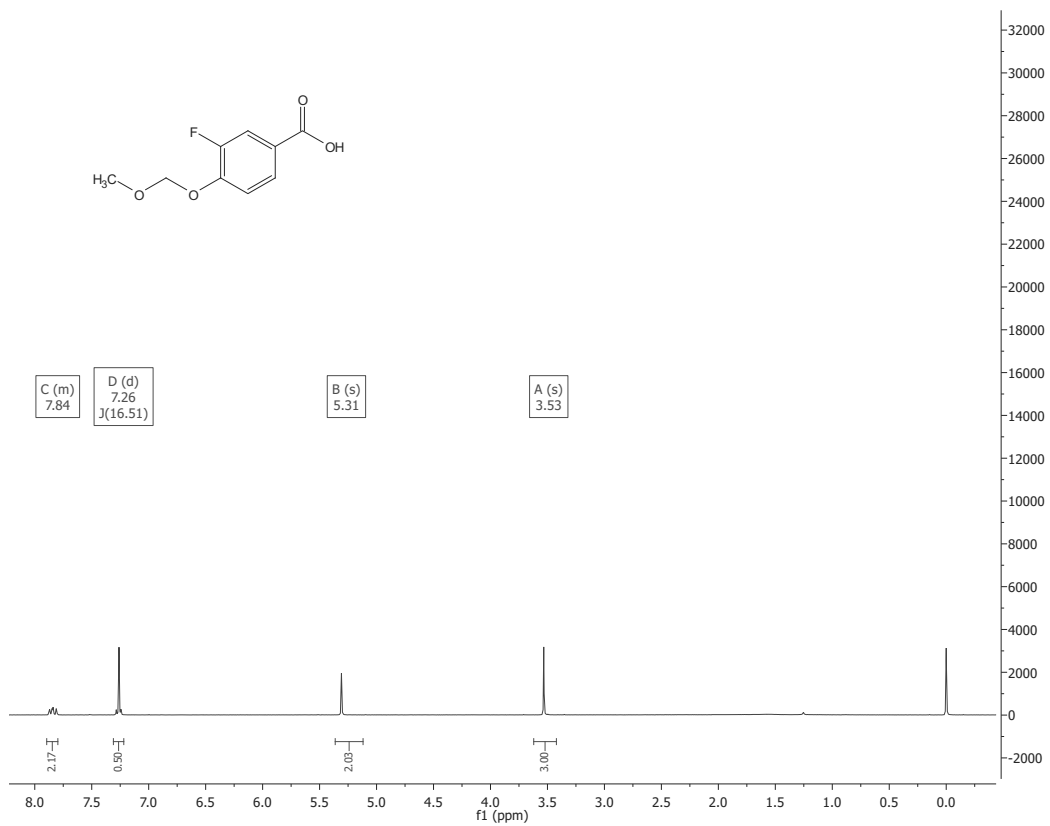


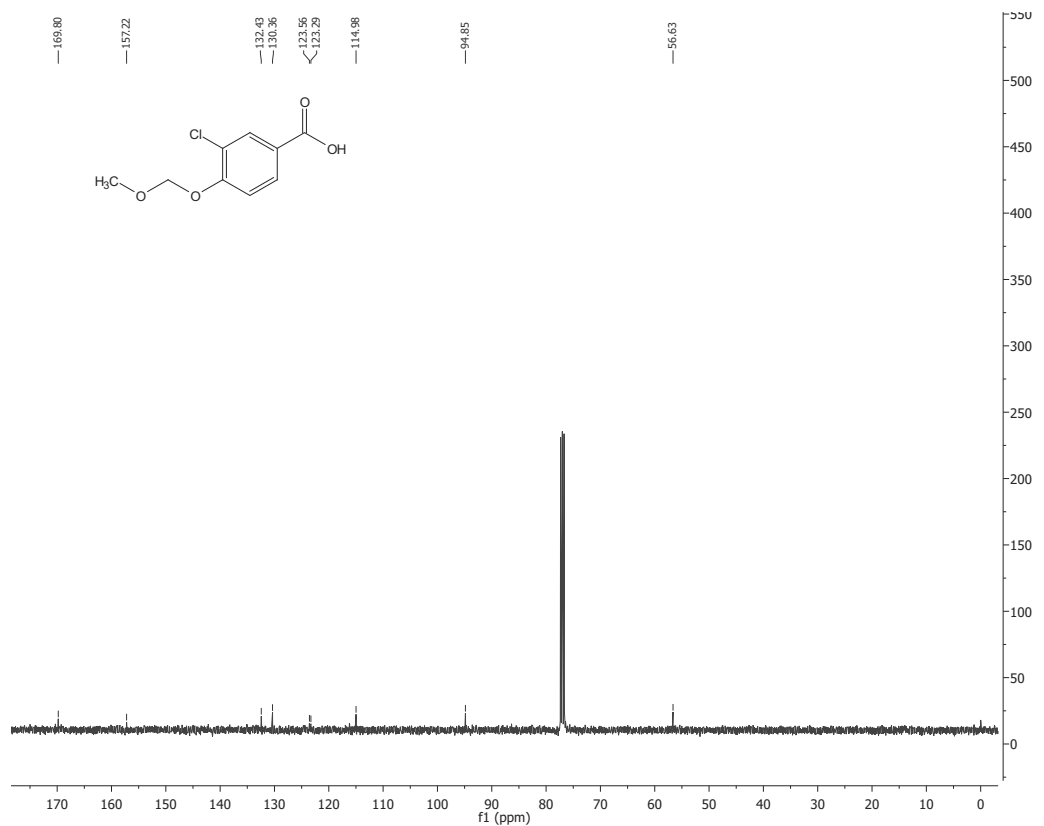
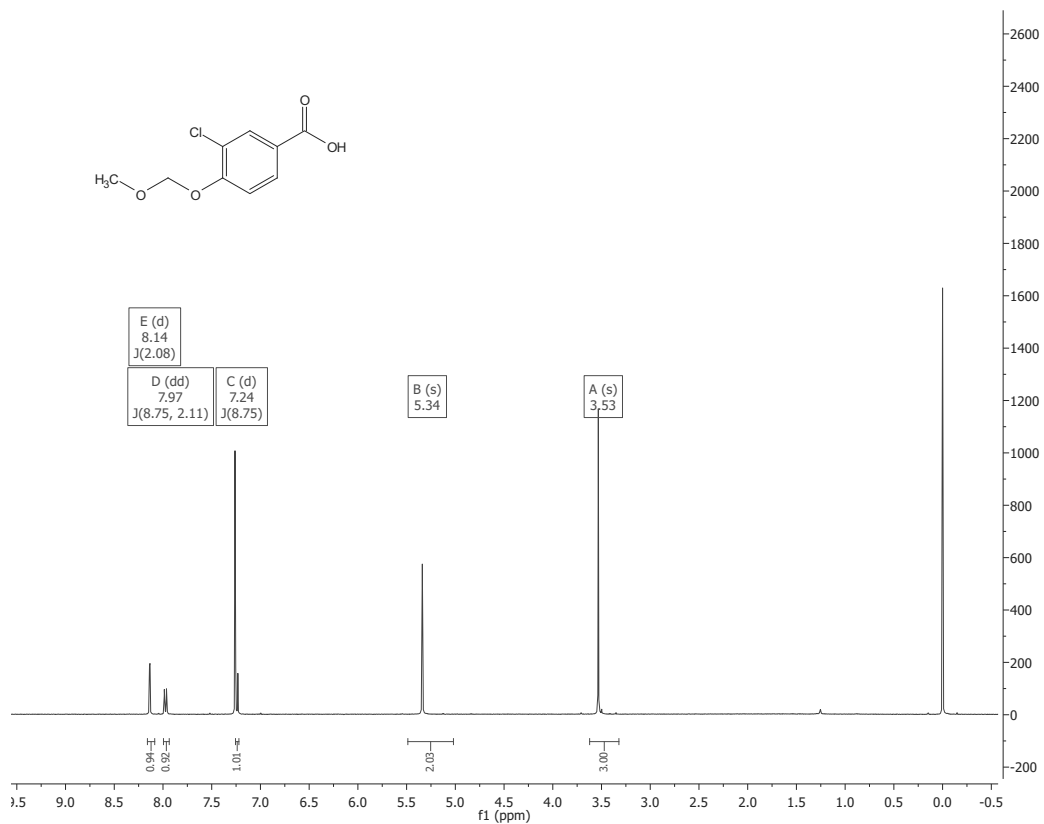


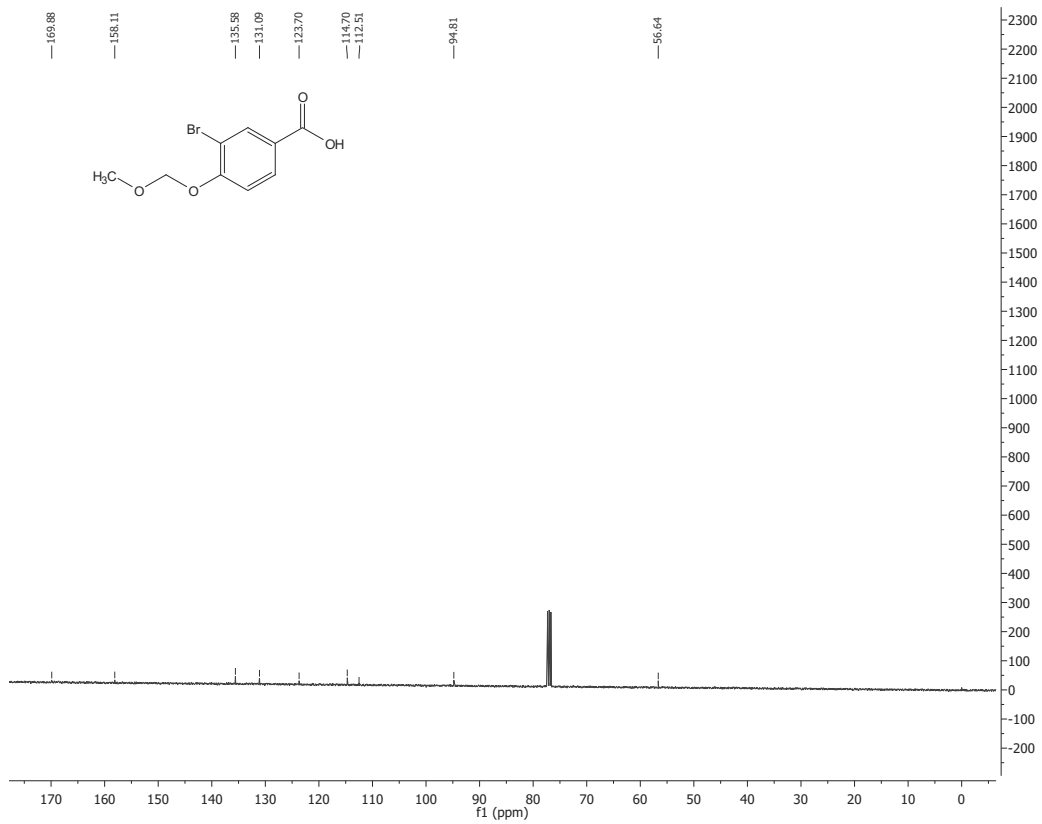
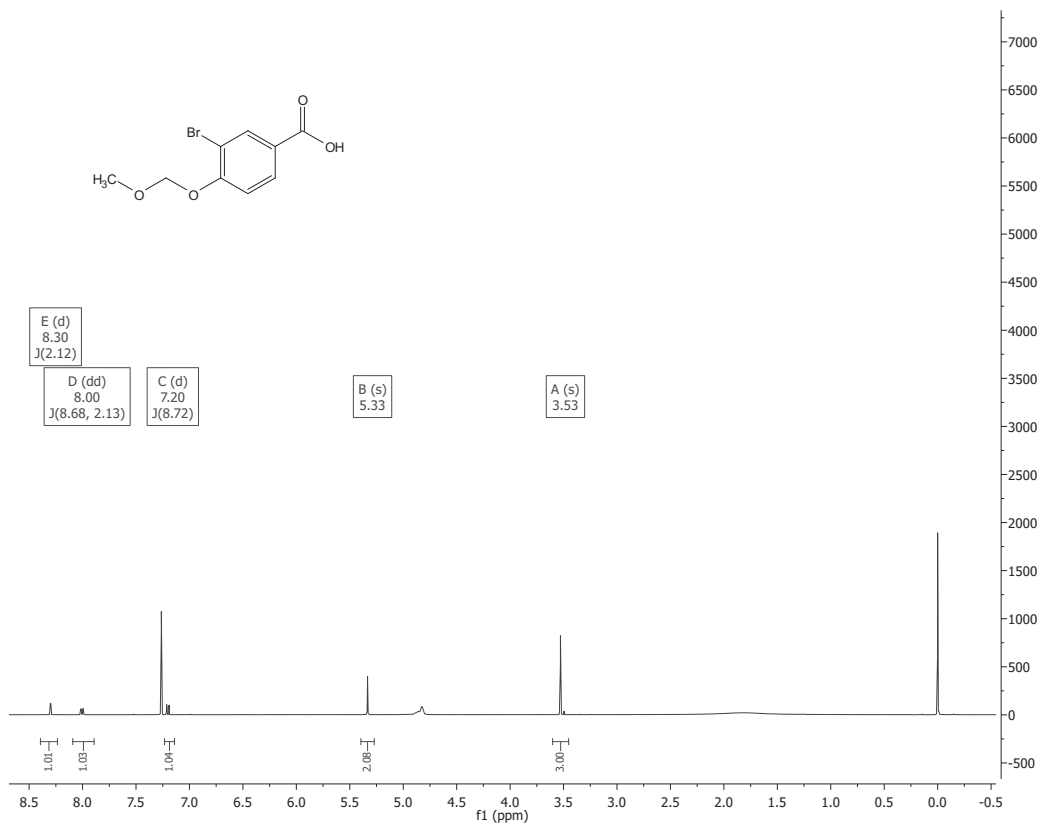


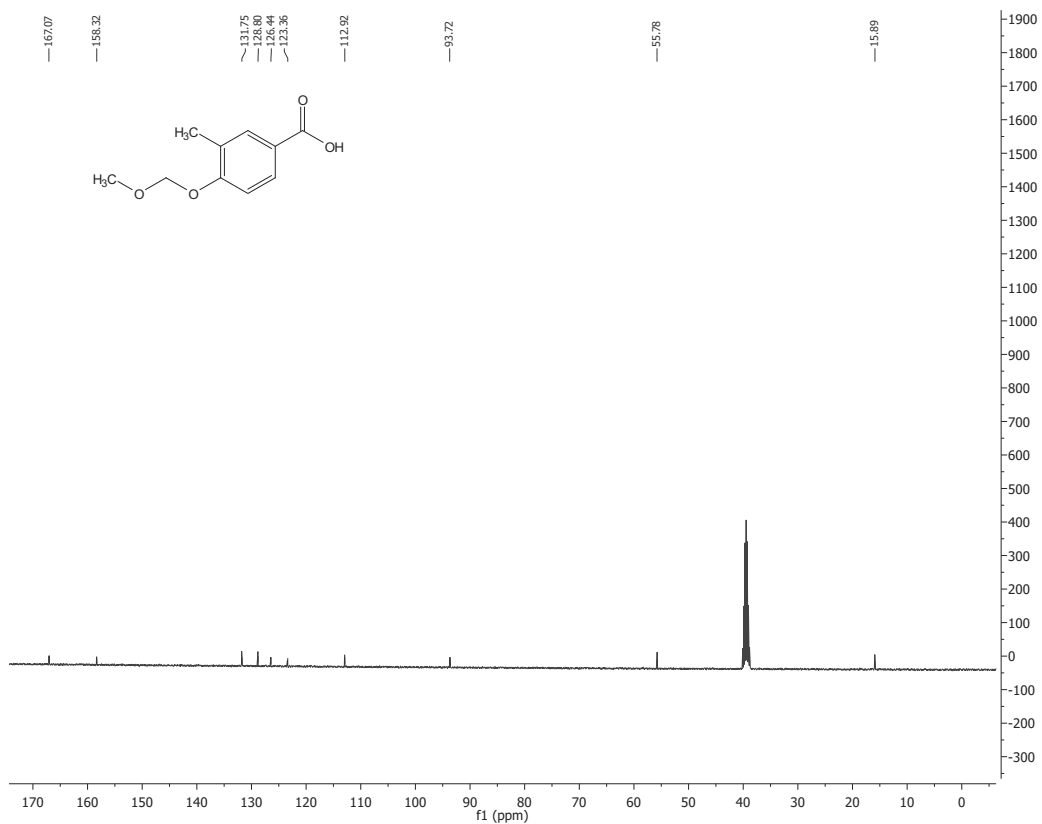
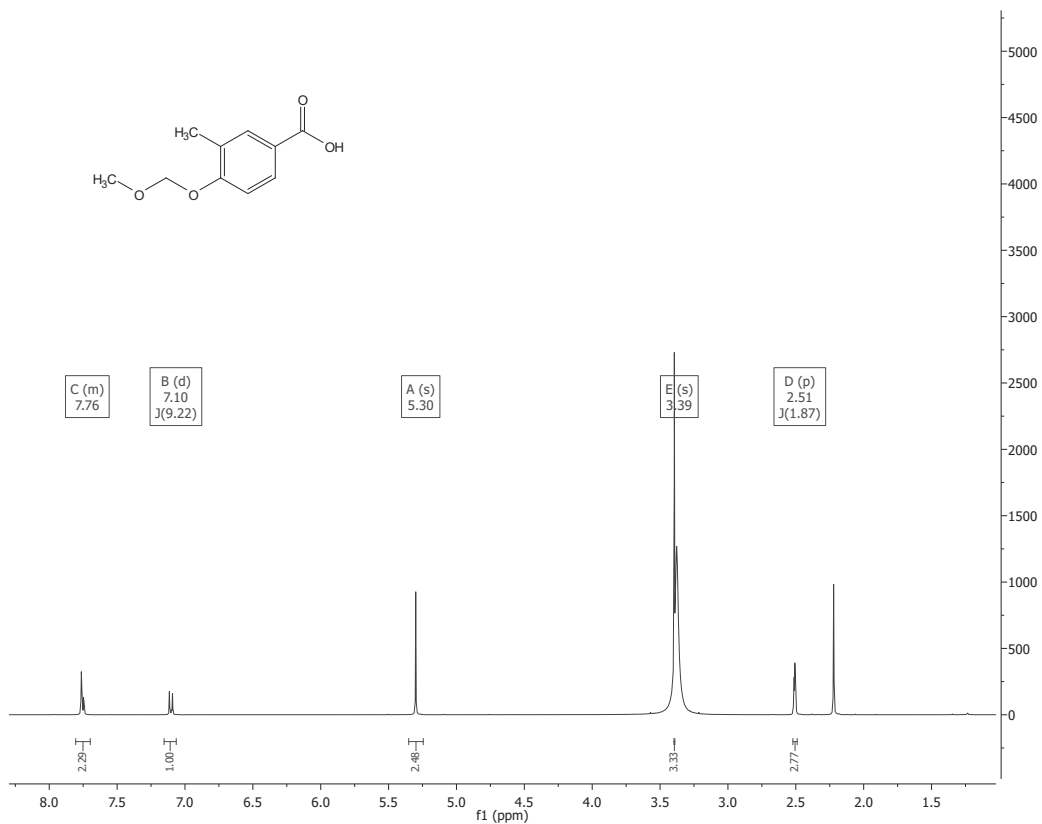


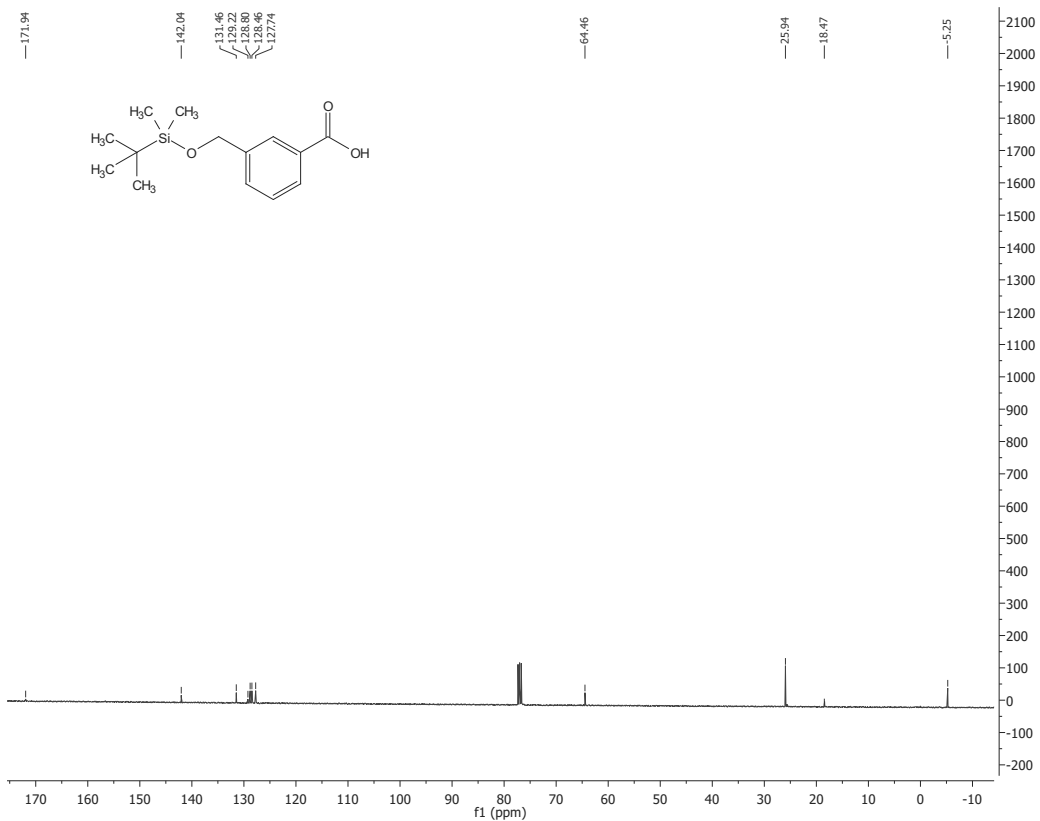
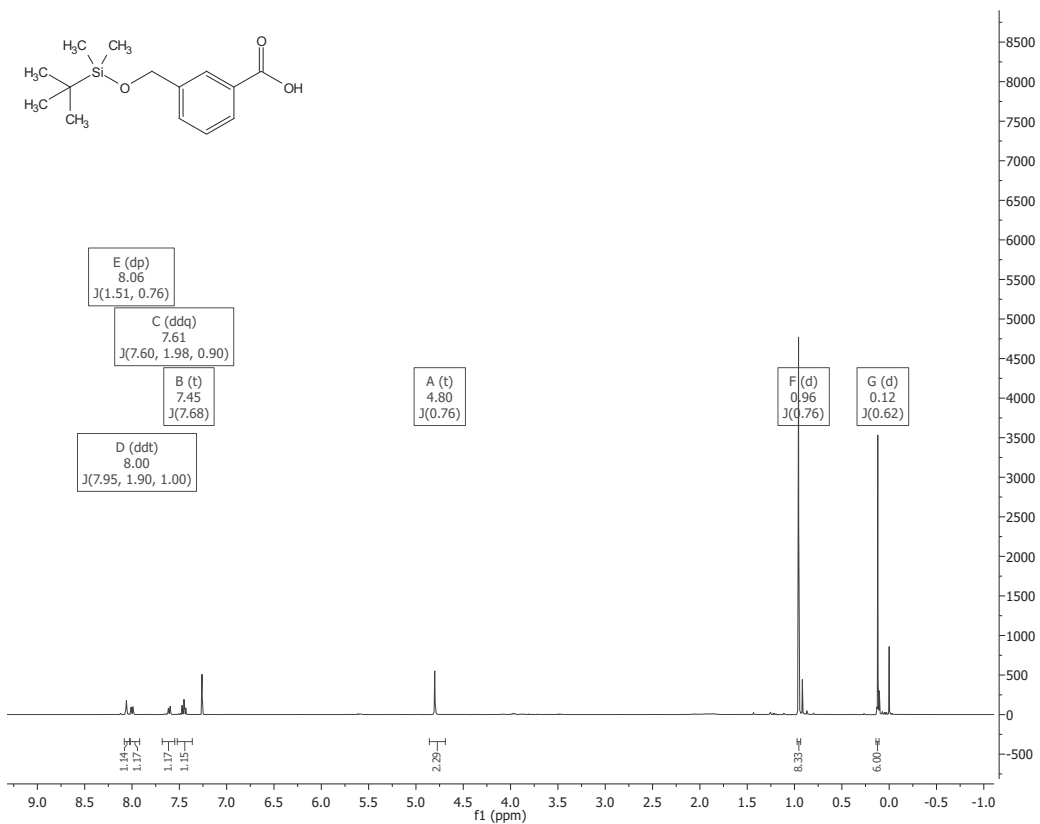


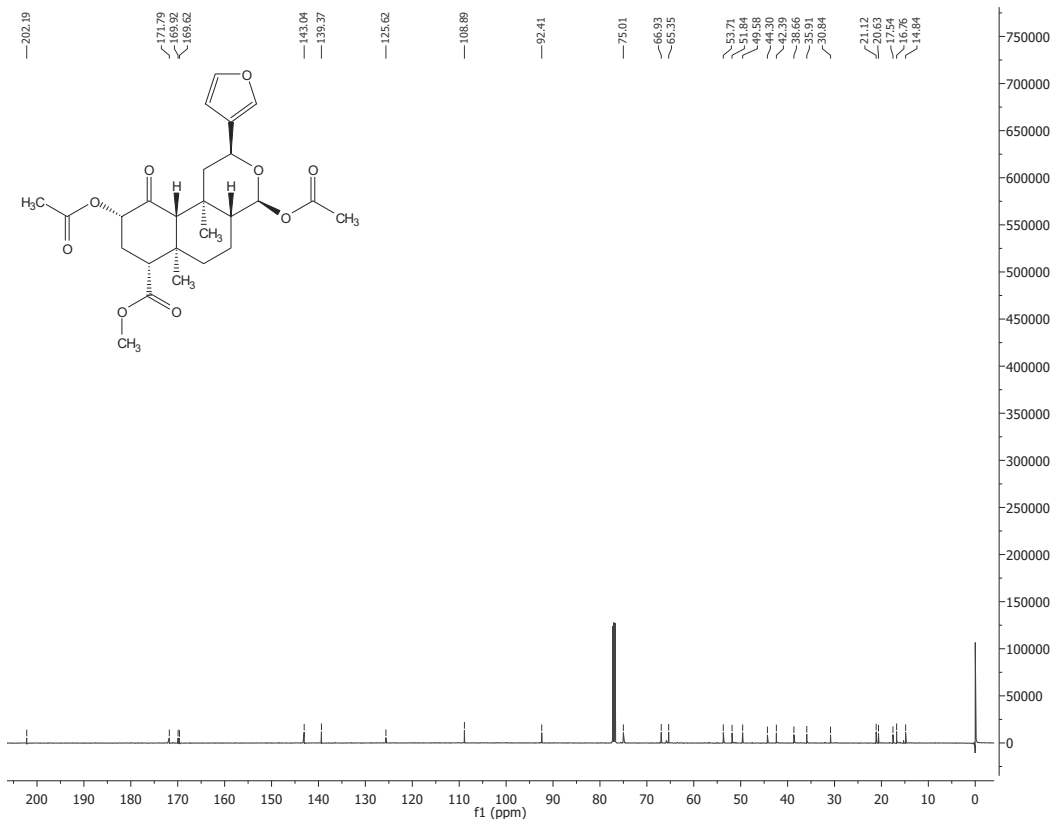
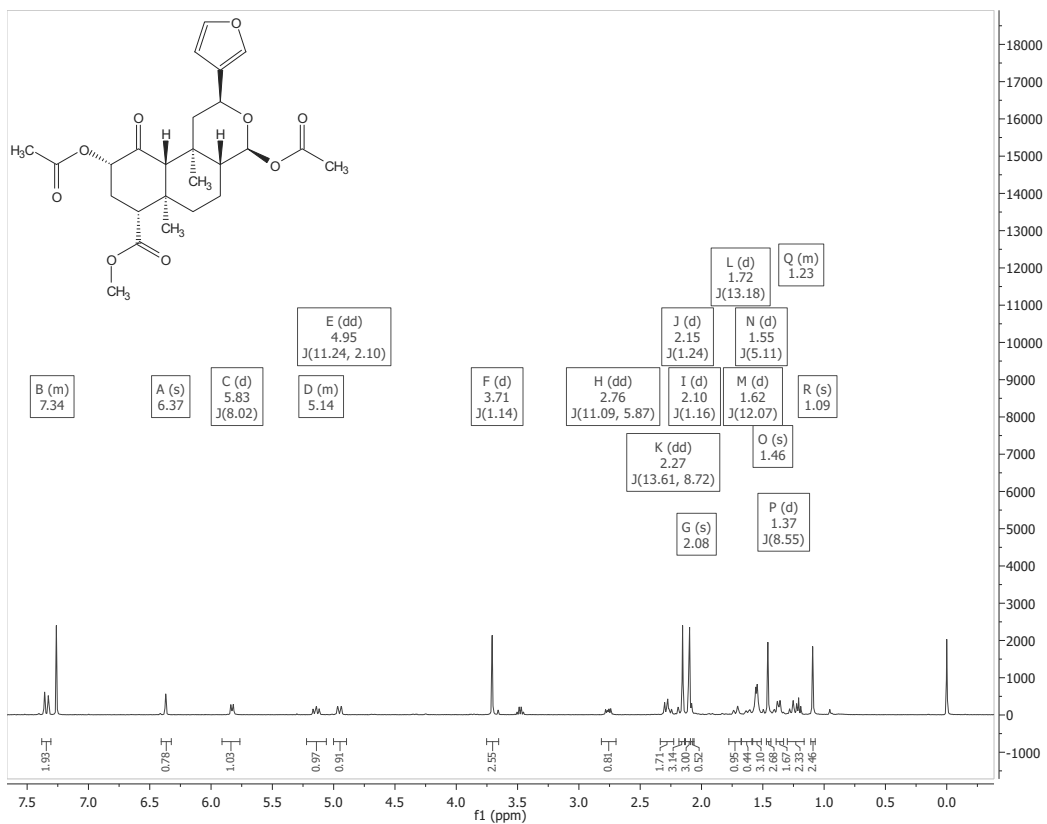




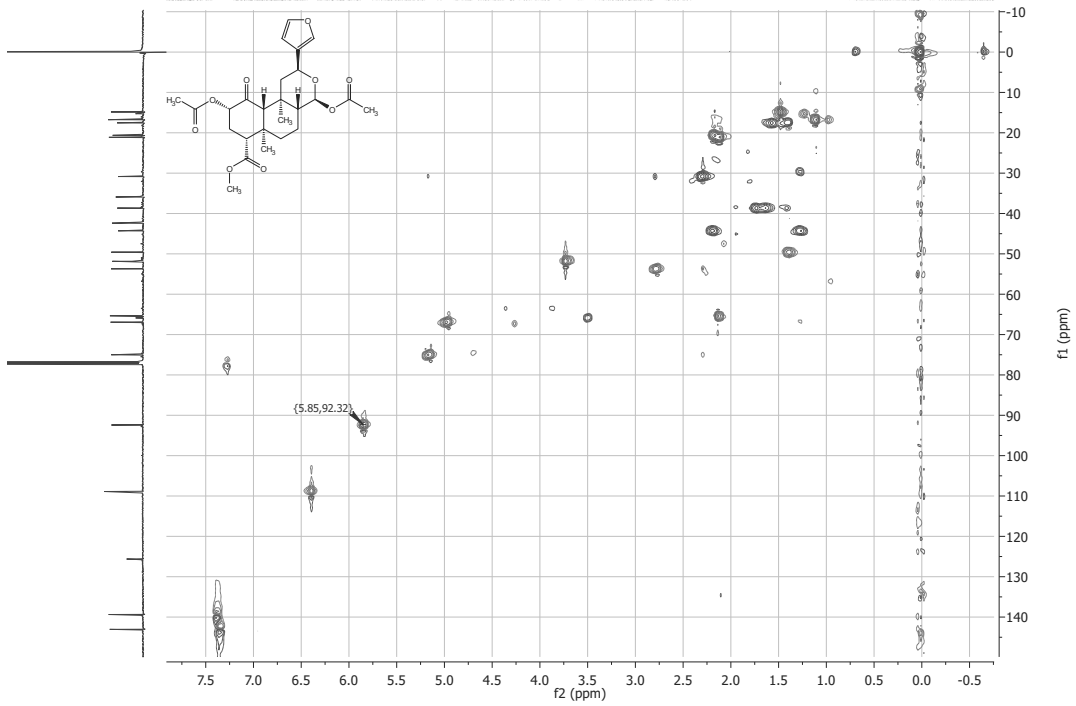




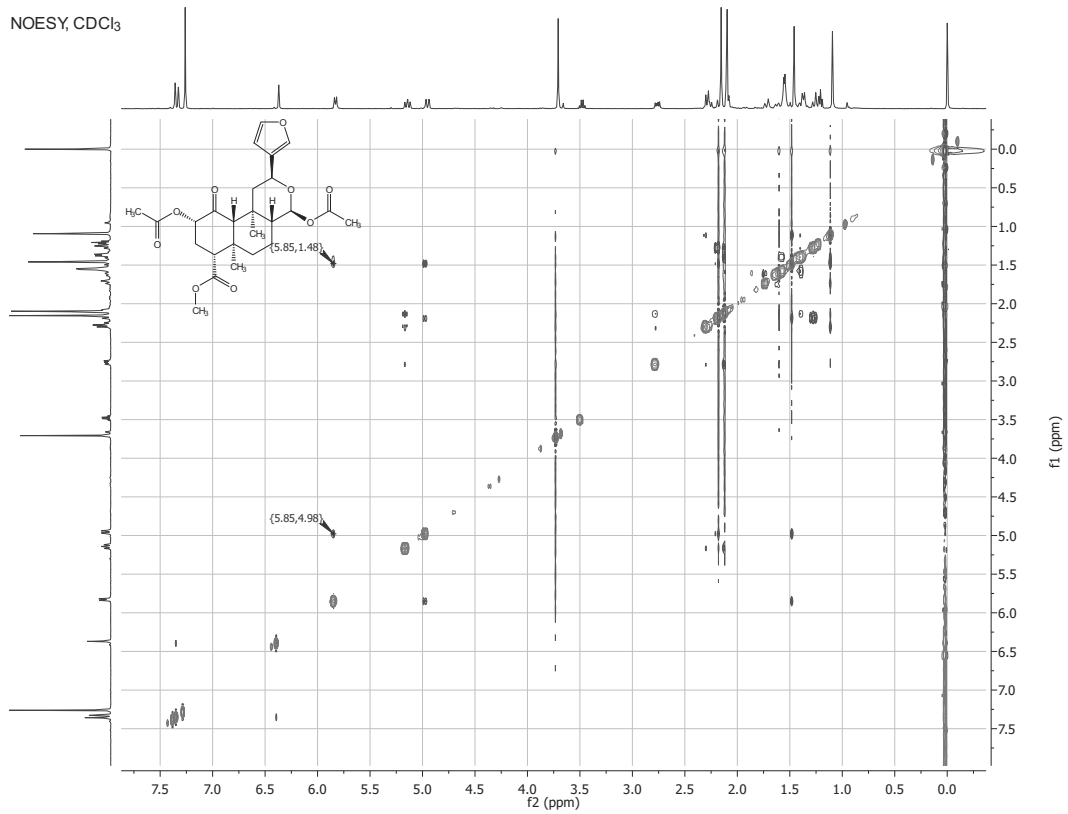


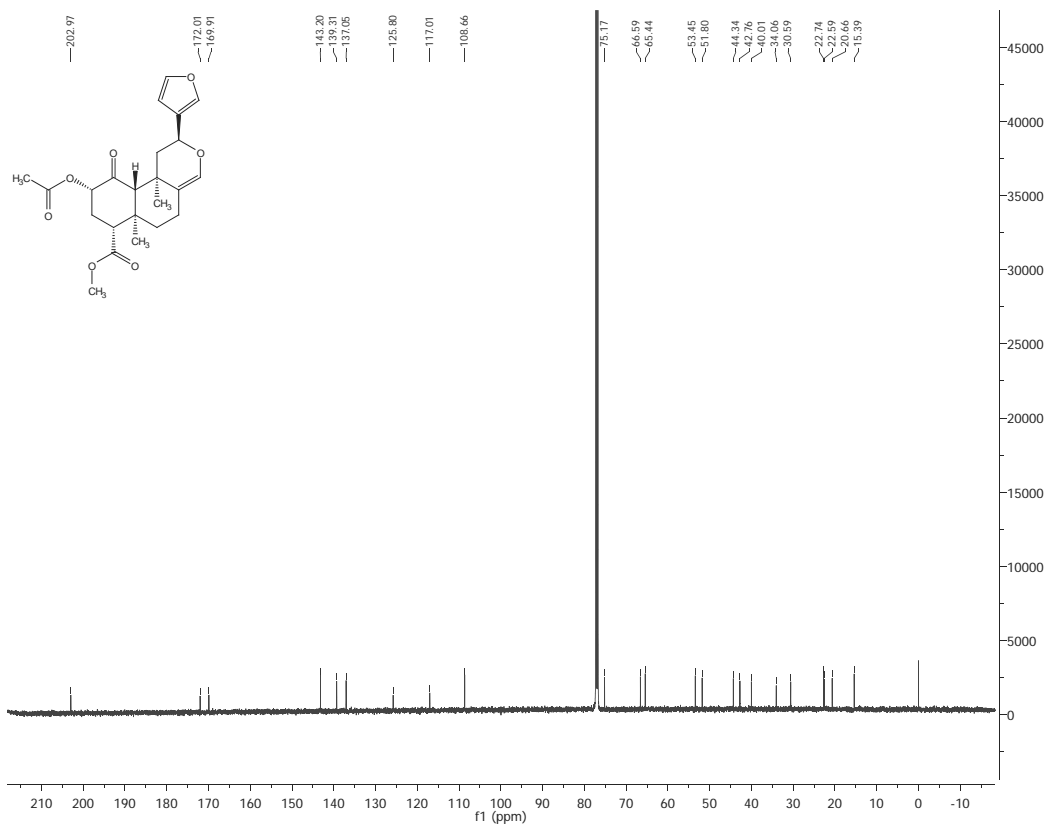
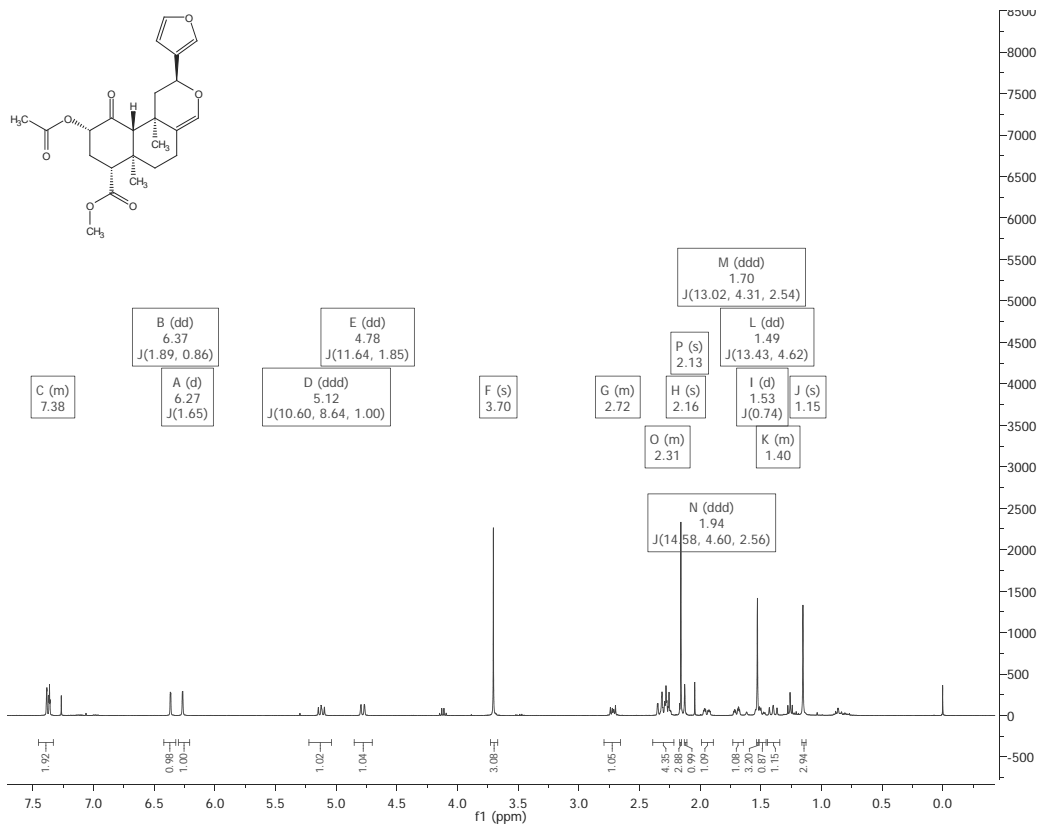


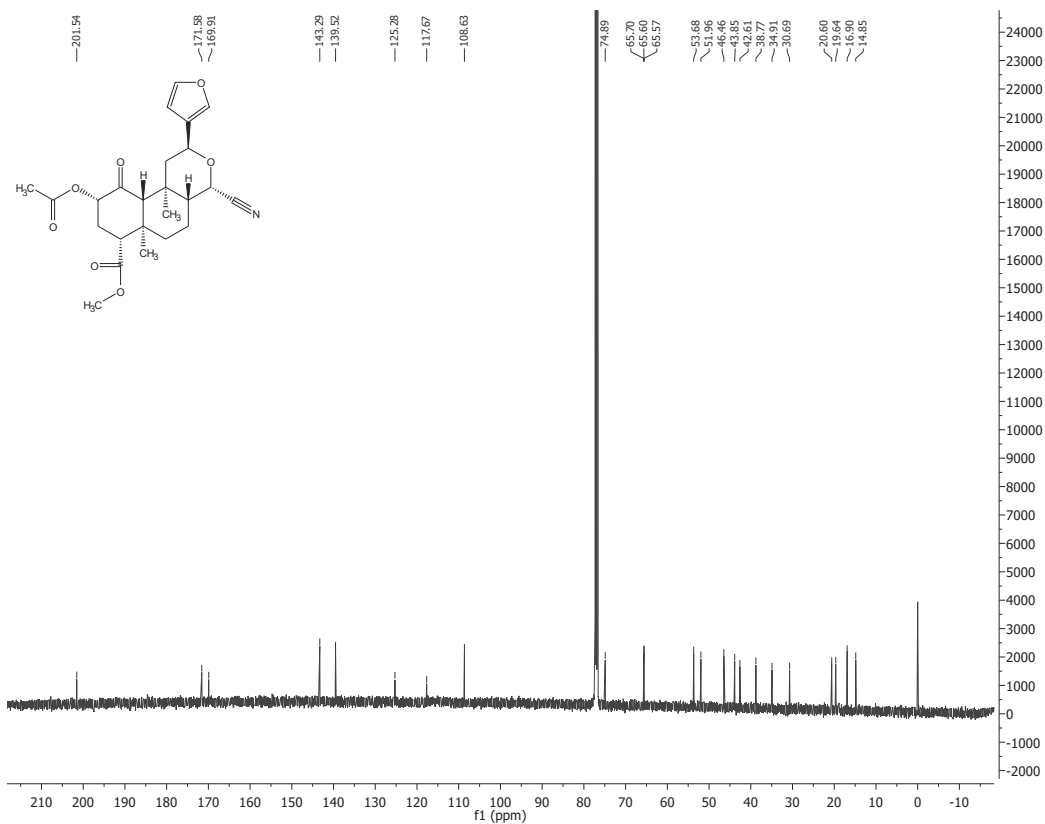
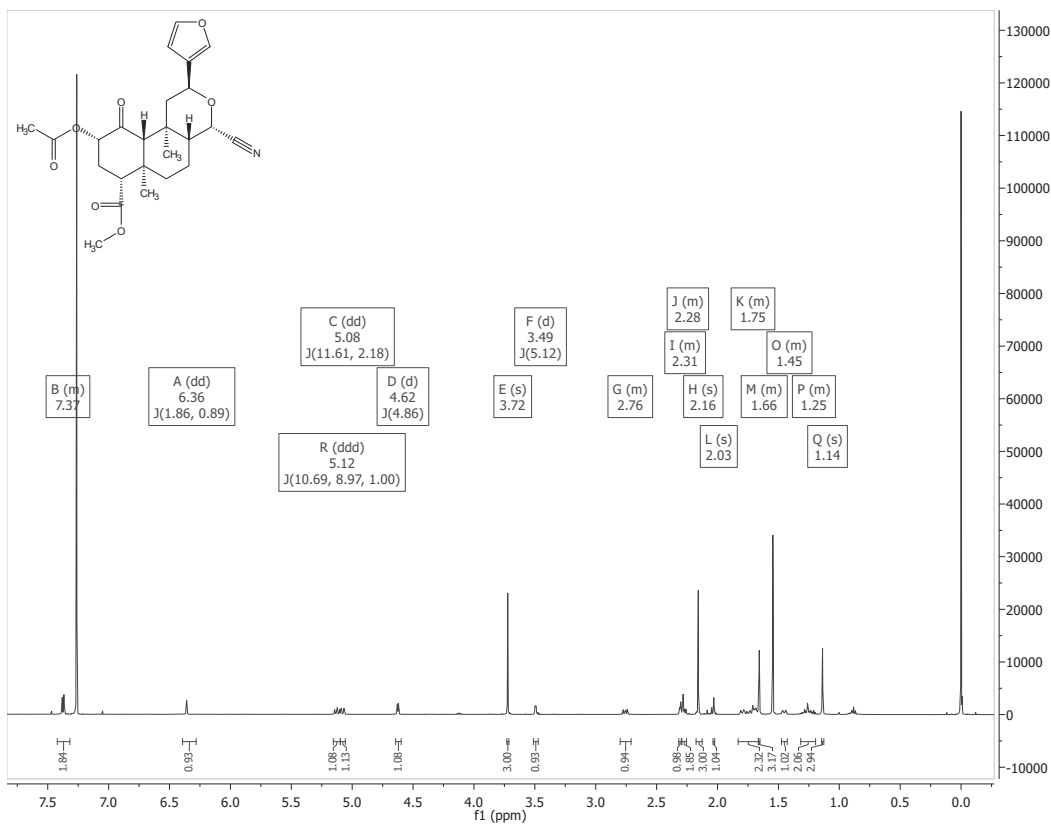
HSQC, CDCl₃



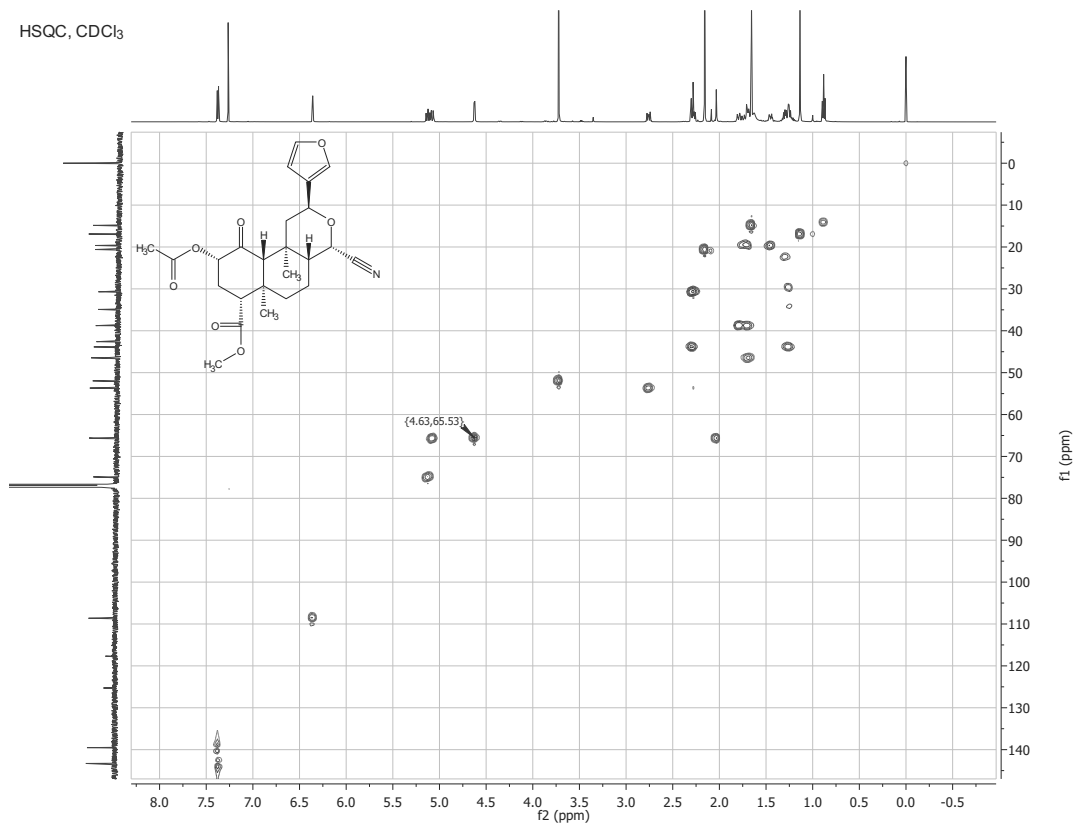
NOESY, CDCl₃



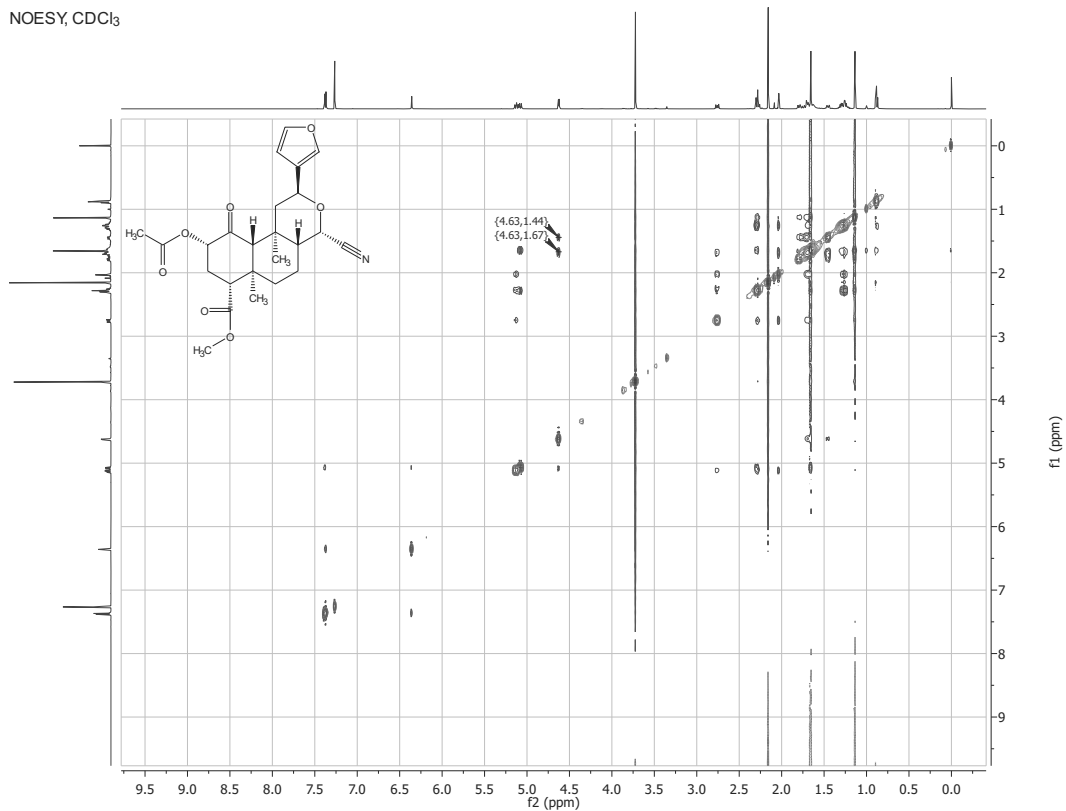


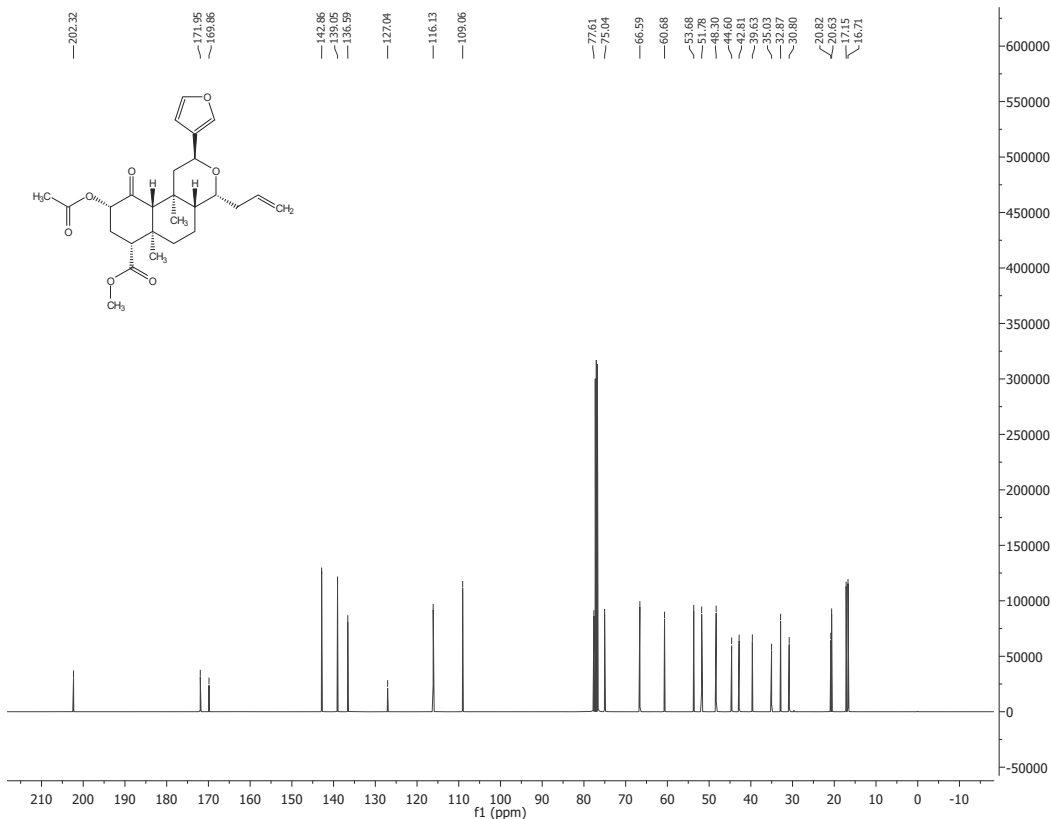
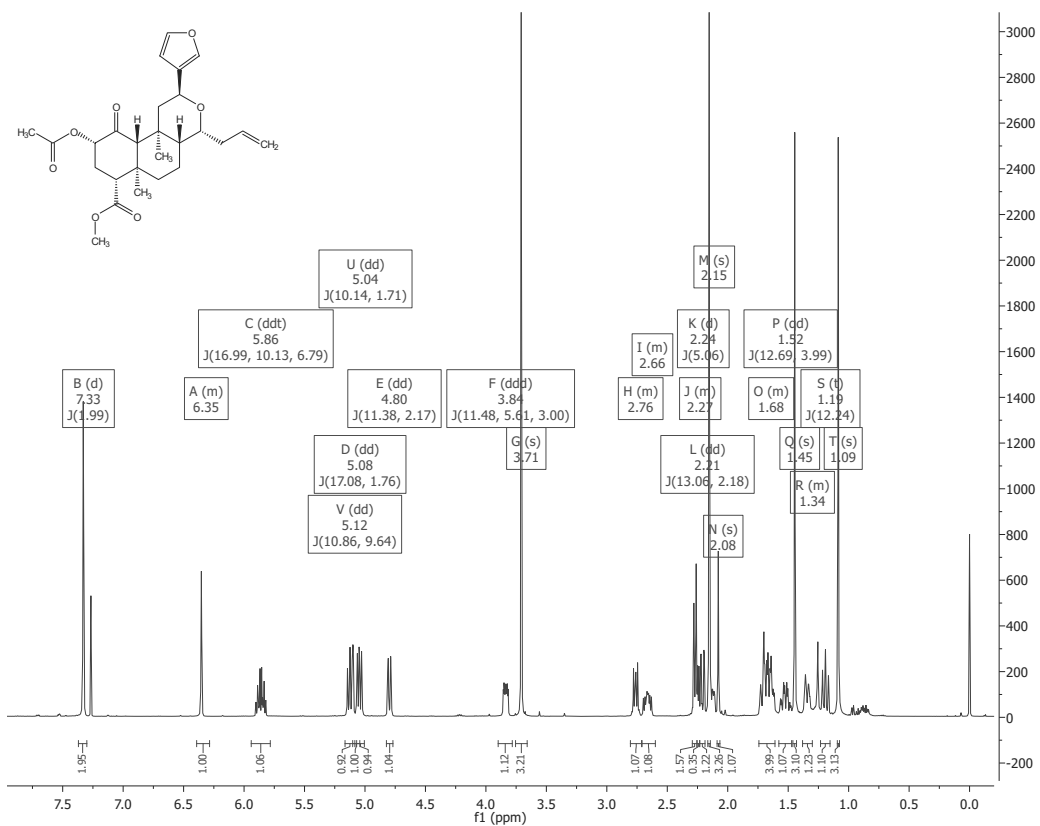


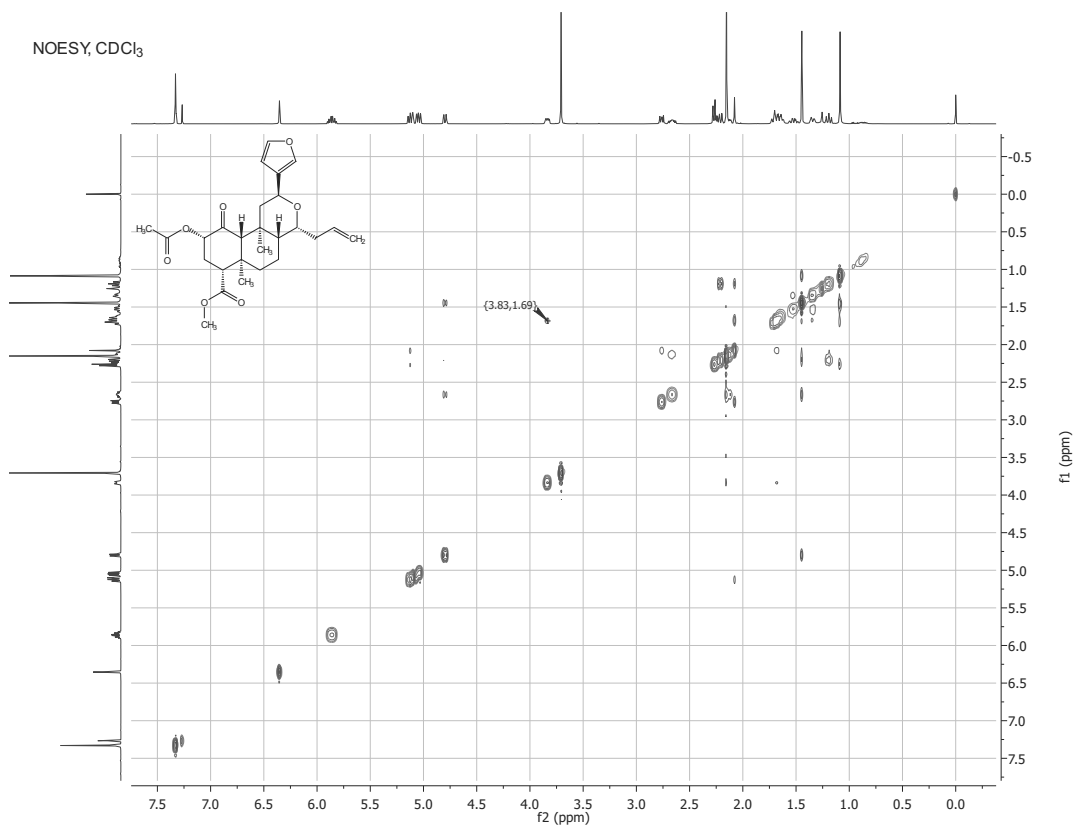
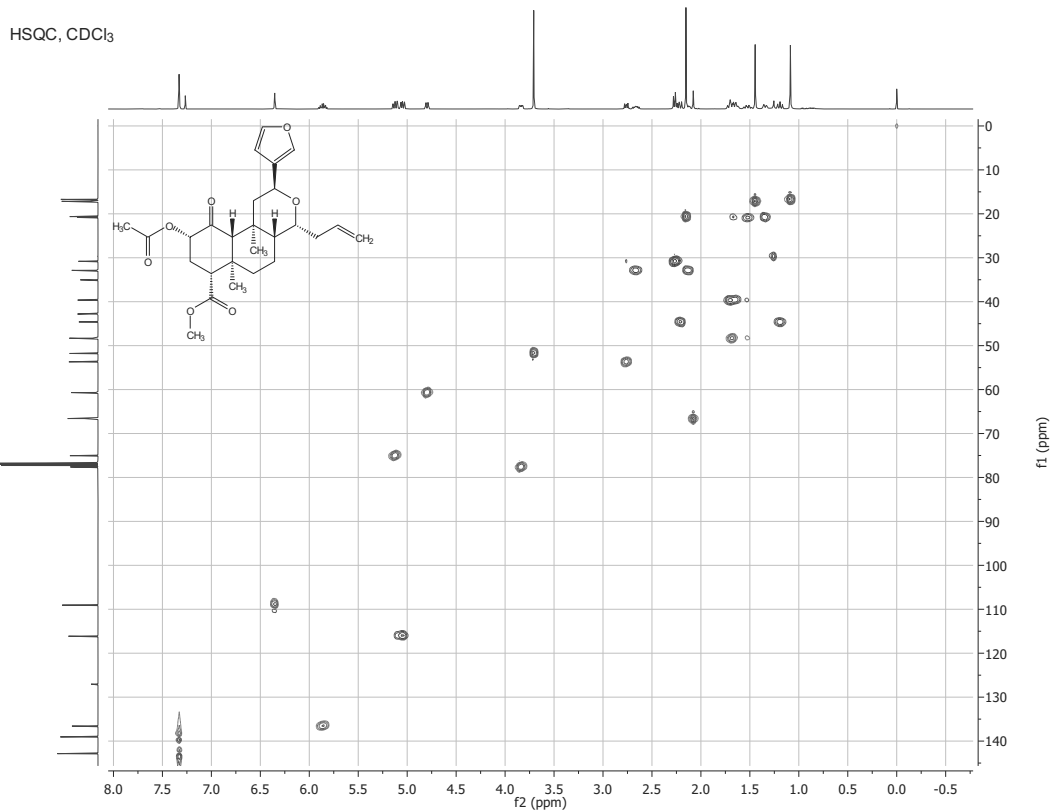
HSQC, CDCl₃

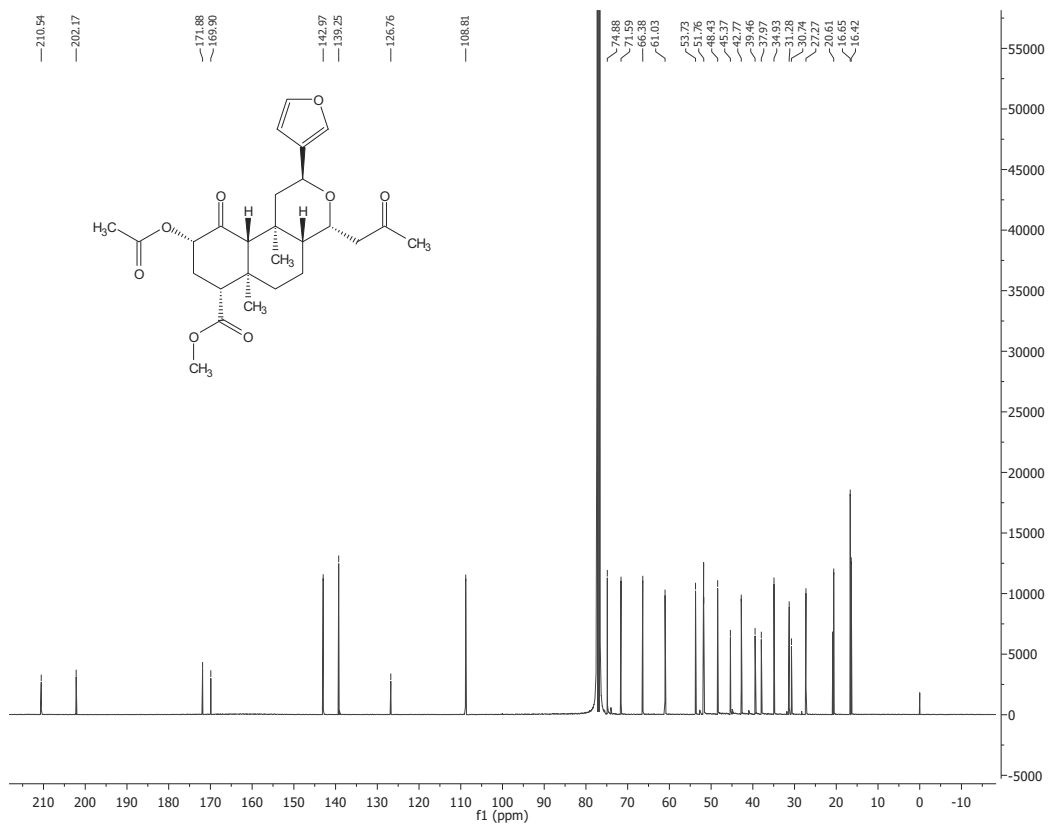
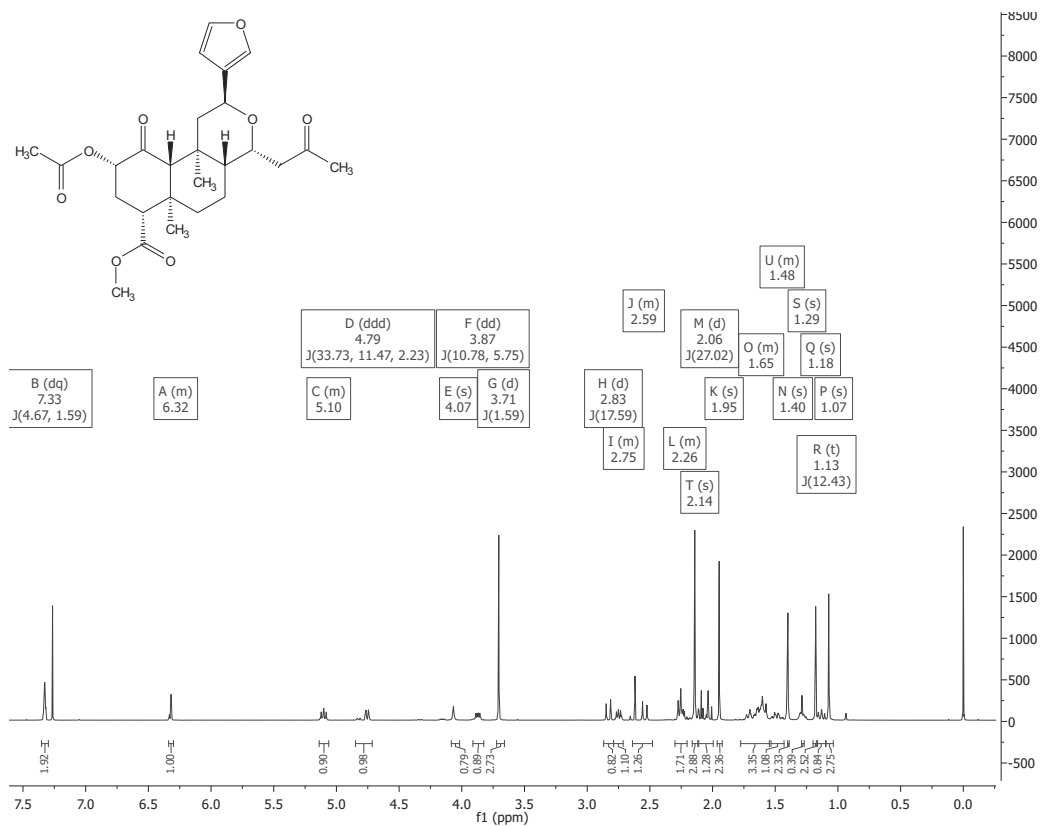


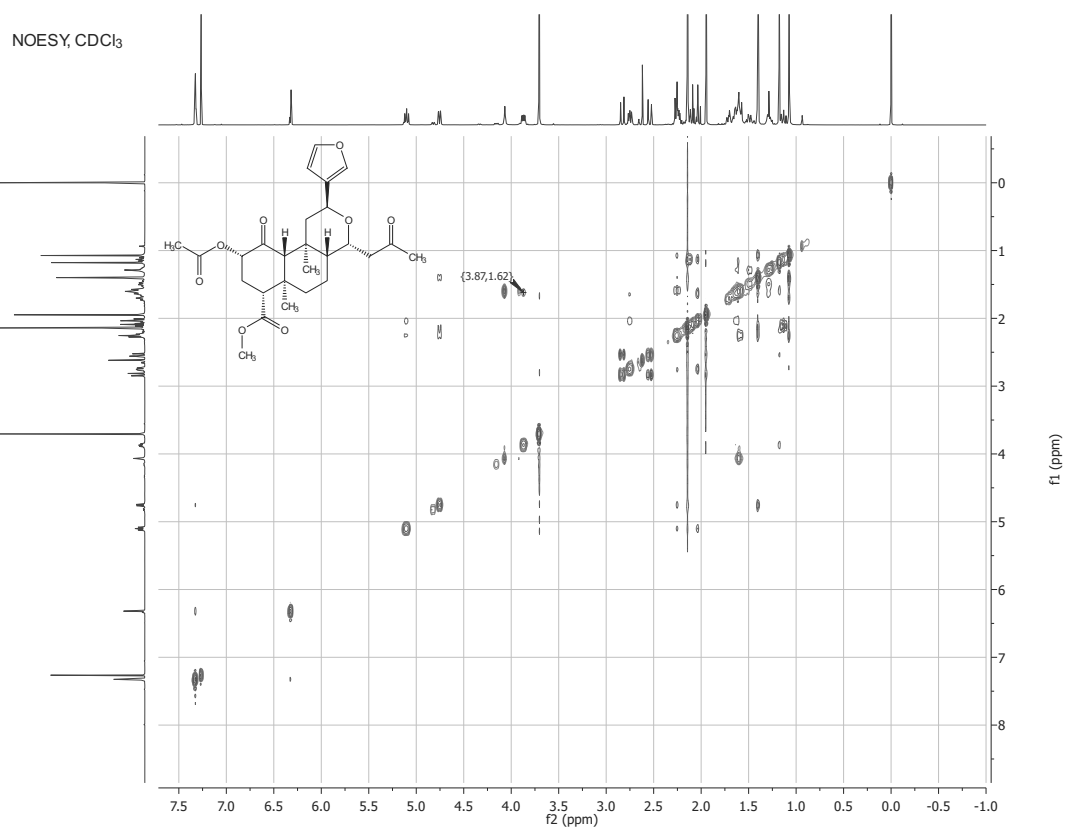
NOESY, CDCl₃

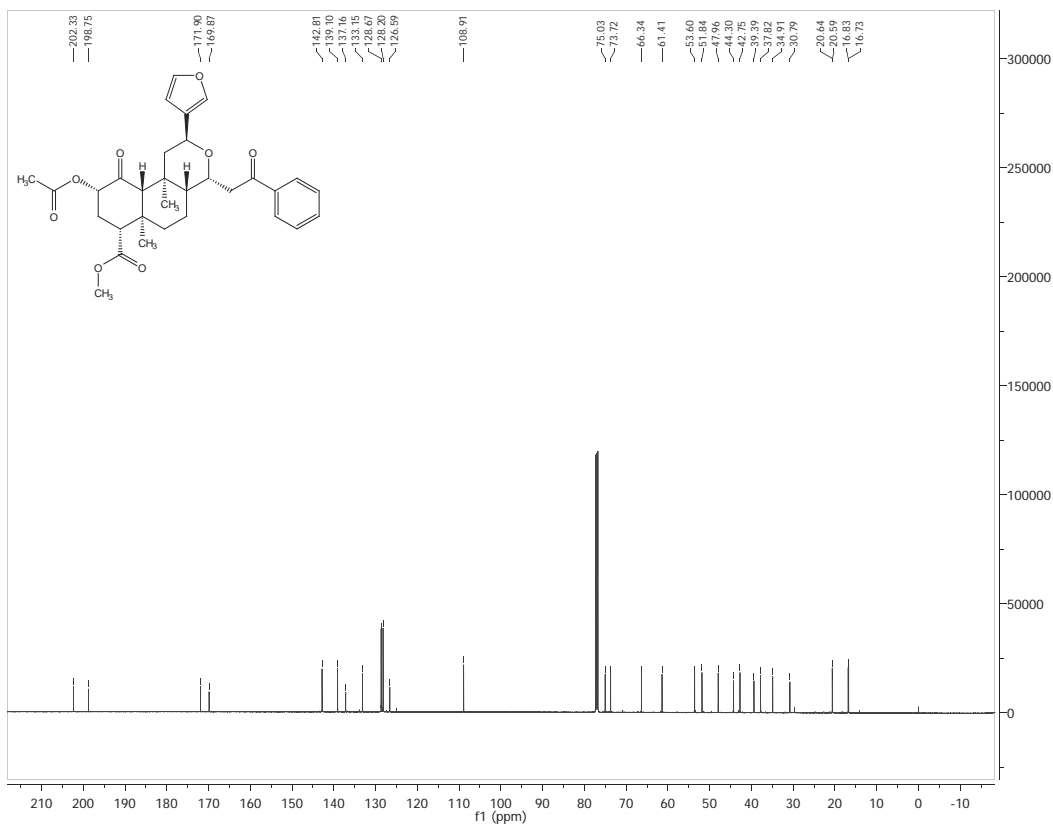
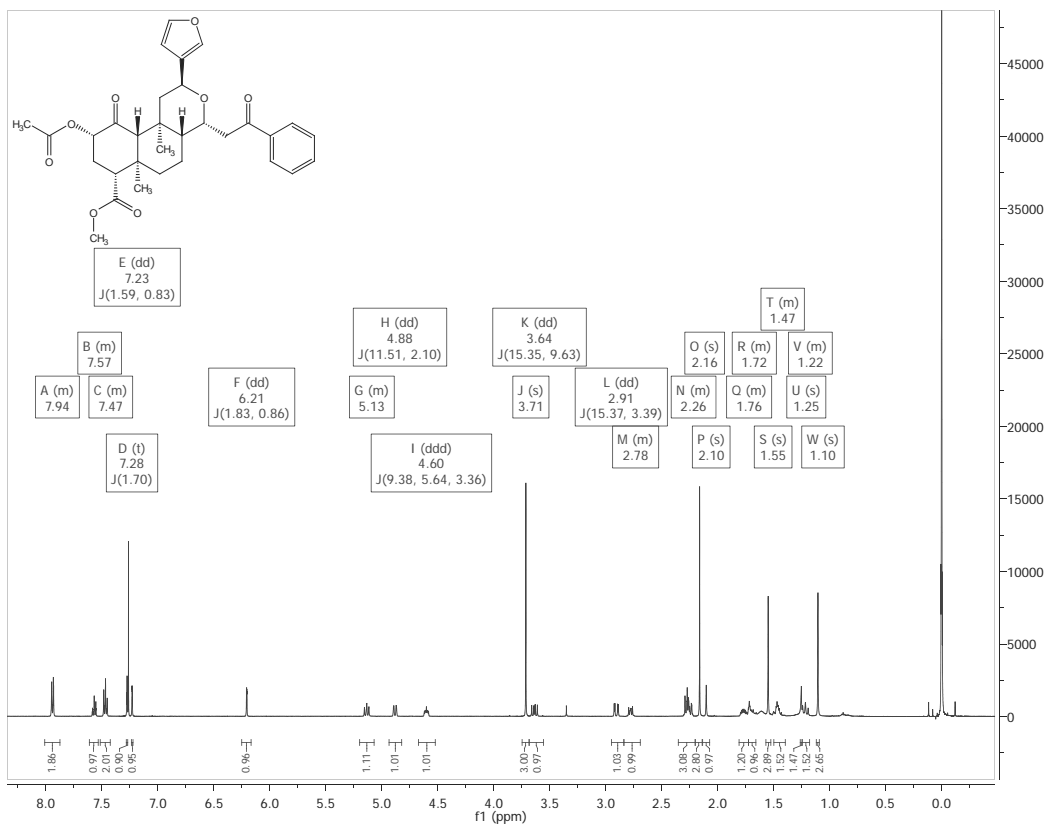




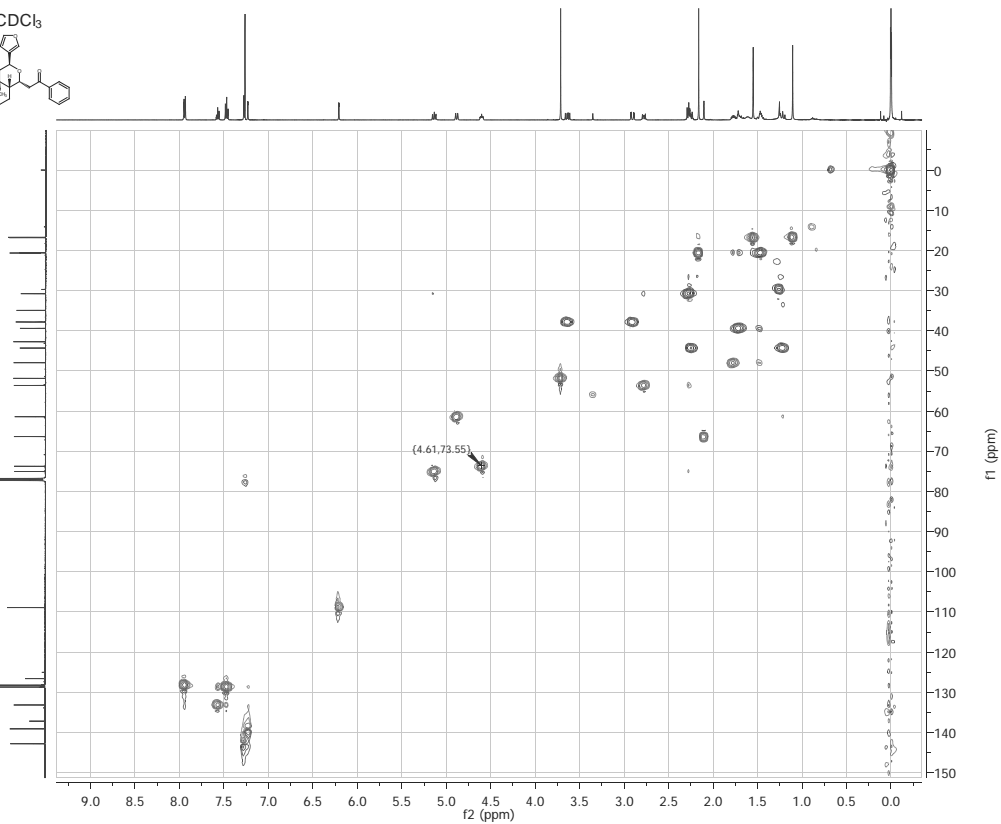
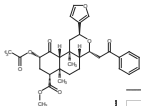




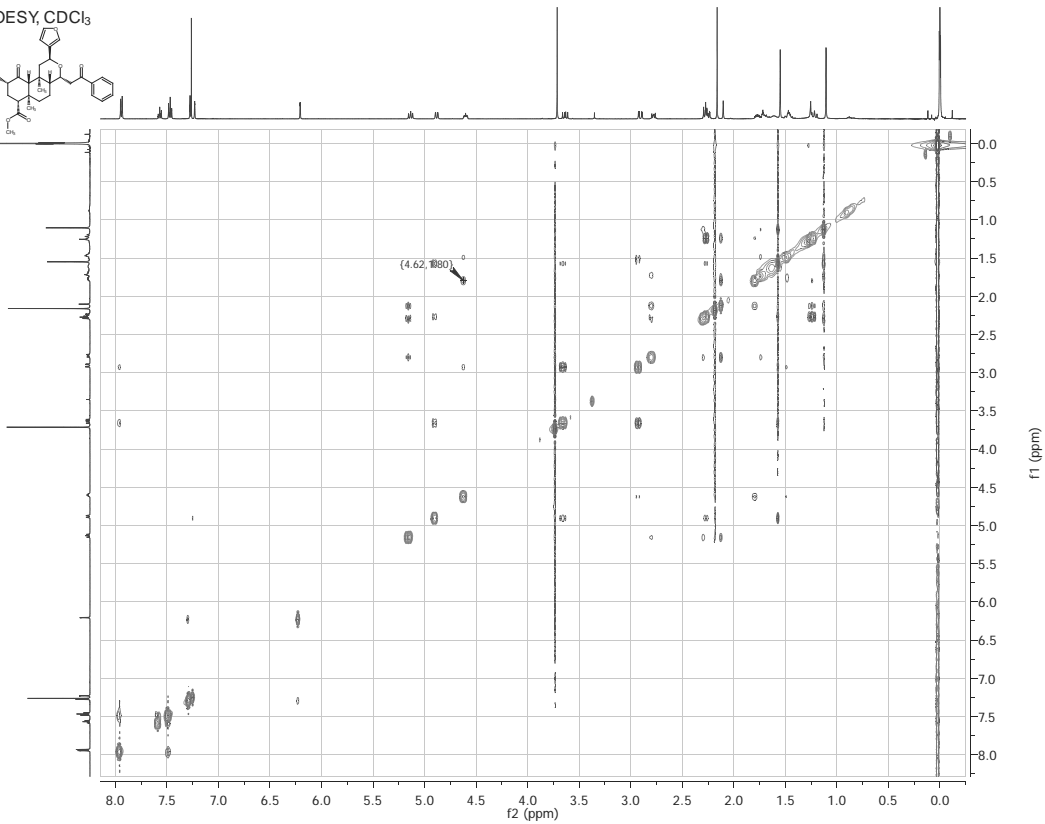
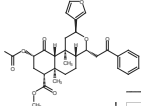


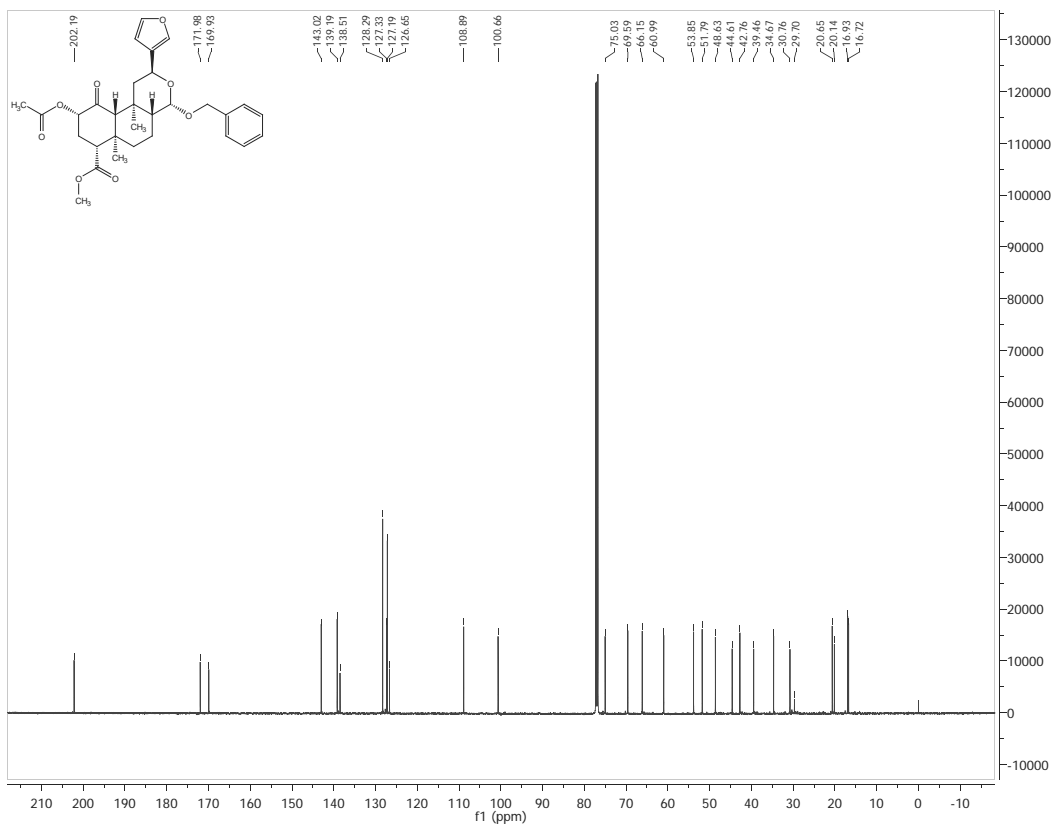


HSQC, CDCl₃

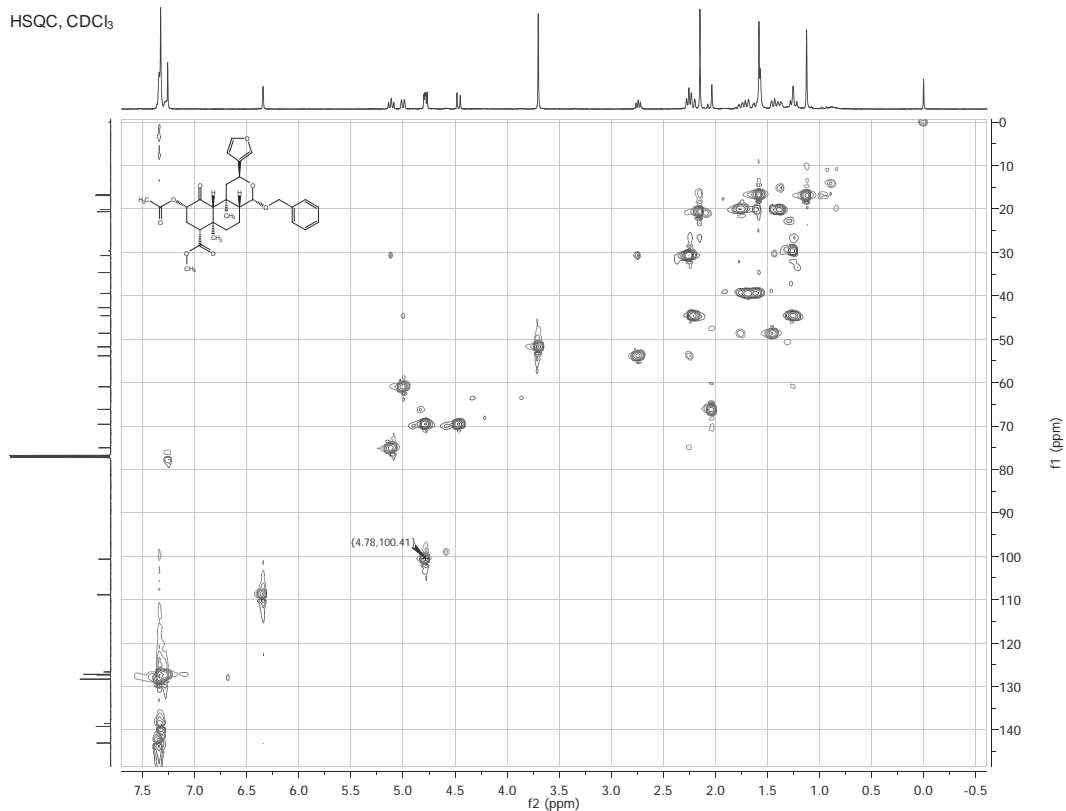


NOESY, CDCl₃

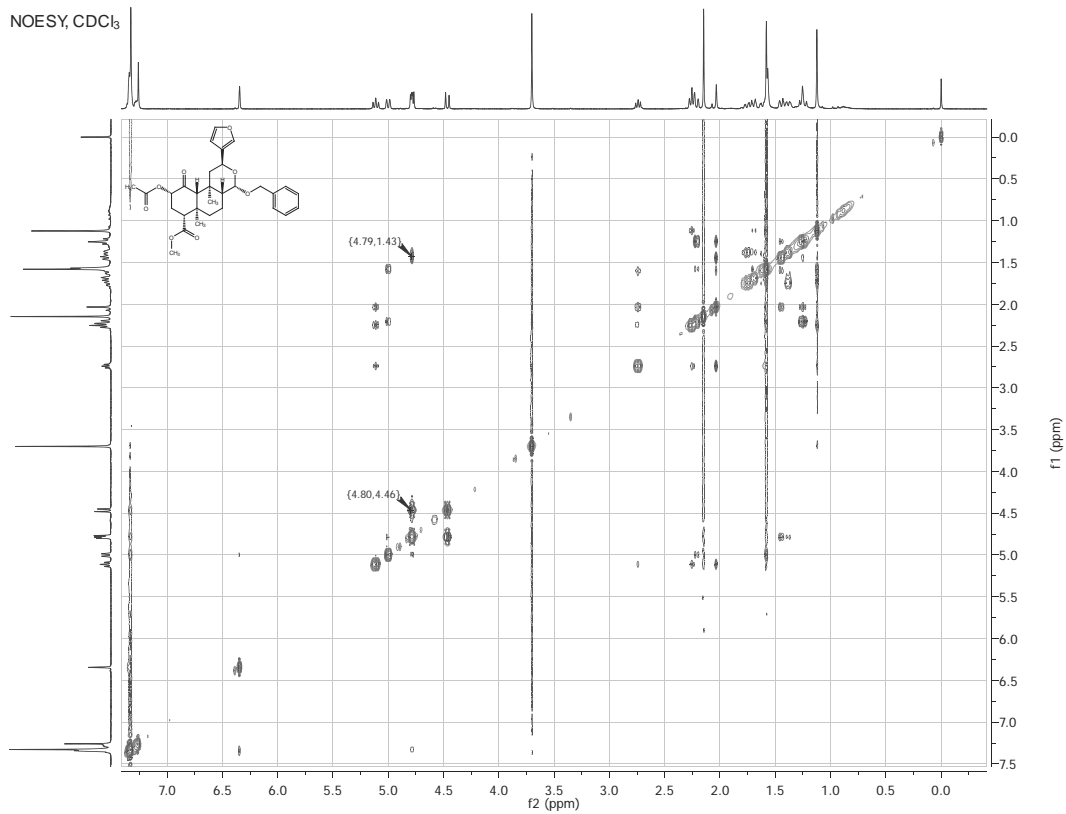


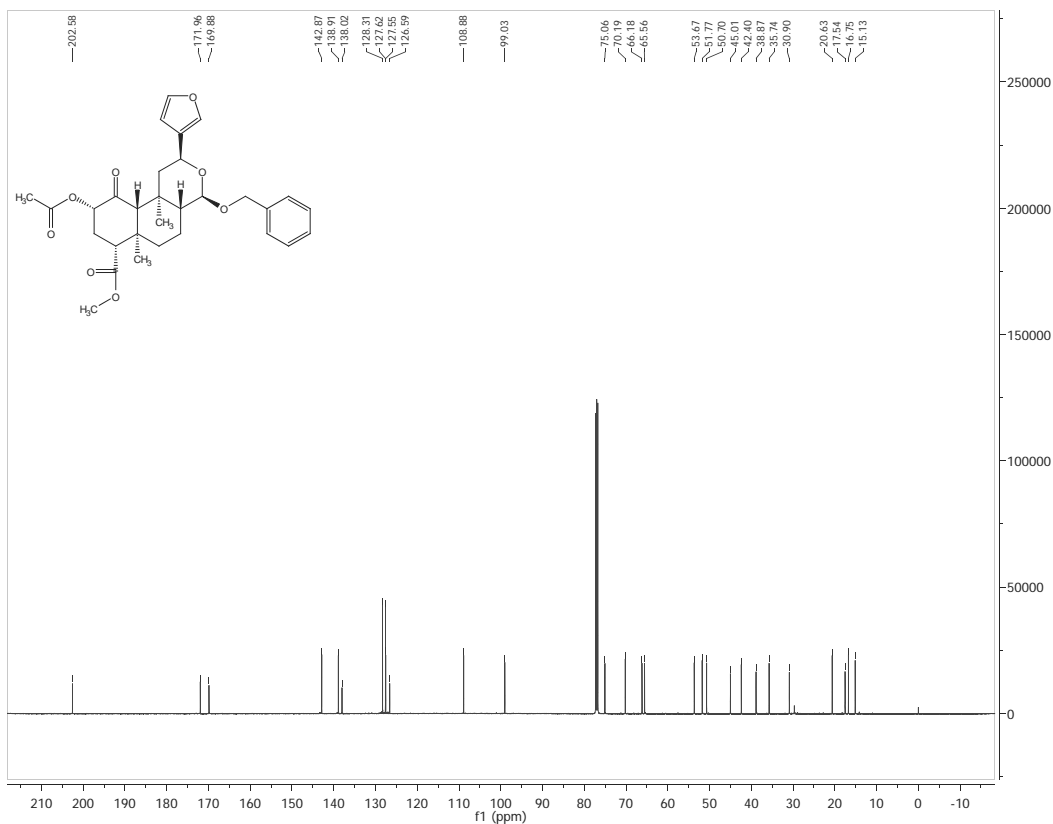
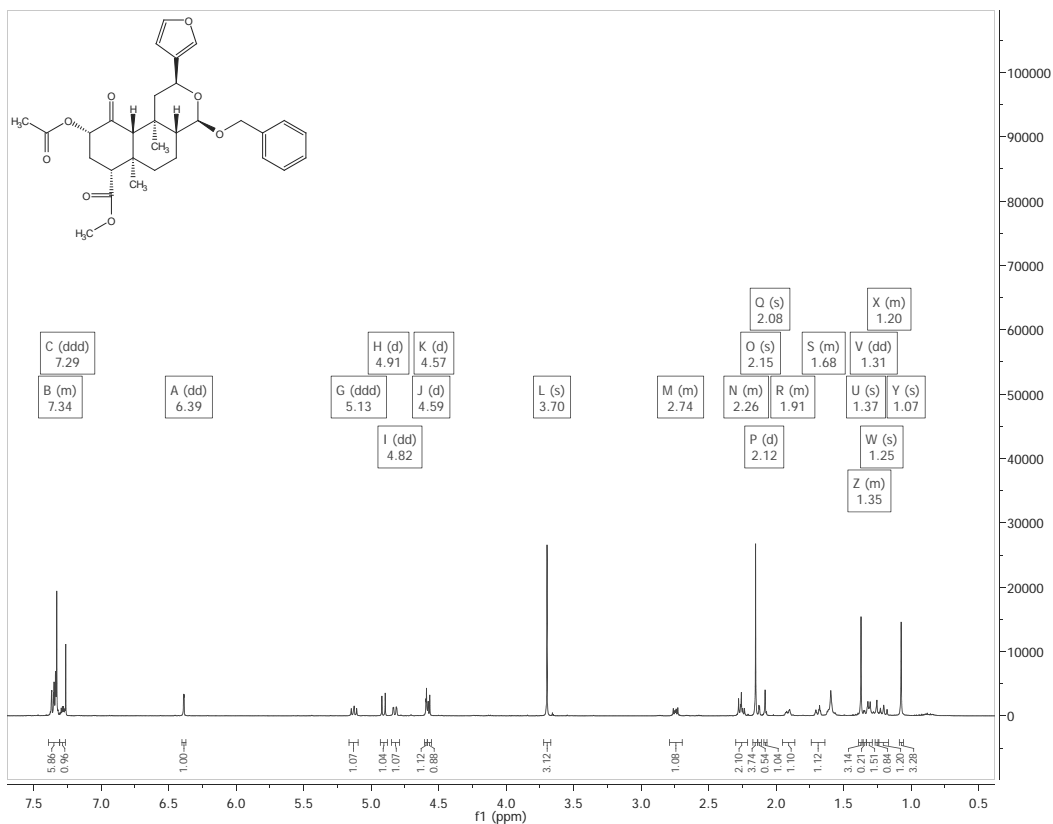


HSQC, CDCl₃

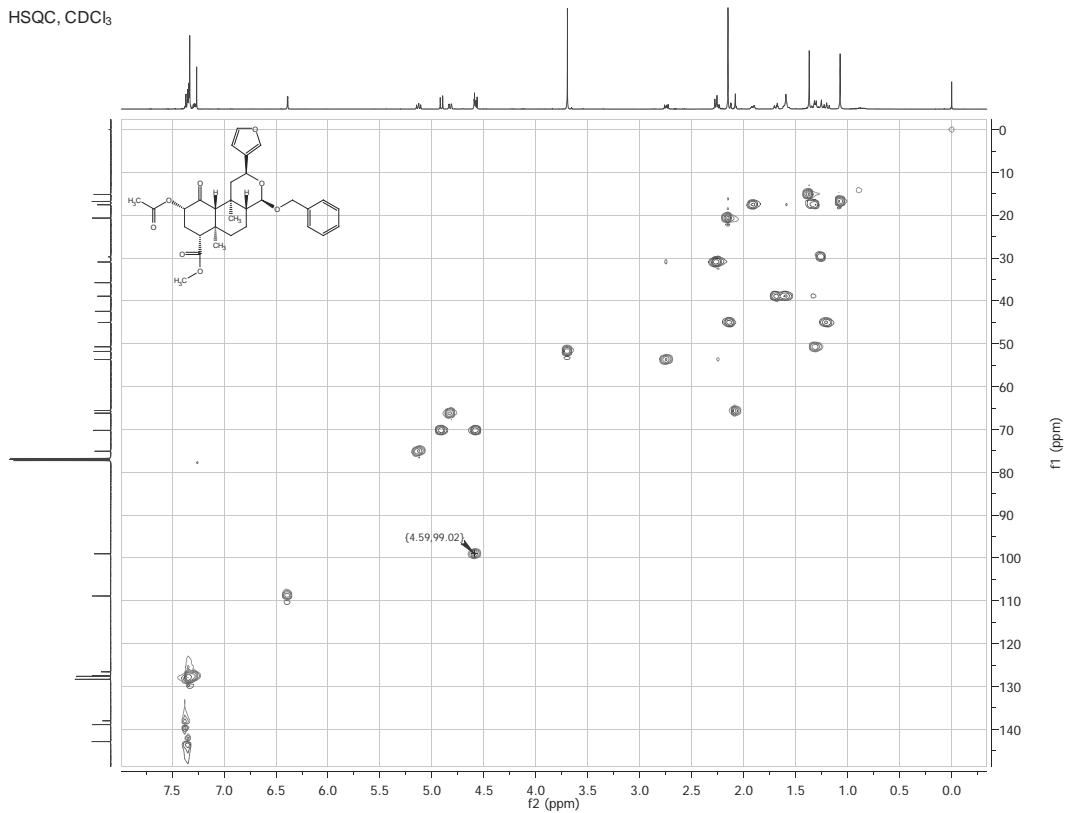


NOESY, CDCl₃

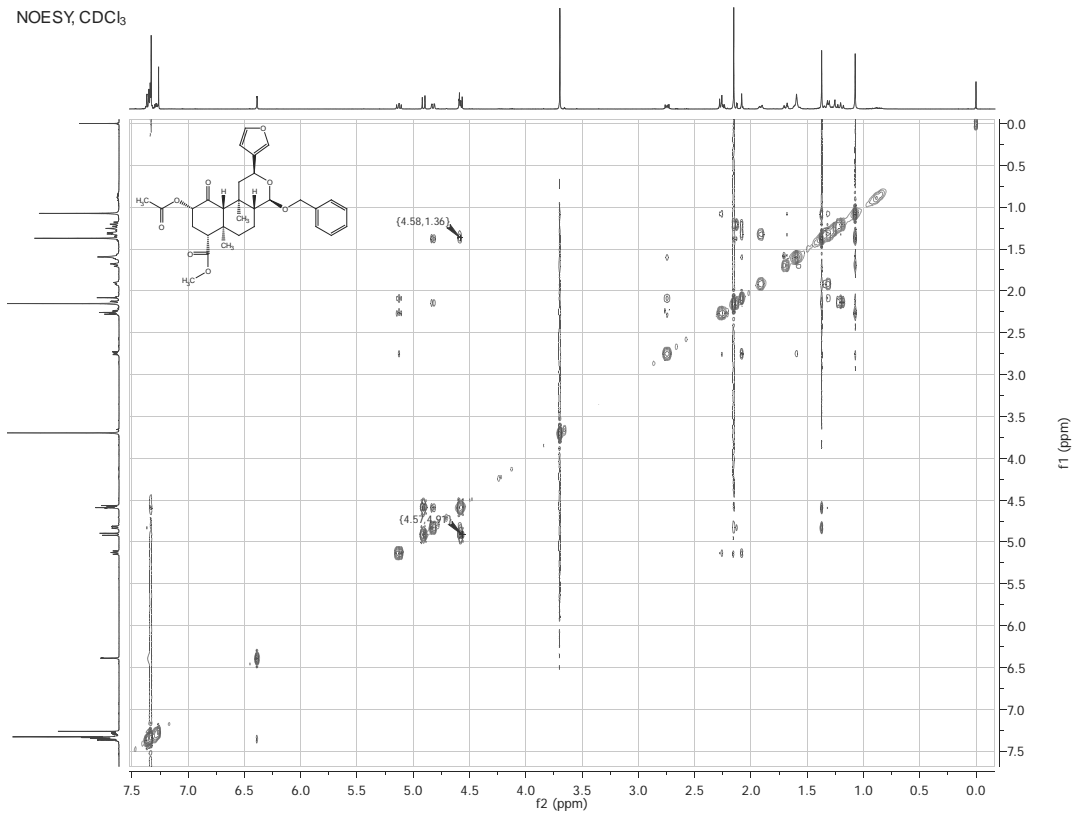


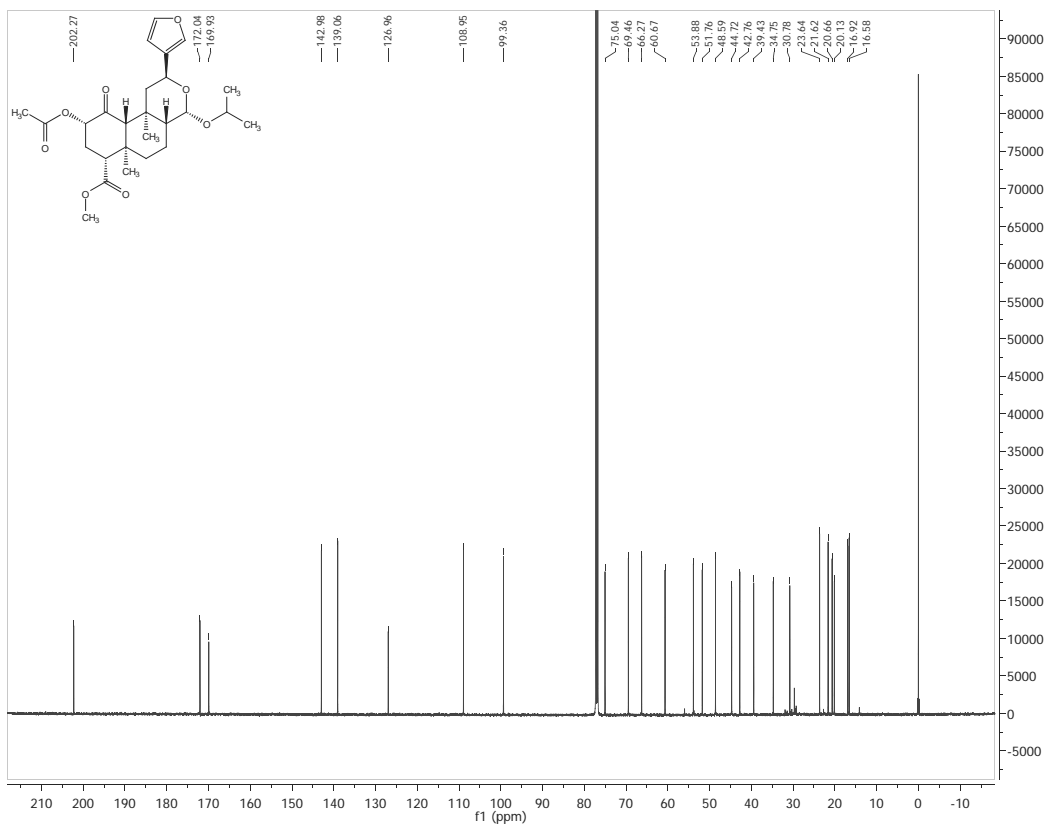
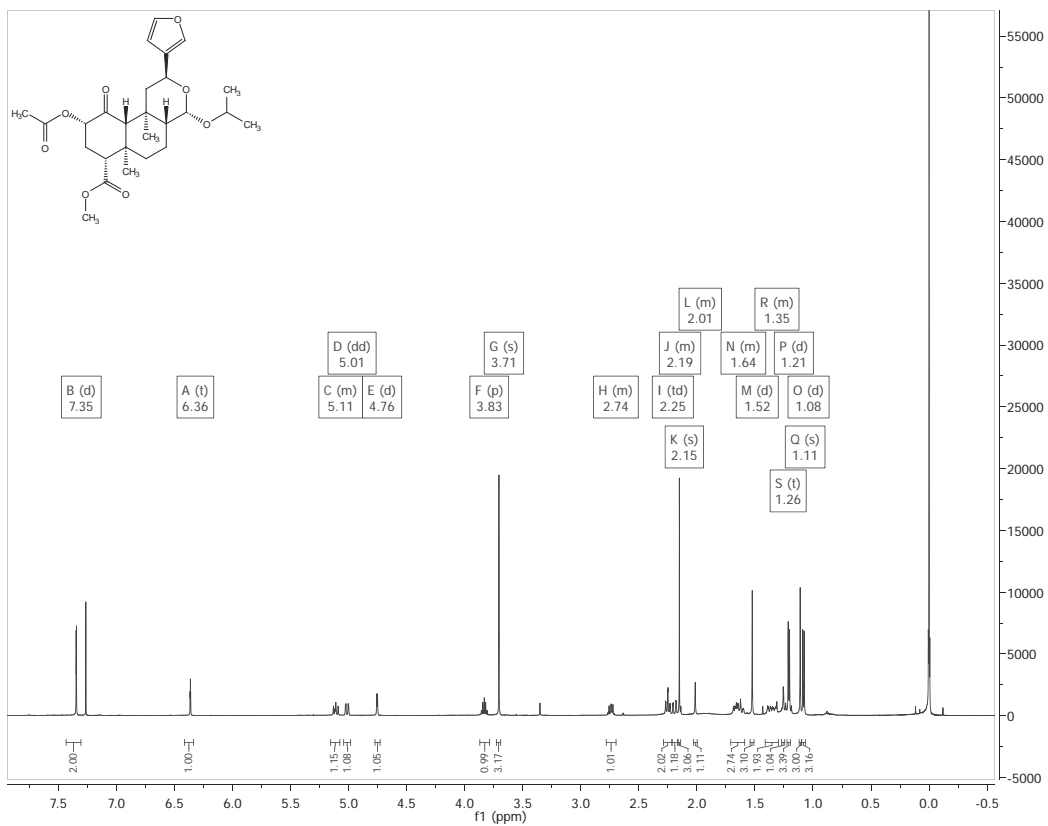


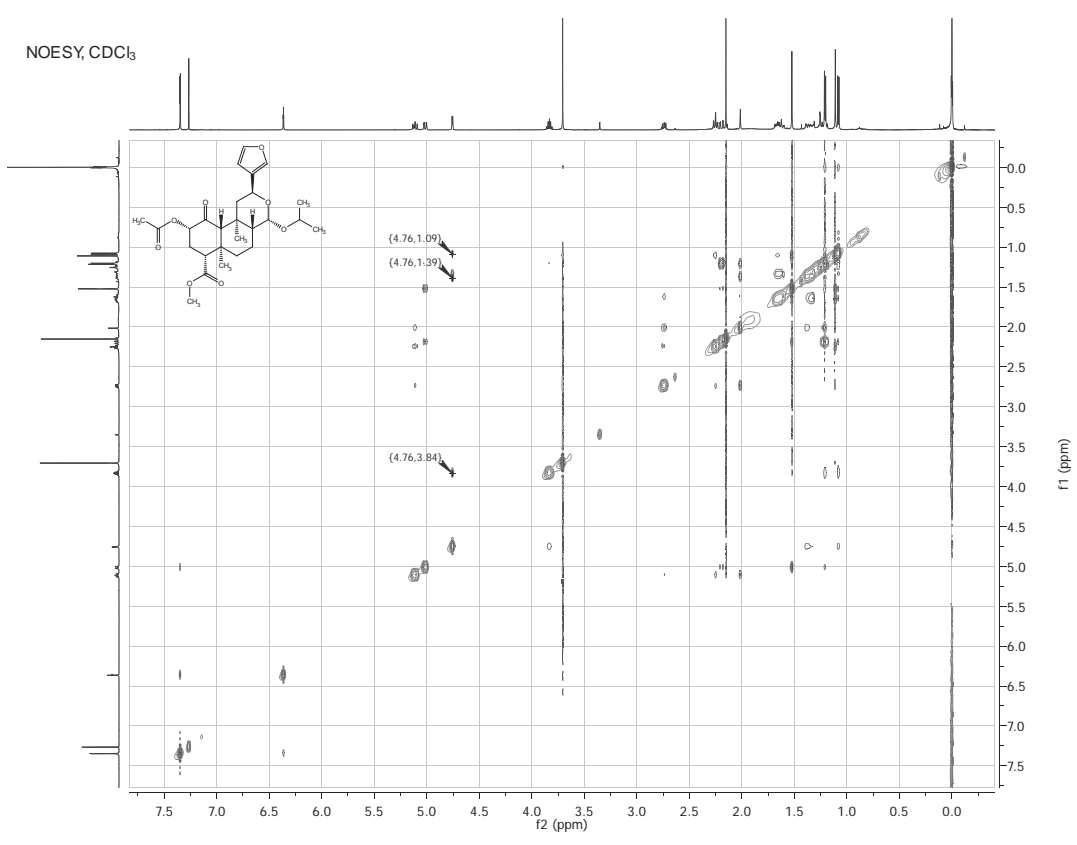
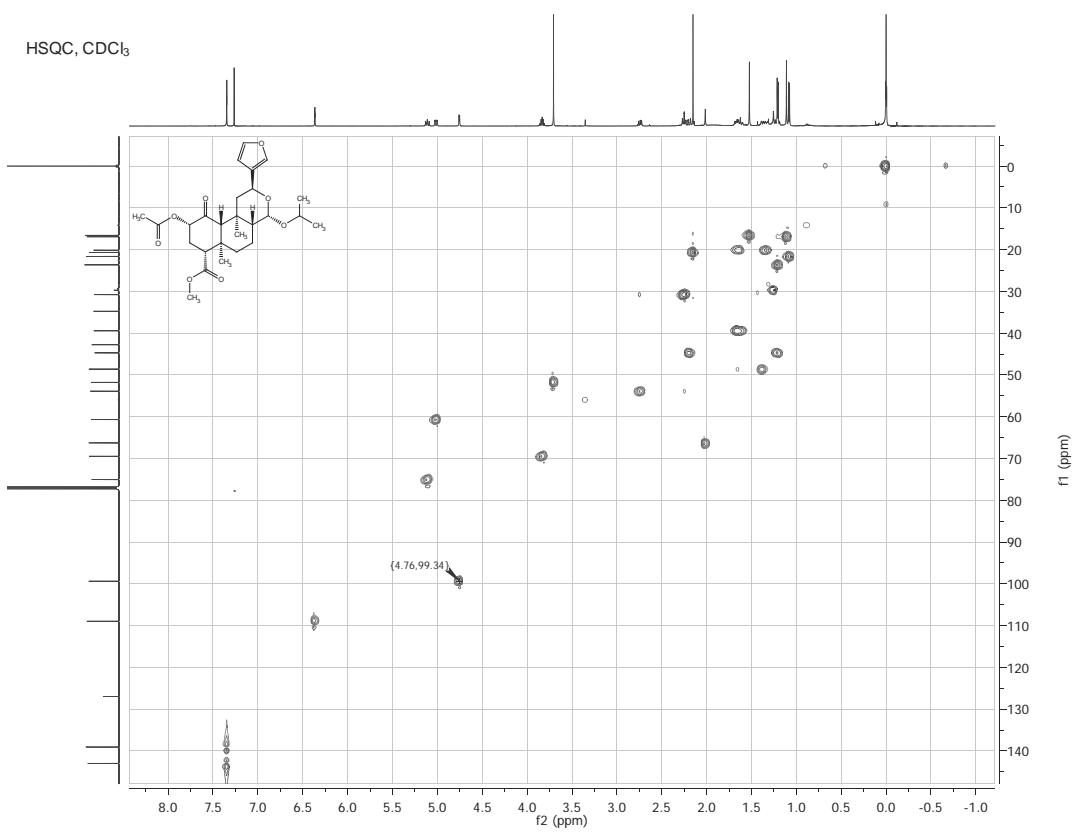
HSQC, CDCl₃

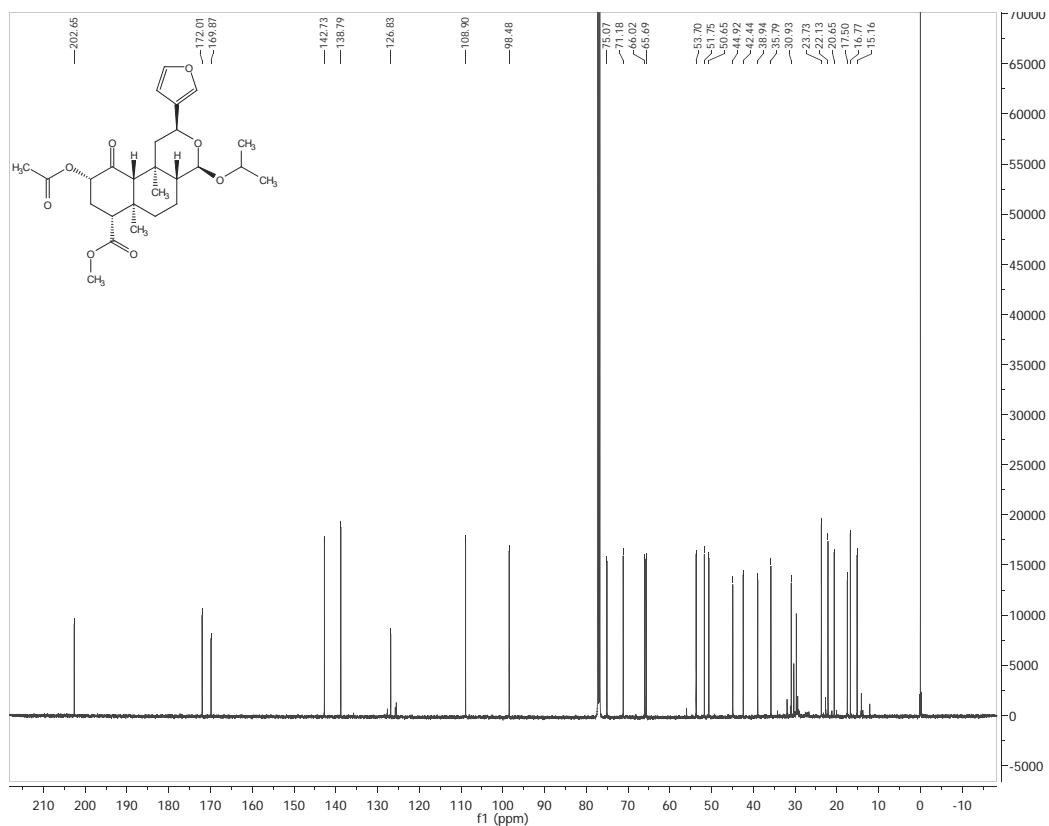
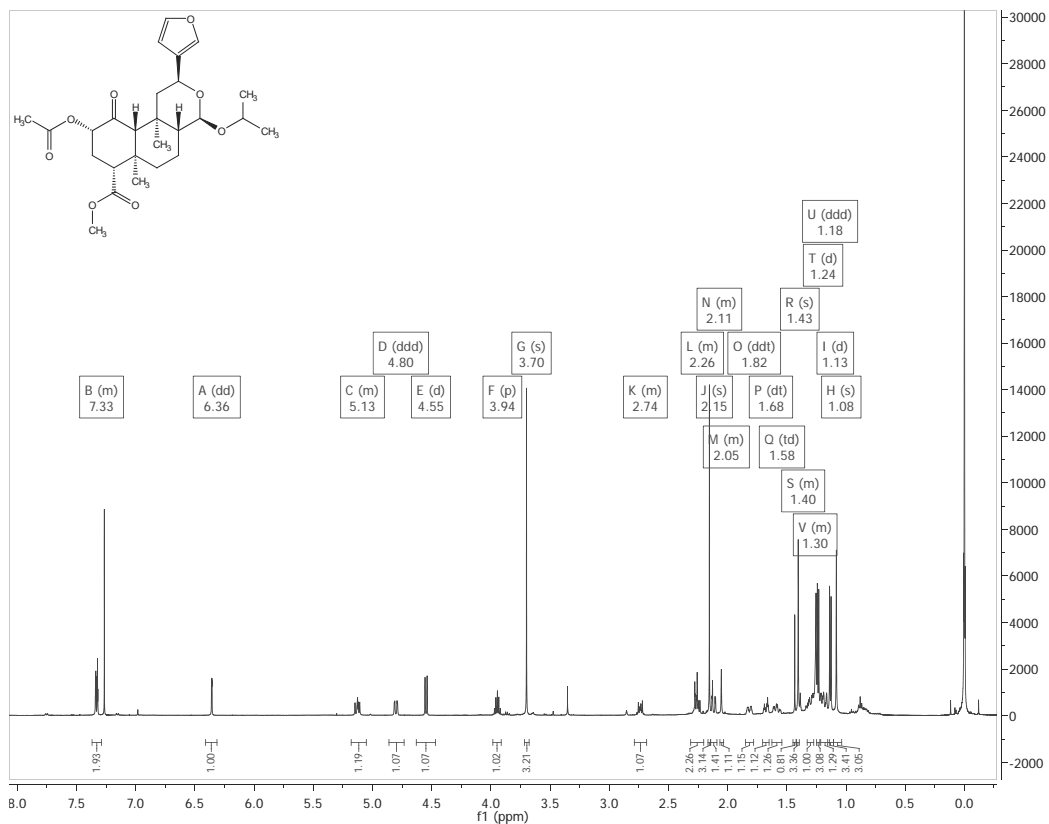


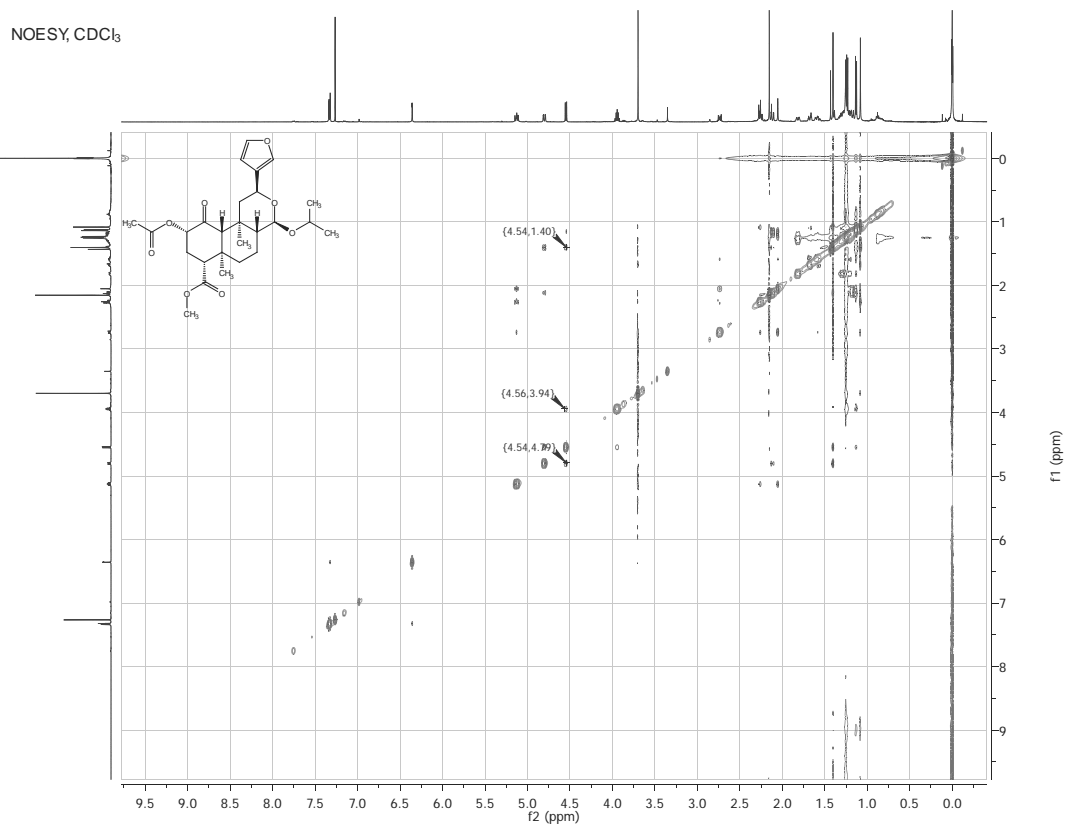
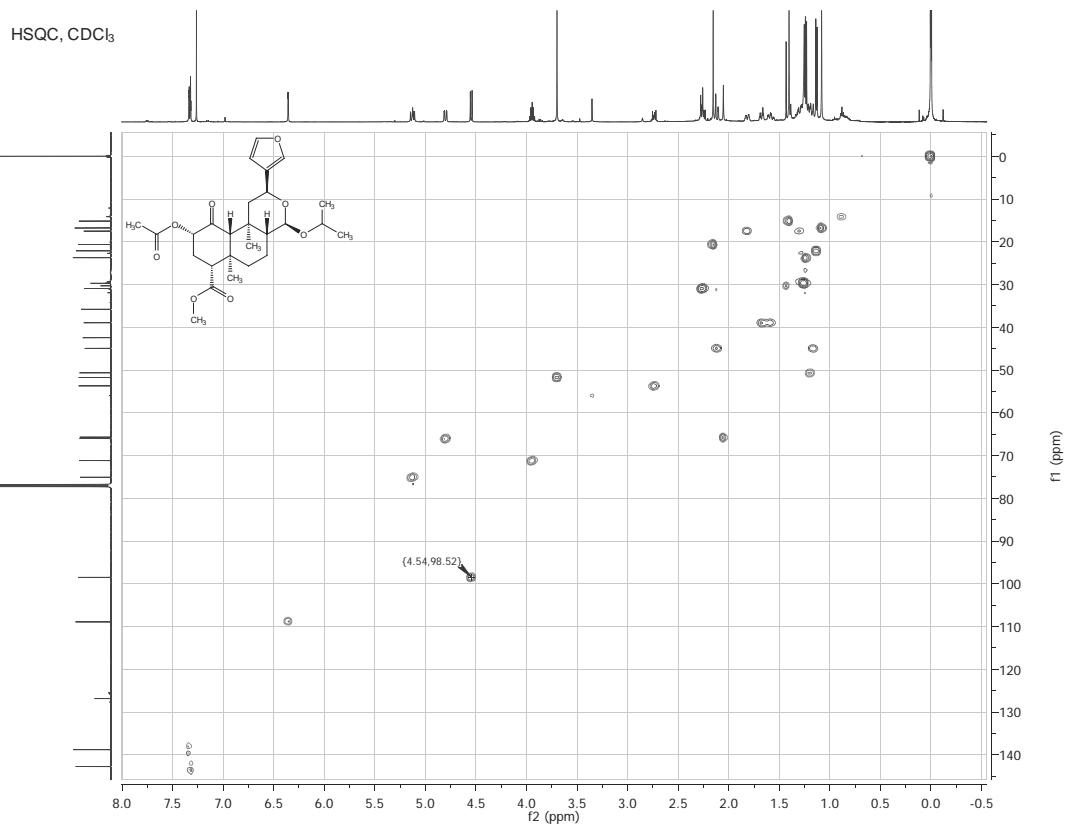
NOESY, CDCl₃

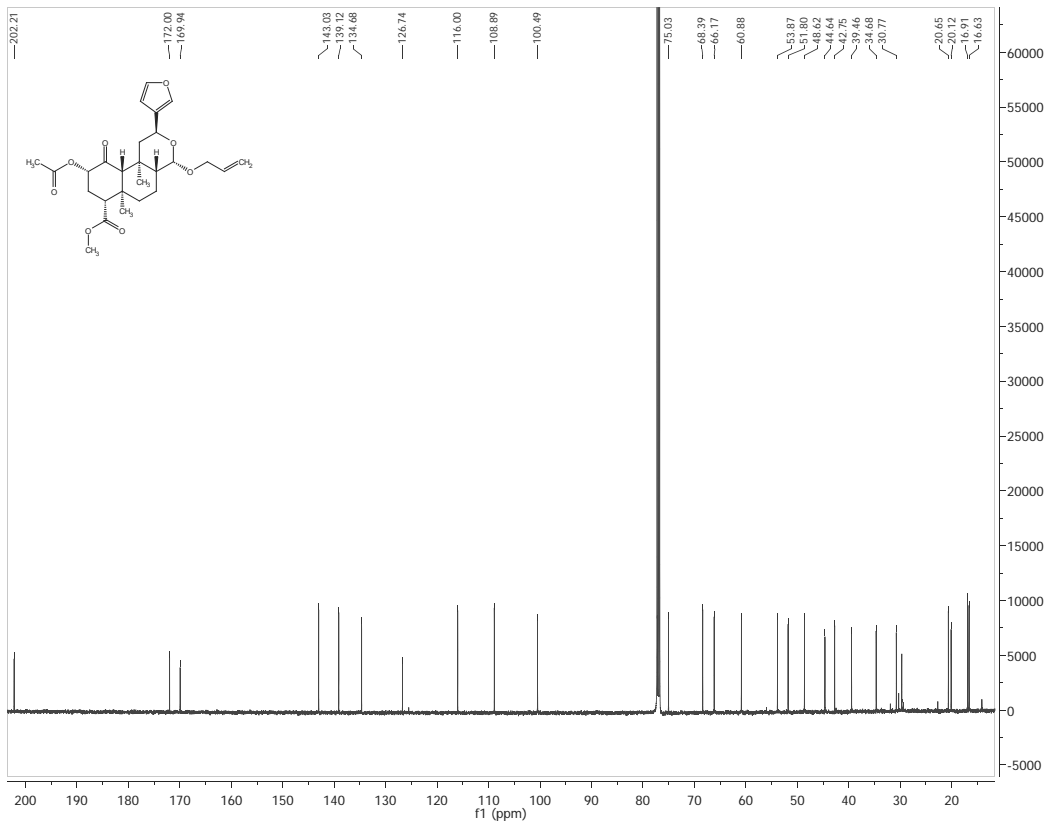
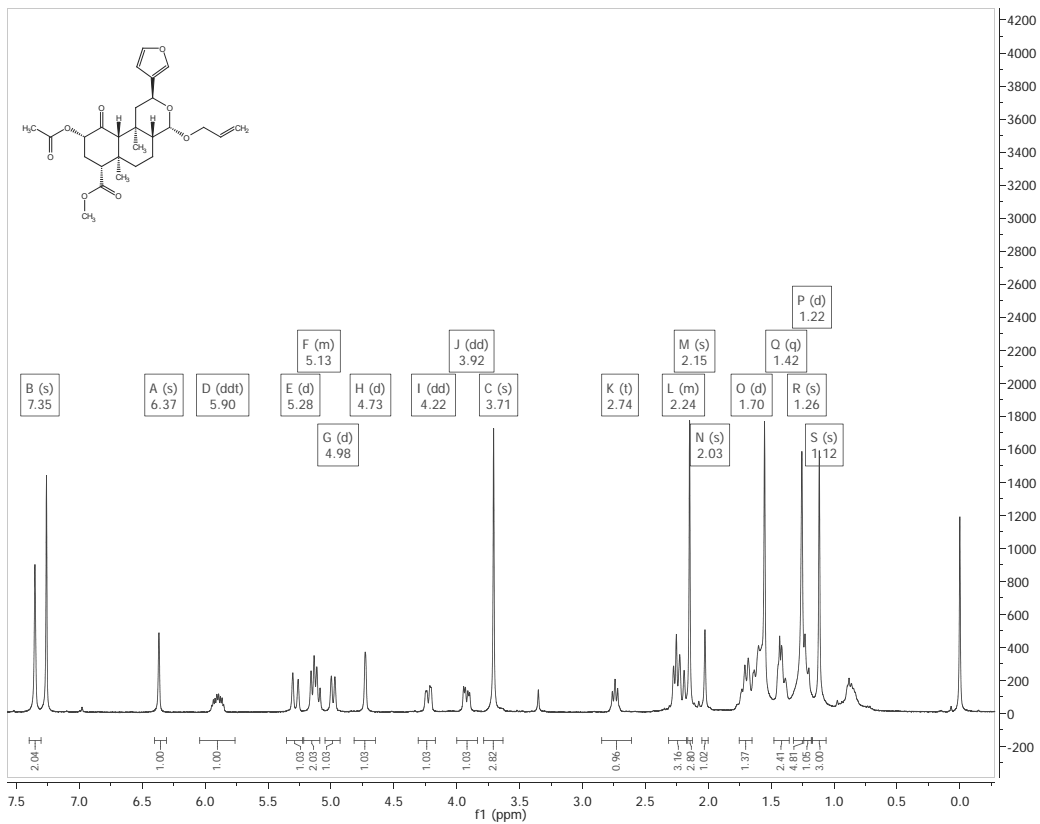




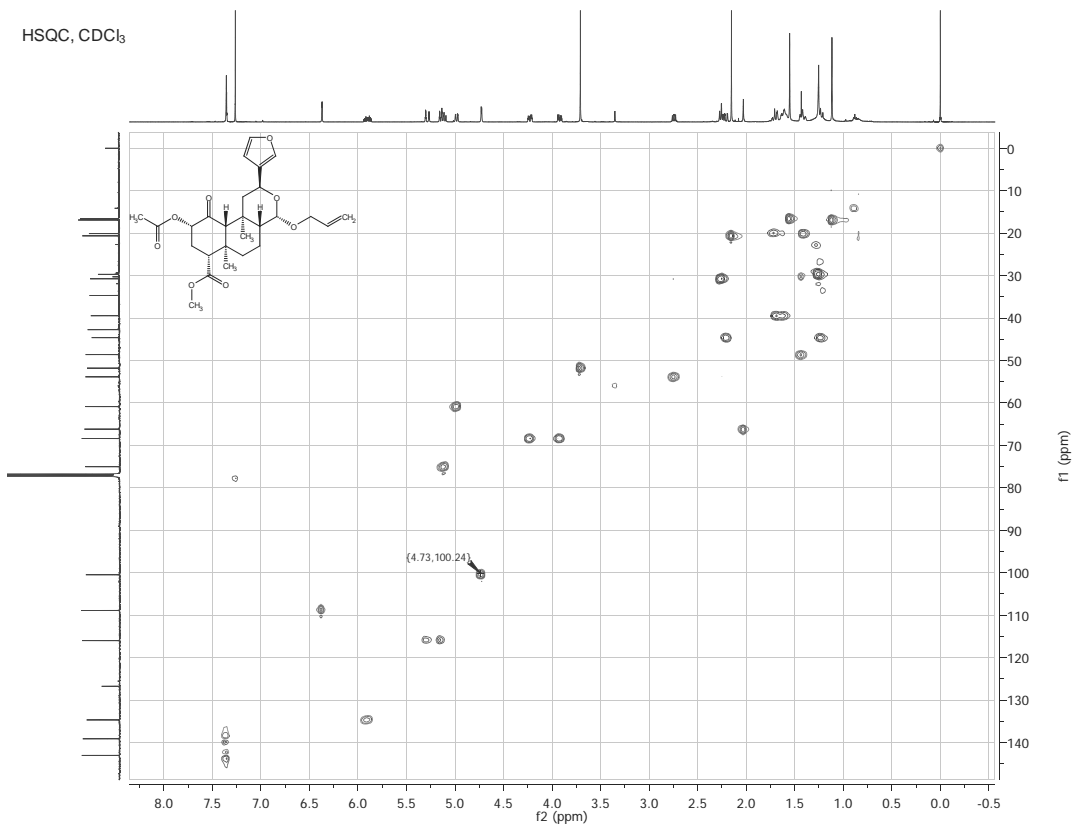




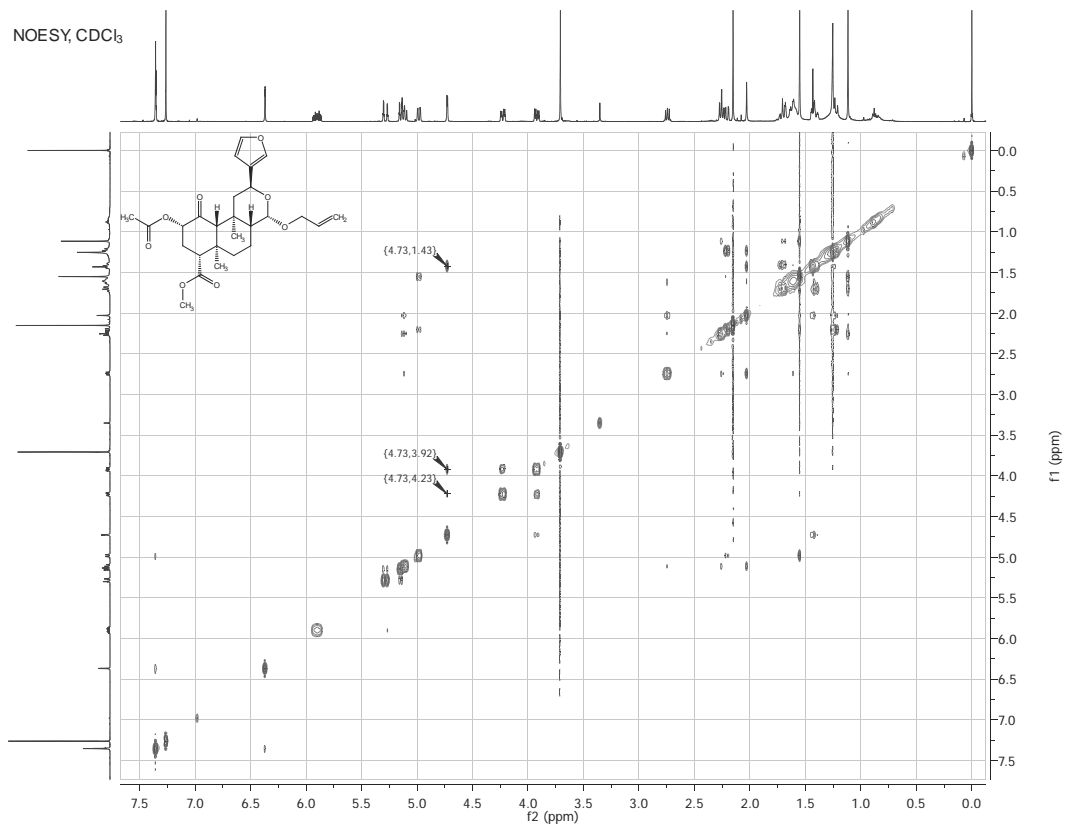


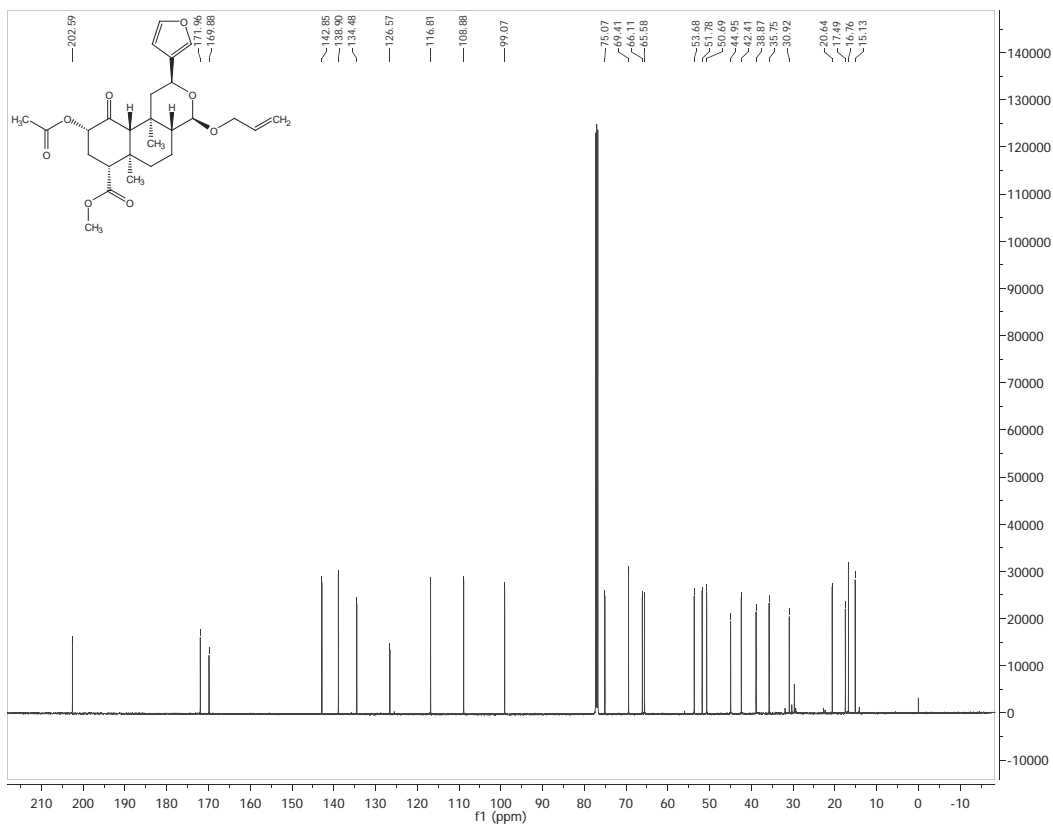
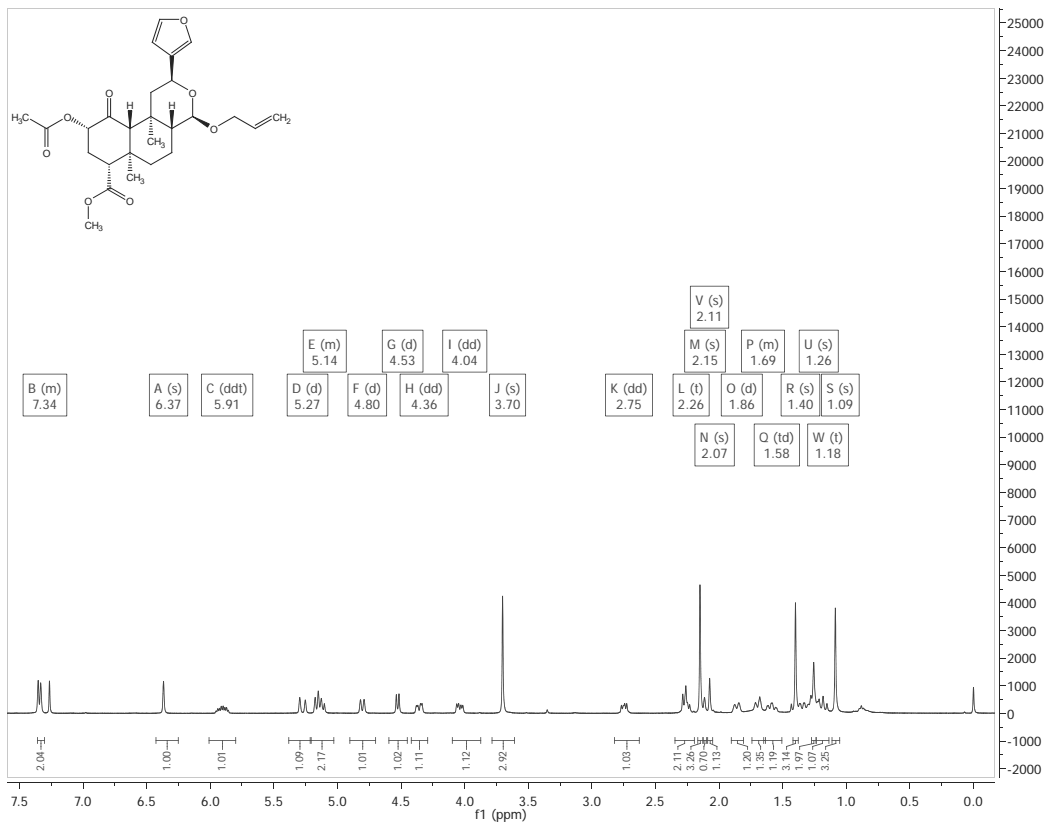


HSQC, CDCl₃

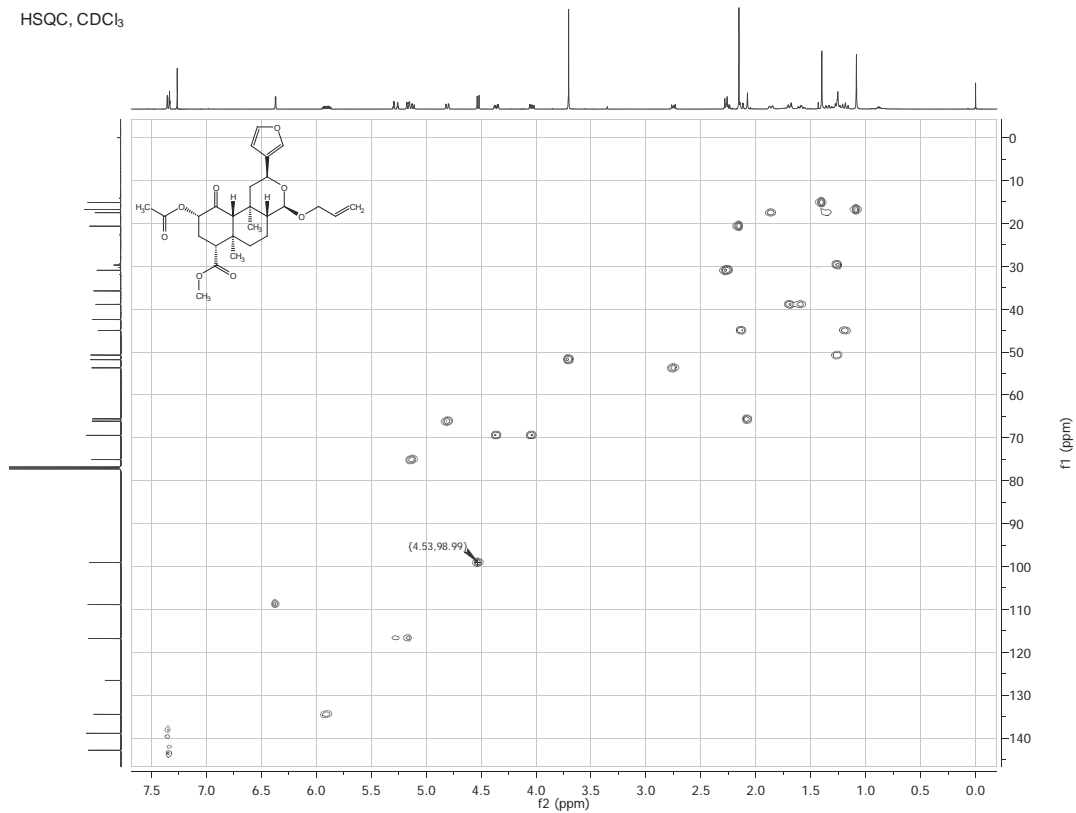


NOESY, CDCl₃

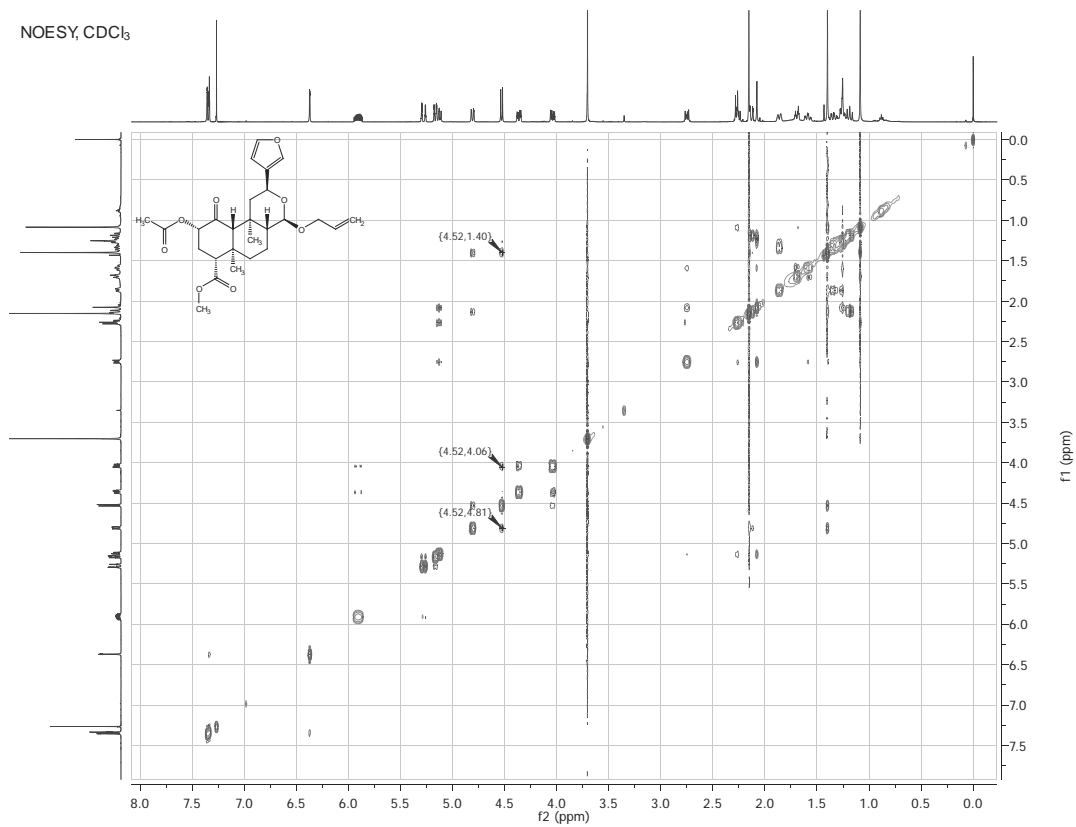


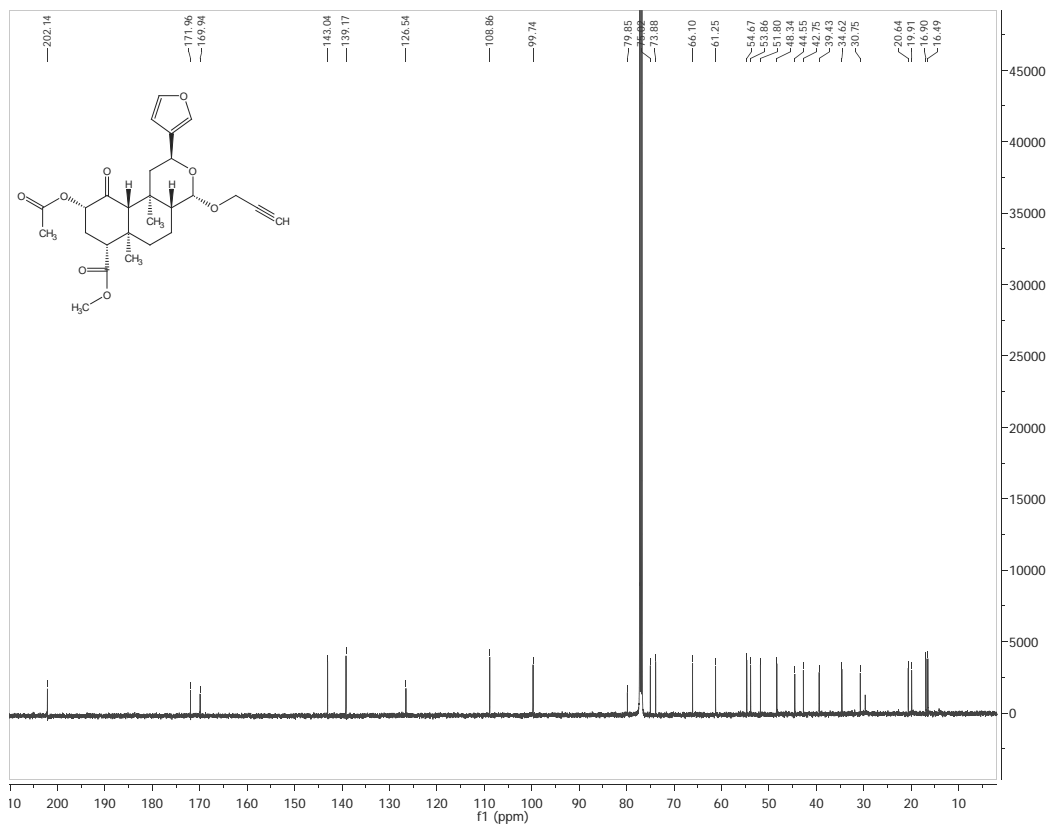
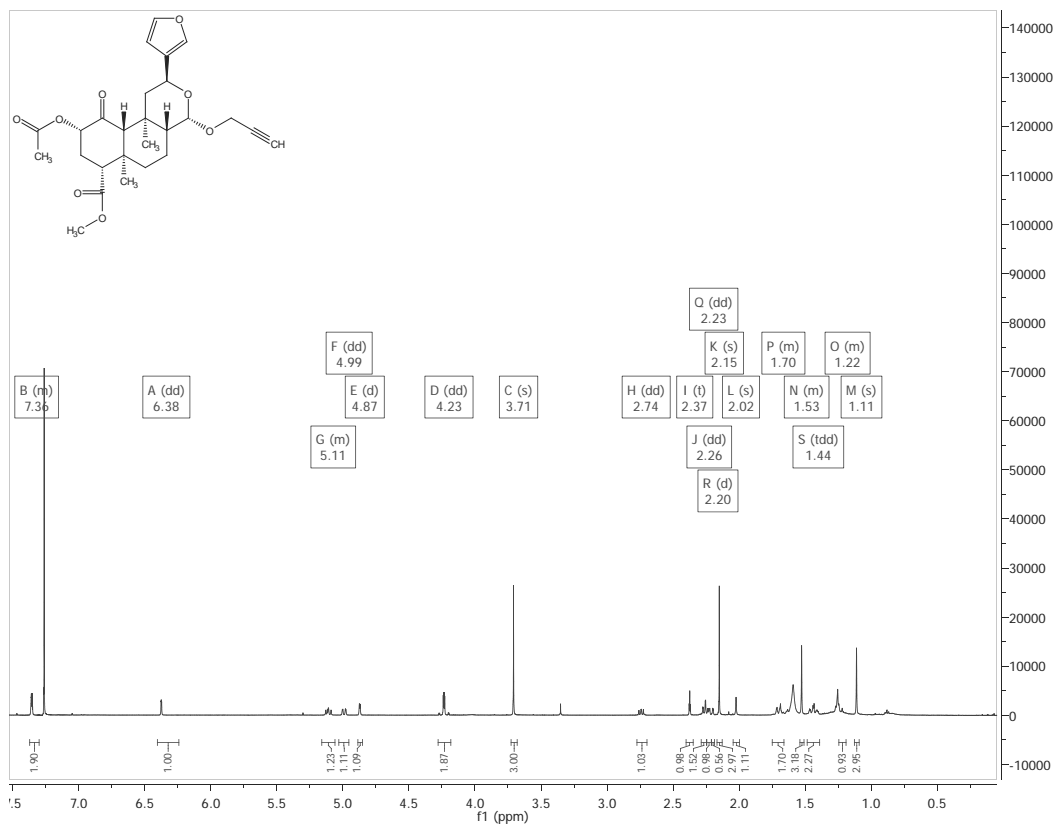


HSQC, CDCl₃

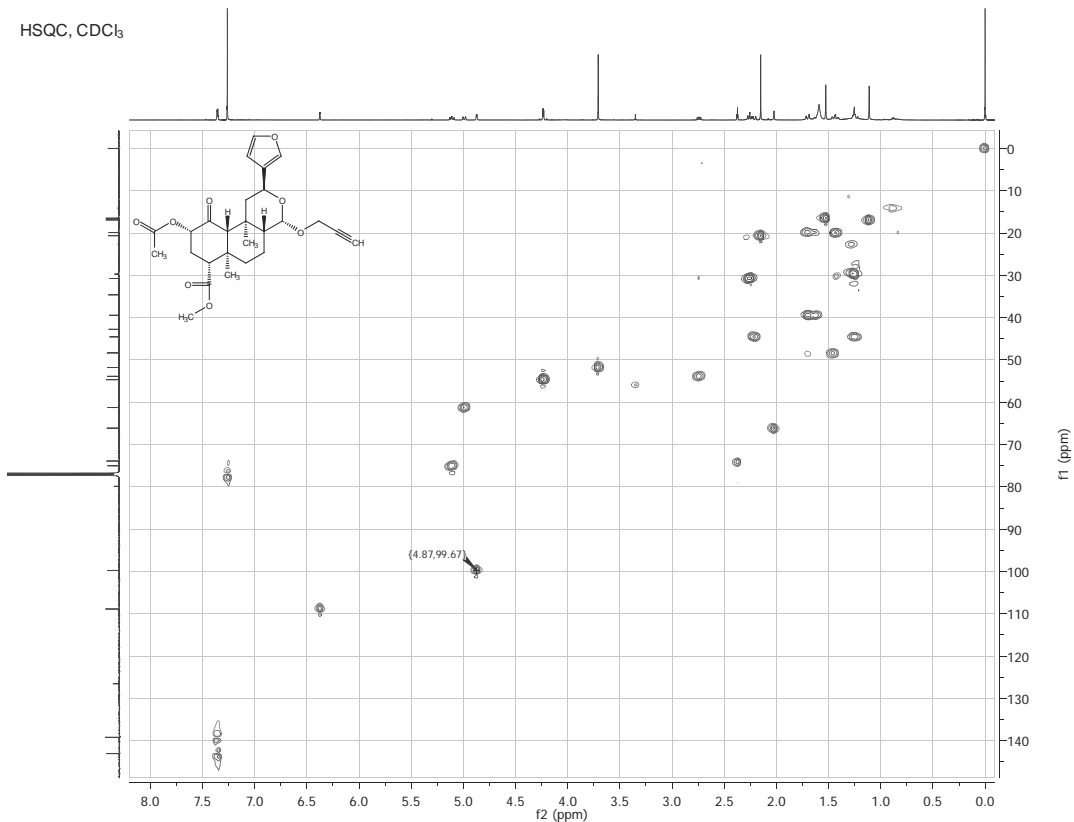


NOESY, CDCl₃

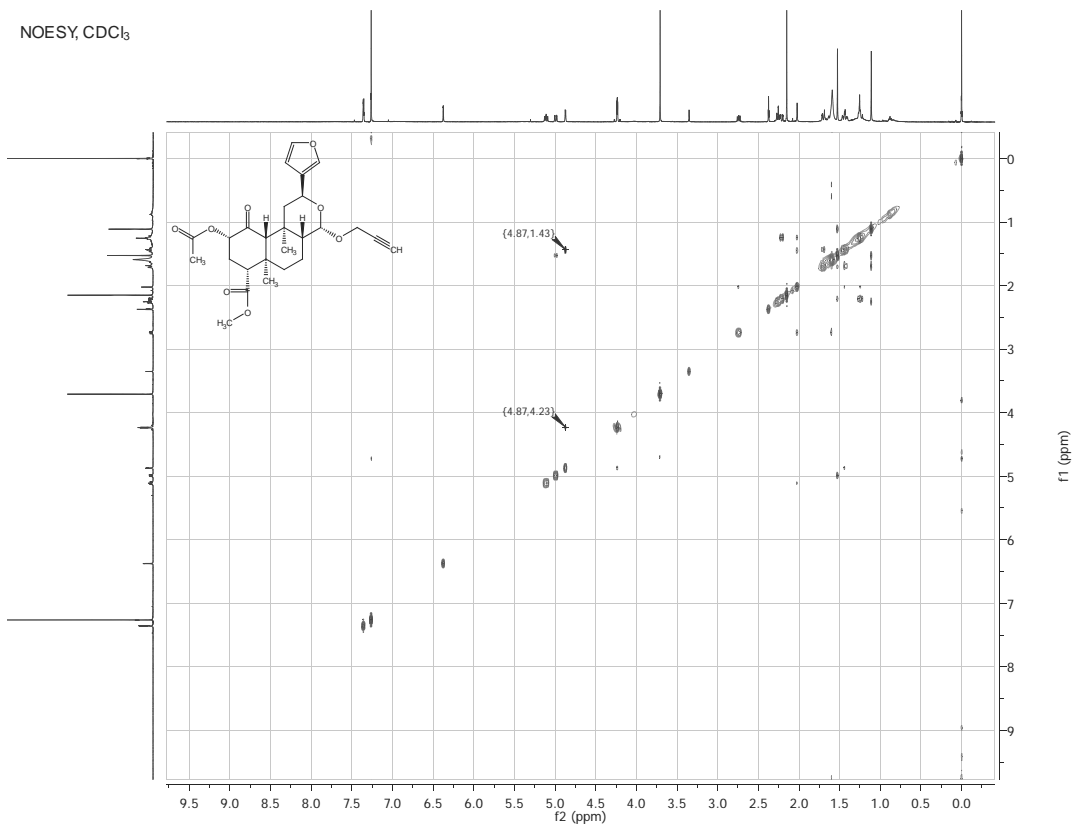


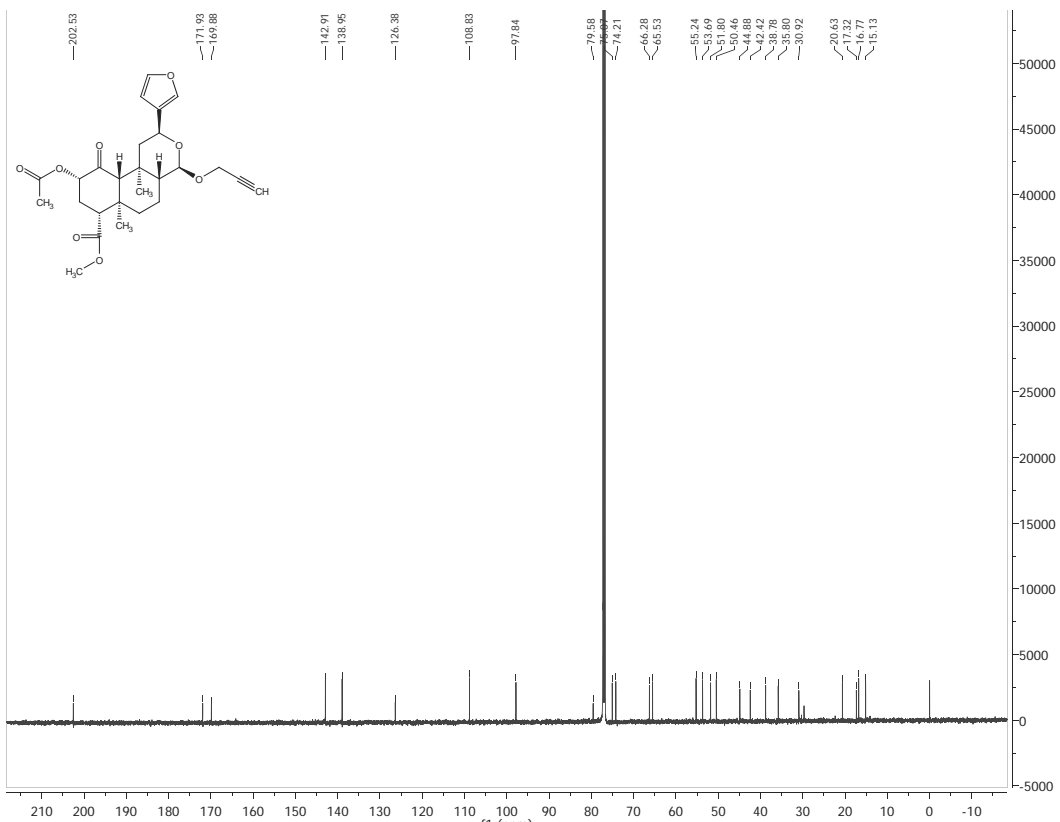
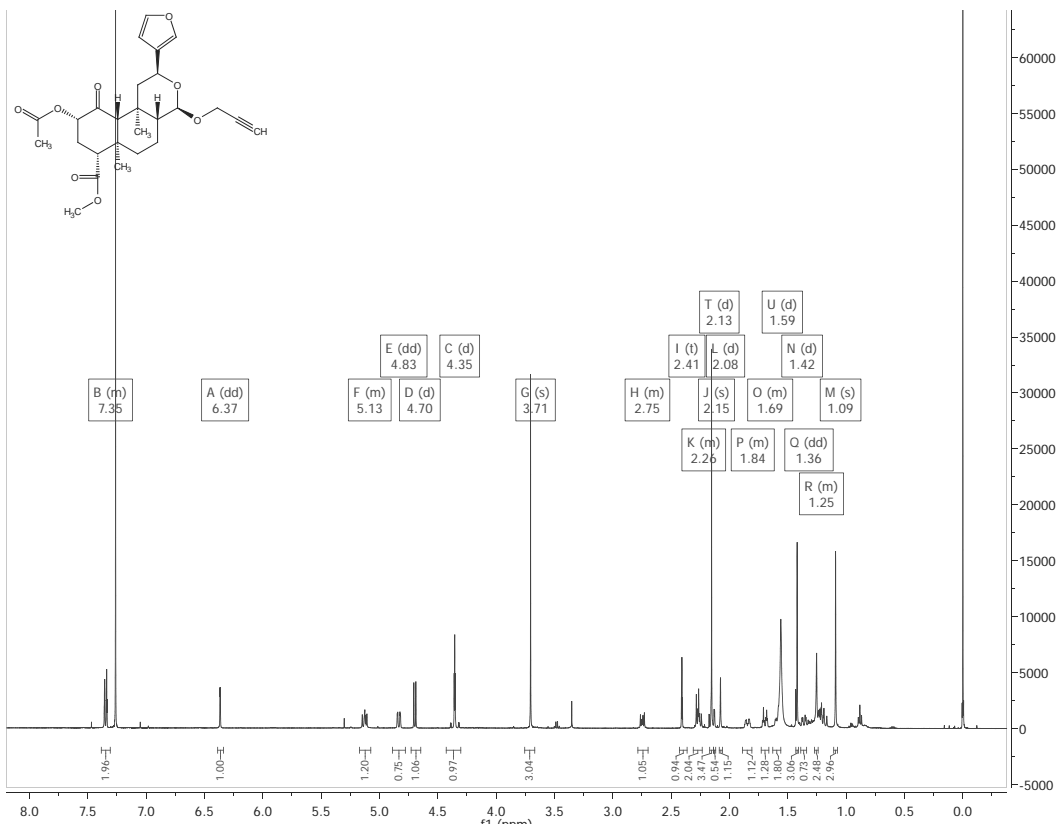


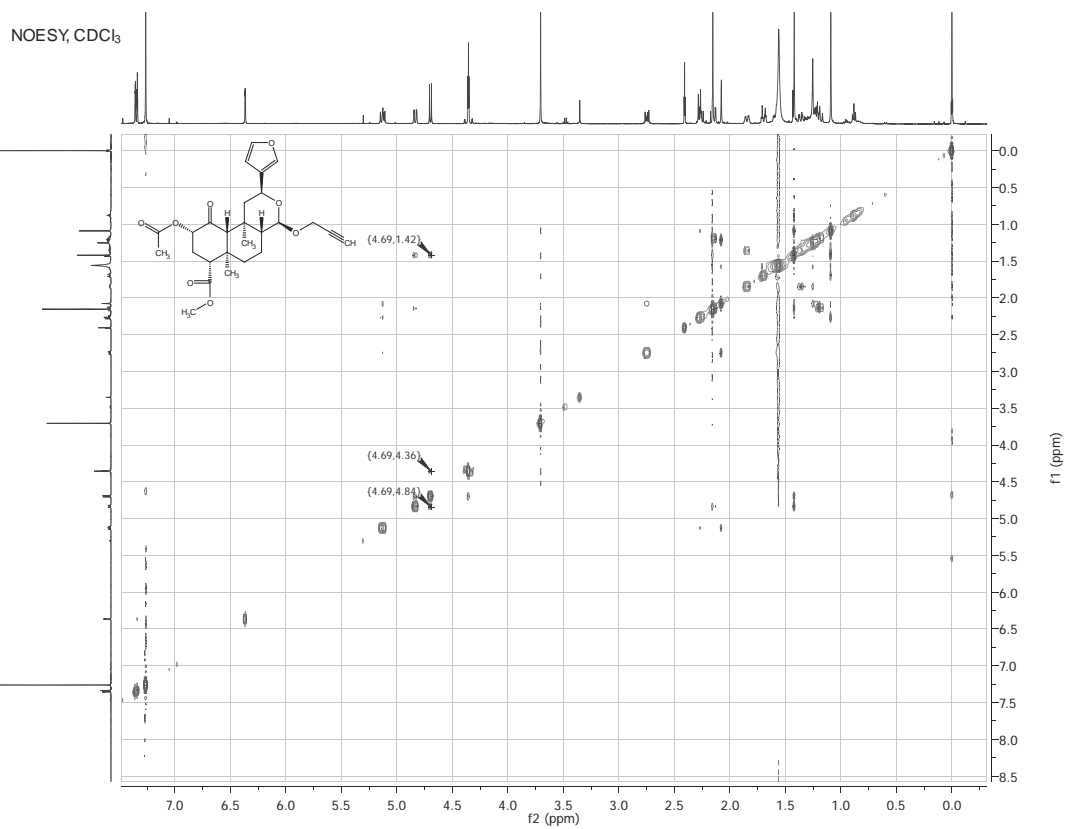
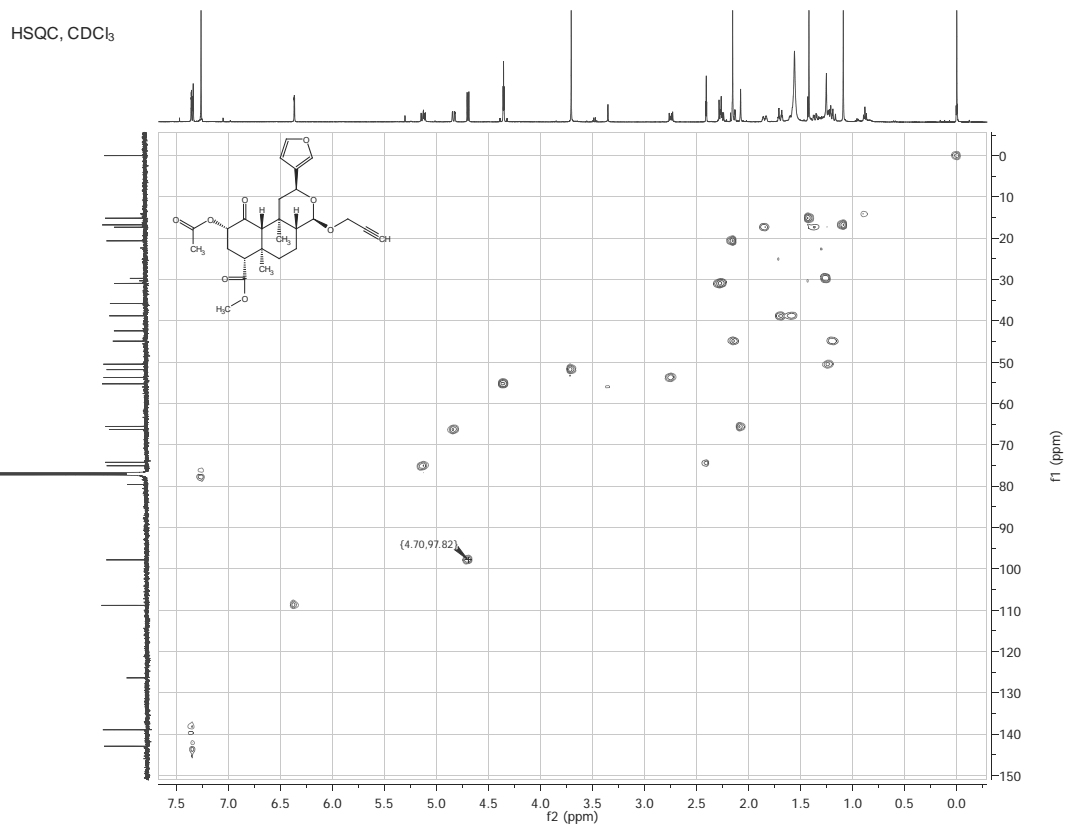
HSQC, CDCl₃

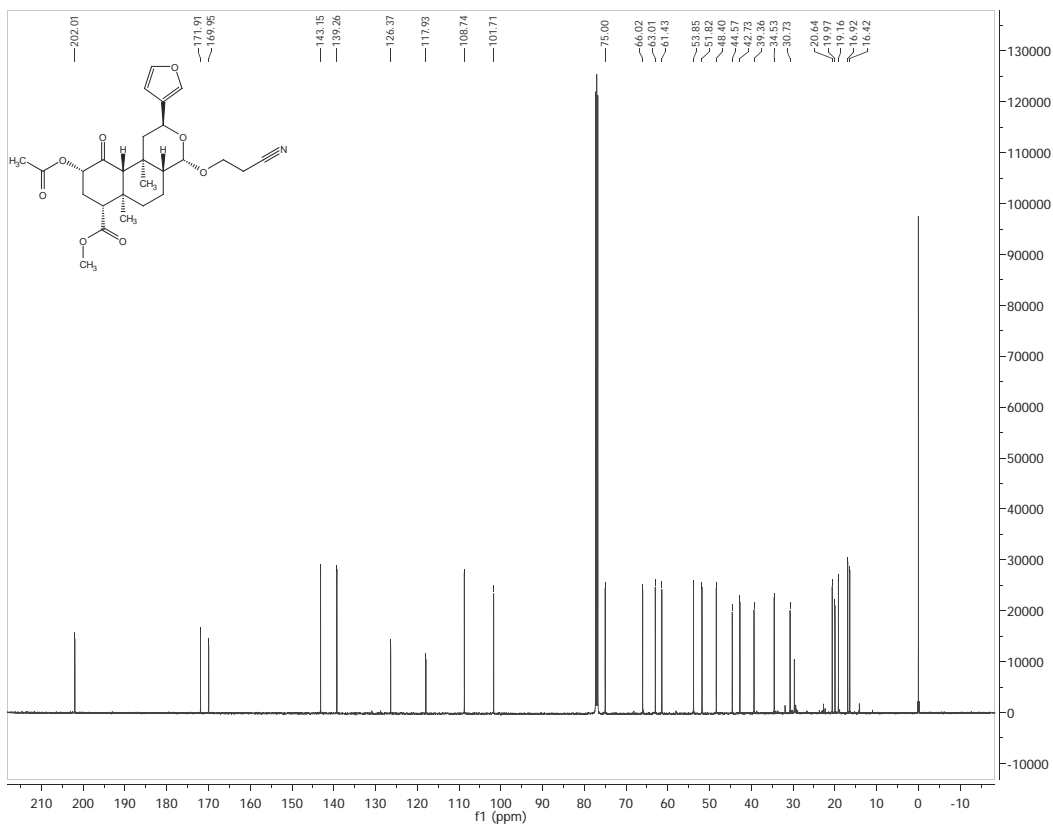
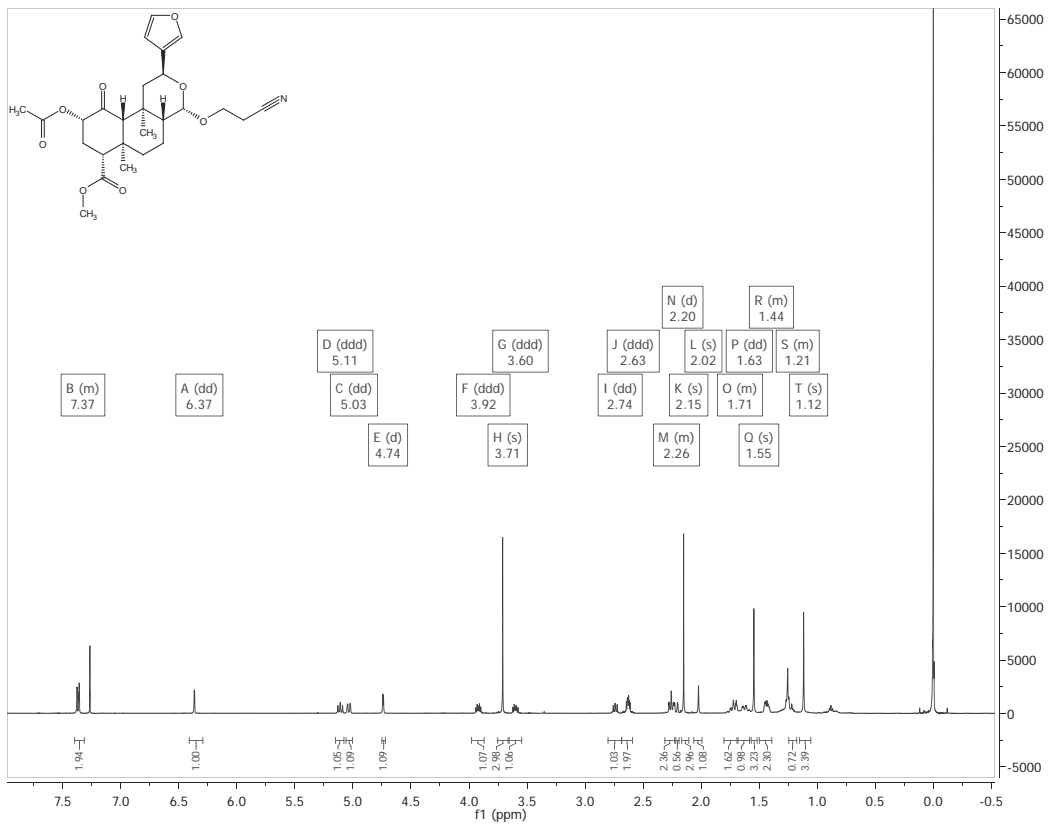


NOESY, CDCl₃

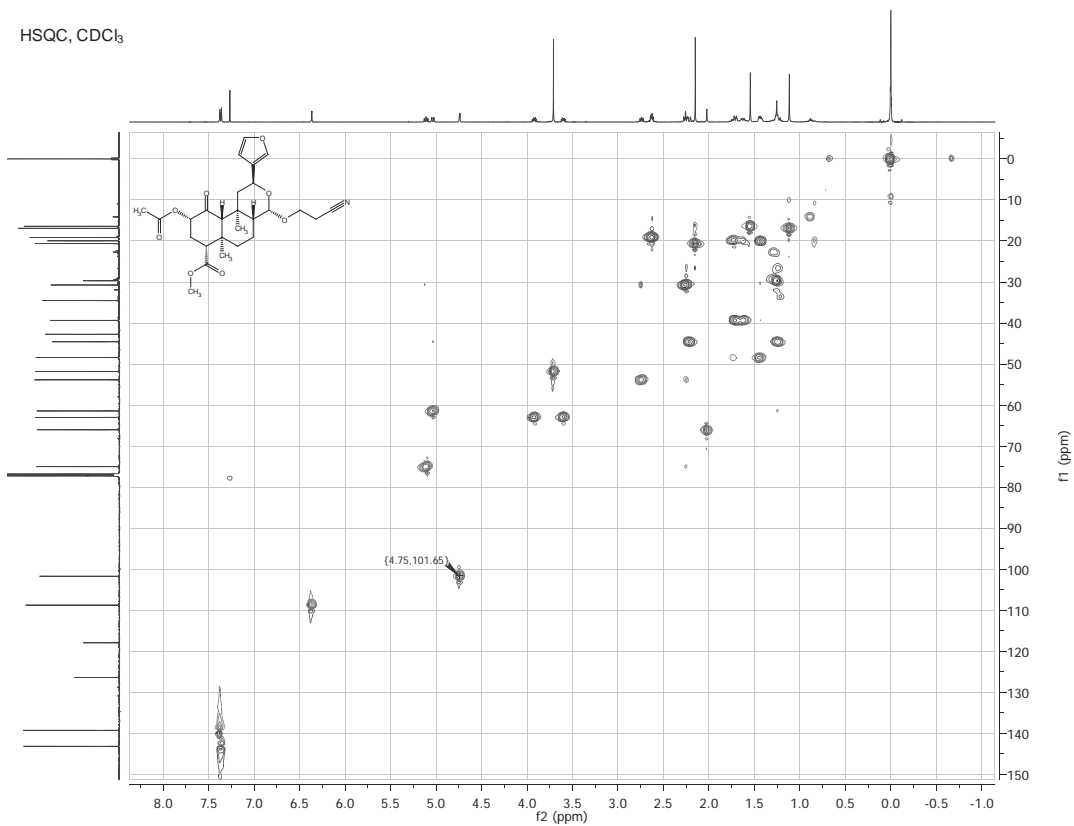




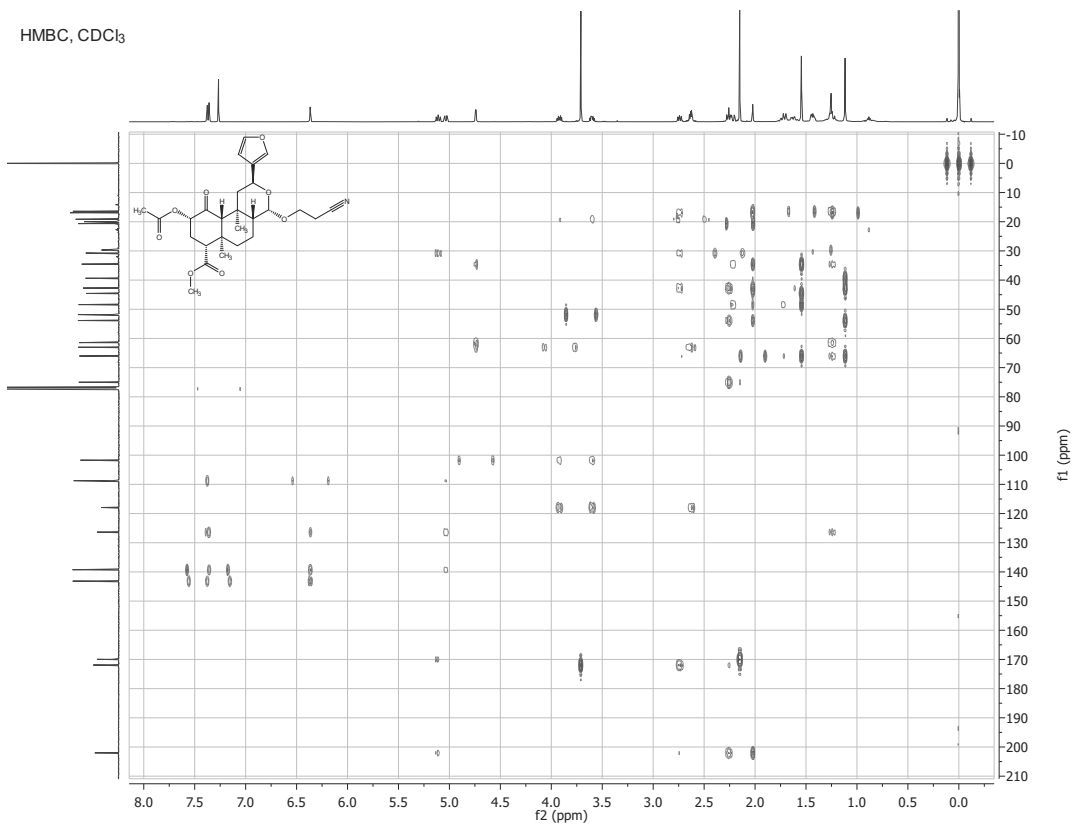


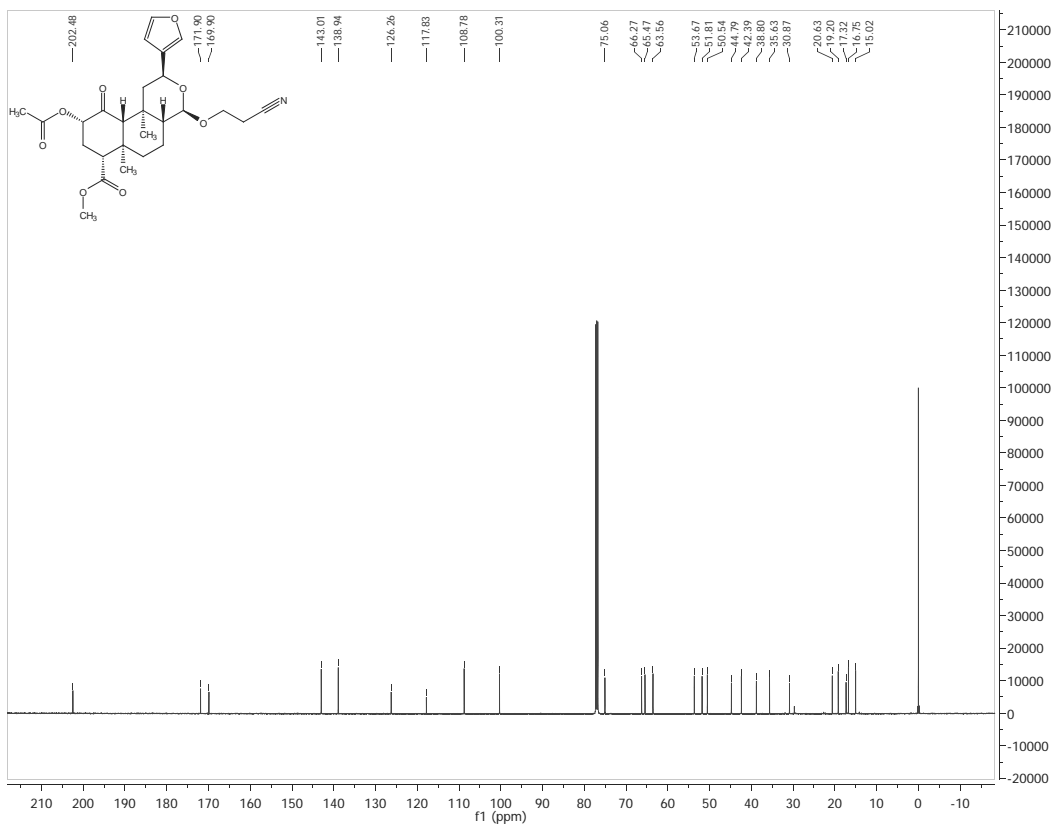
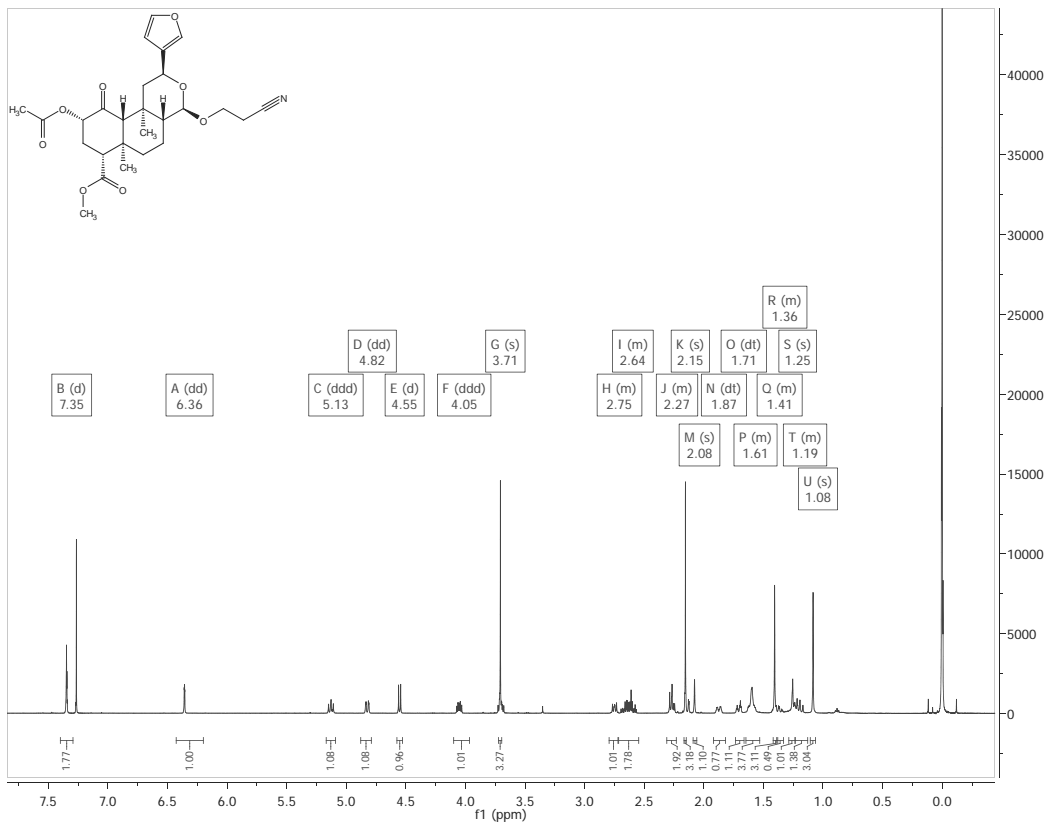


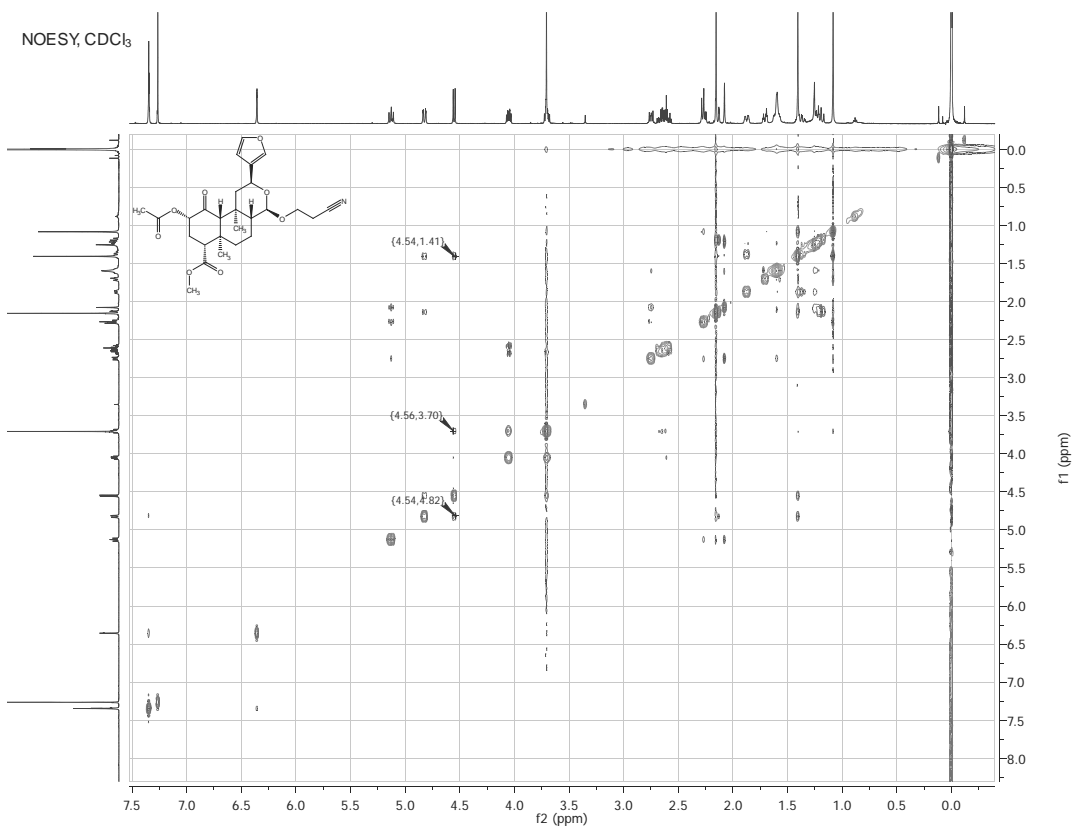
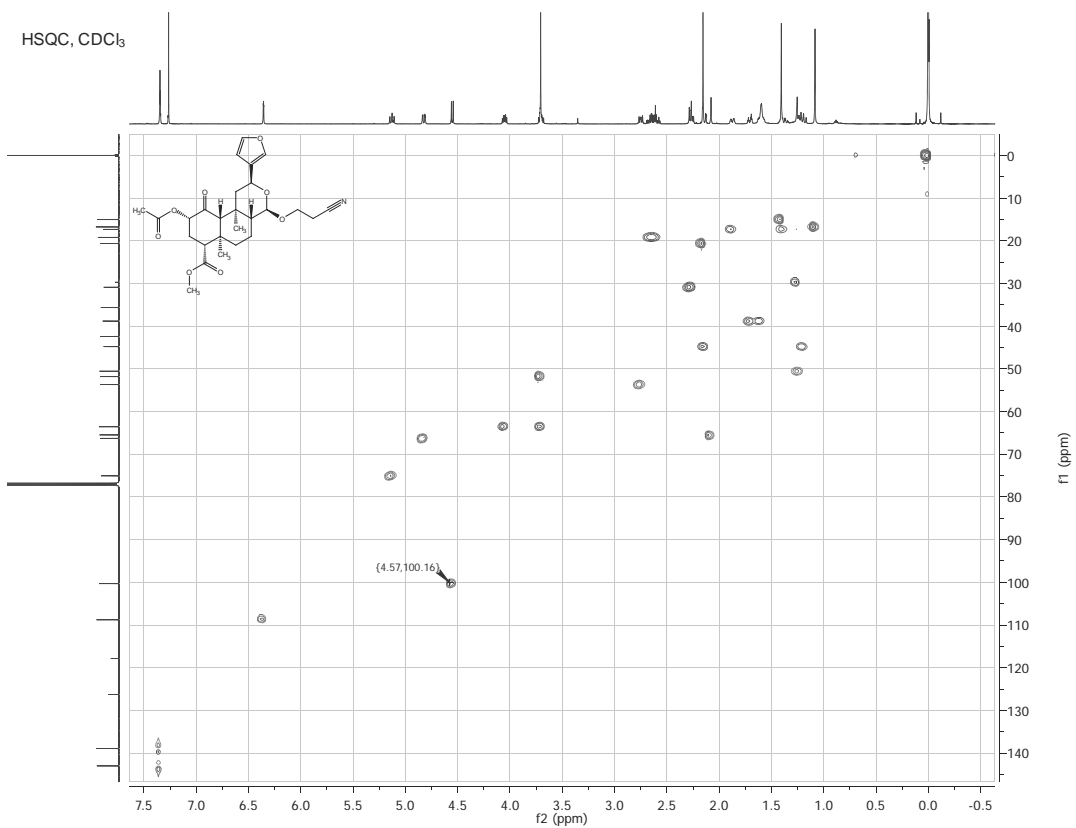
HSQC, CDCl₃

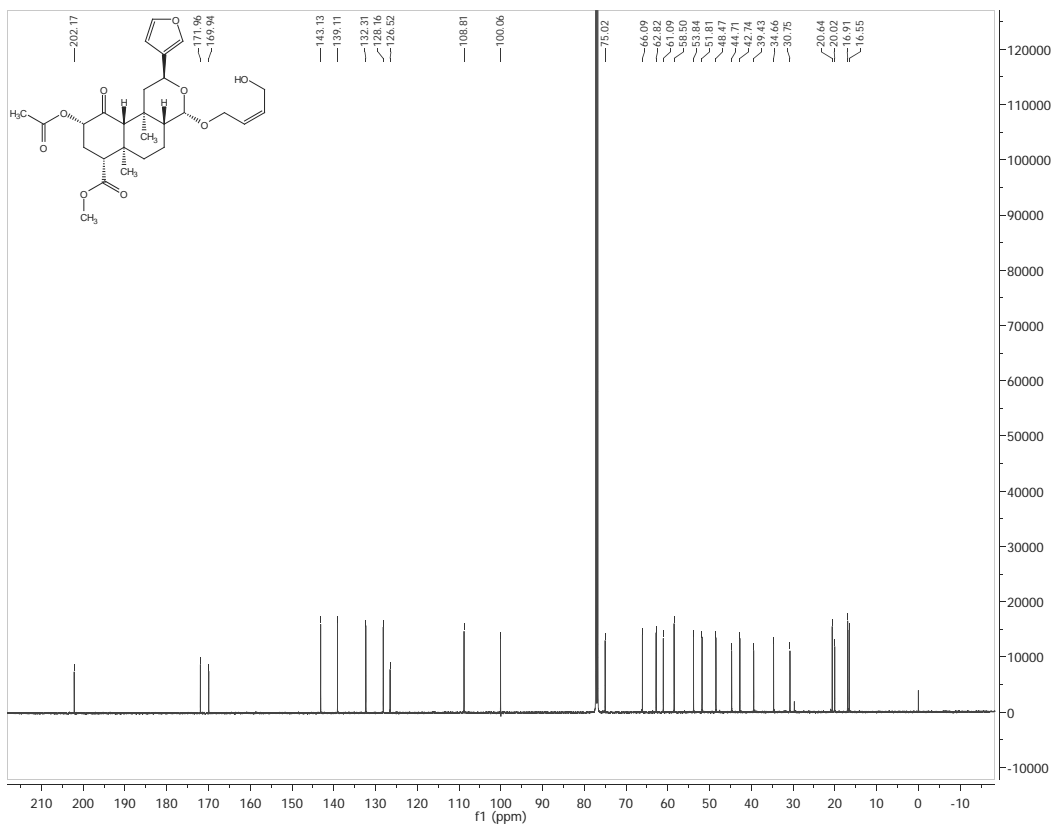
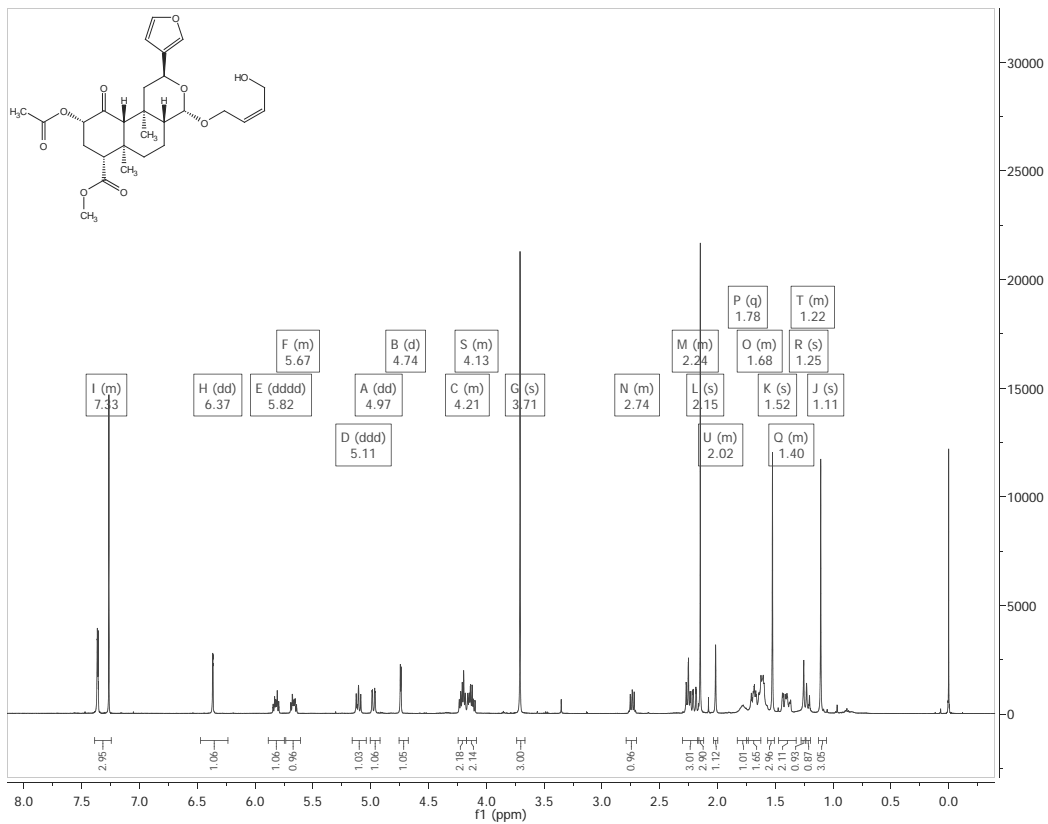


HMBC, CDCl₃

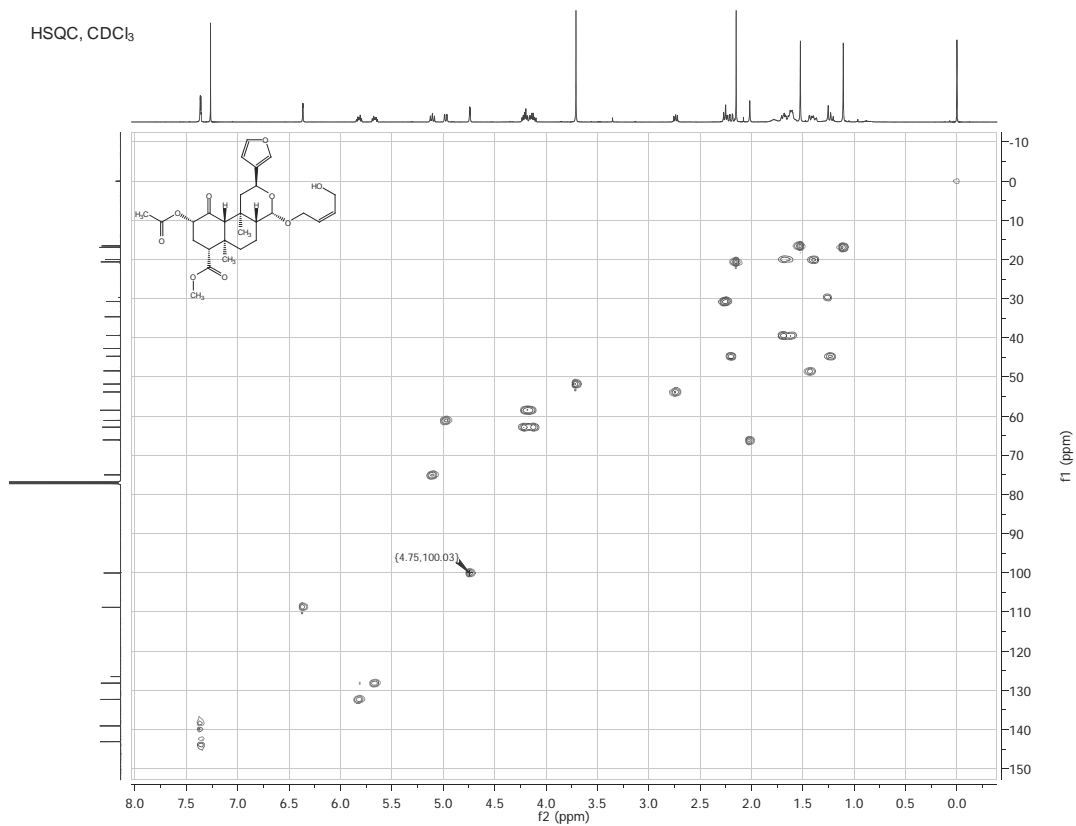




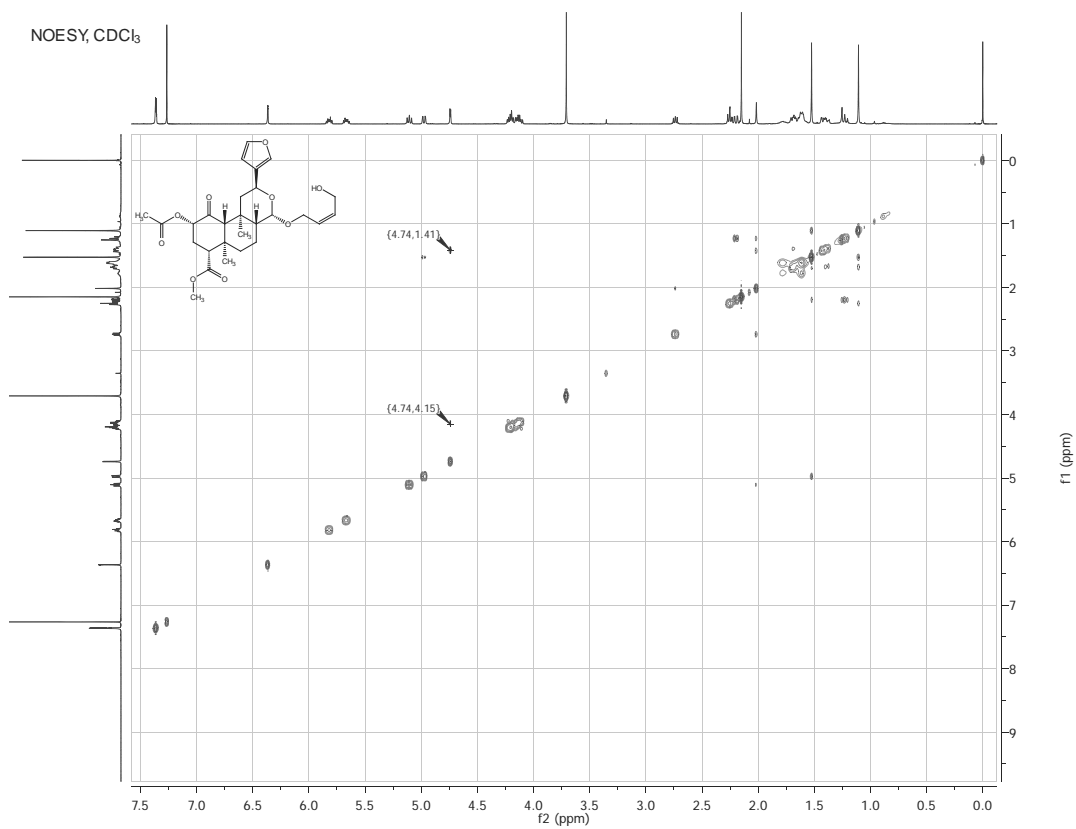


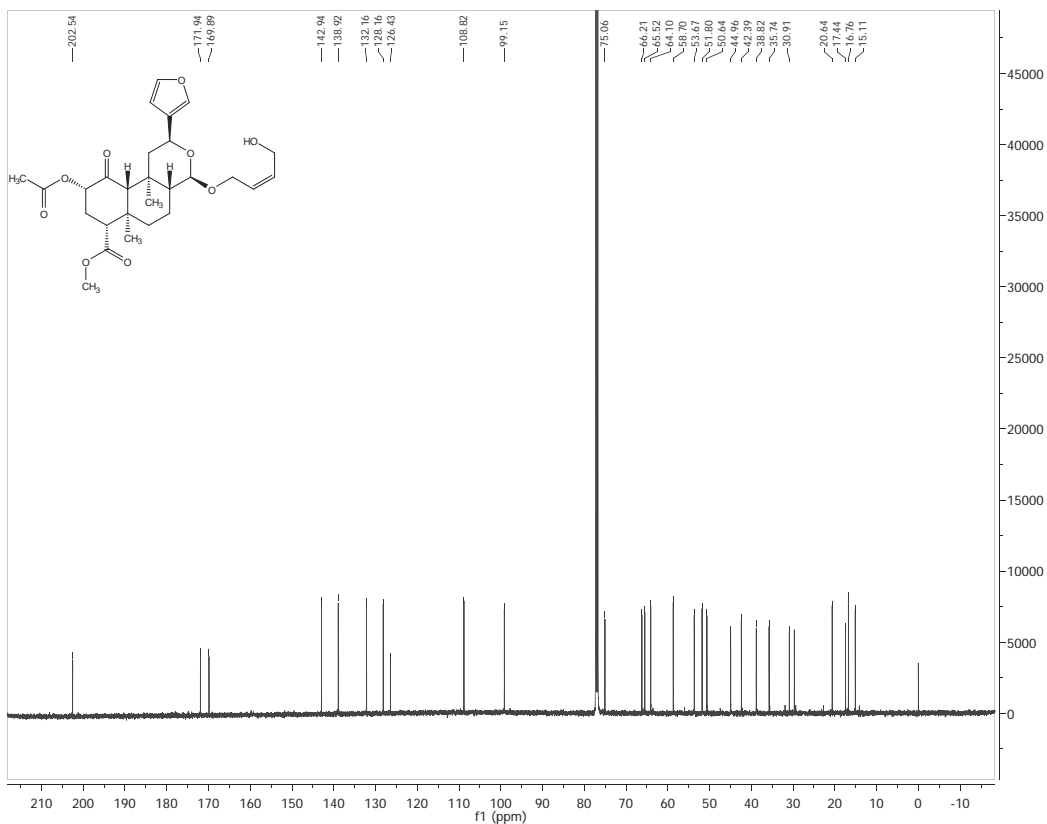
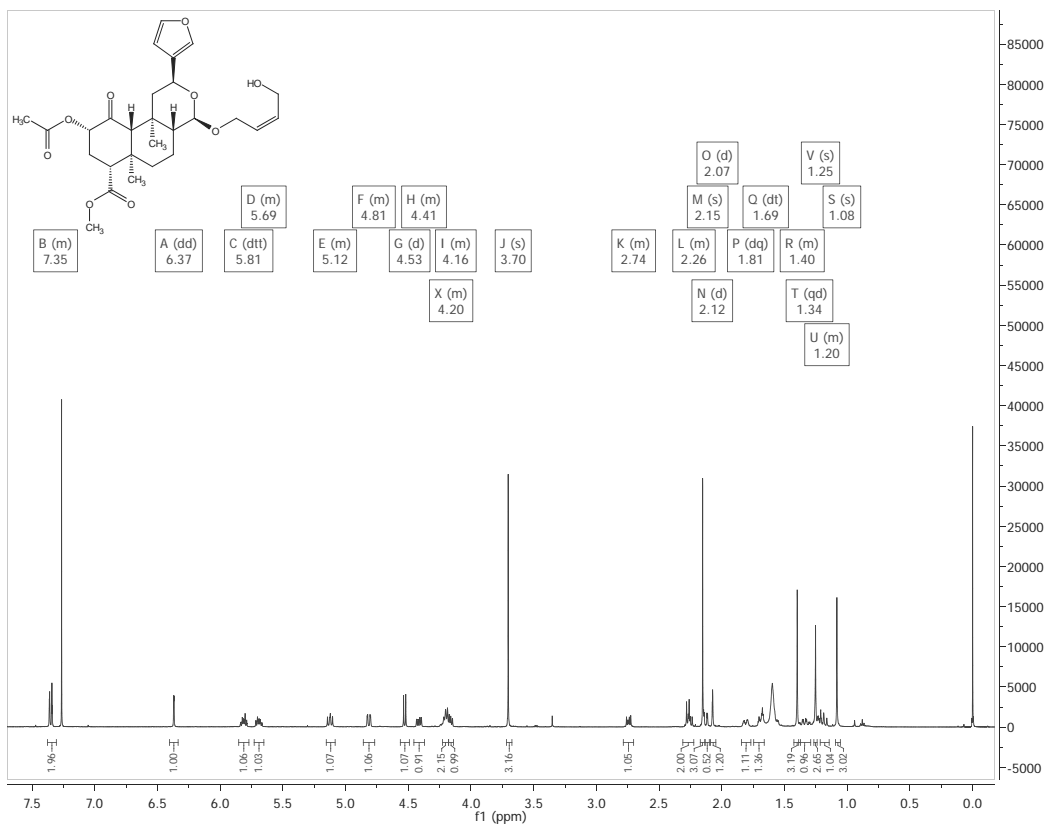


HSQC, CDCl₃

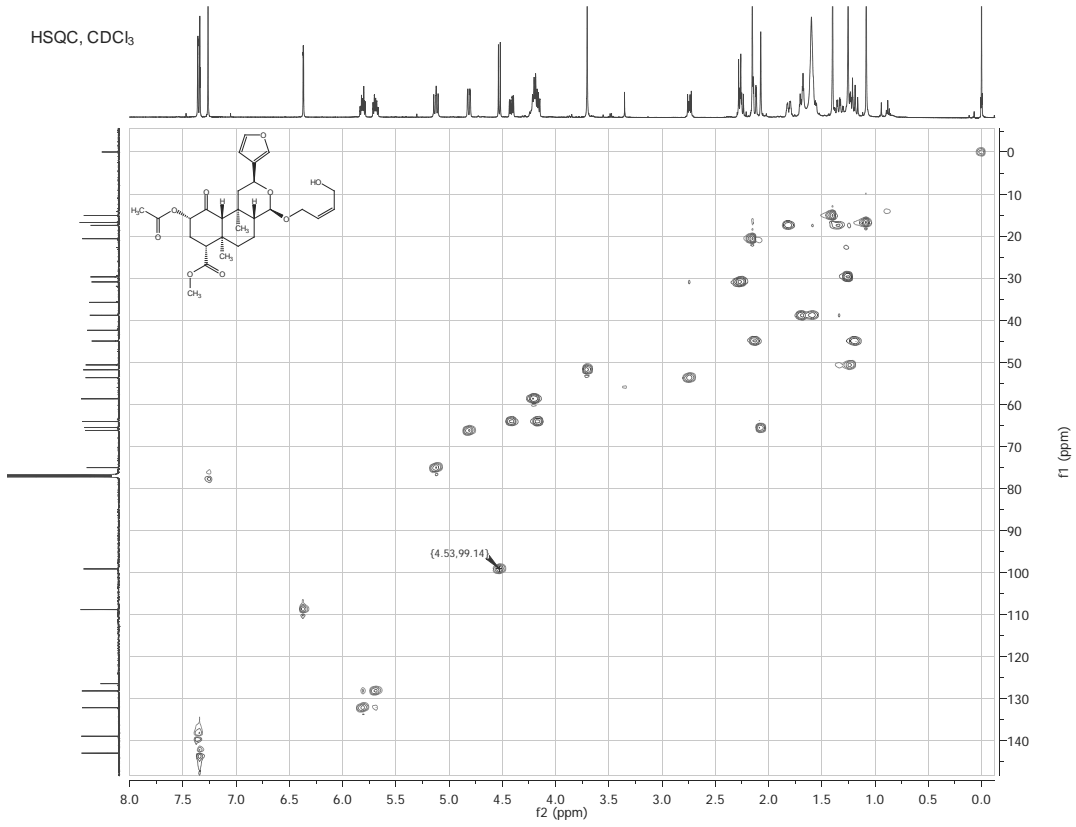


NOESY, CDCl₃

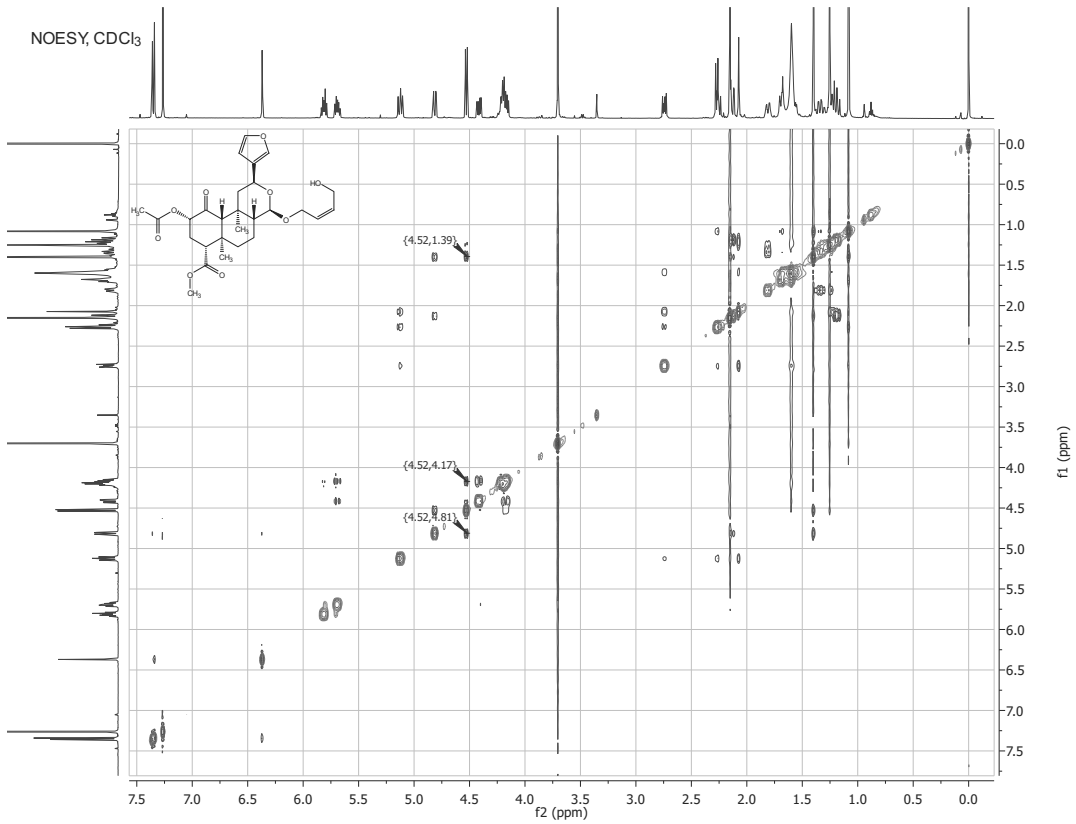


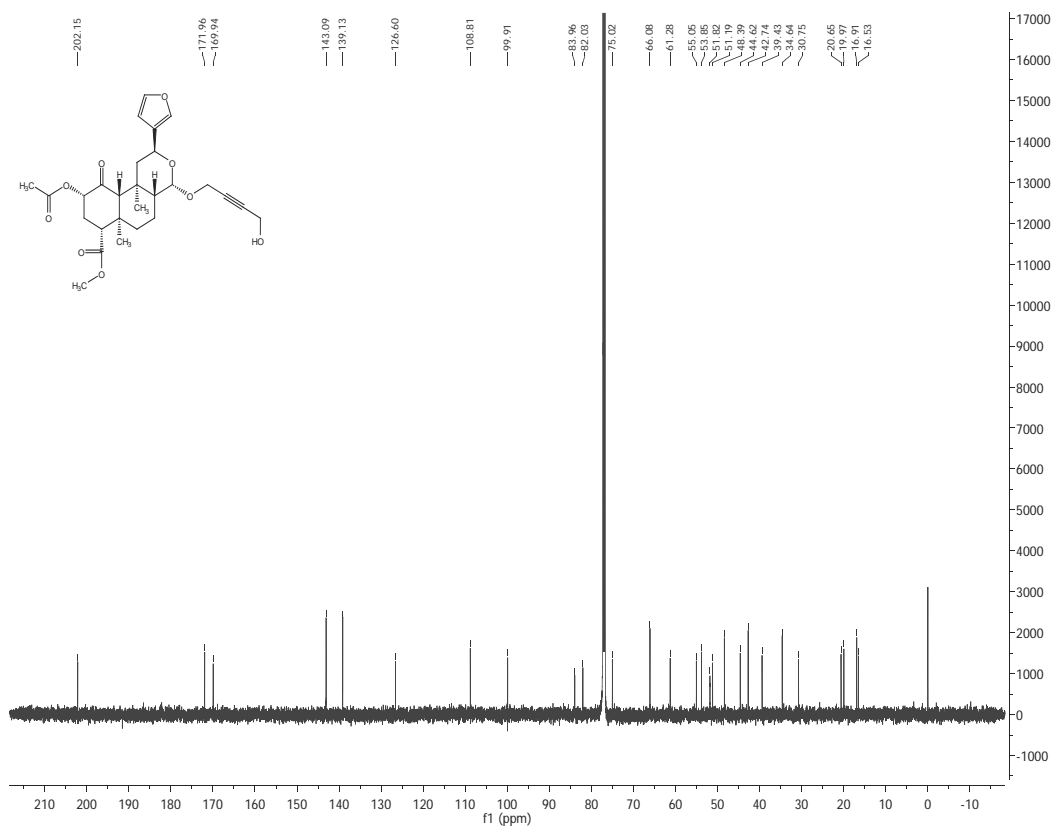
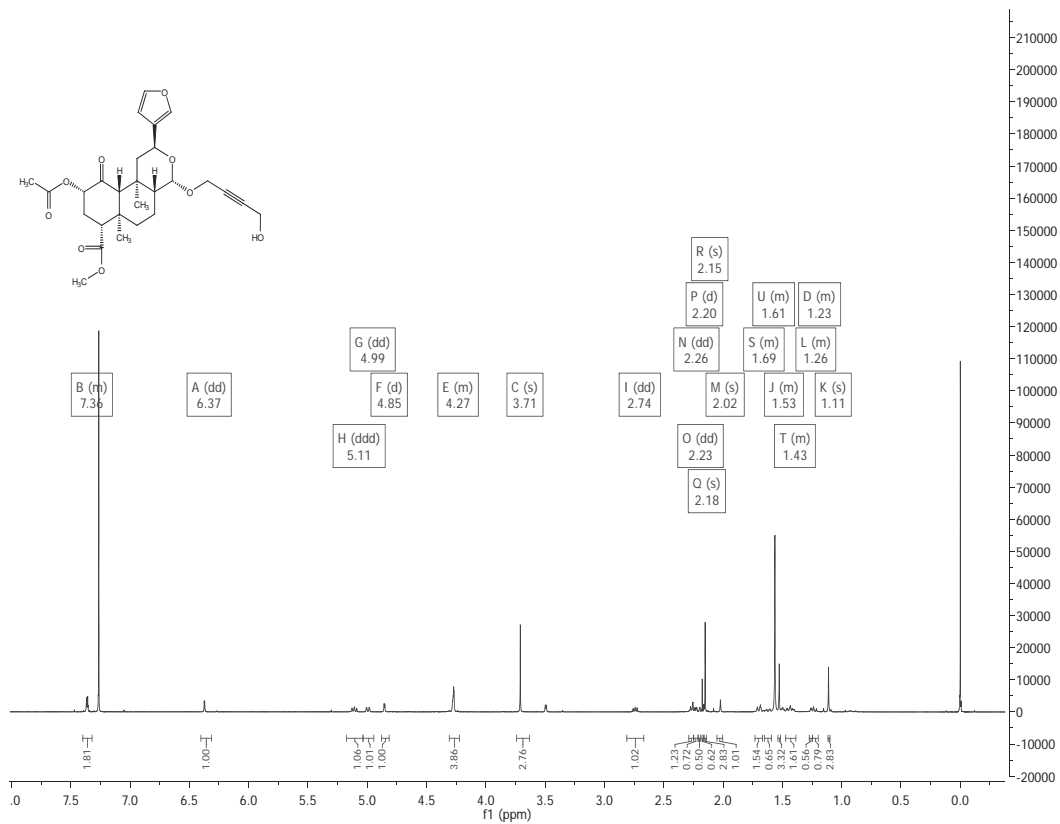


HSQC, CDCl₃

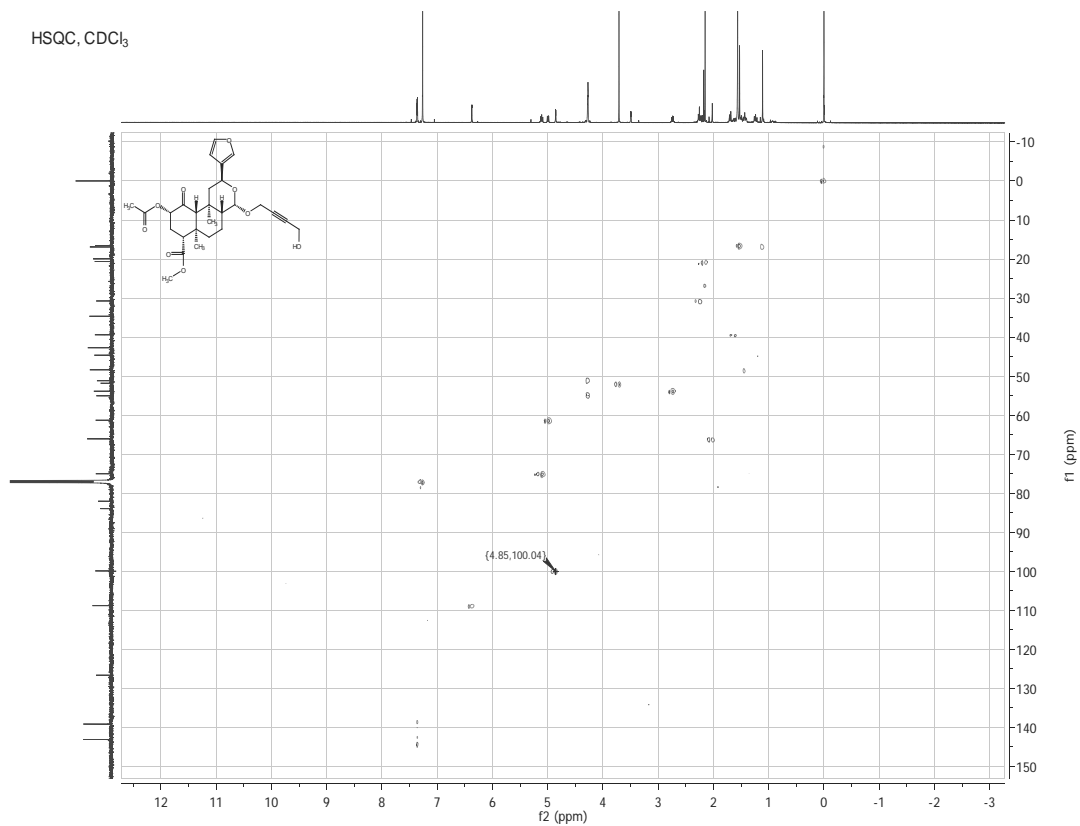


NOESY, CDCl₃

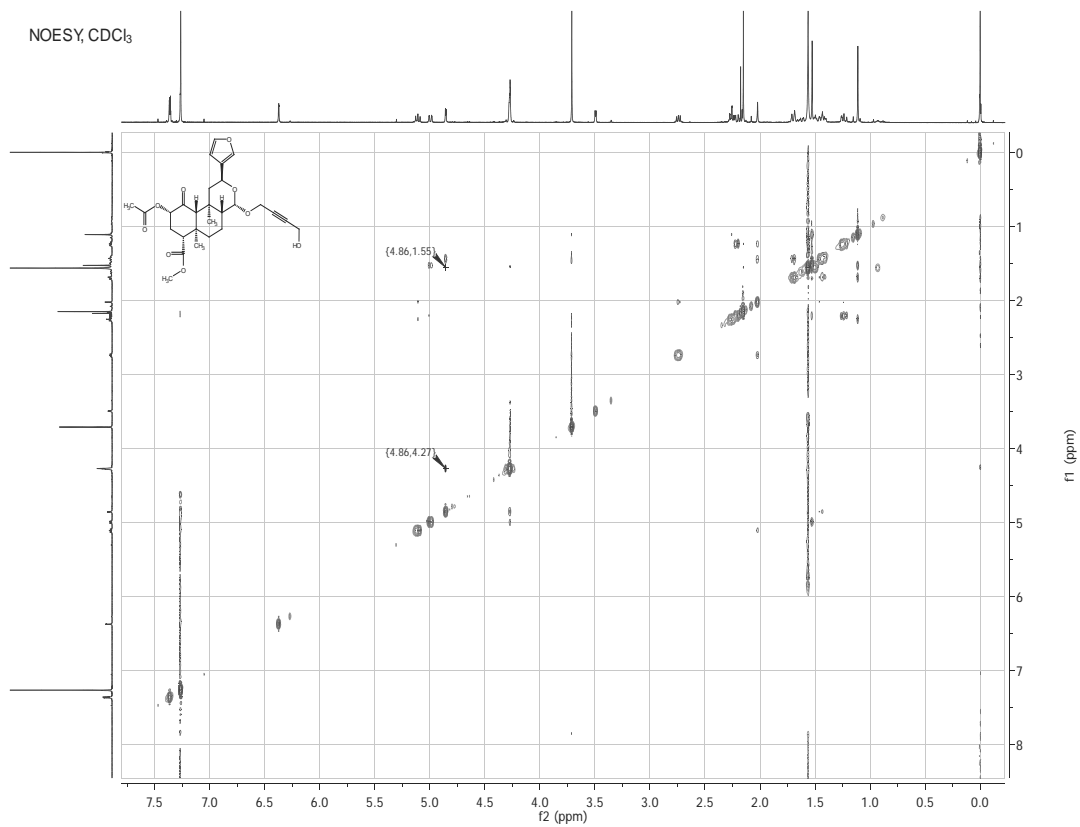


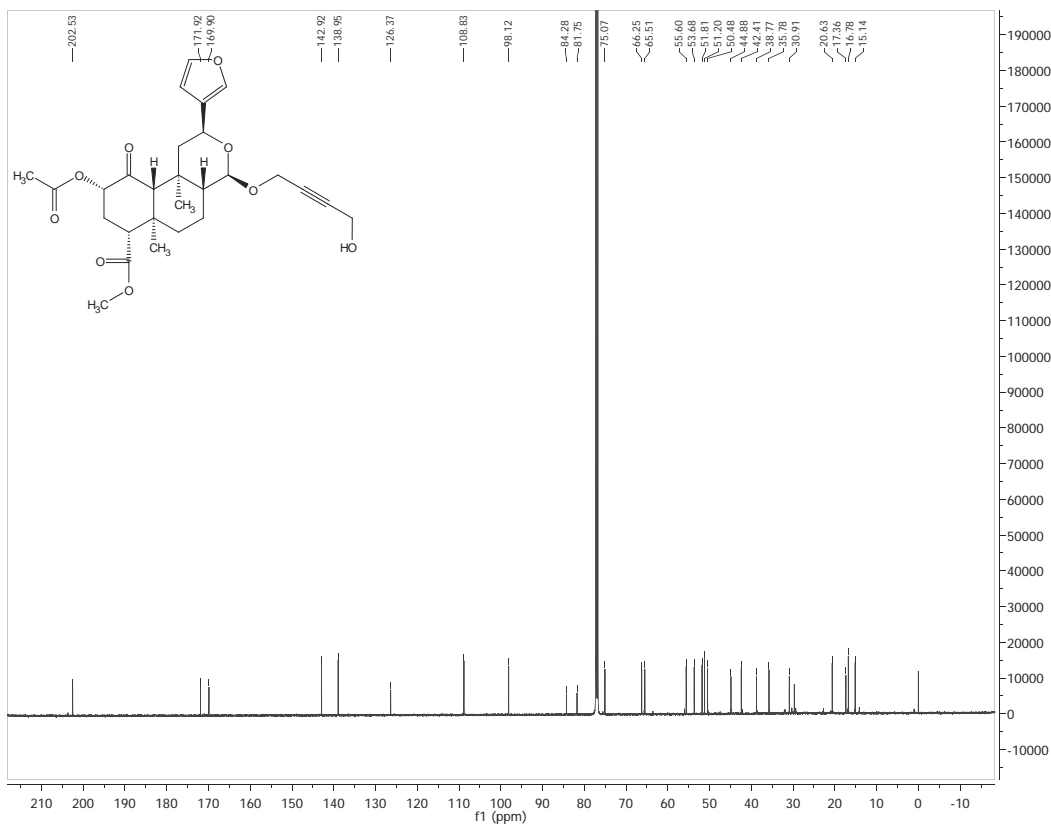
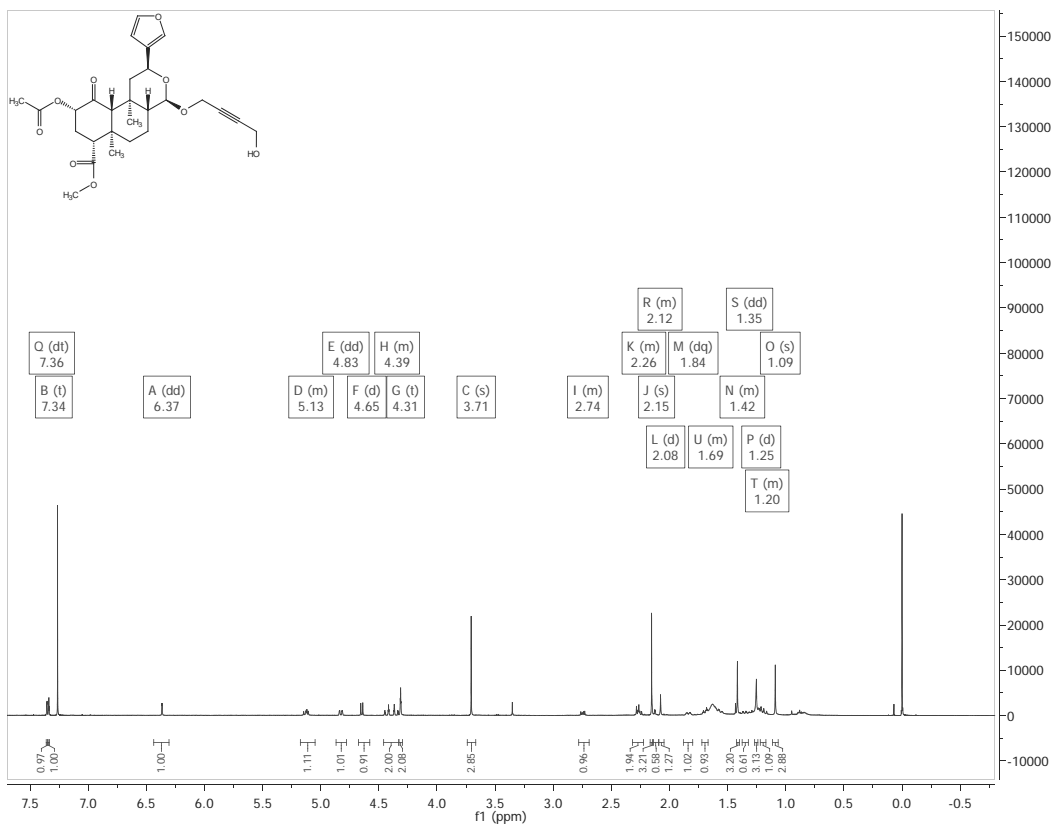


HSQC, CDCl₃

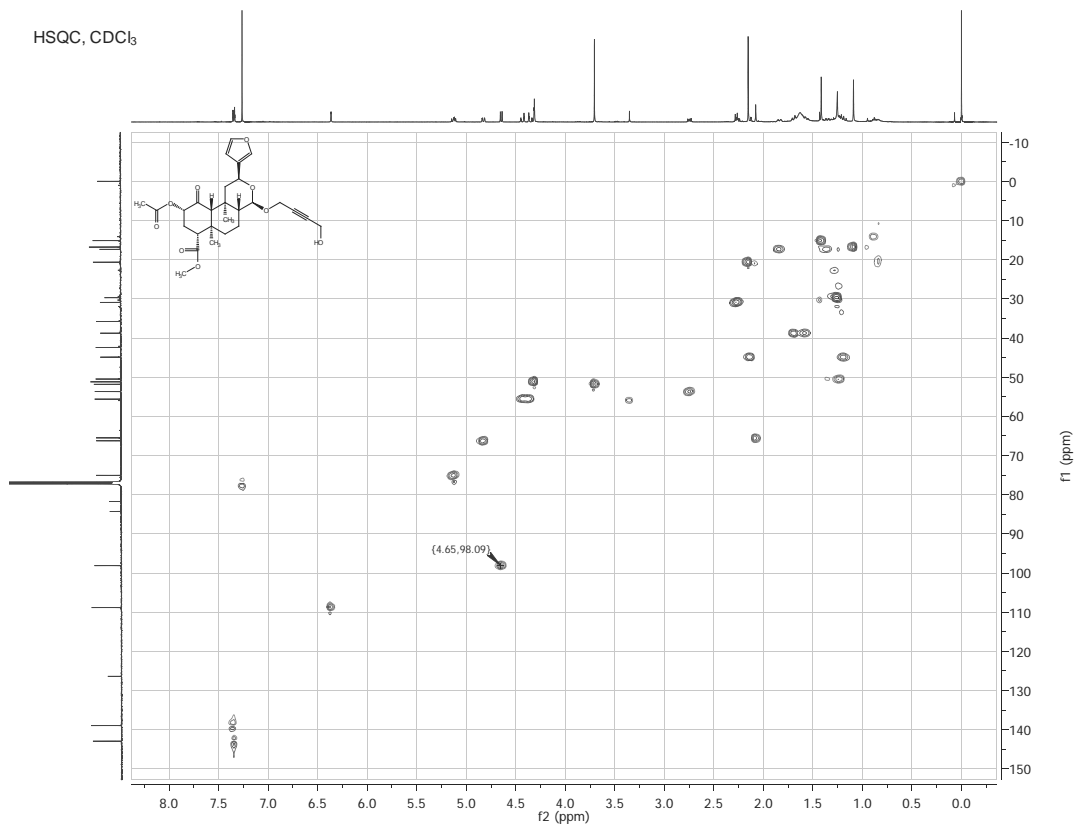


NOESY, CDCl₃

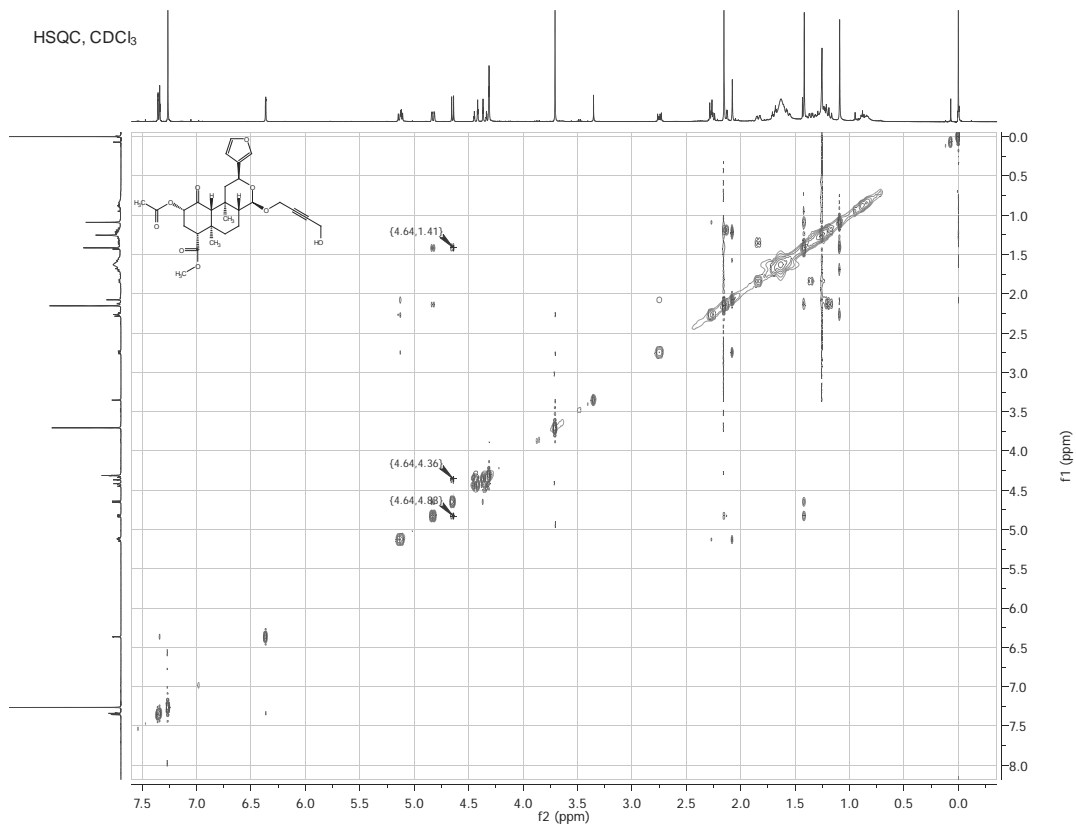


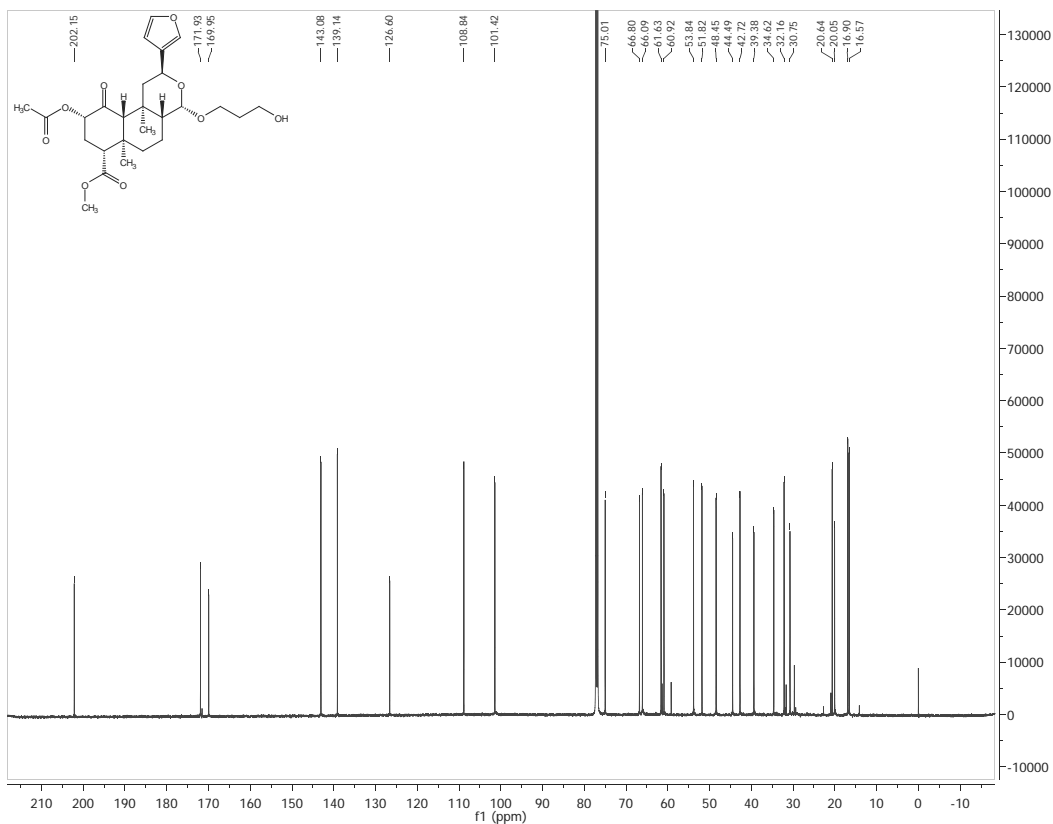
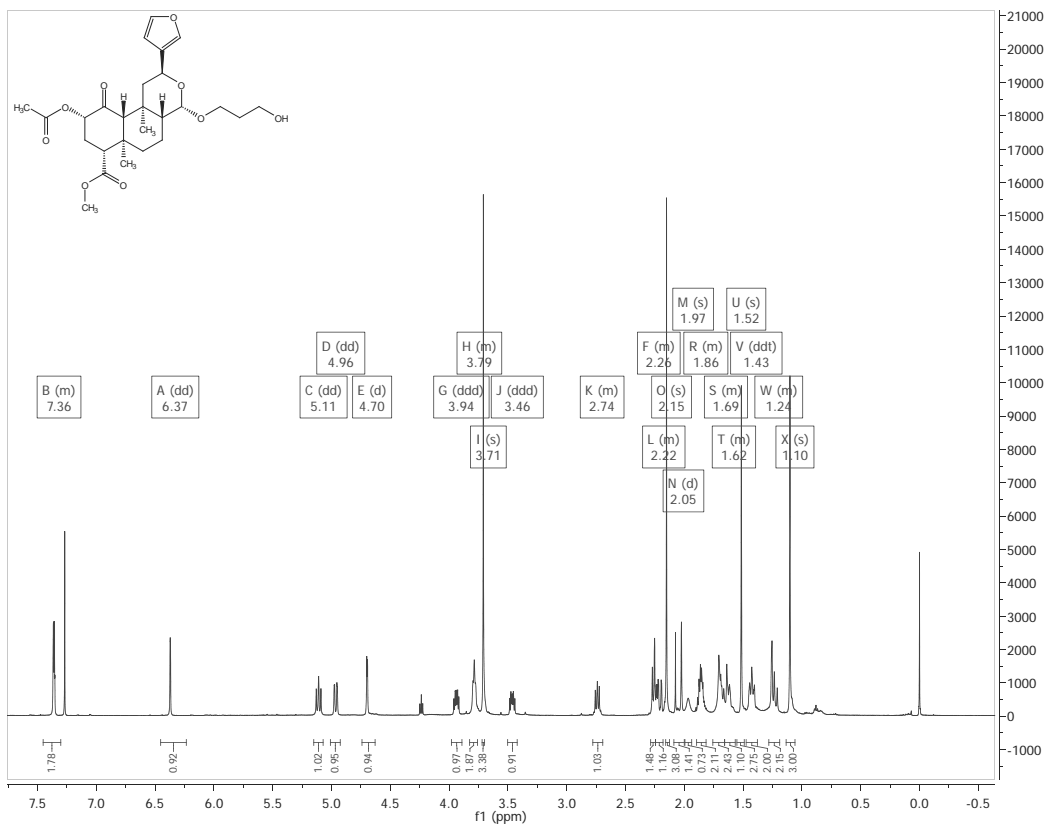


HSQC, CDCl₃

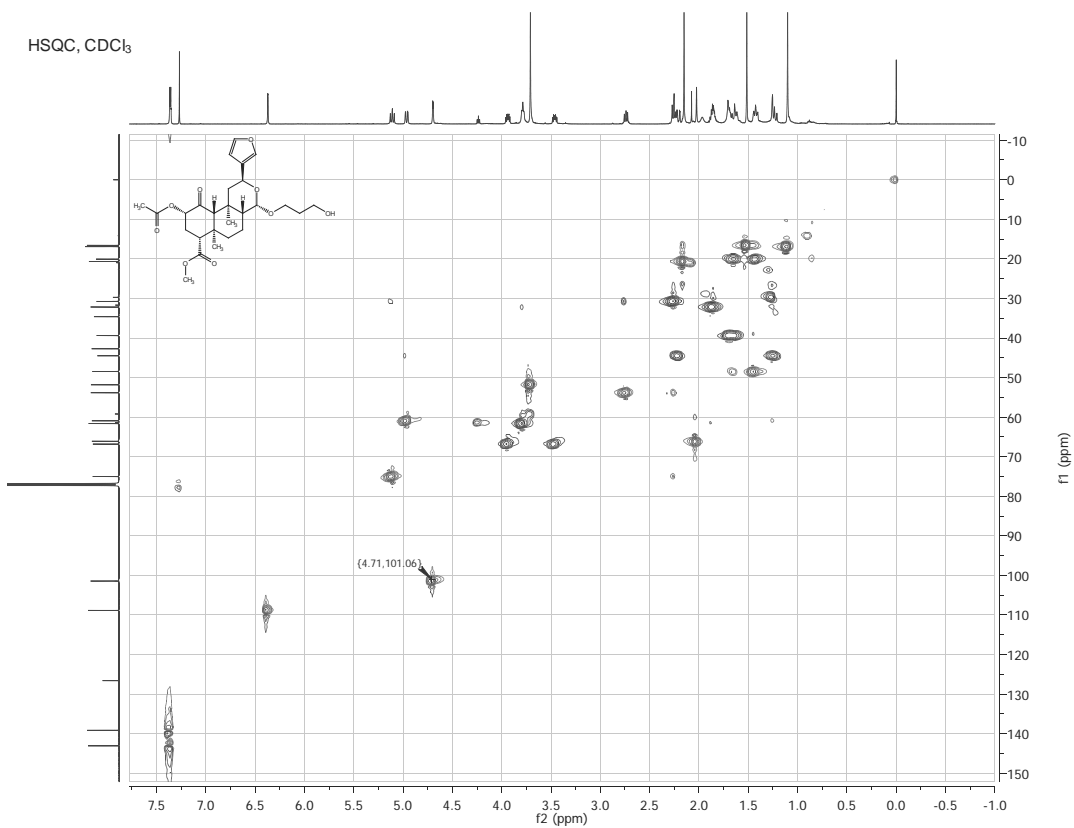


HSQC, CDCl₃

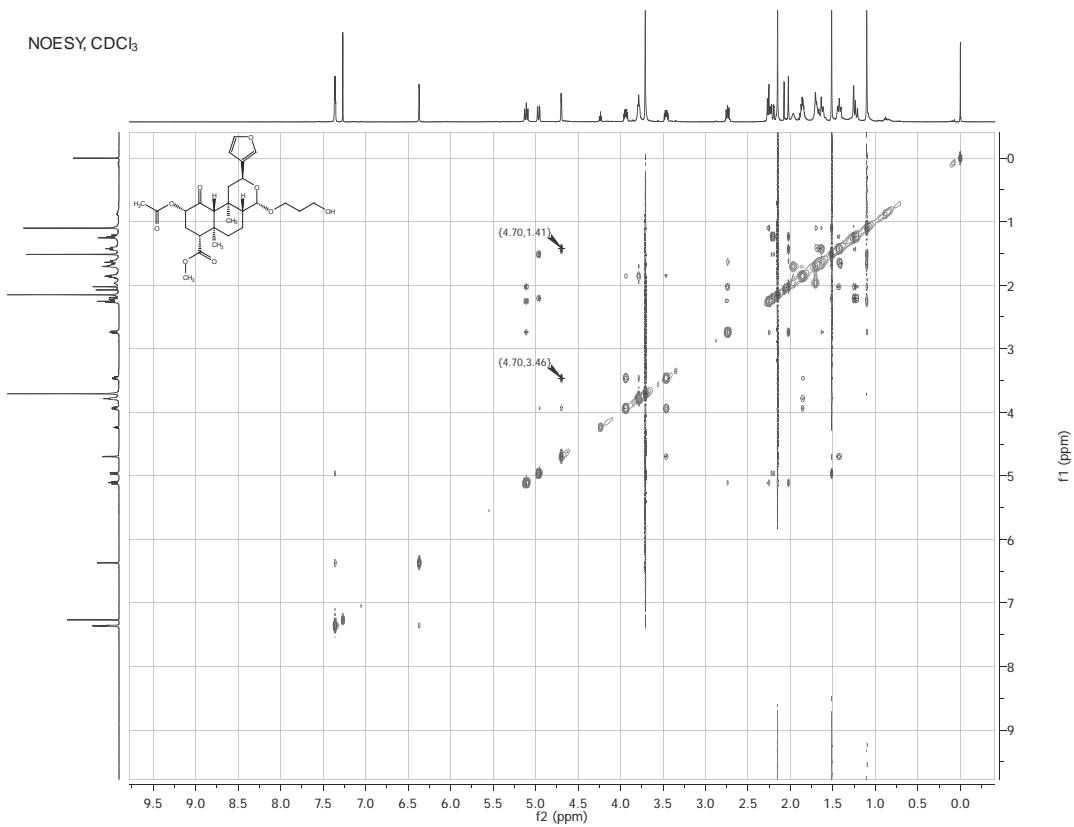


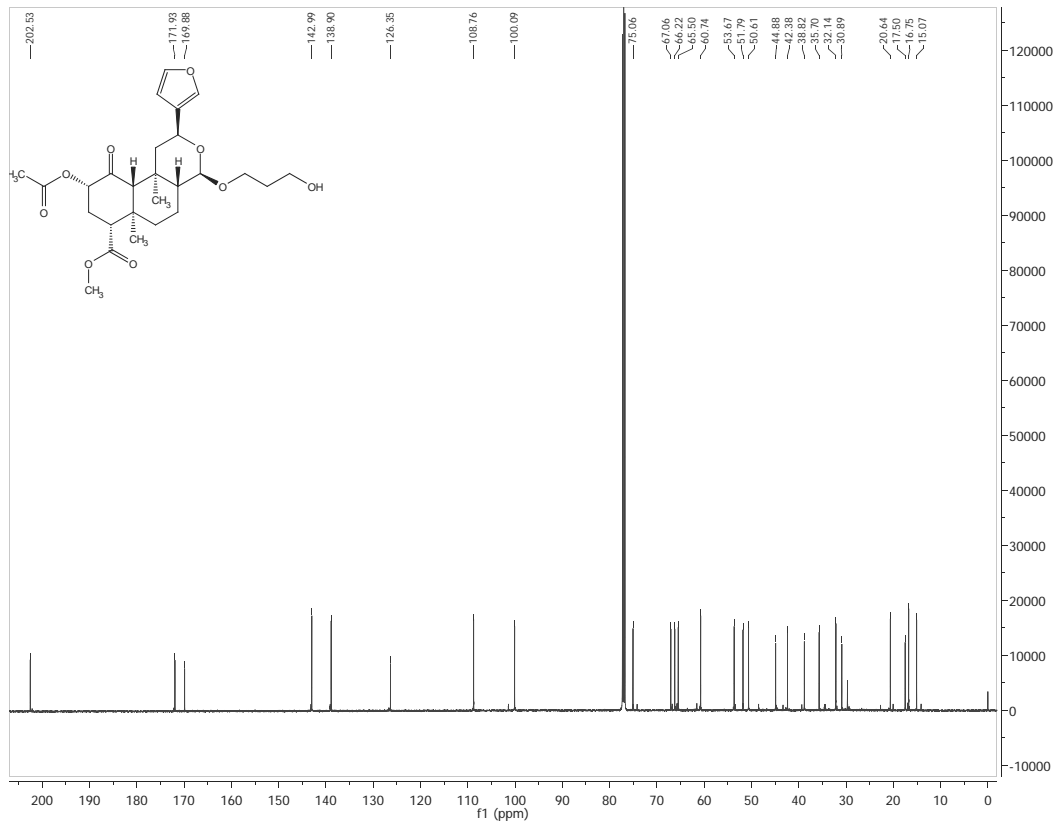
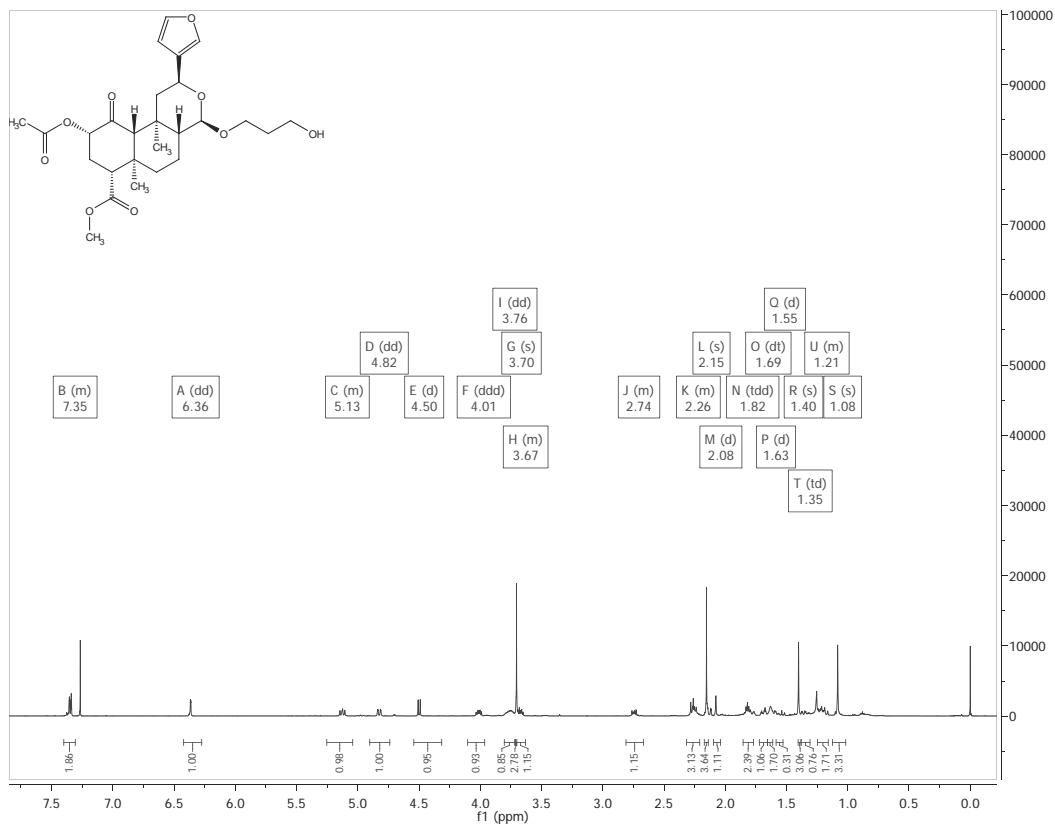


HSQC, CDCl₃

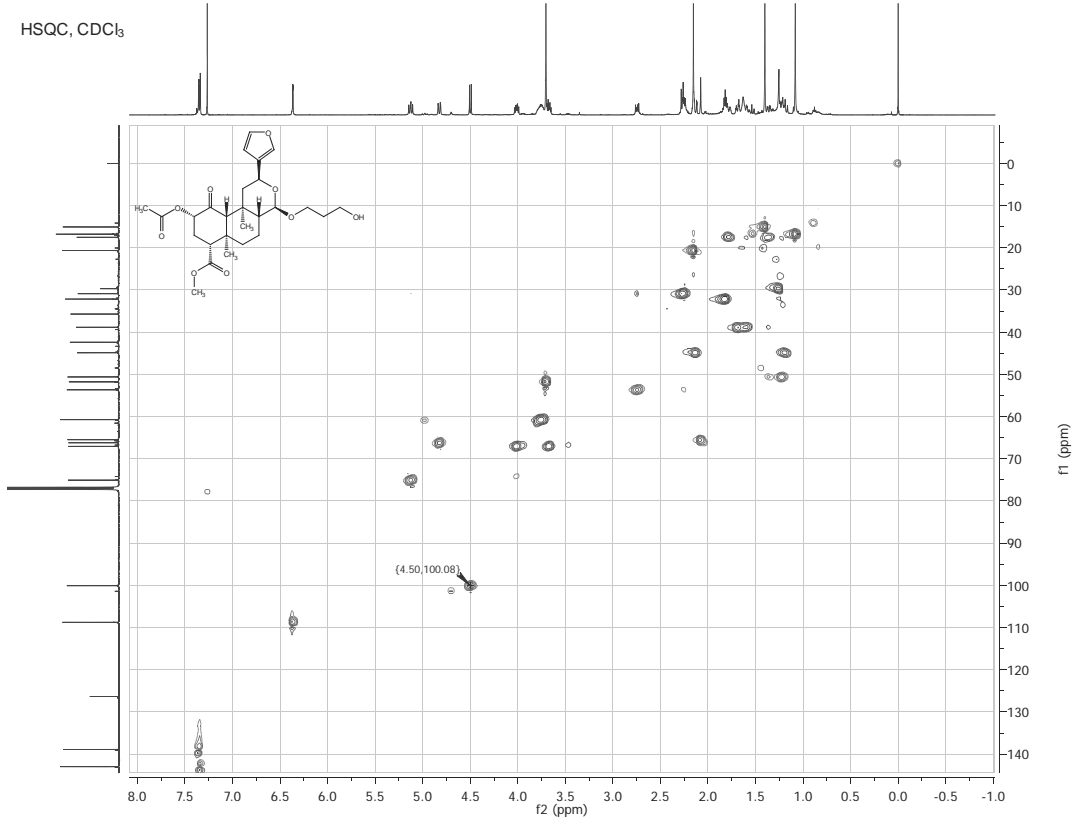


NOESY, CDCl₃

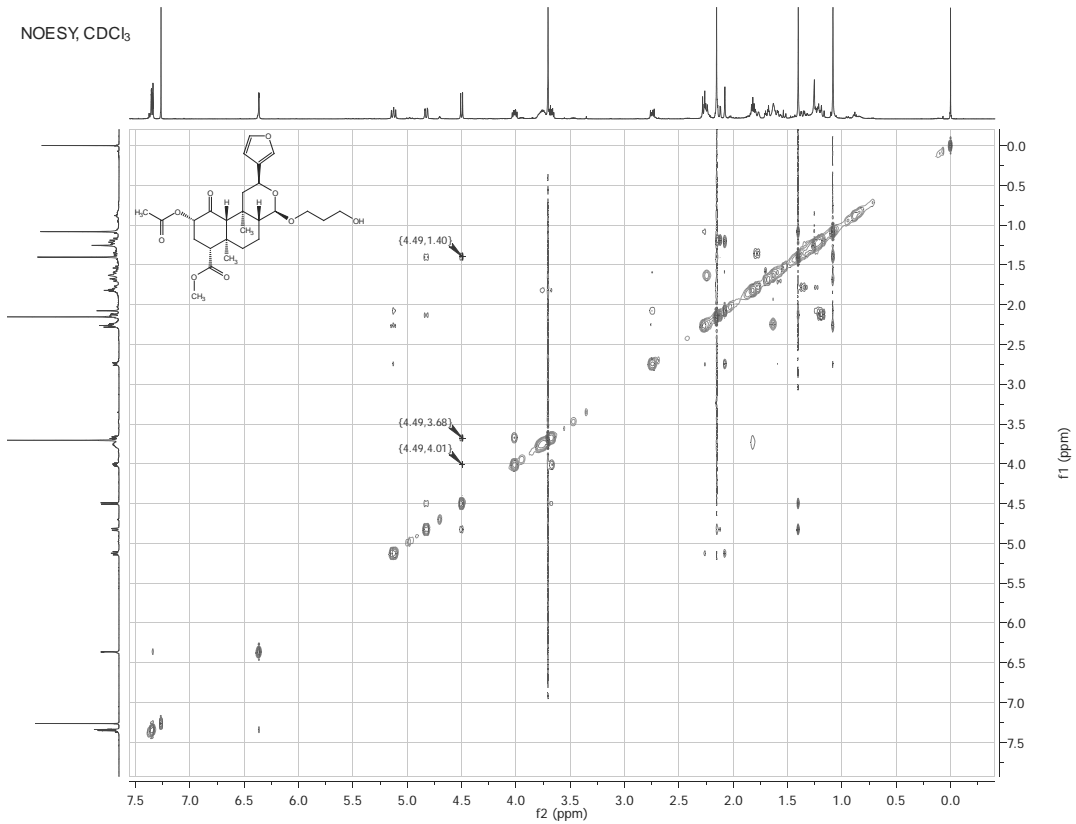


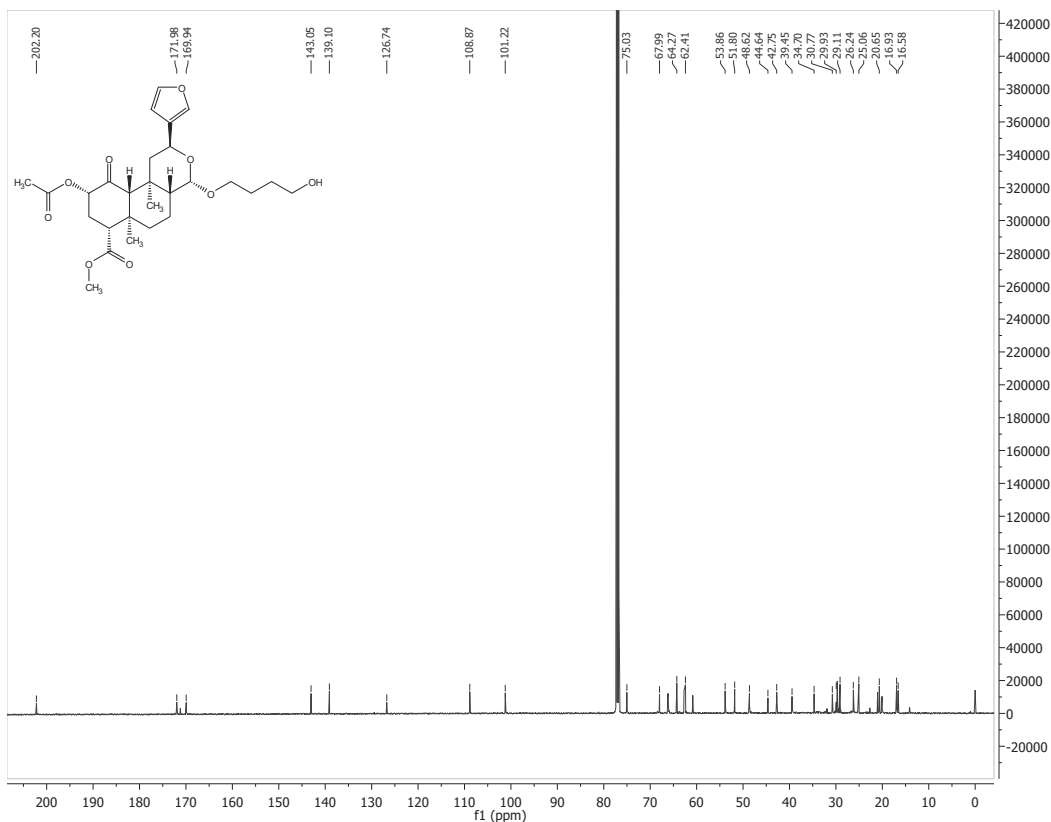
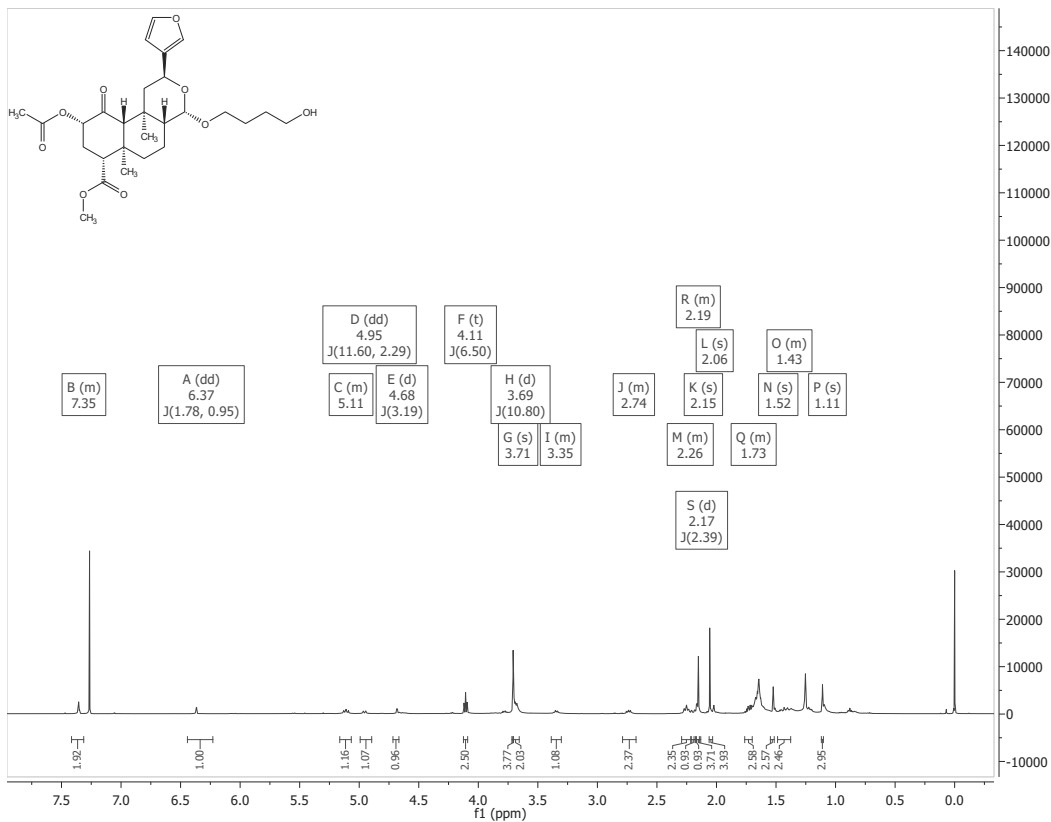


HSQC, CDCl₃

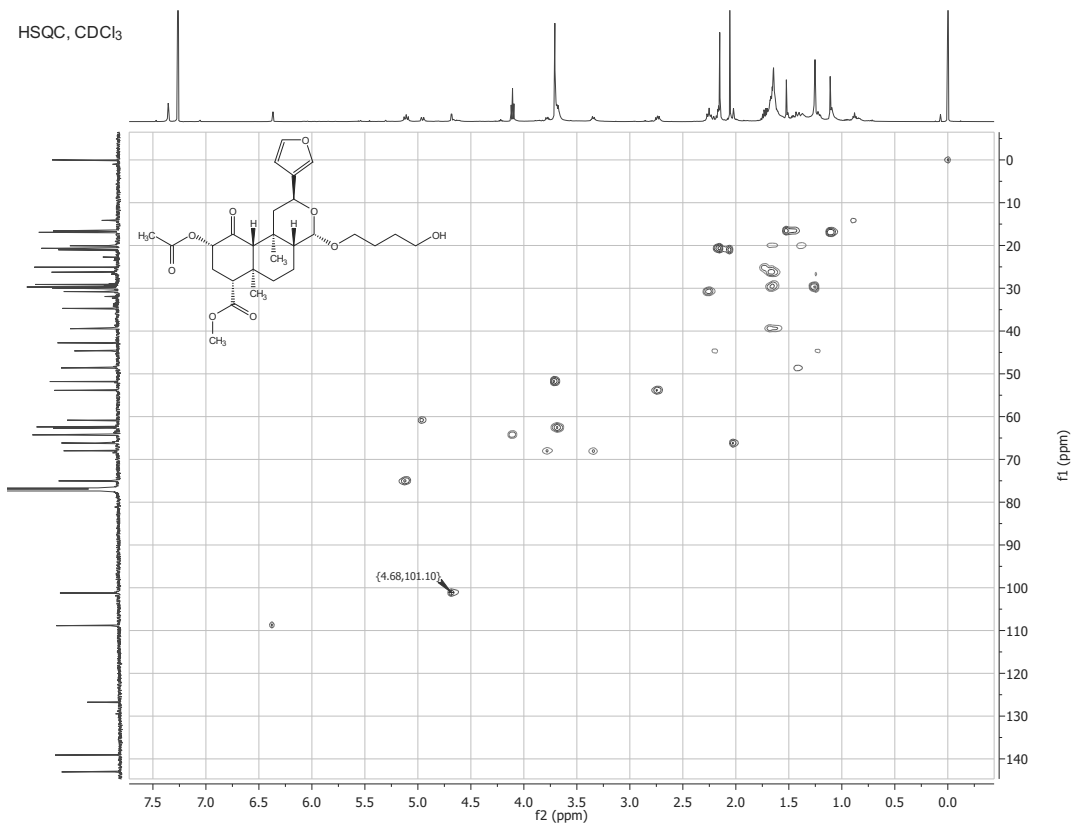


NOESY, CDCl₃

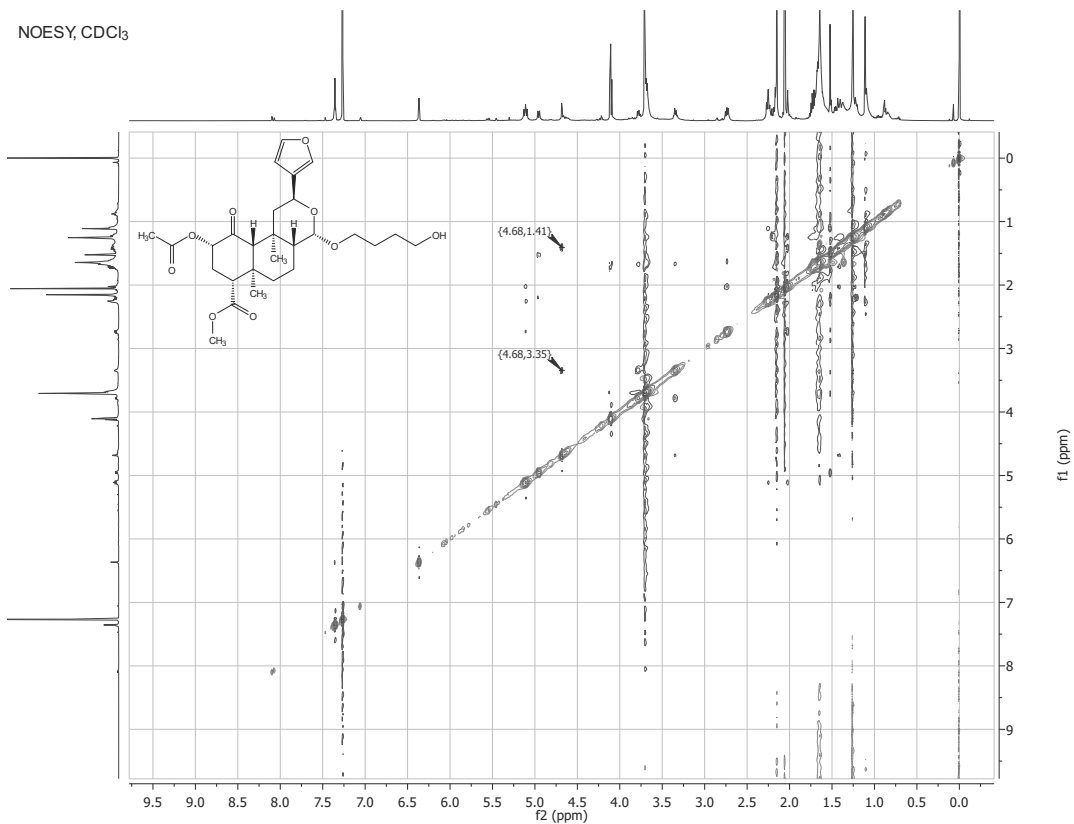


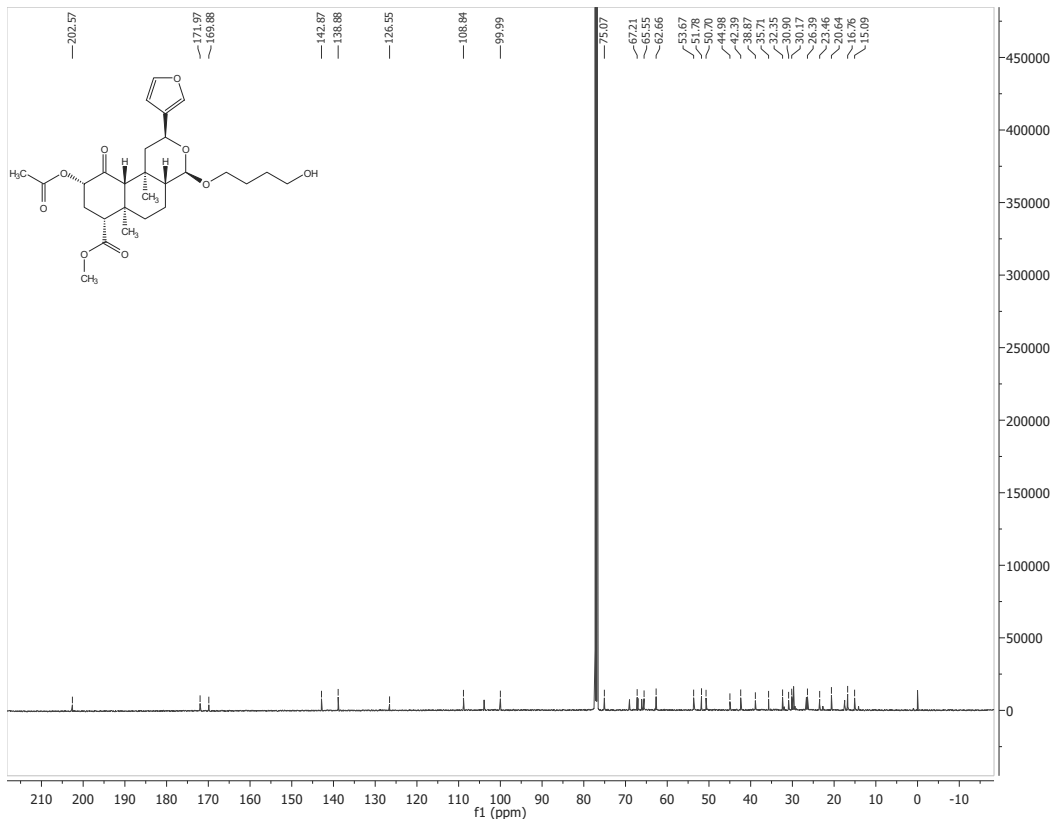
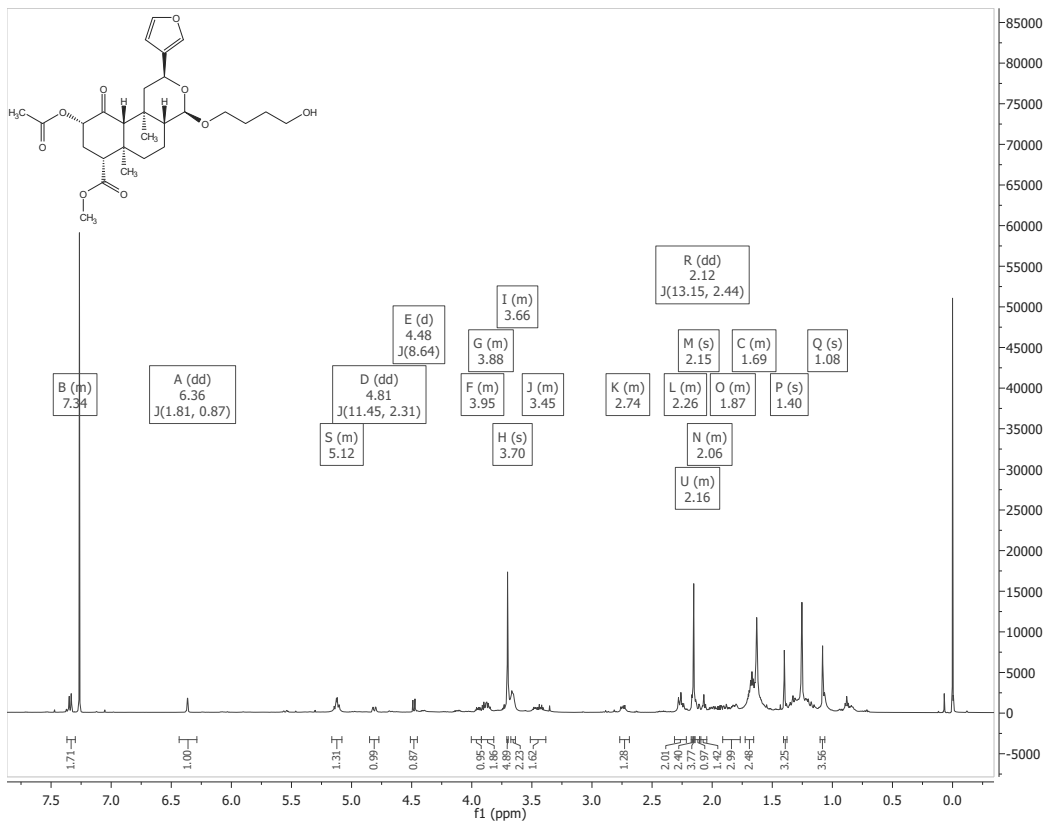


HSQC, CDCl₃

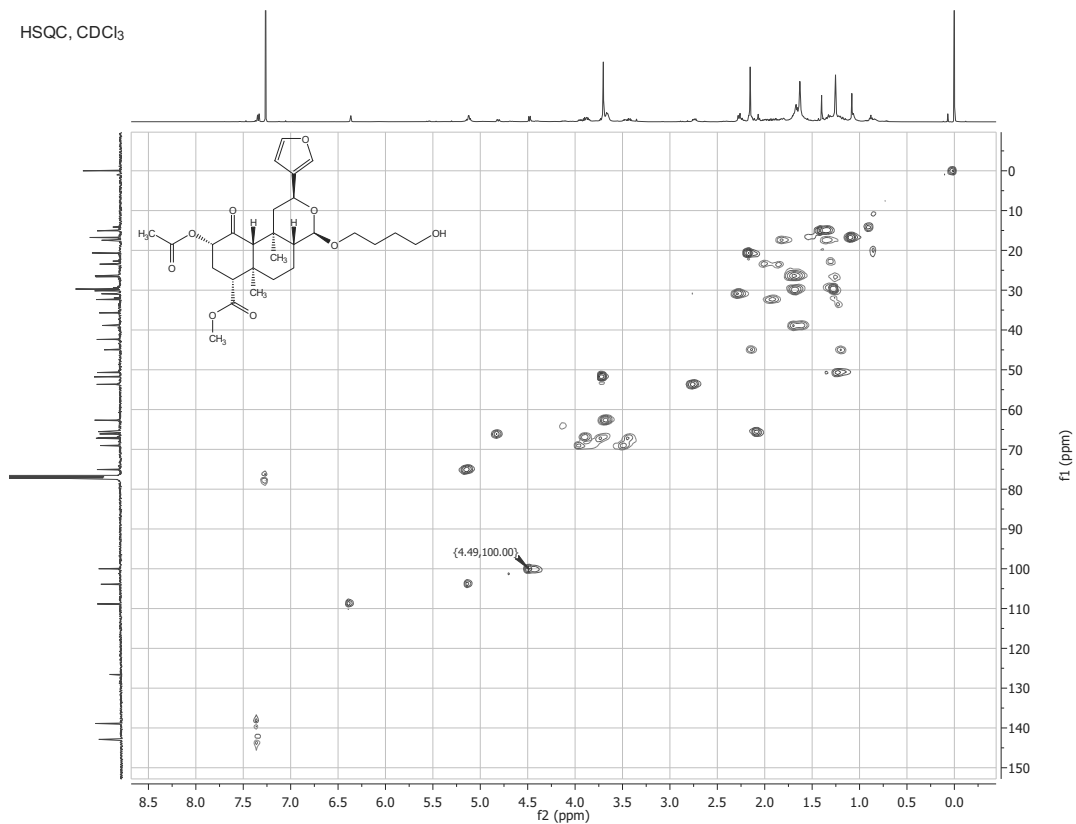


NOESY, CDCl₃

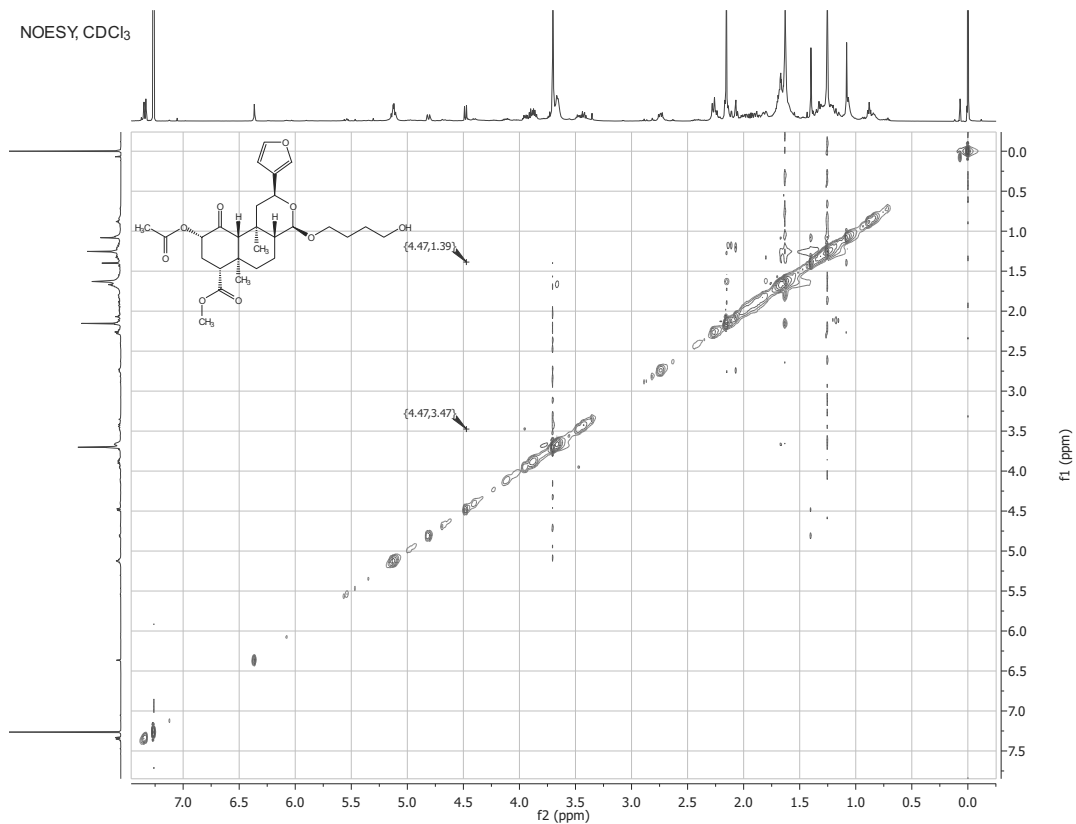


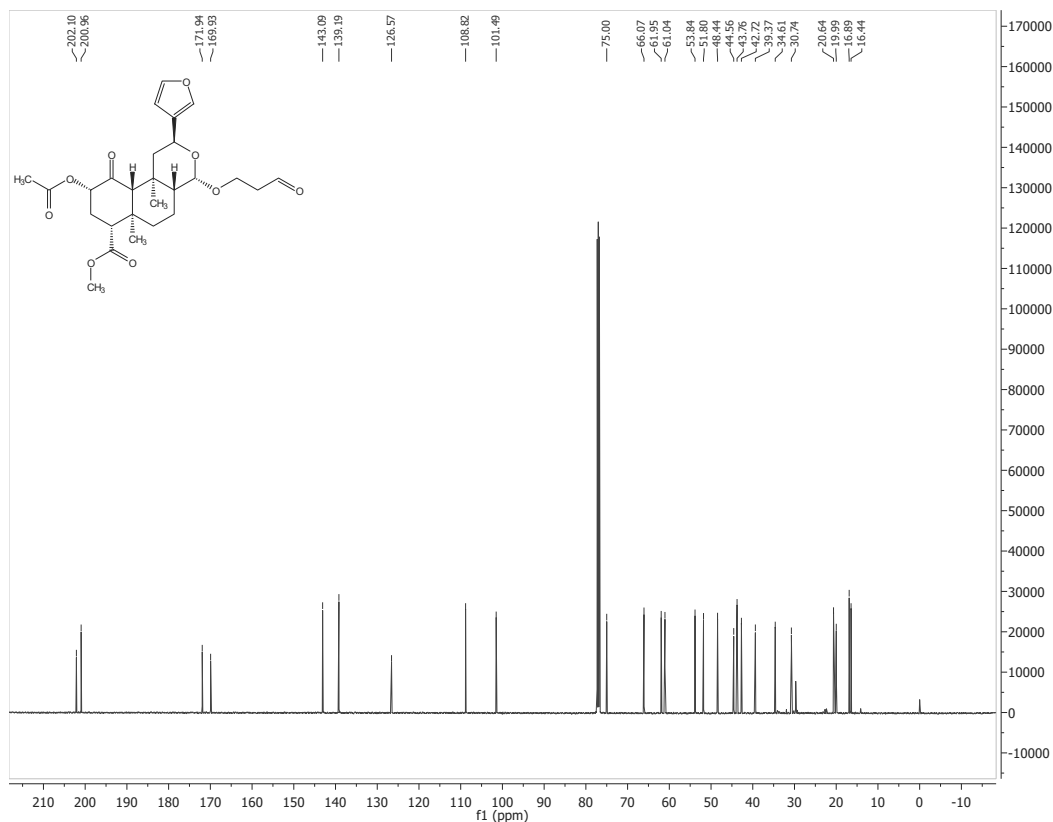
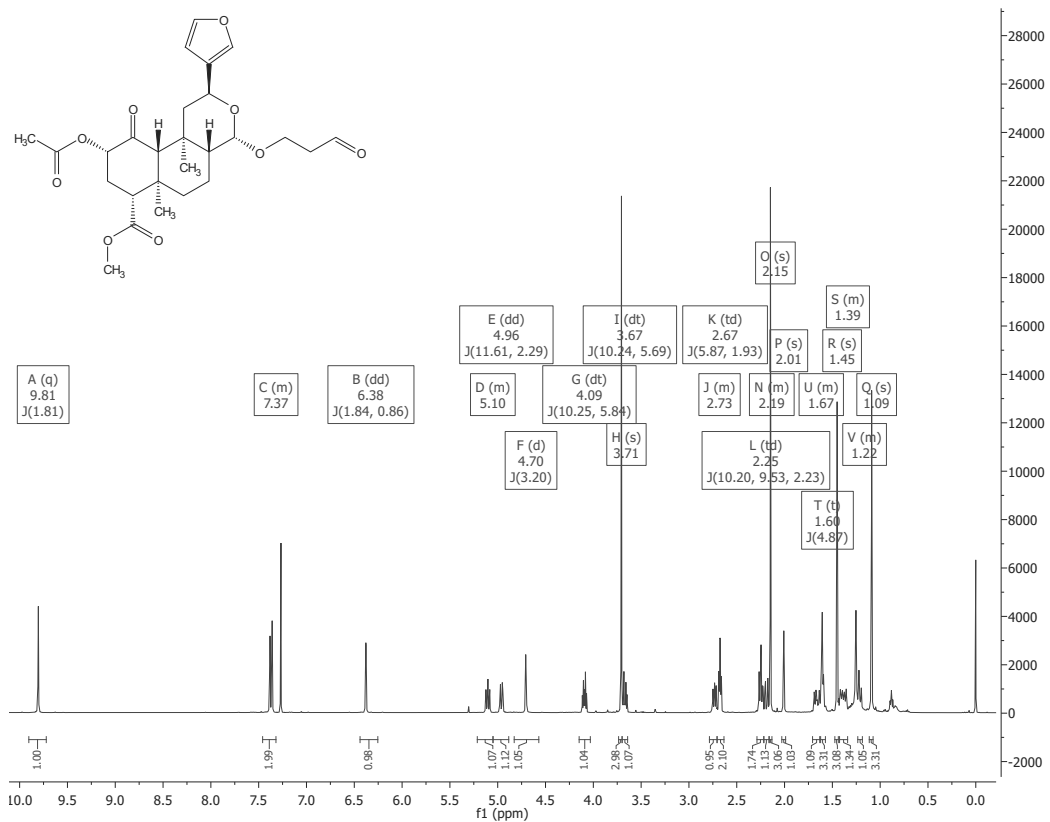


HSQC, CDCl₃

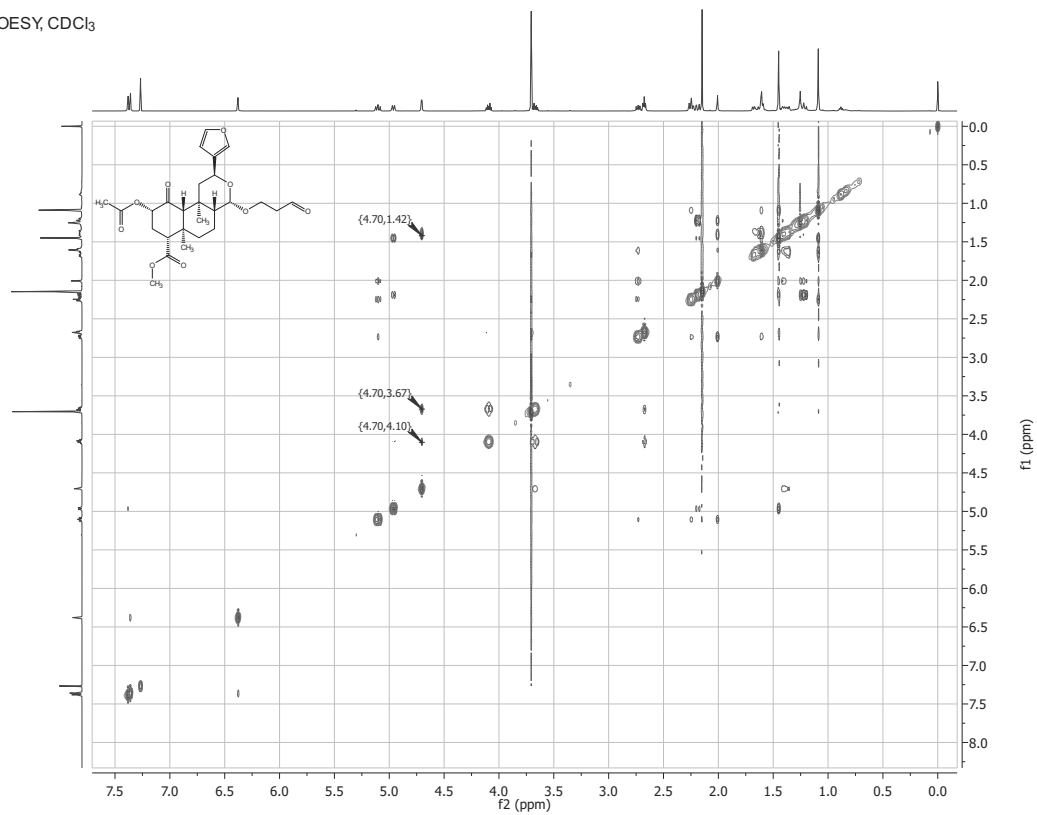


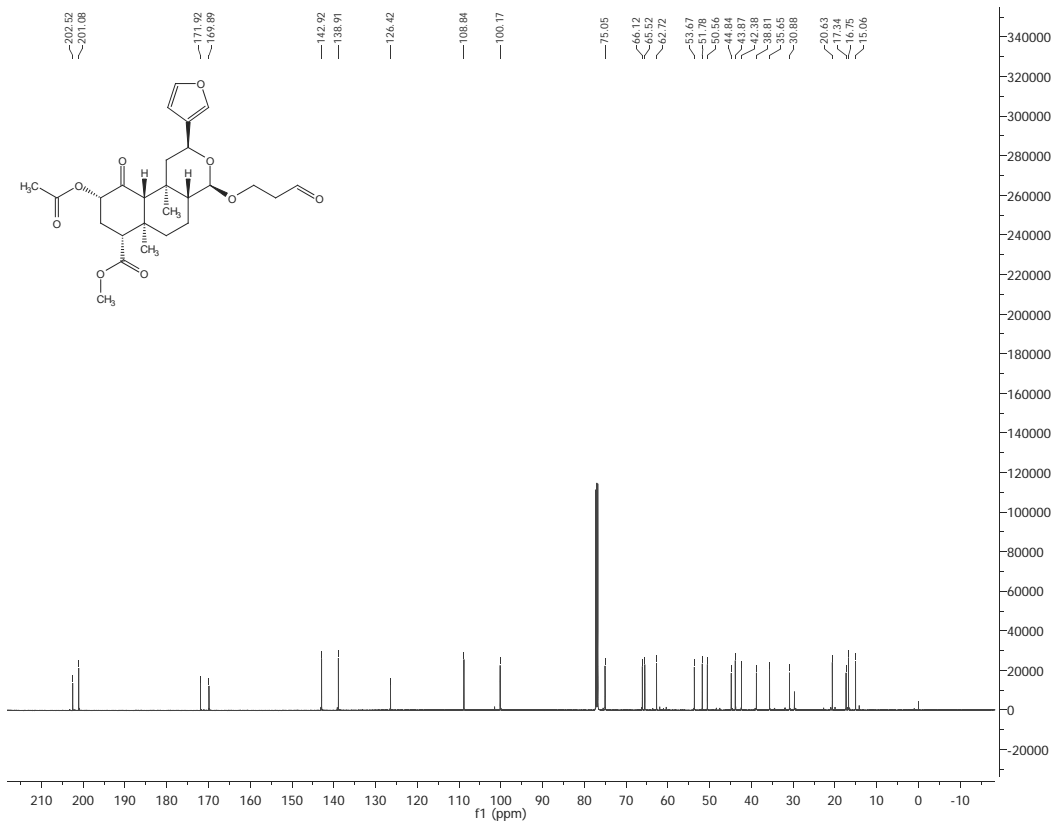
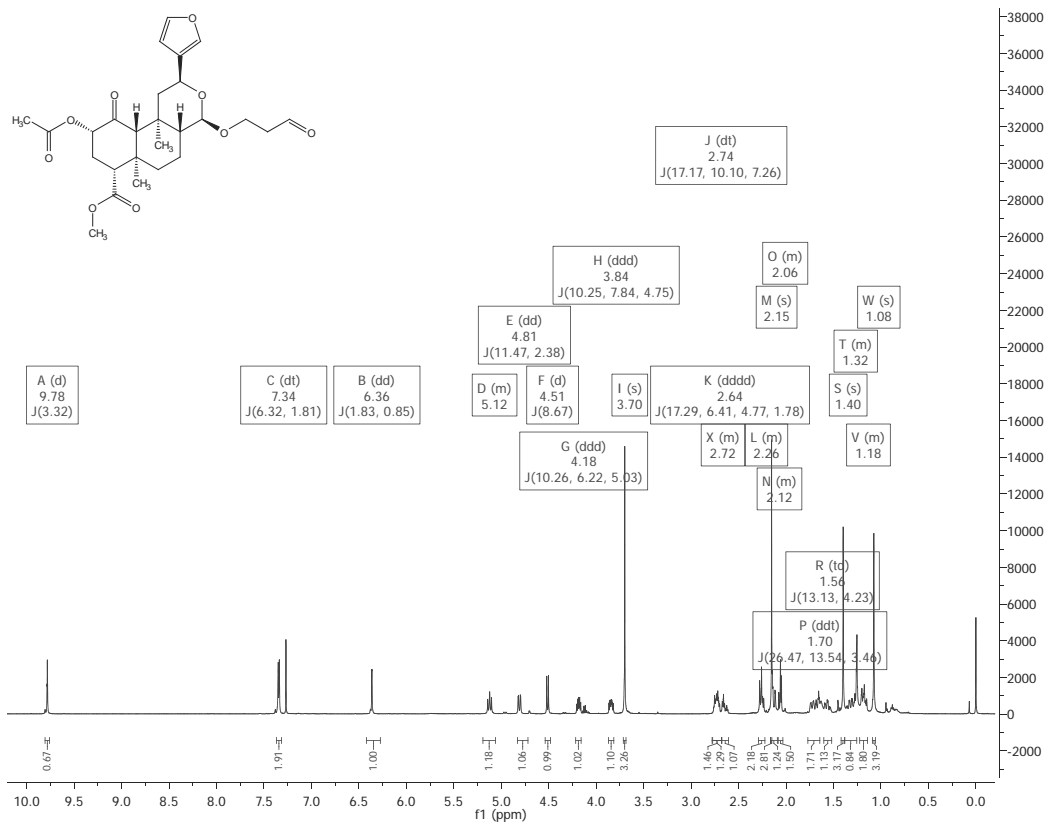
NOESY, CDCl₃



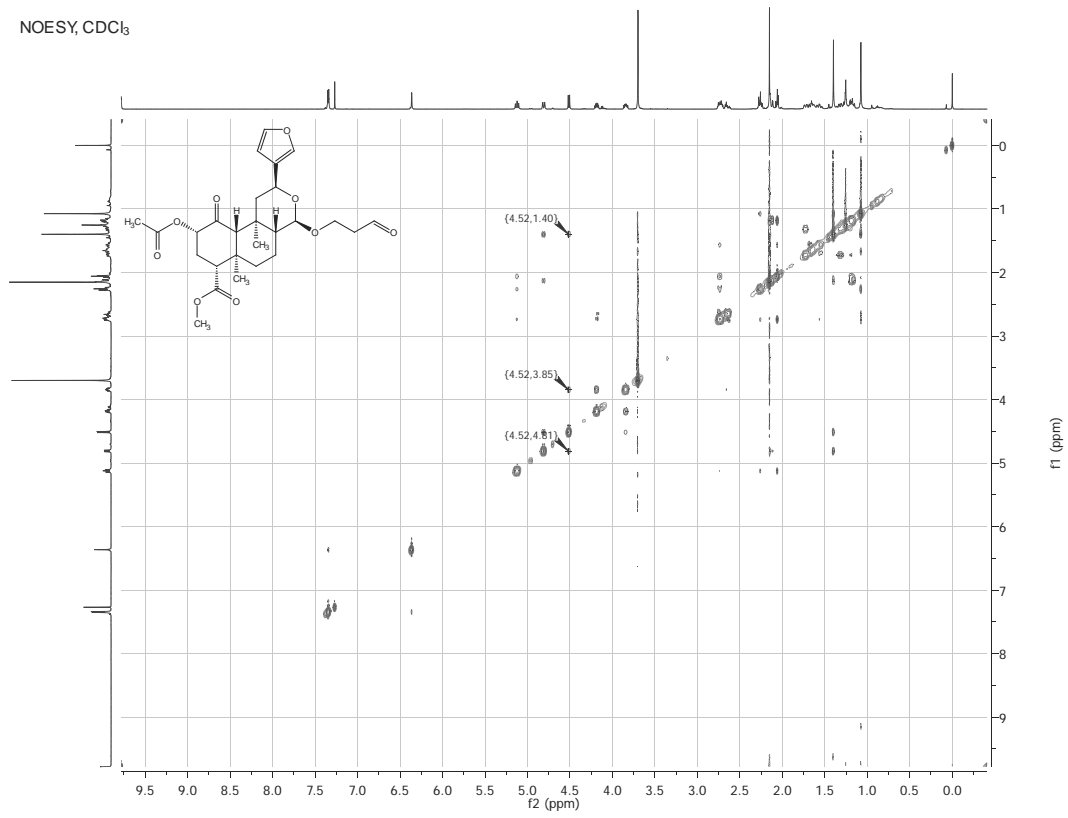


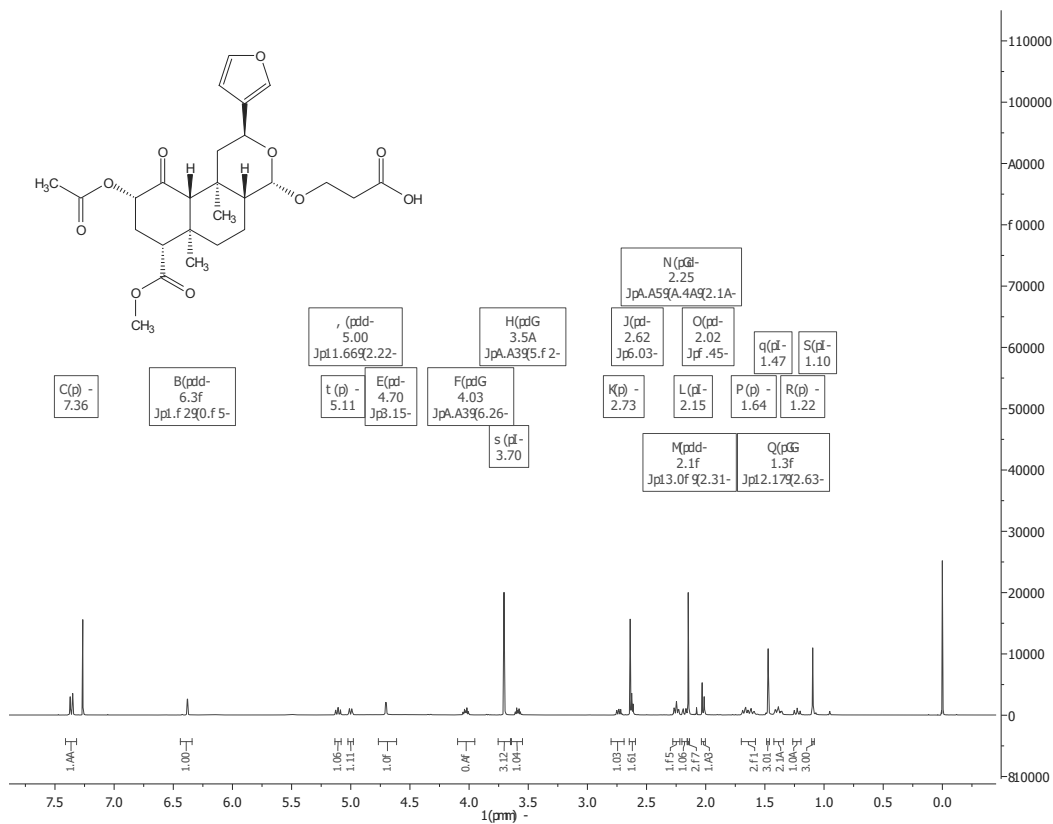
NOESY, CDCl₃





NOESY, CDCl₃





NOESY, CDCl₃

